Diesel Exhaust System Influences on Transient Particulate Emissions and Particle Size Distribution

Cold Start and Fast Acceleration Particulate Mass Emissions and Particle Size Distribution Changes Through a Practical Exhaust System

by

Néstor Y. Rojas

Submitted in accordance with the requirements for the degree of

Ph.D.

University of Leeds

Department of Fuel and Energy

November, 2001

The candidate confirms that the work submitted is his/her own and that appropriate credit has been given where reference has been made to the work of others.

To Ernesto, Martha Lucía, Martha Bibis, Oscar Leonardo and Lucila;

My Beautiful Family.

Abstract

The behaviour of particulate matter emissions from a Ford XLD 4T, passenger car diesel engine through a practical exhaust system in place was investigated during transient conditions, namely cold start and fast acceleration. Particulate emissions were measured at four sampling points through the exhaust system and the changes in particulate total mass concentration, total number concentration, particle size distribution and Carbon/SOF fractions were determined for various engine operating conditions.

Each cold start test consisted of a step-change cold-start with fast acceleration, reaching one of the following target operation conditions: Idle, 1500rpm – 15kW, 2250rpm – 15kW, 2250rpm-35kW and 3500rpm – 15kW. Two preconditioning procedures were designed to provide repeatable cold start tests. These consisted of a) Idle operation for 4 hours the day before the test, followed by overnight soak; and b) 10 minutes at high engine speed operation. Fast acceleration tests consisted of idle preconditioning followed by a step change to the target operation conditions.

The particulate matter changes through the exhaust system were shown to be dependent on the previous operational history of the engine, idle conditions being effective at forming particle deposits. The amount of particulate deposited or blown out from the exhaust system constituted a significant fraction of the total engine exhaust emissions in a significant number of cold start and acceleration tests. The changes in particle concentration did not occur throughout the system in the same fashion. The catalyst produced predominantly particle number and mass reduction and the second silencer was a more efficient particle collector than the first silencer. From the first silencer, particles were resuspended more easily and in many more cases.

Regarding the chemical composition, high-load conditions produced lower Solvent Organic Fraction (SOF) than their low load counterpart. However, the SOF did not change significantly through the exhaust system.

Part of this work consisted of examining the use of the Electrical Low Pressure Impactor (ELPI) to estimate particulate mass emissions. It was observed that the ELPI tended to overestimate the number of particles in the large (>0.1μm) size range. This greatly affected the conversion from total particle number concentration to particle mass concentration. A correction based on comparison between the electrical and gravimetric methods (ELPI vs. Andersen Impactors) in the common size range for both techniques was proposed.

Transient and steady-state tailpipe emission factors, expressed as grams of particulate per unit of engine work in kWh, were calculated from the test results and used to estimate the effect of transients on total cycle emissions in cycles with a different design from those followed in this work.

The ELPI proved to be useful, yet limited for particle collection on Transmission Electron Microscope (TEM) grids in several size ranges. TEM images of particles were analysed and their fractal dimension determined.

Acknowledgements

I would like to express my gratitude to the Department of Fuel and Energy of the University of Leeds, for their support and for giving me the opportunity to do this PhD work.

I wish to give my most sincere thanks to Professor Gordon E. Andrews, for his invaluable guidance and permanent support, his ideas and encouragement. Also I would like to thank Dr. Andrew Clarke for his help with the particle science concepts.

I also would like to thank Mr. Geoff Cole for his support and for all he taught me during the tests. Thanks to Mr. Harry McLeod and Bob Boreham for their help with the engine operation and gas analysis.

I would like to thank my sponsors; the Committee of Vice-Chancellors and Principals of the Universities of the United Kingdom (CVCP) and the Overseas Research Student (ORS) scholarship they awarded me; the University of Leeds for the Tetley and Lupton Scholarship; the Department of Fuel and Energy for the maintenance grant; and the *Corporación para el Futuro de Colombia, Colfuturo*, for the student loan/scholarship that covered the rest of my maintenance.

This work would have not been possible without the shared sponsorship of the EPSRC and Ford Motor Co. through the Joint Research Equipment Initiative, EPSRC grant Grant GR/L26063. Thanks to Ford Motor Co. for donating the diesel test engine and to Tim Sale and Dave Gregory, who offered me their professional support and advise, and gave their permission to publish the papers with the results from this work.

Many thanks to Dr. Rick Brydson and his team at the Electron Microscopy team of the Department of Materials at the University of Leeds for their great help in my learning how to use the TEM and interpret the images.

Finally, I would like to thank all those who gave me their support; my family and my Colombian friends, who were always with me even being on the opposite side of the Atlantic Ocean; and all my friends in Leeds, who will be with me even once they will be all over the world.

Contents

Figures

Tables

Abbreviations

ACEA	Association des Constructeurs Europeens d'Automobiles
AEA	Atomic Energy Authority Research Establishment (AEA Technology)
AFR	Air/Fuel Ratio
atdc	after top dead centre
BLPI	Berner low-pressure impactor
BP	British Petroleum Co.
btdc	before top dead centre
CI	Compression ignition
CMD	Count median diameter
CNG	Compressed Natural Gas
CNC	Condensation Nuclei Counter
CO	Carbon monoxide
CO_2	Carbon dioxide
COMEAP	Committee on the Medical Effects of Air Pollutants
CONCAWE	The Oil Companies European Organisation for Environment, Health and Safety
CPC	Condensation Particle Counter
CVS	Constant volume sampling
DETR	Department of Environment, Transport and the Regions
DI	Direct injection
DOC	Diesel oxidation catalyst
DPF	Diesel particulate filter
DR	Dilution ratio
EGR	Exhaust Gas Recirculation
EI	Emission Index, g/kg fuel
ELPI	Electrical low-pressure impactor

EPA	Environmental Protection Agency
EPEFE	European Programme on Engines, Fuels and Emissions
ESC	European Steady-state Cycle
ETC	European Transient Cycle
EUDC	European Urban Driving Cycle
FID	Flame Ionisation Detector
FTP	Federal Test Protocol
GC	Gas Chromatography
HC	Hydrocarbon (s)
HGV, HDV	Heavy-goods vehicles, Heavy-duty vehicles
IC	Intercooled
IDI	Indirect injection
IEA	International Energy Agency
LDV	Light-duty vehicles
LEV	Low-emission vehicles
LPG	Liquefied Petroleum Gas
MGV	Medium-sized goods vehicles
MOUDI	Micro-orifice uniform deposit impactor
mph	miles per hour
MS	Mass spectrography
N/A	Naturally aspirated
N_2O	Nitrous oxide
NMHC	Non-methane hydrocarbons
NO	Nitrogen oxide
NO_2	Nitrogen dioxide
NO_x	Nitrogen oxides (including NO, NO_2 and N_2O)
OECD	Organisation for Economic Cooperation and Development
OH	Hydroxyl radical
PAC	Polycyclic Aromatic Compounds

PAH	Polycyclic Aromatic Hydrocarbons
PM	Particulate matter
PM_n	Total Particulate matter finer than *n* size (*n* in μm), as in PM_{10}
ppb	parts per billion
ppm	parts per million
QCM	Quartz Crystal Microbalance
QUARG	Quality of Urban Air Review Group
rpm	revolutions per minute
SAE	Society of Automotive Engineers
SEM	Scanning electro-microscope
SI	Spark ignition
SMMT	Society Of Motor Manufacturers And Traders
SMPS	Scanning mobility particle sizer
SO_2	Sulphur dioxide
SOF	Solvent organic fraction
TC	Turbocharged
TCIC	Turbocharged – Intercooled
TEM	Transmission electro-microscope
TEOM	Tappered-element microbalance
TGA	Thermo-gravimetric analysis
THC	Total Hydrocarbons
TWC	Three-way catalyst
UHC	Unburned Hydrocarbons
ULEV	Ultra-low-emission vehicles
ULSD	Ultra-low sulphur diesel
VOC	Volatile organic compounds
WHO	World Health Organisation

Symbols and units

a	aggregate (as a subscript)
A_a	projected area of an aggregate (μm^2, nm^2)
A_p	projected area of a primary particle (μm^2, nm^2)
$\overline{U}$	average velocity in pipe
b	constant in Equation 1.34.
B	particle mobility (cm/s dyn)
C_c	Cunningham slip correction factor
C_{crit}	Threshold concentration for nucleation ($\mu g/m^3$)
C_d	drag coefficient
d	pipe diameter, particle diameter (μm, nm)
d_a	aerodynamic diameter (μm, nm)
d_g	geometric mean diameter (μm, nm)
d_p	particle diameter, mobility diameter (μm, nm)
D_f	fractal dimension
D_v	diffusivity of vapour molecules (cm^2/s)
D	diffusivity, particle diffusion coefficient (cm^2/s)
e	electron charge
E	Capture efficiency, electrical field
F	Force, N
F_c, F_a	forces of collision and adhesion, N
f	friction factor
g	acceleration of gravity, gas (as a subscript)
H	Hamaker constant ($2x10^{19}$ J)
i	undetermined subscript, individual (e.g. N_i, M_i, d_i, etc)
J_d, J_r	particle deposition and resuspension fluxes (kg/m^2s)
k	Boltzmann constant ($1.38x10^{-16}$ dyn cm/K)

k_{fc}, k_m	auxiliary parameters in equation 1.80
K	coagulation coefficient (cm^3/s)
Kn	Knudsen's number
L	maximum length of an agglomerate (μm, nm), tube length (m)
M	molecular weight
m_a	aggregate mass (g, mg, μg)
M_p	particle mass concentration, mg/m^3
m_p	primary particle mass (g, mg, μg)
$\overline{m_s}, \overline{m_t}, \overline{m_c}$	work-specific particulate mass emissions during steady-state, transient or a cycle, g/kWh.
N	particle number concentration, cm^{-3}
N_0	number of particles in smallest aggregate for Equation 1.2.
N_a	number of particles in an aggregate
N_{av}	Avogadro's number
P	penetration rates ratio, Penetration
p	pressure (atm), particle (as a subscript)
pa	particle-aggregate (as a subscript)
p_d	vapour pressure over a particle (atm)
p_s	vapour, or saturation, pressure (atm)
Q	volumetric exhaust flow, flow rate
r_{sa}	surface average roughness (m)
r_{sa}^*	surface critical roughness (m)
R	universal gas constant
Re	Reynold's number
R_g	radius of gyration (μm, nm)
RH	relative humidity
R_p	particle radius (μm, nm)
S	saturation ratio
Sc	Schmidt number

s_g	geometric standard deviation
Sh	Sherwood number
Stk	Stokes number
T	temperature (^oC, K)
t	time, s
U, V	velocity (m/s, cm/s)
ν	*Poisson's ratio*
$\bar{\nu}$	molar volume of a liquid
v_m	molecular volume (m^3)
Vts	terminal settling velocity, m/s
x_{rms}	root mean square distance (m, μm, nm)
w_s, w_t, w_c	work delivered by the engine during steady-state, transient or a cycle, kWh.
W/A	deposition layer particle concentration per unit area (kg/m^2)
Z	electrical mobility
α, β	angles in the definition of deposition and adhesion moments, equation 1.79
χ	particle shape correction factor
ε	rate of energy dissipation
ϕ	pipe bend angle, radiants; equivalence ratio
γ	ratio of the specific heat at constant pressure to the specific heat at constant volume; Dupré energy of adhesion.
η	viscosity of the gas, efficiency
λ	mean free path, μm
θ	pipe inclination, degrees
ρ	density (kg/m^3)
ρ_g	gas density (kg/m^3)
ρ_p	particle density (kg/m^3)
σ	surface tension

σ_g	geometric standard deviation

Chapter 1.
Diesel particulate emissions – A review on recent concerns, measurement techniques and previous results

Emissions from combustion sources, particularly from automotive engines, are responsible for a considerable fraction of air pollution (OECD, 1988; Whitelegg, 1993) and play a very significant role in Global Warming processes (MacLean, 1998), perhaps one of the most disquieting environmental issues of our society in the last decade. In this scenario, the combination of fuel and engine technology that can produce the lowest amount of greenhouse gases per unit of power generated at a reasonable cost will be preferred over other technologies. Diesel engines are extremely efficient power plants and emit about 20% less greenhouse gases than gasoline engines (IEA, 1993), so they would be very strong candidates to become dominant in the market if greenhouse gas emissions were the main selection factor. Another factor, however, put diesel engines in disadvantage: diesel exhaust particulate pollution.

Diesel particulate emissions are one and even two orders of magnitude higher than those from gasoline engines (Ahamed, 1997; Hill, 2000), and such emissions are considered as a threat to public health, according to evidence from numerous toxicological and epidemiological studies (Walsh, 1999). Death rates and concentration of particles with a diameter of less than 10μm (PM10) have shown to be strongly associated, with a 1% increase in the number of deaths caused by a $10\mu g/m^3$ increment in particulate mass concentration. The highest risk is probably due to particles smaller than 2.5μm, PM2.5 (HEI, 1995). Current emissions legislation is for total particulate mass concentration, which is effectively PM10 legislation, as diesel and Spark Ignition (SI) size measurements show that virtually all particles are finer than 10μm, with an additional limit for PM2.5 in the USA since 1999. These legislative controls have forced car companies to achieve important improvements in combustion and aftertreatment technologies. Particulate emissions within Europe have been reduced by about 80% since 1980 and, for the EU-15, a 75% reduction in particulate emissions from diesel vehicles between 1990 and 2010 has been predicted, after the implementation of the Auto-Oil I Programme (CONCAWE, 1999). This includes a 30% predicted growth in road transport, from which diesel passenger cars count for a steadily increasing fraction since 1980 in Europe and a steady fraction in Japan and the USA (Walsh, 1999).

Recently different researchers have shown evidence that particle size distribution, particle number, particle surface area and particle composition are potentially more critical factors than particulate mass, regarding their interaction with lung or alveoli cells (Seaton 1985, Oberdörster 1994). It is not clear that legislation to mass concentration also controls the number of fine particles. This prompts a debate on which of those factors is most important to be regulated and how the new decisions will affect the emission measurement standards (ETH, 2000). Also, for many researchers, current knowledge on measuring diesel particle size distribution is not mature enough for legislative purposes, since there are still uncertainties in the reproducibility and comparability of the results obtained by different groups and technologies. It is estimated that by August 2002 legislative decisions on this matter will have been made in the European Union context, where current limits for particulate matter emitted by new diesel passenger cars are 0.08g/km and will be 0.05g/km in 2000 and 0.025g/km in 2005 (Walsh, 1999). This converts to 0.32 g/kg-fuel (Emission Index) using 79g/km fuel consumption. Over the 160,000km that the 2005 emissions control technology has to be validated for, the total mass emitted will be 4.0kg. If the engine manufacturers develop engines to produce 25% below the standard, as is normal to account for production variability, then the total mass emitted by a diesel passenger car over 160,000km will be 3.0 kg.

Legislation uses driving cycles that try to account for the particulate emissions at different engine operation conditions, representative of urban and/or motorway driving. Some engine conditions provoke higher emission rates of particulate matter to the atmosphere, either by affecting the engine performance or inducing changes in the exhaust system. From these, cold start is, perhaps, the most critical transient state tested in regulated driving cycles, leading to engine particulate and gaseous emissions that are several times higher than steady state emissions. According to Hall et al. 1998, the particulate mass emissions are higher during cold start owing to the production of larger particles during this period. Rapid acceleration transients in these tests produced higher levels of particle number at high speed. These transients can also produce undesirable and unpredictable emissions of visible particulate clouds, a situation experienced by low emission diesel car users of several manufacturers. The latter problem, however, is not present in legislated driving cycles and only occurs in real world driving.

Unpredictable visible levels of particulate emissions have occurred after a new exhaust system has been in operation for typically six months to one year of average use. Drivers that normally only use relatively low power in city driving, with little high speed operation, often find that when they undertake a high speed or high acceleration manoeuvre, a cloud of visible particulates are emitted (Sale, 1998). One

situation where this often occurs is in the acceleration onto a motorway or freeway after relatively slow speed city-street driving over the previous days. Drivers that regularly have fast accelerations and sustained high speed driving as part of their normal driving pattern will not experience the problem as their exhausts are regularly being cleared of any accumulated particles. Low speed commuting journeys, several short duration journeys per day, or peak time journeys in traffic jam conditions are the type of real world driving that will lead to the storage of particulates in exhaust systems on a sustained basis.

Several manufacturers of passenger car diesel engines have experienced this phenomenon of sudden release of particulate in low emission diesel vehicles. The 3.0 kg to be emitted by low emission diesel engines over 160,000km are not a large amount of particulate and could be stored in exhaust systems or traps designed for this purpose. However, the problem is difficult to reproduce in the laboratory and is not a feature of legislated test procedures. The observed phenomenon obviously involves the storage of particulates in exhaust systems, as the equivalent acceleration events in the EUDC part of the test cycle do not give this phenomenon. Evidence can be found that diesel exhaust systems contain accumulated particulate matter in the silencer boxes, which is observed when they are cut open for inspection.

This work investigates the changes suffered by particulate matter through a practical diesel passenger car exhaust system, under the critical cold start and rapid acceleration operation conditions. This was studied in terms of mass concentration, number concentration, size distribution, chemical composition and physical structure, and the aim was to reproduce in the laboratory, the deposition and blow-out phenomena that have been observed only in real driving conditions and have not counted in legislative driving cycles. Techniques used included the procedure of the Society of Automotive Engineers (SAE) for filter mass determination at 52°C, Andersen Impactors sampling at 100°C for mass size distribution, Electrical Low Pressure Impactor (ELPI) for number size distribution, Thermogravimetric Analysis (TGA) for chemical composition, and Scanning Electron Microscopy (SEM) and Transmission Electro-microscopy (TEM) for particulate structure imaging.

From the measurement experience developed in this work, the author has also analysed some aspects of the particle number-to-mass conversion issue, which has been shown to be a difficult problem among the scientific community in this field.

The following chapters develop the investigation as follows:

Chapter 1 contains a brief literature review regarding particulate matter characteristics, measurement techniques and conditions to support the legislative process and technological approaches to particulate reduction.

Chapter 2 describes the experimental techniques and conditions used in the present work.

Chapters 3 and 4 present an analysis of the changes along the exhaust system during cold start, in terms of particle mass, number, size distribution and chemical composition.

Chapter 5 shows a similar analysis of the changes of diesel particulates through the exhaust system for the rapid acceleration tests.

Chapter 6 shows support results from steady-state tests.

Chapter 7 focuses on the discussion on the results.

Chapter 8 presents the conclusions derived from the present work and suggestions for future work.

1.1. Objective of this work

This work investigates the changes experienced by diesel exhaust aerosol through a practical exhaust system during cold start and acceleration periods. This is to be achieved by sampling and characterising the aerosol at four points along the system, and then looking for key changes in some aerosol characteristics such as total mass and number concentration, particle size distribution and, to a certain extent, chemical composition and particulate morphology through image analysis. In the exhaust and sampling systems, the exhaust aerosol is exposed to changes in temperature, flow regime and direction, transport line geometry and roughness, among many others. Measuring its particulate mass concentration and collecting particles for chemical analysis involves the separation of the particulate phase from the gas phase by filtration. Particle number concentration and particle size distribution measurement techniques may require dilution with fresh air, followed by the exposition to electrical and/or inertial fields. Imaging of the particles requires the particulate collection on a suitable substrate and exposition to electron beams in electron microscopes.

As a result of the various conditions present in the transport through the exhaust system, sampling lines and measurement devices, the aerosol undergoes numerous changes. The processes responsible for these include: particle deposition on the surfaces of transport lines and other devices; reentrainment and outgassing from them; particle coagulation to form larger agglomerates; condensation of vapour phase components to form new particles or cause particle growth; chemical reactions within the particles and on their surface, among others. Many of these processes are well understood, but some of them are not, therefore creating uncertainties and

unpredictable events such as those that originated the idea for the present work. This chapter aims to briefly describe the present knowledge around those processes, how they have been used to develop aerosol characterisation techniques and a review of important results emerging from the use of these techniques, after presenting an overview of the health and environmental aspects of particulate matter, as well as the role of transport in particulate emissions.

1.2. Health and environmental impacts of particulate matter

PM10, the total mass concentration of particles smaller than 10μm in an aerosol, is the parameter used for legislative control of particulate emissions and air quality standards and, for their aerodynamic characteristics, these particles can penetrate into the human respiratory system and deposit through it. Practically the totality of the particle mass emitted from diesel engines is below this limit (Table1.1.), which has created a number of concerns over diesel particulate emissions.

It has been found that atmospheric PM10 correlate well with mortality, morbidity, asthma and lung function statistics (COMEAP, 1995; Hall, 1998; Pope, 1992). A $10\mu g/m^3$ rise in PM10 concentration can be associated to a 1% increase in the relative risk of mortality from all causes in the exposed population. The same increase in PM10 is accompanied by a 1.4% increase in mortality from cardiovascular causes and a 3.4% increase in the relative risk of respiratory causes of death (Dockery, 1994). According to the US Six cities study (Dockery, 1993), the rise and fall in non-accidental death rates is linked to daily levels of fine particulates (PM2.5) but not with other pollutants. The correlation held even at low levels.

An important fraction of diesel combustion particles is formed by organic compounds that have been shown to have a carcinogenic effect. Rats exposed to high concentrations of diesel exhaust unmistakably developed lung cancer, giving clear evidence of carcinoginecity (Mauderly, 1994). On the other hand, epidemiological studies have shown that an increased risk of lung cancer was detected in populations heavily exposed to diesel fumes, but this constituted limited evidence only (COMEAP, 1995). Reports by the World Health Organisation (WHO) in 1996 and the California and US EPAs in 1998 coincide in the sufficiency of rat studies in demonstrating the carcinogenicity of diesel exhaust, as well as in the lack of unambiguous evidence for human epidemiology studies (HEI, 1999). Diesel exhaust remains classified by the International Agency for the Research on Cancer (IARC) as probably human carcinogenic (Harrison, 1993; HEI, 1999). It is still unclear if the carcinogenic characteristics of diesel exhaust are due to carcinogenic

volatile compounds, such as benzo(a)pyrene or benzo(a)anthracene, absorbed on the particles, or to the particles themselves, stripped of organic and other materials on the surface (Mauderly, 1994).

Particles deposit in different sections of the respiratory system according to their aerodynamic behaviour, which is dependent on the particle size. Alveolar deposition starts becoming important below 4µm and much more significant below 0.4µm, and the fraction of particles around this size is called 'respirable fraction' by some authors (Hall, 1998). A 'high risk respirable fraction' was also defined by EPA for particles smaller than 2.5µm, or PM2.5, after comparing PM10 and PM2.5; the EPA concluded that ambient coarse fraction particles are either less potent or a poorer surrogate for community effects of air pollution than air fine fraction particles (Baker, 1998), and defined a PM2.5 standard of an annual average level of 15mg/m^3 and a 24-hour standard of 65mg/m^3, to be applied in locations with high natural dust concentrations that can not meet the PM10 standard.

		<2.5µm	<10µm
Petrol cars	Leaded – no catalyst	67	80
	Unleaded – no catalyst	70	90
	Three-way catalyst	90	97
Diesel cars		92	100
Diesel Heavy-Goods Vehicles (HGV)		92	100
Tyre wear		39	55
Brake lining		39	98

Table 1.1. Percentage of size fractions of particulate matter emissions from road transport (USEPA, 1985). *Note of the author*: The apparently low percentage of particulate mass observed in the petrol cars figures of the USEPA report may be misleading. This fraction should be near 100% as in diesel engines. However, no reason for this value was found in the reference.

From the comparison between the effects of PM10 and PM2.5 on health, the importance of studying particle size distribution in emissions from diesel engines becomes greater and several studies have tried to explain the mechanism of action. It has been observed that the mass of suspended particulate matter associated with adverse effects is very small and that particles may have a non-specific action (COMEAP, 1995). It has been suggested that ultrafine particles (smaller than 50 nm), which represent a small proportion of the mass of PM10 but a high proportion

of the number of particles, may play a role. According to Seaton, 1995, nanoparticles and ultrafine particles may provoke alveolar inflammation causing changes in blood coagulability and attacks of acute respiratory illness in susceptible people. Seaton has proposed also that very fine particles may cause adverse health effects regardless of their composition. Posterior examinations, however, have shown the opposite evidence: i.e. no short-term effects following exposure to carbon, silver or iron oxide ultrafine particles were observed in rats, in a study by Ziesenis et al. (Ziesenis, 1998).

Murphy et al. (Murphy, 1998) support this idea showing that carbonaceous particles have a less damaging effect on the lung epithelium than silica, and that the surface chemistry of the particles is more important than the size. They also affirm that small aggregate-in-air particles may have a greater toxicity to the lung than the same mass (but lower total surface area) of larger particles, due to cumulative effects. Oberdörster, 1994, gave evidence that ultrafine particles (50nm) may be far more biologically active in the lung than fine particulate (250nm) with the same chemical composition, and similar experience has been published by other researchers (Kales 1994). Donaldson et al. (Donaldson 1998) showed the importance of particle size in the effects on human health overdosing rats with a relatively inert powder such as TiO_2. No effect was observed when the particle size in the powder was 200nm, but a significant decrease in lung function occurred when the particle size was 50nm. From these results, it can be suggested that particle surface area or particle number is a more relevant parameter for assessing critical exposure levels than particle mass. According to Wilson, 1997, there are very different patterns of personal exposure to the different size fractions of particulate matter and only a few data, as well as some correlation given by Peters, 1997 and Tach, 1997 between lung function and exposure to ultrafine particles, are available on this matter.

Apart from the effects on human health, other environmental concerns over diesel particulate emissions have to do with the effects to the environment, the most important being as follows;

- Visibility reduction. Diesel particulate emissions include particles of a broad size range. Among them, particles between 0.2µm and 2µm have the capacity to scatter light, and those particles around the size of the light wavelength, 1µm, absorb it. The result of these two processes is visibility reduction, not proven a public concern in recent research, but nonetheless an issue to take into account when establishing air quality standards and emissions reduction strategies. Research at the

University of Birmingham found evidence that suggests that particulate matter exerts a strong control on visibility (Harrison, 1996).

- Soiling. Black smoke is the main type of particulate blamed for building soiling, and diesel particulate constitute a significant fraction of the total black smoke emitted to the atmosphere in urban areas. However, the assessment of the exact contribution of diesel particulate emissions to soiling is complex, since it depends on many factors such as blackness per unit of smoke, particle size distribution, chemical nature of the particles, and surface characteristics and orientation, among others. Soiling from transport generates a significant amount of public concern, as has been indicated by research during the 1990s. (Ball, 1983).

1.3. The role of transport in total particulate emissions

According to the Third Report of the Quality of Urban Air Review Group, QUARG (Harrison, 1996), road transport particulate emissions, as PM10, constituted 25% of the national particulate emissions in the UK in 1990. This fraction changed greatly with the type of area, urban or rural, where the estimate was made. In Greater London, perhaps the most dramatic example, road transport accounted for 75% of the total particulate emissions. In this scenario, legislation has become increasingly strict, and the emissions from new vehicles must meet reductions by up to 80% between 2000 and 2008 with the introduction of new technologies. Assuming an increase in road usage, the implementation of stricter emission limits on new vehicles, and a constant contribution of 20% by diesel engines to the new-vehicle market, it has been predicted that the transport contribution to PM10 emissions will have been reduced by about 35% of 1990 levels in the year 2010.

The QUARG indicated that medium- and heavy-goods vehicles (MGV and HGV), mainly powered by diesel engines diesel engines, constituted two thirds of the total road traffic emissions in 1990. As black smoke, the diesel contribution in the same year was 39% of London total emissions. Therefore, any reduction in diesel particulate emissions will affect significantly the total emissions. As an example, the predicted reduction by the year 2010, mentioned above, was mainly due to a reduction in emissions from diesel-powered MGV and HGV.

The contribution of SI engines to the total of particulate emissions, as black smoke, was 3% in the UK and 7.7% in London, in 1991 (Chell, 1993). The scenario is dramatically different in the USA and other countries with a much more

significant use of petrol: 67% of the total black smoke from road transport was emitted from petrol vehicles, mainly due to the low fraction of diesel vehicles in the market. A CONCAWE study (CONCAWE, 1998) found that the gasoline engines emitted 40 – 85 times less particle mass compared with the diesel engines for all test conditions, ranging from idle to high-speed. In terms of particle number, the difference between these fuels depended on the operation conditions: gasoline engines emitted 2000 times lower concentrations than diesel engines at urban speeds, but only about 3 times lower at the higher highway speed tested. This was supported by Rickeard et al, who showed similar number concentrations for spark ignition and diesel vehicles under high-speed cruise conditions: $1x10^{14}$ km^{-1} and $2x10^{14}$ km^{-1} for petrol and diesel, respectively, although for total cycle emissions, SI engines emitted much lower number concentrations (Rickeard, 1996). It is clear, then, that gasoline emissions will have to be considered if the particle number concentration becomes an important parameter in particulate emission control.

1.4. Particulate formation in diesel engines

Diesel exhaust aerosol consists of stable and unstable combustion gases and very unstable particles undergoing a complex series of changes since the moment they are formed until a long time after they are cooled in the exhaust system and diluted into the atmosphere. Particles start to be formed as soon as the fuel is injected to the cylinder. In diesel engines, fuel is introduced into the combustion chamber through hole-type nozzles that make possible the formation of one or several finely divided sprays (Russell, 1997). The fuel leaves the nozzle and travels into the combustion chamber in the form of ligaments and droplets that are formed in a way that depends on the pressure drop across the nozzle, the density, viscosity and surface tension of the fuel and the density and temperature of the air. The fuel droplets mix with hot, compressed air to form a near-stoichiometric mixture and, consequently, are evaporated and heated up to the auto-ignition temperature, provoking a series of chemical reactions in which unstable hydrocarbons and oxygenate species are formed and ignite spontaneously. The time between the start of injection and the start of the auto-ignition is known as ignition delay and lasts 0.0002 to 0.002 seconds (0.02 to 2 milliseconds), depending on the engine speed and the engine piston design. Low-emission engines have ignition delays that are very short, of the order of 0.2 ms. The ignition delay is of major importance for the completion of the combustion reactions and for the engine emissions. It is the only period when auto-ignition can occur, and corresponds to the period during which the piston travels from about 20^{o} crank angle before top dead centre (btdc) to 40^{o} after

top dead centre (atdc). This period can be as short as 2.1ms for a passenger car at up to 4800 rpm.

The auto-ignition process does not occur homogeneously in the whole spray. The fuel in the centre of the spray is heated by combustion of the surrounding fuel, and due to the low concentration of oxygen in this area, it is pyrolysed in the gas as well as in the liquid phase. This all occurs at high pressure, which increases the rate of pyrolysis. The very low oxygen concentration reacts with hydrogen atoms from the fuel and as a result, carbon-rich species remain in the centre of the jet. Some more oxygen entrained causes hydrogen stripping from the enriched species and hence leaves carbon chains, which are the precursors of the particulate (Kittelson, 1978). Agglomeration of the formed particles takes place as a result of intimate contact among them, followed by their binding together, in an area of turbulence generated when the jet blasts through the slower-moving air.

The size of basic soot particles (precursors or embryonic nuclei) is about 0.001 to 0.01μm (1 to 10nm). Then, precursors produce larger particles (between 0.01 and 0.1μm) either by coagulation or interacting with the liquid and vapour "surface growth" species, basically unburned hydrocarbons (Kittelson, 1978). These may remain unburned due to the presence of too-lean or too-rich-to-burn zones, entrapment in the holes downstream of the injection needle and areas near the cylinder head and piston, fuel on the wall not removed by air motion, or lubricating oil present in the combustion chamber in significant quantities. Kazuhisa et al. (Kazuhisa, 1999) showed how the growth of soot particles from 0.02 to 0.1μm occurs between 0.3 and 0.8 milliseconds after ignition.

Oxidation of precursors of soot and growth species opposes the formation and growth reactions (Choi, 1995), and it takes place during diffusion burning processes after ignition. Nearly all the soot produced in fuel rich parts of the spray are consumed while the piston descends at the start of the power stroke due to turbulent mixing of the burning mass with the air above the piston crown (Russell, 1997). The design of the combustion chamber (diameter, depth, profile, etc.) and its matching with the injection equipment are very important for keeping emissions low without a loss in torque and specific power.

After leaving the cylinder, the exhaust is cooled in the manifold, silencers and pipes. Processes of particle deposition (i.e. gravitational, diffusional, inertial, thermophoretic or electrophoretic) and reentrainment through the pipes, occur as the particles interact with the pipe walls. Furthermore, coagulation and gas-to-particle conversion processes (nucleation, adsorption/condensation of H_2SO_4 - H_2O vapour and soluble organic components) take place as the interaction among particles

(Abdul-Khalek, 1999). All these processes produce particles whose size is in the range 0.1 to 1μm, with a changing size distribution as they occur along the exhaust system. A comprehensive explanation of the effects of the exhaust system on particulate is still to be done, although many papers have been published about the effect of aftertreatment devices (oxidation catalytic converters or particulate traps) on the particles.

The cooled exhaust aerosol finally leaves the exhaust system and undergoes further cooling and dilution in the atmosphere, where nucleation, absorption and adsorption processes take place, affecting also the particle size distribution in different ways. A dilution ratio of 1000 may be reached in 1 to 2 seconds, a period long enough to change the total particle number concentration by a factor of 100 or higher due to nucleation process only. More than 90% of the particle number formed are in the nanoparticles range (smaller than 50 nm), and from 5 to more than 50% of the particle mass may form as nanoparticles and adsorbed material, as it has been confirmed in dilution experiments (Abdul-Khalek, 1999).

1.5. Particle and aerosol characteristics

As a result of the processes briefly described above, diesel exhaust aerosols exhibit an extremely wide range of particle sizes, shapes, densities, concentrations, chemical composition, etc. According to their individual characteristics, particles react in different ways to various forces applied over the aerosol, which can be used to allow their classification and characterisation. This, however, also contributes to the very high sensitivity shown by the aerosol to sampling and measuring conditions, transport, changes in temperature, dilution, etc.

This section describes particle and aerosol characteristics and properties that determine the aerosol behaviour in the exhaust system of a diesel engine. The object of this study is to examine particle mass and size distribution changes in a practical exhaust system.

1.5.1. Particle size, shape, density and fractals

Particle size is the main characteristic that determines the behaviour of the particle in an aerosol. Given the wide range of particle sizes in diesel exhaust aerosols, from a few nanometers to 10μm or even larger, their behaviour is governed by different physical laws. Nanoparticles, for example, respond primarily to Brownian motion, whereas large particles are governed by inertial and gravitational forces (Willeke et al., 1993).

Diesel exhaust particles also exhibit a varied range of shapes, from spherical to very long, branched particle agglomerates. With this diversity in particle shape, each particle would need a set of parameters to characterise its size. However, it is preferred to establish an equivalent diameter or equivalent area. Some examples are shown in Figure 1.1. The definitions of these dimensions are related to the visual appearance of individual particles, so they are relevant when using powerful optical techniques like SEM and TEM, which will be described later.

The definition of particle size has gone beyond the optical appearance of the particles. Based on the differential behaviour of the particles under various forces, diffusion, aerodynamic, electrical and optical equivalent diameters have been defined, each representing a measurable index of the particle. The aerodynamic diameter, d_a, for example, is defined as

$$d_a = \sqrt{\frac{C_c(d_p)}{C_c(d_a)}} \frac{\sqrt{\rho_p}}{\sqrt{\rho_a}} d_p, \qquad \text{(Equation 1.1.)}$$

where $C_c(d_p)$ and $C_c(d_a)$ are the Cunningham slip correction factors when the particle size is represented by the mobility and aerodynamic diameters, d_p and d_a, respectively; ρ_p is the particle effective density and ρ_p, the particle aerodynamic density, normally equal to 1 kg/m^3. The Cunningham slip factor is the function of the particle diameter that accounts for the discrete character of the aerosol, in contrast with a continuous fluid.

Likewise, particle equivalent diameters have been defined based on particle properties, like the projected area and the volume-to-surface ratio diameters. The bases for the definitions are shown in Table 1.2. Here, the particle shape is important in determining the particle behaviour. For example, in the case of long diesel particle agglomerates, the surface area per unit mass or volume and hence the charging characteristics of the particle are affected, which would determine the particle behaviour under electrical forces. Also, the large voids of the volume enclosed by the particles change the effective density of the agglomerate (the total volume, including voids, is taken into account), and this affects the particle behaviour under forces that are proportional to the particle mass. In these cases, it is sometimes convenient to define a mass-equivalent diameter, which does not take into account the voids, or an envelope-equivalent diameter, which includes the voids. Several of the equivalent diameters mentioned in this section will be used throughout this work.

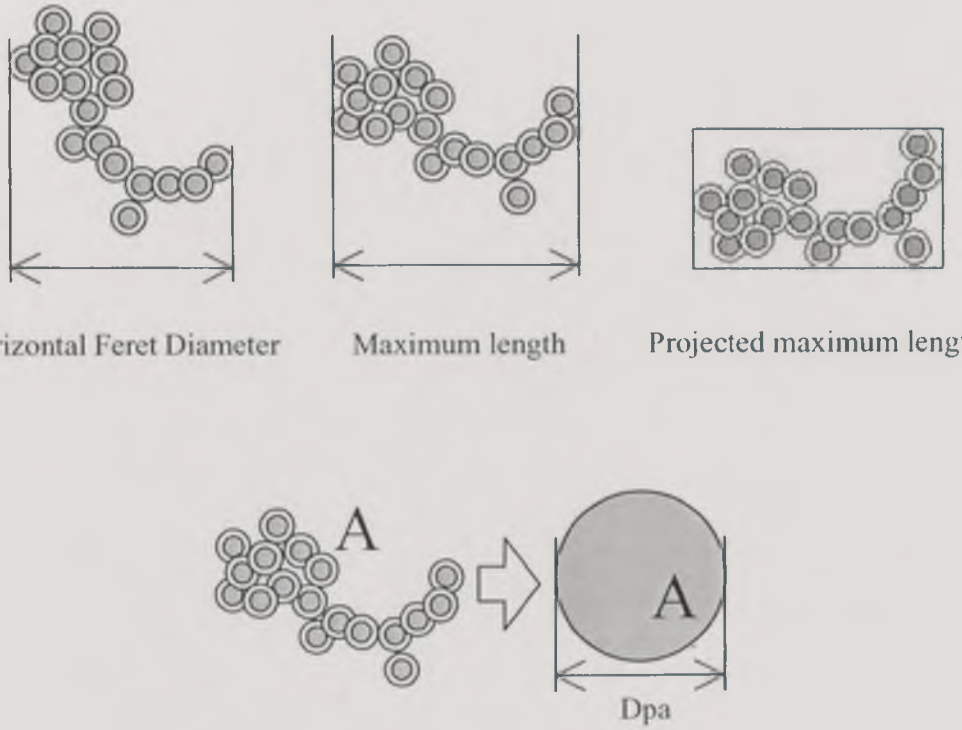

Figure 1.1. Examples of equivalent particle dimensions used in particle sizing.

Long branched diesel exhaust particles can be described as fractal-like aggregates, and their density and mass can be calculated from this description. The fractal definition takes into account the complexities introduced by the shape of the aggregates when calculating their perimeter, surface area or mass. The fractal dimension, D_f, is the key parameter in the characterisation of the aggregates (Brasil, 1999). It gives the information about how compact or open, branched, etc, an aggregate is. A $D_f = 3.0$, for example, would represent a perfectly compact, spherical aggregate. Diesel particles have been found to show D_f values between 1.8 and 2.7, indicating long branched aggregates as well as more compact ones, respectively.

Defined equivalent diameter	Particle behaviour / property
Diffusion diameter	Brownian motion
Aerodynamic diameter	Gravity, Inertial field
Electrical mobility diameter	Electrically-induced motion
Optical diameter	Light scattering
Projected area diameter	Particle surface

Sauter mean diameter	Particle volume-to-surface ratio
Mass diameter	Long aggregates, excluding internal voids
Envelope diameter	Long aggregates, including internal voids

Table 1.2. Equivalent diameters used to describe particle behaviour or properties in an aerosol.

By assuming that primary particles are spherical and having an experimental indicator of their density, the mass of an aggregate was defined by Gorbunov et al. (Gorbunov, 1999) as:

$$m_a = m_p \times N_o \times \left[\frac{R_g}{R_p}\right]^{D_f} \qquad \text{(Equation 1.2.)}$$

where R_g is the radius of gyration of the agglomerate formed by primary particles of radius R_p; m_p is the mass of a primary particle; D_f is the fractal dimension of the agglomerate; and N_o is the average number of primary particles in the smallest aggregate for which the expression is valid. There are some problems with this equation, however, because it is not valid when the number of particles equals N_o, as suggested by Clarke (Clarke, 2001). Gorbunov (Gorbunov, 1999), based on measurements of the changes in SMPS number distributions of a 1.8L turbo diesel exhaust aerosol collected in a Teflon bag, and following an integrating method, found that during the first 80 minutes of age of the aerosol, the average values of the parameters were: $D_f = 1.92 \pm 0.8$, $N_o = 2.5 \pm 0.6$, when accepting the density of a 12.5nm radius primary particle to be $1.50 g/cm^3$, as suggested by Weingartner et al (Weingartner, 1997).

The shape of a particle carries information about the formation and history of the aggregate: primary nanometric spherules, which diffuse very rapidly, coagulate into more or less branched chains, and these chains intercept one another to form larger clusters. The aggregation depends on the formation and flow conditions, and can be described by different models, such as ballistic, diffusion-limited, particle-to-cluster and cluster-to-cluster aggregation. One of these may be more significant than the others at different growth stages and various engine operation conditions. The first particles agglomerate ballistically, particle to particle and particle to cluster, producing compact aggregates, with high fractal dimensions. As the aerosol cools down and the aggregate size increases, for example through the exhaust manifold and exhaust pipe, diffusion-limited aggregation becomes more important and the fractal dimension of the agglomerate becomes lower. At high load conditions,

cluster-cluster aggregation occurs faster, and, as a result, the aggregates have a very low fractal dimension (Skillas, 1998; Brasil, 2001).

Most of the studies to find the fractal dimension of soot aggregates have involved the analysis of structural parameters in two-dimensional, projected images of particles produced by TEM, therefore requiring the establishment of a relationship with three-dimensional properties such as the number of primary particles in the aggregate, the radius of gyration, the aggregate surface, the fractal dimension and the fractal pre-factors, whose definitions are not included in this thesis, but can be found elsewhere (Friedlander, 1993 and 2000; Nyeki, 1994; Brasil, 1999; Skillas, 1999; Gorbunov, 1999; Kostoglow, 2000). Brasil et al. (Brasil, 1999) have compiled the considerations and corrections needed to do this, and defined a recipe to characterise both structural and fractal properties from projected images as a result. From basic measurements such as the maximum length of the agglomerates, projected areas of agglomerates and primary particles, and the mean diameter of the primary particles, the following procedure is followed:

- Calculate the number of particles per agglomerate,

$$N_a = \left(\frac{A_a}{A_p} \right)^{\alpha} \qquad \text{(Equation 1.3.)}$$

where A_a is the projected area of the agglomerate and A_p, the projected area of a primary particle; α can be reasonably assumed to be equal to 1.09 for diesel engines (Brasil,1999; Lee, 2000).

- Calculate the radius of gyration for each agglomerate,

$$R_g = \frac{L}{3}, \qquad \text{(Equation 1.4.)}$$

where L is the maximum length of the agglomerate. This relationship is generally valid for diesel engines, for which Brasil et al (Brasil, 1999) found that $(L/R_g)=1.50\pm0.05$.

- For each agglomerate, calculate the relationship

R_g/d_p (Equation 1.5.)

where d_p is the average diameter of the primary particles.

- Finally, plot N vs. (R_g/d_p) in logarithmic scale and adjust the best power function fit, the slope of which is the fractal dimension, D_f.

1.5.2. Particle size distribution

Diesel exhaust, as many other natural aerosols, is polydisperse, i.e. it is composed by particles of very different sizes. To describe this size diversity, it is necessary to use a particle size distribution function, perhaps the most important of the physical characteristics of this kind of aerosols (Friedlander, 1977).

The particle size distribution is, essentially, a statistical concept. It is formed by contiguous size intervals, each containing information about a certain particle parameter, namely number, mass surface area, volume, chemical composition, etc. Therefore, it is possible to have a number-weighed particle size distribution, a mass-weighed particle size distribution, and so forth. The particle size will be given by the measurement technique, as an equivalent diameter such as those already mentioned: aerodynamic diameter, electrical mobility diameter, etc. The information can be shown in different ways: a tabulated set of data, a histogram, a continuous frequency curve, a cumulative curve or a mathematical continuous function, as illustrated with an example in Figure 1.2. When plotting these graphs, it is usual to normalise the data by dividing the measured parameter (N, number concentration; M, mass concentration; etc) of a defined interval *i* by the size difference in that interval, for example $\frac{\Delta N_i}{\Delta d_i}$ or $\frac{\Delta N_i}{\Delta \log_{10} d_i}$ if the size axis is in logarithmic scale. From this point on, the logarithm will be always considered as $\log_{10}$, but only log will be used. For $\log_e$, ln will be used.

In a normalised histogram, the area of the rectangle in each size interval is proportional to the total number (or mass, volume, etc.) of particles. This can be converted to a smooth curve by selecting a characteristic size for each size interval and making the area under the curve proportional to the number (or mass, volume, etc) of particles. This can also be converted into a cumulative distribution curve by adding the number (or mass) of particles of all the size intervals under a certain size. The experimental size distribution may be fitted to continuous statistical distribution functions, such as Gaussian, log-normal, Poisson, power-law, among other distributions. For detailed information about generating and representing particle size distributions, the readers are referred to the literature (Friedlander, 1977; Hinds, 1982; Willeke, 1993). Here, the most important characteristics of diesel exhaust aerosol size distribution are described.

Figures 1.2. and 1.3. show a typical, normalised, size distribution of a diesel exhaust aerosol, in its two main components: number-weighed and mass-(or volume-) weighed size distributions. Distributions are bimodal, that is, they have two modes or characteristic sizes where the distributions have a local maximum. The

first, around 0.007μm to 0.02μm, is normally called nucleation mode, and the second, around 0.1μm, accumulation mode. The mass distribution may show a third mode, around 10μm or more, called the coarse mode. The distribution around each mode fits very well to a log-normal distribution, which means that they show the well-known bell shape of the Gaussian distribution when the size-axis scale is logarithmic.

This distribution can be easily represented mathematically and summarised with a few parameters, namely the geometric median diameter and the geometric standard deviation:

$$F(d) = \frac{1}{\sqrt{2\pi}\log s_g} \exp\left[-\frac{1}{2}\left(\frac{\log d - \log \overline{d_g}}{\log s_g}\right)^2\right], \qquad \text{(Equation 1.6.)}$$

where $\overline{d_g}$ is the geometric mean diameter and s_g is the geometric standard deviation:

$$\overline{d_g} = \left[\pi d_i^{N_i}\right]^{1/N} \qquad \text{(Equation 1.7.)}$$

$$\log s_g = \left[\frac{\Sigma N_i (\log d_i - \log d_g)^2}{N}\right] \qquad \text{(Equation 1.8.)}$$

The distributions in Figures 1.2. c) and 1.3. show the relative characteristics of the number and mass distributions of diesel exhaust aerosol: most of the particle numbers is in the nucleation mode, but they might contribute very little to the mass distribution. Figure 1.2. c) shows the nuclei and accumulation modes in the volume-weighed distribution, which is equivalent to the mass distribution. The corresponding number-weighed distribution, however, shows that the nuclei mode was predominant over the accumulation mode when both are plotted on a linear scale.

A recent study of number and mass size distributions in emissions from European light-duty vehicles (Hall et al, 1998) showed that 99% of the particles were below 1μm, which corresponded to 85% of the mass.

Differences in the combustion characteristics cause differences in the particle size distribution of exhaust aerosol from various sources. The distribution may then become a fingerprint which allows the identification of the sources of apportionment of particulate pollution in a certain region. As an example, Figure 1.4. shows the particle size distributions of exhaust aerosols from several diesel and petrol vehicles

studied in the DETR/SMMT/CONCAWE Particulate Research Programme 1998-2001 (Andersson, 2001). The highest number concentrations were found in exhaust aerosols from Conventional Diesel vehicles, compared with Direct Injection (DI) Gasoline, Multi-point Injection (MPI) and Liquefied Petroleum Gas (LPG) vehicles, as well as Trap-equipped Diesels, at idle and 50 km/h in Figures 1.4. a) and 1.4.b).

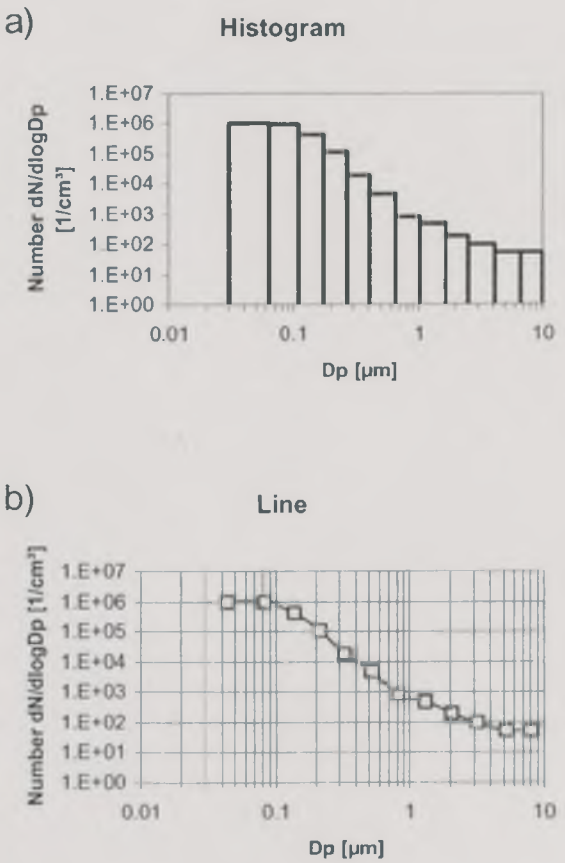

Figures 1.2.a) and 1.2.b). Examples of size distribution diagrams. a) Histogram and b) line.

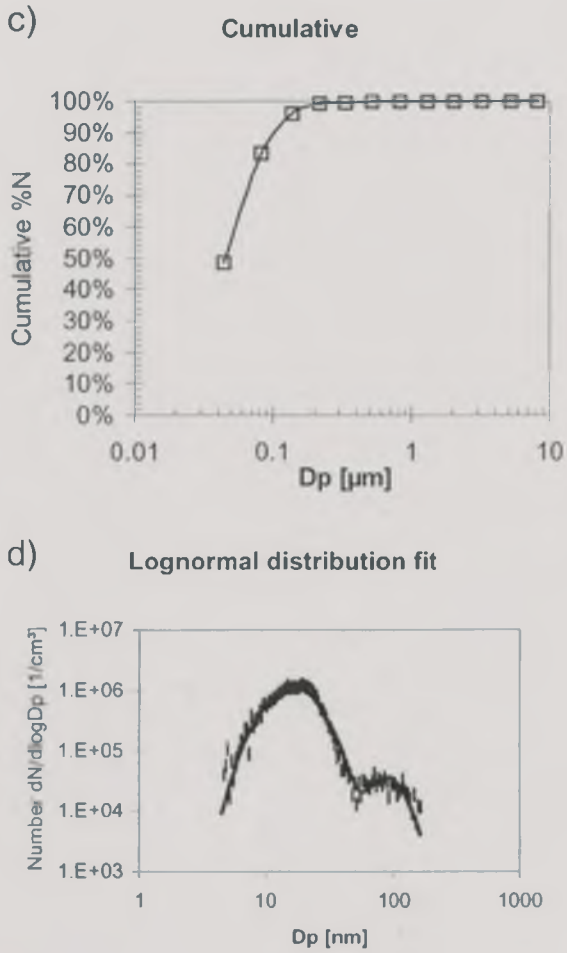

Figures 1.2.c) and 1.2.d). Examples of size distribution diagrams. c) Cumulative distribution and d) lognormal distribution fit.

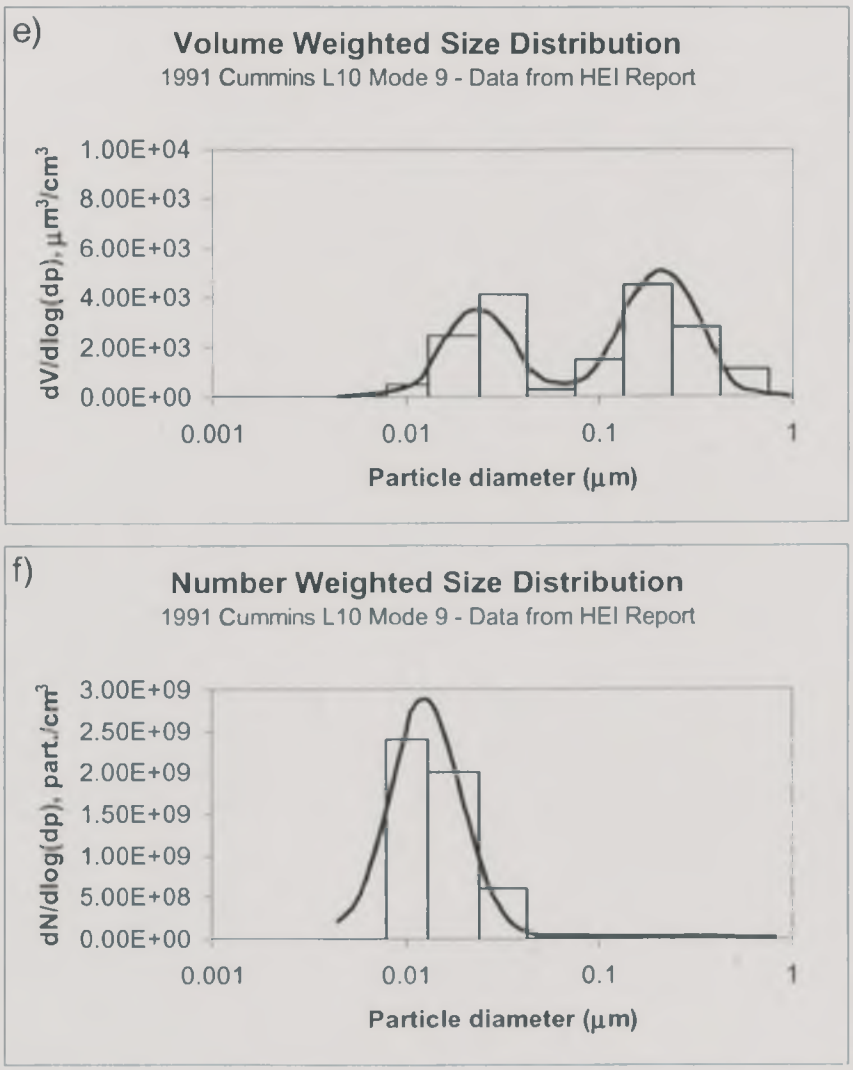

Figures 1.2.e) and 1.2.f). Examples of size distribution diagrams. e) Volume-weighted size distribution and f) number-weighed size distribution from dynamometer studies on diesel engines (Kittelson, 1998).

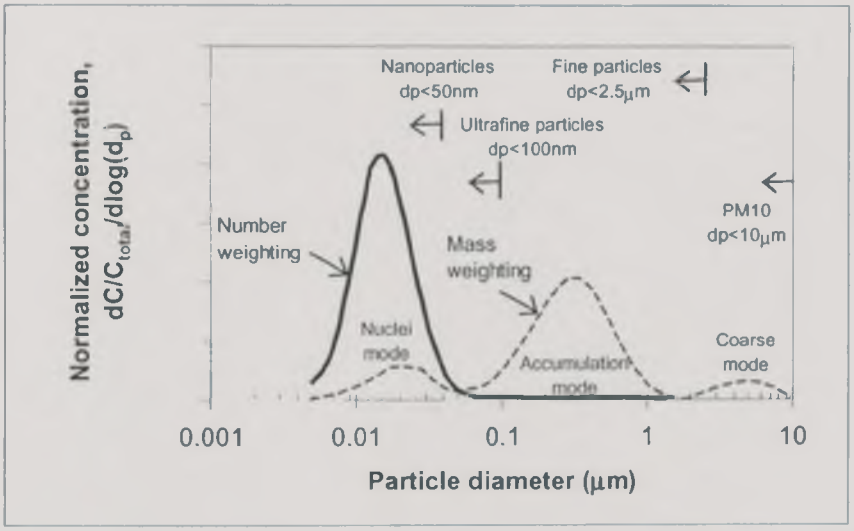

Figure 1.3. Typical size distribution of a diesel exhaust aerosol (Kittelson, 1998).

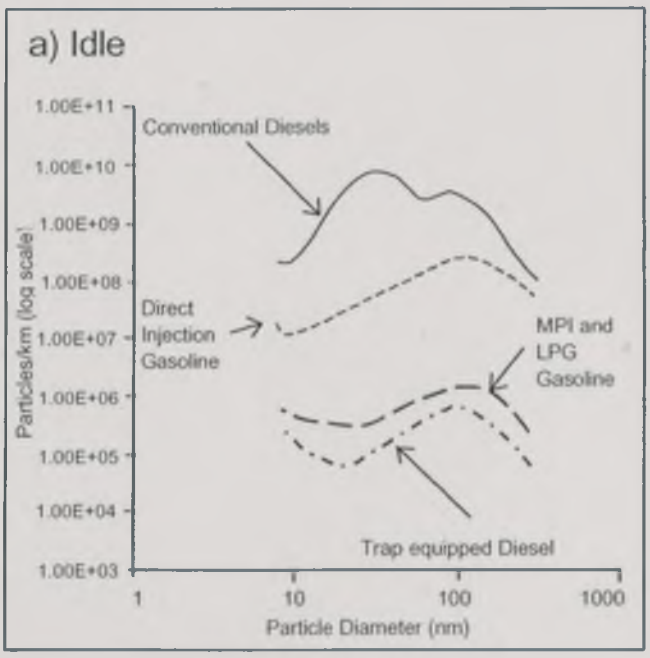

Light Duty Vehicles
Particle Number and Size at Idle

Figure 1.4.a). Particle size distributions from diesel and petrol light-duty vehicles (Andersson, 2001). Idle

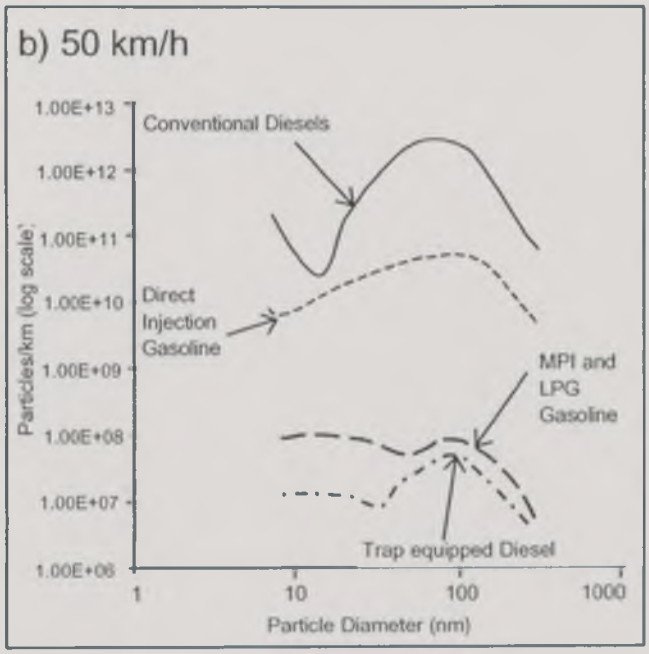

Light Duty Vehicles
Particle Number and Size at 50km/h

Figure 1.4.b). Particle size distributions from diesel and petrol light-duty vehicles (Andersson, 2001). 50 km/h.

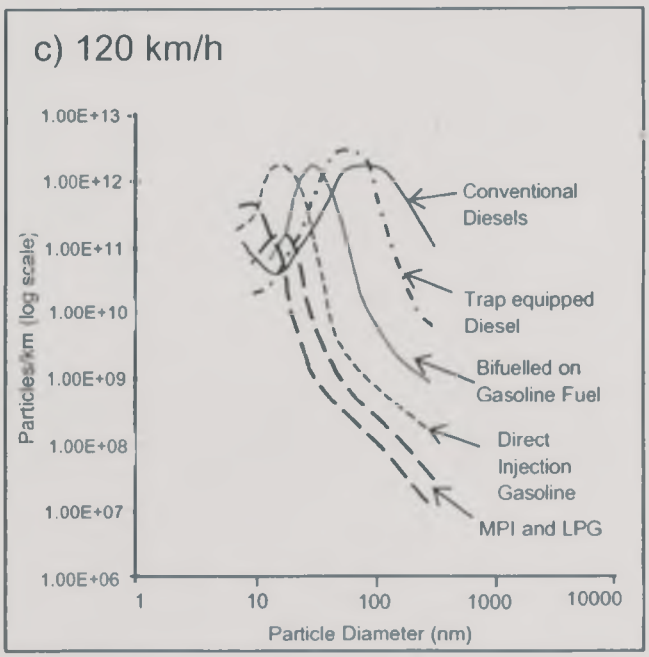

Light Duty Vehicles
Particle Number and Size at 120 km/h

Figure 1.4.c). Particle size distributions from diesel and petrol light-duty vehicles (Andersson, 2001). 120 km/h.

However, at 120 km/h, there was a significant increase in the particle number concentration for all the vehicles that previously showed low number concentrations.

This was due to a clear increase in the number of particles in the nucleation mode, nanoparticles (<50nm).

1.5.3. Mass and number concentration

Total mass and number concentration can be either derived from the size distribution described above or measured directly using a suitable technique. From the total size distribution, it is clear that the total mass or number can be calculated by adding the number at each size range. Following the nomenclature used above,

$$N = \Sigma N_i \qquad \text{(Equation 1.9.)}$$

$$M = \Sigma M_i, \qquad \text{(Equation 1.10.)}$$

where M_i is measured directly or calculated from the particle number N_i:

$$M_i = N_i \pi \frac{d_i^3}{6} \rho_{pi}, \qquad \text{(Equation 1.11.)}$$

if the particle density is known.

If a continuous particle size distribution function is used instead, the total number and mass for sizes below a certain value can be calculated using the cumulative number and mass distribution expressions, respectively:

$$N(d_p) = \int_0^{dp} N_d(d_p) d(d_p), \text{ where } N_d = \frac{dN(d_p)}{d(d_p)} \qquad \text{(Equation 1.12.)}$$

$$M(d_p) = \int_0^{dp} M_d(d_p) d(d_p), \text{ where } M_d = \frac{dM(d_p)}{d(d_p)} \qquad \text{(Equation 1.13.)}$$

where the suitable definition of the upper limit of the integral, d_p, can be used for various purposes. For example, legislative limits have been set for several years for particle mass below 10μm or PM10. New limits have been imposed in California legislation, for particle mass below 2.5μm, or PM2.5. Hence, having the information for the whole size distribution, it is possible to calculate these mass values and compare them with the legislated values, as long as the errors due to the differences in the measurement techniques are taken into account.

Since the particle density is a very difficult parameter to measure, the measurement of total mass concentration and total number concentration is achieved separately by very different techniques. High efficiency filtration at suitable conditions, followed by the gravimetric determination of the filtered mass, is the currently standard technique for total mass concentration, although other techniques

are also available. Total number concentration can be determined by optical counting of the particles if they are large enough to scatter light. Ultrafine particles and nanoparticles can be made to grow by condensation of alcohol on their surface, and then counted. Other counting methods include charging the particles to a known charge distribution and then detecting the current generated when the particles impact on a conductive stage connected to an electrometer. These techniques are explained later in this chapter.

1.5.4. Particulate chemical composition

As a result of the combustion process, as well as physical and chemical changes through the exhaust system, the chemical analysis of a diesel exhaust particulate sample is a complex task. The particulate chemical composition includes organic and inorganic compounds, their nature and relative amount depending on the fuel used, the engine technology level, and the operational conditions.

Normally, the chemical analysis of diesel particulate is carried out over a filtered mass of particulate, from which the total mass concentration is also determined, so the concentration of each component is expressed as an average concentration in the sample, regardless of the particle size distribution. However, the composition of individual particles may change depending on various factors such as the particle size and the exact moment and conditions when they are produced. Therefore, the size distribution of chemical compounds and important changes in particulate composition with time become significant aspects to be investigated.

The composition of diesel particulate matter has been typically expressed as the fractions of solid carbon, soluble organic fraction (SOF), sulphates, water and ash (metals, others). The SOF is formed by unburned hydrocarbons from both diesel fuel and lubricant oil, as well as pyrosynthesised compounds, which can be adsorbed over the solid phase, or condense forming particles that aggregate to solid particles. The extent to which these hydrocarbons become part of the particulate matter is strongly affected by the sampling conditions. Therefore, these conditions must also be taken into account so the analysis can be comparable among different research groups.

A typical composition of diesel particulate matter from a LD engine is shown in Figure 1.5. In it, the SOF fraction is 32% (25% from the fuel and 7% from the lubricant oil), but it can actually vary between 10% and 80%. This is possibly the most important fraction of particulate matter related to health effects, since it includes polyaromatic hydrocarbons (PAH), some of which have been classified as proven or probably carcinogenic. By definition, the SOF is the fraction soluble in an organic solvent. The reference method, therefore, is the Soxhlet extraction, for

which the use of Methylene Chloride or benzene/alcohol is recommended. This method is time consuming (8 hours) and requires a high degree of analytical expertise, for which reason alternative methods have been developed. These include vacuum oven sublimation, purge vacuum oven sublimation, thermogravimetric analysis (TGA), pyrolisis – gas chromatography and differential on-line gaseous hydrocarbon analysis at two temperatures (Abbass, 1990; Williams, 1988). These methods agree to a certain degree with the extraction method, the main differences being related to the sulphate content of the particulate matter, which is much higher for vacuum sublimation and TGA than for extraction.

Apart from the determination of total SOF in the particulate matter, the speciation of SOF is required when identifying individual compounds that may be responsible for higher health hazards. Some SOF determination methods allow having an extract or effluent that can be analysed with advanced separation techniques, such as visible, infrared and UV spectrometry; atomic adsorption and flame photometry; mass spectrometry and gas and liquid chromatography, among others, which can be combined to increase the resolution and range of the analysis. The extract from the Soxhlet extraction method is readily available for these analyses. The gaseous effluent from the vacuum sublimation and the TGA methods can be fed to an FID to identify the hydrocarbons constituting the SOF. Detailed descriptions of the analytical techniques can be found elsewhere (Willeke, 1993; Harrison, 1998; Lipkea, 1979; Abbass, 1989).

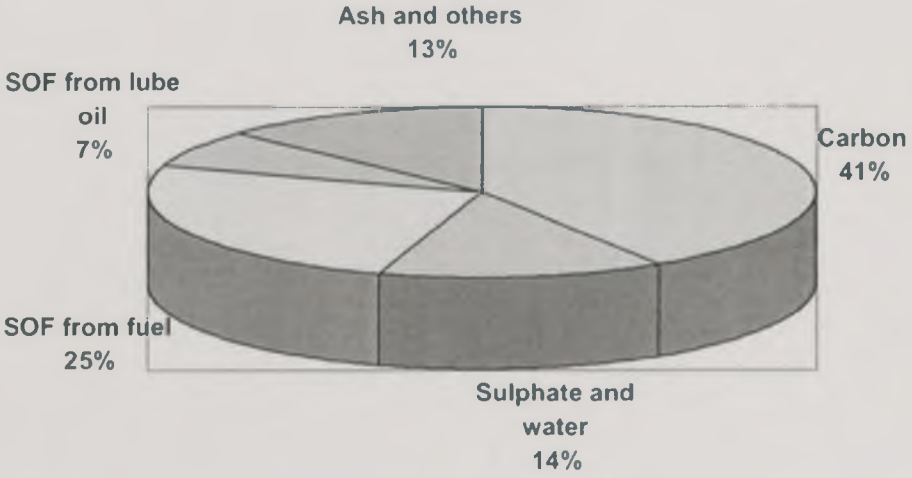

Figure 1.5. Typical chemical composition of diesel exhaust particulate matter (Ahamed, 1999).

As stated above, chemical compounds might not be distributed evenly among particles of different sizes. If a collection technique in different size ranges allows having enough particulate mass to perform an accurate chemical analysis, the

chemical composition can be also expressed as a distribution of a specific component as a function of particle size. Some examples of this are given by Venkataraman et al. (Venkataraman, 1994), Tanaka et al. (Tanaka, 1999) and Westerholm et al. (Westerholm, 1999), who have determined the size distribution of PAH in diesel exhaust aerosol from a passenger car engine using low pressure impactors. The latter, using the electrical version (ELPI) evaluated different collection substrates, but even in the best case, the results showed a difference by a factor of 3 between PAH from conventional filter sampling and ELPI sampling. The technique they used was an extraction in dichloromethane and fractionation according to polarity, followed by gas chromatography – mass spectrometry (GC-MS) analysis. PAH size distribution was parallel to the mass-weighed particle size distribution, with the largest mass being emitted at 0.1μm and 70% of the mass between 0.05μm and 0.4μm. The more important PAH found were phenanthrene, 2-methyl-phenanthrene, 1-methyl-phenanthrene, fluoranthene, pyrene, benzo(ghi)-fluoranthene, and chrysene/triphenylene, from a total of 24 identified components ranging from three-ringed to six-ringed PAH.

1.6. Particulate physical and chemical processes

Diesel exhaust aerosol is highly unstable, owing to the multiple changes through the exhaust pipes and the subsequent dilution in the atmosphere. Various physical and chemical processes occur continuously in the particulate phase, therefore changing the particle concentration, size distribution and chemical composition. The processes take place as a result of the thermodynamic properties of the particulate components, which cause mass transfer between the particulate and gas phases, in either direction, and between particles. This section starts describing some concepts given by the equilibrium thermodynamics, and then applied to the different physical and chemical processes. Afterwards, the processes of nucleation, condensation, evaporation and coagulation are briefly explained.

1.6.1. Thermodynamic properties

In an ideal situation, the exhaust aerosol could be considered as a system in which the particulate and vapour phases are in equilibrium, that is, there is no net mass transfer between those phases, or between particles. In the vapour phase, the concentration of each of the exhaust gas components is expressed by its partial pressure. The sum of the partial pressures of all the components is the exhaust pressure, so the partial pressure of a certain component divided by the exhaust pressure becomes the fractional concentration of the component in the exhaust gas. The liquid fraction of the particulate phase consists of the same components of the

vapour phase, and each vapour component exerts such a pressure over the liquid of the same component that no mass transfer occurs. This is called vapour, or saturation, pressure, which is a unique property of a liquid, and is a function of temperature: $p_s(T)$.

In real situations, ash particles e.g. metals play the role of condensation nuclei. However, if the number of nuclei is not sufficient, the equilibrium condition may not be met, and the actual partial pressure of each component would differ from the saturation pressure as a result. Therefore, the ratio of the actual pressure of a component in vapour phase to its saturation pressure at the same temperature may become a very important parameter called the saturation ratio:

$$S = \frac{p}{p_s(T)}, \qquad \text{(Equation 1.14.)}$$

For S=1, the mixture is saturated; for S>1, it is supersaturated; and for S<1 it is unsaturated. There are two particularly important saturation trajectories in diesel aerosols, which are i) the reversible adiabatic expansion and ii) the dilution with cooler air, which may lead to the formation of small liquid droplets or nuclei particles. For the adiabatic expansion, the following conditions along the trajectory are met:

$$\frac{p_2}{p_1} = \left(\frac{T_2}{T_1}\right)^{\gamma/(\gamma-1)}, \qquad \text{(Equation 1.15.)}$$

where 1 and 2 refer to the conditions before and after the expansion, respectively, and γ is the ratio of the specific heat at constant pressure to the specific heat at constant volume.

Particle size has an interesting effect on the vapour pressure, called the Kelvin effect. In a small particle or droplet, the resistance offered by neighbouring molecules to a molecule that has reached the sufficient energy to separate from the liquid phase and become part of the vapour phase, is lower than the resistance of the liquid molecules on a plane surface. Therefore, the vapour pressure is higher on the particulate or drop than on the plane surface. For a drop of diameter d_p,

$$\ln\frac{p_d}{p_s} = \frac{4\bar{v}\sigma}{d_p RT} = \frac{4\sigma v_m}{d_p RT}, \qquad \text{(Equation 1.16.)}$$

where p_d is the vapour pressure over the particle, $\bar{v}$ is the molar volume of a liquid, v_m is the molecular volume

($v_m = \bar{v}/N_{av}$, being N_{av} Avogadro's number), (Equation 1.17.)

and σ is the surface tension. From this definition, it can be inferred that there is a minimum droplet size for a particle to form and grow. Under this size no condensation will occur, unless an extremely high supersaturation exists in vapour phase. For the organic vapours present in diesel exhaust, particles much larger than 0.2μm are needed for condensation to occur on them in a 1% supersaturation (Willeke, 1993).

1.6.2. Nucleation

Nucleation is the formation of droplets from the vapour phase in the absence of previous condensation nuclei. This requires large saturation ratios, e.g. 2 to 10, present only in chemical process and combustion situations. The formed droplets, which become condensation nuclei, are agglomerations of molecular clusters that have reached the minimum size established by the Kelvin effect mentioned above. Molecular clusters under that size are formed continuously, but are unstable and disintegrate quickly, so they do not become condensation nuclei. The supersaturation required for this process to occur is a property of a certain vapour at a given temperature and is called the critical saturation ratio.

Various gas-to-particle conversion processes can cause nucleation. Between the physical process, adiabatic expansion, mixing or dilution, conductive cooling and radiative cooling are found. Chemical processes in the gas phase can also originate nucleation, when new condensable species are formed. This is the case of photochemical smog, which is the result of the formation of nitric acid, sulphuric acid and condensable organic compounds from NO, SO_2 and organic compounds emitted in the automotive exhaust, reacting with tropospheric ozone, under the action of ultraviolet light.

Two theories have been used to explain nucleation from gas phase reaction: the classical theory, for single condensable species; and the heteromolecular theory, or multicomponent condensation. For the last case, if two or more condensable species are present simultaneously and interact strongly, their condensation can occur at much lower vapour pressures than that for the single species.

The most important nucleation species in exhaust aerosol is sulphuric acid, in its system with water vapour (Friedlander, 1977). Sulphuric acid's threshold concentration for its nucleation may be estimated by the following equation developed by Seinfeld and Pandis (Abdul-Khalek, 2000):

$$C_{crit} = 0.16e^{0.1T-3.5RH-27.7}$$ (Equation 1.18.)

where C_{crit} is the threshold concentration (in $\mu g/m^3$) of H_2SO_4, T is the absolute temperature and RH is the relative humidity. Hydrocarbons can also provoke significant nucleation, the potential for which is represented by the saturation ratio.

1.6.3. Condensation

Once nucleation has taken place generating condensation nuclei, and/or there are previously formed particles larger than the Kelvin diameter, molecules from the vapour phase can condense on their surface making the particles grow. The growth rate depends on the saturation ratio and the particle size. For particles smaller than the mean free path of the gas, λ, the particle growth is controlled by the kinetic theory of the gases. The mean free path of the gas, λ, is the average distance travelled by a particle without colliding against any gas molecule. For larger particles, on the other hand, the particle growth depends on the molecular diffusion to the particle surface. The growth rate is expressed as follows, for each case:

$$\frac{d(d_p)}{dt} = \frac{2(p - p_d)}{\rho_p \sqrt{2\pi RT / M}}, \text{ for } d_p<\lambda \qquad \text{(Equation 1.19.)}$$

$$\frac{d(d_p)}{dt} = \frac{4D_v M(p - p_d)}{\rho_p d_p RT}, \text{ for } d_p>\lambda \qquad \text{(Equation 1.20.)}$$

where D_v is the diffusivity of the vapour molecules (Willeke, 1993). The integration of the latter equation allows calculating the time required for growth from a certain size to another:

$$t = \frac{\rho_p RT(d_2^2 - d_1^2)}{8D_v M(p - p_s)}, \text{ for } d_1>\lambda. \qquad \text{(Equation 1.21.)}$$

Unlike nucleation, condensation on previously formed condensation nuclei or particles does not require high saturation ratios. Only a few-percent supersaturation is enough for the process to take place.

The knowledge of condensation has lead to the development of particle counting techniques such as the Condensation Nuclei Counter, CNC, as will be seen later. In them, the particles are exposed to a supersaturated atmosphere and then cooled by a rapid expansion, so they grow to a size of about 10μm, regardless of their initial size, and can be detected by a single-particle optical counter. In this way, it is possible to count particles that originally are below the detection limit of optical devices and could not be measured otherwise.

In the field of diesel exhaust emissions, Kittelson et al. (Kittelson, 1991) and Khalek et al. (Khalek, 1999, 2000) have investigated experimentally and assessed theoretically the growth processes by nucleation and condensation during cooling and dilution. Their study started when investigating the high variability in particulate measurements during transient tests. Particle number concentration was found to be strongly dependent on dilution conditions such as temperature, saturation ratio, dilution ratio and residence time in the dilution tunnel, owing to the formation of nanoparticles. Different dilution conditions can generate differences in particle number concentration of up to two orders of magnitude, represented in a huge nanoparticles mode. Most of the nanoparticles formed during cooling and dilution of the exhaust aerosol consist of sulphuric acid and hydrocarbons, the former being the main nuclei precursor and the latter the main growth species by condensation. The use of low sulphur fuel can reduce significantly the number of new nuclei although it does not always eliminate the nuclei mode. A very important result from their work is that carbonaceous particles play a significant role in the depletion of gas-phase condensing species such as sulphuric acid and hydrocarbons. When carbon particulate emissions are reduced, as in the case of ultra-low emission engines, the condensing species, sulphuric acid and hydrocarbons, stay in vapour phase and can nucleate as droplets of less than 50nm in size. These are considered, then, as nanoparticles, which become the most significant fraction of the total particulate. To avoid the formation of nanoparticles, the emissions of the condensing species must be reduced.

The increased nucleation trends described by Abdul-Khalek et al. explain the observations by other researchers, in which increasing particle number and formation of nucleation mode occur as the exhaust aerosol passes through particulate traps (Mayer, 1995, 1996; Abdul-Khalek, 1996; Matter, 1999; Dementhon, 1997; Baumgard, 1991).

1.6.4. Evaporation

The mass transfer between the particulate and gas phases can occur in either direction, and the previous sections examined the gas-to-particle transfer processes of nucleation and condensation. The opposite process, particle-to-gas transfer, is evaporation and is governed by the same laws.

As an opposite process, evaporation needs the opposite condition for nucleation or condensation to occur, that is, the partial pressure of vapour, p, is lower than the saturation pressure p_s. The equation for the size decrease rate, or evaporation rate, is just a readjustment and correction of the equation for growth by condensation:

$$\frac{d(d_p)}{dt} = \frac{4D_v M}{\rho_p d_p R}\left(\frac{p}{T_\infty} - \frac{p_d}{T_d}\right), \text{ for } d_p > \lambda \qquad \text{(Equation 1.22.)}$$

where the subscript d refers to the particle surface and ∞, away from the surface (Willeke, 1993). λ is the mean free path, defined in section 1.6.3. The difference between T_∞ and T_d facilitates the correction for surface cooling due to rapid evaporation.

For small particles, the Fuchs correction factor for diffusion is introduced, being very important for particles smaller than 1μm (Willeke, 1993):

$$\frac{d(d_p)}{dt} = \frac{4D_v M}{\rho_p d_p R}\left(\frac{p}{T_\infty} - \frac{p_d}{T_d}\right)\left[\frac{2\lambda + d_p}{d_p + 5.33(\lambda^2 / d_p) + 3.42\lambda}\right],$$

for $d_p < \lambda$ (Equation 1.23.)

If the conditions are favourable, evaporation of droplets without insoluble material can occur with no limit, that is, zero diameter, in contrast to the minimum nuclei size for condensation to occur. The time needed for the particle to dry out is calculated as:

$$t = \frac{R\rho_p d_p^2}{8D_v M\left(\frac{p_d}{T_d} - \frac{p_\infty}{T_\infty}\right)}, \text{ for } d_p > \lambda \qquad \text{(Equation 1.24.)}$$

However, most particles formed by nucleation will not dry to zero diameter, but to the diameter of the original nuclei (Willeke, 1993).

1.6.5. Coagulation

Particulate aggregates are formed as a result of the predominant action of van der Waals forces at the surface of particles with liquid and sticky components. The action of these forces was explained in a previous section. The process by which the aggregates interact with others to form larger aggregates is called coagulation, and it can occur in two ways. The first is called thermal coagulation, and is due to Brownian motion of the particles. The second is kinematic coagulation, in which the action of external forces, as those described in a previous section, are responsible for causing the relative motion among particles. Regardless of the particle motion mechanism, the result from the coagulation process is particle growth and a decrease in particle number concentration.

1.6.5.1. Thermal coagulation

The simplest way to study thermal coagulation is assuming that the aerosol is monodisperse, and then correcting the equations for polydisperse aerosols with known characteristics from the log-normal particle size distribution. For a monodisperse aerosol, the diffusion of one particle to another causes a decrease in particle number concentration. The rate at which this occurs can be expressed by:

$$\frac{dN}{dt} = -KN^2 \qquad \text{(Equation 1.25.)}$$

where K is the coagulation coefficient and N is the particle number concentration. For particles larger than the mean free path of the gas,

$$K = 4\pi d_p D = \frac{4kTC_c}{3\eta} \qquad \text{(Equation 1.26.)}$$

where D is the particle diffusion coefficient, k is the Boltzmann's constant and η is the viscosity of the gas. From this, it is inferred that the coagulation rate is very high at high number concentrations and slow at low number concentrations. For particles with $C_c \approx 1$, the coagulation coefficient would be independent of particle size. Considering that K is constant, as it is in the extent of particle size increase normally observed, the integration of the Equation 1.26. with the initial condition $N=N_0$ when $t=0$ gives the change in number concentration in a defined period t, which can be calculated as:

$$N(t) = \frac{N_0}{1 + N_0 Kt} \qquad \text{(Equation 1.27.)}$$

where the subscript 0 represents the initial conditions. If spherical particles were considered, the final particle size in the period t would be given by:

$$d(t) = d_0(1 + N_0 Kt)^{1/3} \qquad \text{(Equation 1.28.)}$$

The equations are correct for liquid droplets, since they are derived for perfectly spherical particles. Diesel particles are aggregates of unit solid particles slightly different from spheres. The equations become approximately valid for them as long as they form compact clusters, but this is not usually the case, so a correction for aggregate shape must be included, and the use of the fractal dimension becomes likely.

The previous considerations for monodisperse aerosols can be applied to polydisperse aerosols such as diesel exhaust, if some adjustments are applied. In

polydisperse aerosols, the diffusion of small particles to others with a larger size, and therefore a larger surface area, is enhanced in comparison to diffusion of small particles to others of the same size. Therefore, the coagulation rate can be reasonably expected to increase in a polydisperse aerosol with respect to the monodisperse aerosol. If the former has a log-normal particle number size distribution, then its size can be represented by the geometric median diameter (GMD) and the geometric standard deviation σ_g. Using these parameters, the diffusion coefficient for the particles in the polydisperse aerosol can be calculated as:

$$\overline{K} = \frac{2kT}{3\eta}\left[1 + e^{\ln^2\sigma_g} + \left(\frac{2.49\lambda}{GMD}\right)\left(e^{0.5\ln^2\sigma_g} + e^{2.5\ln^2\sigma_g}\right)\right], \quad \text{(Equation 1.29.)}$$

and replace K in the equation for monodisperse aerosols. It is assumed that σ_g remains constant, which is reasonable for moderate particle size changes. If large changes occur, the growth analysis can be made in several smaller size intervals where the assumption is acceptable, a value of K being calculated for each interval (Willeke, 1993). Then the change in the number concentration of particles in a certain size d_i, N_{di}, with time, in an aerosol with the size ranges d_1, d_2, d_3... d_n, can be expressed as:

$$\frac{dN_{d_j}}{dt} = \frac{1}{4}\sum_{d_i=d_1}^{d_{j-1}} K_{d_i(d_j-d_i)} N_{d_i} N_{d_j} - \frac{1}{2}\sum_{d_i=d_1}^{d_n} K_{d_j d_i} N_{d_j} N_{d_i}, \quad \text{(Equation 1.30.)}$$

where the first term on the right hand side of the equation corresponds to the increase due to combination of smaller particles making a d_j-th size particle, and the second term, to the loss of d_j-th particles by combination with other particles (Reist, 1993). K_{didj} is the coagulation coefficient for the polydisperse aerosol formed by size ranges d_i and d_j. The change in the total particle number concentration, considering all size ranges is the sum of the changes in individual size ranges, which becomes:

$$\frac{dN_{d_j}}{dt} = -\frac{1}{4}\sum_{d_j=1}^{d_n}\sum_{d_i=d_1}^{d_n} K_{d_j d_i} N_{d_j} N_{d_i}, \quad \text{(Equation 1.31.)}$$

According to Reist, 1993, the main limitation of this approach is that the it may be required to solve a set of very many equations simultaneously when coagulation proceeds, and even so, there may be inaccuracy in the numerical solution. Therefore, he recommends the use of nonlinear integrodifferential equations, which convert the discrete model of equations 1.30. and 1.31. into a continuous model. The reader is invited to read the references to have a deeper

knowledge on this approach and others out of the scope of this work (Reist, 1993; Willeke, 1993; Friedlander, 2000).

1.6.5.2. Kinematic coagulation

The different response of particles of various sizes to external forces such as gravity, create relative motion, collisions and hence coagulation. The prevailing collision mechanisms between large and small particles are inertia and interception. Since the smaller particles tend to follow the gas flow around larger particles owing to their lower inertia, the particle collection of the large particles is lower than it would be if the small particles did not follow that flow, which defines the collection efficiency, E. Taking this into account, the capture rate for particles under the effect of gravity is expressed as:

$$n_c = \frac{\pi}{4} d_d^2 V_{ts} NE, \qquad \text{(Equation 1.32.)}$$

where d_d is the diameter of the large particle and V_{st} is the settling velocity or relative velocity between large and small particles. The capture efficiency, E, can be calculated by the empirical expression (Hinds, 1982):

$$E = \left(\frac{Stk}{Stk + 0.25} \right)^2, \text{ for Stk} \geq 1 \qquad \text{(Equation 1.33.)}$$

where the Stokes number, $Stk = \frac{\rho_p d_p^2 C_c V}{18 \eta d_d}$. (Equation 1.34.)

Particles of the same size have a zero relative settling velocity, so their capture efficiency becomes also zero.

In diesel exhaust-aerosol transport systems, such as the exhaust pipe and sampling systems, the coagulation can be significantly enhanced owing to flow velocity gradients for particles following different, neighbouring streamlines. This process is called shear coagulation and, for a laminar flow in a tube, it can be expressed as:

$$\frac{V_{shear}}{V_{thermal}} = \frac{d_p^2 \Gamma}{6 \pi D}, \qquad \text{(Equation 1.35.)}$$

where $\frac{V_s}{V_t}$ is the ratio of the shear coagulation rate to thermal coagulation rate, and Γ is the velocity gradient at that point (Hinds, 1982). In many practical situations, however, the flow is not laminar but turbulent, and thus the coagulation can be

enhanced even further. This is called turbulent coagulation, and is due to the increase in velocity and change in direction of the velocity gradients, owing to inertial effects in the turbulent eddies. The ratio of turbulent coagulation to shear coagulation for a monodisperse aerosol is given by:

$$\frac{V_{turb}}{V_{shear}} = \frac{bD_p^2}{64\pi D}\left(\frac{\rho_g \varepsilon}{\eta}\right), \qquad \text{(Equation 1.36.)}$$

where b is a constant of order 10 and ε is the rate of energy dissipation per unit mass of gas (Hinds, 1982). In a pipe of diameter d_t, this parameter is:

$$\varepsilon = \frac{2f\overline{U^3}}{d_t}, \qquad \text{(Equation 1.37.)}$$

where $\overline{U}$ is the average velocity in the pipe and f is the friction factor.

According to Hinds, 1982, turbulent coagulation is negligible for particles below 0.1μm and very important for particles around and larger than 10μm. Complex geometries and flow direction changes such as those present in the exhaust pipe, catalyst and silencers can be expected to increase the extent of turbulent coagulation.

1.6.6. Chemical reactions

Multiple reactions take place between the particulate – including solid and liquid - and gas phases. The high specific surface area (surface area per unit mass) plays a very important role in the diversity of reactions, which can occur between compounds within a particle, between particles with different composition and between particles and various species in the gas phase. At diesel exhaust conditions, the number and complexity of the reactions are extremely large.

Different processes control the rate at which these reactions occur. Between compounds within the particles, reaction rates are controlled by chemical kinetics. The rate of reactions between particles with different chemical composition is mostly controlled by the coagulation rate. Between particles and species in the gas phase, the reaction rate is predominantly controlled by the condensation rate. As a reminder, some of the species that condense from the gas phase onto the particle surface are sulphuric acid and associated water, and a complex mixture of semi-volatile hydrocarbons. Extracts from particulate matter analysed by gas chromatography showed two peaks at the equivalent n-alkane carbon number distributions for hydrocarbon species of C_{16} and C_{25}. The first was derived from diesel fuel and the second, from lubricating oil (Abdul-Khalek,2000). A

representative hydrocarbon, just in the middle of the SOF range in particulate matter is nonadecane.

The process through which gas molecules dissolve in the liquid component of the particle is called absorption, which is normally extremely fast and thus not a controlling process when compared to diffusion from the gas to the particle surface or diffusion within the particle. It carries on until the solubility limit of the gas in the liquid is reached. If mass transfer occurs between the gas phase and solid components of the particles, the process is called adsorption, which may or may not include chemical reactions, in which cases it is called physisorption and chemisorption, respectively. Physisorption is the result of the action of van der Waals forces when the temperature is below the critical temperature of the gas. It is similar to condensation in its analysis. Chemisorption involves the creation of chemical bonds, and it can occur at temperatures higher than the critical temperature of the gas.

1.7. Forces acting on particles

Particles suspended in the exhaust aerosol are in continuous motion, and respond to the flow of the exhaust gas, which largely governs their behaviour, as well as to various external forces that originate through the exhaust pipe, such as inertial, thermophoretic, or electrophoretic forces. This section describes the concepts involved with the particle motion in the diesel exhaust aerosol. Since the particle size extends from a few nanometers to several micrometers, different physical laws govern their motion: the kinetic theory of gases is closely related to the motion of submicron particles, especially those smaller than 0.1μm, affected by the motion of gas molecules; and fluid dynamics is applied to intermediate and large particles immersed in the continuous gaseous medium. The section concludes with the application of these forces to the aerosol flow through the exhaust and sampling lines, expressed as the overall particulate transport efficiency.

1.7.1. Particle adhesion, detachment and bouncing

The adhesive forces that keep the particles together are extremely important but poorly understood. They are normally several orders of magnitude stronger than common external forces applied on the particles, and may depend on particle size, shape, surface roughness, chemical composition, etc; the surrounding-gas properties as humidity and temperature; and the mechanics of other particles that make contact with them, the time of contact between one another and their relative velocity.

Diesel exhaust particles are formed by carbonaceous solid material and liquid components, condensed and/or adsorbed from the gas phase. The liquid component facilitates the action of London - van der Waals forces, which are the main adhesive forces for sticky particles. These act over extremely short distances, in contrast to gravitational, inertial, thermophoretic and electrical forces, and decrease rapidly to zero away from the particle surface (Friedlander, 1977). The random motion of electrons creates instantaneous dipoles at the particle surface in the electrically neutral material, and these induce dipoles in neighbouring materials, creating attraction forces (Hinds, 1982; Willeke, 1993). The forces are inversely proportional to the square of the separation distance between two surfaces. After an initial contact, they deform to reduce the separation distance and increase contact area, until the attractive forces balance those that resist deformation. This occurs between neighbour particles, as well as between a particle and an object surface, for example, exhaust walls, a filter or an impactor stage.

Detachment forces can break the adhesion of the particles. Vibration, as well as gas currents over a layer of deposited particles, contributes to particle detachment. The vibration detachment force is proportional to the particle diameter cubed, d_p^3, and that due to a gas current, to the exposed area, or d^2. As the opposed force, adhesion, is in linear proportion to the diameter, d, large particles become more likely to be detached than the fine ones. According to some authors, particles smaller than 10μm, which constitute virtually the totality of diesel exhaust aerosol, are not likely to be removed by vibration or exhaust gas flow, but once those particles have formed a deposition layer over a surface, e.g. the walls of an exhaust pipe, larger pieces, namely around 100μm to 10mm, may be removed from the layer by those mechanisms (Hinds, 1982; Willeke, 1993). Other authors (Ziskind, 1995) have pointed out that particles as small as 2μm can be reentrained in turbulent pipe flow. The phenomenon of reentrainment in turbulent flows is discussed in more detail later in this chapter.

Adhesion and detachment, as suggested above, occur because of the liquid component of the particles. The solid component, on the other hand, originates a different phenomenon, particle bounce. The stronger force resisting the surface deformation in solid particles may be greater than the adhesion force of the liquid component, so the particle ends up moving away after making contact with another particle or a solid surface. This characteristic is undesirable for particulate collection techniques based on inertial impaction, although it can be improved by applying grease or oil to the collection surface, as it will be seen later.

1.7.2. Gas flow and particle motion in the gas

According to the engine speed, in the case of exhaust aerosol flow through the exhaust system, or the sampling flow rate, in the case of aerosol characterisation equipment, the aerosol flows at various flow rates, which affect its flow pattern, from smooth or laminar, to highly turbulent. This pattern is governed by the ratio of the inertial force of the gas to the friction force between the gas and the exhaust pipe walls, expressed by the Reynolds number,

$$\mathrm{Re} = \frac{\rho_g V d}{\eta}, \qquad \text{(Equation 1.38.)}$$

where ρ_g is the gas density, V the velocity of the gas, η the gas viscosity and d the pipe diameter. Suspended in this gas, particles are in continuous motion, its flow pattern being defined by its own particle Reynolds number, Re_p, with a similar definition to Re, changing the pipe diameter for the particle diameter, d_p. The gas flow pattern, and therefore Re, is affected by direction and geometry changes in the pipe, the inclusion of the catalytic converter honeycomb channels, orifices and bends in the exhaust silencers.

Diesel exhaust particles interact with the exhaust gas molecules, so to analyse the motion of the particles whose motion can be significantly affected by this interaction, the discontinuous nature of the gas must be taken into account.

Following the reasoning by Stokes, it is possible to develop an expression for the force resisting the motion of a spherical particle of diameter d_p, moving through the gas at a constant velocity V, when the particle is away from surfaces. The force is called particle's drag force, and is given by the Stokes' law:

$$F_{drag} = 3\pi\eta V d_p, \qquad \text{(Equation 1.39.)}$$

where η is the gas viscosity. For this expression to be valid, the particle Reynolds number, Re_p, must be much less than unity, and the particle diameter must be much larger than the mean free path of the gas molecules. The mean free path, λ, is a characteristic of the gas, as defined previously in section 1.6.3., is the average distance travelled by a molecule between successive collisions. It depends on the gas density, and increases with increasing temperature and decreasing pressure. It is related to the particle diameter through the Knudsen number:

$$Kn = \frac{2\lambda}{d_p}, \qquad \text{(Equation 1.40.)}$$

Therefore, the Stokes' law, as expressed in Equation 1.39., is applicable to spherical particles with a Knudsen number Kn << 1. In this case, the gas is considered as a perfect *continuum*.

Stokes' law becomes incorrect when the assumptions of spherical particles, Reynolds numbers much smaller than unity and particles much larger than the gas molecules (Kn<<1) are not met. For these situations, corrections may be applied.

For very small particles, approaching the mean free path of the gas molecules, this is Kn≈2, the gas is no longer a perfect continuum. The drag for a given velocity becomes less than predicted by Stokes' law and continues to decrease with particle size (Friedlander, 2000). This can be corrected by a factor called the Cunningham correction factor, C_c, so Equation 1.39. becomes:

$$F_{drag} = \frac{3\pi\eta V d_p}{C_c}, \qquad \text{(Equation 1.41.)}$$

where

$$C_c = 1 + Kn\left[A + Q\exp\left(-\frac{b}{Kn}\right)\right]. \qquad \text{(Equation 1.42.)}$$

The constants A, Q and b are given by an empirical fit for a certain gas. For air, the values A=1.252, Q=0.399 and b=1.100 were published by Jennings in 1988 (Reist, 1993). The Cunningham correction factor equals unity in the continuum regime and is bigger than unity for decreasing particle size in the transition regime. For solid particles in air at normal conditions, C_c = 1.02 for 10μm particles, 1.15 for 1μm particles, and 2.9 for 0.1μm particles (Reist, 1993; Willeke, 1993).

Additionally, a dynamic shape factor, χ, may be introduced to account for the non-sphericity of the particles:

$$F_{drag} = \frac{3\pi\eta V \chi d_p}{C_c}. \qquad \text{(Equation 1.43.)}$$

χ can be between 1.12 and 1.32 for branched particle clusters of spheres such as diesel particles (Willeke, 1993; Reist, 1993).

When particles much smaller than λ, this is, in the free molecular range (Kn>>1), they can flow very close to surfaces such as pipe or channel walls, orifices, etc, without being disturbed by gas molecules. An expression for the drag force can be derived from kinetic theory:

$$F_{drag} = \frac{2}{3} d_p^2 V \rho_g \left(\frac{2\pi kT}{m_g} \right)^{1/2} \left[1 + \frac{\pi\alpha}{8} \right], \qquad \text{(Equation 1.44.)}$$

where k is the mass transfer coefficient, ρ_g is the gas density, m_g is the molecular mass of the gas molecules. α is an accomodation coefficient that must be normally evaluated experimentally, but is usually near 0.9 for momentum transfer (Friedlander, 2000).

1.7.3. Diffusion

In the presence of a particle concentration gradient, e.g. between the centreline of the exhaust pipe and the boundaries of the pipe walls, small particles migrate from the higher to the lower concentration, as gas molecules do, owing to the random movement of the particles. This is known as diffusion or Brownian motion. A diffusion coefficient or diffusivity, is thus defined as

$$D = \frac{kTC_c}{3\pi\eta d_p} = kTB, \qquad \text{(Equation 1.45.)}$$

where k is the Boltzmann constant (1.38×10^{-16} erg/K) and B is the mechanical mobility of the particle in the surrounding gas. The diffusivity can be used to estimate the root mean square distance, which is the distance the particle can travel in a given time t,

$$x_{rms} = \sqrt{2Dt}. \qquad \text{(Equation 1.46.)}$$

1.7.4. Settling velocity, aerodynamic diameter and inertial impaction

Particles are attracted by the gravitational force

$$F_{grav} = m_p g = (\rho_p - \rho_g) v_p g. \qquad \text{(Equation 1.47.)}$$

This force equilibrates quickly with particle drag, so the particle reaches a constant settling velocity, defined as

$$V_{ts} = \frac{\rho_p d_p^2 g}{18\eta}, \qquad \text{(Equation 1.48.)}$$

for $d_p > 1\mu m$ and $Re < 1.0$. The settling velocity of spherical particles is easily expressed mathematically. Since such particles, e.g. droplets, are also easy to produce, their settling velocity is used as a reference to compare their behaviour with that of non-spherical diesel exhaust and atmospheric particles. This is the origin

of the definition of the aerodynamic diameter, d_a, which is the diameter of a unit-density sphere that has the same settling velocity as the particle in question.

Similarly, the Stokes diameter, d_s has been defined as the diameter of a spherical particle with the same density and settling velocity as the particle in question. Therefore,

$$\rho_p d_s^2 = \rho_a d_a^2 . \qquad \text{(Equation 1.49.)}$$

$$\text{For Re} > 0.1,\ V_{ts} = \sqrt{\frac{4\rho_p C_c d_p g}{3\rho_g C_d \chi}}, \qquad \text{(Equation 1.50.)}$$

This equation must be solved iteratively, since C_d is dependent on settling velocity (Willeke, 1993). An initial value for V_{ts} is assumed to calculate C_d. This value is re-introduced in equation 1.49. to calculate V_{ts}, which is used for a new C_d value. This is repeated until successive values for each parameter converge.

From the definition of the settling velocity, some other parameters have been defined. The relaxation time,

$$\tau = \frac{V_0}{g}, \qquad \text{(Equation 1.51.)}$$

indicates the time a particle needs to reach (1/e) of its final velocity in a gravitational field. It is used to calculate the stopping distance of a particle that is injected into a gas, as

$$S = V_0 t, \qquad \text{(Equation 1.52.)}$$

where V_0 is the initial velocity of the particle. This is extremely useful in the design of particle collectors, i.e. impactors, in which the aerosol flow negotiates a 90°C bend at an initial velocity V_0, so particles above a certain size do not follow the gas flow owing to their inertia, and thus can be collected on an impaction stage at a distance S. The initial velocity, V_0, is determined by the size of a jet nozzle upstream of the collection stage. This kind of system can be represented by the Stokes number:

$$Stk = \frac{S}{d} = \frac{\rho_p d_p^2 V C_c}{9\eta d_j}, \qquad \text{(Equation 1.53.)}$$

where d is a characteristic dimension as the nozzle radius, and d_j=2d, the nozzle diameter. A schematic diagram of inertial deposition is shown in Figure 1.6.

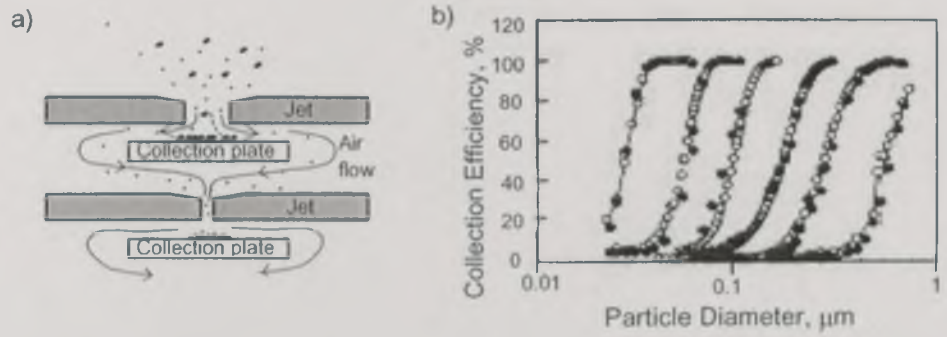

Figure 1.6.a) Schematic diagram of inertial deposition as it occurs in two impactor stages. b) The curves on the right (Keskinen, 1999) represents the typical collection efficiency values for various collection stages in an impactor. The particle diameter at which the collection efficiency of a stage is 50% is the cut-off diameter for that stage.

1.7.5. Thermophoresis

Since the gas molecule motion increases with increasing gas temperature, particles in a thermal gradient have more contact with gas molecules in the hotter side and, as a result, they are forced towards the colder side. The thermophoretic force is defined as:

$$F_{th} = \frac{-p\lambda d_p^2 \Delta T}{2\rho_g T}, \text{ for } d_p < \lambda \qquad \text{(Equation 1.54.)}$$

$$F_{th} = \frac{-9\pi\eta^2 d_p H \Delta T}{2\rho_g T}, \text{ for } d_p > \lambda \qquad \text{(Equation 1.55.)}$$

where DT is the temperature gradient and H includes the effect of the thermal gradient inside the particle, and it is given by:

$$H \cong \left(\frac{1}{1+6\lambda/d_p} \right) \left(\frac{k_a/k_p + 4.4\lambda/d_p}{1+2k_a/k_p + 8.8\lambda/d_p} \right), \qquad \text{(Equation 1.56.)}$$

where k_a and k_p are the thermal conductivities of air and particle, respectively (Willeke, 1993).

The thermophoretic velocity is given by

$$V_{th} = \frac{-0.55\eta\Delta T}{\rho_g T}, \text{ for } d_p < \lambda \qquad \text{(Equation 1.57.)}$$

$$V_{th} = \frac{-3\eta C_c H \Delta T}{2\rho_g T}, \text{ for } d_p > \lambda. \qquad \text{(Equation 1.58.)}$$

In the former case, it is independent of particle size, and in the latter, it is a weak function of particle size.

Thermophoretic velocity can exceed settling velocity for submicron particles as well as deposition due to thermophoresis can be more significant than deposition by diffusion for particles larger than 0.2μm.

1.7.6. Electrophoresis

Particles carry electric charge, and can be charged in a controlled way. An electrostatic field originates an electrostatic force that may be higher than other external forces, depending on the number of charges on the particle:

$$Felec = neE\,, \qquad \text{(Equation 1.59.)}$$

where n is the number of electrons with charge *e*, and E is the electric field. An equilibrium between F_{elec} and F_{drag} leads to a terminal velocity,

$$V_{elec} = \frac{neEC_c}{3\pi\eta d_p} \qquad \text{(Equation 1.60.)}$$

From here, it is possible to relate the mobility mechanical mobility with the electrical mobility, as

$$Z = neB, \qquad \text{(Equation 1.61.)}$$

$$\text{so } V_{elec} = ZE\,. \qquad \text{(Equation 1.62.)}$$

Electrical mobility has been used to classify particles by size, as long as a known charge distribution with particle size exists, as will be seen in the next section.

1.7.7. Transport efficiency

As a result of the study of the effect of the various forces explained above, several authors have derived correlations for the transport of aerosol through lines with a circular cross section, such as those used normally for aerosol transport and sampling, and applied in this work. The transport efficiency, $\eta_{transport}$, as defined by Brockmann in the compilation by Willeke and Baron (Willeke, 1993), is "the product of the transport efficiencies in each flow element for each mechanism":

$$\eta_{transport} = \prod_{mechanism} \eta_{mechanism} \qquad \text{(Equation 1.63.)}$$

The expressions to estimate the transport efficiency due to each of the most common and significant mechanisms are given below.

1.7.7.1. Gravitational settling

The transport efficiency for an aerosol in laminar flow in a straight tube with an inclination θ is expressed by:

$$\eta_{tube\_grav} = 1 - \frac{2}{\pi}\left[2\kappa\sqrt{1-\kappa^{2/3}} - \kappa^{1/3}\sqrt{1-\kappa^{2/3}} + \arcsin(\kappa^{1/3})\right] \qquad \text{(Equation 1.64.)}$$

$$\kappa = (3/4)Z\cos\theta = (3/4)(L/d)(V_{ts}/U)\cos\theta$$

for $V_{ts}\sin(\theta/U) \ll 1$, where $Z=(L/d)(V_{ts}/U)$ is the gravitational deposition parameter, L is the length of the tube and d is the inside diameter of the tube (Willeke, 1993).

For turbulent flow, the expression becomes:

$$\eta_{tube\_grav} = \exp\left(\frac{-4Z\cos\theta}{\pi}\right) \qquad \text{(Equation 1.65.)}$$

also for the condition $V_{ts}\sin(\theta/U) \ll 1$. It has been shown that if the tube through which turbulent flow exists is a bending tube, the transport efficiency due to gravitational settling is equal to that through a horizontal tube with the same diameter and the length projected by the bending tube on the horizontal plane. This is not valid for laminar flow through the bending tube. Nevertheless, the flow at the diesel exhaust conditions is turbulent virtually all the time, so the expression is applicable.

1.7.7.2. Diffusional deposition

The walls of the exhaust pipe act as a sink for diffusing particles owing to the particle concentration gradient inside the pipe. At the walls, the particle concentration can be considered as zero, so those particles would deposit on them. The transport efficiency with diffusive deposition is given by the expression:

$$\eta_{diff} = \exp\left(\frac{-\pi d L V_{diff} Sh}{Q}\right) \qquad \text{(Equation 1.66.)}$$

where Sh is the Sherwood number; V_{diff} the deposition velocity due to diffusion, d is the tube diameter, L is the tube lenght and Q is the volumetric exhaust flow (Hinds, 1982). The Sherwood number is related to the Reynolds number for the gas, Re, and the Schmidt number, Sc. For turbulent flow,

$$Sh = 0{,}0118\,\mathrm{Re}^{7/8}\,Sc^{1/3} \qquad \text{(Equation 1.67.)}$$

where:

$$Sc = \frac{\mu_g}{\rho_g D}.$$

1.7.7.3. Turbulent inertial deposition

Particles with large inertia can be deposited on wall pipes under the effect of the turbulence in the center of the pipe. The transport efficiency with turbulent inertial deposition can be expressed in a very similar way to that due to diffusional deposition, just replacing V_{diff} by V_t:

$$\eta_{inertial} = \exp\left(\frac{-\pi d L V_t}{Q}\right) \qquad \text{(Equation 1.68.)}$$

The turbulent inertial deposition efficiency, V_t, has been better studied by comparing it to the carrying gas velocity, U, through the definition of the dimensionless turbulent inertial deposition velocity, V_+:

$$V_+ = 5.03(V_t / U)\,\mathrm{Re}_f^{1/8} \qquad \text{(Equation 1.69.)}$$

Then, the dimensionless velocity is an indicator of how fast the particles are with respect to the velocity of the carrying gas. The dimensionless velocity is related to the dimensionless relaxation time τ_+:

$$V_+ = 0.0006\tau_+^2 \qquad \text{(Equation 1.70.)}$$

The dimensionless relaxation time is defined by:

$$\tau_+ = 0.0395 Stk\,\mathrm{Re}_f^{3/4} \qquad \text{(Equation 1.71.)}$$

1.7.7.4. Inertial deposition at a bend

The change in the aerosol flow direction causes the particles with higher inertia to deposit on the pipe walls. The transport efficiency with inertial deposition at a bend for turbulent flow is given by:

$$\eta_{bend\ inertial} = \exp(-2.823 Stk\phi) \qquad \text{(Equation 1.72.)}$$

where ϕ is the bend angle in radiants. It is independent of the Reynolds number, depending only on the bend angle. For laminar flow, the transport efficiency is affected by the Reynolds number and the curvature ratio, the latter defined as the ratio between the bend radius and the tube radius. Nevertheless, for exhaust aerosol flow, only turbulent flow will be considered, so the curvature ratio and the Reynolds number do not affect the transport efficiency.

1.7.7.5. Thermophoretic deposition

The transport efficiency with thermophoretic deposition is given by:

$$\eta_{th} = \exp\left(-\frac{\pi d L V_{th}}{Q}\right) \qquad \text{(Equation 1.73.)}$$

where V_{th} is the thermphoretic deposition velocity. This is dependent on the particle size, expressed by the Knudsen number.

$$V_{th} = \frac{-0.55\eta\nabla T}{\rho_g T}, \text{ for Kn>2} \qquad \text{(Equation 1.74.)}$$

$$V_{th} = \frac{-3\eta C_c H \nabla T}{2\rho_g T}, \text{ for Kn<2.} \qquad \text{(Equation 1.75.)}$$

Thermophoresis has been shown to have a significant effect on the amount of soot mass deposited on the combustion chamber and exhaust system walls (Abraham, 1996; Kittelson, 1990)

1.7.8. Results from previous studies on particle deposition

Particle dispersion and deposition has been studied theoretically, experimentally and using computer simulations. Several authors include compilations of various studies in the field (Chunhong, 1998; Willeke, 1993; Hinds, 1982; Friedlander, 1977). Other authors (Berger, 1995) have remarked that thermophoresis plays a significant role in the deposition of particles through vehicle exhaust systems. Here, some conclusions from selected studies are presented, given their relevance to the application in vehicle exhaust.

Computer simulations by Chunhong et al. (Chunhong, 1998) evaluated the aerosol particle deposition in duct flows using the computational fluid dynamics code FLUENT®, which allowed the inclusion of models for Brownian motion diffusion, thermophoresis, lift force and gravity in laminar and turbulent aerosol flow. For the turbulent case, representative of vehicle exhaust, they found that, when the particles are beyond the viscous sublayer near the tube wall, thermophoresis and Brownian motion diffusion are negligible, owing to the increased particle dispersion produced by the turbulence. Close to the wall, inside the viscous sublayer, thermophoresis has a strong effect on deposition and transport of particles below a few micrometers in size, and Brownian motion is the dominant dispersion mechanism. The thermophoretic force decreases with increasing particle size above 0.1μm and the range of particle sizes affected by this force expands as the temperature gradient increases.

Chunhong also found that, for turbulent hot gas flow in a duct with cold walls, the deposition velocity increases significantly for particles smaller than 0.1μm, owing to thermophoresis. For particles between 0.1μm and 4μm, thermophoresis was the dominant deposition mechanism. Deposition of larger particles was more importantly influenced by turbulent eddy impaction and the effect of thermophoresis became insignificant.

In their study on thermophoretic deposition in turbulent flow, Romay et al. (Romay, 1998) aimed to determine the way different mechanisms acted together over particles between 0.1μm and 0.7μm, particularly thermophoresis and turbulent eddie impaction. They developed an expression to predict the total particle deposition and assumed that both mechanisms were independent and acted in series. The preditions agreed well with experimental results for small particles and Reynolds numbers around 5000, but deposition was underestimated by as much as 50% of the experimental values for higher Reynolds numbers. This was attributed to an unaccounted turbulent effect in the theoretical prediction, indicating the need to develop a more detailed theoretical model.

Berger et al (Berger, 1995), in a realistic study of particle deposition on a diesel exhaust pipe, used a model including thermal and turbulent eddy diffusion as well as thermophoresis, and compared its results with experimental data involving particle size distribution measured with cascade impactors. They found that, for the fine particle mode, with a median diameter of 0.12μm and accounting for 75% of the total particle mass, the penetration rate through the pipe was 88%. On the other hand, the penetration for the coarse particle mode, with a median diameter of 2.4μm and 25% of the mass, was just 64%. The effect of turbulent diffusion was more significant for large particles when the flow is turbulent, but just the opposite occurs when this is laminar. Thermophoresis was a very important deposition mechanism, depending on the temperature gradient near the wall. When insulating the pipe, the gradient was reduced and the penetration rates ratio $P_{insulated}/P_{non\text{-}insulated}$ was around 93%.

The studies mentioned above pointed out the importance of thermophoresis in the region near the walls for turbulent flows. The dynamics of aerosols in this region has been modelled by Zaichik et al. (Zaichik, 1995), who analysed the effect of droplet size and concentration on the deposition rate in turbulent pipe flows. They found that the deposition coefficient was a function of the dimensionless relaxation time for large particles only. For small particles, it depends on the inertia parameter.

1.7.9. Reentrainment of particles in turbulent flows

Reentrainment of particles from the deposition layer, also called resuspension by several authors, is not yet a well characterised process (Adhiwidjaja, 2000; Phares, 2000; Ziskind, 1995; Willeke, 1993; Kittelson, 1991), although it has been subject of theoretical and experimental studies covering different approaches to its several behavioural aspects. Resuspension is a consequence of deposition processes. Reducing deposition through isolation, preheating and using short lines would diminish the deposition rate and, therefore, the resuspension rates, as Kittelson explained. This approach, however, was focused on the measurement, and not on the emissions in the real world. Exhaust pipe isolation and preheating is not practical, so particulate deposition, and hence resuspension, cannot be controlled this way. As a result, particles deposit and are reentrained through the exhaust system.

Excellent reviews and analysis of the phenomenon have been made by Ziskind et al. (Ziskind, 1995) and Phares et al. (Phares, 2000), to which the reader is referred to for a detailed explanation of the phenomenon. Here, the most relevant aspects from these reviews are summarised, although their application to resuspension in real exhaust systems is still quite impractical.

Two kinds of forces have been proposed to cause particle resuspension of particles in turbulent flows, namely normal lift forces and tangential shear forces (Phares, 2000). These forces act over the particles producing various modes of motion involved in particle separation: lift-off from the surface, sliding and rolling. The most widely accepted models explaining the involved processes in equilibrium are the JFK and the DMT theories, which describe the detachment of particles from a planar surface, assuming that the particles are originally spherical but are flattened against the surface because of the action of attractive forces. The theories predict a critical pull-off force that depends on particle size:

$$F_{pull-off}^{DMT} = \pi \gamma d_p \qquad \text{(Equation 1.76.)}$$

$$F_{pull-off}^{JKR} = \frac{3}{4}\pi \gamma d_p \qquad \text{(Equation 1.77.)}$$

where γ is the Dupré energy of adhesion (Phares, 2000). The difference between both forces is small, although they were derived from different principles: in the DMT theory (developed by Derjaguin et al.), the contact area decreases gradually to zero, whereas in the JKR theory (developed by Johnson et al.), there is a finite contact radius at the moment of detachment, caused by crack propagation due to high tensile stresses along the particle/plane contact surface. These theories do not include the effect of elastic moduli of the particle and the surface. Another model is

necessary for this, which is the TPL theory (developed by Tsai et al.), whose equations are not included here, but are shown elsewhere (Phares, 2000). This theory assumes that the contact area between surfaces is dependent on the elastic modulus of the particles and so is the pull-off force over the particles. As a consequence, a decrease in the elastic modulus produces an increase in the pull-off force, which begins to resemble the separation of two flat surfaces.

Phares et al. (Phares, 2000) investigated the validity of the equilibrium theories by converting the threshold tangential forces involved in particle reentrainment to a threshold shear stress, and comparing them with experimentally measured threshold shear stress values. These are calculated from the particle Reynolds number, and thus are size-dependent. Phares et al. pointed out that the equilibrium theories, in which detachment forces are applied infinitely slowly, are not successful in predicting accurately the size dependence of the threshold shear stress, since resuspension occurs suddenly, too quickly to maintain the equilibrium. Therefore, they undertook a resuspension dynamics analysis, by changing the applied force duration and intensity in their experiments and developing a dynamic resuspension model based on crack propagation kinetics. In this way, they found an explanation for the deviations of the equilibrium theories' predictions, but lack of information did not allow producing a quantitative reliability for the dynamic model.

Although Phares et al. stated in their recent study that resuspension takes place suddenly, several researchers have based their studies on the assumption that reentrainment has a statistical origin associated with the turbulent flow character, as has been indicated by experimental measurements, described as random turbulent "bursts". Turbulent flow involves the repetition of similar events or "coherent structures" in time, such as low speed streaks in the viscous sublayer, ejections of low-speed fluid, sweeps of low-speed fluid, vortical structures, sloping near-wall shear layers, formation of near-wall pockets and large scale motions and discontinuities in the streamwise velocity. These structures, and their possible role in particle resuspension, were described in detail by Ziskind et al. (Ziskind, 1995). Here, it is relevant to say that their action differs for different particle sizes.

The importance of the dynamic analysis on particle resuspension is reflected in the fact that unsteady conditions such as turbulent flow with eddies impinging on the wall and the start-up and shutdown of flows are much more significant causes of reentrainment than steady conditions. Cold start, fast acceleration and deceleration would be the most influencing events on particle reentrainment in the diesel exhaust system. In them, deposition and reentrainment usually occur simultaneously. Adhiwidjaja et al. (Adhiwidjaja, 2000) described the formation of deposition layers

as a result of simultaneous particle deposition and reentrainment, using an aerosol with coarse particles (median diameters between 3.5μm and 5.6μm). They observed how the deposition layers formed striped patterns that, under certain conditions, moved streamwise at a velocity V_{dl}, proportional to the flux of colliding particles J_d, dependent on the aerosol concentration:

$$V_{dl} \approx k_m J_d \qquad \text{(Equation 1.78.)}$$

where k_m is the proportional constant.

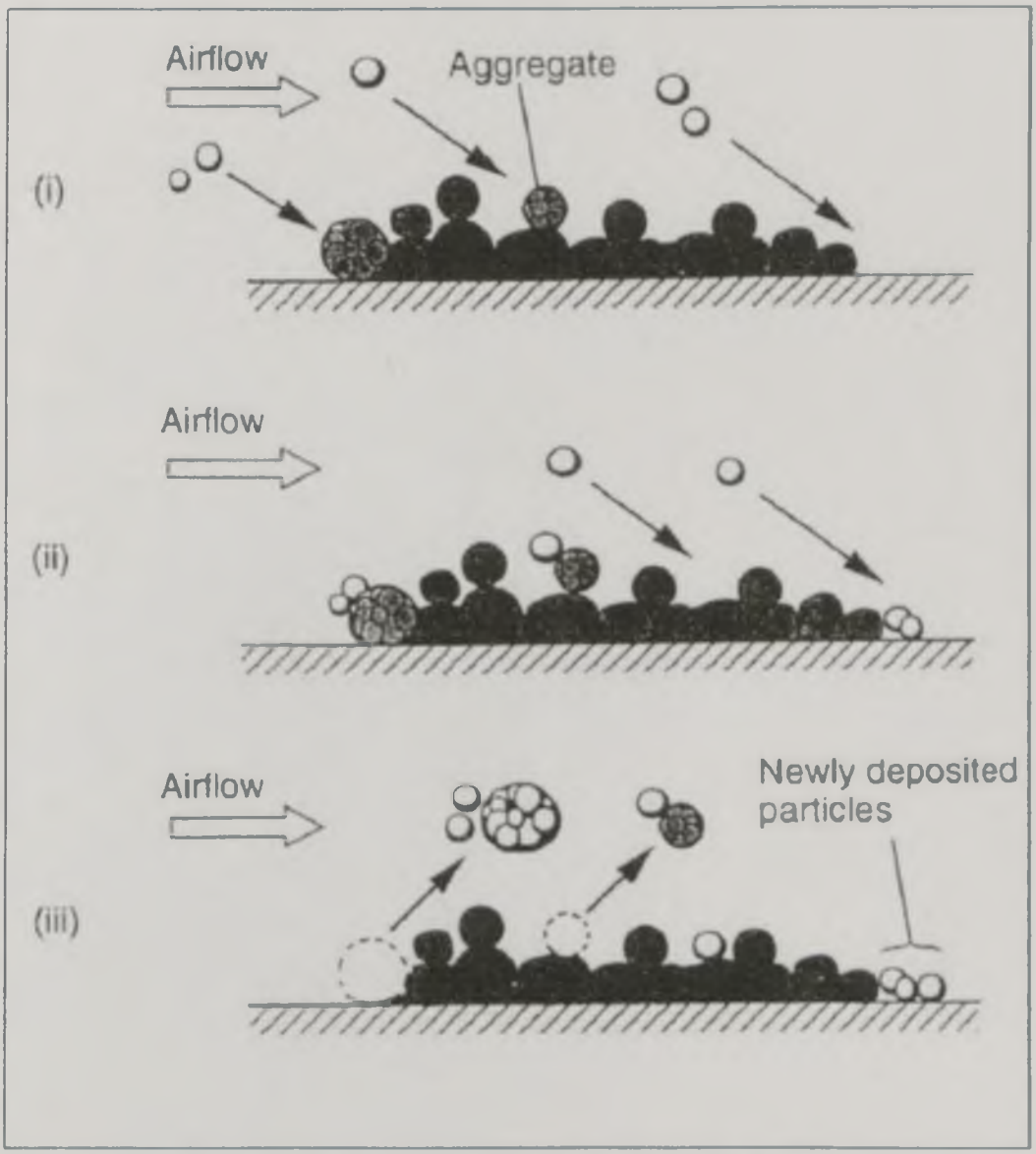

Figure 1.7. Mechanism of striped deposition layer movement (Adhiwidjaja, 2000).

The mass of the deposited particles per unit area (W/A) was a function of the gas velocity V_g an is constant at steady conditions, as a result of the equilibrium between deposition and reentrainment phenomena:

$$\frac{W}{A}\left(V_g, r_{sa}, N\right) = J_d - J_r \qquad \text{(Equation 1.79.)}$$

where r_{sa} is the surface average roughness and J_r, the resuspension flux. The resulting mechanism they proposed is shown schematically in Figure 1.7.

An increase in the roughness of the tube material reduced the interval between strips as well as the thickness of the layer. The roughness also affected the velocity at which the layer moved downstream of the pipe, taking it down to zero at a critical roughness r_{sa}^{*}. They also found that the proportional constant k_m could be characterised by the ratio between the collision and adhesion moments, as shown in Figure 1.8.

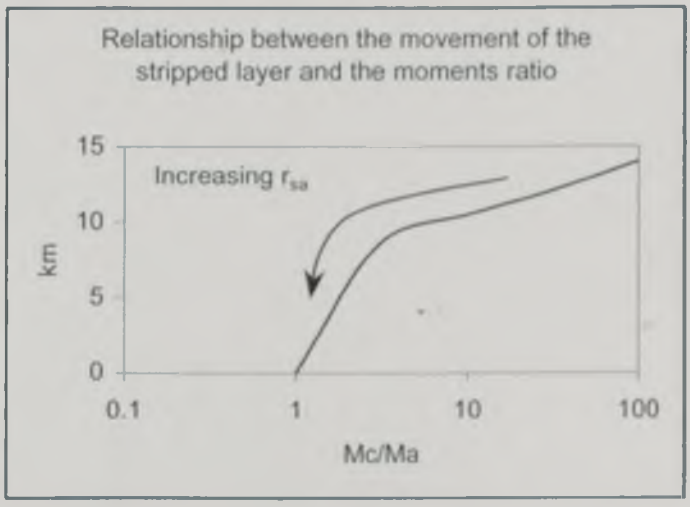

Figure 1.8. Relationship between the movement of the deposition layer and the collision/adhesion moments ratio.

The following expression for the collision/adhesion-moments ratio M_c/M_a was derived:

$$\frac{M_c}{M_a} = \frac{\cos(\alpha+\gamma)+\sin(\beta-\gamma)}{2\sin\alpha}\frac{F_c}{F_a} \qquad \text{(Equation 1.80.)}$$

where F_c is the collision force and F_a, the adhesion force, and α and β, angles in Figure 1.9. These are defined as:

$$F_c = 1.12 k_{fc}^{-2/5} m_{pst}^{3/5} d_{pst}^{1/5} v^{8/5} \qquad \text{(Equation 1.81.)}$$

and

$$Fa = \frac{A_{pa} d_{pa}}{12 z^2} \qquad \text{(Equation 1.82.)}$$

where $k_{fc} = \frac{1-\nu_p^2}{E_p} + \frac{1-\nu_a^2}{E_a}, m_{pa} = \frac{m_p m_a}{m_p + m_a}, d_{pa} = \frac{d_p d_a}{d_p + d_a}, H_{pa} = (H_p H_a)^{1/2}$. E is the Young modulus; H, the Hamaker constant; and ν, the Poisson's ratio. The subscripts a and p designate the deposited aggregate and the colliding particle, respectively.

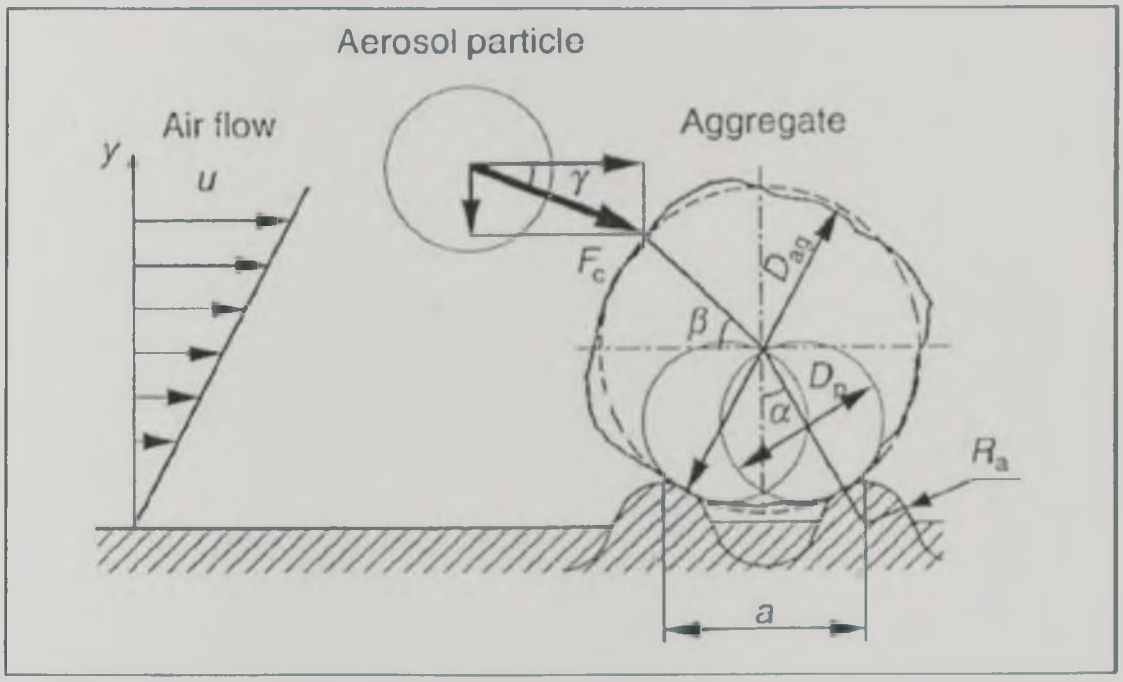

Figure 1.9. Schematic representation of a particle impacting upon an aggregate particle on the rough surface (Adhiwidjaja, 2000).

Another study by the same group (Adhiwidjaja, 2000) showed that, for charged particles, electrostatic forces enhanced the particle deposition, increasing the deposited mass on the tube walls to a certain value, irrespective of the applied voltage to the tube. The use of a wide electrode or an array of electrodes at intervals or in spiral along the tube eliminated the filmy deposition layers.

1.8. Aerosol characterisation techniques

1.8.1. Total mass concentration

The separation of the particulate and gas phases is the most straightforward technique to determine the total particulate mass concentration in an aerosol. Normally, this involves the filtration of the aerosol and the gravimetric

determination of the mass collected, which is therefore related to the total concentration by dividing by the total volume of aerosol passing through the filter. This is not a continuous monitoring procedure, since a rather large mass is needed to be collected for the technique to be accurate with the current laboratory microbalances.

Given the significance of transient emissions, other techniques have been developed to allow rapid and even continuous determination of total particulate mass concentration. Examples of these techniques are the Tapered Element Oscillating Microbalance (TEOM), the Quartz Crystal Microbalance (QCM), light scattering and extinction techniques. Although these have been extensively tested and correlate to a certain extent well with the gravimetric determination, the legislated technique is still based on the gravimetric determination at 52°C, using a Constant Volume Sampling (CVS) system. Researchers in industry, the universities and official institutions are working hard on techniques that allow the measurement of transient emissions for legislative purposes.

The following sub-sections describe briefly the most important total mass determination techniques, namely filtration-gravimetric determination and the TEOM. The former has been extensively used at the Department of Fuel and Energy for many years, and the latter, although not used in the present work, will be part of future projects on engine emissions at the same Department.

1.8.1.1. Exhaust filtration – gravimetric mass determination

Owing to its simplicity, flexibility and economy, filtration is perhaps the most widely used mass collection technique for aerosol characterisation (Willeke, 1993). It provides the virtually complete separation of the particulate phase from the gas phase, through a combination of mechanisms such as inertial impaction, interception and diffusion of the aerosol particles onto a fibrous or membrane filter (Hinds, 1982). The technique involves a pump, a proper sampling probe at the exhaust -or the exhaust dilution- system, an efficient transport line, a filter holder, a flow measurement device and a flow regulator. The temperature of the transport line, the filter holder and the flow measurement device is of utmost importance, so it must be controlled to meet a well-defined standard.

Filters for gravimetric mass determination of exhaust aerosol must be nearly 100% efficient in the particulate separation from the gas phase. The materials that have offered the best performance at the standard testing conditions are glass fibre, quartz and microporous membranes, from which the former are preferred because of the very low pressure drop across them and have become the standard filter media. They consist of fibres with diameters between 0.1μm and 100μm, have a 60% to

99% porosity, and their thickness can be between 0.15mm and 0.5mm. For a high collection efficiency to be achieved, the aerosol sample velocity must be kept low.

The gravimetric mass determination requires the change in the filter weight before and after sampling to be attributable only to the particulate from the aerosol. For this condition to be met, the filter weight should not be affected by temperature, age or moisture of the surrounding atmosphere. This is difficult to achieve, since both the filter material and the collected particles are hygroscopic and, therefore, they adsorb/absorb water vapour. This makes the technique particularly sensitive to the relative humidity of the surrounding atmosphere. Since it can be very changeable in an open space, the technique must include the conditioning of the filters in a closed constant-temperature-and-humidity atmosphere for 24 to 48 hours before their weighing, as well as the use of a blank filter. The use of the Teflon-coated version of glass fibre filters reduces significantly the sensitivity to moisture conditions, since Teflon reduces the inherent reactivity of glass fibre.

1.8.1.2. Real time mass measurement: TEOM

The TEOM uses the principle according to which the frequency of a vibrating object depends on the object's mass. The element in question is a special glass tapered tube that holds a filter where particulate matter from the flowing aerosol is deposited. The element vibrates at its natural frequency, dependent on the total mass (tapered element plus particulate), and this vibration frequency is continuously measured electronically. Using the vibration frequency difference between two instants t_1 and t_2 in time, the mass deposited on the filter in that period can be determined:

$$m_{1,2} = \frac{K_o}{(f_1^2 - f_2^2)}, \qquad \text{(Equation 1.83.)}$$

where K_o is a characteristic of the element and f_1 and f_2 are the vibration frequencies at t_1 and t_2, respectively.

1.8.2. Particulate imaging

The shape, size and count of individual particles can be determined from images of collected samples. Optical imaging has a very limited use, since it can not be used for measurements of particles smaller than the wavelength of light, 0.5μm, which constitute a great majority of the particles in number. More powerful techniques, such as Scanning Electron Microscopy and Transmission Electron Microscopy are used for those purposes. Practical applications in the use of these microscopes are presented by Watt et al. (Watt, 1985).

1.8.2.1. Transmission Electron Microscope (TEM)

The TEM was exactly derived from the optical microscope. In it, light has been replaced by electrons, and optical lenses by their electromagnetic equivalent (Watt, 1985; Lipkea, 1979). The electron illumination has a much shorter wavelength, 0.01μm, which allows high magnifications (x 300000) and, therefore, the measurement of much smaller particles than its optical counterpart. Measuring particles larger than 10μm, however, is not practical because of the small field of view at low magnifications. Electrons are produced by an electron gun, concentrated on the sample by a condenser lens, then focused by an objective lens into an intermediate image, and finally enlarged by a projector lens to produce a resulting image on a fluorescent screen or photographic film. The system works at high vacuum pressures, normally 10^{-4} mbar or below, since the electron gun must be protected from the atmosphere and electron scatter by air molecules must be minimised. The energy supplied to the lenses is very high, in the order of 1000kV or higher. The combination of high vacuum and high-energy systems make the microscope very bulky, needing separate rooms, or even buildings. Samples must be collected on thin membranes supported by fine metallic grids to be mounted over a standard sample holder of the TEM. The membranes must be transparent to the electron beam, and the materials used vary from carbon to metals and oxides.

1.8.2.2. Scanning Electron Microscope (SEM)

The SEM has little in common with the TEM, although it also uses an electron gun and a condenser lens system to produce the electron beam. The difference is that the SEM does not use the objective and projector lenses as the TEM does. The electron beam produced, with energies around 40keV, is very fine and focused on a narrow portion of the sample surface. It is then scanned across the surface in a pattern of parallel lines or a "raster". From the sample surface, secondary electrons with energies of a few tens of eV are emitted, and high-energy backscattered electrons from the primary beams are re-emitted and reflected (Watt, 1985). Then they are collected, amplified and used to produce an image of the sample surface in a cathode-ray tube. Since the intensity of emission of electrons from the sample surface is very sensitive to the incidence angle of the primary beam, topographical information about the sample surface can be obtained. The resolution of the SEM is not as good as that of the TEM, being around 0.1μm, but it allows determining the shape and elemental composition of large agglomerates. The samples can be taken from filters previously covered by a thin layer of a conductive material to avoid irregular charging.

1.8.3. Size distribution measurement techniques

Particle size classification can be achieved by applying the knowledge on the size-dependent behaviour of the particles under the action of external forces, such as those described in a previous section. The diffusion battery, for example, classifies particles between 0.002μm and 0.2μm, according to their diffusion onto cylindrical tubes or screens. Impactors use the inertial behaviour of the particles to make them impact onto several stages according to their size: the aerosol is accelerated in a jet and then the flow direction changes abruptly over an impaction stage, so particles with high enough inertia escape the flow streamlines, impact on the stage, and stay there if bounce is not significant. Electrical sizers use the charging principles and the electrical mobility of the particles with the same objective. There are some additional techniques based on other principles such as thermophoretic deposition.

This section will describe the most widely used techniques for exhaust aerosol analysis, namely the Andersen inertial impactor, the Electrical Low-Pressure Impactor and the Scanning Mobility Particle Sizer. The former two were used in this work, and the latter will be used in future projects of the Department, and is one of the most widely used techniques at the moment.

1.8.3.1. Andersen Impactor

The Andersen Impactor classifies particles in seven stages with the median aerodynamic diameters in Table 1.3.

Stage	Median Diameter, μm
0	9
1	5.8
2	4.7
3	3.3
4	2.1
5	1.1
6	0.7
7	0.4

Table 1.3. Andersen Impactor median aerodynamic diameters.

The particle size distribution is determined gravimetrically, using 7 cm ϕ glass fibre or Teflon filters as the collection media. These are to be weighed before and after sampling so, a 24- to 48-hour conditioning period in a constant temperature-and-humidity atmosphere is recommended to reduce the technique sensitivity to water adsorption by the filter and the sample.

The top impactor stages consist of a single central orifice, whereas the lower stages have gradually more and smaller orifices in a radial configuration. The diameter of the nozzles determines the size of the particles to be collected on the corresponding stage, through the definition of the Stokes number:

$$Stk = \frac{\rho_p C_c d_p^2 U}{9\eta d_n} \qquad \text{(Equation 1.84.)}$$

where d_n is the diameter of the orifices or nozzles of the stage. Normally, it is calculated as Stk_{50}, which is the Stokes number of particles with a size d_{50}. This is called the cut diameter of a stage, that is, the diameter of the particles collected with 50% efficiency on that stage.

1.8.3.2. Electrical Low Pressure Impactor (ELPI)

The ELPI classifies particles in 12 impactor stages. The median size range (as aerodynamic diameter) for each impactor stage is shown in Table 1.4. The fractions are defined by the median diameter of the particles deposited on each stage.

Stage	Median Diameter, nm	Stage	Median Diameter, nm
1	42	7	834
2	82	8	1326
3	141	9	2084
4	219	10	3270
5	333	11	5270
6	525	12	8234

Table 1.4. ELPI Impactor Size Fractions

1.8.3.2.1. Instrument description and operation

In the ELPI, a vacuum pump generates an absolute pressure of 100mbar. In this way, it makes it possible for the impaction of particles below the lowest cut-off size of an Andersen Impactor, which works at atmospheric pressure. A previous version of this technique was the Berner low-pressure impactor (BLPI), which allowed the measurement of particles in the same range as that resolved by the ELPI. The BLPI, however, is still a gravimetric technique as the Andersen Impactor is, so long sampling times are needed to collect an accurately weighable mass, and the technique is subject to a great variability due to the sensitivity of the filters to

humidity and temperature conditions. To avoid these problems, the ELPI includes an electrical particle counting technique, that also allows measuring the particle size distribution in real time. If the ELPI is used for the collection of particulate mass for chemical analysis, it must be considered that sampling under vacuum conditions can degas the particles, and therefore the fraction of volatile compounds may be underestimated, particularly for very fine particles.

In the ELPI, shown schematically in Figure 1.10. the aerosol particles are charged with a unipolar charge in a diode-type corona charger before entering the actual impactor. This consists of a cylindrical tube, through which the aerosol flows, with a 5 mm long tungsten wire electrode in the centre. When a 5kV positive voltage is supplied to the wire, a corona discharge is generated around the wire and thus ions are produced. Positive ions migrate towards the cylinder walls, that is, perpendicular to the particle flow, building a unipolar positive charge on the particles as a result. The remaining ions, as well as charged particles below 20 nm, are removed in an electrical trap. This particle loss is the main disadvantage of this charging system (Keskinen, 1992, Marjamäki, 2000).

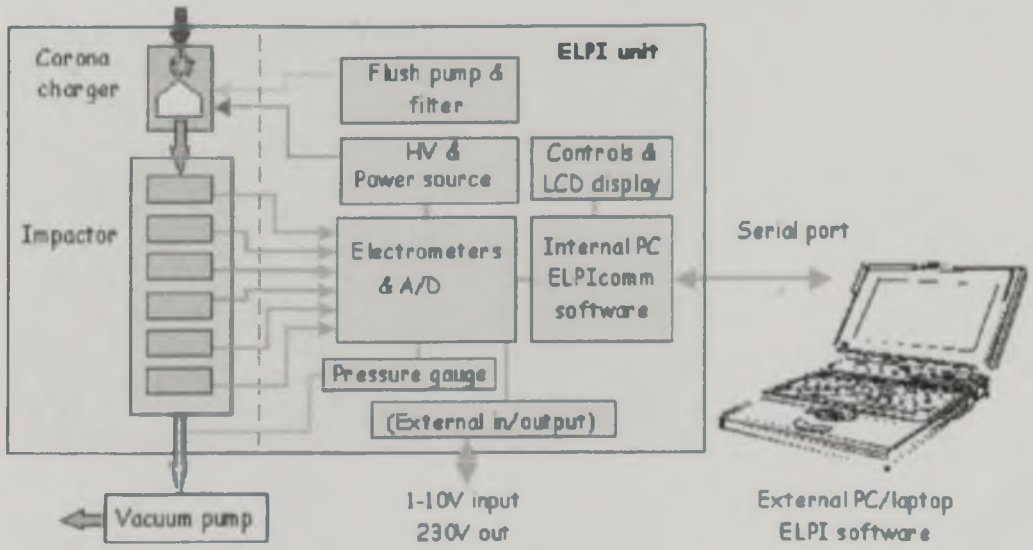

Figure 1.10. Schematic representation of the ELPI (Dekati®).

After passing the ion trap, the aerosol is fed into the impactor. Each stage of the impactor is insulated from the previous and next stages by Teflon O-rings, and each is connected to an electrometer. When the particles impact on a stage, their charge is transferred to the stage, so an electrical current is generated, which is measured by the electrometer of the corresponding stage. The current signals from each stage is then converted into particle number concentration at each size by applying:

$$N = \frac{I}{PneQ} \qquad \text{(Equation 1.85.)}$$

where N is the particle number concentration, I is the measured current, P is the penetration through the charger, e is the charge of the electron, n is the average number of charges per particle and Q is the flow rate.

The charger's efficiency is a power function of the particle diameter, which is a result from the calibration of the charger. Including this function, the group *PneQ* in the previous equation for this unit becomes:

$$PneQ = \begin{cases} 277.52 d_p^{3.179}, \text{ for } d_p < 0.0482\mu m \\ 3.557 d_p^{1.741}, \text{ for } 0.0482\mu m < d_p < 0.141\mu m \\ 1.335 d_p^{1.241}, \text{ for } d_p > 0.141\mu m \end{cases} \qquad \text{(Equation 1.86.)}$$

Diffusional losses of particles occur through the impactor. Marjamäki et al. (Marjamäki, 1999) showed that particle loss increases rapidly as particle size decreases, and they reach 6% for particles around 0.038μm. These losses are taken into account in the number calculation by means of a correction matrix, Table 1.5.

Stage	1	2	3	4	5	6	7	8	9	10	11	12
1	1											
2	0.016	1										
3	0.016	0.008	1									
4	0.013	0.007	0.004	1								
5	0.012	0.007	0.004	0.003	1							
6	0.011	0.006	0.004	0.003	0.003	1						
7	0.011	0.006	0.004	0.003	0.003	0.003	1					
8	0.007	0.004	0.003	0.002	0.002	0.001	0.001	1				
9	0.007	0.004	0.003	0.002	0.002	0.001	0.001	0.001	1			
10	0.007	0.004	0.003	0.002	0.002	0.001	0.001	0.001	0.001	1		
11	0.007	0.004	0.003	0.002	0.002	0.001	0.001	0.001	0.001	0.001	1	
12	0.007	0.004	0.003	0.002	0.002	0.001	0.001	0.001	0.001	0.001	0.001	1
	0.891	0.947	0.969	0.981	0.984	0.992	0.995	0.996	0.997	0.998	0.999	1

Table 1.5. Correction matrix for particle diffusional losses in the ELPI.

Stages in the ELPI are numbered from fine to large particles, so the bottom stage is number 1 and the top stage is number 12. The values in the correction matrix correspond to the fractional loss of particles, the columns representing the stage on which particles should be collected, and the rows, the stages on which they are actually collected. Particles finer than the cut-off diameter of a stage are lost by diffusion in all stages designated by a higher number (upper stages), and they contribute to a increase in the current measured for each of those stages. Two corrections are, therefore, necessary: the first correction has to account for the diffusional loss of the particles through the upper stages; and the second, for the increase in the current measured at a certain stage, caused by particles that should be counted in lower stages. The transport efficiency through each stage is calculated as

(1 - fractional loss), and the overall transport efficiency, shown at the bottom row of Table 1.5., is the product of the efficiencies for all the stages. The original current measured at each stage is then corrected by subtracting the additional current transferred by the diffusing particles deposited.

Another particle loss mechanism through the ELPI that has been recently evaluated is space charge, since the particles flowing through the ELPI are charged and, therefore, they are subject to electrical forces in the impactor (Virtanen, 2000). It becomes important for large particles at high particle concentrations, but it has not been taken into account in the software provided by the equipment supplier used for the data analysis of this work.

From the simultaneous second-by-second measurement of the currents at all the stages, the particle size distribution for all 12 stages is determined; hence the changes during transient engine operation can be followed in nearly real time. Other technologies have been suggested for this objective, such as the combination of an electrostatic classifier – TEOM – condensation particle counter described by Ristovski et al. (Ristovski, 1998) but, at the moment of writing this thesis, the ELPI is the only particle size instrument used extensively to do this.

The ELPI produces results in terms of number-weighed particle size distribution. The conversion into mass units for comparison purposes with gravimetric techniques and legislated limits involves a set of assumptions, e.g. unit density, constant density over the whole size measurement range and spherical particles regardless of the particle size, assumptions that are all fairly far from being certain. Hence, mass concentrations may be overestimated, as re-calculated mass-based size distributions can be strongly biased towards large particles. Furthermore, if the particle density is unknown, high errors in measured number distributions may be expected, as observed by Moisio et al. and other authors (Moisio, 1997; Tsukamoto, 2000). It is necessary to find methods that can increase the reliability and the validity of the re-calculation of particle number from current data and particle mass from particle number data.

Unlike electrical mobility techniques, the ELPI allows collecting mass in the different stages to determine the mass-based particle size distribution for comparison or analysis purposes. The collection is normally carried out on aluminum foil substrates, over which vacuum grease is applied to reduce particle bounce. Mass collection allows comparing directly steady-state size distributions from particle count and gravimetric determinations. This is not, however, a trivial issue and special conditions regarding mass collection must be taken into account. First of all, it is recommended to run the mass collection as a separate test from the number

distribution determination and operate the ELPI with the charger off, in order to avoid mass losses in the charger, otherwise corrections should be applied. Secondly, the mass collection test has to be long enough to collect a relatively large mass for it to be reliably measured with a 0.01mg sensitivity balance. With a modern low emission engine, this means a 15- to 50-hour test using a 100:1 dilution ratio, implying a very high consumption of fuel, dilution air, etc. Sampling time can be reduced significantly by reducing the dilution ratio, but this should never be lower than 7:1 to avoid reaching the sulphuric acid dew point. Finally, substrates greasing and handling must be extremely careful to minimise the error for grease or aluminium foil losses in the gravimetric determination.

Some evaluations have shown significant overloading problems arising from the use of greased aluminium foil substrates for the stages (van Gulijk, 2000). The overloading is due to the fluffy structure of diesel particles impacting on the stages, and is followed by particle bounce. As a consequence, the count of small particles is lower and the count of large particles larger than the count without overloading. The proposed solution has been the use of vacuum-oil greased, sintered, porous metal stages (Marjamäki, 2000), which prevent particle bounce and blow-off much more effectively than aluminium foil substrates, and increase very significantly the maximum load on the stages.

1.8.3.2.2. Evaluation comparisons of the ELPI with other techniques.

Not many direct comparisons between calculated and gravimetrically measured mass from the ELPI have been published: most of the studies involving measurements with the ELPI report only number-based distributions, which are very useful owing to their real-time characteristics. One of the few studies reporting mass values obtained with the ELPI used the TEOM for comparative purposes (Moisio, 1995). Real-time mass concentrations from both instruments agreed relatively well when measuring emissions from a pulverised coal power plant, ranging from $1mg/m^3$ to $3mg/m^3$. In his PhD thesis, the same author (Moisio, 1999) includes a comparison of mass calculated from ELPI number distribution data with gravimetric mass distribution from a BLPI, showing a fairly good agreement, although some tendency to mass overestimation in the large size range can be observed. The electrometers sensitivity together with the current correction in the large size range can exacerbate a small error when calculating the mass distribution.

For comparison purposes, it may be safer converting a gravimetrically measured mass distribution into the corresponding number distribution and comparing it to the ELPI number distribution. Westerholm et al. (Westerholm, 1999) published an example of this procedure, when evaluating the use of fibreglass filters

for mass collection with an ELPI. He observed a mass distribution with a maximum around 100nm aerodynamic diameter and number concentrations were higher when measured than when calculated from mass. The divergence was much higher in the large size range, being of one order of magnitude for particles around 0.6μm and more than three orders of magnitude for particles around 8μm.

Tsakumoto et al. (Tsakumoto, 2000) evaluated the agreement between the total particulate mass determined gravimetrically and that calculated with the ELPI. They found that both methods were equivalent at low-load conditions, but the ELPI measurements were 1.5 to 2 times greater than the gravimetric for 25% load or higher, owing to the decrease in SOF content during high-load operation. The assumptions of constant charger efficiency, regardless of the properties of the particles, as well as constant density, are considered to be the reasons for the total mass overestimation.

Evaluations of the ELPI have been focused on comparing its results with SMPS, DMPS, DMA and EAA, which also produce the number-weighed size distribution, although this is due to electrical mobility, not aerodynamic behaviour. In their performance evaluation of the ELPI, Marjamäki et al. (Marjamäki, 2000) showed that, when converting aerodynamic diameter into mobility diameter using the bulk density of a calibration aerosol (di-octyl stabate, DOS), a good agreement between the measured distributions was achieved, thus concluding that the ELPI performance was good. This statement, however should not be extended to real world aerosols.

Ahlvik et al. (Ahlvik, 1998) pointed out that, despite the agreement with calibration aerosols, comparisons between these techniques must be interpreted more carefully, since real aerosols, and particularly diesel exhaust aerosol, have a much more complex behaviour because of the high complexity of their shape and density changes with size. They found that, when comparing the ELPI and the DMPS distributions in the mobility size base (that is, converting the aerodynamic diameter to mobility diameter), the ELPI size distribution shifted. To make the distribution match, the particle density values were iterated until the number data from the ELPI equated the number data from the DMPS, thus obtaining a function of the effective particle density vs. particle size that must be taken into account. Ahlvik's effective particle density function decreases dramatically with particle size for particles larger than 1μm. Furthermore, a tandem experiment by the same author demonstrated that, for diesel particles, "a well defined mobility of a monodisperse diesel aerosol classified by the SMPS does not lead to a specific aerodynamic

diameter, but to a wide range of aerodynamic diameters". Therefore, any agreement between the SMPS and the ELPI can be considered fortuitous (Maricq, 1999).

1.8.3.3. Scanning Mobility Particle Sizer (SMPS)

The SMPS is the most widely used electrical mobility sizing technique nowadays. It measures the particle size distribution of the aerosols with a great resolution in the range 0.003μm to 1μm by using three units in series: a Kr-85 bipolar source for particle charging, a differential mobility analyser (DMA) and a Condensation Nuclear Counter (CNC), as shown schematically in Figure 1.11. The bipolar ion source brings the polydisperse aerosol to charge equilibrium. The DMA consists of a central rod and an annular cylinder of aerosol surrounding a core of air but instead of collecting the particles of a desired size on the rod, the DMA produces a monodisperse aerosol around that size. This is possible due to a gap between the rod and a collection tube at the lower part of the analysis tube, which only particles of a certain size, defined by their mobility, pass through. Particles smaller than those are collected on the rod, and those larger are exhausted, whereas the particles that passed through the gap are counted by a CNC.

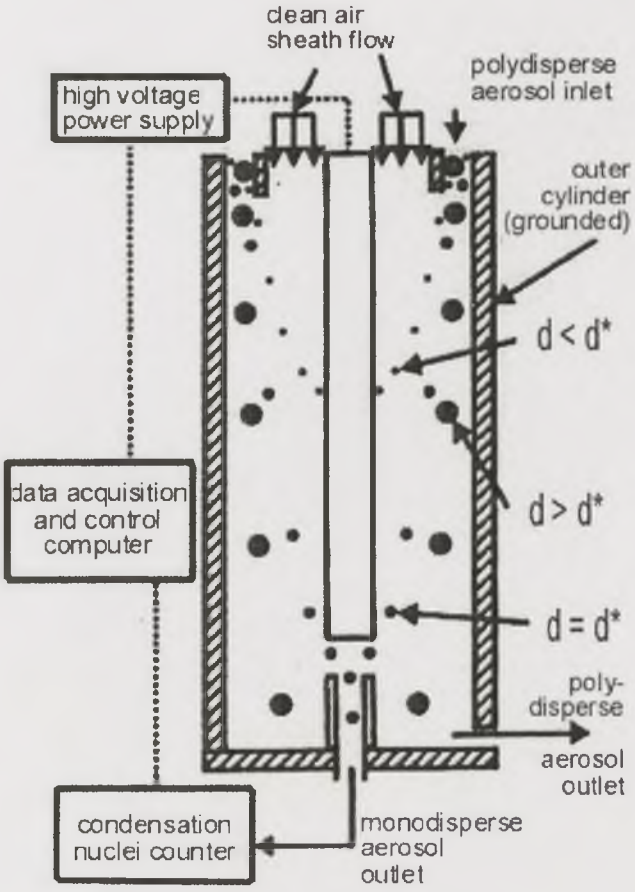

Figure 1.11. Schematic representation of the SMPS.

In the CNC, particles of the aerosol are put in contact with a saturated alcohol vapour atmosphere, created by a pool of alcohol kept at 35°C. The particles are then carried to a condenser tube at 10°C, hence the particles grow due to alcohol condensation on their surface, until becoming large enough to be counted by an optical device. By applying successive discrete voltages on the rod, monodisperse aerosols with particles of different sizes are generated by the DMA and counted by the CNC in short, successive periods, thus completing a whole distribution of 105 size classes classified in less than 60 seconds. This response, unfortunately, is not good enough when measuring the whole size distribution during engine transient operation. Transient response can be achieved only if the measurement is limited to a narrower range, in which case it would be necessary to run the transient test several times to build the size distribution over the whole range. Another limitation of the SMPS is that it does not measure particles larger than 1μm, so the accumulation mode and particles up to 10μm, important for legislative purposes, are left out.

1.8.4. Recommendations for Exhaust Sampling in Particulate Characterisation

The main difficulties related to the sampling and measurement of particulates from diesel engines are due to the unstable character of their compounds in the changing physicochemical conditions they find from the very moment they are produced. Measurement of the exhaust volume emitted by the engine is also a big problem to overcome. Sampling systems have been developed to manage these difficulties and provide the measurement equipment with a representative, stable and reliable sample. An example of such a system is the Constant Volume Sampler (CVS), which does not require the measurement of the exhaust volume (Hill, 1999). A CVS system involves a dilution process that brings about several other advantages over the raw exhaust measurement. It slows the chemical interaction of the various species present in the gas. Furthermore, its measurement accuracy is not affected by leaks in exhaust and sampling systems. However, it is not intended to reproduce atmospheric dilution. In transient cycle tests, CVS systems are used to proportionally sample from a mean bag aerosol sample and so determine the gaseous pollutants and total particulate mass concentration over the cycle.

Despite the CVS system advantages, several studies have shown how diesel particulate composition (Abbass, 1991) and particle size distribution (Kittelson, 1991) change along the exhaust and sampling systems involving dilution tunnels. The main processes involved in the loss and gain of particles during sampling are diffusion, thermophoresis, particle charging, reentrainment, outgassing. Studies have

defined certain guidelines to design and set up sampling systems so that the effect on the measurement can be reduced to less than 10%, e.g. avoiding sharp bends as well as long and narrow tubes, avoiding thermal gradients and using clean tubes. They have also remarked the necessity for standardisation of size distribution measurement, since comparison of different data sets is not possible due to problems with artifact formation.

Kittelson et al. (Kittelson, 1991) produced a set of recommendations on the design and operation of measurement facilities involving dilution tunnels, based on the analysis of the sources of variability in the Heavy-Duty Test Procedure. In order of higher to lower importance, recommendations related to the dilution tunnel and sampling system are summarised as follows:

a) Reduction of heat transfer to reduce thermophoresis.

b) Tunnel conditioning.

c) Temperature and/or dilution ratio control, to minimise or eliminate the effect of the saturation ratio, which is the driving force for condensation and/or absorption of SOF.

d) Improvement in flow measurements to and from the secondary dilution tunnel, to achieve a ±0.5% accuracy.

e) Improvement of filters and handling procedures.

f) Conditioning of combustion and dilution tunnel air.

g) Deposition analysis.

Kittelson remarked also on the lack of understanding of the reentrainment of particles from the walls of the engine, exhaust system and sampling system, which may change the nature and quantity of particles emitted by the engine.

In one of the most recently published studies, Maricq, 1999 compared the effect of two different dilution systems on the particle size distribution of emissions from petrol and diesel engines. One was a conventional dilution tunnel that dilutes the whole exhaust and the other, an ejector-pump diluter that can be used to measure distributions directly at different points along the tailpipe. It was found that the size distribution depends on the transfer line temperature, the ultrafine particle number concentration increasing when using an insulated stainless steel line. Particle number emissions measured in a dilution tunnel are higher than measured by diluting with an ejector pump, especially in the size range below 100nm. The use of a silicon rubber coupler promotes ultrafine mode formation due to desorption and/or pyrolisis of material by hot exhaust gases. In the case of diesel engines emissions, the dilution

tunnel causes the particles to grow around 20nm in size. This artifact is due to heating of the transfer hose. On the other hand, the use of an ejector pump as a dilution system causes a transient artifact due to residual hydrocarbons on the j-tube sample probe used, which condensate onto the particles' surface.

1.9. Effect Of Engine Performance And Pollutant Reduction Technologies On Exhaust Particulate Emissions

Different engine performance enhancing strategies and emission reduction technologies affect particulate emissions either positively or negatively. Trade-offs exist and it is necessary to look for a compromise among engine power output, driveability, fuel consumption and emissions of different pollutants. There is a vast amount of literature regarding all diesel processes that influence particulate formation, from which only the most important aspects are summarised below. References are given for those interested in deepening their knowledge in these aspects.

For its formation characteristics, particulate formation is reduced effectively by increasing the Air/Fuel ratio (AFR) -that is, reducing the Equivalence Ratio-. Increasing the Equivalence Ratio is convenient to reach high Mean Effective Pressures (MEP), but it increases fuel consumption and, above a certain limit – around 0.5, AFR below 24-, produces a catastrophic increase in soot emissions (Kittelson 1994, Perkins 1999). Lean combustion is, then, desirable to keep low fuel consumption levels. However, because of the high availability of oxygen originated by lean combustion, NOx emissions increase, which is by all means undesirable.

The following are among the technological responses to these trade-offs: Turbocharging, Aftercooling, very-high-pressure Fuel Injection, Flexible Injection Timing and Cooled Exhaust Gas Recirculation (EGR).

1.9.1. Exhaust Gas Recirculation (EGR)

The EGR is a NOx emission reduction technique based on lowering the combustion peak temperature. A fraction of the exhaust gases is drawn into the combustion chamber, displacing a fraction of the air. During the fuel injection and subsequent combustion, the exhaust gas acts as an inert sink of the heat released by the reacting air-fuel mixture, allowing a lower peak combustion temperature. The NOx formation potential decreases, so that emissions of this pollutant are reduced by up to 25%.

The EGR has a potential problem at high load or power, since it may increase particulate emissions to undesirable levels, owing to a reduced Air/Fuel ratio. For

this reason, the EGR rate control strategy is biased towards low loads (Baert, 1999; Leet, 1998; Suzuki, 1997; Dickey, 1998).

1.9.2. Aftertreatment

Aftertreatment devices have been introduced into the exhaust system of petrol and diesel engines in order to meet emission limits imposed by regulations. The introduction of DeNOx catalysts and particulate traps appears to be forced by 2005 for diesel heavy-duty vehicles. Diesel oxidation catalysts (DOC) have been installed in recent models of passenger cars, and particulate traps have been under study. Advanced oxidation catalysts similar to the one installed on the Ford 1.8L passenger car diesel engine of the used in this work have been designed to operate as a hydrocarbon adsorber during cold start and as a catalytic reactor after warming up.

1.9.2.1. Diesel Oxidation Catalysts (DOC) and DOC with hydrocarbon adsorber

Catalysts have been applied for cleaning automotive exhaust emissions for 25 years now. Their application on diesel engines, however, has been delayed nearly 15 years with respect to their petrol counterpart, since diesel vehicles could meet the emissions standards without using aftertreatment technologies. As legislation has become stricter, and owing to the difficulties encountered in removing NOx from diesel exhaust, the efforts to improve catalysts for diesel engines have increased significantly in the last 10 years (Shelef et al., 2000; Webster, 2000). The large excess of oxygen used by diesel engine does not allow using three-way catalysts (TWC), since these require a stoichiometric mixture to remove HC, CO and NOx. Therefore, efforts have been focused on developing oxidation catalysts for lean combustion, but able to reduce NOx. At the same time, diesel catalysts must deal with particulate matter, either removing them or, at least, not increasing their concentration in number or mass. Also, as diesel exhausts are much cooler than petrol ones, the catalyst must light-off at lower temperature. Aditionally, stricter emission limits make necessary developing a technology that can reduce emissions during cold start, before reaching the catalyst light-off temperature. The answer to this is HC adsorption at cold temperatures.

Highly porous materials, such as zeolites, have been used as HC adsorbers in diesel oxidation catalysts since the 1990s (Engler, 1993; Adams, 1996; Leyrer, 1996). The adsorption is temporary, so the hydrocarbons are desorbed once the catalytic active material (Pt, Pd) has lit off, and therefore are oxidised.

Particulate matter consists mainly of large hydrocarbon molecules adsorbed on a carbon core, as well as a small amount of sulphate compounds. DOCs have the

ability to oxidise the carbonaceous material, hence reducing the total particulate mass. However, together with the carbonaceous material, DOCs can oxidise SO_2 from the gas phase at temperatures about 3500 °C, forming SO_3 and then H_2SO_4. This is either adsorbed by the particles or condensed to form new particles. In either case, the particle number and mass concentrations can increase with the presence of the catalyst. Fortunately, with the use of ultra-low sulphur fuels, which are now widespread in Europe, this risk is overcome. The catalyst reduces the particulate matter concentration in the exhaust at all exhaust temperatures. In these conditions, the hydrocarbon adsorber has been shown to improve the particulate matter conversion by the catalyst, reaching 40% to 50% in small diesel engines (Adams et al., 1996).

The effect of DOCs on particle size distribution has been described by some authors as a decrease in mass concentration, but at the same time an increase in number concentration of nanoparticles, coinciding with an increase in sulphates concentration. Krüger et al., 1998 tested an improved design, optimised for low sulphur conversion, which showed a huge reduction in sulphates and nanoparticles downstream of the catalyst compared to the non-optimised model. Klein et al., 1998 showed that the oxidation catalyst reduces the SOF content over the whole temperature range of a diesel car. In the low temperature region SOF content is reduced by the catalyst and no sulphate is formed, which causes a shift to lower particulate sizes due to a lack of adhesives after the catalyst. In the high temperature region SOF content is reduced by the catalyst but sulphate is formed, so that an enlargement of particulate is observed due to the sulphate that acts as a glue.

Kittelson and Abdul Khalek, 1998, also observed an increase in particulate number concentration produced by the oxidation catalytic converter at high temperature operation conditions of the engine, i.e. high speed and high load. Formation of nanoparticles by the catalyst was evident in the range 7 – 13nm and suggested the mechanism of particle nuclei formation by $H_2SO_4 - H_2O$. Bagley, 1998 suggested a different mechanism for the formation of these tiny particles, due to carbonaceous nuclei. Kittelson found the presence of calcium and pointed out that nuclei may be metallic ash from oil and fuel additives.

1.9.2.2. Particulate traps.

Diesel particulate traps, also called Diesel Particle Filters (DPFs) are designed to store particulate matter from the engine for relatively long periods, followed by a regeneration period consisting of burning the particulate off by thermal and/or catalytic processes. DPFs significantly reduce particulate mass concentration, but some authors have shown that they may increase significantly the number

concentration of nanoparticles by promoting the nucleation of hydrocarbons and sulphates. Without the trap, these species condense and are adsorbed by solid particles. Not all the studies have shown the increase in nanoparticle concentration trough traps; Hawker et al., 1996, tested a continuously regenerating DPF that showed no formation of nanoparticles and a reduction in particle number concentrations by 1 to 2 orders of magnitude in each size class from 10 to 210nm. In the same year, Mayer et al. (Mayer, 1996) tested various trap designs efficiency at different particle sizes, and found a low efficiency for the surface filter and a high efficiency for the deep-bed filter, at trapping fine particles, and Dementhon, 1997, confirmed these differences among various trap designs. He detected a high particulate stripping rate during regeneration with all traps, and generally, the particle mean diameter observed downstream of the trap was slightly smaller than the one detected upstream of the trap. Deep bed traps were found to lose more particulates around 100nm during regeneration. Further work by Pattas et al., 1998, showed a reduction in total mass and number concentration through a ceramic trap, although a relatively high penetration of ultrafine was observed. High peaks of particles were generated when using the trap during accelerations of an urban driving cycle, probably due to desorption of condensed hydrocarbons.

Perhaps the most important factor influencing particle size distribution changes through particulate traps is the residence time of the exhaust aerosol in the trap, according to Abdul Khalek, 1998, who found higher concentrations of nanoparticles when residence times were longer, due to nucleation inside the trap and, for some models, downstream of the trap. In the same study, it was shown that, in early stages of the regeneration process of the trap, a dramatic increase in the concentration of nanoparticles occurred. Then, it decreased as the agglomerates concentration increased, indicating that the penetration along the trap increased as the trap regenerated. Finally, a better performance of the trap was observed when the trap was loaded, due to the increased contact between the particles and the trapping material when particles are already closing the porous structures of the traps.

1.9.2.3. Exhaust pipe and silencers

The exhaust pipe offers some of the conditions required for the particles in the exhaust aerosol to deposit on its walls: it is normally horizontal, so gravitational forces act fully (they are perpendicular) over the particles; its walls are colder than the exhaust gas, so thermophoretic forces are created promoting particle deposition. The exhaust has bends that create the turbulence that can enhance the deposition. Nevertheless, the ultimate result of various deposition processes is its opposite: particle resuspension, or reentrainment. This has been identified as a significant

source of variability in transient tests. Its processes are not thoroughly understood although it is known that certain parameters such as the wall shear stress, the nature of the particle-surface and particle-particle bonding, and surface vibrations, play an important role. Kittelson et al. (Kittelson, 1991) considered minimizing deposition as the best approach to reduce reentrainment, and therefore variability in the tests.

Kittelson showed that the tailpipe caused the highest thermophoretic deposition loss in the exhaust – dilution system combination: 2.6%, the total system loss being just over 5%. Modifications to the tailpipe were applied to reduce this loss with the results shown in Table 1.6.

The exhaust silencers include complex internal components in their design, such as extended inlet/outlet tubes, thin baffles with eccentric holes, internal connecting tubes, perforated tubes, perforated baffles, flow plugs and sound-absorbing materials. All these components increase the area exposed to the exhaust aerosol as well as the turbulence in the flow and, therefore, heat and mass transfer coefficients, factors that are intimately related to the enhancement of particle deposition. Reentrainment, and with it test variability, can then be expected to be enhanced as a result.

Modification	Mass fractional particulate loss from raw exhaust by thermophoresis
Base case, no insulation	0.026
Base + Perfect insulation = B	0.019
B + thinner wall	0.013
B + dilution air, 2:1 DR, constant flow	0.012
B + 200°C preheating	0.010
B + dilution air, 3:1 DR, constant flow	0.009
B + dilution air, 2:1 DR, proportional flow	0.007
Base + Normal insulation + 150°C preheating + dilution to limit Tmax = 150°C	0.003

Table 1.6. Thermophoretic deposition losses. Influence of tailpipe modifications. (Kittelson, 1991).

1.9.3. Influence of Cold Start

Vehicle engine emissions are much higher when the engine is cold than when fully warmed. Under urban driving conditions, the vehicle may need to be driven for

a considerable distance to warm up, 5km in the case of diesel engines, 10km for petrol engines, so that a significant number of urban journeys are made with a cold engine, therefore increasing the emissions. The effect is dramatic for gaseous emissions of petrol engines, such as volatile organic compounds (VOC) and CO emissions, for which one third of total emissions during these typical journeys occur during cold start (Farrow, 1993). This figure can increase significantly for petrol engines fitted with a three-way catalyst, since the engine runs on rich mixtures when it is cold and the catalyst requires stoichiometric mixtures to be highly efficient.

Particulate matter emissions from diesel engines are also affected by cold start. Table 1.7. shows that cold-start particulate emissions are 20% higher than those from a hot engine. In addition, the low temperature of the pipes, together with its subsequent fast warm-up and the sudden disturbance caused by switching on the engine, mainly manifested as vibration, may affect the deposition and reentrainment processes. As a result, sudden emissions during the cold-start may occur and be considerably higher than for a hot engine and exhaust system.

	CO	THC	NOx	PM
Standard Petrol	1.6	2.0	1.0	-
Petrol + TWC	9.6	11.0	1.3	-
Diesel	1.6	1.0	1.2	1.2

Table 1.7. Ratio of average Cold:Hot emissions in real urban conditions for petrol and diesel cars. The cars were driven over the same urban trip for both cold and hot conditions to make the comparison (Farrow, 1993).

1.9.4. Legislative driving cycles

At this point, it is worthwhile to have a closer look at the design of the legislative driving cycles over which the emission standards are defined. The test conditions and procedures defined for this work, which are described in Chapter 2, were not devised to reproduce any specific condition or mode of a legislative driving cycle, and therefore no direct comparison can be made. However, it will be tried to find some relationship, so the impact of the results can be suggested.

The cycles examined here correspond to the European context for both heavy-duty and light diesel vehicles. Cycles for heavy-duty vehicles include the ECE R49, the ESC (European Stationary Cycle), and the ETC (European Transient Cycle). On the other hand, cycles for light vehicles include the ECE 15 (or UDC, Urban Driving Cycle) and the EUDC (Extra Urban Driving Cycle). There are fundamental differences among cycles. Firstly, some of them are performed on engine

dynamometers and others on chassis dynamometers. Secondly, some of them are multi-mode steady-state tests and others are fully transient. And finally, the results are expressed in different units, some in g/kWh and others in g/km. All this makes difficult to make comparisons of the integrated emissions obtained from them. The main objectives and characteristics of the tests are described below.

1.9.4.1. ECE R49 for heavy-duty vehicles

The ECE R49 is a 13-mode steady-state diesel engine test cycle used for certification of heavy-duty engines through the Euro II emission standard. It is performed on an engine dynamometer, which is operated through a sequence of 13 steady-state load and speed conditions, shown in Figure 1.12., each known as a test mode. The emissions are measured and expressed as g/kWh over each mode, and then they are wheighted averaged to produce an overall result. The conditions are identical to those of the US 13-mode cycle, although the weighting factors, also shown in Figure 1.12, are different. In the European weighting, high loads, and therefore high exhaust temperatures, are the emphasized characteristics.

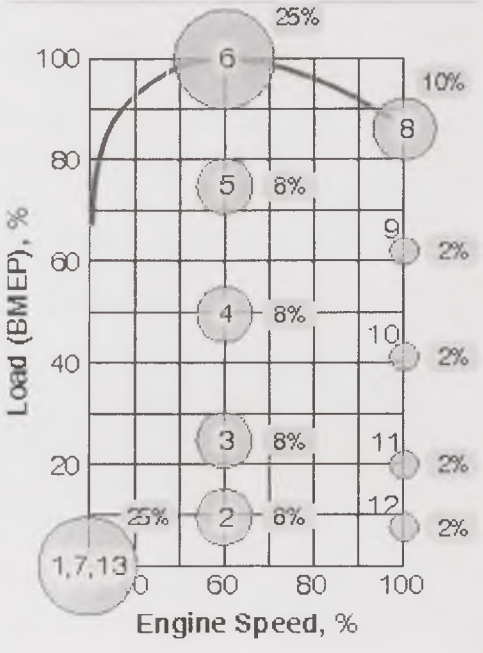

ECE R49 and US 13-mode Cycles

Mode No.	Speed	Load, %	Weighting Factors	
			R49	US
1	idle	-	0.25/3	0.20/3
2	maximum torque speed	10	0.08	0.08
3		25	0.08	0.08
4		50	0.08	0.08
5		75	0.08	0.08
6		100	0.25	0.08
7	idle	-	0.25/3	0.20/3
8	rated power speed	100	0.10	0.08
9		75	0.02	0.08
10		50	0.02	0.08
11		25	0.02	0.08
12		10	0.02	0.08
13	idle	-	0.25/3	0.20/3

Figure 1.12. Conditions and weighting factors for the ECE R49 driving cycle.

From October 2000, with the introduction of Euro III standards, the R-49 cycle is replaced by the ESC.

1.9.4.2. ESC (European Stationary Cycle) for heavy-duty vehicles

The ESC cycle is a 13-mode cycle that replaced the R49 from 2000. Conditions and weighting factors are, however, quite different, as shown in Figure 1.13. The operation also differs from that in the R49, being stricter. Each mode has a prescribed operation time, completing engine speed and load changes in the first 20 seconds.

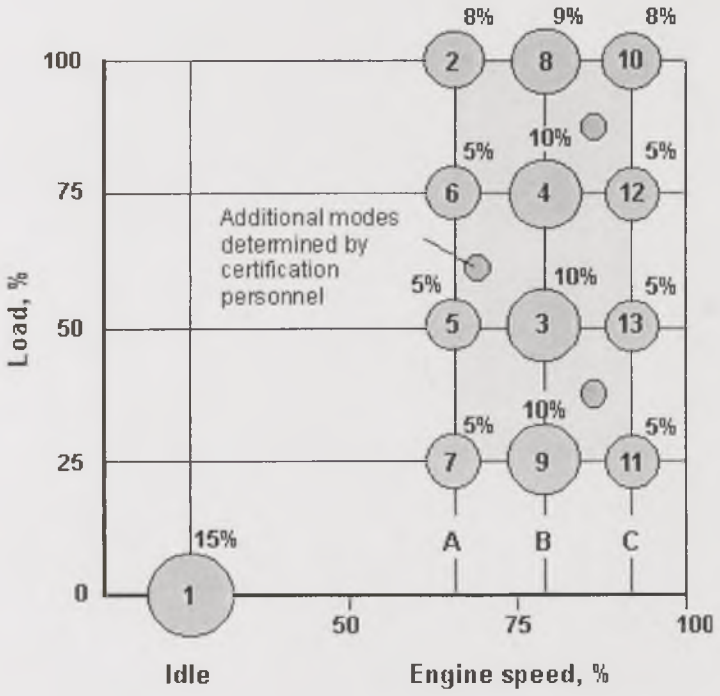

ESC Test Modes

Mode	Engine Speed	% Load	Weight factor, %	Duration
1	Low idle	0	15	4 minutes
2	A	100	8	2 minutes
3	B	50	10	2 minutes
4	B	75	10	2 minutes
5	A	50	5	2 minutes
6	A	75	5	2 minutes
7	A	25	5	2 minutes
8	B	100	9	2 minutes
9	B	25	10	2 minutes
10	C	100	8	2 minutes
11	C	25	5	2 minutes
12	C	75	5	2 minutes
13	C	50	5	2 minutes

Figure 1.13. Conditions and weighting factors for the ESC.

The speed should be within ±50rpm of the specified value and the torque, within ±2% of the maximum torque at the specified speed. Additional random tests around the certification area may be required by the certification personnel. In the ESC, a single filter is used for particulate emissions for the 13 modes. The results are expressed as g/kWh.

The engine speed conditions A, B and C are defined taking the speed at maximum power as a reference:

- The high speed n_{hi} is determined by calculating 70% of the declared maximum net power. The highest engine speed where this power value occurs (i.e. above the rated speed) on the power curve is defined as n_{hi}.
- The low speed n_{lo} is determined by calculating 50% of the declared maximum net power. The lowest engine speed where this power value occurs (i.e. below the rated speed) on the power curve is defined as n_{lo}.
- The engine speeds A, B, and C to be used during the test are:

$$A = n_{lo} + 0.25(n_{hi} - n_{lo})$$
$$B = n_{lo} + 0.50(n_{hi} - n_{lo})$$
$$C = n_{lo} + 0.75(n_{hi} - n_{lo})$$

The ESC test is characterized by high average load factors and very high exhaust gas temperatures.

1.9.4.3. ETC (European Transient Cycle) for heavy-duty vehicles

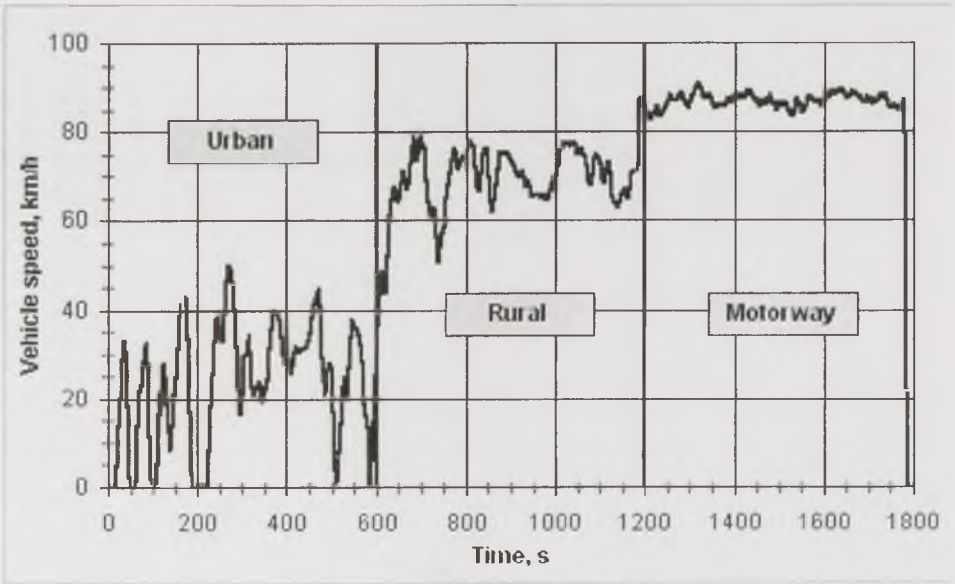

Figure 1.14. Vehicle speed vs. time for the chassis dynamometer variant of the ETC.

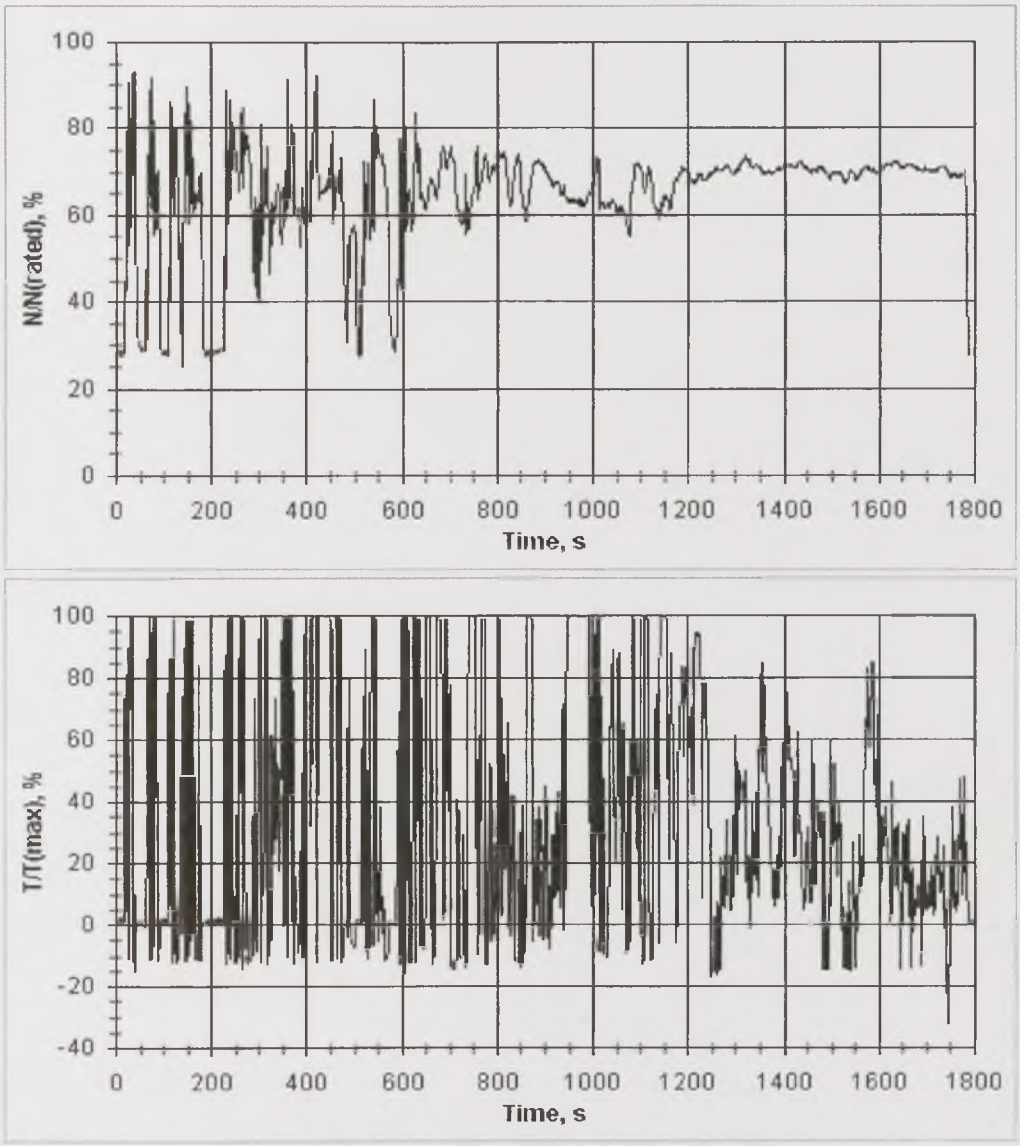

Figure 1.15. Engine speed (upper chart) and torque (lower chart) for the engine dynamometer variant of the ETC.

The ETC was introduced together with the ESC for emission certification of heavy-duty diesel engines in Europe through EURO III standards, in 2000. It was based on real road measurements, and consists of three parts that represent urban, rural and motorway driving. The duration of the entire cycle is 1800s, and the duration of each part is 600s. Urban conditions are characterised by a maximum speed of 50km/h, frequent starts, stops, and idling. Rural driving starts with a steep acceleration segment. The average speed is about 72 km/h. Motorway driving uses an average speed of about 88 km/h. The emissions are sampled following the Constant Volume Sampling technique and expressed in g/km.

The ETC has two variants, one for chassis dynamometer and another for engine dynamometer. For the former, vehicle speed vs. time is shown in Figure 1.14. For the latter, engine torque and speed are shown in Figure 1.15.

1.9.4.4. ECE and EUDC (Extra-Urban Driving Cycle) for Light duty vehicles

The ECE+EUDC cycle is a chassis-dynamometer test used for emission certification of light-duty vehicles in Europe. The entire cycle includes four ECE segments repeated without interruption, followed by one EUDC segment. The basic segments are shown in Figure 1.16.

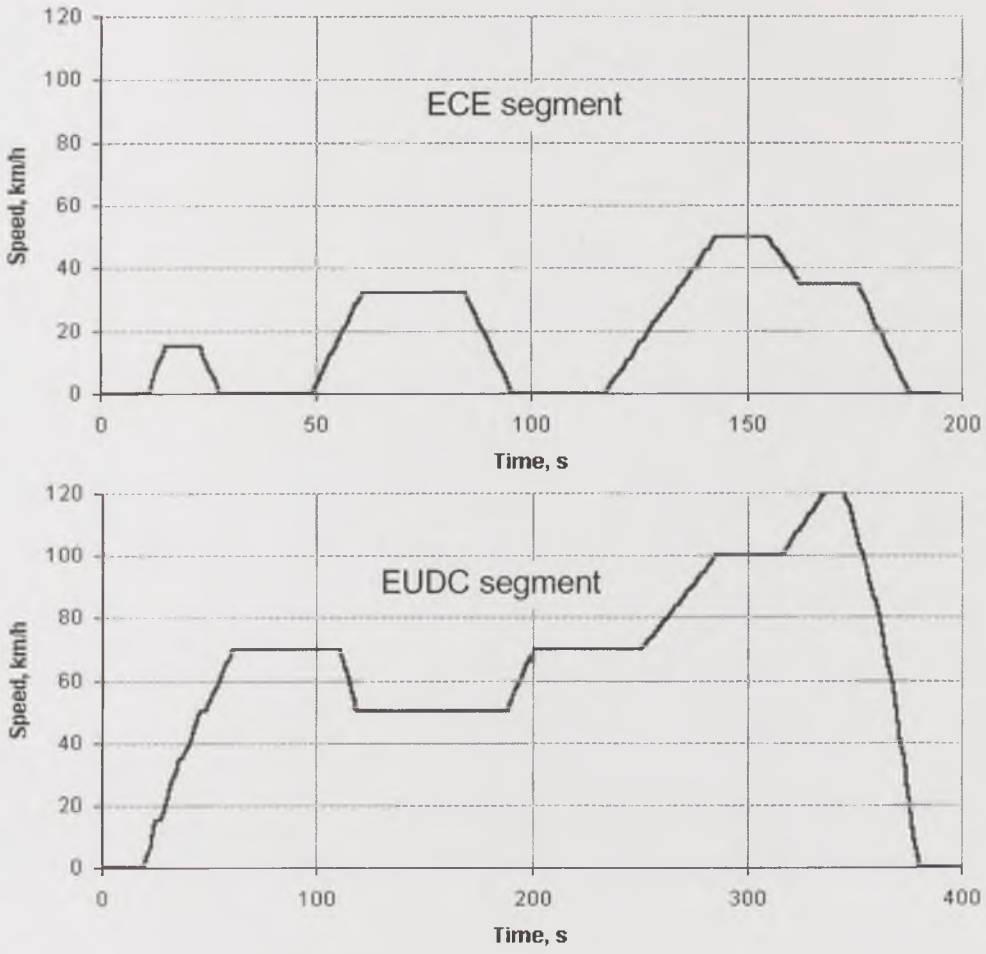

Figure 1.16. Speed conditions vs. time for the ECE and EUDC segments of the European cycle for light-duty vehicles.

The ECE (also known as UDC, Urban Driving Cycle) was designed to represent typical city driving conditions, characterized by low vehicle speed, low engine load, and low exhaust gas temperatures. The EUDC segment, added after the fourth ECE cycle, accounts for more aggressive, high speed driving modes. The maximum speed of the EUDC cycle is 120 km/h or, as an alternative for low-power vehicles, 90 km/h, observed in Figure 1.17.

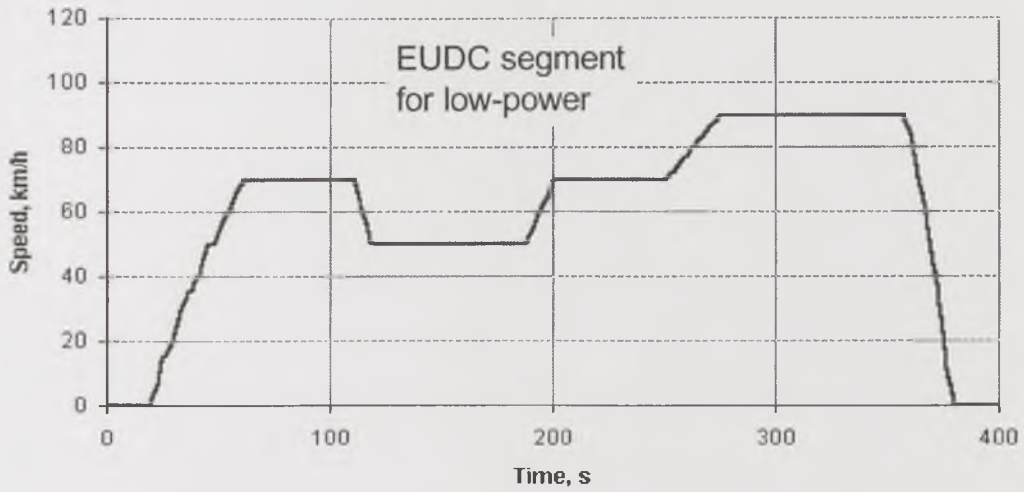

Figure 1.17. Speed conditions vs. time for the alternative EUDC segment for low-power vehicles.

The following are the summarised conditions for the whole cycle:

Characteristics	Unit	ECE 15	EUDC
Distance	km	4×1.013=4.052	6.955
Duration	s	4×195=780	400
Average Speed	km/h	18.7 (with idling)	62.6
Maximum Speed	km/h	50	120

1.9.5. Influence of Transients: acceleration and deceleration

Particulate emissions from diesel engines increase dramatically for richer combustion with a decrease in the Air/Fuel ratio (AFR). During transient events, the AFR is likely to suffer this kind of excursions, therefore increasing particulate emissions (Tanin, 1999). The situation is clearly reflected in the differences between legislated steady-state and transient driving cycles. Transient tests demand much more from the performance of an engine regarding its ability to keep emissions low. Therefore, emissions from a transient test are generally higher than from steady-state tests.

In Europe, a calibration of a EURO II DI/TCI Heavy Duty Diesel Engine was carried out comparing the steady-state EURO II (ECE R49) and EURO III tests (13-Mode – ESC), and the transient EURO IV test (ETC). Particulate matter emissions increased for the transient test in such a way that the EURO-II limit was exceeded, as observed in Figure 1.12. The emissions from the transient test exceeded those from the ECE R49 by 40%, whereas the emissions from the 13-mode cycle were 25% lower.

Since transients affect the combustion process, they may have an effect on the chemical composition of the particles and the particle size distribution of the exhaust

aerosol. Results from the DETR/SMMT/CONCAWE Research Programme for Heavy-Duty Emissions (Wedekind, 2000), showed that in the first part of the R49 cycle the nanoparticles were most abundant, but in the second part, the accumulation mode dominated, which seemed to be related to chemical composition: conditions with high levels of carbon produced a dominating accumulation mode, since the carbon cores promote the accumulation of nanoparticles. On the other hand, over the ETC, nanoparticles were readily produced in response to virtually all the transient excursions, including increases and decreases in load. "Accumulation mode particles were produced mostly across the urban phase and reduced across the rural and motorway phases, suggesting a positive relationship between the severity of transients within a cycle and the particle number."

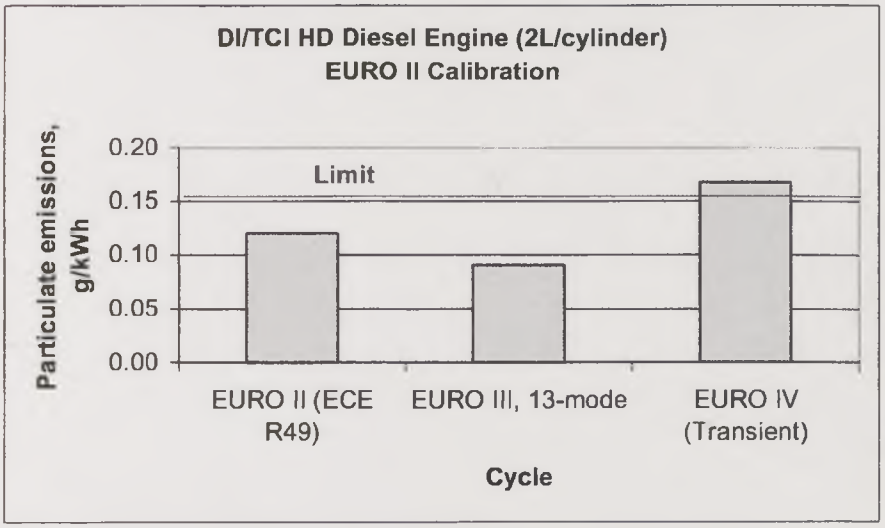

Figure 1.18. Effect of the European Test Cycles on Particulate Emissions from a EURO-II Engine (Zelenka, 1998).

Increase in particle number concentration and Emission Index as a consequence of transient changes has also been observed in spark ignition engines. Kayes et al. (Kayes, 1999) showed that "during controlled start-up tests, particulate matter emissions were consistent with a peak just at start-up, followed by a period of relatively level emissions during which time the particle size distribution may shift upward and/or along the particle size axis in response to the equilibration in the intake, in-cylinder or exhaust processes. When the ignition and injection are simultaneously shut-off, PM emissions may peak again, but quickly decrease."

Also in Spark Ignition engines, a study by Hall et al. (Hall, 2000) showed that, during acceleration transients from 50km/h to 140km/h ,and even from 120km/h to 140 km/h, bursts of particles were blown out from the tailpipe and clear increases in particle number concentration occurred. It was found that the emission rates from

the engine were not the same as those at the tailpipe, since particles deposited on cool surfaces within the exhaust system during cool operation and were released when the vehicle warmed up. It was concluded that sustained periods of high temperature operation would clean the exhaust system and reduce the particle number concentration to low levels within minutes. However, this process would be more significant for Spark Ignition, since the temperatures reached are higher than in Compression Ignition engines.

Chapter 2.
Experimental Techniques and Procedures Used in This Work

2.1. The Low-Emission Ford 1.8L IDI Diesel Engine

The engine used was a Ford XLD 418T. It is a Turbocharged 1.8 litre indirect injection engine, designed to meet the ECE 15.04 and 5th Amendment emission control standards, with a high performance even at high-speed conditions and a good fuel economy. A picture of the engine in the test bed and the engine power curves are shown in Figures 2.1. and 2.2., from which the maximum power is 55kW@4500rpm and the maximum torque is 152Nm@2250rpm. A detailed description of the engine can be found in the Ford XLD Range Engine Specification Brochure (Ford, 1992).

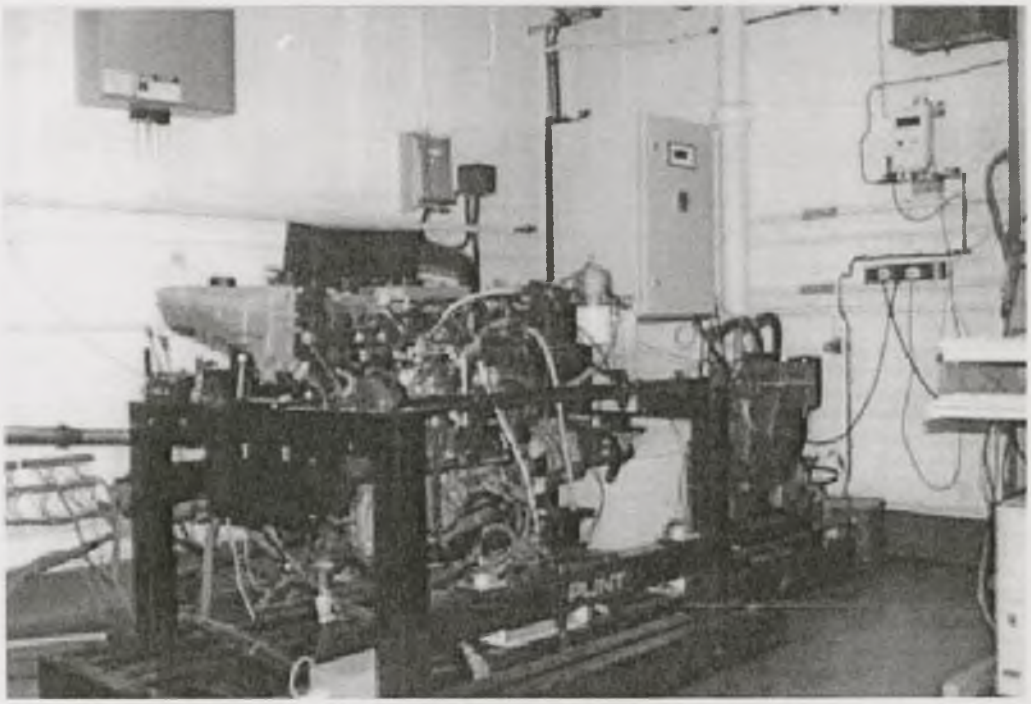

Figure 2.1. The Ford XLD 418T engine in the test bed.

Figure 2.2. shows the power curves for the Ford XLD 418T engine and the test conditions used for this work. The conditions do not correspond to any specific selected mode in a legislative driving cycle.

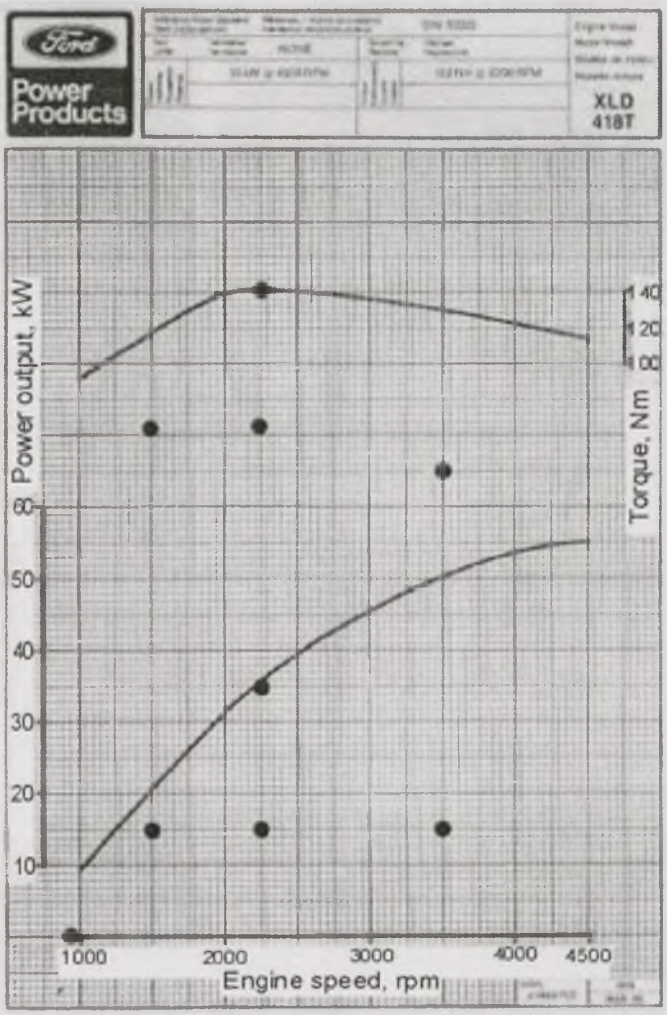

Figure 2.2. Power curves for the Ford XLD 418T engine. The dots represent the test conditions used for this work.

Each test for this work, as will be explained in more detail later, consisted of a cold start with a step change to one of the conditions shown in Figure 2.2 or an acceleration with a warm engine from idle to one of those conditions. The engine was kept running at the same condition for a period between six and ten minutes. Afterwards, the engine was decelerated and shut down in the case of cold start tests, or decelerated to idle in preparation for a second acceleration, in the case of the acceleration tests.

The first part of the tests for this work was transient, and the second, after reaching the target speed and power condition, steady. The steady part may be associated to one of the steady-state modes of the R49 or the ESC, as shown in Figure 2.3., although these are designed for heavy-duty engines and not for light-duty engines such as the Ford XLD 418T. On the other hand, the transient part cannot be associated to a complete transient legislative test such as the ETC, since

the latter involves several acceleration/deceleration cycles and not only one step change. However, some similarity can be found in terms of speed with the rural segment of the ETC, between 600s and 1200s in Figure 2.4. Most of the speeds used in this work are below the speed of that segment of the ETC, and one –3500rpm- is above it.

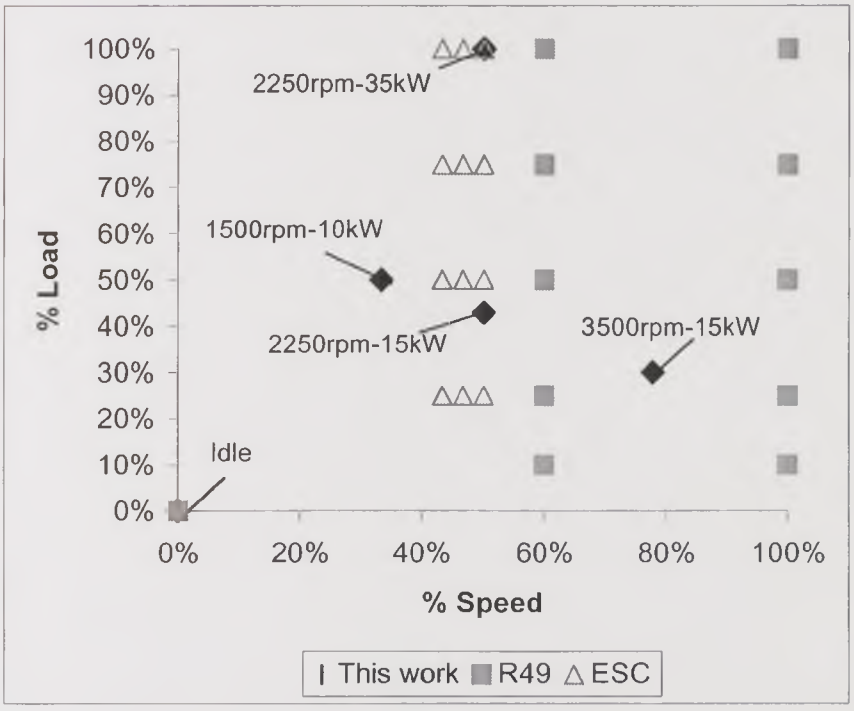

Figure 2.3. Test conditions for this work, as compared to the various modes of the legislative driving cycles for heavy-duty engines.

Regarding the light-duty legislative driving cycle, the ECE+EUDC, or real-world conditions, there is no direct reference that allows a comparison with the steady-state test conditions reached in this work. Engine dynamometer test conditions of engine speed and load do not correspond to a single speed condition in chassis dynamometer tests, mainly because of the influence of the gear changes. In spite of this limitation, a relationship between the steady-state conditions targeted in this work and real-world conditions could be attempted qualitatively as follows:

Target Test conditions	Related ECE+EUDC conditions	Related real-world conditions
Idle	Idle segments	Idle
1500rpm – 10kW	50-100s ECE (30km/h)	Very slow urban driving conditions
2250rpm – 15kW	140-170s ECE (50- 35km/h)	Slow urban driving conditions
3500rpm – 15kW	50-100s EUDC (70km/h)	Medium speed urban/rural driving conditions
2250rpm – 35kW	300s EUDC (100-120km/h)	Medium speed motorway conditions

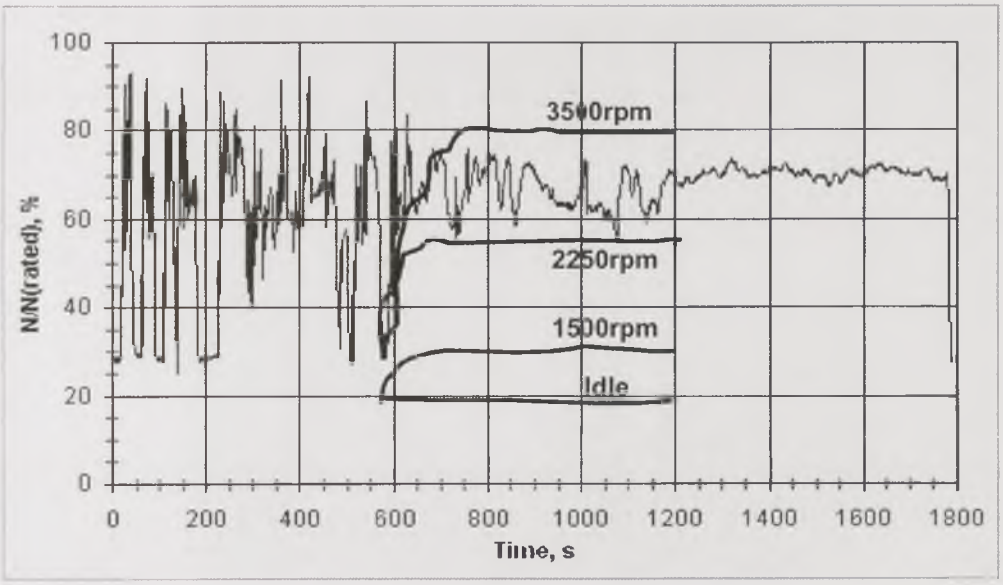

Figure 2.4. Section of the ETC, in grey, for which the tests for this work show similarity (N is speed in rpm).

2.1.1. Turbocharger and Intercooler

In the Ford XLD 418T, the engine output and mechanical efficiency are increased by increasing the density of the air drawn into the engine, in order to achieve a performance level closer to that of the gasoline engine. A compressor driven by an exhaust gas turbine increases the air density. This technique is known as turbocharging and the compressor, as turbocharger. In addition to this, a heat exhanger that uses air as cooling medium, known as intercooler, is also used in order to avoid a decrease in density caused by temperature rise in the compression process.

The use of turbocharging and intercooling reduces fuel consumption and also particulate and NOx emissions when compared with naturally aspirated engines. Mori et al. (Mori, 1997) and Tanin et al. (Tanin, 1999) showed that particulate and NOx emissions could be reduced by around 25% and 15% respectively, and at the same time fuel economy increased, when using turbocharging and intercooling.

2.1.2. Exhaust Gas Recirculation (EGR)

EGR is another emission control technique in the Ford XLD 418T. As explained in the previous section, NOx emissions are reduced by decreasing the peak combustion temperature by introducing a fraction of the exhaust gas to the combustion chamber.

2.2. The Exhaust System

The engine exhaust pipe is a single 45mm (Internal diameter) x 2mm-wall pipe connected to the exhaust manifold. The maximum backpressure is 100mbar (Ford, 1992). Figure 2.5. shows a view of part of the exhaust sytem as installed in the test bed. The components of the exhaust system are described below.

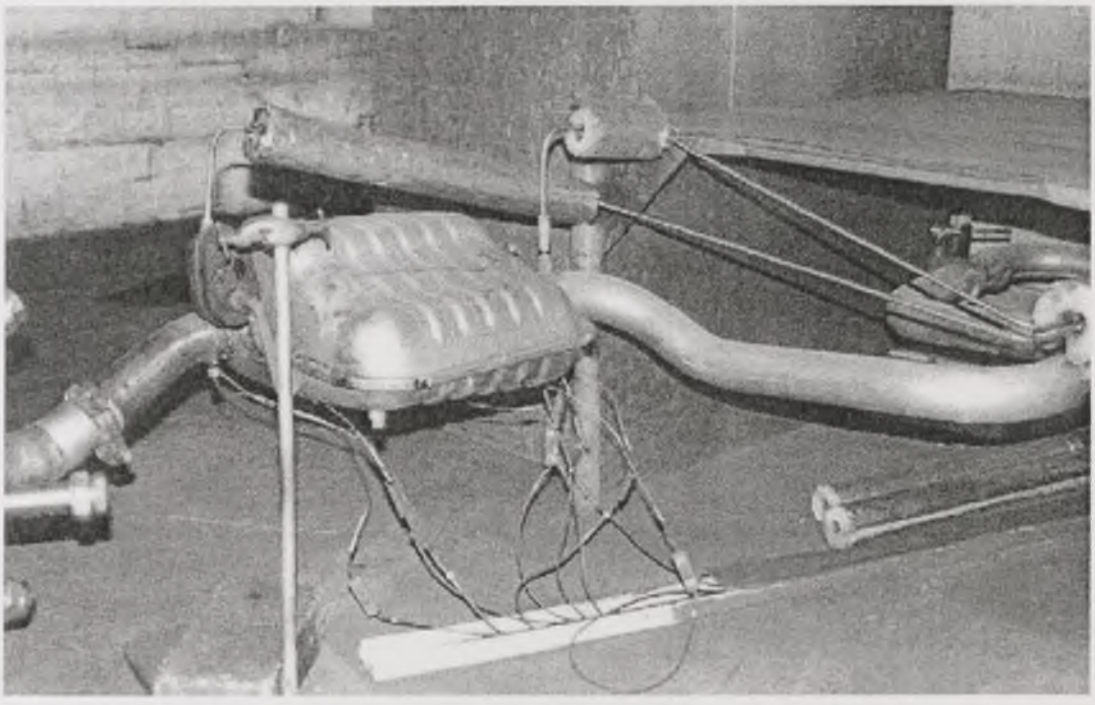

Figure 2.5. The exhaust system as installed in the test bed.

2.2.1. Close-Coupled Diesel Oxidation Catalyst (DOC) with Hydrocarbon adsorber.

The catalyst installed in the exhaust system of the Ford XLD 418T has the following characteristics:

Substrate: 300 cells/in^2, cordierite, 8 mil. wall

Volume: 60% swept volume (1.08 litres)

Coating: Engelhard IEX531

Loading: 10 g/ft^3 Platinum

The catalyst formulation includes a zeolite for hydrocarbon adsorption during cold start, whose characteristics were explained above. A picture of the catalyst is shown in Figure 2.6.

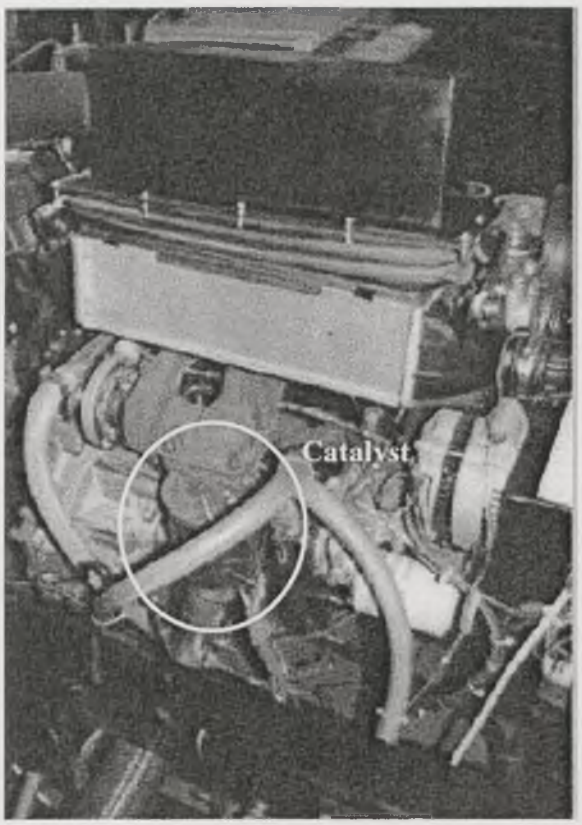

Figure 2.6. Side view of the close-coupled diesel oxidation catalytic converter as installed in the exhaust system.

2.2.2. Silencers

The exhaust Ford XLD 418T has two serial silencer boxes of different design downstream of the catalyst. The first silencer consists of two parallel partially perforated tubes, each having the same exhaust pipe diameter, separated 1/3 diameter from each other, enclosed in a box. The second is an S-shaped tube enclosed in a corrugated box. The perforated and bent tubes are characteristic discontinuities of reactive silencers, whose performance is determined by their geometrical shape. The discontinuities provoke a reflection of part of the acoustic energy back to its source, or back and forth through the pipe until it is dissipated. Hence, the acoustic energy penetrating the system is reduced. Figures 2.7. and 2.8. show cut-open silencers identical to those installed in the exhaust system.

The use of perforations, bends and baffles in the design of reactive silencers modifies the flow pattern of the exhaust aerosol and increases the surface area on which particles can be deposited, either temporarily or definitely.

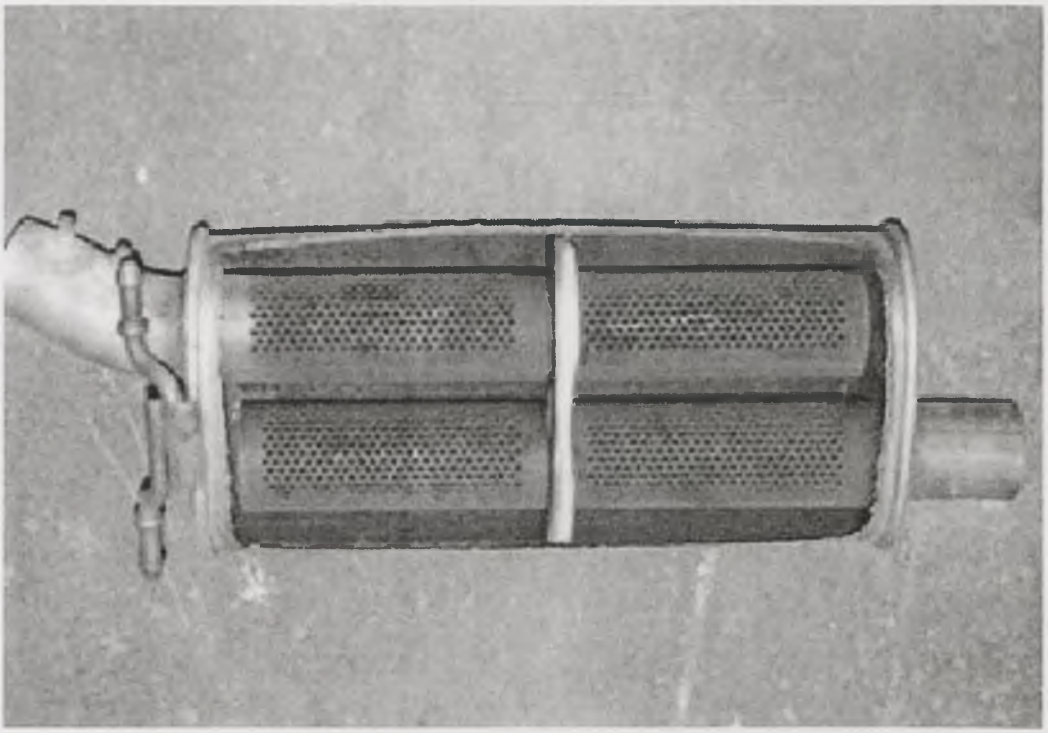

Figure 2.7. Cut-open silencer 1.

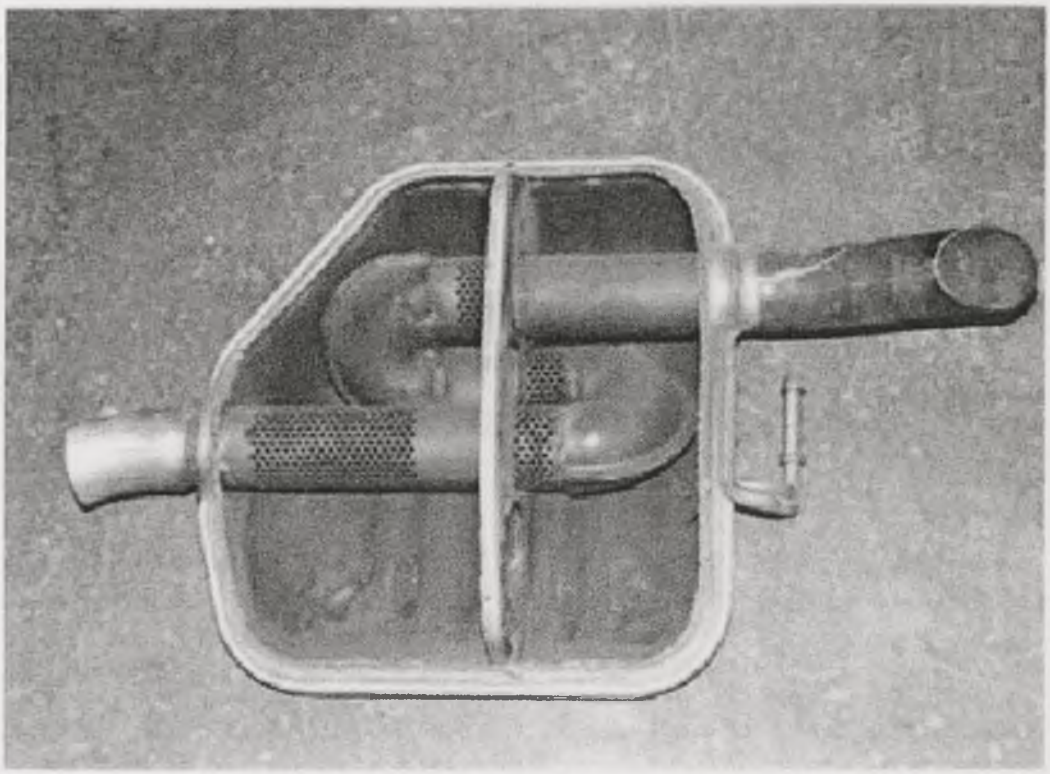

Figure 2.8. Cut-open silencer 2.

2.3. Ultra-low Sulphur Diesel Fuel

The diesel fuel used in this work was ultra-low sulphur fuel, known and sold in the UK and other European countries under the generic name "City Diesel". A complete specification sheet is shown in Table 2.1.

Property and Units	Limit		Test Method Note (1).
Appearance	Clear and bright, free from visible sediment and water		Visual
Colour	Max	2.5	D1500 - IP196
Odour		Merchantable	
Density @ 15°C, g/ml	Min-Max	0.820 – 0.835	D4052
Cold Filter Plugging Point Winter, °C (2) Summer, °C (2)	 Max Max	 -15 -5	EN 116 / IP309
Cloud Point Winter, °C (2) Summer, °C (2)	Max Max	+3 56	D2500 / IP219
Flash Point (PMCC), °C	Min	49	ISO 2719
Cetane Number	Min	49	ISO 5165 / IP380 / D613
Cetane Index	Min	46	ISO 4264 / IP380 / D4737
Viscosity, cSt @ 40°C	Min – Max	2.0 – 4.5	ISO 3104
Sulphur, %W	Min	0.005	ISO 8754
Copper Corrosion (3h. @ 50°C)	Max	1	ISO 2160
Micro Carbon Residue: Residue weight on 10% Bottoms	Max	0.30 (Note 3)	ISO 10370 / IP398
Ash, %W	Max	0.01	ISO 6245 / IP4
Particulate Matter, mg/kg	Max	24	DIN 51 419
Water, mg/kg	Max	200	D1744
Distillation, %Vol Rec @ 250 °C	 Max	 65.0	 ISO 3405
%Vol Rec @ 345 °C	Min	95.0	
Oxidation Stability, mg/100ml	Max	2.5	D2274

Table 2.1. Ultra-low Sulphur Autodiesel (ULSD) Specification Sheet (taken from Bayford Thrust, Energy. Bayford & Co. Ltd.

2.4. The Froude DPX Type Hydraulic Dynamometer with remote control

The Froude DPX-Type Hydraulic Dynamometer used in this work was an electrically controlled version of the manually operated original dynamometer. The modifications were made by Plint and Partners ®, although the principle, design and construction remained the same. The dynamometer is accurate, though its control

response is slow and, therefore, it is not the ideal dynamometer for transient test cycles. However, the cold start and fast acceleration tests designed for this work do not involve cyclic operation, but only one step change in speed and load, so the dynamometer performance was considered good enough if helped by manual acceleration to make it faster. In the tests the step-change target condition was reached between 30 and 90 seconds from the disturbance of the system.

Compared to real-world driving, the manual acceleration achieved was still somewhat slow and gentle, so the results were not really comparable to real-world conditions, where much more aggressive accelerations take place. Furthermore, real world driving involves gear changes that were not simulated by the dynamometer. All this would mean that much more dramatic changes could be expected in real-world driving than those found in this work.

2.5. Temperature Monitoring Along the Exhaust System

Temperature gradients between an aerosol and a solid surface, e.g. between exhaust aerosol and the inner walls of the exhaust system, generate a thermophoretic force acting on the aerosol particles, in addition to the drag, gravimetric and Brownian motion forces (Chunhong, 1998). Thermophoresis leads to particle deposition on the walls and, when the temperature gradient is high, the thermophoretic force may become the main deposition driving force. Thermophoresis depends on particle size, as well as on the relation between particle size and the mean free path, i.e. the Knudsen number, $Kn = \frac{2\lambda}{d}$, where λ is the mean free path and d_p, the particle diameter. Berger et al. built an approximate model to observe the changes in the particle size distribution of a hot diesel exhaust aerosol due to thermophoretic deposition through a pipe (Berger, 1994). They found that thermophoresis played the major part only in rather slow flows, and diffusion was more important elsewhere.

K-type thermocouples, some pressed against the metal or ceramic surfaces, and some exposed to the exhaust gas, monitored continuously the temperatures along the exhaust system. A total of 32 thermocouple readings were possible, located through the exhaust system as shown in Table 2.2. and Figure 2.9.

2.6. Exhaust Gas Analysis

Exhaust Gas Analysis was carried out downstream of the catalyst. Total Unburned Hydrocarbons Concentration was determined by using Flame Ionisation

Detectors at three temperature levels: 190°C (hot FID), 90°C (medium FID) and 56°C (cold FID). Chemiluminiscence was used to determine NO_x. Non-Dispersive Infra Red analysis was used for CO, O_2 and CO_2.

Upstream Catalyst	1.Metal Turbo Out Gas Side	Downstream Silencer 1	13.Skin bottom out
	2.Gas Turbo out		14.Skin top-out
	3.CAT Face US		15.Metal-Out M1 Gas-side
Downstream Catalyst	4.CAT Face DS		16.Gas Out, M1
	5.Metal Gas side DSCat	Upstream Silencer 2	17.Metal Gas side in M2
	6.Gas sample DS Cat		18.Gas In, Silencer 2 (rear)
	7.Metal intersection		19.Skin top-in
Upstream Silencer 1	8.Metal Gas side in M1		20.Skin bottom-in
	9.Gas In, Silencer 1		21.Gas-mid section M2
	10.Skin bottom in	Downstream Silencer 2	22.Skin top-out
	11.Skin top in		23.Skin bottom-out
	12.Gas-mid section M1		24.Metal for tail pipe
			25.Gas, Tail Pipe

Table 2.2. Location of thermocouples along the exhaust system.

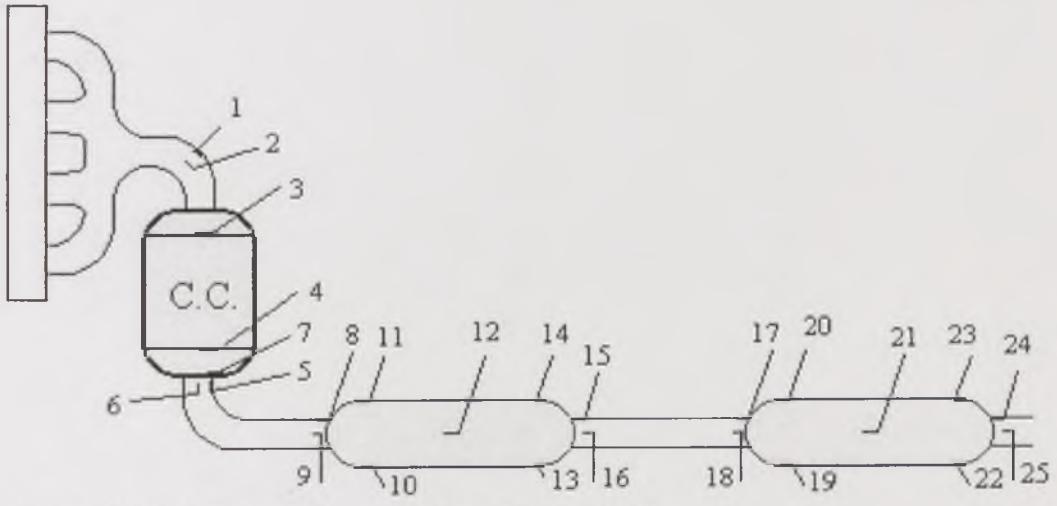

Figure 2.9. Thermocouples along the exhaust system.

Sample ports, which were common to all measurement techniques, consist of sample pipes 6.3mm OD located on the exhaust pipe centreline, with a curved section to exit through the exhaust pipe wall, normal to the wall. The particulate sample pipe was made of stainless steel.

2.7. Mass Concentration Filter Determination

Exhaust samples were taken using the heated SAE smoke measurement technique, shown in Figure 2.10., which is manufactured in the UK by Richard Oliver Ltd. This was modified to include separate heating of the filter paper housing as well as the constant temperature oven. This was particularly suitable for sampling directly from the exhaust of low emission diesel engines. The constant temperature sampling (CTS) technique used includes uncooled stainless steel pipes inserted with a bend onto the centreline of the exhaust pipe. Each sample was transported through heated flexible sample lines to the CTS system into a heated oven set at 50°C. The sample was cooled in the oven to 50°C and then passed through a Whatman 40mm-diameter GF/F glass fibre filter, located in a heated filter mount at 50°C and having a sample spot size of 25mm. The exhaust flow rate through the filters was 5 L/min. Figure 2.11. shows schematically the mass-measurement set up through the exhaust system.

Figure 2.10. Mass filter in the SAE smoke measurement technique.

The particulate mass concentration was determined by measuring the increase in weight of the filter. Weights were recorded to 10-mg accuracy after a 24-hour conditioning period in a constant humidity enclosure, before and after the test. The mass collected was divided by the sample volume to obtain the particulate

concentration as mg/L or g/m^3. This was then converted into mass of particulate per mass of fuel burnt using the equation:

$$EI\ (g/kg\text{-}fuel) = (M_p/1.18)(1 + A/F)/1000 \qquad \text{(Equation 2.1.)}$$

Where,

M_p= Particulate Matter mg/m^3.

A/F = Air/Fuel ratio by mass.

The constant 1.18 kg/m^3 is the density of the sample gas at the sample flow meter temperature and pressure.

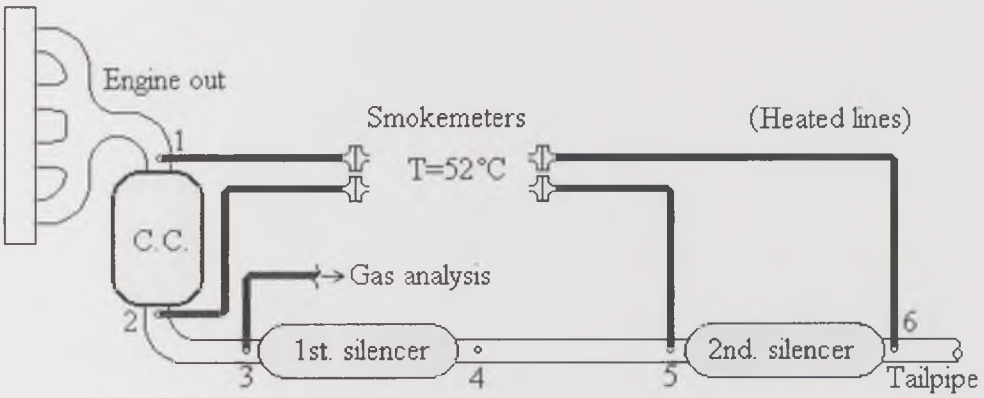

Figure 2.11. Experimental set-up for mass concentration measurements.

2.8. Particle Size Distribution Measurement

2.8.1. SEM and TEM imaging

Table 2.3. shows the characteristics of the TEM and SEM used in this work, both at the Department of Materials of the University of Leeds.

Instrument	Model	Features
SEM	Hitachi S700	Field-Emission Gun Secondary Electronic Imaging
TEM	Phillips CM20	LaB6 Source Bright-field Imaging

Table 2.3. Characteristics of the TEM and SEM used in this work.

Samples for the SEM were taken from Andersen impactor collection filters, in a 2-hour sampling at 100°C, with the engine running at 2250rpm and 15kW. A 0.5cm square was cut from the filter on stage 4 of the impactor and covered by a

gold film before the observation under the microscope, in order to make the sample conductive.

Samples for the TEM were taken using carbon film in gold grids 200 mesh/in^2. The grids were put over aluminium foil collection substrates of the ELPI, greasing only a very small portion of the collection substrates to hold the grids by the edge, and avoid them to be lifted by the aerosol flow. The engine was run at 2250rpm and 15kW for two hours, as in the case of particulate collection with the Andersen impactors, using a 10:1 dilution ratio (one dilution stage with Dekati® ejector-type diluter). Normal greasing on the collection substrates was not used owing to the interference that the grease may produce in the image formation. No mounting wax was used to hold the grids either, since this can break them as a result. The grids were then kept on the stages just by a very small amount of grease on the grid edge. Two grids per stage were used.

2.8.2. Andersen Impactor

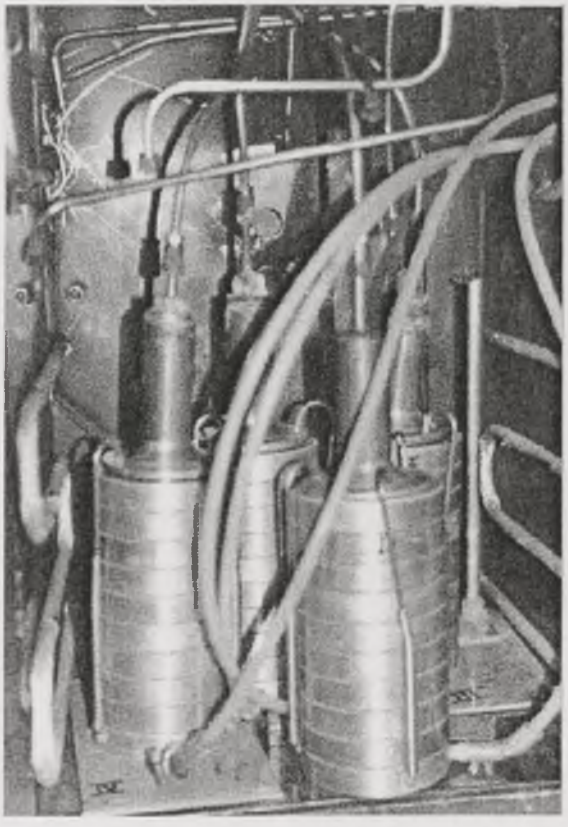

Figure 2.12. Andersen impactors as located into an oven at 100°C.

Four Andersen Impactors were used simultaneously at four sampling points along the exhaust system, to determine the mass-weighed particle size distribution in steady-state conditions. The sampling flow through each impactor was 28.32L/min, and it was carried directly from the exhaust, with no dilution involved. To

accomplish this, heated lines at 180°C were used to transport the samples, and the impactors were kept in an oven at 100°C, as seen in Figure 2.12., so the condensation of exhaust water vapour was avoided.

Teflon coated fibreglass filters were used as collection substrates on each stage of the impactors. Filter weight was recorded to 10-μg accuracy after a 24-hour conditioning period in a constant humidity enclosure, before and after two-hour tests. This period was needed to collect enough mass on the filters. The mass collected was divided by the sample volume to obtain the particulate concentration as mg/L or g/m^3, and converted into Emission Index in g/kg-fuel. Subsequently, the particle size distribution was derived by a simple data reduction technique.

2.8.3. Electrical Low Pressure Impactor (ELPI)

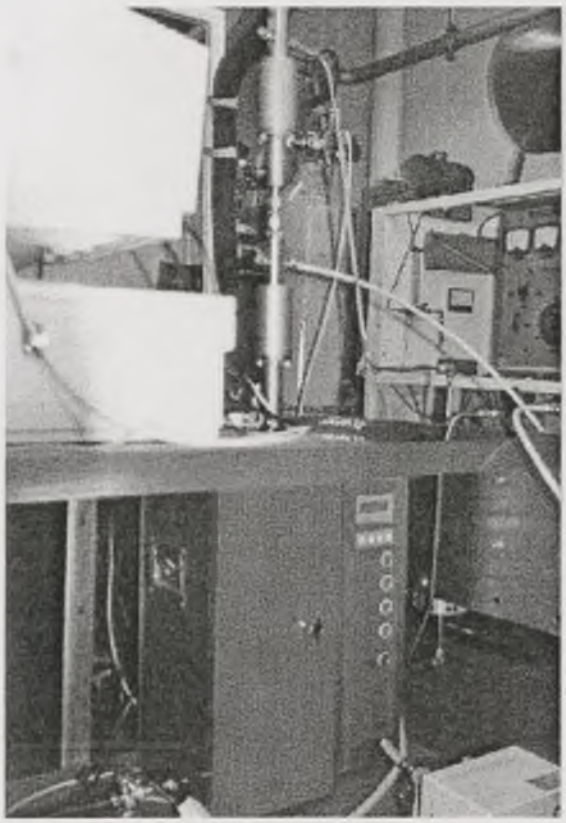

Figure 2.13. The ELPI with the double-stage ejection-type dilution system.

The Dekati® ELPI was briefly described in Chapter 1 and is shown in Figure 2.13. It was used to determine the particle size distribution between 0.038μm and 10μm on a second-by-second basis. The same four sample ports used for the filter mass determination equipment and the Andersen Impactors along the exhaust system were used for the ELPI in non-simultaneous tests.

Dilution is necessary when using the ELPI owing to:

a) the exhaust particle number concentrations are well over the equipment operation threshold;

b) the exhaust must be kept above the sulphuric acid dew point to protect the instrument from physical deterioration.

In this work, two dilution systems were used in series to produce an adequate aerosol to be analysed by the ELPI. The first was a whole-exhaust two-stage dilution tunnel. The second, Dekati's ® two-stage minidilution system. These systems are explained below.

2.8.3.1. Whole Exhaust Dilution

The whole exhaust was mixed with air at the normal tailpipe exit. A two-stage air dilution tunnel system was used with a 4/1 dilution at the tailpipe. This used air taken downstream of the air filter on the main dilution tunnel and separately metered. A sample from this primary full flow dilution was then further diluted to give an overall dilution ratio of 180/1. The dilution ratio was determined using NOx analysis as well as airflow metering. The dilution airflow was manually controlled so that the dilution ratio was constant during the engine acceleration period. At 3.5m from the sample inlet in the secondary dilution tunnel the diluted particles were sampled into the ELPI size analyser.

The dilution ratio of 180:1 selected for whole exhaust dilution was within the range used in laboratory studies, which rank between 5:1 and 1000:1. Dilution ratios between 5 and 50 are considered critical for gas-to-particle conversion processes, and are not recommended. So the dilution ratio of 180:1 used in this study for whole exhaust dilution was considered safe. This value is, however, much lower than real-world dilution conditions. Measurements by Kittelson et. al., showed that in atmospheric dilution, the exhaust passed through the critical dilution ratio values between 5:1 and 50:1 in less than 0.4s and was diluted above 1000:1 in aproximately 1s (Kittelson, 1998).

The present double dilution system, shown schematically in Figure 2.14. was not ideal in its design. The primary whole exhaust dilution was at rather a low dilution ratio of 4/1. Abdul-Khalek et al. 1998, 1999 have shown that low primary dilution ratios can influence the particle number and volume concentrations for particles below about 80nm. Also the considerable length of the primary dilution tunnel could produce large particle losses due to deposition on the walls (Kittelson, 1991). This length was unavoidable due to the distance between the test bed and the secondary tunnel and the length of the exhaust system at 90° to the engine. However, it was considered important to use whole exhaust flow in the primary

dilution so that all the particles blown out from the wall region were collected. The secondary dilution tunnel was fed with a sample from the primary dilution stage, to yield high overall dilution ratios, around 150:1 to 200:1.

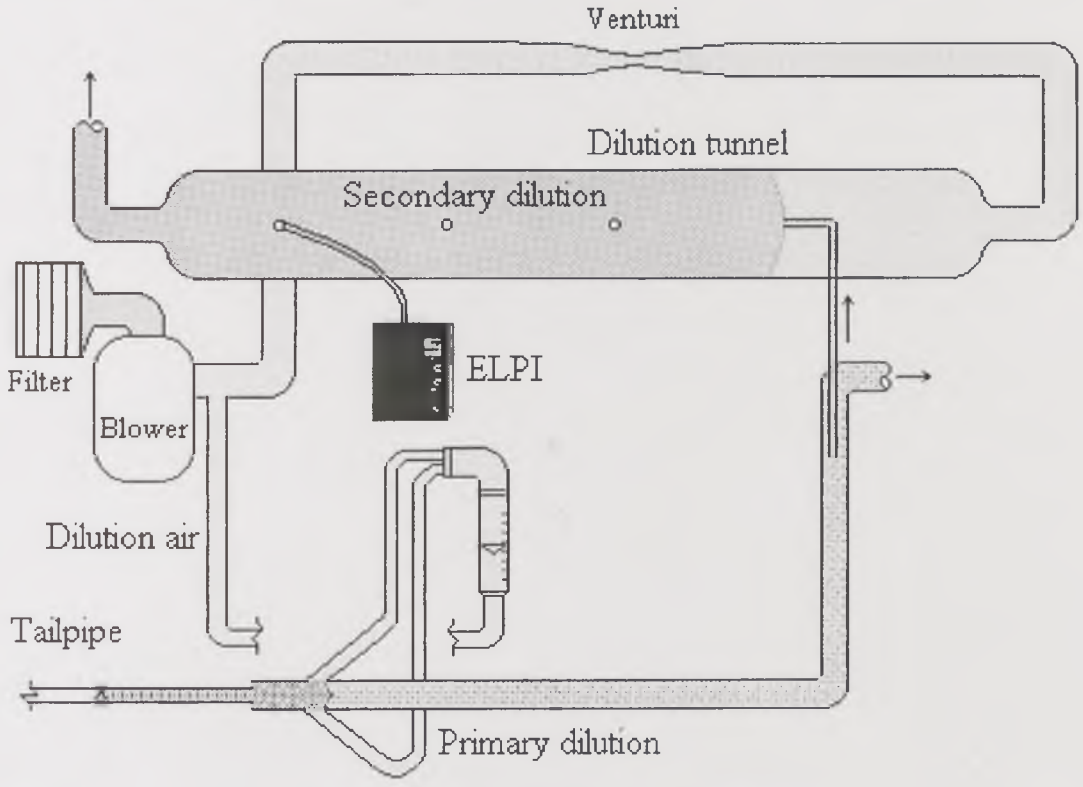

Figure 1. Experimental set-up, dilution tunnel and ELPI sampling point location

Figure 2.14. Experimental set-up for particle size distribution measurement with ELPI and a whole exhaust dilution system.

2.8.3.2. Two-Stage Minidilution

Since the objective of this work was identifying the changes through the exhaust system, a direct exhaust dilution was needed. This was achieved by using a double minidilution system provided by Dekati®. Each diluter consists of an ejector in which zero grade air at 2 bar overpressure generates a vacuum at the exhaust sample position. The ejector draws the exhaust particle sample into a dilution chamber in which air and exhaust gases mix together. Part of this diluted exhaust is drawn to the atmosphere and the rest into the second diluter, as shown schematically in Figure 2.15. The second dilution is identical to the first one, and part of its product is drawn into the ELPI at a nominal flow rate of 10L/s. In this work, each dilution stage had a dilution ratio of 10/1, yielding a 100/1 overall dilution ratio. Water vapour condensation was avoided in the first diluter by heating the dilution air to 100°C. The second dilution air was not heated, so the resulting temperature of the aerosol entering the ELPI was approximately 28°C.

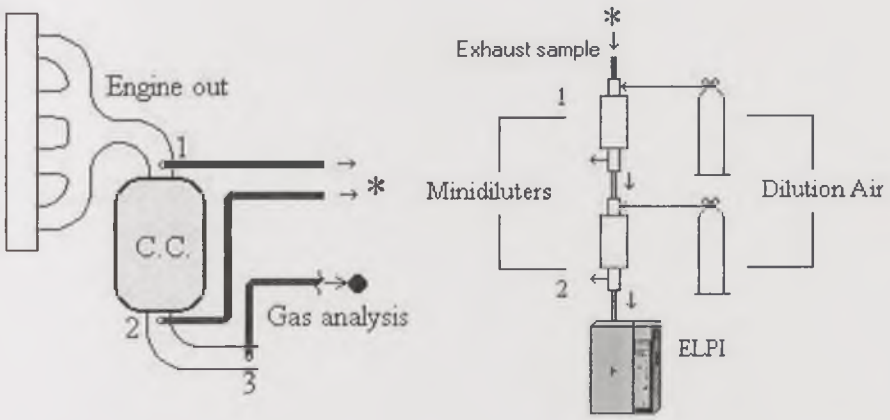

Figure 2.15. Experimental set-up for particle size distribution with ELPI and a double-stage ejection-type dilution system.

2.9. Particulate Analysis

2.9.1. Thermal-Gravimetric Analysis (TGA)

The thermal-gravimetric analysis uses the difference in phase and volatility of various groups of chemical compounds to give general information regarding the chemical composition of a particulate sample. The application of this technique to the analysis of diesel particulate matter collected on filters allows determining the carbon content, ash, water and soluble organic fraction (SOF), together with the differentiation of the source of SOF from fuel or lubricant oil technique, developed at the University of Leeds by Abbass et al. (Williams, 1988; Abbass, 1991).

The TGA apparatus consists of a highly sensitive microbalance that reads continuously the sample weight. The sample is hanging into a oven whose temperature and heating/cooling ramps can be closely-controlled and through which flows a controlled atmosphere created from known gases. The sample weight is recorded at all times, so any change in sample weight can be related to changes temperature and/or reaction with the flowing gases.

The TGA technique was developed for liquid or solid samples to be put into a 5mm diameter ceramic pan including a metallic pan holder. The adaptation for particulate matter on filters consists of cutting the 25mm inner circle where particulate matter is actually collected from the 55mm collection filter, folding it and wrapping it with an aluminium wire hook to be hung instead of the pan holder. The sample is heated at a rate of 20°C/min until reaching a temperature of 550°C in a Nitrogen atmosphere, so all materials that are volatile under this temperature, virtually all SOF, are removed from the sample and are exhausted. Keeping the temperature at 550°C, the flow of nitrogen is stopped and, instead, air starts flowing.

The oxygen reacts with the particulate carbon remaining on the filter. Any residue on the filter is due to the ash content of the particulate matter.

The differentiation between the SOF from lubricant oil and the SOF from the fuel is achieved by running the analysis with samples of pure fuel and lubricant oil, as well as mixtures of both, spiked on filters, and then comparing the temperatures at which they start and finish their volatilisation. In their work, Abbass et al. (Abbass, 1991) found that all virtually all the fuel was volatilised at 290°C, virtually the same temperature at which the lubricant oil started its volatilisation. Despite the fact that a narrow overlap was found, the calibration with mixtures showed that the contribution can be calculated from the difference of the mass loss fractions below and above 290°C. The results from this technique agreed with those from other thermal methods such as vacuum oven sublimation, purged vacuum oven sublimation and pyroprobe/gas chromatography, but all the others produced higher SOF values than the Soxhlet extraction method due to the sulphate content of the samples being more efficiently extracted by thermal methods than by solvent extraction.

2.9.2. Pyrolisis – Gas Chromatography

This technique consists of a very rapid volatilisation of hydrocarbons from the particulate matter and their subsequent analysis by gas chromatography (Williams, 1988). It uses very small scratched-from-filter samples into a 20mm X 3mm quartz tube, which is heated rapidly to 660°C and held at that temperature for 20 seconds in a stream of inert gas. The volatilised material from the sample is carried by the inert gas to a chromatographic column, which analyses the sample for individual compounds. If the quartz tube is weighed before and after the analysis, the weight difference represents the SOF of the particulate.

2.10. Tests Description

This work was focused in two types of tests, Cold Start and Fast Acceleration. Preconditioning of the exhaust system was carried out before these tests to simulate the effect of either prolonged city-driving conditions or regular motorway driving. Additional tests were also needed to study the number-to-mass conversion when determining particle size distribution. The description of the tests follows.

2.10.1. Preconditioning Procedures

The application of preconditioning procedures in this work was the result of the hypothesis that the sudden particulate blow out observed in real-world driving was due to particulate storage under prolonged low speed, low power city-driving

periods, followed by a fast acceleration period. Regular high-speed, high-power driving would lead to virtually no storage in the exhaust, as any deposit would be repeatedly cleared out. Hence, the effect of the recent history of the engine was considered an important factor in this study.

The first preconditioning procedure was designed to simulate prolonged low speed and low power City Driving. It consisted of a Four-hour Idling Period prior to the test, which henceforth will be referred to as 'Idle Preconditioning'. If followed by a Cold Start Test, an overnight soak after preconditioning was also applied. In contrast, continuous operation was applied for the hot fast acceleration tests.

The effect of high-speed motorway driving for a short period, e.g. commuting, was achieved by using a 'High Speed Preconditioning'. It consisted of a ten-minute operation at 3500rpm, with the objective of clearing out the exhaust system by blowing off fluffy particle deposits. After this, the engine was left for an overnight soak to run a cold-start test the morning after.

2.10.2. Cold Start Procedures

Cold start tests were run after the overnight soak at ambient laboratory temperatures following the preconditioning procedure. The goal in each test was to reach a certain condition just after starting the engine. The time the engine takes to reach the condition was longer for either high speed or high load than for low speed or low load, but it never exceeded one and a half minutes. Measurements with Andersen Impactors were extended for as long as twenty minutes from cold start. Measurements with the ELPI were no longer than ten minutes, and many times they were shorter, since once stabilisation in particle number concentration was reached, the tests were stopped, as will be shown later.

The engine operation conditions at which the cold start tests were performed were typical of low power (0-15kW) and high power (35 kW) city driving:

- Idle, that is, 800rpm - 0kW
- 1500rpm - 10kW
- 2250rpm - 15kW
- 2250rpm - 35kW
- 3500rpm - 15kW

2.10.3. Fast Acceleration Procedures

Fast acceleration tests were run immediately after a four-hour preconditioning at Idle. They consisted of two six-minute step-change cycles to high engine speed or

load conditions in less than one and a half minutes, with a ten-minute idle period between consecutive cycles.

Three target conditions in these tests were selected from the cold start tests to perform the fast acceleration tests:

- 2250rpm - 15kW
- 2250rpm - 35kW
- 3500rpm - 15kW

2.10.4. Mass Collection Procedures with Andersen Impactors and ELPI

Particle size distribution determination using Andersen Impactors needs a long sampling time to collect enough mass. At moderate conditions, two hours are needed when sampling undiluted exhaust. This size distribution is, therefore, representative of steady state conditions.

Mass collection with the ELPI was carried out for the same period and the same conditions as that using the Andersen Impactor. In this case, however, the exhaust was diluted to a 10:1 ratio. The charger was off at all times to avoid particulate mass losses, as recommended by Marjamäki et al. (Marjamäki, 2000).

2.11. Supporting results

2.11.1. Theoretical penetration efficiencies through the exhaust system

In this section the effect of some parameters on the transport efficiencies through a pipe similar to that of the exhaust system used in this work were calculated using real temperatures, engine speed and Air/Fuel ratio profiles as measured in the tests, in order to observe the deposition trends of the particulate matter. This does not aim to be a detailed model, but only a very basic model that can give more elements of analysis. The complex geometry of the catalyst, for example, was not taken into account; hence this is not a realistic result. However, it is useful to observe the trends produced in order to observe the contrast with the experimental results. The work in this PhD thesis had an experimental nature, so the development of a realistic and complete model for the particulate deposition and reentrainment in exhaust systems is beyond its scope. This would be for future work.

The gravimetric, thermophoretic, inertial and diffusive depositions were calculated as penetration or transport efficiency through the system. The overall transport efficiency is defined in the equation 1.62. and is the fraction of the entering particulate into the system that penetrates it. The calculation was made over 12 size

ranges corresponding to the ELPI impaction stages, Table 1.4., in order to detect size-dependent effects, and at different times during the transients. The dimensions and characteristics of the exhaust system used in the model are shown in Table 2.4. and Figure 2.16. Specific features of the devices, such as the honeycomb geometry of the catalyst and the multiple orifices of the first silencer were not taken into account. The devices were considered as portions of pipe with the same exhaust diameter of the exhaust pipe, so the results of the model will be expected to produce higher transport efficiencies than the real system. More realistic estimations would demand a much more complex model.

	Section 1: Catalyst	Section 2: First silencer	Section 3: Second silencer
Device Length (m)	0.14	0.39	0.34
Associated Pipe length (m)	--	4.10	0.34
Number of 90°C bends	0	7 (+4 inside the device)	4 (inside the device)

Table 2.4. Dimensions and characteristics of the exhaust system used in the deposition calculations.

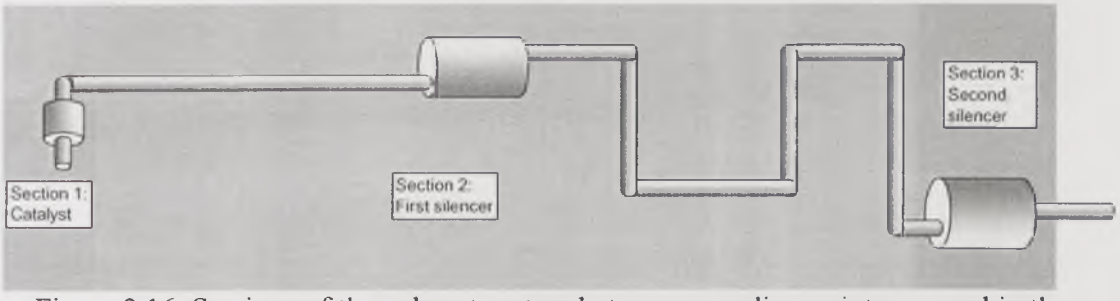

Figure 2.16. Sections of the exhaust system between sampling points, as used in the experimental results and in the deposition calculations.

The penetration efficiencies were calculated using equations 1.63. and 1.64. (gravimetric), 1.65 (diffusional), 1.67 (inertial), 1.71 (inertial in bends), and 1.72 (thermophoretic), with their corresponding auxiliary equations shown in Chapter 1, i.e. dimensionless numbers.

Real temperatures measured during the tests were used in the estimation of the properties of the aerosol system, such as viscosity and density. Simplified equations for these properties in the exhaust system were provided by Dekati® (Dekati, 1999) in the ELPI Excel® calculations spreadsheet, and used as follows:

Gas viscosity:

$$\mu = 0.01 \times \left(\frac{1069.15[O_2] + 963.02[CO_2] + 420.35[H_2O] + 873.1[N_2]}{5.66[O_2] + 6.93[CO_2] + 4.24[H_2O] + 5.29[N_2]} \right)$$ Equation 2.2.

where [ ] indicates the volumetric fraction of each component of the exhaust gas.

Temperature correction for viscosity:

$$\mu_{corr} = \mu * \left(\frac{273 + T}{273} \right)^{1.5} \times \left(\frac{383.4 + T}{383.4} \right)$$ Equation 2.3.

Molecular mass:

$$M_g = 32[O_2] + 44[CO_2] + 18[H_2O] + 28[N_2]$$ Equation 2.4.

Gas density:

$$\rho_g = \frac{M_g P}{R \times (T + 273)}$$ Equation 2.5.

Mean free path:

$$\lambda = 6.6 \times 10^{-8} \left(\frac{T + 273}{293} \right) \times \frac{1.3768}{1 + \frac{110.4}{(T + 273)}}$$ Equation 2.6.

The fuel consumption was measured experimentally by an automatic fuel timer and the Air/Fuel ratio (AFR) calculated from the gas analysis. With these two parameters, the exhaust mass flow was calculated:

$$\dot{m}_{exhaust} = \dot{m}_{fuel} \times (1 + AFR)$$ Equation 2.7.

The volumetric exhaust flow was then:

$$\dot{v}_{exhaust} = \frac{\dot{m}_{exhaust} R(T + 273)}{M_g}$$ Equation 2.8.

And the exhaust gas linear speed, considering a countinuous rather than a pulsing flow:

$$V_{exhaust} = \frac{v_{exhaust}}{A_{pipe}}$$ Equation 2.9.

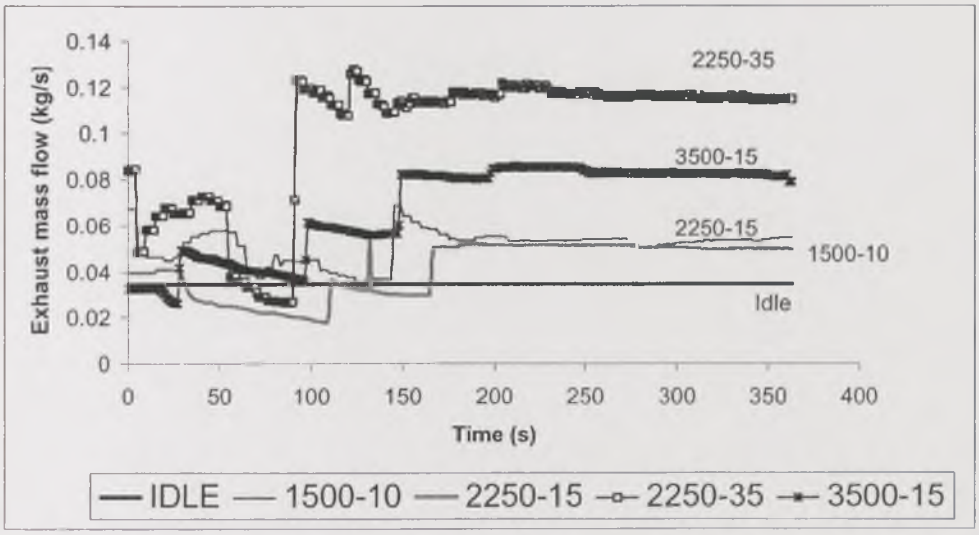

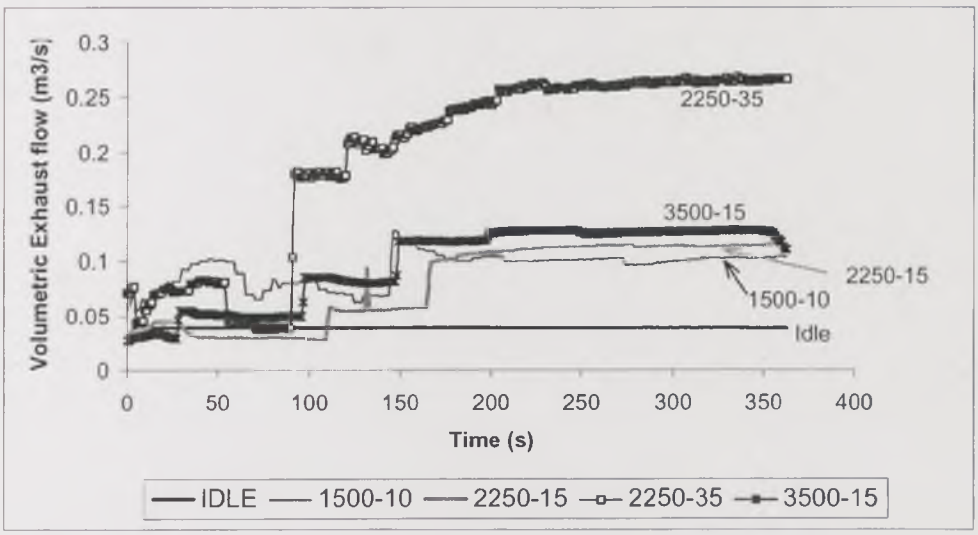

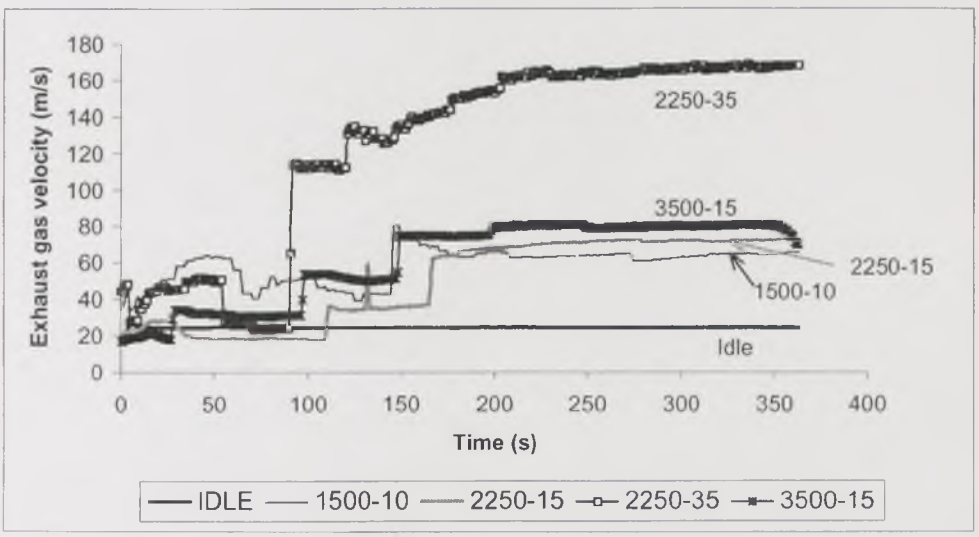

Figure 2.17. Real exhaust mass and volumetric flow vs. time, and exhaust gas velocity vs. time for the engine operational conditions in this work.

The cross sectional area of the 0.045m I.D. of the exhaust pipe, A_{pipe}, is 0.0015904 m^2.

Figure 2.17. shows the resulting exhaust mass and volumetric flows, as well as the exhaust gas speeds for the various engine operational conditions investigated in this work. The exhaust flow and the exhaust gas velocity increase with the engine speed at similar load levels. Idle operation showed the lowest steady exhaust flow and velocity. These increase slightly with increasing speeds for 1500rpm - 10kW, 2250rpm - 15kW and more significantly for 3500rpm - 15kW. High load operation, 2250rpm - 35kW, showed the highest exhaust flow and gas velocity of all conditions. These changes respond to the operation of the turbocharger. In a turbocharged engine such as the Ford XLD 418T, air is pumped into the combustion chamber to increase the air density and the volumetric efficiency, reducing the emissions. The mixture is kept lean, i.e. the AFR is kept higher than in naturally aspirated engines for all conditions. At high load conditions, the extra air pumped to the engine and the high fuel consumption result in the increased exhaust mass and volumetric flows, and hence higher exhaust gas velocity observed in Figure 2.17.

During the first 150 seconds in Figure 2.17., the various step-change cycles in Exhaust flow and gas velocity reflect the response of the engine control strategy to the acceleration during cold start, including a repeated decrease in exhaust flow, which is counteracted by corresponding increases in AFR and therefore in exhaust flow and gas velocity. After 150 seconds, a stabilisation was reached.

2.11.1.1. Effect of the time from cold start

According to the theoretical prediction, the penetration efficiency through the exhaust system during a cold-start-like transient should have the following characteristics, as shown in Figures 2.18. and 2.19.:

- The calculated total penetration efficiency of very fine particles, below 0.1μm, is always higher than that of particles larger than 1.0μm. Mid-sized particles have normally intermediate penetration efficiencies, although under some conditions they show higher penetration efficiencies than finer particles.
- The dominant process for the deposition of very fine particles, those below 0.1μm, is thermophoresis. Therefore, the highest penetration efficiency of very fine particles occurs during the first 30 seconds of cold start, when the difference between the exhaust-gas and metal temperatures reaches a maximum. Afterwards, the penetration efficiency reaches a minimum between 60 and 120 seconds from cold

start, when the gas-metal temperature difference is the highest, and then, the penetration efficiency increases again, until reaching a stable value, which is often higher than that in the period between 30 and 60 seconds from cold start.

- Particles larger than 1.0μm deposit through the exhaust system mainly under the action of gravitational forces. Low gas velocities, and therefore long residence times in the exhaust system, reduce the penetration of these particles through the exhaust system due to gravitational forces. Consequently, the lowest penetration efficiency for these particles occurs in the first thirty seconds, when the engine gas velocity is also the lowest. Then, as the gas velocity increases to the target condition, the penetration efficiency increases steadily, reaching a maximum between 5 and 6 minutes from cold start, which remains constant afterwards.
- Particles between 0.1μm and 1.0μm are affected by both thermophoretic and gravitational forces alike. The smaller particles in this range tend to behave the way particles smaller than 1.0μm do, whereas larger particles behave more like particles larger than 1.0μm.

Figure 2.18. illustrates the changes of the penetration efficiency with time for the various particle-size ranges, for a target condition of 2250rpm - 15kW, through the first section of the exhaust pipe.

2.11.1.2. Effect of the target operation conditions

For the stabilisation period, the deposition model showed idle operation to cause the lowest total penetration efficiency for particles of all sizes, as shown in Figure 2.19. Medium speed and low load conditions, namely 2250rpm - 15kW and 1500rpm - 10kW, showed the second and third lowest total penetration efficiency, although thermophoretic deposition for these conditions was more significant than for idle conditions, owing to the higher temperature differences. High engine speed conditions showed just slightly higher total penetration efficiency than 1500rpm - 10kW and 2250rpm - 15kW. For all these low load conditions, the penetration efficiency in the large size range was controlled by gravimetric effects. The total penetration efficiency was higher in the large size range and lower in the fine size range for high load conditions, 2250rpm - 35kW.

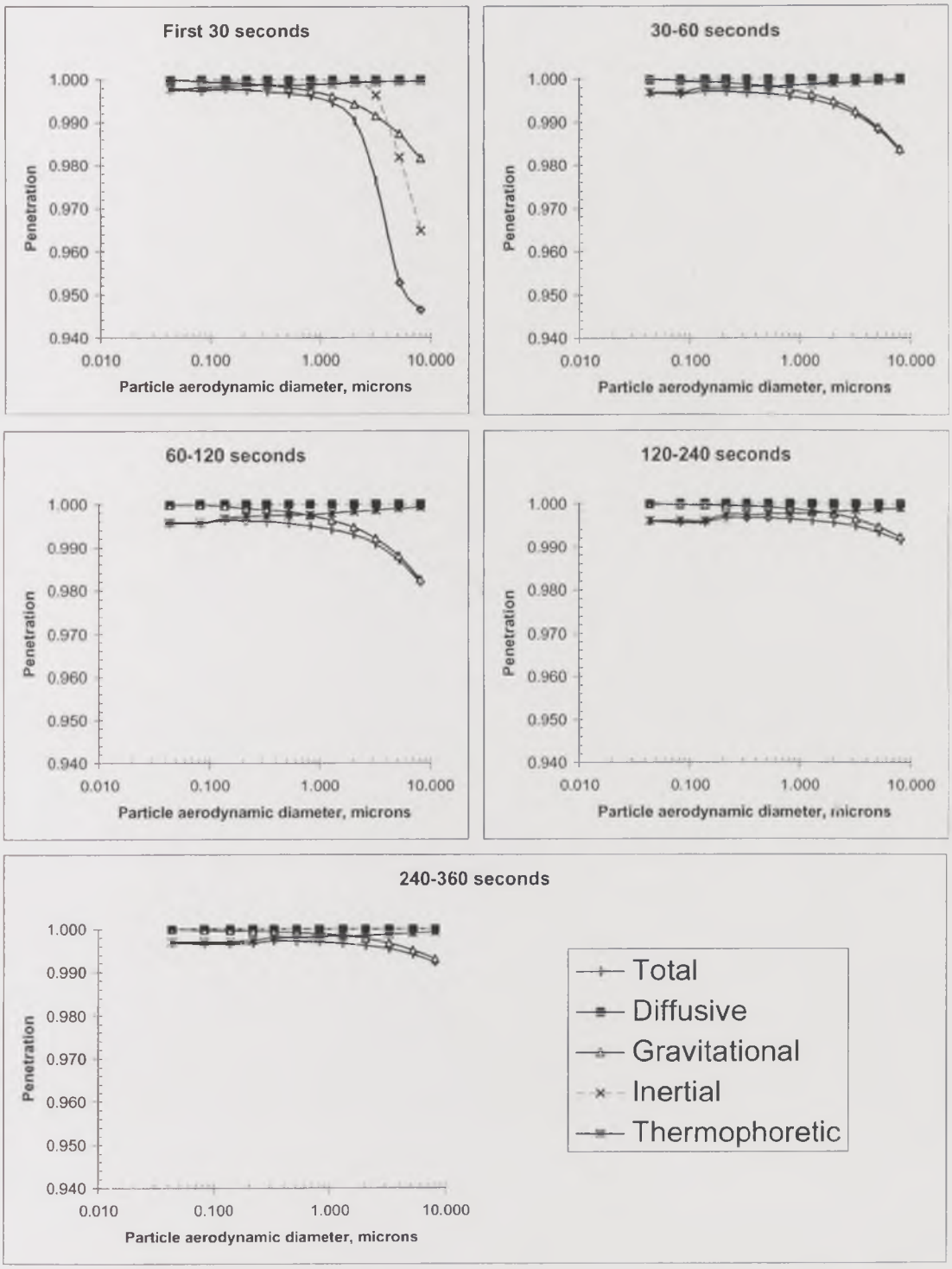

Figure 2.18. Penetration efficiency through the system vs. particle size for various periods from cold start. Target conditions: 2250rpm - 35kW.

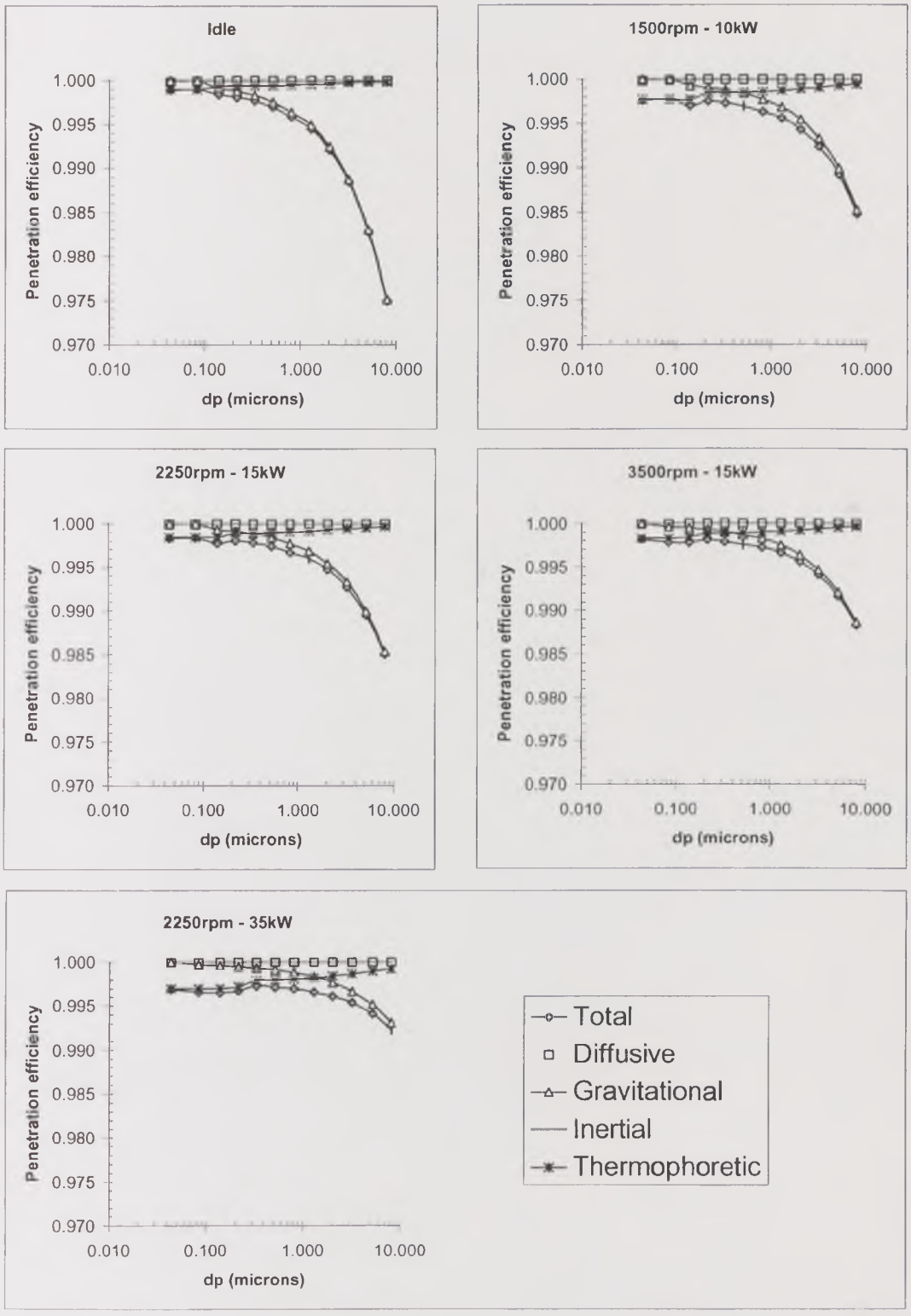

Figure 2.19. Penetration efficiency vs. particle size for various engine operation conditions after 4 minutes from cold start.

The exhaust gas velocity is higher at these high load conditions owing to the turbocharger, thus increasing the penetration of large particles. On the other hand,

the higher temperatures and gas-metal temperature differences under these conditions account for the increased thermophoretic deposition of fine particles, reducing their penetration.

2.11.2. The correction of the particle number-to-mass conversion used in this work

A comparison between the particulate mass size distributions from the Andersen Impactors and the ELPI at different points along the exhaust system and with the engine running at 2250rpm – 15kW are shown in Figure 2.20. A comparison with the mass distributions calculated from ELPI numbers was made, using the spherical particle and unity density assumptions. The shape of the mass distributions from the gravimetric determinations was substantially different from that derived from the ELPI number distribution. This would suggest that the assumptions of unit density and spherical particles were not valid.

Apparent densities in the different size ranges were then calculated from the comparison of the measured and calculated mass at the four sampling points. This calculation still assumes spherical particles. The results are given in Figure 2.21. as average values of density vs. particle diameter. Since four Andersen Impactors at four points were used for the comparison with the ELPI, error bars are given as an indication of the variability of the density determination. Particles collected on each stage of the ELPI had, then, a density range. The calculated densities in the upper stages of the ELPI showed little error, whereas their variability at lower stages was greater because they were the product of an extrapolation using the trend of the stages 5, 6 and 7, which correspond to the lower stages of the Andersen Impactors. The shape of the resultant curve in Figure 2.21. was very similar to the shape of the effective density reported by Ahlvik et al., although they represent somewhat different parameters. The resulting mass per particle using unit and apparent densities is shown in Figure 2.22. The mass distribution changed after applying the calculated apparent density values and the total mass concentration agreed well with the gravimetric determination, as seen in Figure 2.23.

These results were made assuming that the ELPI number distributions were totally reliable in all size ranges and that the disagreement with the gravimetric mass measurements was entirely due to the density and shape assumptions. However, Figure 2.24. show the comparison in the opposite direction. The original ELPI number distributions are compared with the number distributions calculated from the gravimetrically derived mass distributions, assuming unit-density spherical particles. This shows that not only the shape, but also the values of the distributions, agreed very well in the middle size range covered by the ELPI. The distributions

diverge for particles bigger than 1μm by up to two orders of magnitude and to a lesser extent for particles smaller than 0.1μm.

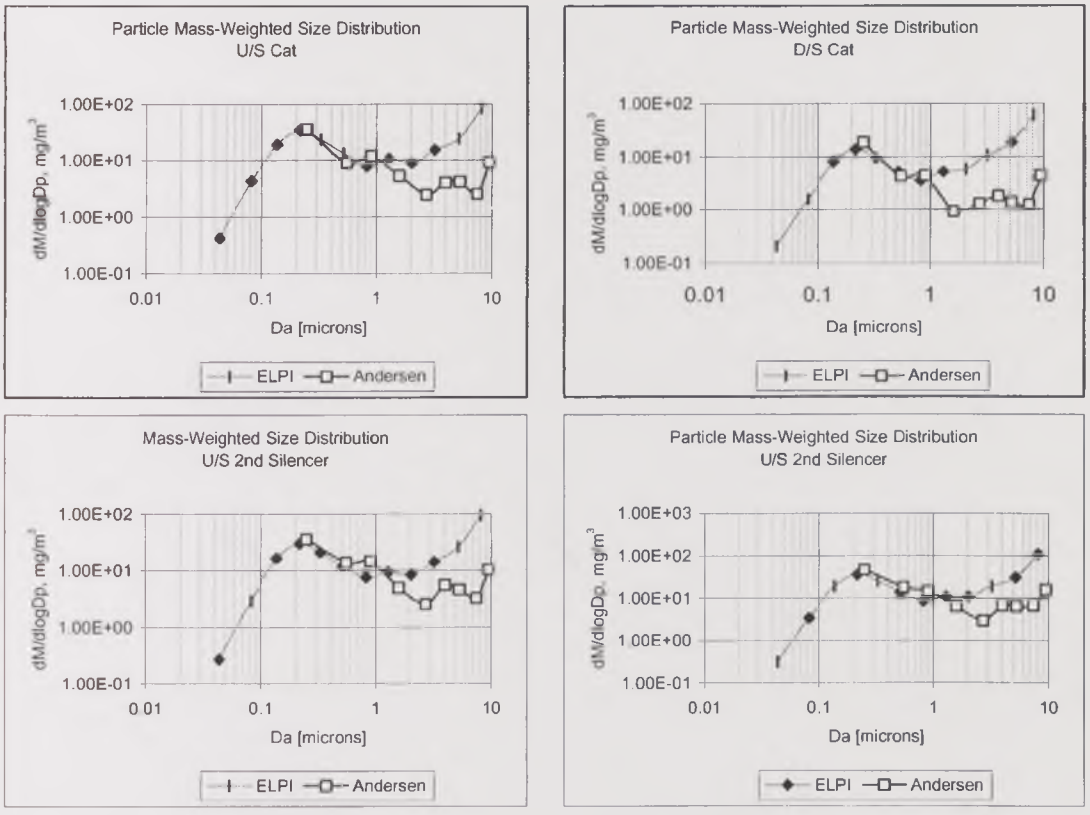

Figure 2.20. Comparison between mass size distributions as measured with the Andersen Impactors and the ELPI.

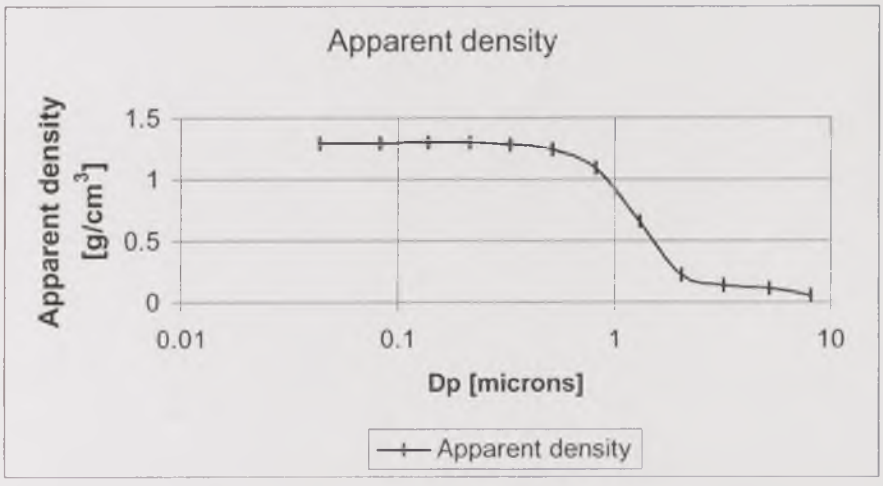

Figure 2.21. Apparent Density vs. Size derived in this work, by comparison between the ELPI and Anderson Impactors.

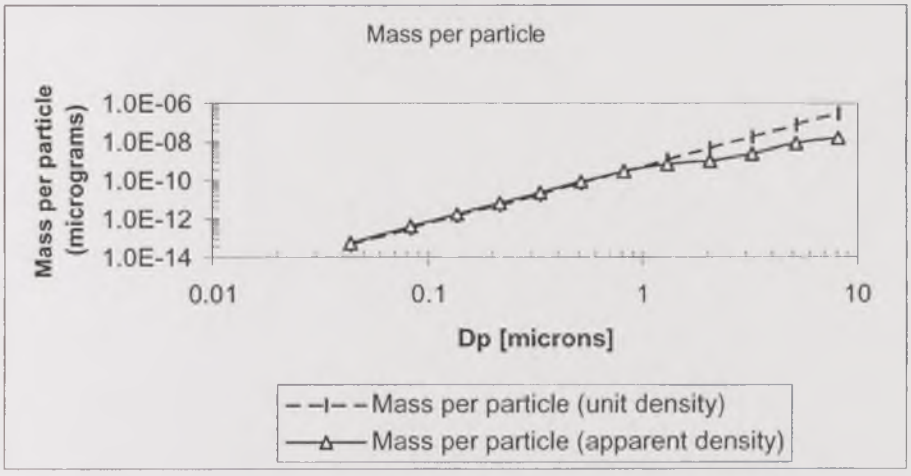

Figure 2.22. Mass per particle calculated with unit and apparent densities.

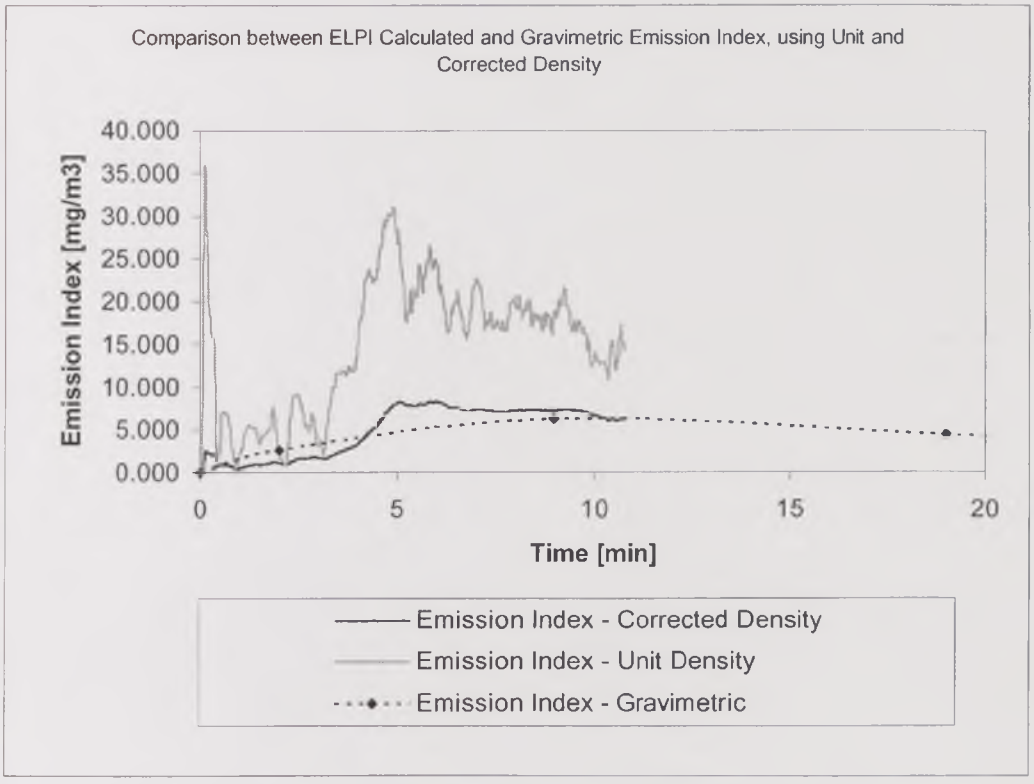

Figure 2.23. Comparison between ELPI Calculated and Gravimetric Emission Index, using Unit and Corrected Density.

In the ELPI, the measured current in every stage is corrected for fine particle losses according to a correction matrix that depends on the type of stages that is used. Corrections for teflon and metal-shielded teflon insulators, with sintered metal collection subtrates are available with the instrument. The measured stage current is then converted into number or mass concentration values by applying the charger efficiency power function, dependent on particle size. This function is a result of the

calibration of the charger, which is made with a calibration aerosol (DOS, NaCl) and a DMA to generate monodisperse aerosols. The total number of particles is determined from the electrometer measurements and APS number concentrations. The latter is used for particles bigger than 1μm, which is the range showing the biggest divergence in our test, as well as in the study by Weingartner, 1997.

An evaluation of the ELPI [Marjamäki, 2000] showed that in that size range, the charger efficiency differed from that specified by the manufacturer, owing to the decrease in counting efficiency of the APS. Also, it is possible that differences in dielectric properties between calibration and test aerosols make big unknown particles more likely to be more densely charged than calibration aerosol particles. Therefore, particles are counted in higher numbers than they actually are. Regarding these difficulties, Donald et al. (Donald, 1997) suggested that better algorithms for the conversion of current signals into number concentrations should be developed.

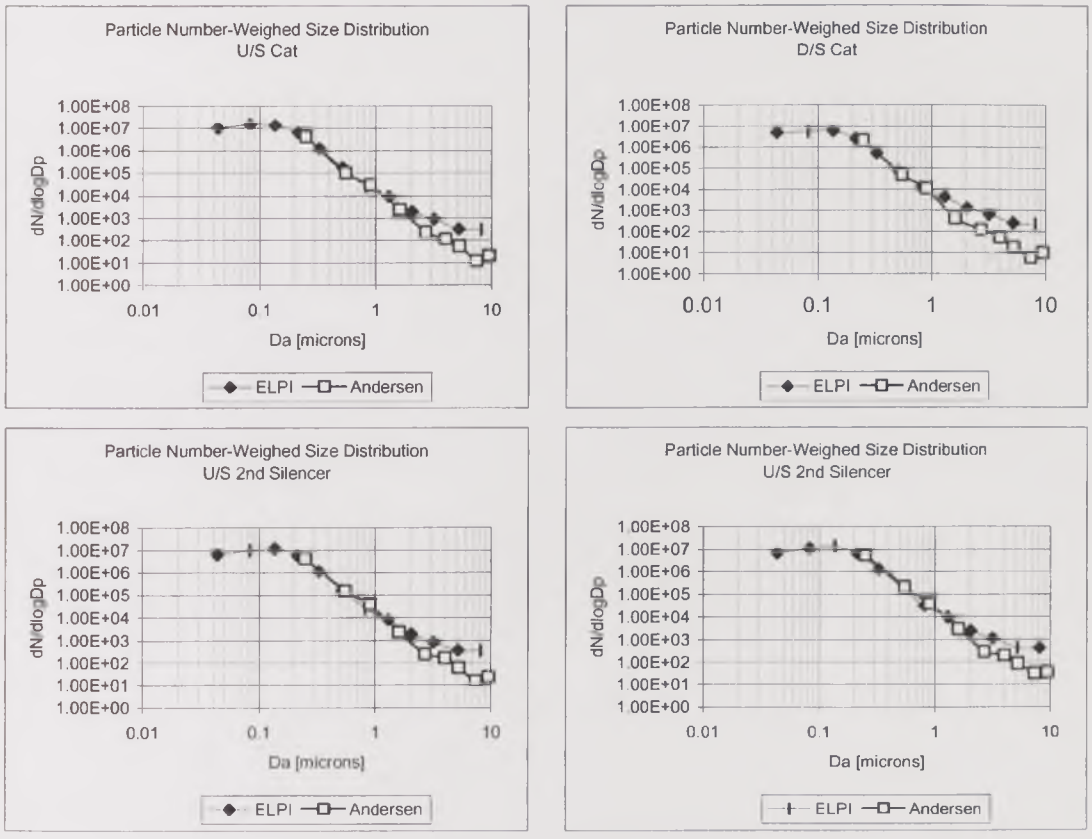

Figure 2.24. Comparison of the number size distributions as derived from Andersen Impactors and ELPI measurements.

2.11.3. Analysis of SEM and TEM images of diesel particles

Particles from the Ford 1.8L IDI diesel engine were analysed by SEM and TEM after collection on various stages of one Andersen Impactor and the ELPI, respectively. The collection technique based on impaction has been used successfully for many years (Lipkea, 1978), although it implies long collection periods to have enough material on the filter, and is normally carried out with dilution of the exhaust. Long collection periods can affect the particle structure, since the particles are exposed to the interaction with other impacting particles. Furthermore, the formation of various layers of particles is likely, which is not convenient for the image analysis. Dilution and cooling affect the particle structure because of the condensation of hydrocarbons, as shown by Lipkea et al. (Lipkea, 1978). To avoid these disadvantages, other authors have used the thermophoretic sampling technique, in which a cold grid holder is exposed to the hot exhaust aerosol for a very short period (a few milliseconds), thus promoting thermophoretic deposition of particles onto the grid.

An attempt was made to evaluate the particle separation in the Andersen and the Low-Pressure impactors through microscopic-image analysis. Although this separation is based on the aerodynamic behaviour of the particles, a relationship with the microscopic-image sizing may not be discarded. There is a limitation, however, which is that the microscopic image is a bidimensional measurement, whereas the aerodynamic sizing depends on a combination of parameters defined in three dimensions.

Samples from the Andersen Impactor stages were collected on glass-fibre filters, from which portions were cut off and covered by a layer of gold to make them conductive. Those from the ELPI were collected on TEM carbon-film grids placed on the impaction stages. For both cases, the collection took 2 hours, without dilution for the Andersen impactors, and a 10:1 dilution for the ELPI. The engine ran at high-load conditions, 2250rpm – 35kW.

Figure 2.26. shows examples of the SEM images from stage 4 of the Andersen impactor upstream of the catalyst at two magnification levels. Because of the formation of two or more layers of particles on the particulate filter, it was not possible to achieve images of individual particles but in few cases. The resulting image had good tridimensional characteristics, although the resolution was poor compared to that achieved with the TEM, examples of which are shown in Figure 2.27. Nevertheless, it was possible to measure the size of primary particles from them, by using the KS400® image analysis software. TEM images had an excellent resolution, allowing not only measuring the size of the primary particles, but also

observing the layers of fullerenes that consitute their basic carbonaceous structure at high magnifications (310000X). At lower resolutions (38000X, 27500X) the projected area of many individual agglomerates was measured, so the calculation of the fractal dimension was possible. Unlike the SEM images, those produced by the TEM do not show a clear tridimensionality.

The size of the primary particles showed some variations, depending on the technique and the magnification used, but it was not clear whether this reflected a real change in the particle size or an artifice of the analysis. The smallest primary-particle diameters, shown in Table 2.5. and Figure 2.25., were measured in high-magnification TEM pictures, around 25nm. At low magnifications with the same technique, diameters were around 35nm to 40nm. The highest value was measured with the SEM, around 70nm.

	Primary particles		Agglomerates	
	Average Dp (nm)	Std. Dev. (nm)	Median Dp (nm)	Geom. Std. Dev.
TEM High mag. (310k X) a.	23.76	3.58		
TEM High mag. (310k X) b.	25.67	6.05		
TEM Low mag. (38k X) a.	39.40	12.72	73.66	1.17
TEM Low mag. (38k X) b.	33.98	5.62	68.54	1.22
SEM	69.68	19.11		

Table 2.5. Average primary-particle diameters from SEM and TEM images.

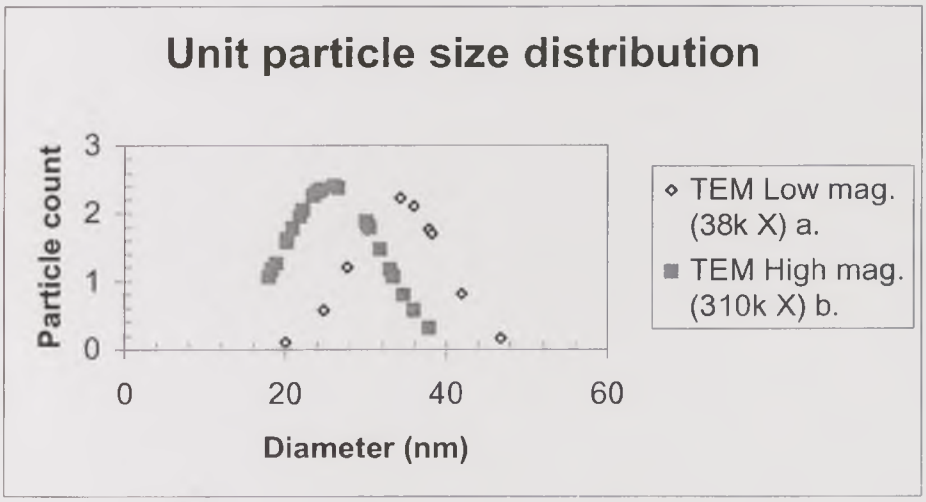

Figure 2.25. Primary-particle size distributions for high and low TEM magnifications.

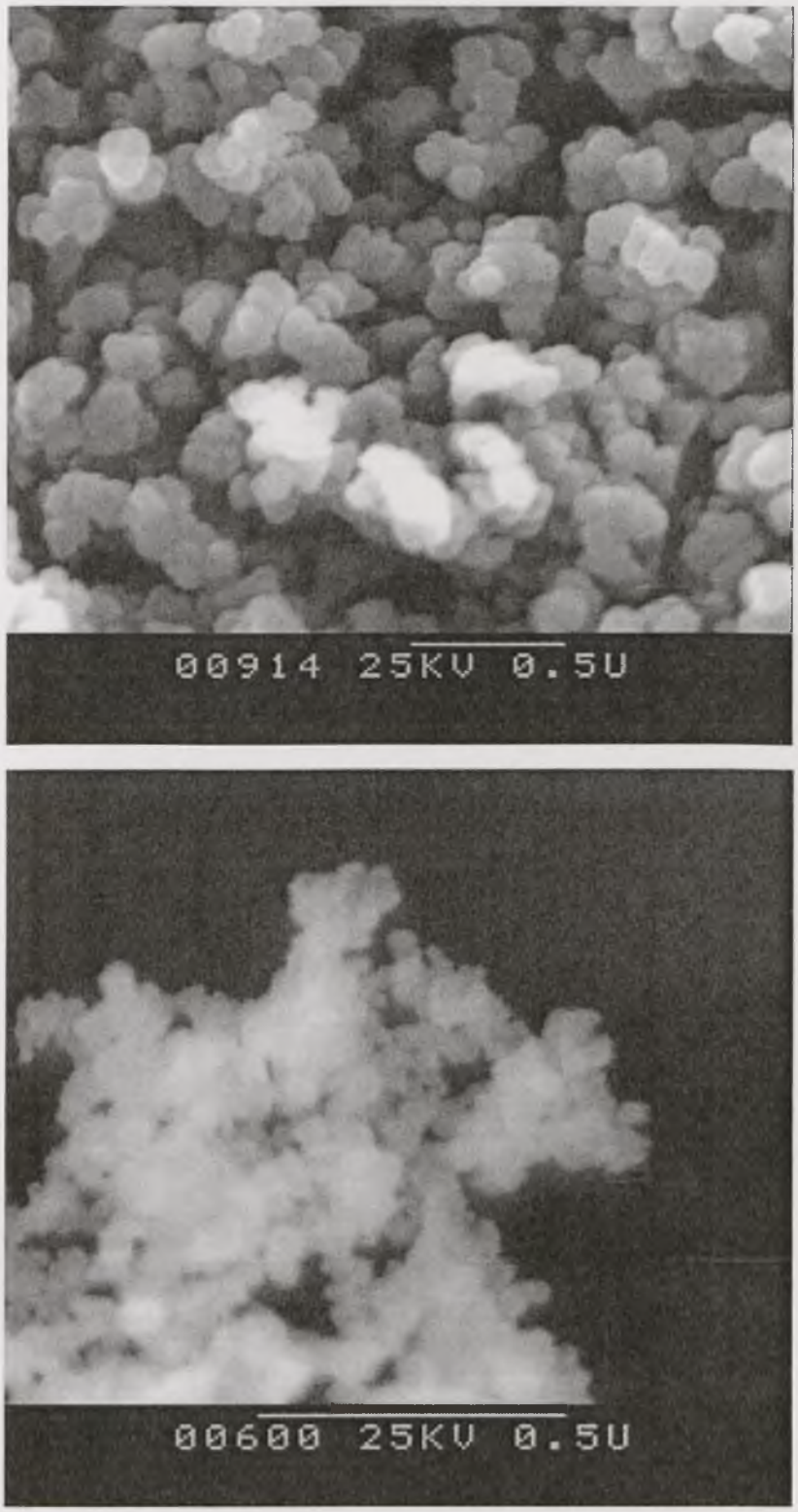

Figure 2.26. SEM images of particles collected on Andersen Impactor stages. The grey line under each image corresponds to 0.5μm.

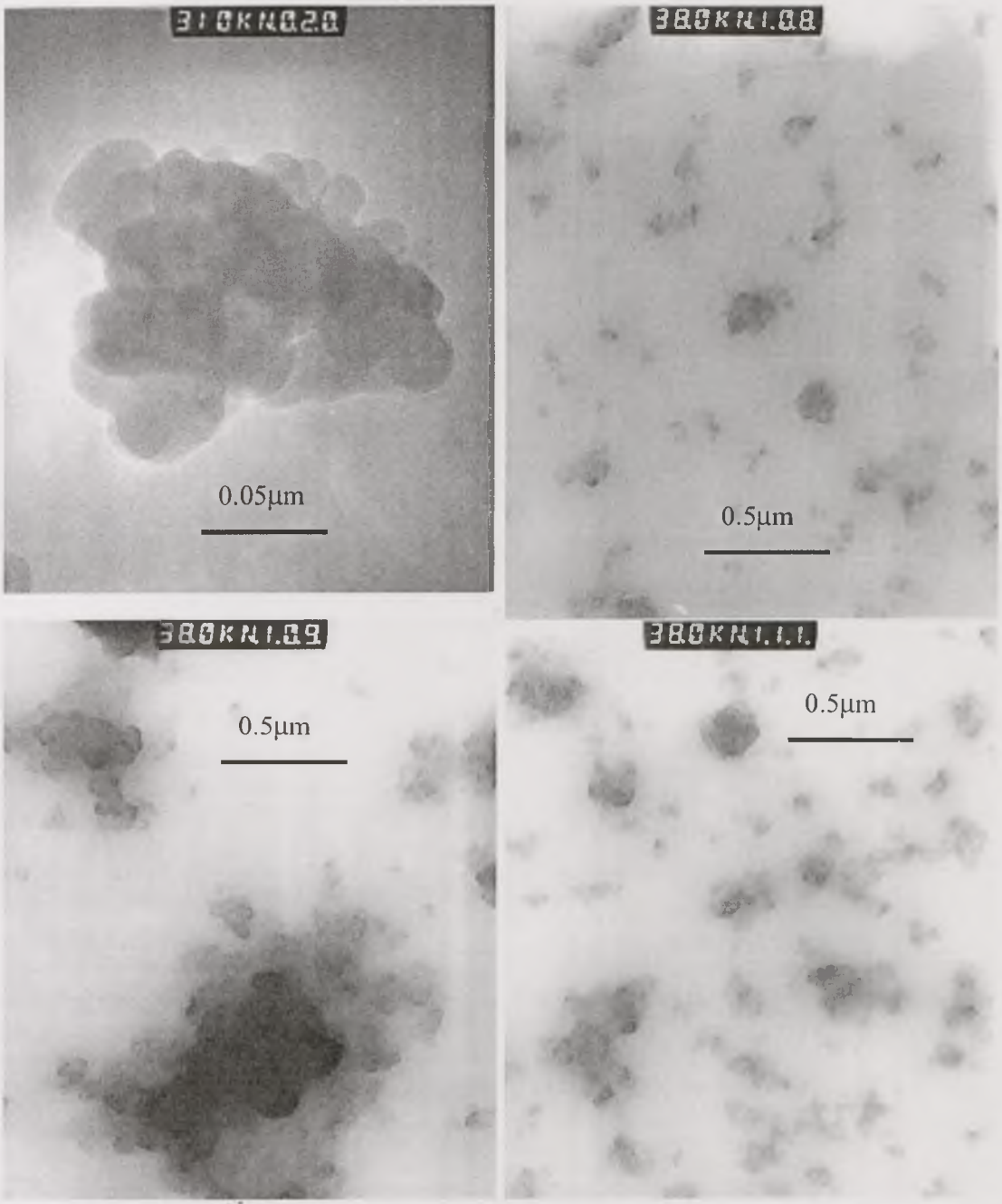

Figure 2.27. TEM images of particles collected on ELPI stages.

The particle size distribution for the agglomerates was built from statistical data of the equivalent circle diameters of nearly 150 individual particles, based on projected area measurements of the low-resolution TEM images. Results are shown in Table 2.5. and Figure 2.28. In addition, projected area data, together with the maximum Feret Diameter and the average diameter of the primary particles, were also used to determine the Fractal Dimension of the agglomerates, assuming a value of $\alpha = 1.09$ in Equation 1.03 (Lee, 2000) and calculating the radius of gyration in Equation 1.04 as $R_g = F_{max}/3$ (Brasil, 1999). The resulting value of $D_f = 1.82$ (Figure

2.29.) was comparable to that of 1.83 found by Lee on a Caterpillar single cylinder diesel engine at 1400rpm - 0% load (Lee, 2000), but lower than the 1.88 for the same engine at 1400rpm - 50% load, which would be the equivalent condition in this work.

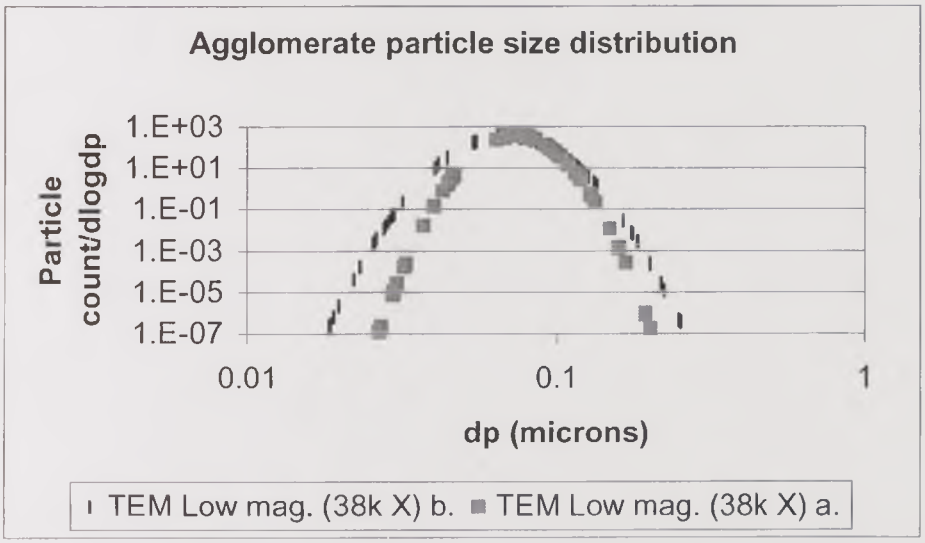

Figure 2.28. Particle size distributions of the agglomerates from low-resolution TEM pictures.

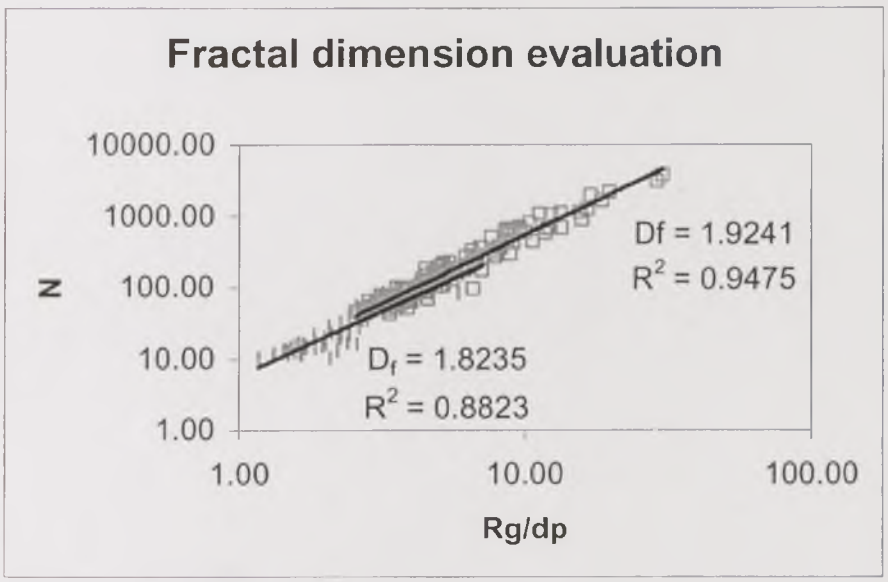

Figure 2.29. Fractal dimension determination from TEM image analysis.

Chapter 3.
Cold Start Particulate Mass Emission and Particle Size Distribution Changes Through a Practical Exhaust System – Preliminary Tests

3.1. Introduction

Preliminary tests were run at Idle, 1500rpm - 10kW and 2250rpm - 15kW, in two sets of tests that differed in the immediate previous history of the engine. Initially, the engine was idling for four hours the day before the test. It was then left to cold soak overnight at 11 to 15°C prior to the cold-start tests the next day. Test series Set 1 in Table 3.1. were carried out with this preconditioning at idle prior to the first test. After each cold-start test at a fixed condition, the engine was shut down and left to cold-soak until the next day. Thus each test in the sequence had a cold start and the previous operational condition of the engine was known. The end test condition of Set 1 tests was 15 kW power output and this was considered to be representative of a low power city driving with the possibility of accumulating deposits. It would leave the exhaust systems with much less deposits than at the idle condition.

The second test sequence, Set 2, was carried out with a 15kW extended test followed by a cold soak overnight at 11 to 15°C, in reverse order from Set 1, ending with the idle condition on the third day. This was designed to start with a 'cleaner' exhaust and end with deposition at idle. Finally, the tests in Set 3 were carried out with the same procedures followed in Set 2, but with the catalyst and adjacent exhaust pipe work cooled overnight, using an external temperature controlled cooling system controlled at 2°C. The coolant was circulated through pipes wrapped around the catalyst and the adjacent exhaust pipe work. The temperature of the catalyst and pipe at the start of the test was 3-5°C. This was designed to enhance particle deposition through the catalyst and delay light off.

3.2. Exhaust Temperature Changes During Cold Start

Exhaust aerosol and system wall temperatures were monitored during cold-start tests at all conditions. Temperatures upstream and downstream of the catalyst are useful to determine the catalyst light off as well as the temperature gradient between the exhaust aerosol and the metal in contact with it, which together with the flow characteristics, determine the thermophoretic deposition potential.

	Uncooled catalyst		Cooled catalyst
	Set 1	Set 2	Set 3
Day 1	Idle	High	High
Day 2	Low	Low	Low
Day 3	High	Idle	Idle

Table 3.1. Test Procedure for the preliminary tests.

3.2.1. Catalyst light-off temperature

Since the oxidation reactions are exothermic, they produce an increase in the gas temperature through the catalyst. Gas temperatures in the catalyst are plotted in Figure 3.1. as a function of time from cold start. Only the first 10 minutes of the test have been plotted, as the temperatures were constant after this period. This is the duration of many short city driving journeys and is 50% of the European passenger car test cycle. Hence, the exhaust warm-up period is significant. The catalyst light-off temperature was approximately 300°C for the tests at 1500rpm - 10kW and 2250rpm - 15kW. During the cold start at Idle, the catalyst was not active for oxidation. The gas temperature in this did not reach above 140°C and the temperature downstream of the catalyst was below the gas temperature upstream. In contrast, the gas temperature increased clearly through the catalyst at 1500rpm - 15kW, showing that the catalyst was active. At 2250rpm - 15kW, however, the temperature difference as the gas passed through the catalyst was very small, indicating that there was a lower energy release by CO and UHC oxidation. As it shall be seen later, the hydrocarbon levels out of the engine at 2250rpm were substantially lower than at 1500rpm, which explained the lower heat produced.

3.2.2. Metal temperature differences and thermophoretic particle-deposition potential

Temperature differences between the exhaust aerosol and the metal in contact with it were used to estimate the particle deposition due to thermophoresis. Aerosol and metal temperatures for the tests are plotted against time in Figures 3.1., 3.2. and 3.3, at the inlet of the catalyst and of each silencer. The temperature difference at all these points increased rapidly during the first minute or two minutes for all conditions, reaching a maximum temperature difference and then decreasing gradually to a fairly constant value. At idle, the maximum temperature difference in the catalyst was around 120°C, and the equilibrium temperature difference around 40 to 60°C. Maximum and equilibrium aerosol-metal temperature differences were

reduced to just 50°C and 20°C respectively at the inlet of the first silencer, and 30°C and 20°C at the inlet of the second silencer, thus reducing substantially the thermophoretic deposition potential, already very low upstream of the catalyst.

At 1500rpm - 10kW, the temperature difference upstream of the catalyst was above 200°C for about one minute, reaching a maximum at 250°C. The equilibrium temperature was around 100°C. Upstream of the first silencer the maximum and equilibrium temperature differences were around 150°C and 70°C respectively, and decreased to 80°C and 50°C at the inlet of the second silencer. The thermophoretic deposition potential was clearly increased from idle conditions, particularly upstream of the catalyst.

Aerosol – metal temperature differences during cold start at 2250rpm - 15kW were not very different from those at 1500rpm - 10kW. A maximum temperature difference of 240°C was reached upstream of the catalyst before two minutes from cold start, decreasing to 50°C - 60°C six minutes later. Maximum and equilibrium temperatures were 150°C and 50°C - 60°C respectively upstream of the first silencer, and 90°C and 35°C respectively downstream of the second silencer.

3.3. Hydrocarbon Emissions During Cold Start

The total hydrocarbon emissions as measured at the sampling point downstream of the oxidation catalyst are shown in Figure 3.4. for the three test conditions of Set 1 and 2 in Table 3.1. Only the first ten minutes from cold start are shown.

3.3.1. Idle

The previous day to the cold-start test at Idle conditions of Set 1, the engine was operated at idle for a period of several hours, so the hydrocarbon-adsorbing zeolite was saturated. This caused a peak in hydrocarbon emissions of around 4000ppm downstream of the catalyst during cold start. The peak was followed by a decrease in hydrocarbon emissions to 1000ppm after one minute, and a subsequent increase due to thermal desorption of hydrocarbons by the zeolite when reaching 150°C, Figure 3.1. The catalyst did not show evidence of reaching the light-off temperature during the Idle test, and hence there was no reduction in the hydrocarbon emissions associated with catalytic oxidation.

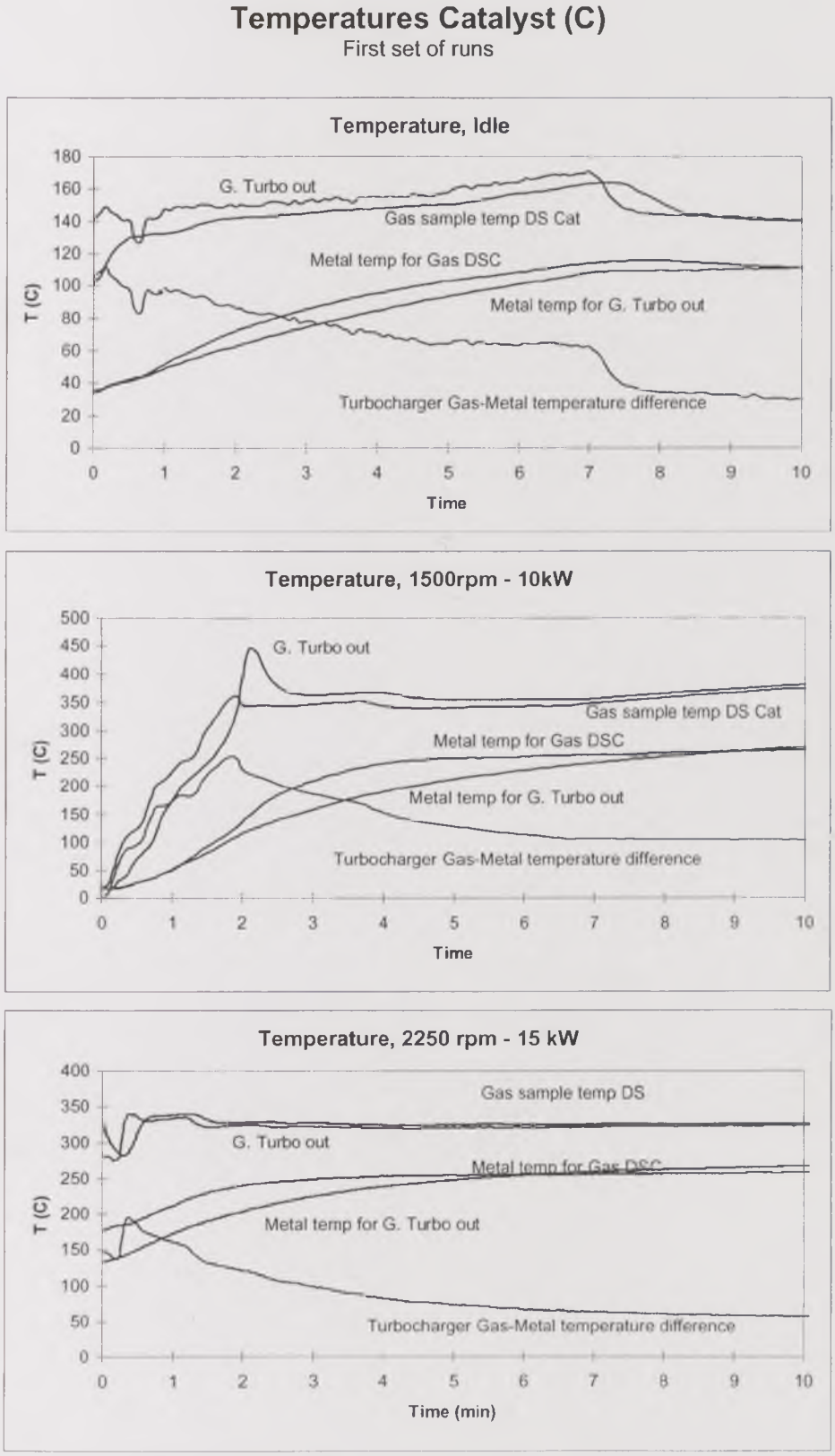

Figure 3.1. Catalyst temperatures during cold start at idle, 1500rpm - 10kW and 2250rpm – 15kW. a) First set.

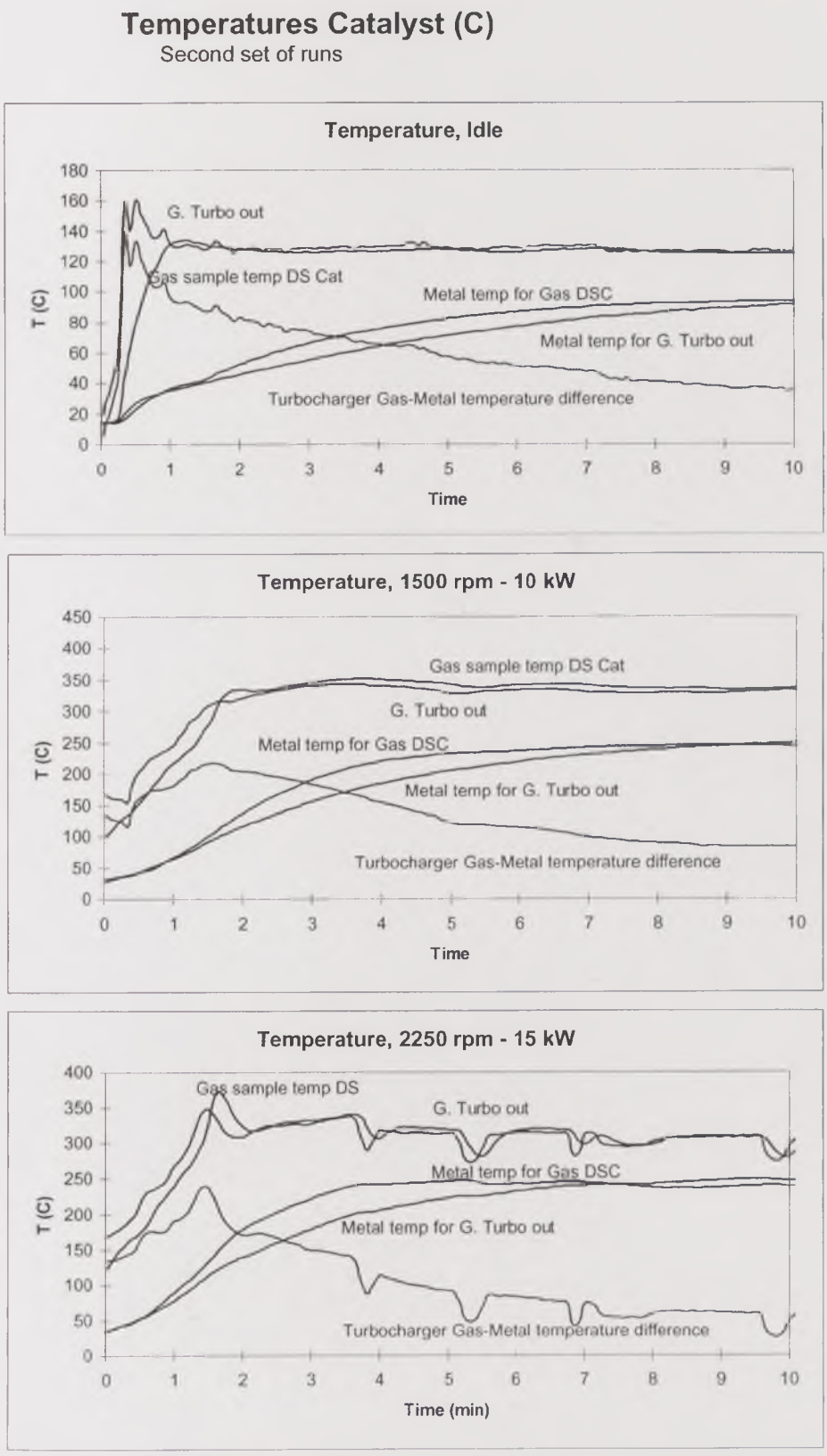

Figure 3.1. Catalyst temperatures during cold start at idle, 1500rpm - 10kW and 2250rpm – 15kW. b) Second set.

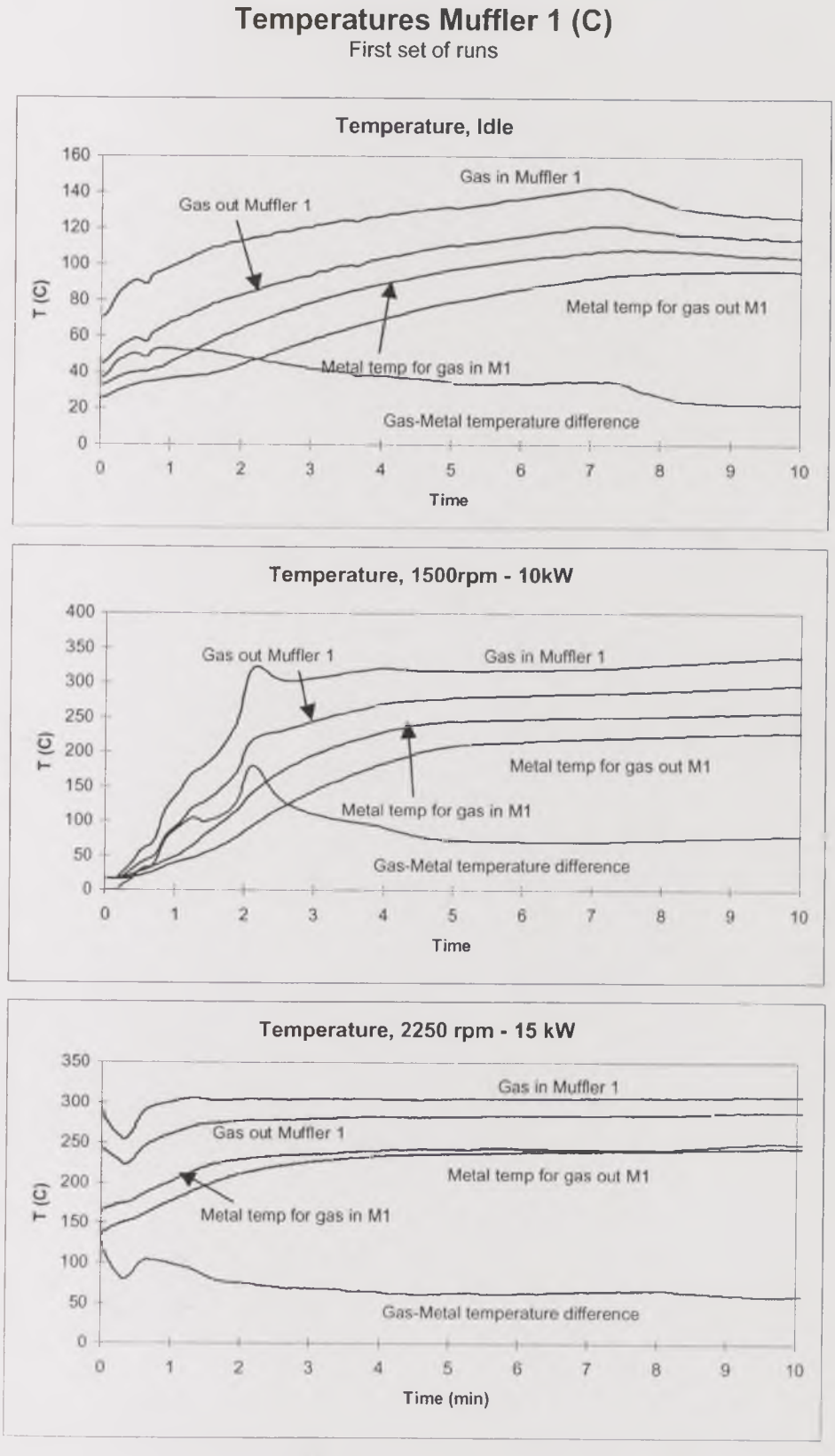

Figure 3.2. Exhaust gas and wall temperatures and temperature differences through the exhaust system. a) First silencer, first set.

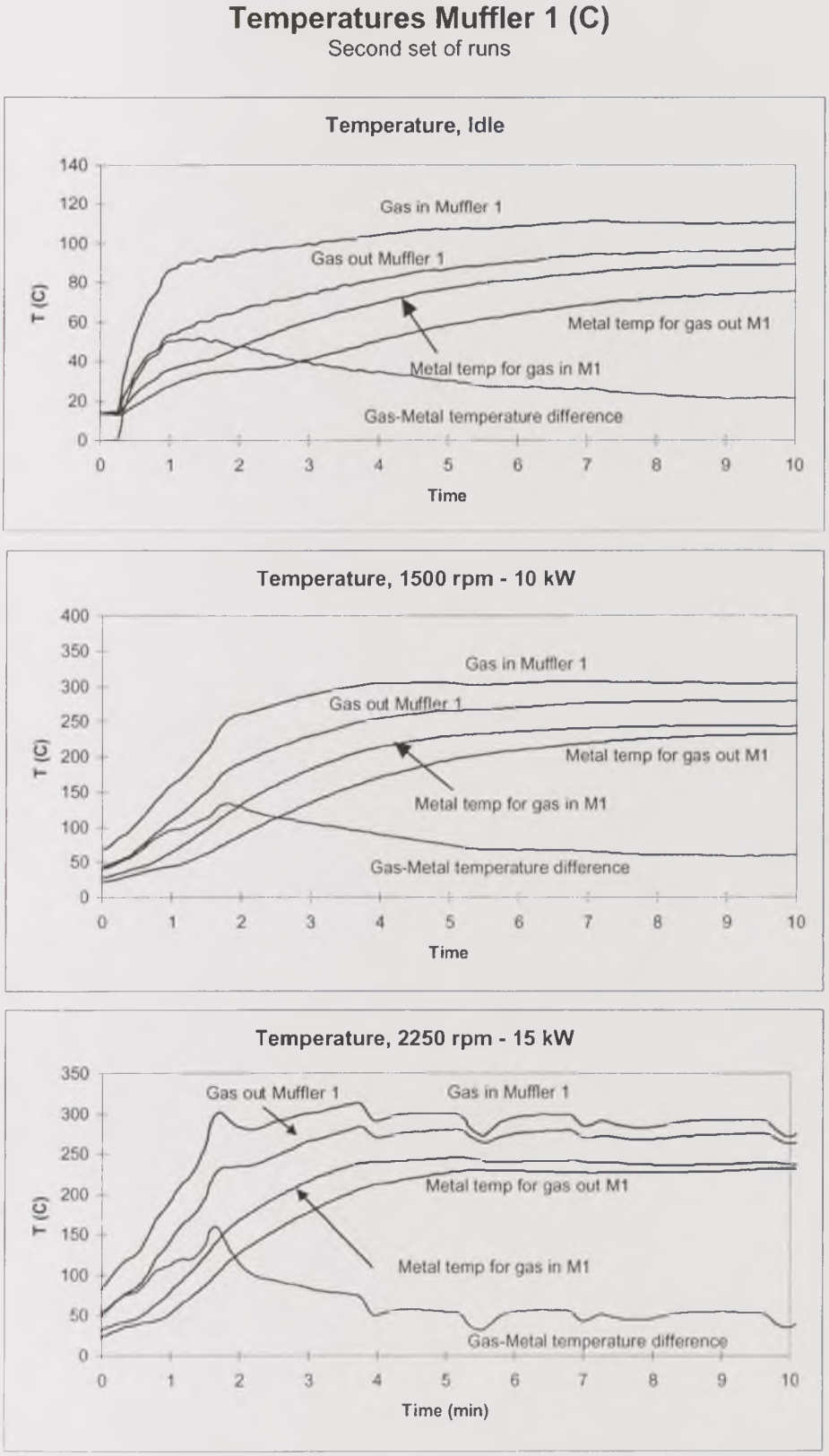

Figure 3.2. Exhaust gas and wall temperatures and temperature differences through the exhaust system. b) First silencer, second set.

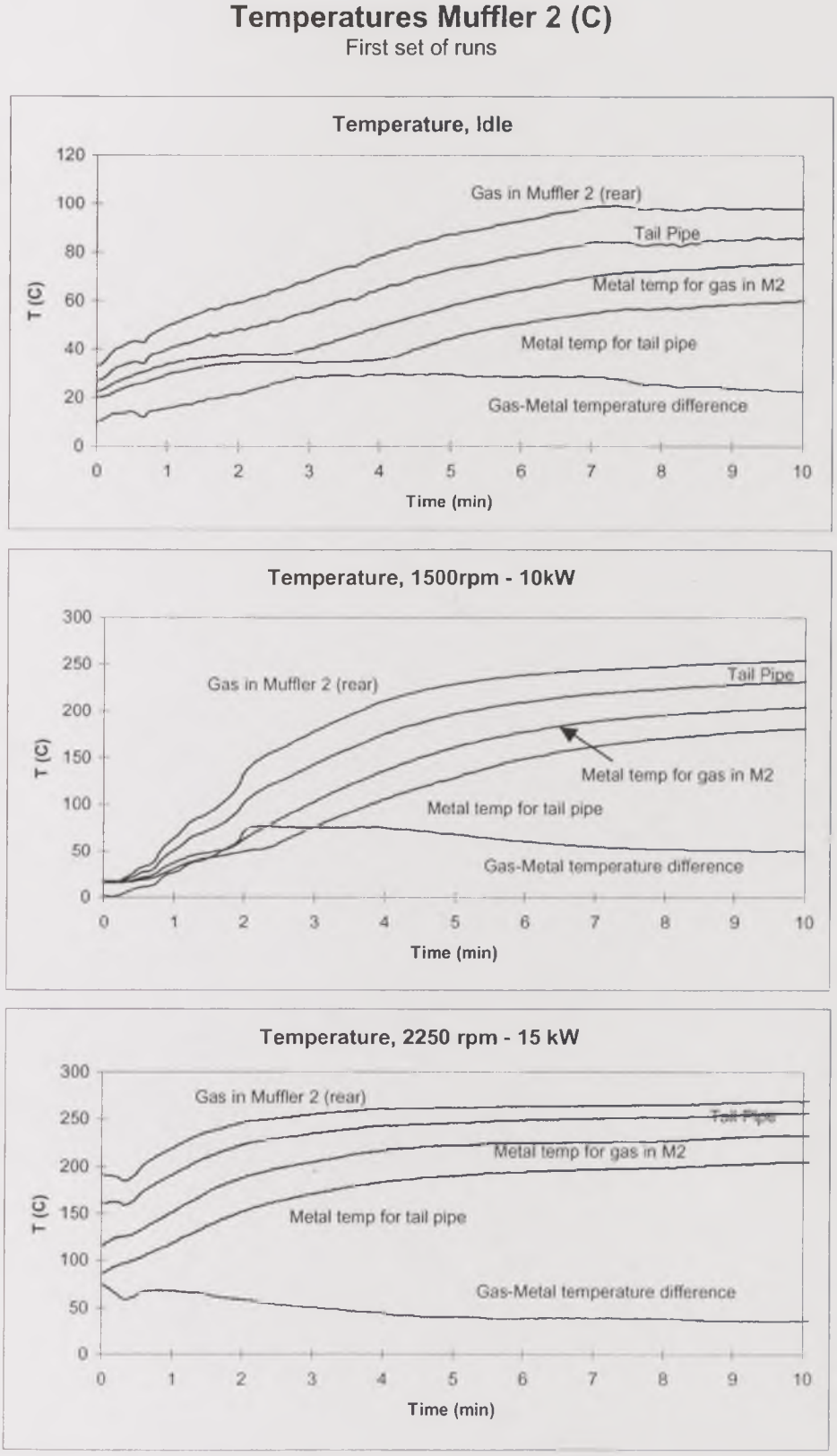

Figure 3.3. Exhaust gas and wall temperatures and temperature differences through the exhaust system. a) Second silencer, first set.

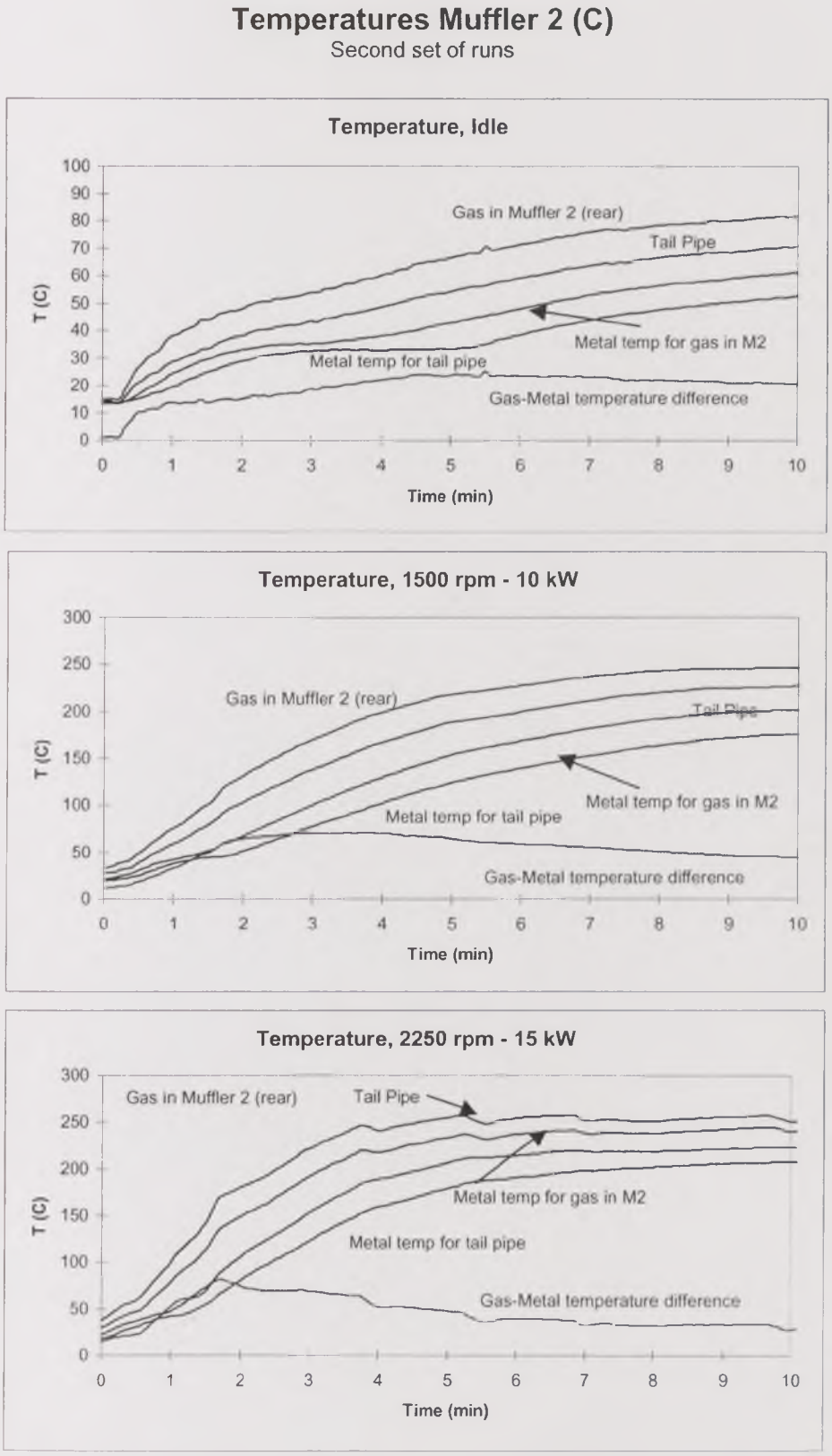

Figure 3.3. Exhaust gas and wall temperatures and temperature differences through the exhaust system. b) Second silencer, second set.

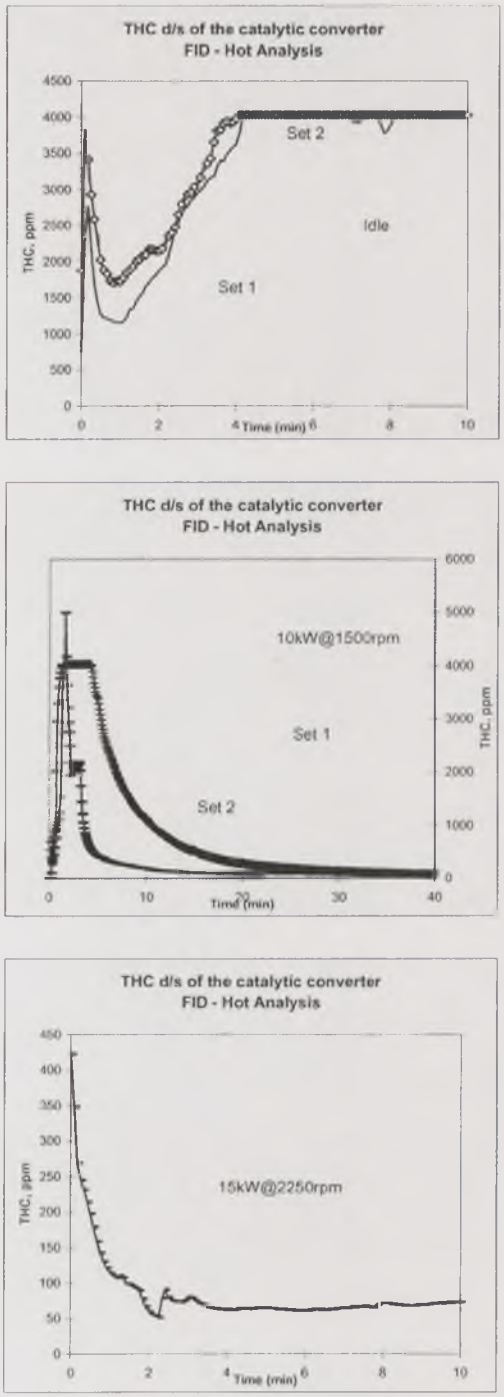

Figure 3.4. Hydrocarbon emissions during cold start measured downstream of the catalyst.

The Set-2 hydrocarbon results were very similar to those in Set 1, but with slightly higher values. The three-day test sequence in Set 2 was to start with the high-load 15kW condition, followed by the 10kW condition, and to end the sequence with the idle test. The 10kW test had a catalyst temperature above 300°C and this was above the hydrocarbon adsorber desorption temperature. Therefore, the

adsorber should have been completely desorbed prior to the test. The hydrocarbon peak during cold start in Set 2 is thus difficult to explain for the cold-start Idle tests in Set 2, as it should have been eliminated by the hydrocarbon adsorber. The zeolite would not have carbon particles deposited on it, as the previous higher temperature test conditions should have 'cleaned' the zeolite. This effect was not seen at Idle, but it was at the 10kW conditions, whose description follows.

3.3.2. 1500rpm - 10kW

At the 10 kW cold-start test of Set 1, despite having been run one day after an adsorber-saturating idle test, the hydrocarbon adsorber showed its effectiveness for the first minute, when the catalyst face temperature was below 200°C. Hydrocarbon emissions were kept under 1000ppm downstream of the catalyst during that period. At the same time, the catalyst heated up rapidly and was above 200°C after the first minute, causing desorption of hydrocarbons from the zeolite during the following four minutes. The hydrocarbon concentration during that period reached 4000ppm. Afterwards, the catalyst controlled the hydrocarbon emissions, decreasing the concentration to 1000ppm by the tenth minute of test. This decreasing trend was kept for the following 15 minutes, down to less than 200ppm.

For the cold-start test at the same condition of Set 2, which was preceded by a 15kW cold-start test, there were no previously-stored hydrocarbons in the adsorber and hence the hydrocarbon desorption peak lasted for a much longer period than for the equivalent test of Set 1. The peak in hydrocarbon emissions, which reached 5000ppm, was rapidly controlled after the catalyst lit off, decreasing to 2000rpm around three minutes from cold start, below 1000ppm before ending the fourth minute, and below 200ppm at ten minutes from the start of the test.

3.3.3. 2250rpm - 15kW

At 15 kW the temperatures rose faster and the cold start hydrocarbon peak was below 500ppm. The catalyst reduced the hydrocarbon emission continuously from start up, as at these conditions the catalyst was above 200°C after just 30s and above 300°C after 90s. After 2 minutes the UHCs were well below 100ppm and the oxidation catalyst was at its most effective condition.

3.4. Filter Mass Concentration Changes Through the Exhaust System During Cold Start

3.4.1. Particulate Concentrations at Different Positions in the Exhaust Pipe System

The particulate mass emissions expressed as an Emission Index, g/kg fuel, against time from cold start are shown at the four simultaneous sampling positions in the exhaust in Figure 3.5., for the three test conditions of Sets 1 and 2. These results as emission rate in g/hr are shown in Figure 3.6. The data points are shown for the middle of the time period for which the filter papers were sampled over.

These results show that, for all of the tests, there was considerable difference in the particulate emissions among the four sample positions. The differences changed with time, being greatest at the first particulate sample, this is, during the first two or three minutes from cold start, when the most important disturbance due to changes in speed and acceleration occurred.

Owing to the effect of the silencers, the Emission Index measured at the sampling point downstream of the catalyst differed from that that at the tailpipe. At all conditions tested, the tailpipe emissions were higher than those downstream of the catalyst, which indicated a particulate blow-out from the silencers section. Particulates re-entrained from the first silencer and then a fraction of them deposited in the second silencer. This problem was greatest for the Set 2 idle results, where the exhaust had been operated at the 15 and 10 kW conditions prior to the test and should have been relatively free of deposits. The particulate emissions downstream of the catalyst were extremely low, at approximately 1 g/kg of fuel or 2 g/hr. However, particles already in the exhaust were still entrained by the low flow velocities at Idle with high particulate emissions upstream of the second silencer and lower emissions at the tailpipe. This indicated that deposition of particles removed from the first silencer occurred in the second silencer. This movement of particulates from one silencer to the other was also apparent at the 10kW condition.

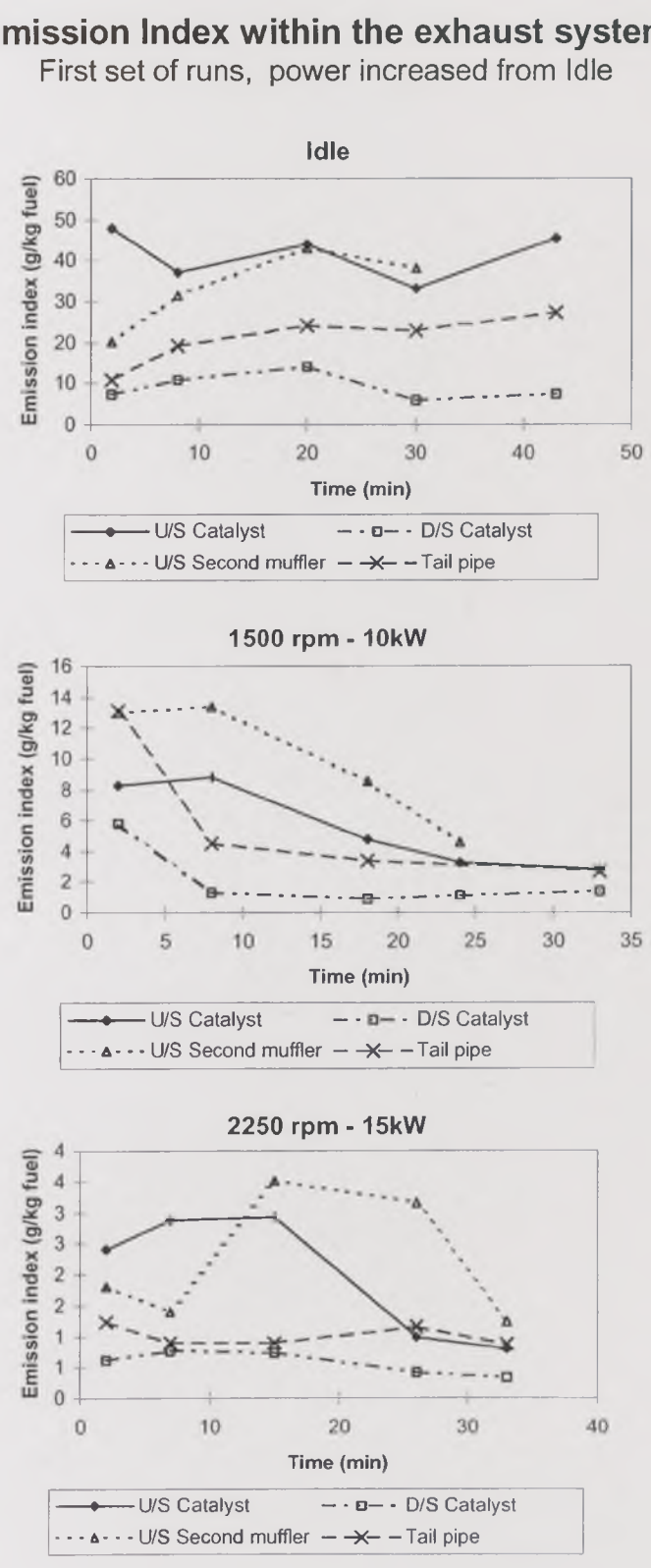

Figure 3.5. Emission Index during cold start through the exhaust system. a) First set.

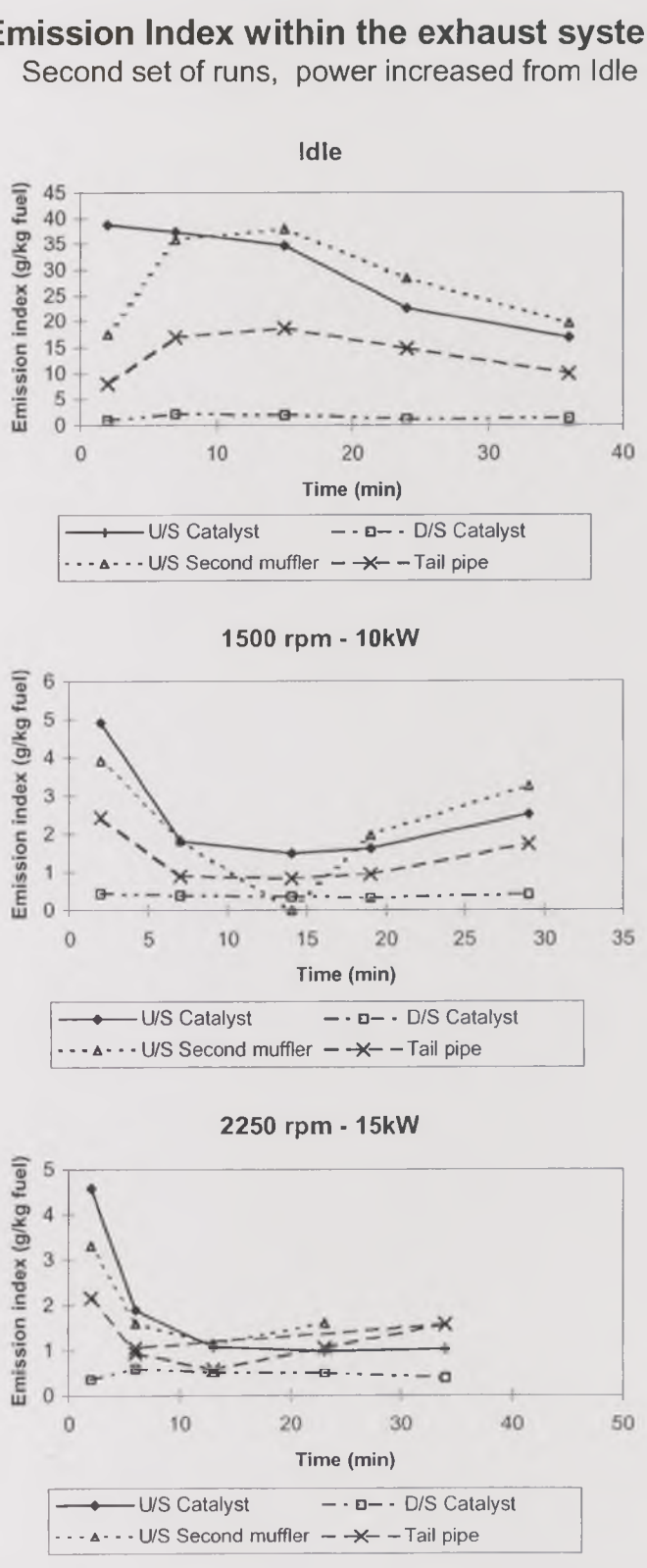

Figure 3.5. Emission Index during cold start through the exhaust system. b) Second set.

The same events occurred for the 15kW condition for the Set 1 tests, which had started with the Idle test and the engine preconditioned at idle. For the Set 2 tests that started at 15 kW, with preconditioning at 15kW, the results were different. The first particulate samples showed evidence of particulate deposition under cold start conditions. However, after 30 minutes the tailpipe emissions were the highest and greater than those emerging from the engine, upstream of the catalyst. This is direct evidence of exhaust system blow-out.

The largest particulate emissions rate over the test period occurred for Idle, which also had the greatest particulate deposition rate in the second silencer. It was these high emission rates at Idle that led to the choice of long periods of engine idle as a means of exposing the exhaust system to high soot loadings. This did not have a direct equivalence to real world driving, but enabled deposits in the exhaust to be established the day prior to the tests. The preconditioning procedure was practical for laboratory conditions and was thus adopted as a repeatable method of accumulating deposits in an exhaust pipe on a short timescale. It would reproduce the deposition achieved by driving at low-power, urban driving conditions for about a week, assuming a pattern of 1-2 driving hours a day for five days. As an example, it is reasonable to think of this as the working week, which would be followed by a weekend when the driver would take a motorway to drive to the countryside, blowing out a fraction of the deposits when driving at higher speed and power.

At Idle, 20-30g/hr of particulate would be deposited in the exhaust with about 100 g stored over the 4-hour idle preconditioning. At 15 kW this was reduced to 5 g/hr to 10 g/hr. An average exhaust deposition rate of 10 g/hr is reasonable to assume for the low-power conditions used in this work. If a vehicle were used at these conditions for two hours per day and five days per week then 100g per week would accumulate in the exhaust. This is a significant deposit level and if this is blown out in one fast acceleration then a large soot cloud will be produced. It was shown above that for a low-emission engine, which will meet Euro 4 passenger car regulations, 4kg of particulates would be emitted in 160,000km. Hence, the 100g accumulated by storage in the exhaust in about a week would represent the emissions of a low-emission vehicle for 4,000km. In this way, this work succeeded in reproducing in the laboratory the events that have been observed in real world driving.

3.4.2. Particulate Storage and Blow-out in the Exhaust Downstream of the Catalyst

Particulate storage and blow-out results are expressed as a mass loss from the aerosol between two given sampling positions. If the result is positive, then

particulate loss or storage between the sampling positions has occurred. If it is negative, then there has been a particulate gain or blow-out between them.

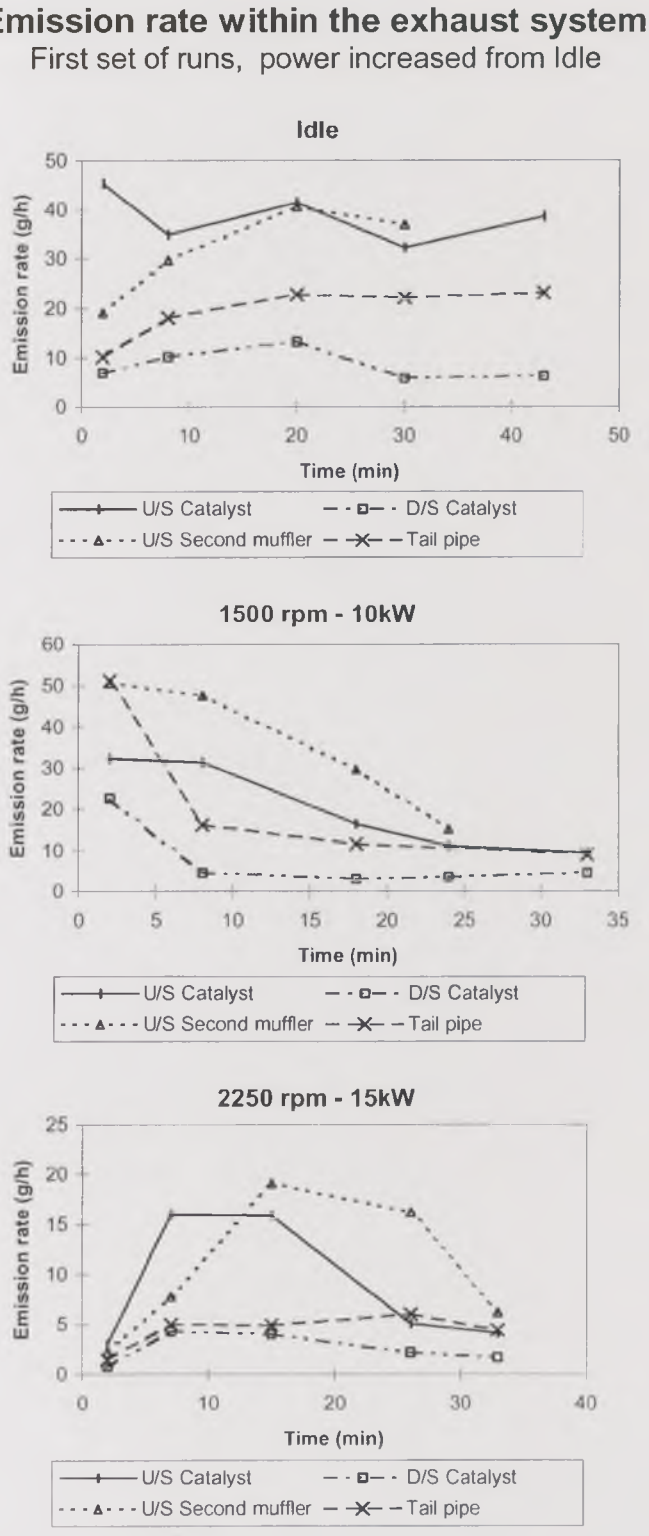

Figure 3.6. Emission rate during cold start through the exhaust system. a) First set.

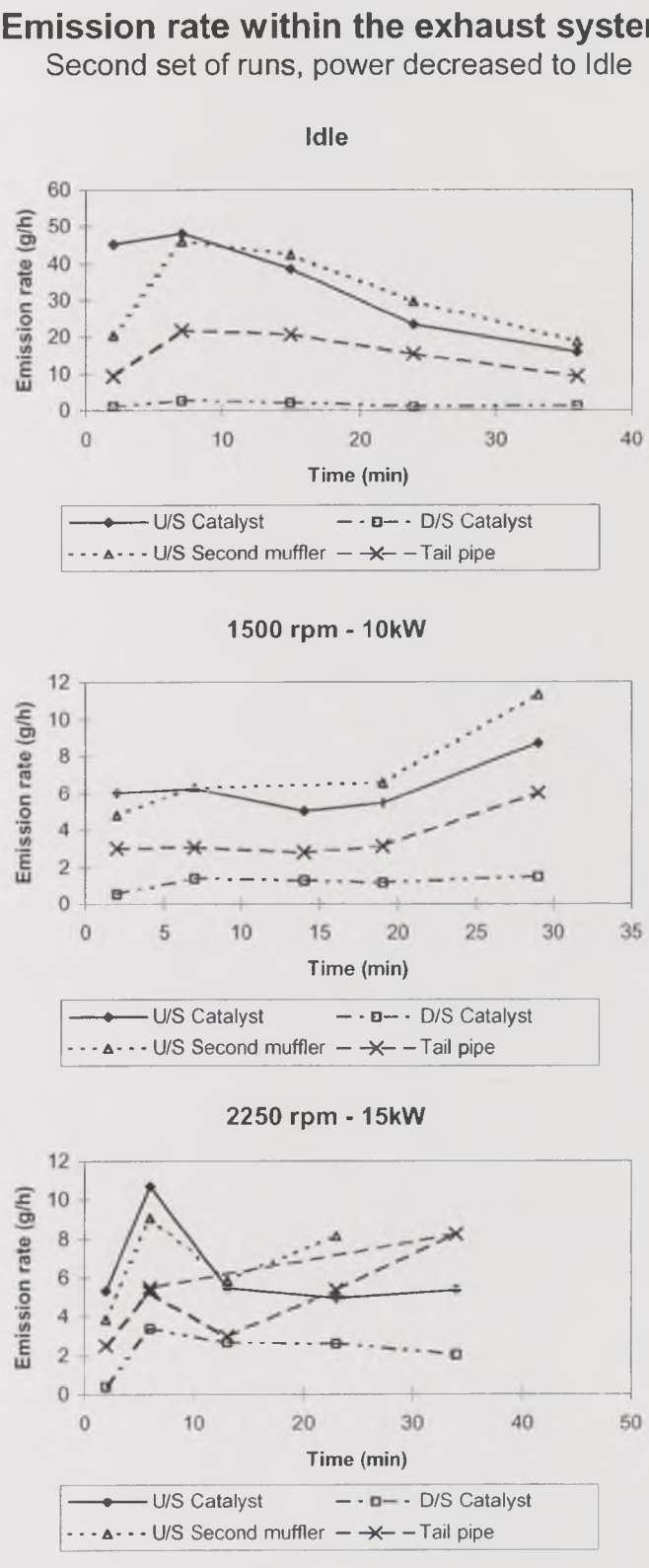

Figure 3.6. Emission rate during cold start through the exhaust system. b) Second set.

The particulate mass blow-out between downstream of the catalyst to downstream of the first silencer and then between that point and downstream of the second silencer are shown in Figures 3.7. (Idle), 3.8. (1500rpm – 10kW) and 3.9. (2250rpm – 15kW) for the three sets of tests and the three test conditions. The results are expressed as a) Emission Index, g/kg of fuel, and b) the equivalent results as Emission rate in g/hr. The results show that, in most of the conditions tested, there was particulate blow-out from the first silencer and deposition in the second silencer. The particulate blow-out from the first silencer was greater than the deposition in the second silencer and was a significant fraction of the tailpipe emissions. This is shown clearly in Figure 3.10., which plot the net particulate blow-out from the exhaust downstream of the catalyst as a percentage of the tailpipe emissions. Also plotted is the particulate deposition in the second silencer as a percentage of the tailpipe emissions.

At idle, Figure 3.7. and 3.10. show that deposition occurred across the second silencer for Sets 1 and 2 tests and this was at a peak rate of 20g/kg of fuel or about 20 g/hr. The maximum deposition rate occurred after 20 minutes. At the initial cold start most of the particles deposited on the catalyst and the movement of particles from one silencer to the other was about half the peak deposition rate. Overall, from downstream of the catalyst to the tailpipe there was a net blow-out of particulate material. This was due to a large blow-out from the first silencer, much of which was deposited in the downstream silencer and the rest was emitted from the tailpipe.

The particles emitted from the tailpipe that originated in the deposits in the first silencer were 30% of the tailpipe emissions after 2 minutes, and this fraction increased to 70% after 30 - 45 minutes. Clearly the existing deposits in the exhaust were a major factor in the tailpipe emissions at cold start idle conditions.

For the tests of Set 2, for which the engine had a previous operational history of 10 and 15 kW tests prior to the idle test, the first silencer exhaust deposition was at a higher rate than for Set 1 after 8 minutes from cold start. The deposition peaked at 35 g/kg after 8-15 minutes, compared with 30 minutes to reach this deposition rate in the Set-1 tests. These results showed that the first silencer was releasing more particulate material than that being deposited in the second silencer. The net blow-out of particulates from the exhaust downstream of the catalyst, as a percentage of the tailpipe emissions, was approximately 90% after 7 minutes and close to 100% after 15 minutes. The tailpipe emissions were close to 100% and they were all generated by the first silencer blow-out throughout the 35 minute test. Consequently, it may be concluded that the 15 kW and 10 kW conditions prior to this idle test of Set 2 was not sufficient to blow out all of the exhaust deposited material.

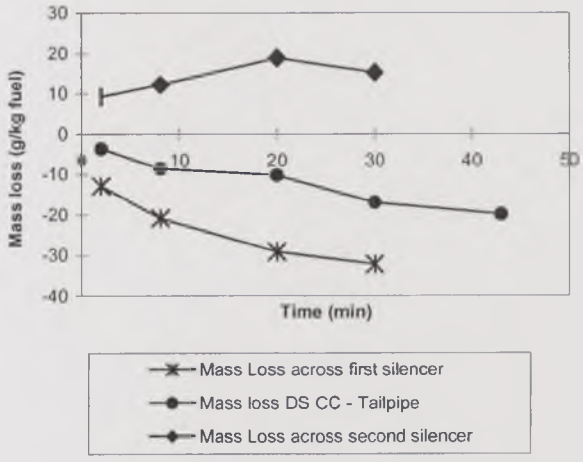

Idle, first set.

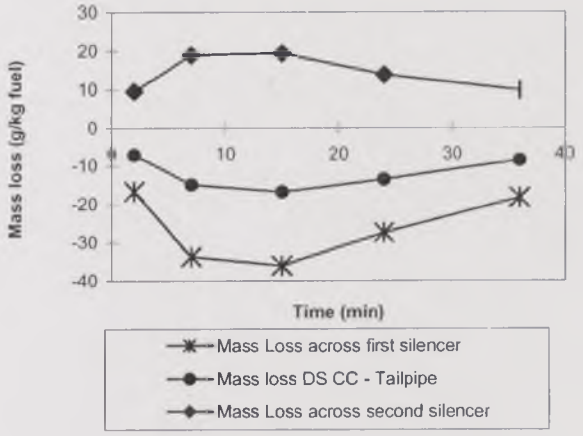

Idle, second set.

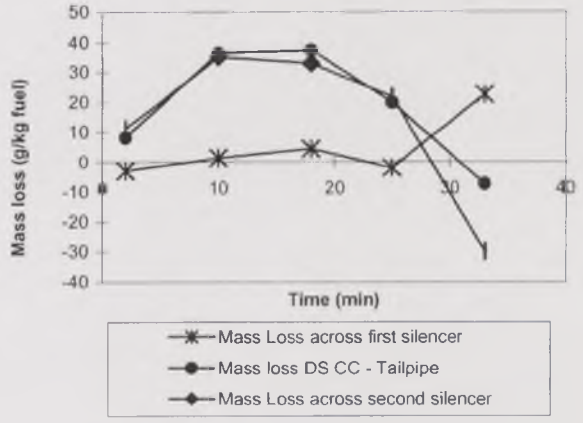

Idle, cooled exhaust.

Figure 3.7. Mass loss in the exhaust system section downstream of the catalyst during cold start at idle. a) Emission Index.

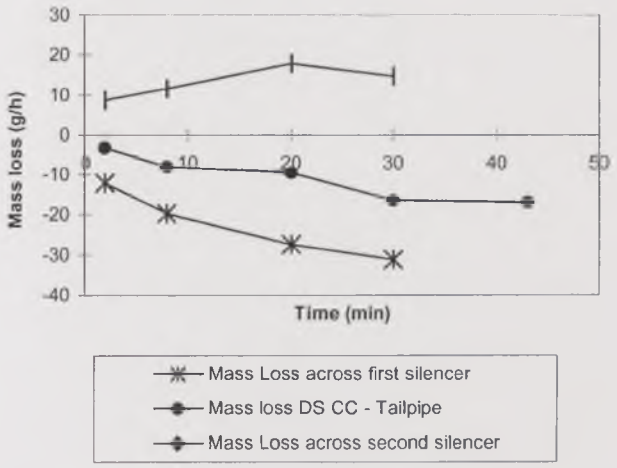

Idle, first set.

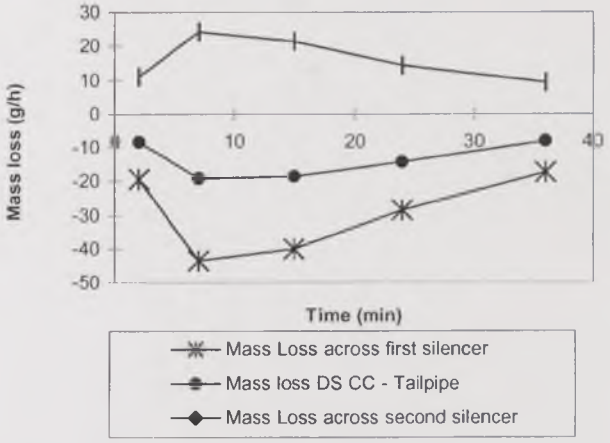

Idle, second set.

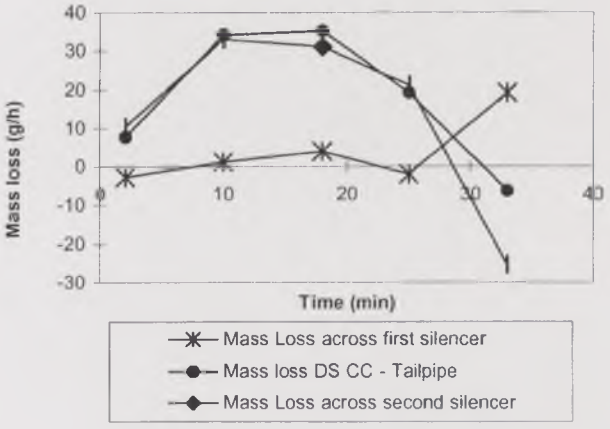

Idle, cooled exhaust.

Figure 3.7. Mass loss in the exhaust system section downstream of the catalyst during cold start at idle. b) Emission rate.

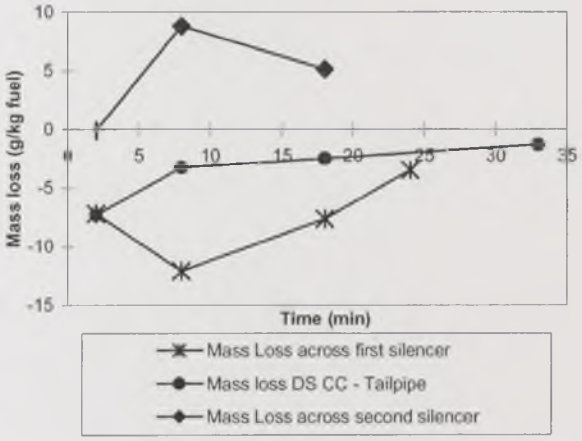

1500 rpm, 10 kW, first set.

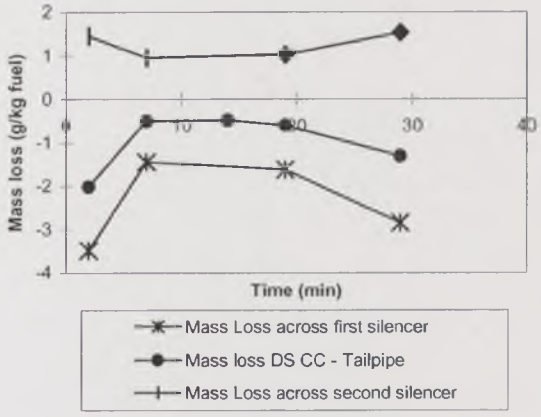

1500 rpm, 10 kW, second set.

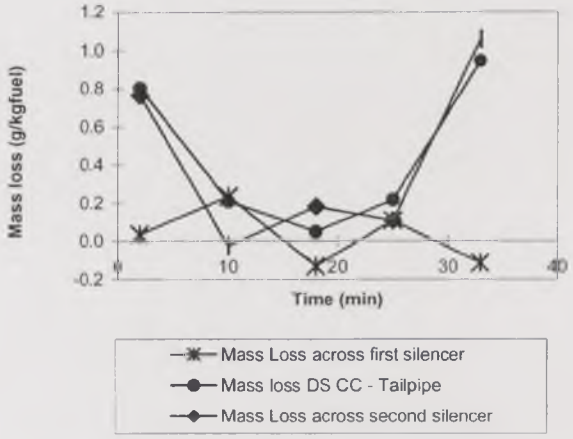

1500 rpm, 10 kW, cooled exhaust.

Figure 3.8. Mass loss in the exhaust system section downstream of the catalyst during cold start at 1500rpm – 10kW. a) Emission Index.

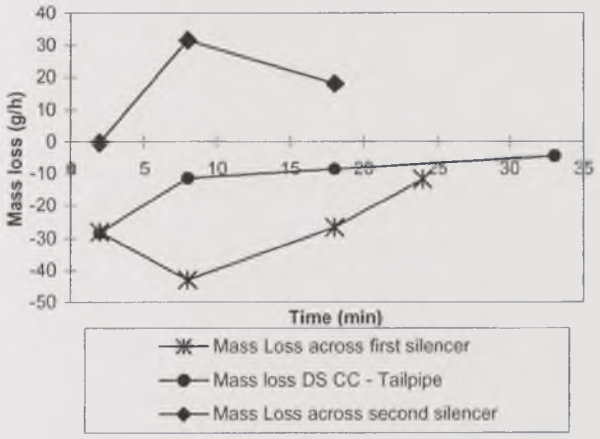

1500 rpm, 10 kW, first set.

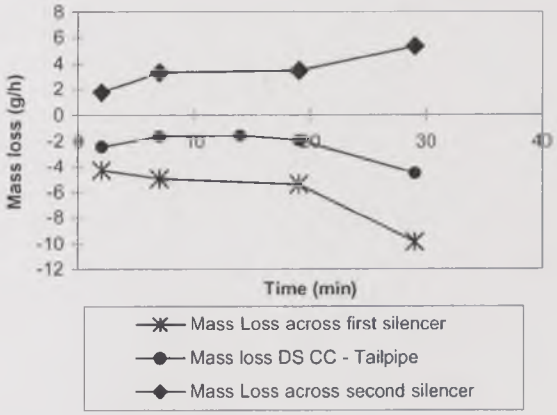

1500 rpm, 10 kW, second set.

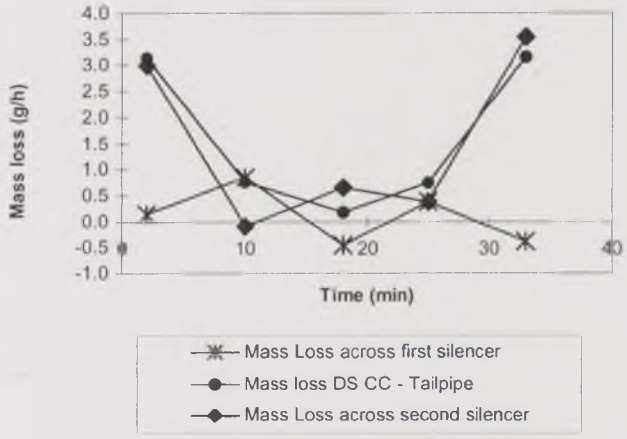

1500 rpm, 10 kW, cooled exhaust.

Figure 3.8. Mass loss in the exhaust system section downstream of the catalyst during cold start at 1500rpm – 10kW. b) Emission rate.

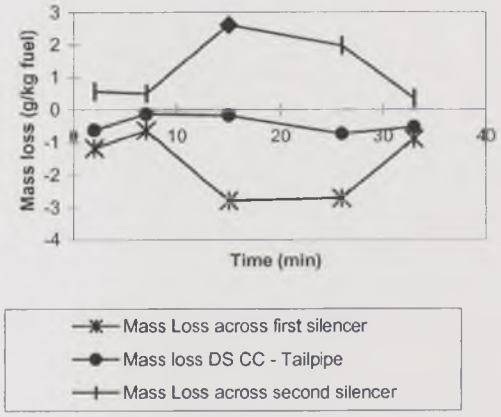

2250 rpm, 15 kW, first set.

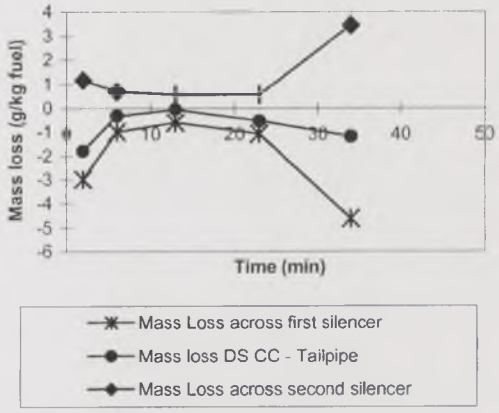

2250 rpm, 15 kW, second set.

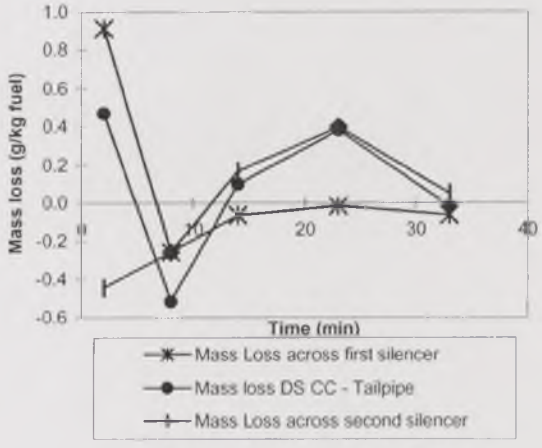

2250 rpm, 15 kW, cooled exhaust.

Figure 3.9. Mass loss in the exhaust system section downstream of the catalyst during cold start at 2250rpm – 15kW. a) Emission Index.

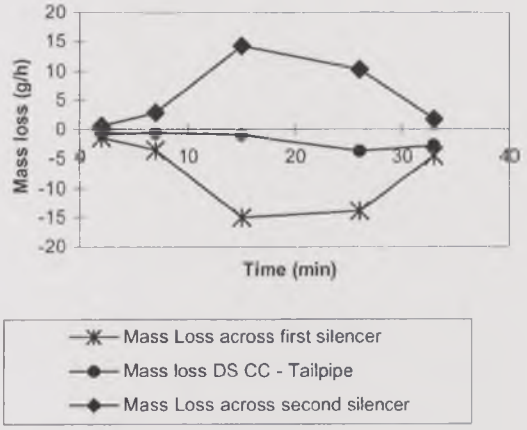

2250 rpm, 15 kW, first set.

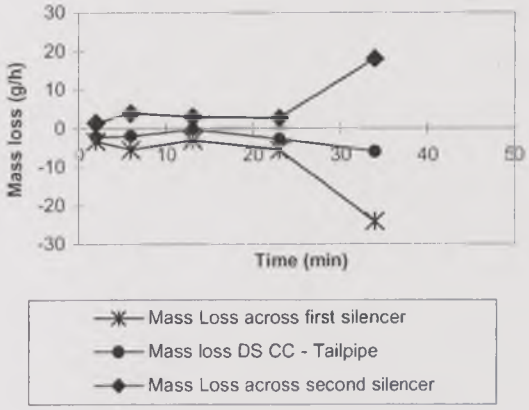

2250 rpm, 15 kW, second set.

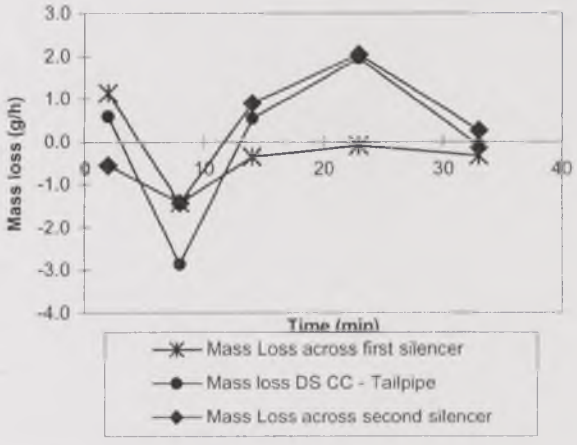

2250 rpm, 15 kW, cooled exhaust.

Figure 3.9. Mass loss in the exhaust system section downstream of the catalyst during cold start at 2250rpm – 15kW. b) Emission rate.

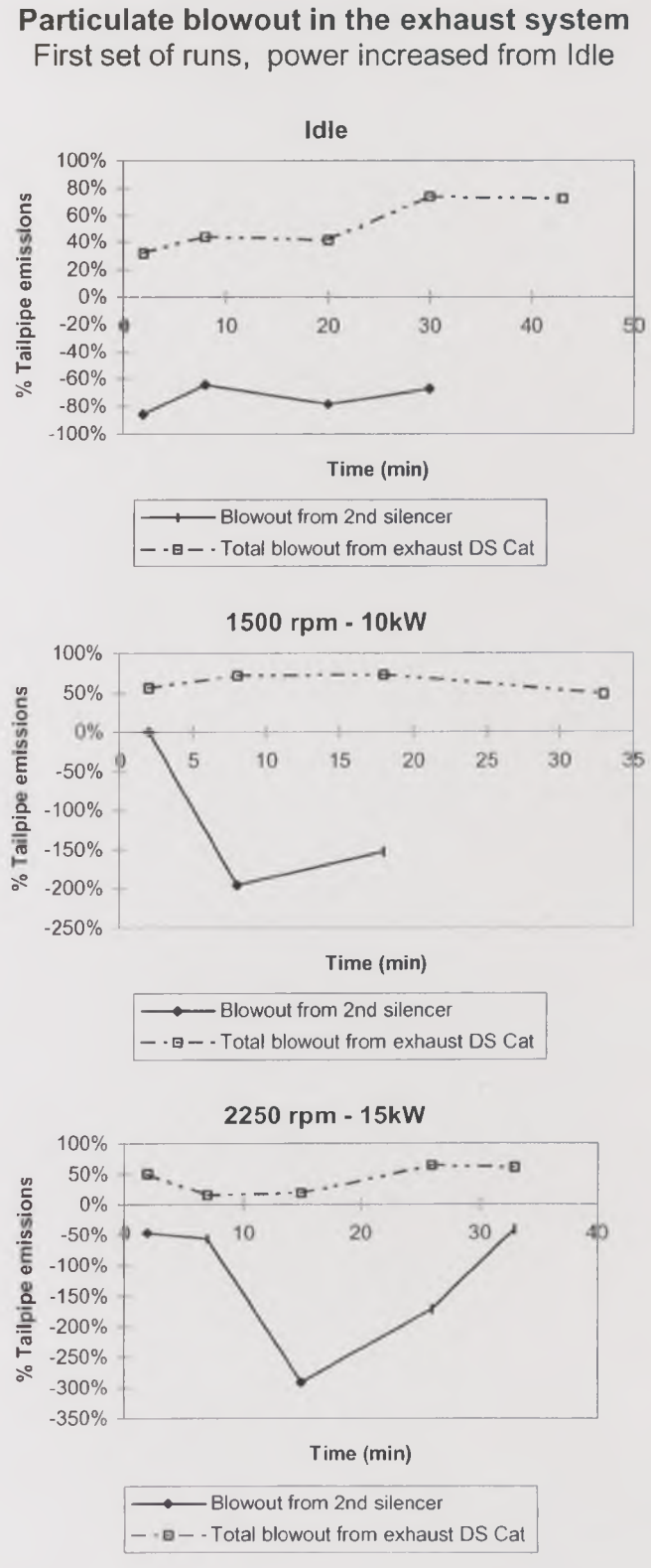

Figure 3.10. Particulate blow-out from the exhaust system section downstream of the catalyst during cold start as a percentage of the tailpipe emissions. a) First set.

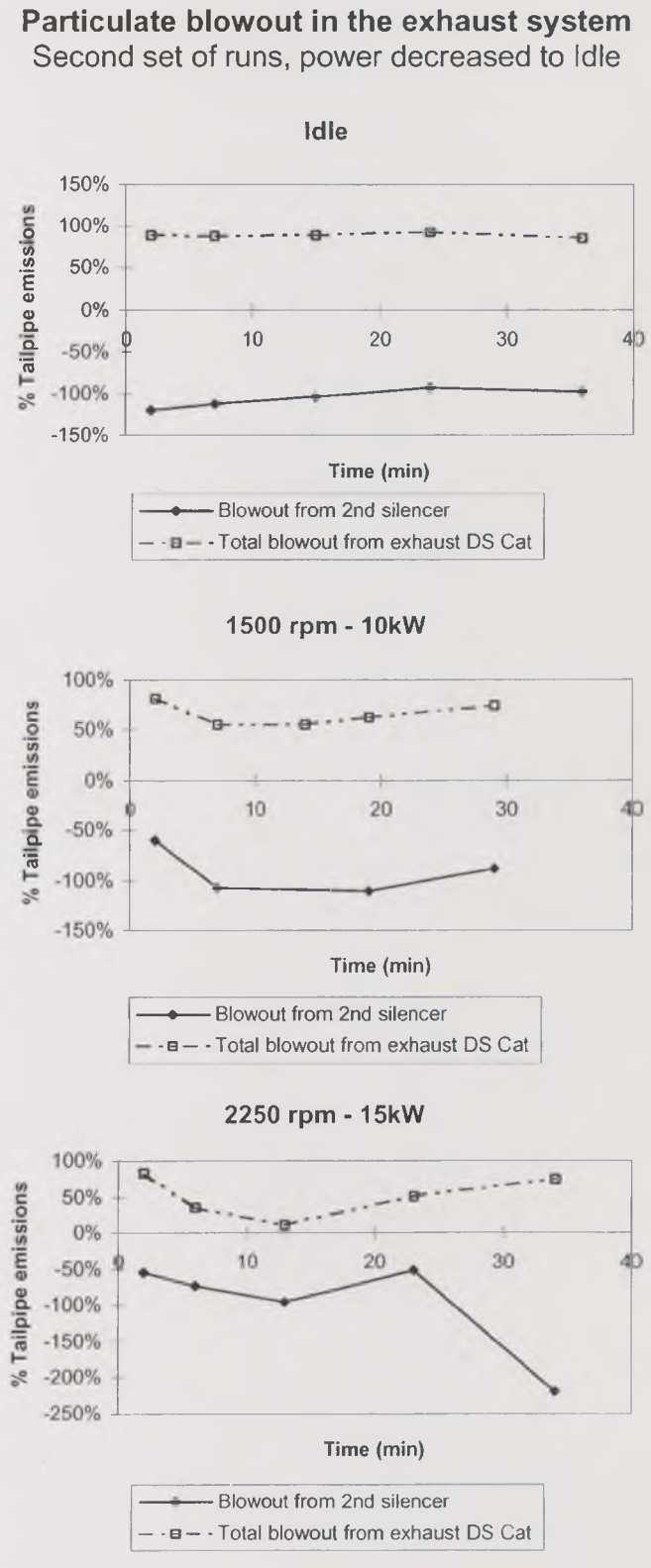

Figure 3.10. Particulate blow-out from the exhaust system section downstream of the catalyst during cold start as a percentage of the tailpipe emissions. b) Second set.

For the cooled catalyst and associated exhaust pipe, there was no blow-out of particles in the first silencer, and there was the highest deposition in the second silencer, 35 g/kg. Also there was net deposition in the exhaust downstream of the catalyst. This was a substantially different result to that at the other Idle conditions. The whole exhaust was not cooled, only the catalyst region and hence a specific influence of catalyst temperature was not expected to influence the results. It is possible that the change in behaviour of the exhaust in terms of the location of the particulate storage was due to the differences in the previous history of the use of the engine. The tests of Set 3, although carried out in the same order as Set 2, had an 8-day prior test sequence of Idle - 10kW - 15kW - 15kW - 10kW - Idle - 15kW - 10kW compared with the 5 day prior test sequence of Idle - 10kW - 15kW - 15kW - 10kW - Idle for the Set-2 Idle tests. It will be shown below that at 15kW, deposits were moved from the first silencer to the second silencer and this could have been the cause of the blow-out of the first silencer and the filling of the second silencer. This then left the second silencer with the deposits that were blown out in the final Set-3 Idle test.

At the 10kW condition, Figure 3.8. shows that deposition rates were much lower than at Idle. However, the trends of the results were similar, with deposition in the second silencer and blow-out of particles by the first silencer. The deposition rate in the second silencer after 7-8 minutes was about 3 g/hr for Set 2 and 35 g/hr for Set 1. The associated blow-out of particles by the first silencer was 5 g/hr and 45 g/hr for Set 2 and 1 tests respectively. This produced net particulate blow-out rates, from the exhaust downstream of the catalyst, of 2 g/hr and 10 g/hr respectively.

For the test at 10kW of Set 1, the net blow-out of particulates from the first silencer that was not deposited in the second silencer was about 50% of the tailpipe emissions after 2 minutes. This increased to 75% after 8 minutes and was then reduced to 50% after 18-33 minutes. Thus, the exhaust deposits had a major role in determining the tailpipe emissions, just as they did at Idle. For the Set-2 results the exhaust pipe deposits had a greater role in the tailpipe emissions, accounting for 80% of the tailpipe emissions after 2 minutes. This was reduced to 50% after 7 minutes and then increased again to 70% after 30 minutes.

For the Set 3 tests with the catalyst cooled to about 3°C, there was little deposition or blow-out from the first silencer. At the first cold-start sample, there was about 0.8g/kg fuel deposition in the second silencer, but this was rapidly reduced to negligible amounts by the time of the second particulate sample at 10 minutes. These results showed that a cold catalyst appears to influence the particulate deposition downstream of the catalyst in a way that decreases the

deposition in the exhaust system. This may be because at the lower catalyst temperature the hydrocarbon adsorber is more efficient and this produces a lower particulate SOF. This would then make the particles less sticky and hence with a reduced tendency to become part of the deposition layer of the exhaust pipe surfaces.

At the 15kW condition, Figure 3.9., the mass storage and blow-out rates were lower than those at 10kW. For Set 1 tests, the initial blow-out rate was 25% of the storage rate in the catalytic converter. This decreased to nearly zero over the whole exhaust downstream of the catalyst, between 5 and 15 minutes after the cold start. Subsequently there was a small increase in the overall blow-out rate over the exhaust pipe length downstream of the catalyst. However, there was a large blow-out of particulates from the first silencer and deposition in the second and the two rates were very similar, which was why the overall storage was low. This had a greater effect in the first few minutes after the cold start than at 10kW. The net blow-out of particulates from the exhaust system was a lower proportion of the exhaust tailpipe emissions than at 10kW. However, the 15kW condition was not a sufficiently high exhaust velocity to clear out the exhaust, but it was very effective at moving particles from the upstream silencer to the downstream.

The Set-2 tests at 15kW had similar results to those of Set 1. Higher initial rates of storage in the second silencer and blow-out from the first silencer occurred in the first five minutes and after 35 minutes. Between 5 and 25 minutes the movement of particulates in the exhaust was less than 1 g/kg. Over all the exhaust, after the catalyst to the tailpipe, there was a net blow-out of particulates that averaged 1 g/kg. This was a very large fraction of the tailpipe emissions. In the first 5 minutes 90% of the tailpipe emissions were accounted for by the blow-out of particulates from the exhaust. The lowest overall exhaust blow-out rate occurred at 13 minutes and this coincided with the minimum tailpipe emissions. However, the exhaust was undergoing mass deposition in the second silencer during this time and this was then followed by a blow-out at 35 minutes from the first silencer, not all of which was deposited in the second silencer. This was responsible for the increase in the tailpipe emissions at 35 minutes.

With a pre-cooled catalyst and connecting exhaust pipe at 15kW, the particulate storage and blow-out in the exhaust system was relatively small. Most of the deposition occurred across the catalyst. However, in the first 3 minutes there was a large mass deposition in the first silencer but a mass blow-out from the second silencer out of the tailpipe. This was followed by a mass blow-out from both silencers after 8 minutes. The first silencer then had no further blow-out or

deposition up to 33 minutes. However, there was a significant deposition in the second, cooler silencer over the period 10-25 minutes.

3.4.3. Particulate Removal Efficiency of the Diesel Oxidation Catalyst with Hydrocarbon Adsorber

Particulate matter concentration can be reduced by the DOC with hydrocarbon adsorber in these ways:

- Storing particulates deposited on its walls by thermophoresis, diffusion or inertial deposition.
- Adsorbing hydrocarbons from particles in its zeolite component during cold start and cold operation of the engine.
- Oxidizing hydrocarbons that are adsorbed on the carbon cores of the particles by its catalytically active component, Pt, during hot operation.
- Oxidizing gaseous hydrocarbons that could get adsorbed on the particles due to cooling.

Combined mechanisms of deposition, adsorption and oxidation all contribute to the catalyst particle removal efficiency. As a combined unit, the catalyst efficiency is thus defined as the fraction of particulate matter at the engine outlet that does not penetrate the catalyst due to those processes. An additional potential effect of the oxidation catalyst, as mentioned in the previous chapter, would be the generation of new particles by $H_2SO_4 \cdot H_2O$ nucleation, but since the sulphur content of the fuel used is so low, this contribution is negligible. These particle-removal catalyst efficiency results are shown in Figure 3.11.

3.4.3.1. Idle

During cold start at Idle with the catalyst starting at ambient temperature, the catalyst efficiency was over 70% in the first set of tests and over 90% in the second set. There was little dependence of the efficiency on time from the cold start, indicating a good retention of particles by the hydrocarbon adsorber during cold start. For 35 minutes there was no evidence that the particulate storage capacity of the catalyst had been exhausted. The particle storage must be due to surface deposition on the very large surface area of the catalyst, under conditions where the catalyst is not hot enough to oxidise hydrocarbons.

A different result was found when the catalyst temperature was 5-8°C when the test started. The catalyst efficiency for storing and oxidising particulates was only 50% after 2 minutes, much lower than for the Sets 1 and 2 test sequences. Subsequently the efficiency was reduced to zero for 10-20 minutes after the cold

start and then returned to 50% for 25-35 minutes. The reason for this unusual behaviour of the catalyst with time as a particulate store is not known. It had been anticipated that the catalyst would more effectively store hydrocarbons and particulates when it was colder. Further work is required on the effect of the catalyst initial temperature on particulate deposition.

3.4.3.2. Low speed and power (10kW)

At 1500 rpm and 10 kW in the first set of tests, the catalyst efficiency was low (30%) during the first few minutes, increasing rapidly with time until it reached a maximum of about 85% after 10 minutes, with a decrease to 50% after 30 minutes. In the second set, the catalyst efficiency was over 90% during the first few minutes and decreased to a minimum of around 75% after 15 minutes, showing a further increase over 80% towards the end of the test, after 30 minutes. At 10 kW, the catalyst temperature was 350°C after 2 minutes. Hence, the main contribution to the catalyst efficiency was from a reduction in the gaseous hydrocarbons and hence in the particulate volatile fraction.

When the catalyst was cooled below 5°C prior to the test, the catalyst efficiency was much lower than when it was started at ambient temperature. This was the same trend as found at Idle for the 5°C catalyst temperature. Even though the exhaust temperatures after 5 minutes were not significantly different in both cases, the catalyst efficiency was well below the values for Set 2 at the same conditions.

3.4.3.3. High speed and power (15kW)

For the first set of tests, with the exhaust preconditioned the previous day by the 10 kW test and idle test the day before, The catalyst particulate removal was above 50% at all times, and was 75% for the first 15 minutes after the cold start. At 15kW the catalyst was above 350°C after 2 minutes and hence most of the efficiency would be due to oxidation by the catalyst. The 75% removal efficiency after the cold start could have been increased due to particulate deposits during the two minutes the catalyst was not at its light-off temperature.

For the Set-2 tests at 15kW, with preconditioning the previous day at 15 kW, the initial cold start results had a catalyst removal efficiency of 90% in the first two minutes. This was probably contributed to by large particulate deposition on a catalyst that was cleaned prior to the test by operation above 350°C the previous day.

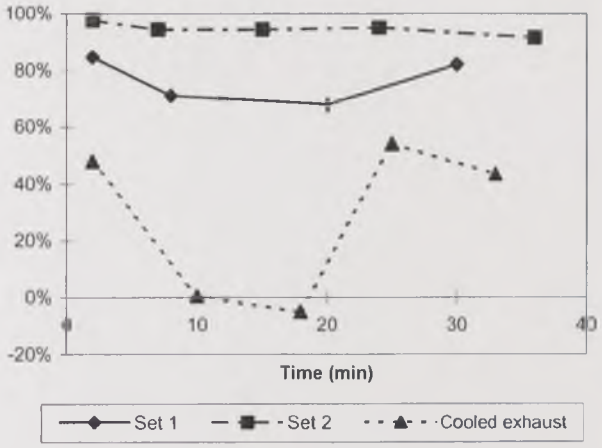

Idle.

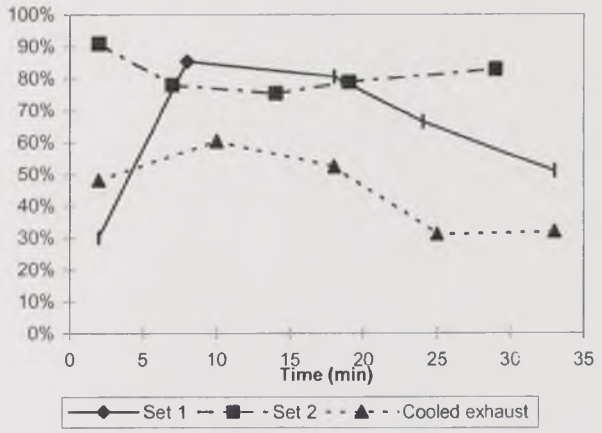

1500 rpm, 10 kW.

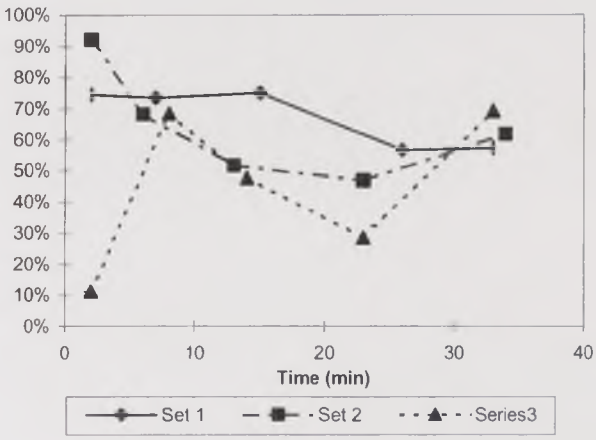

2250 rpm, 15 kW.

Figure 3.11. Catalyst particle removal efficiency during cold start at various conditions.

After five minutes the catalyst particulate removal efficiency had fallen to 70% and then 50% after 13 minutes. It is not clear why the efficiency should be different once the catalyst had lit off for Sets 1 and 2 tests and this needs further investigation.

With the catalyst pre-cooled at 3°C, its initial removal efficiency was very low, only 10% after two minutes. The main difference from the test of Set 2 was that the prior test was idle rather than 15kW. At idle the Set 2 tests had over 90% removal efficiency. This was due to particulate deposition and adsorption of hydrocarbons. This state of the catalyst produced then little trapping capability for the 15kW test, and possibly the blow-out of the previously stored particulates from the idle test. The influence of the 3°C catalyst temperature was small in comparison with the influence of the previous history of the operation of the catalyst. Once the 15kW high exhaust temperatures had heated the catalyst and desorbed the hydrocarbons and particulates the catalyst particulate oxidation efficiency reached 70% and then roughly followed the Set-2 efficiency results.

3.5. Chemical composition by TGA

Particulate filters were collected with the Richard Oliver Particulate Mass Determination Instrument during cold-start tests at idle and at 2250rpm - 15kW, as well as with Andersen Impactors at steady-state conditions at 2250rpm - 15kW. The filters were analysed for their chemical composition using the TGA instrument. The results are presented as SOF and carbon fractions. In this section, the carbon fraction will be used as the parameter to evaluate the changes in particulate composition against the time from cold start and the location in the exhaust. It is expressed here as a percentage of the total mass fraction lost in the TGA, i.e. Carbon + SOF. This does not correspond to the total particulate mass, since the ash was not taken into account owing to errors in the laboratory procedure. Therefore any change in the ash fraction was not detected. According to Ahamed (Ahamed, 1999), the ash fraction in the exhaust particulate from the same engine was as low as 2%. The author has estimated that it may rise up to 14%, and at idle conditions it may be as high as 50%.

3.5.1. Chemical composition vs. particle size

The particulate collection with the Andersen Impactors was carried out at 2250rpm – 15kW at the four selected points along the exhaust system, for a period of two hours with the impactors in an oven at 100°C. A portion of each particulate filter was cut and analysed in the TGA instrument, following the procedure explained in Chapter 2.

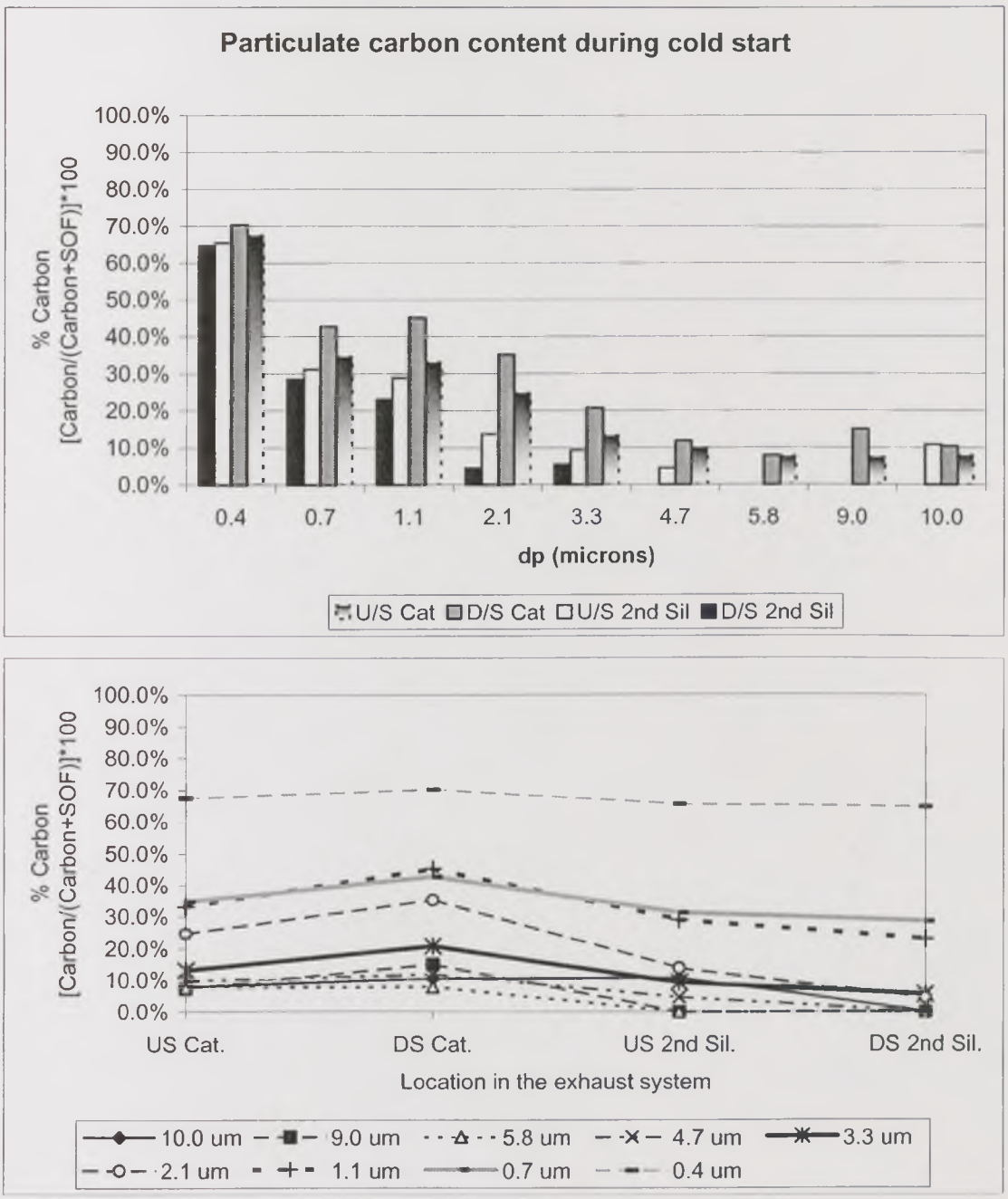

Figure 3.12. Exhaust particulate carbon content vs. particle size and location in the exhaust. 2250rpm - 15kW.

Figure 3.12. shows the results of the analysis as carbon content for the 8 stages of each impactor. The corresponding carbon size distribution, calculated from the Emission Index and the TGA carbon content is shown in Figure 3.13. For all the stages, the carbon content decreased with increasing particle size. Its maximum was 65% to 70% for particles collected on the back filter (smaller than 0.4μm aerodynamic diameter), and particles above 0.7μm have a carbon content not higher than 45%. Above 4.0μm, the carbon content was 15% or less. This decrease in the

carbon content indicated that particle growth in the range measured was due to condensation of volatile material.

The particles experienced changes in the carbon content as they pass through the exhaust system. In all the stages, the carbon content increased through the catalyst, owing to oxidation or storage of the hydrocarbons that form the SOF, and then consistently decreased through the silencers. This was evidence that a fraction of the particulate SOF was transformed by the catalyst, and that further hydrocarbon condensation occurred as the exhaust aerosol cooled down through the silencers.

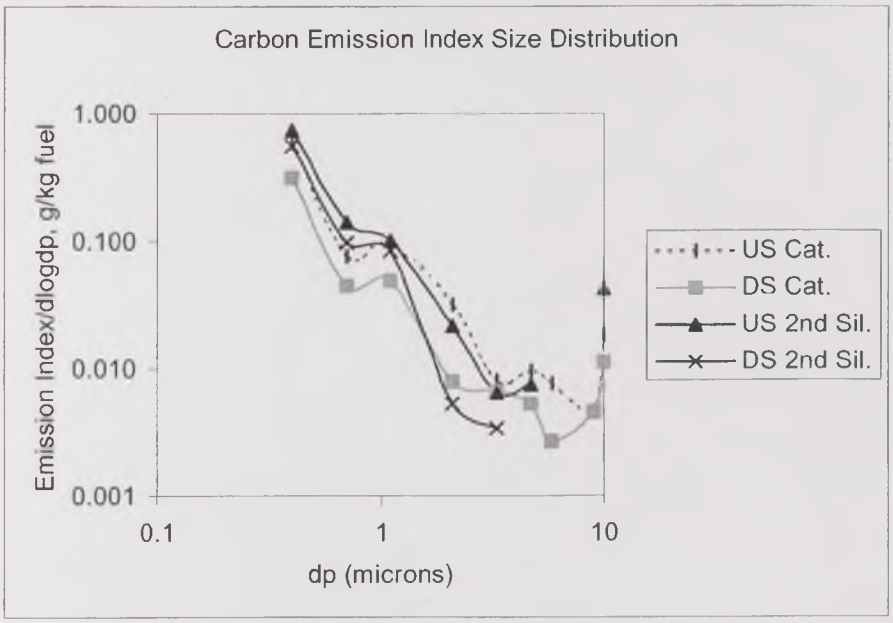

Figure 3.13. Particulate Carbon Emission Index size distribution at 2250rpm - 15kW.

3.5.2. Cold start at Idle

Particulate mass filters collected at four points through the exhaust system, at various times during cold start, were analysed with the TGA instrument using the procedure explained in Chapter 2.

The exhaust particulate carbon content during cold start at idle conditions was below 15% for the totality of samples, as observed in Figure 3.14. At the start of the cold start, the carbon content of the particulate at the entrance of the exhaust system was just 7.1%. Through the catalyst, it increased to 12.5%, owing to the transformation of some of the particulate SOF. There was no significant change through the first silencer, but through the second silencer, the carbon content decreased to 10.1%, indicating that SOF condensation occurred mainly through the second silencer, which was colder than the first silencer.

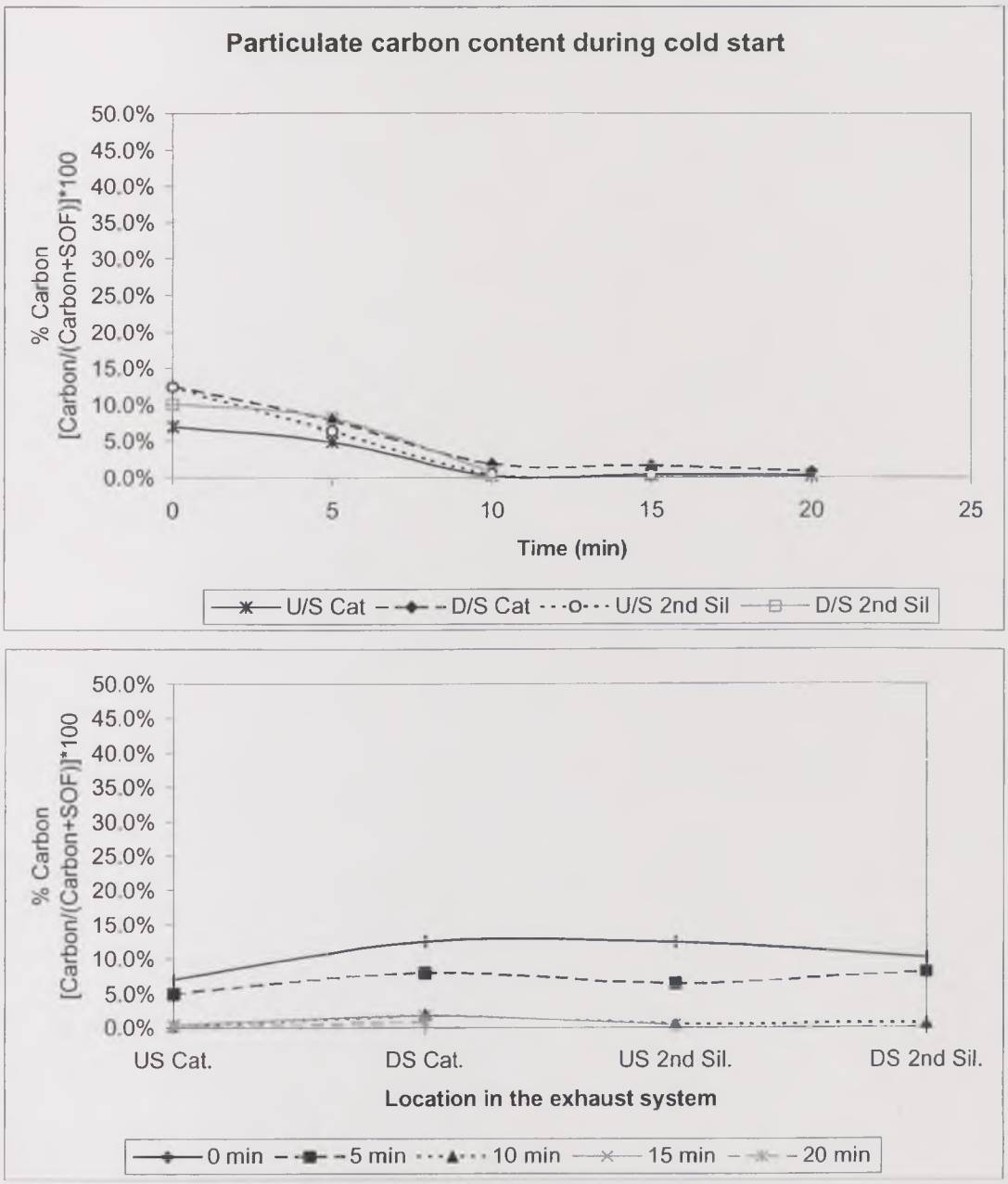

Figure 3.14. TGA particulate carbon content during cold start at idle conditions.

At five minutes from the cold start, the carbon content had decreased to 5.0% upstream of the catalyst, 7.9% downstream of the catalyst, 6.4% upstream of the second silencer and 8.1% downstream of the second silencer. The increase in carbon content through the second silencer might have been due to some particulate resuspension since, as seen above, that carbon content should have decreased through the second silencer.

From 10 minutes onwards, the carbon content throughout the system was very low, just around 0.2% upstream of the catalyst, 1.6% downstream of the catalyst, and 0.5% downstream of the silencers.

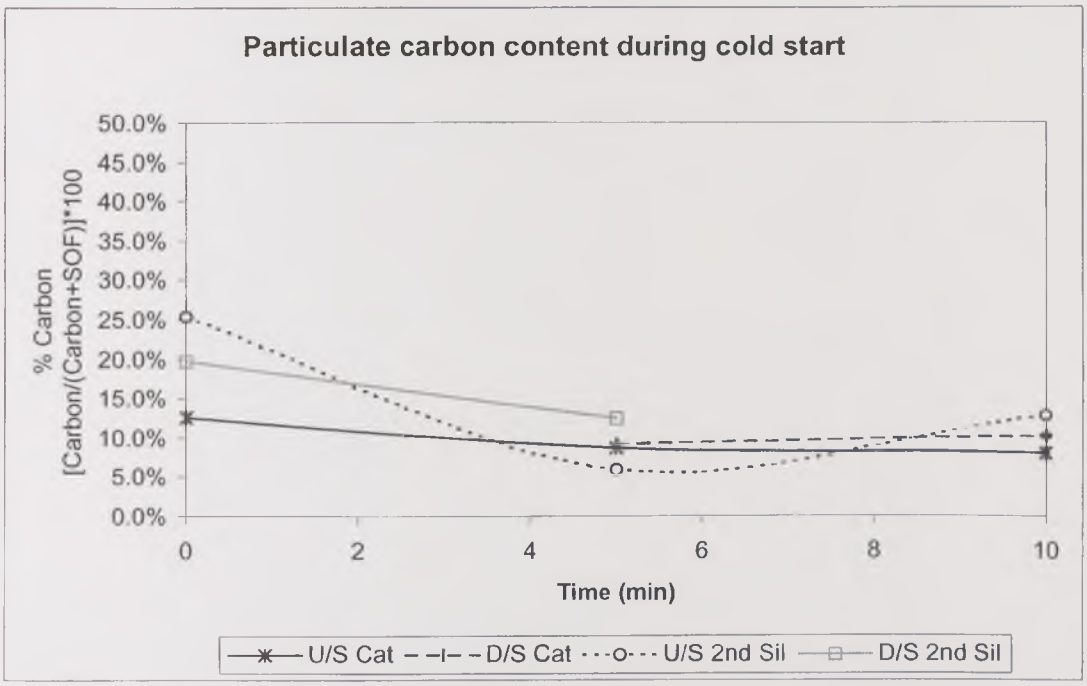

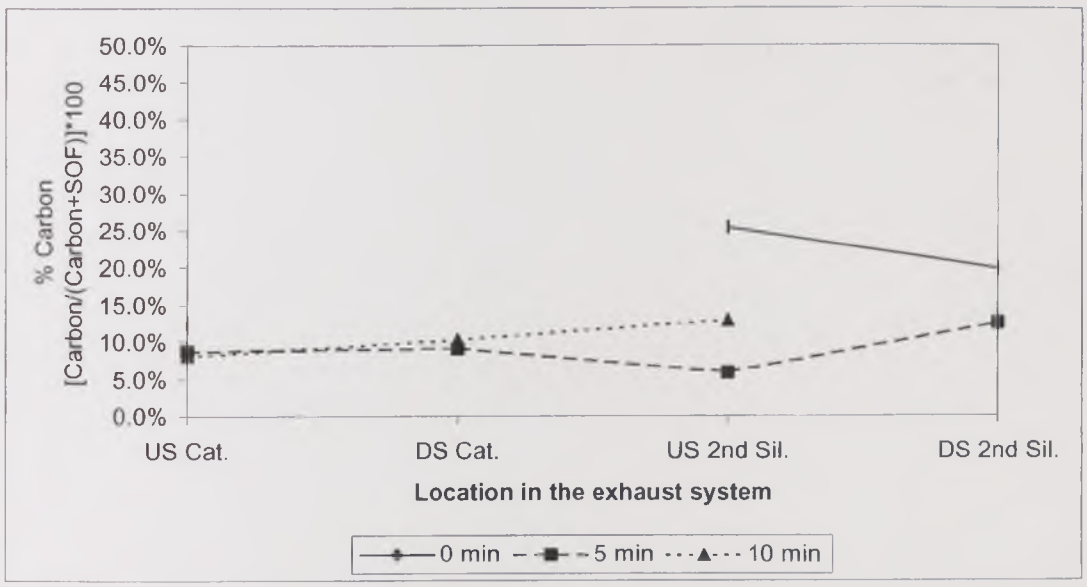

Figure 3.15. TGA particulate carbon content during cold start at 2250rpm - 15kW.

3.5.3. Cold start at 2250rpm –15kW

The particulate carbon content at the cold start, as observed in Figure 3.15. was 12.5% at the exhaust system entrance. The analysis of the sample downstream of the catalyst was, unfortunately, unsuccessful, but the evidence suggests that the

particulate carbon content increased through the catalyst to not less than 25%, which was the value upstream of the second silencer. Through the second silencer, the carbon content decreased to 19.7%.

The carbon content decreased with time from cold start, so after 5 minutes it was lower than 8.7% upstream of the catalyst and between 9% and 10% downstream of the catalyst. Upstream of the second silencer, however, the carbon content had a minimum at 5.9% at five minutes from cold start, then increasing to 12.9%. Downstream of the catalyst, the carbon content was 12.5% at five minutes.

The values found for the particulate content of the mass filter samples once the stabilisation condition has been reached, around 12%, were very low when compared to those measured for the Andersen Impactors at the same engine operation conditions, which suggested an overall carbon content not lower than 50%. This difference was presumably due to the difference between collection temperature used for the Andersen Impactors and that used in the Richard Oliver mass determination technique. At a temperature of 100°C, the particulate collected on the Andersen Impactor substrates included much less condensable material than the particulate on the mass filters, collected at 52°C. As a result, the relative amount of carbon in the Anderson samples became higher than in the mass filters. Therefore, a direct comparison between the carbon content of the samples from these techniques was unreasonable.

3.6. Total Number Concentration, Mass Concentration and Particle Size Distribution Changes Through the Exhaust System During Cold Start Using the ELPI

The engine cold start introduces a disturbance into the exhaust system and the particle deposits of its walls, bringing them from a cold, quiet rest to a vibrating, warm state, in which they interact with the flowing exhaust aerosol. Its transient effects, as measured with an ELPI on a second-by-second basis, are described in this section.

Before starting the analysis, however, it is necessary to explain the implications of assumptions and limitations inherent to the use of the ELPI to produce particle mass distributions.

In the aerodynamic classification of aerosols, the diameter of a particle is the equivalent diameter to that of a unit-density sphere with the same aerodynamic mobility as the particle in question. Therefore, the mass of a particle deposited on a stage with a defined aerodynamic diameter range is calculated as follows:

$m_p = \rho_p \left(\frac{\pi D_p^3}{6} \right)$, being ρ_p the particle density, that is, unit-density in assumptions for aerodynamic sizing. The real particle density, however, is not known, but has an effect on the resulting size distribution (Maricq, 1998; Ahlvik, 1998; Moisio, 1997).

The particle mass distribution, calculated using the above expression involves the potential risk of exacerbating any small error in the detection of large particles, i.e. 1.0μm to 10.0μm; only one 10μm particle extra detected by an electrometer of the ELPI is 10^6 times as heavy as a 0.1μm particle and 10^9 times as heavy as a 0.01μm particle. In addition, the ELPI has potential calibration and detection problems in the large size range. Therefore, the mass distribution is very likely to be unreliable in a number of cases. In order to make the data useful for the purposes of this research work, a correction is attempted, as described in Chapter 6. Hence, the mass-distribution change analysis shown from this point onwards will use both the uncorrected and corrected mass calculated from ELPI number concentrations. Although both are mentioned, the author, anticipating one of the conclusions, will consider the **corrected** values as the most realistic from this point on, since they are closer to the gravimetric mass determination. The reader is asked to take this into account when examining the results. A detailed comparison with gravimetric results will be found in Chapter 7.

Another point that is worth mentioning at this point has to do with the various size-dependent phenomena taking place as a result of the interaction between the exhaust aerosol and the system walls. In the analysis, particles will be evaluated in three groups, corresponding to size ranges that show differences in particle growth and transport behaviour, since they are affected differently by physical processes, as observed in Chapter 1. These groups will be referred to as ultrafine or very fine particles (<0.01μm), mid-sized particles (0.1 to 1.0 μm) and large particles (1.0 to 10.0 μm). Within the ultrafine size range, a subgroup of nanoparticles will occasionally be mentioned. Throughout the description of the tests results many examples of the complex combination of the various physical processes will be observed. They will involve the increase or decrease in particle number and mass concentrations of the exhaust aerosol through the exhaust system devices.

In the fine size range, the increase in the number of particles may be due to the formation of new particles by nucleation, particularly at low temperatures, although the extent at which this occurs with a low-sulphur fuel is very limited. In the fine size and mid-size ranges, particles grow by coagulation, and this also results in an increase in the number of particles. The ELPI does not detect particles under

0.035μm, but if these grow by coagulation, the number of particles between 0.035μm and 1.0μm will increase as a result. Coagulation virtually stops occurring over 1.0μm. Therefore, any increase in the number of large particles is due to reentrainment of deposits from the exhaust system deposits. Reentrainment does not occur for particles smaller than 1.0μm, so this size becomes a clear limit in the consideration of physical processes affecting the interaction between the exhaust aerosol and the exhaust system walls.

On the other hand, the decrease in the particle number concentration is due to deposition, which can occur at all size ranges, and coagulation in the fine and mid-size ranges. Deposition will be mostly thermophoretic for very fine particles; gravimetric and inertial for large size ranges; and a combination of both for mid-sized particles.

3.6.1. Idle

The lowest degree of disturbance is reached when the engine is just started and no further acceleration is applied. Particulate number and mass emissions during cold start with no further acceleration showed the following characteristics, common to all sampling points:

- An initial mass burst for the first five seconds of start, represented by a local particle mass concentration peak with time, followed by a decrease to a much lower level.
- An increase in particle number concentration, having a peak 10 to 15 seconds after the initial mass peak. At about the same time, a second mass peak appeared, although not necessarily similar to the first mass peak.
- A decrease in number and mass concentration to stabilisation levels.

Figure 3.16. shows the total number and mass concentration for all four sampling points against time. They show the different events described above and the point-to-point differences in mass and number concentration, particularly in the number-peak event. However, the concentration changes analysis is better visualised in a simplified chart for total number and mass concentration, as shown in Figure 3.17., plotting the total number and mass concentration changes against the position in the exhaust. Each line in this figure represents a cold-start event.

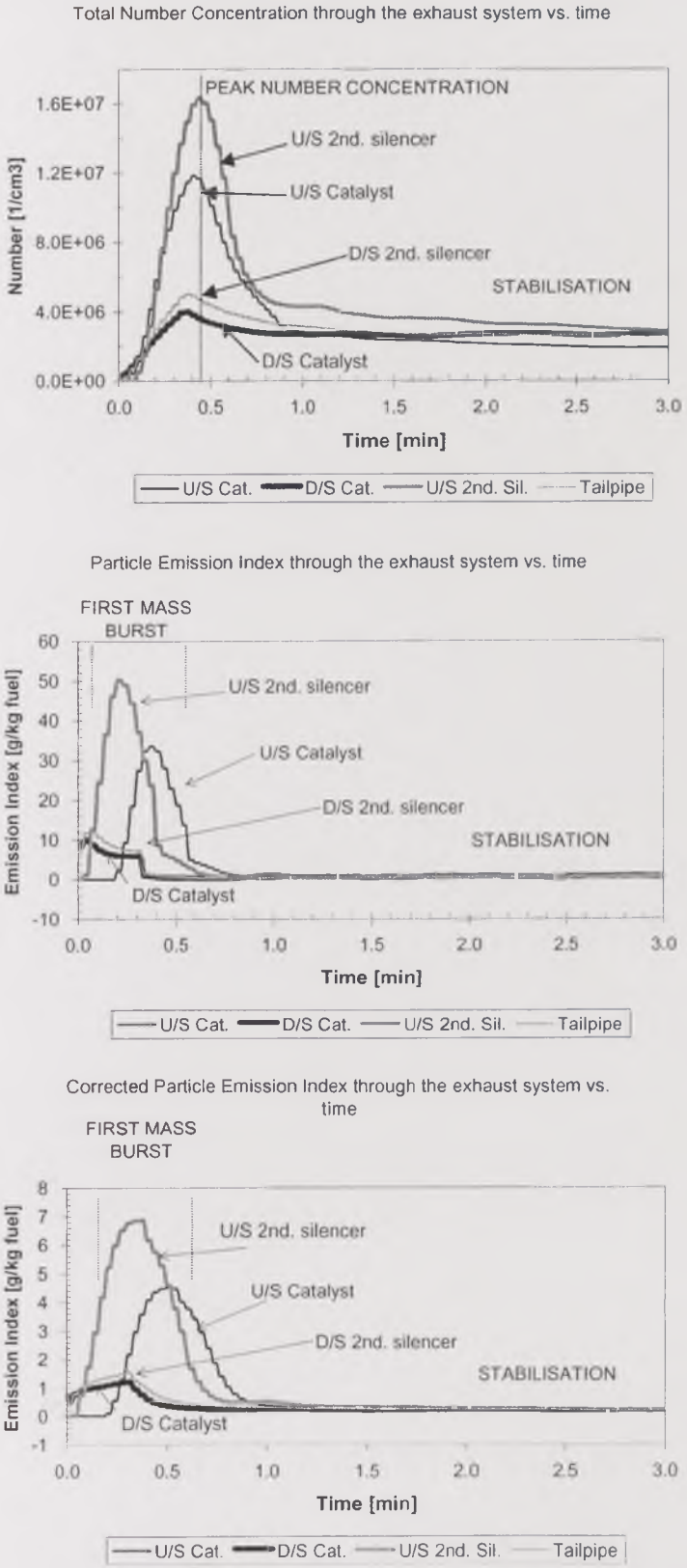

Figure 3.16. Total number and mass concentrations through the exhaust system against time during cold start at Idle. a) Concentrations at sampling points.

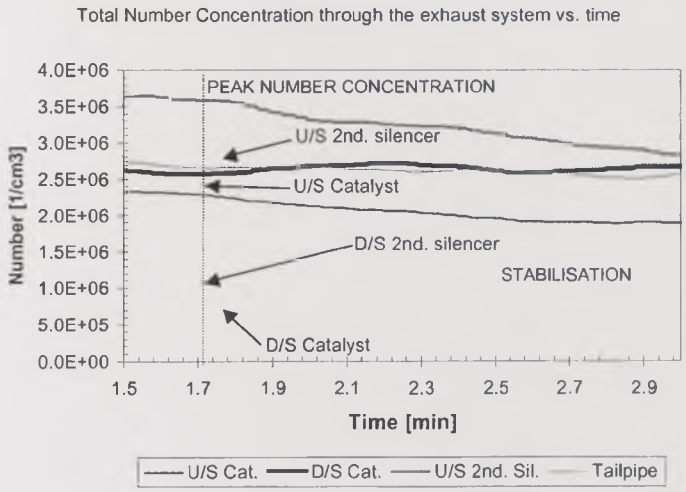

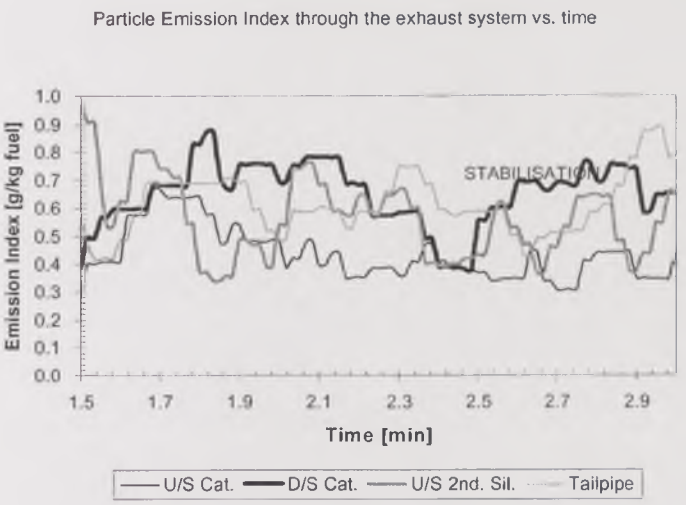

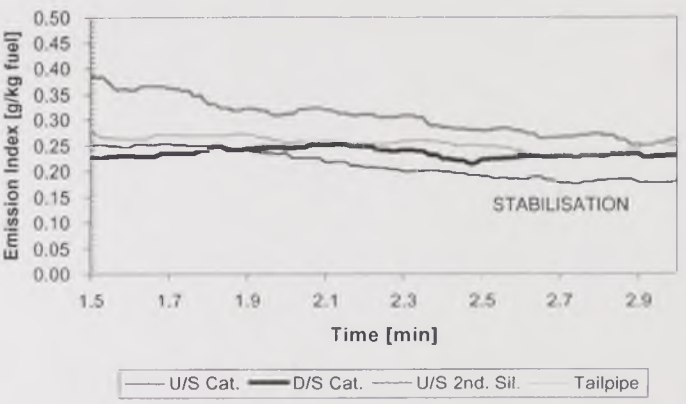

Figure 3.16. Total number and mass concentrations through the exhaust system against time during cold start at Idle. b) Detail of concentrations at sampling points during stabilisation.

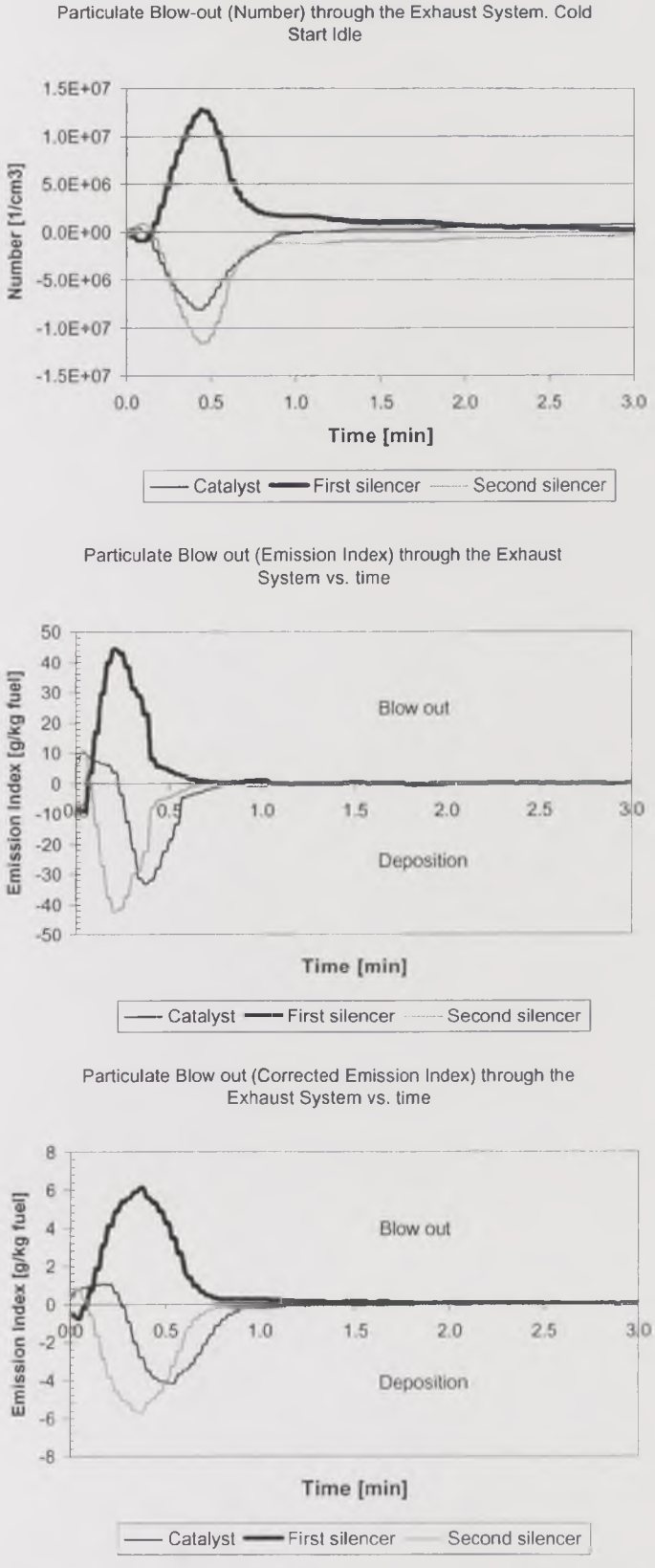

Figure 3.16. Total number and mass concentrations through the exhaust system against time during cold start at Idle. c) Blow-out through the system.

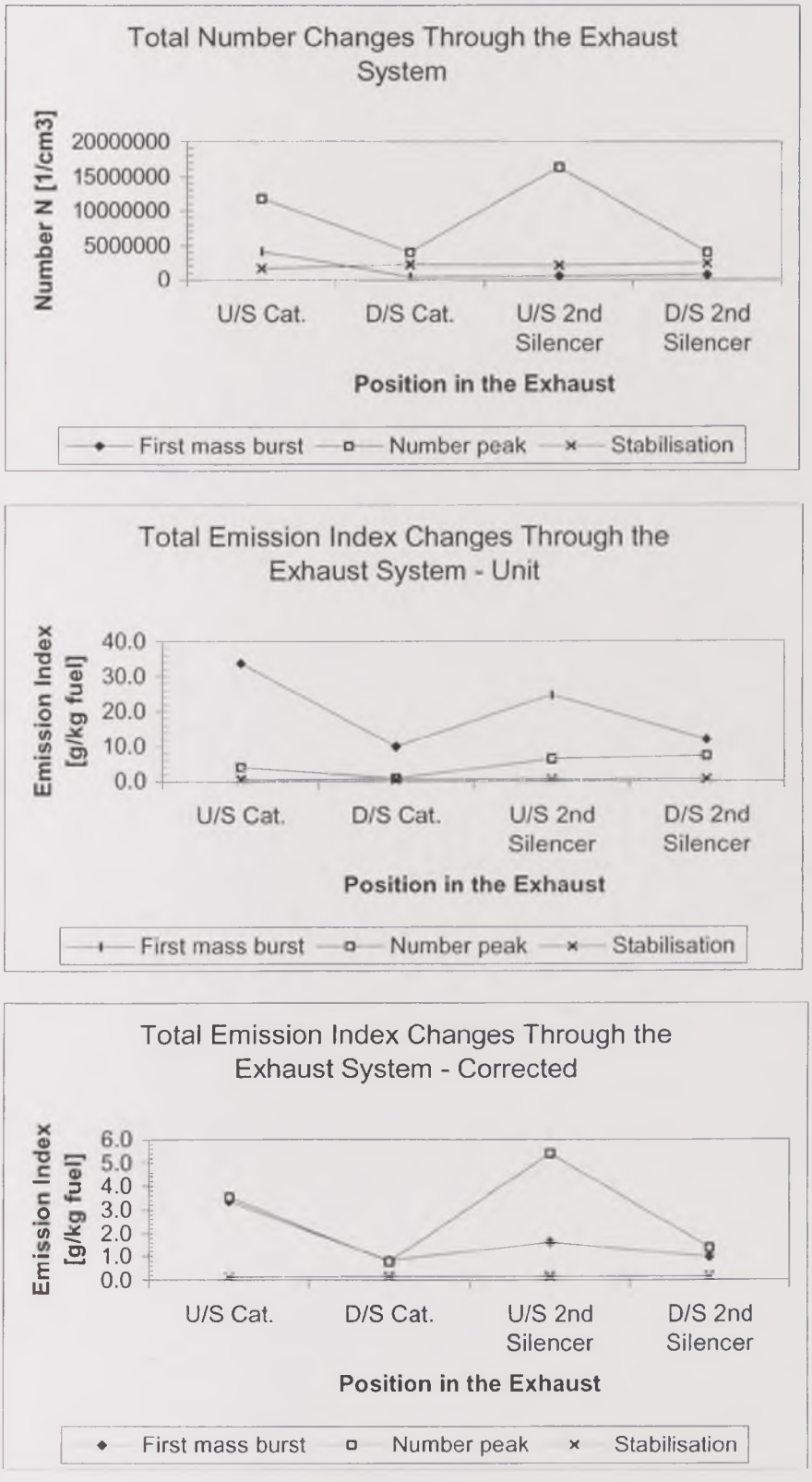

Figure 3.17. Total number and mass concentrations for the main events during cold start at Idle against the position in the exhaust.

3.6.1.1. First mass burst

During the first mass burst, the particle number concentration upstream of the catalyst was just over $4.0x10^6$ cm^{-3}, decreasing to just above one tenth of this value when passing through the catalyst, $4.7x10^5$ cm^{-3}. This level increased by 10% through the first silencer, and increased through the second silencer to $7.5x10^5$ cm^{-3}, that is, a 50% increase. According to this, a great number of particles grew by coagulation, deposited and/or were adsorbed through the catalyst, and a much smaller number of particles were reentrained from the deposition layer on the walls of the second silencer, as a consequence of the first disturbance to the system.

The decrease in number concentration through the catalyst during this event occurred for all size ranges measured; the decrease was much more significant for particles between 0.1μm and 0.5μm. In contrast, through the first silencer, the number of particles between 0.1μm and 10μm increased as a result of particle growth by coagulation and particle blow-out from the walls, respectively, in the first mass burst event. The contribution of these particles was very significant to the total particle number concentration downstream of the silencer, which nearly doubled that upstream. Finer particles, between 0.030μm and 0.2μm, increased in number through the second silencer, most likely by coagulation of smaller particles and condensation of volatile species, thus accounting for the 50% increase in particle number in the exhaust. About 5% of the larger particles entering the second silencer, in contrast, deposited through the device.

This first analysis showed that the simplest disturbance originated by the cold start has a complex effect on the transient growth (by coagulation and condensation), adsorption, deposition and re-entrainment of particles of different sizes through the exhaust system. Each device showed a different effect on the particle growth, deposition or blow-out, not coincident even in the size of particles being deposited or reentrained. Naturally, the significance of the fine particles, that is, particles in the 0.030μm to 0.2μm range, is larger when analysing changes in particle number concentration, owing to the characteristics of the number size distribution. But no single trend seemed to appear.

The uncorrected Emission Index decreased from 33.6 g/kg fuel upstream of the catalyst to 9.99g/kg fuel downstream of the catalyst. A new increase to 24.5g/kg fuel occurred through the first silencer and then it decreased again to 11.9g/kg fuel through the second silencer. The corresponding corrected Emission Index were 3.4g/kg fuel to 0.8 g/kg fuel through the catalyst, then up to 1.6 g/kg fuel through the first silencer, and down again to 1.0 g/kg fuel through the second silencer.

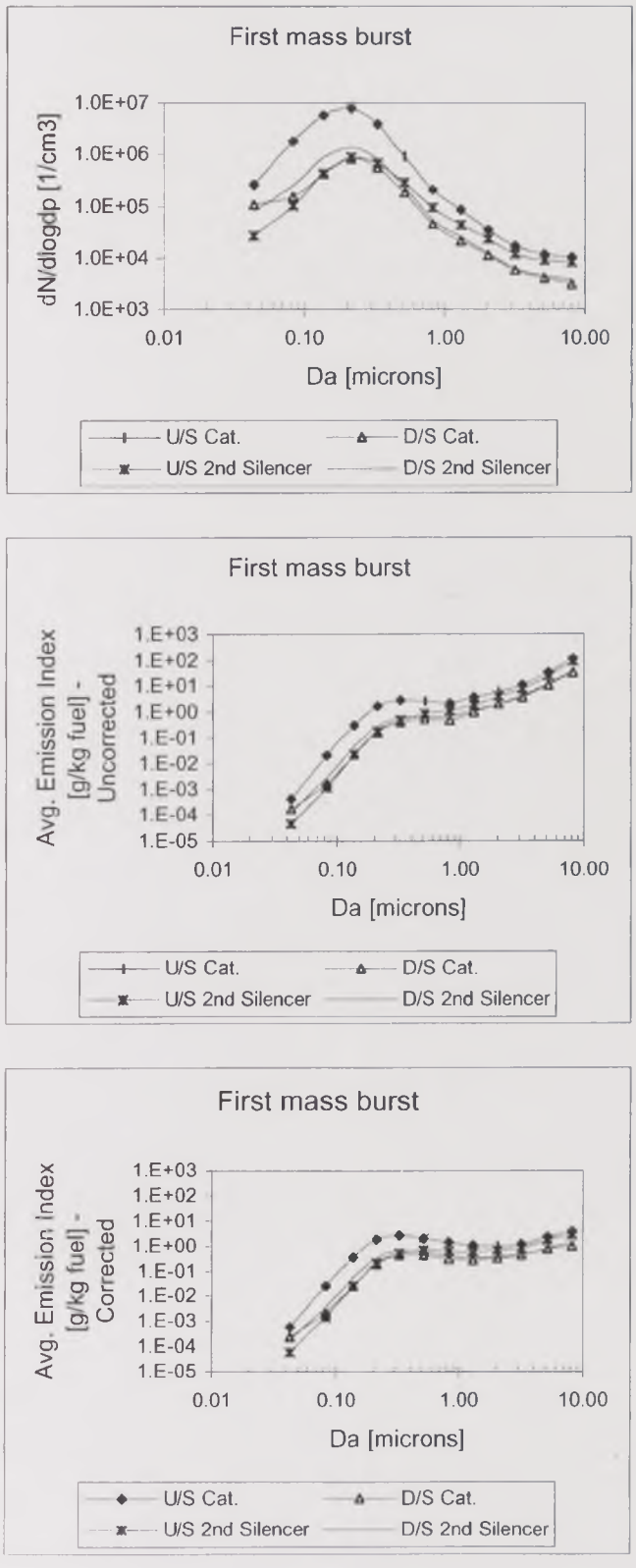

Figure 3.18. Particle size distributions for the first mass burst at various points through the exhaust system (Idle).

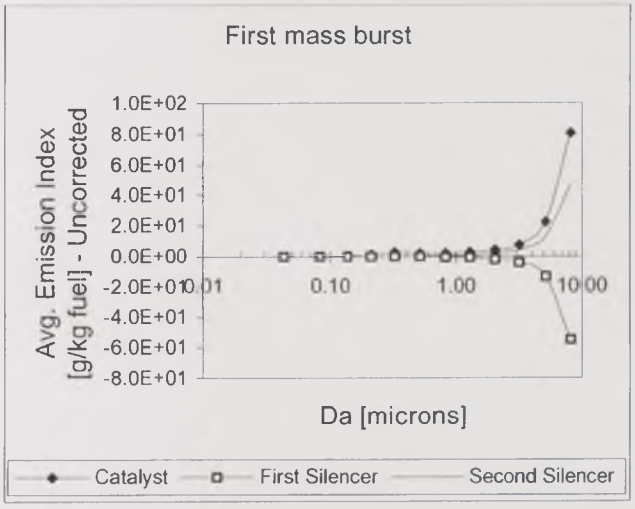

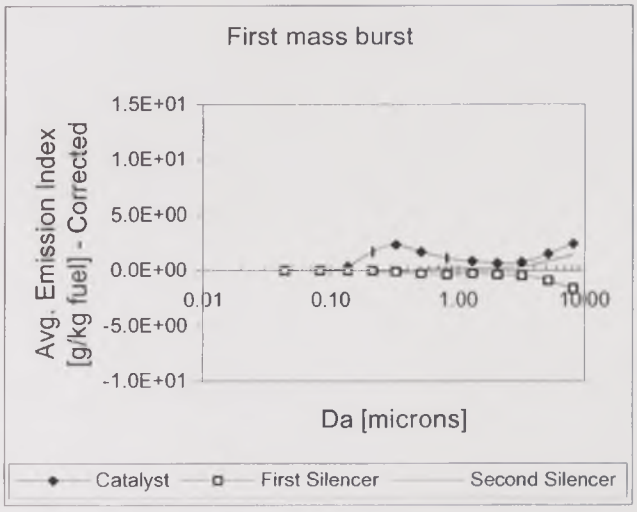

Figure 3.19. Particle blow-out through three sections of the exhaust system, for different size ranges, during the first mass burst event of the cold start (Idle).

The effect of the correction on particle mass concentration along the exhaust system when converting particle number concentration in the calculation process is shown in the mass distribution charts of Figures 3.18. and 3.19. The total mass concentration expressed as Emission Index, g/kg fuel, became one order of magnitude lower when using the correction, being more significantly affected by the calculated mass of particles in the large size range. This is the origin of the initial disagreement between the Emission Index calculated from numbers and that measured gravimetrically. The use of the uncorrected function attributes most of the mass to particles larger than 0.5μm, and therefore it is this size range in which significant deposition and release changes are found. In contrast, the use of the corrected function estimated that total particle mass as well as mass changes in the middle size range, 0.1 to 1.0μm, were as significant as the mass of large particles.

During the first mass burst, the catalyst adsorbed about 70% of the total particle mass, as calculated by either corrected or uncorrected functions, which was in agreement with the reduction in total particle number. Mostly the deposition of large particles contributed to this change, although the corrected function suggests that mass changes in the middle size range were also significant.

The particle blow-out through the first silencer was also observed in particle mass, being more significant when using the uncorrected conversion into mass: 150% against 50% increase in total mass through the silencer. Contrary to the blow-out expressed number, which was due to middle sized particles, the change in mass was invariably due to large particles, with a small contribution, 15%, of middle-sized particles, when using the corrected mass conversion.

The increase in particle number through the second silencer was strongly affected by the conversion into mass. Middle-sized and, mainly, large particles were actually deposited, so the total particle mass decreased through this silencer. The increase was more likely due to particle growth towards 0.030μm to 0.050μm particles than to fine particle blow-out.

In summary, the significant changes through the exhaust system during the first mass burst event were:

- particles deposited and coagulated through the catalyst with hydrocarbon adsorber;
- very fine particles became part of the deposition layer and large particles were released from it through the first silencer; and
- large particles deposited through the second silencer. Through the same device, ultrafine particles (around 0.030μm) were formed by gas-to-

particle conversion (nucleation by condensing species) and coagulation of these ultrafine particles owing to exhaust cooling.

3.6.1.2. Peak particulate emissions by number

The particulate number peak showed some problems in the electrical detection of the particle current by the ELPI. The instrument's software is designed to correct the original current for fine particle losses by subtraction, so when the correction is as large or larger than the original current itself, a correction warning is produced, as negative currents are generated. Then, the corrected currents, and therefore the particle number concentration and emission index, adopt a zero value. This problem was unfortunately seen quite often in the large size range, 1.0μm to 10.0μm, during very rapid major transients, for example, the number-peak event during cold start with no acceleration, Figure 3.20. Total number concentration was normally not affected by this problem, since the largest numbers were in the fine size range, but mass concentrations could have been affected, since they were normally strongly biased towards particles in the large size range.

The high reduction in particle number through the catalyst persisted during the number-peak event: only 33% of the 1.2×10^7 cm^{-3} penetrated the catalyst. Particles between 0.030μm and 1.0μm deposited, but no data were available for larger particles owing to transient detection problems, as explained above. In contrast, there were more particles downstream of the first silencer than upstream of it, owing to particle growth and blow-out. The particle number increased by 300% through the silencer, to 1.6×10^7 cm^{-3}. An extrapolation of the size distribution curves in Figure 3.20. may well suggest that larger particles were blown-out, although the exact numbers were not measured.

The second silencer acted during this event in a very similar way to the catalyst, particle number concentration decreasing to 4.0×10^6 cm^{-3}, which was a reduction by 75%. The total particle mass concentration and the particle mass distribution showed the same trends as their number equivalent, but this can not easily be taken as a certain result, owing to the lack of data in the large size range. However, it was observed that only the corrected values are in the same order of the gravimetrically determined Emission Index, whilst the uncorrected values were one order of magnitude higher.

In brief, the number by peak event of the cold start at idle provided evidence of particle deposition, both thermophoretic and gravitational, through the catalyst and the second silencer. Particle blow-out occurred in the first silencer. Apparently, the deposition layer in the first silencer was more fragile than that in the second silencer or the thermal shock in the deposits in the first silencer was greater than in the

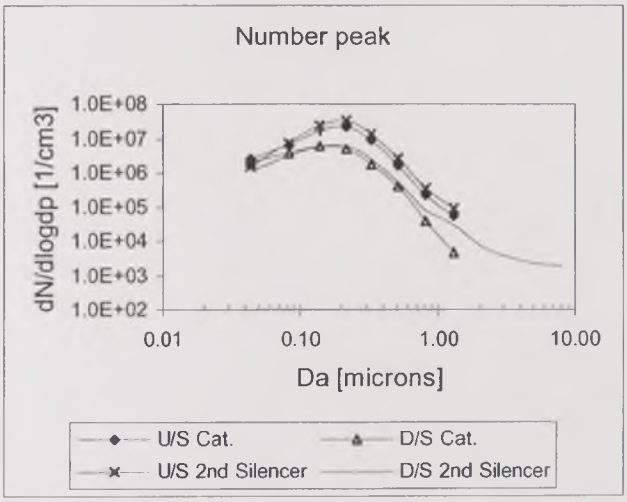

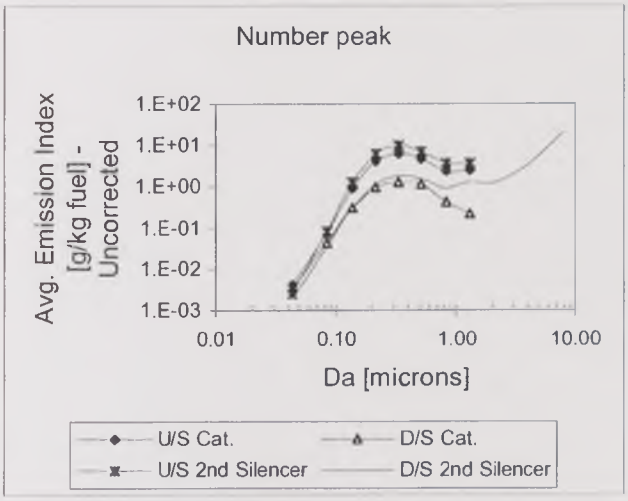

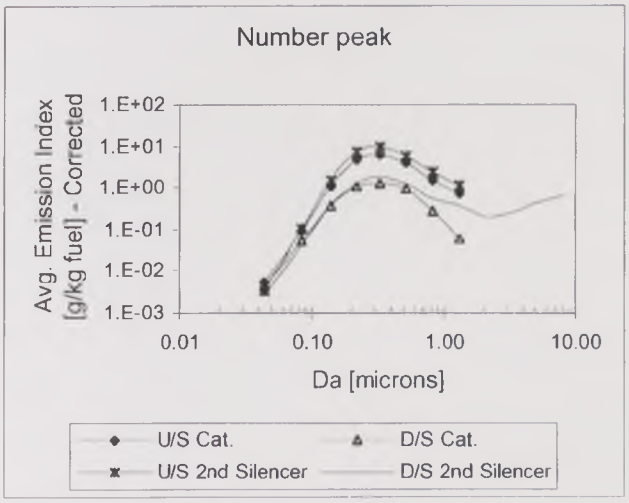

Figure 3.20. Particle size distributions for the peak number at various points through the exhaust system (Idle).

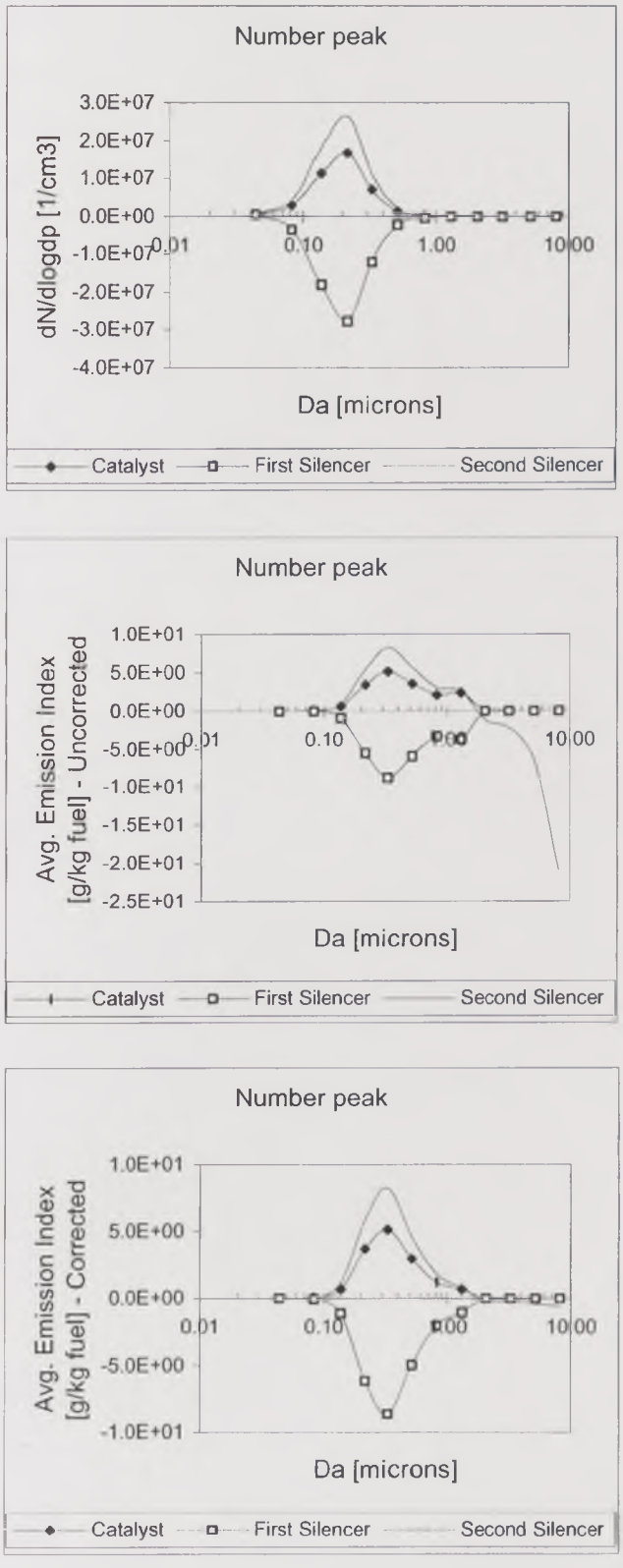

Figure 3.21. Particle blow-out through three sections of the exhaust system, for different size ranges, during the peak number event of the cold start (Idle).

second. The particle size distribution shifted slightly towards smaller sizes through the exhaust system. The uncorrected Emission Index tended to overestimate the gravimetric results and the corrected Emission Index to underestimate them.

3.6.1.3. Stabilisation

Total number and mass concentration decreased with time at all sampling points after the number-peak event, until they reached a stabilisation level. This reduction was by 40% downstream of the catalyst and downstream of the second silencer, and nearly by 90% upstream of the same devices. The changes observed through the exhaust system after the stabilisation were much smaller than those in the previous events, so the total number and mass concentration profiles against position in the exhaust in Figure 3.17. look quite flat, at very similar concentration levels. However, there were still differences that could contribute to have an effect over the deposition layer if this condition was kept for a long period.

After reaching the stabilisation period at about 2 minutes from the cold start, both total number and mass concentrations increased through the catalyst by around 30%, from $1.7x10^{6}$ cm^{-3} to $2.2x10^{6}$ cm^{-3} and from 0.42 g/kg fuel to 0.54 g/kg fuel (corrected 0.133 g/kg fuel to 0.169 g/kg fuel), respectively. The increase in number concentration was due to a blow-out of large particles from the catalyst surface, and nucleation – coagulation processes in smaller size ranges. The change in mass, when using the uncorrected conversion, had a significant contribution of large particles, around 8µm, and, less importantly, particles around 0.2µm, as observed in Figures 3.22. and 3.23. Nevertheless, the corrected conversion diminished, without neglecting, the significance of large particle contribution, so the mass released was estimated to be mostly due to particles around 0.2µm.

When passing through the first silencer, 6% of the particles -by number- were reduced, 14% by mass was deposited without correction and 9% by mass was deposited with the correction. The concentrations downstream of this silencer were then $2.1x10^{6}cm^{-3}$, and 0.47 g/kg fuel or 0.15 g/kg fuel, respectively. The reduction by deposition occurred for all sizes, and, as in the analysis of the blow-out through the catalyst, it was more significant in the very fine and middle-size ranges by number, in the large and middle size ranges by uncorrected mass and in the middle size range by corrected mass. Again, the significance of the large particles on the total uncorrected mass change diminished when including the corrected conversion.

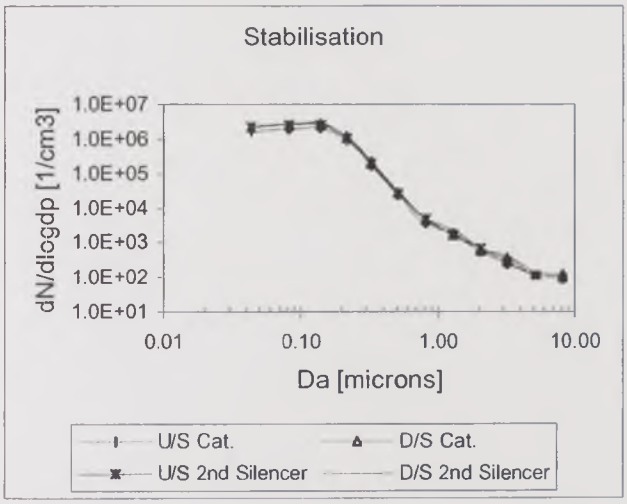

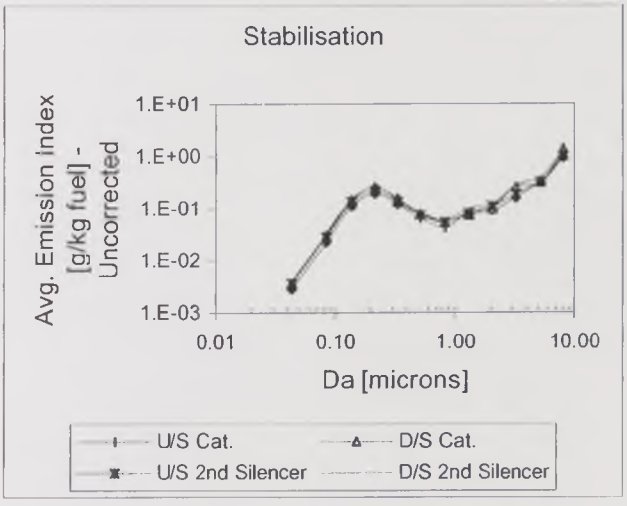

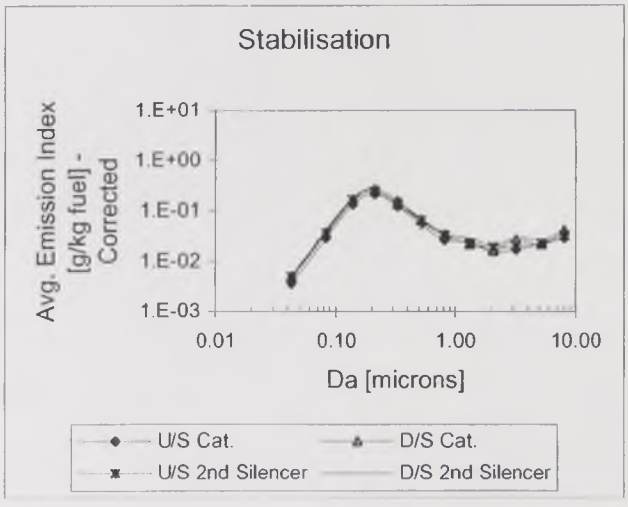

Figure 3.22. Particle size distributions for the stabilisation event at various points through the exhaust system (Idle).

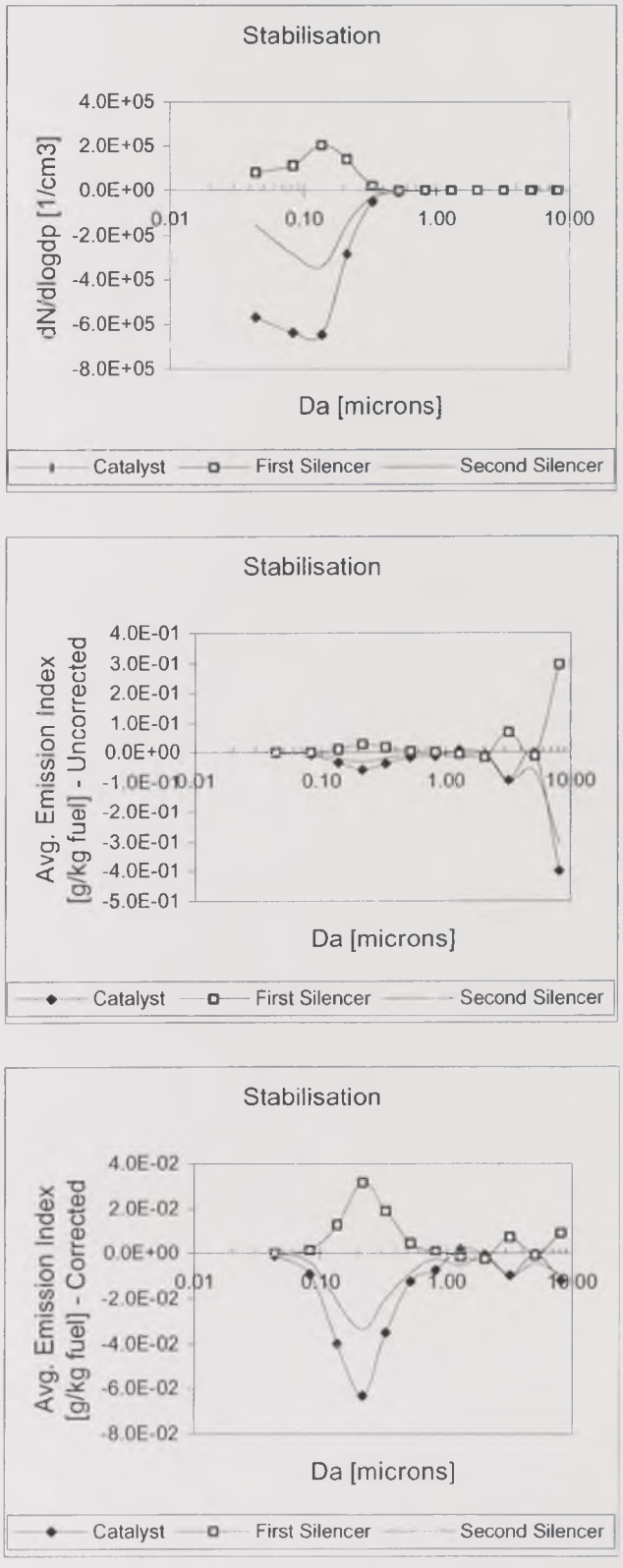

Figure 3.23. Particle blow-out through three sections of the exhaust system, for different size ranges, during the stabilisation event of the cold start (Idle).

Through the second silencer, the aerosol showed a very similar behaviour to that through the catalyst after the stabilisation at idle. Number, uncorrected and corrected mass increased by 11%, 24% and 15% respectively, the concentrations at the tailpipe being $2.3x10^{6}cm^{-3}$, 0.58g/kg fuel and 0.18g/kg fuel, respectively.

To sum up, the stabilisation period of the cold start with no acceleration showed all the devices behaving differently from the critical transient events of the first mass burst and the number peak. Particles were released from the catalyst and the second silencer, and deposited on the walls of the second silencer. No significant change occurred in particle size distribution. The corrected Emission Index was closer to the gravimetric results than the uncorrected Emission Index.

3.6.2. 1500 rpm and 10 kW

To the basic disturbance to the exhaust system during cold start analysed in the previous section, which did not involve any acceleration of the engine, a new disturbance was introduced, to observe the changes in particulate emissions. The acceleration was applied just after starting the engine, until the target conditions of 1500rpm and 10kW were reached. This will be referred to as a low-power condition. Owing to the slowness of the hydraulic dynamometer when using automatic control of the throttle, the manual acceleration was preferred, since a rapid acceleration is needed to produce a more realistic effect. This practice, however, involves the potential risk of reducing the repeatability of the experiment, because a manual operator is very likely to actuate on the throttle at a different speed in every test, which in real driving would correspond to different levels of aggressiveness. As it will be shown, the effect of different acceleration speeds due to manual operation was manifested as a lack of synchronization of the various events along the exhaust system or an introduction of apparent irregularities in the concentration profiles with time.

The cold start with acceleration to low-power conditions showed, at all sampling points, total particle number and mass concentration profiles with the following characteristics against time (Figures 3.24. and 3.25.):

- an initial mass burst during the first few seconds from start;
- a peak in total number concentration, between 30 seconds and one minute after the mass burst;
- a valley following the peak by number, which had a tendency towards stabilisation in total particle number and mass, from 2 to 5 minutes from start; and,

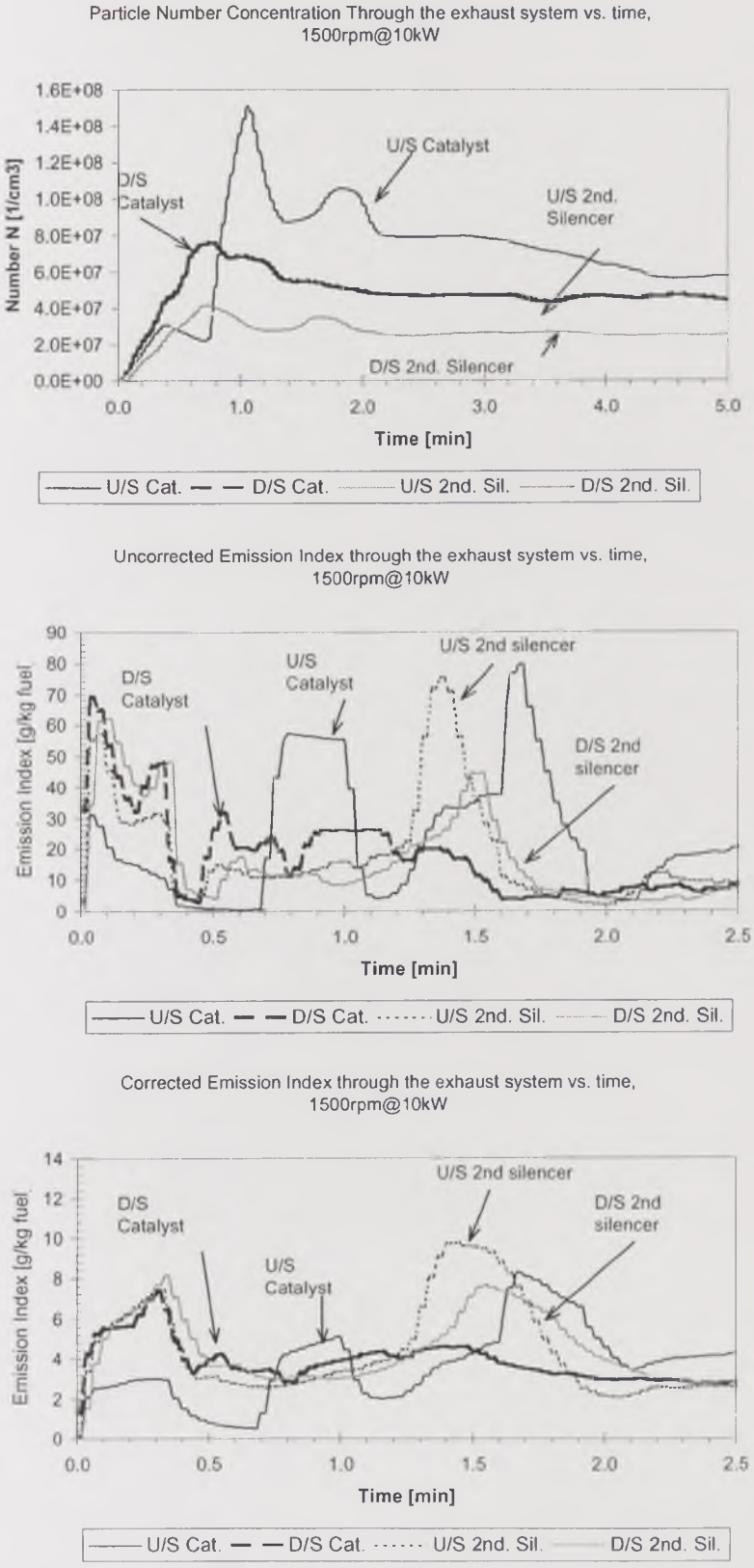

Figure 3.24. Total number and mass concentrations through the exhaust system against time during cold start at 1500rpm – 10kW. a) Concentrations

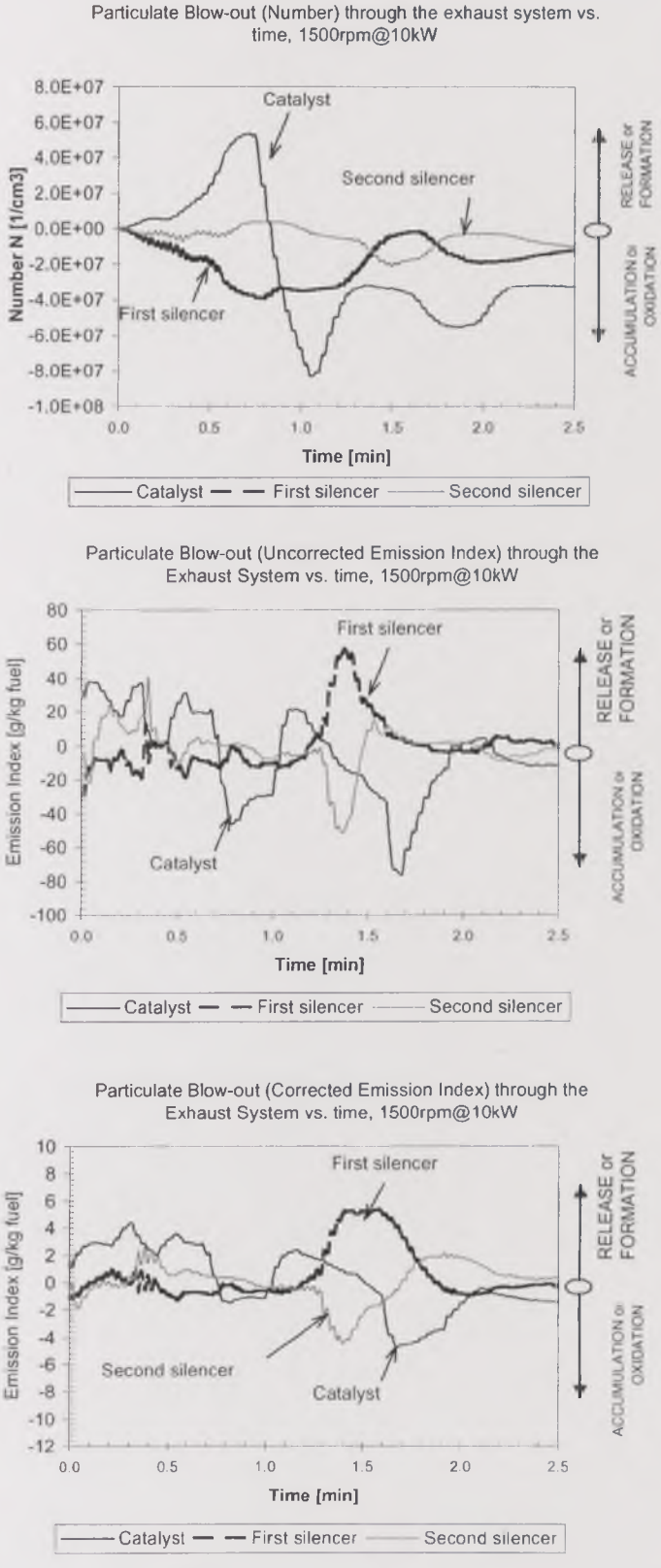

Figure 3.24. Total number and mass concentration changes through the exhaust system against time during cold start at 1500rpm – 10kW. b) Blow-out

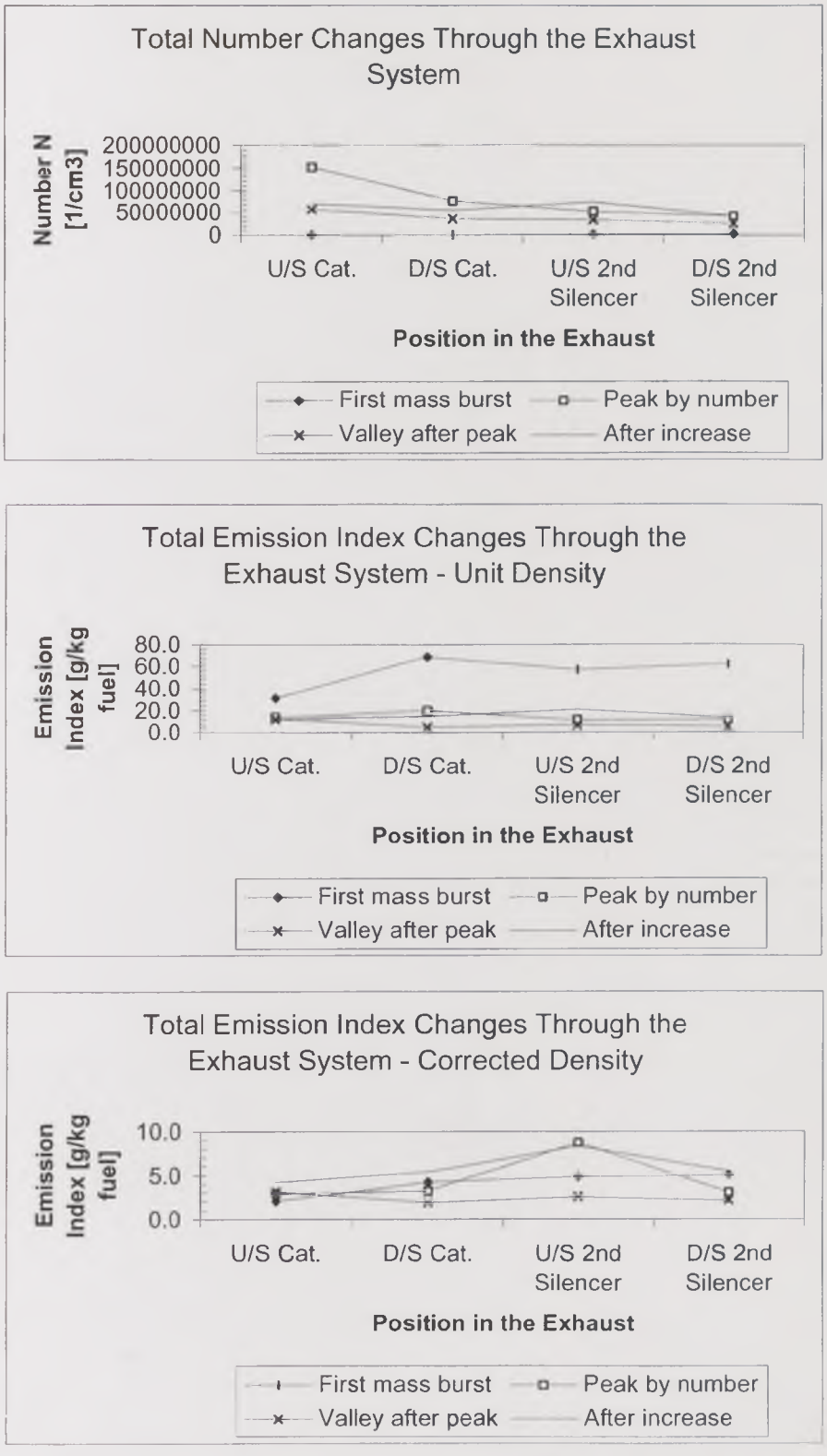

Figure 3.25. Total number and mass concentrations for the main events during cold start at 1500rpm – 10kW against the position in the exhaust.

- a new slow increase in total number and mass concentration, after which a new stabilisation level appeared to be reached, at 15 minutes from cold start.

The first three events were analogous to those observed during cold start without acceleration, the valley corresponding to the stabilisation at idle. The increase after minute 5 from cold start was a new feature introduced by the engine acceleration, and it was due to the opening of the EGR valve. This event was observed only in two of the four sample points, namely upstream of the catalyst and upstream of the second silencer, which was considered as evidence that the EGR valve opening was not reproducible during the various repeat tests. The valve opening responds to a complex set of parameters in the engine control strategy, and one or more of such parameters may have not been met when running the tests in which the valve did not open. Nevertheless, this part of the present work will analyse cold start only, so it will be restricted to the first 5 minutes from start, before the increase event took place.

3.6.2.1. First mass burst

As in the test at 1500rpm - 10kW, the first seconds of the cold start showed at all points an initial mass burst. The total particle number concentration of the exhaust aerosol coming out from the turbocharger in that period was just 2.2×10^5 cm^{-3}, giving a mass concentration of 31.1 g/kg fuel (uncorrected) or 2.1 g/kg fuel (corrected). The number concentration an Emission Index increased to $9.86 \times 10^5/cm^3$, 68.8 g/kg fuel (uncorrected) and 4.2 g/kg fuel (corrected), respectively, through the catalyst, corresponding to a 339%, 121% and 104% increase, also respectively.

Large particles were released and many fine particles were formed by very rapid nucleation-condensation-coagulation combined processes. This differed with the same event in the test at Idle, in which particles were not blown out as in this case, but deposited through the catalyst, although the conditions were not very different in these first few seconds. Blow-out of large particles, 5.0μm to 8.0μm, was significant even when calculating Emission Index with the corrected conversion. This is observed in Figures 3.26. and 3.27.

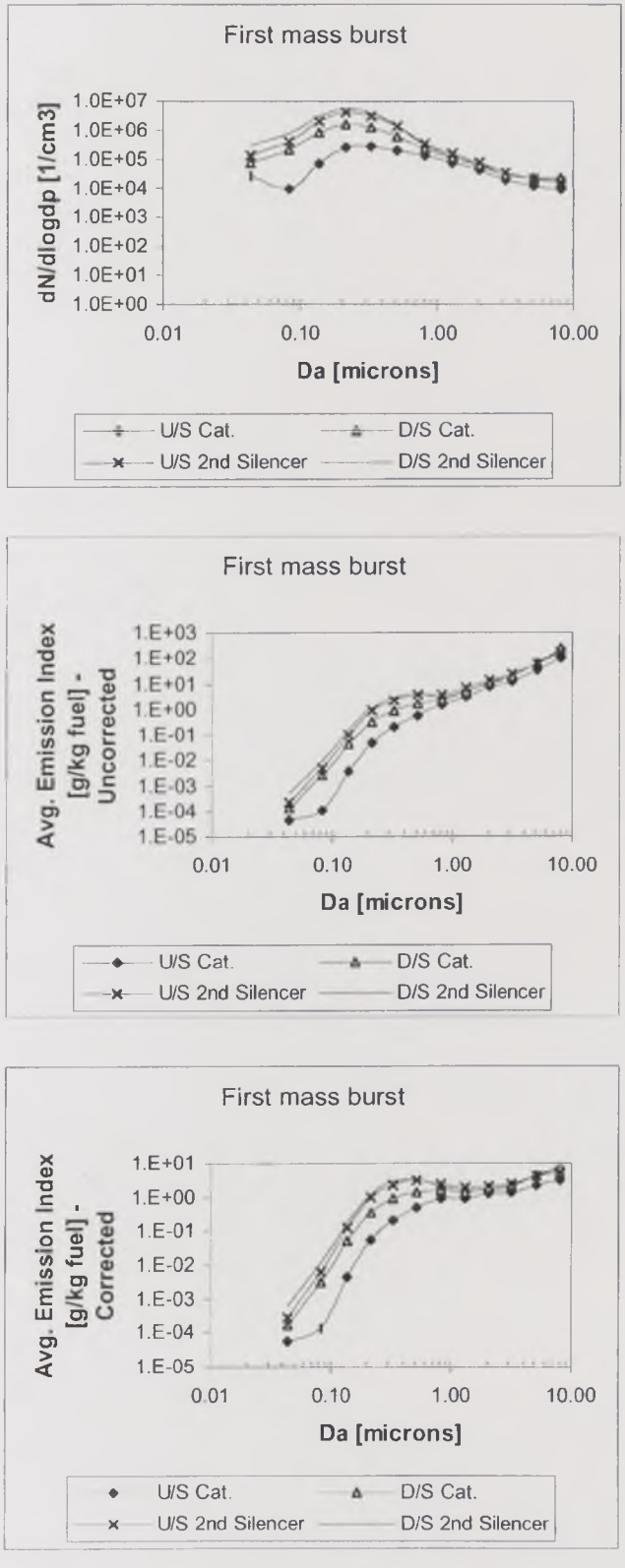

Figure 3.26. Particle size distributions for the first mass burst at various points through the exhaust system (1500rpm – 10kW).

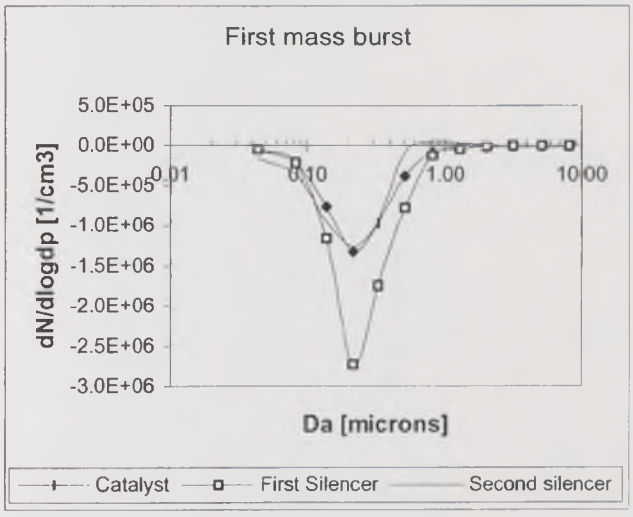

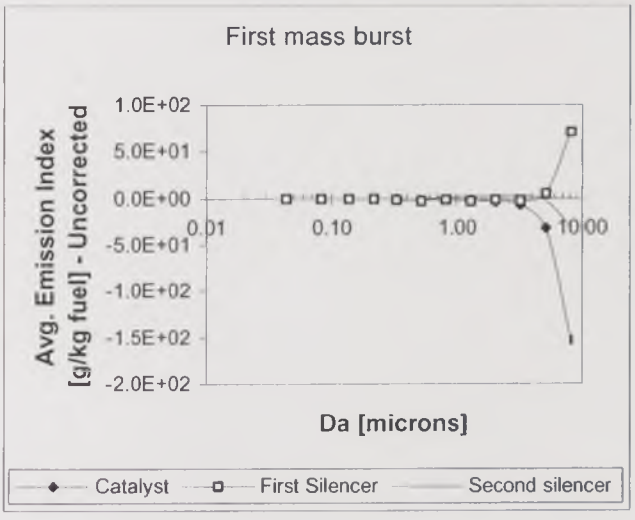

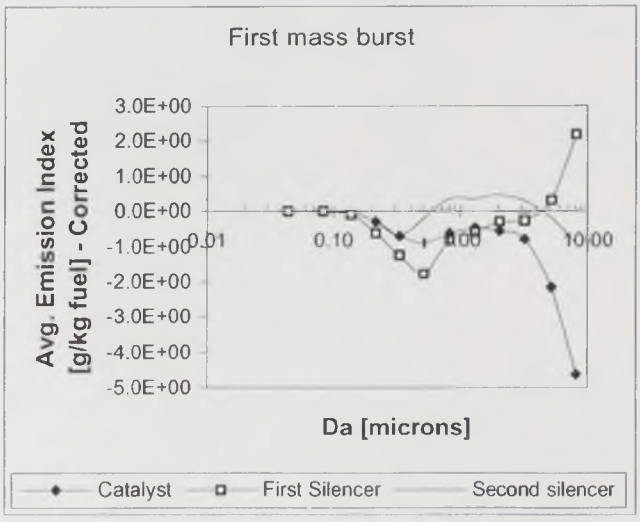

Figure 3.27. Particle blow-out through three sections of the exhaust system, for different size ranges, during the first mass burst event of the cold start (1500rpm – 10kW).

Owing to the still low temperatures, fine particles were formed from the first silencer in this event, increasing the total number concentration by 135%, to $2.3x10^6$ cm^{-3}. In contrast, the total mass concentration calculated with the uncorrected conversion decreased to 57.1 g/kg fuel, by 17%, owing to the deposition of particles larger than 5.0µm. The use of the corrected function, however, reduced the significance of the large-particle mass deposition, making the overall mass concentration to increase by 15%, to 4.9 g/kg fuel downstream of the silencer. It is clear, then, that there was a different behaviour of particles in different size ranges, fine particles were formed through the silencer and large particles deposited presumably by gravimetric and inertial separation.

A 30% increase in particle number concentration took place through the second silencer, to $3.0x10^6$ cm^{-3} at the tailpipe. The mass concentration also increased, by 8% and 3% with and without the corrected conversion, respectively. This was equivalent to 61.9 and 5.0 g/kg fuel. The behaviour of the particles through this silencer was very similar to that through the catalyst, even in the size of particles released, mainly around 0.2µm by number and 0.5µm by mass. Nevertheless, particles between 0.8µm and 1.2µm were actually deposited through the silencer, although not as significantly to affect the overall mass change.

In summary, the first mass burst event of the cold-start test with acceleration to 1500rpm and 10kW showed that, unlike the cold-start in the Idle test, a particle blow-out from the catalyst and the second silencer occurred. The apparent similarity in the behaviour of the particles through these two devices, as well as the opposite, off-phase behaviour through the first silencer as already observed during the cold-start test at idle, were confirmed.

3.6.2.2. Peak by number

The aerosol leaving the turbocharger during the number-peak event had a total concentration of $1.5x10^8$ cm^{-3}, one order of magnitude higher than the corresponding number concentration in the cold-start test at Idle. This converted to a 14.1 g/kg fuel (uncorrected) or 3.3 g/kg fuel (corrected) Emission Index. Through the catalyst, the number concentration was reduced by 50%, down to $7.6x10^7$ cm^{-3}, owing to the deposition and coagulation of very fine particles, those below 0.1µm. Particles larger than this size were blown out, but their number concentration was not significant compared to that of the very fine particles. Their effect on the total mass concentration, however, was important, changing the decrease in number for an increase by 38% (up to 19.4 g/kg fuel, uncorrected) or 12% (up to 3.3 g/kg fuel, corrected) in particle mass through the catalyst. The particle size distribution shifted towards larger sizes through this device.

Particle number concentration continued decreasing through the first silencer, this time by 31%, to $5.2x10^7$ cm^{-3} downstream. Fine particles, below 0.1μm, grew, and the particle size distribution shifted towards larger sizes in the middle-size range. Particles larger than 1.0μm were deposited. This deposition was likely to be thermophoretic. Such behaviour differences among particles in different size ranges, shown in Figures 3.28. and 3.29., caused uncertainty in the net effect on total particle mass concentration. If the uncorrected conversion to mass is used, the particle mass showed to decrease by 44% (down to 10.9 g/kg fuel), owing to the deposition of large particles. In contrast, the corrected conversion to mass reduces the significance of this deposition and increased that of the middle-sized particles that were formed and/or blown-out, so the total particle mass showed to increase by 167%, up to 8.8 g/kg fuel. This is a major question mark in the use of the ELPI to determine transient mass emissions, owing to the trend to overestimate the number of large particles, which account for most of the mass when constant density throughout the size range is assumed.

The deposition and blow-out patterns through the second silencer differed greatly from those found through the previous devices during the number-peak event. Fine and large particles were blown out from the silencer, whereas middle-sized particles deposited on its walls. As a result, the total number concentration decreased to $4.1x10^7$ cm^{-3} (21% decrease), and the total mass increased to 11.4 g/kg fuel (4% increase) when using the uncorrected conversion to mass, although it actually decreased to 3.0 g/kg fuel (66% decrease), if it is calculated with the corrected conversion.

In summary, during the number-peak event of the cold-start test accelerating to 1500rpm and 10kW the behaviour of the aerosol particles was size-dependent, and it may be possible now to associate the change in behaviour to different size-dependent deposition and reentrainment mechanisms. The parallel behaviour of the fine and middle size particles through the catalyst and the first silencer, differing from that through the second silencer, suggests a relationship with the temperature level, –higher in the former devices, lower in the latter–, enhancing the thermophoretic force. Unlike their fine and middle-sized counterpart, large particles showed a parallel behaviour through the catalyst and the second silencer, so a different mechanism affected them. Large particles are less strongly affected by thermophoresis than their finer counterpart. Therefore, flow characteristics determined their deposition and reentrainment patterns. The parallel behaviour, in this case, occurred between the catalyst and the second silencer. This parallelism was observed previously, when the conditions were also more favourable to flow effects than they were to thermophoretic effects at all sizes.

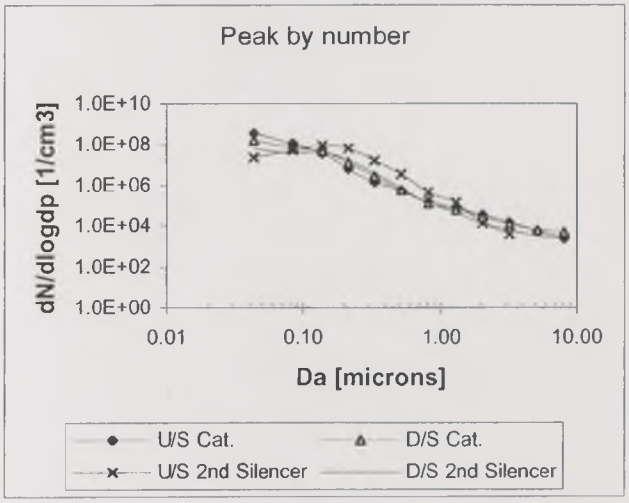

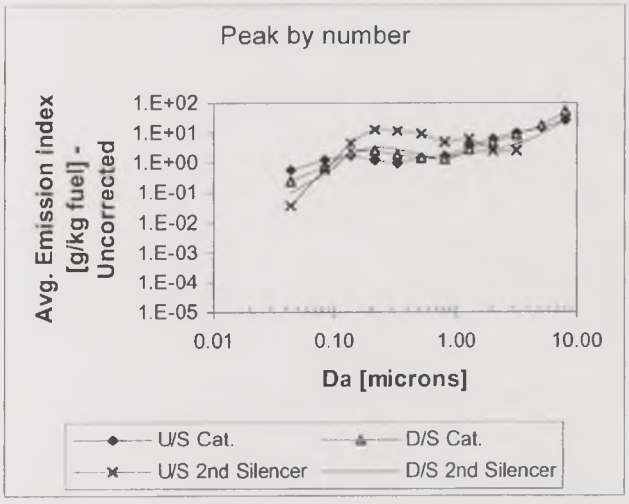

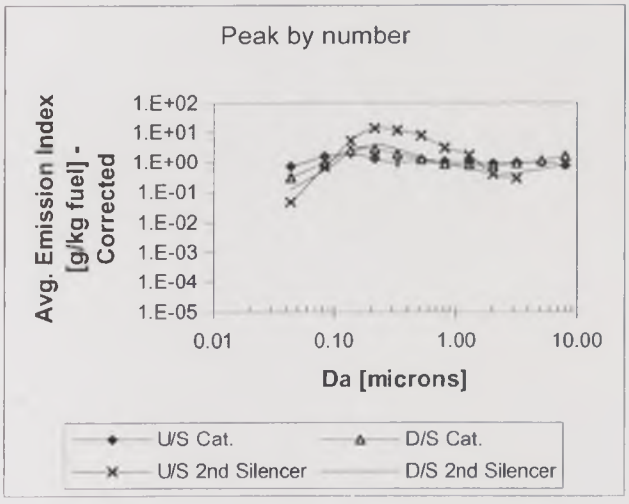

Figure 3.28. Particle size distributions for the peak number at various points through the exhaust system (1500rpm – 10kW).

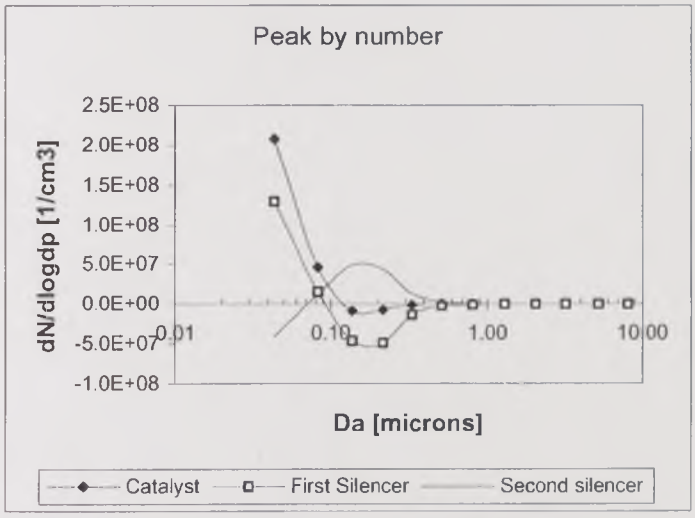

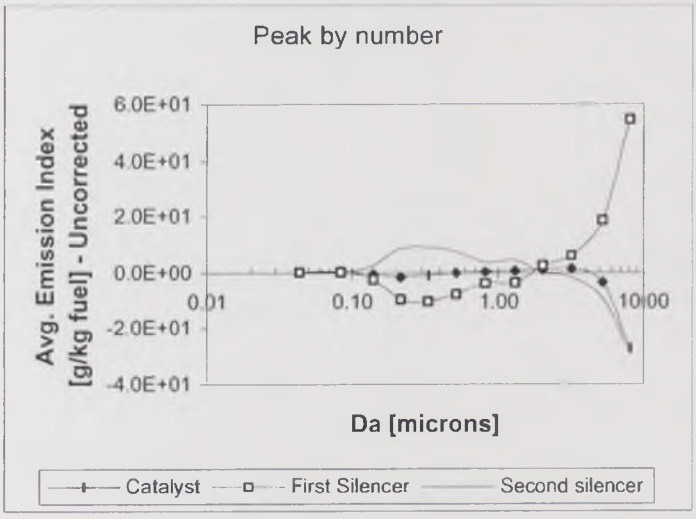

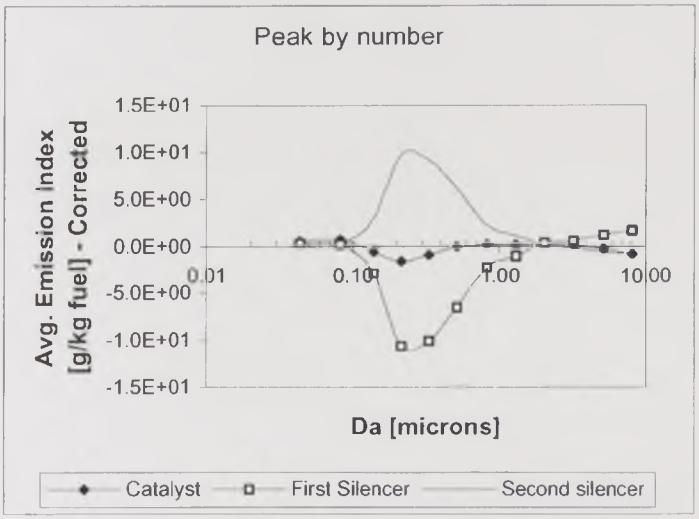

Figure 3.29. Particle blow-out through three sections of the exhaust system, for different size ranges, during the peak number event of the cold start (1500rpm – 10kW).

3.6.2.3. Valley after peak

The valley-after-peak event at the 1500rpm 10kW condition was equivalent to the stabilisation event at idle. The total particle number concentration leaving the turbocharger was $5.7x10^7$ cm^{-3}, roughly 30% of the number concentration at the same sampling point in the number-peak event. The corresponding Emission Index was 12.0 g/kg fuel (uncorrected) or 3.1 g/kg fuel (corrected). The total number concentration decreased through the catalyst by 39%, to $3.5x10^7$ cm^{-3}. Similarly, the total mass concentration decreased by 54% (to 5.5 g/kg fuel, uncorrected) or 36% (to 1.9 g/kg fuel, corrected). This decrease in total number and mass concentration occurred for all size ranges, except those around 0.5µm, which did not change their concentration through the catalyst.

Through the first silencer, total number concentration decreased to $3.4x10^7$ cm^{-3} (2% decrease). The mass concentration, however, increased to 6.7 g/kg fuel (22% increase, uncorrected) or 2.5 g/kg fuel (31% increase, corrected). Only very fine particles, below 0.1µm, deposited and coagulated through the silencer, accounting for the decrease in particle number. Larger particles, in contrast, were blown out, therefore increasing the mass concentration downstream of the silencer. The number and mass concentration of particles around 0.2µm – 0.3µm barely changed. The size distribution shifted slightly towards larger particle sizes (Figures 3.30. and 3.31).

Particles deposited through the second silencer during this event. The number concentration decreased by 28%, to $2.5x10^7$ cm^{-3}, as the particle emission index did by 22% or 18%, that is, to 5.3 g/kg fuel (uncorrected) or 2.1 g/kg fuel (corrected), respectively. As in the case of the catalyst, the deposition occurred for all size ranges. The concentration of particles around 0.2µm, however, barely changed.

In summary, particle deposition occurred through the catalyst and the second silencer at 1500rpm 10kW condition during the apparent stabilisation period after the peak number. Through the first silencer, a decrease in the number of very fine particles indicated deposition and growth by coagulation. Larger particles were blown out from the first silencer.

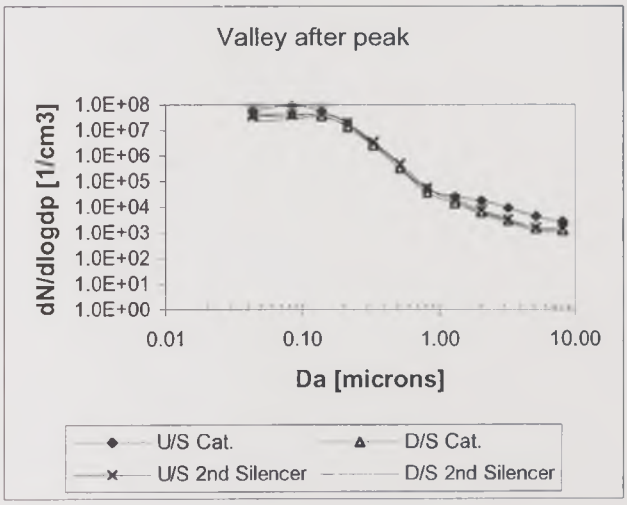

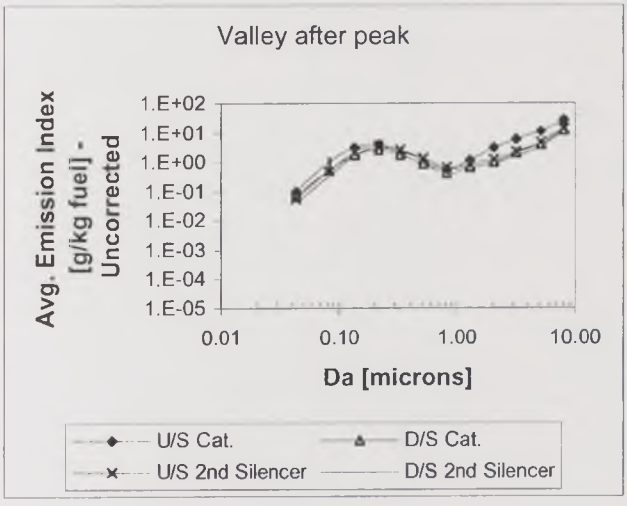

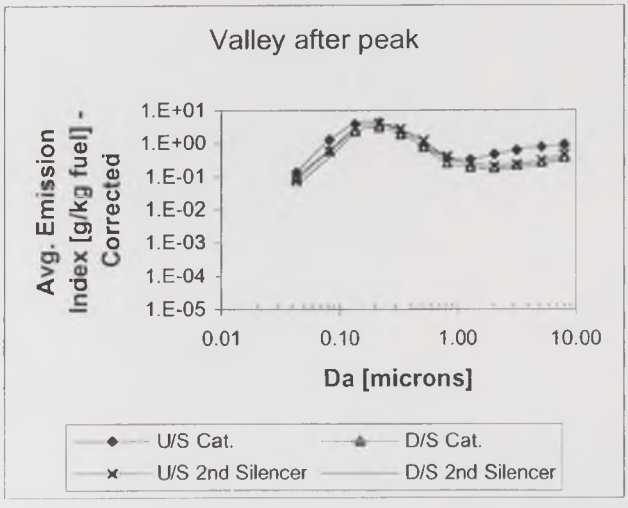

Figure 3.30. Particle size distributions for the valley-after-peak event at various points through the exhaust system (1500rpm – 10kW).

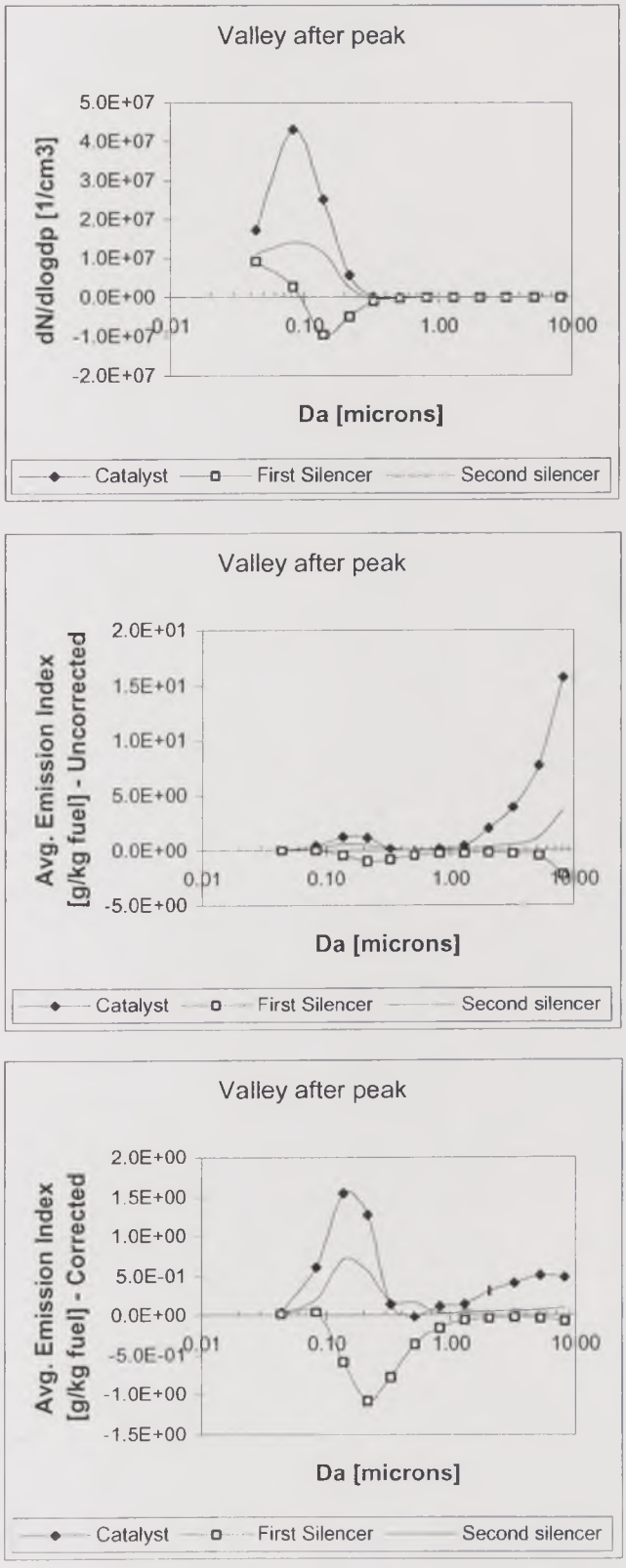

Figure 3.31. Particle blow-out through three sections of the exhaust system, for different size ranges, during the valley-after-peak event of the cold start (1500rpm – 10kW).

3.6.2.4. Increase after EGR

During the test at 1500rpm 10kW, the EGR valve opened after 5 minutes from cold start. By then, the temperatures along the exhaust system had reached steady state and the catalyst had lit off. Therefore, the cold start period could be considered terminated and the analysis of the changes in this period done. However, the total particle number and mass concentration levels after the EGR valve opened were significantly higher than those during the apparent stabilisation in the valley-after-peak event described above. For this reason, the new event is presented and discussed here.

After the EGR valve opened, the total particle number concentration of the exhaust leaving the turbocharger reached a new stabilisation at $7.0x10^7$ cm^{-3}, 25% higher than the previous stabilisation with the EGR valve closed. The corresponding Emission Index was 2.5% higher than the previous stabilisation, 12.3 g/kg fuel, uncorrected; or 36% higher than the previous stabilisation, 4.2 g/kg fuel, corrected). Through the catalyst, the number concentration decreased to $5.5x10^7$ cm^{-3} (22% decrease). In contrast, the Emission Index increased to 14.5 g/kg fuel, uncorrected (18% increase) or 20.6 g/kg fuel, corrected (28% increase). Particles smaller than 0.1μm deposited and coagulated, changing greatly the number concentration, whereas a few particles larger than 0.1μm, with a large mass, were blown out, this being the reason for the change in trend between total particle number and total mass.

Total number concentration increased through the first silencer by 34%, to $7.3x10^7$ cm^{-3}. The corresponding increase in Emission Index was by 42% or 54%, to 20.6 g/kg fuel (uncorrected) or 13.1 g/kg fuel (corrected). Particles of all sizes were blown out, with the exception of those around 40nm, which did not change in number or mass.

Through the second silencer, the total number concentration decreased to $4.3x10^7$ cm^{-3} (41% decrease), which converted to an Emission Index of 13.1 g/kg fuel (37% decrease) or 5.5 g/kg fuel (33% decrease). Particles of all sizes deposited through the silencer. (Figures 3.32. and 3.33.)

In summary, after the EGR valve opened, large particles were blown out from the catalyst and the first silencer and very fine particles through the catalyst were deposited and grew. On the contrary, fine particles coagulated and large particles deposited through the second silencer. The particle size distribution shifted slightly towards larger particles as a result.

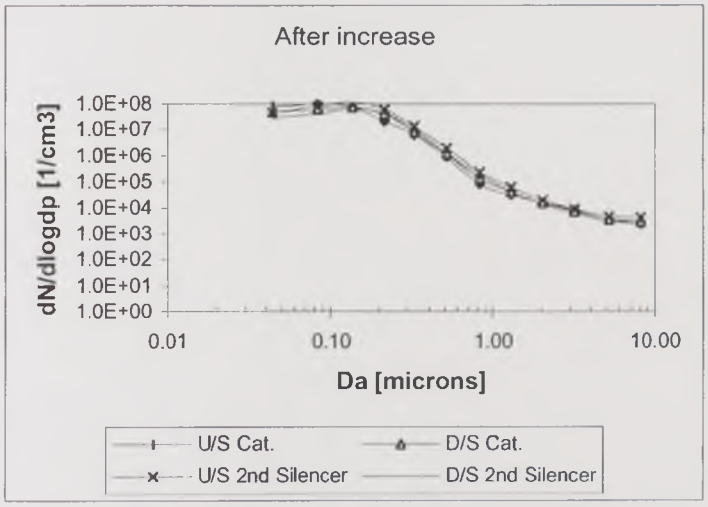

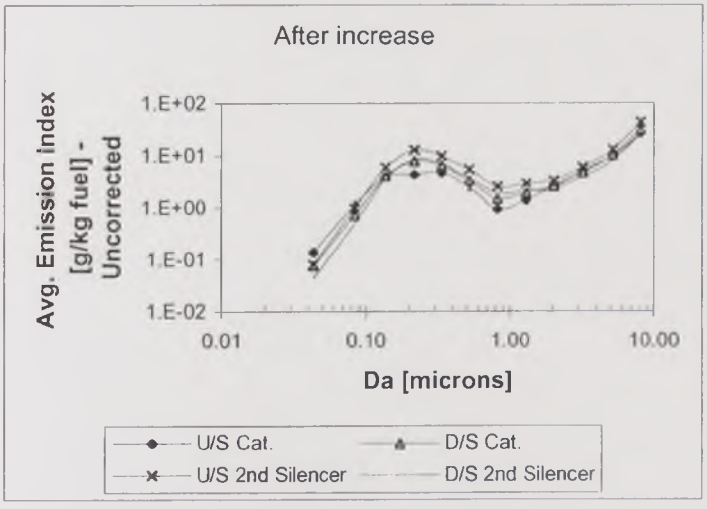

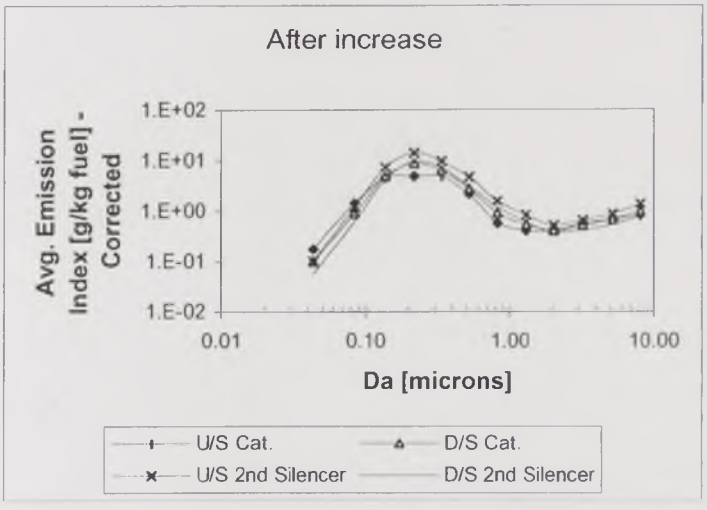

Figure 3.32. Particle size distributions for the increase-after-EGR event at various points through the exhaust system (1500rpm – 10kW).

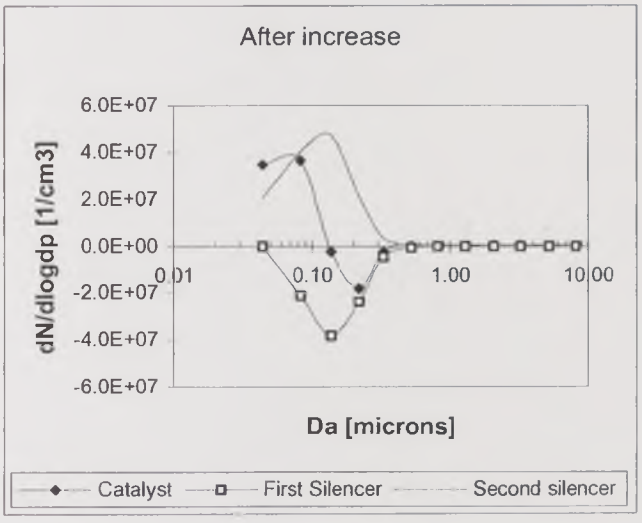

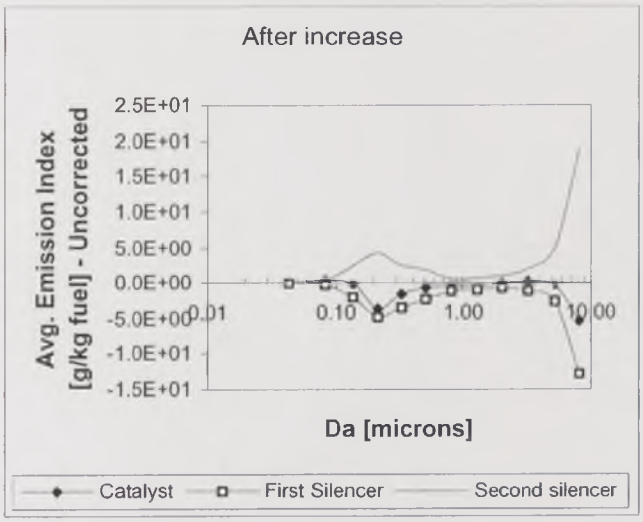

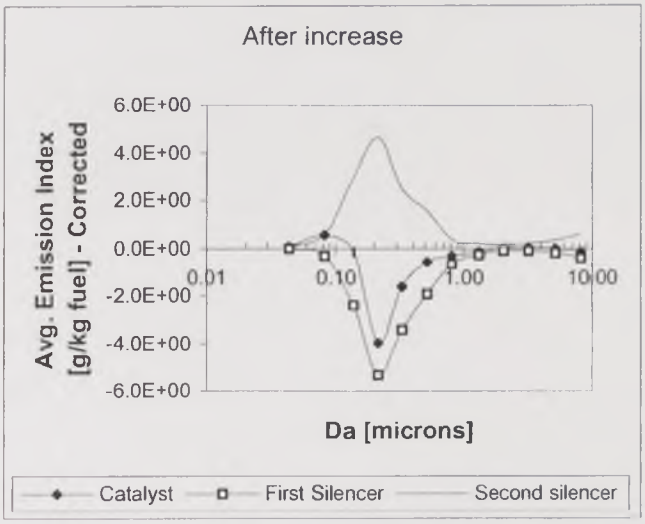

Figure 3.33. Particle blow-out through three sections of the exhaust system, for different size ranges, during the increase-after-EGR event of the cold start (1500rpm – 10kW).

3.6.3. 2250 rpm and 15kW

After analysing the changes that occurred through the exhaust system at 1500rpm and 10kW, a cold start involving a step change to a higher speed and power condition was tested, 2250rpm and 15kW. The expected effects were:

- Higher turbulence in the system, favourable for turbulence-enhanced deposition by diffusion.
- Enhanced particle blow-out of particles due to more significant particle reentrainment from the deposition layer at higher speed.
- Quicker warming-up of gas and metal, with an increased temperature gradient during acceleration, and therefore an enhanced effect on thermophoresis.
- Increased potential for particle agglomeration due to turbulence, owing to the increase in the number and frequency of collisions among particles. However, at the same time, the residence time through the exhaust system decreased, so changes due to coagulation would be seen only if the coagulation occurred in a shorter period than the residence time.

During the cold start with the step-change to 2250rpm - 15kW, the total particle number and mass concentration (as Emission Index) profiles with time in Figure 3.34. showed the same general features as the test at 1500rpm 10kW, namely First mass burst, Number peak, Valley after peak and Increase after the EGR valve opened. Once again, the events were not perfectly synchronised, owing to the test-to-test variability of the manual operation of the throttle during acceleration, so the event-to-event analysis is preferred to a second-by-second one.

3.6.3.1. First mass burst

The total particle number concentration at the turbocharger outlet during the first mass burst was 1.1×10^5 cm^{-3}, which converted to an Emission Index of 8.4 g/kg fuel (uncorrected) or 0.6 g/kg fuel (corrected). From these levels, the number concentration increased to 5.3×10^6 cm^{-3}, and the Emission Index to 59.5 g/kg fuel (uncorrected) or 7.0 g/kg fuel (corrected), through the catalyst. This corresponds to a 47-fold increase in number concentration, and a 6-fold or 11-fold increase in Emission Index, uncorrected and corrected, respectively. The increase in number and mass through the catalyst was expected, since the exhaust system was pre-conditioned at idle for a long period the day before the test, overloading the catalyst channels with particles.

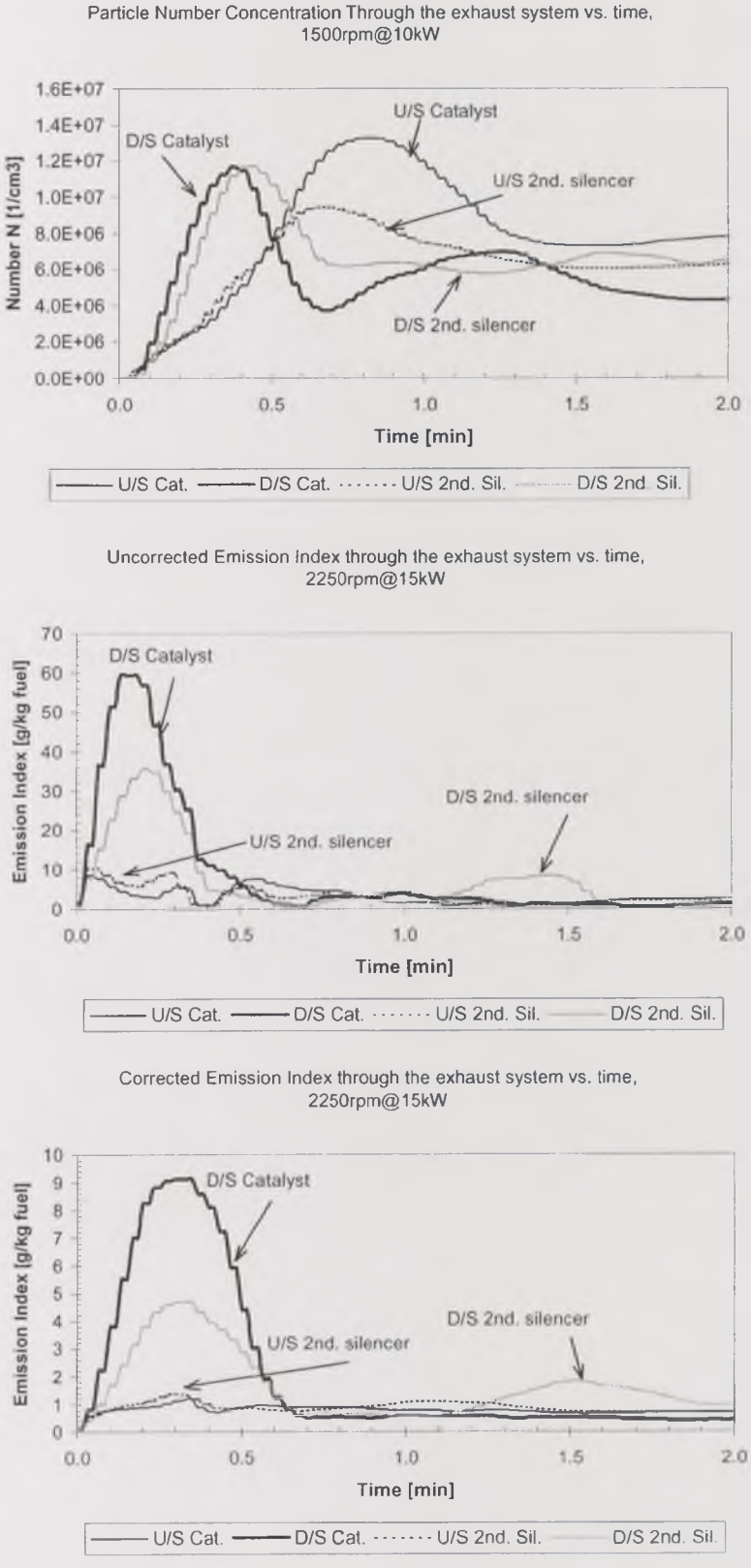

Figure 3.34. Total number and mass concentrations through the exhaust system against time during cold start at 2250rpm – 15kW. a) Concentrations.

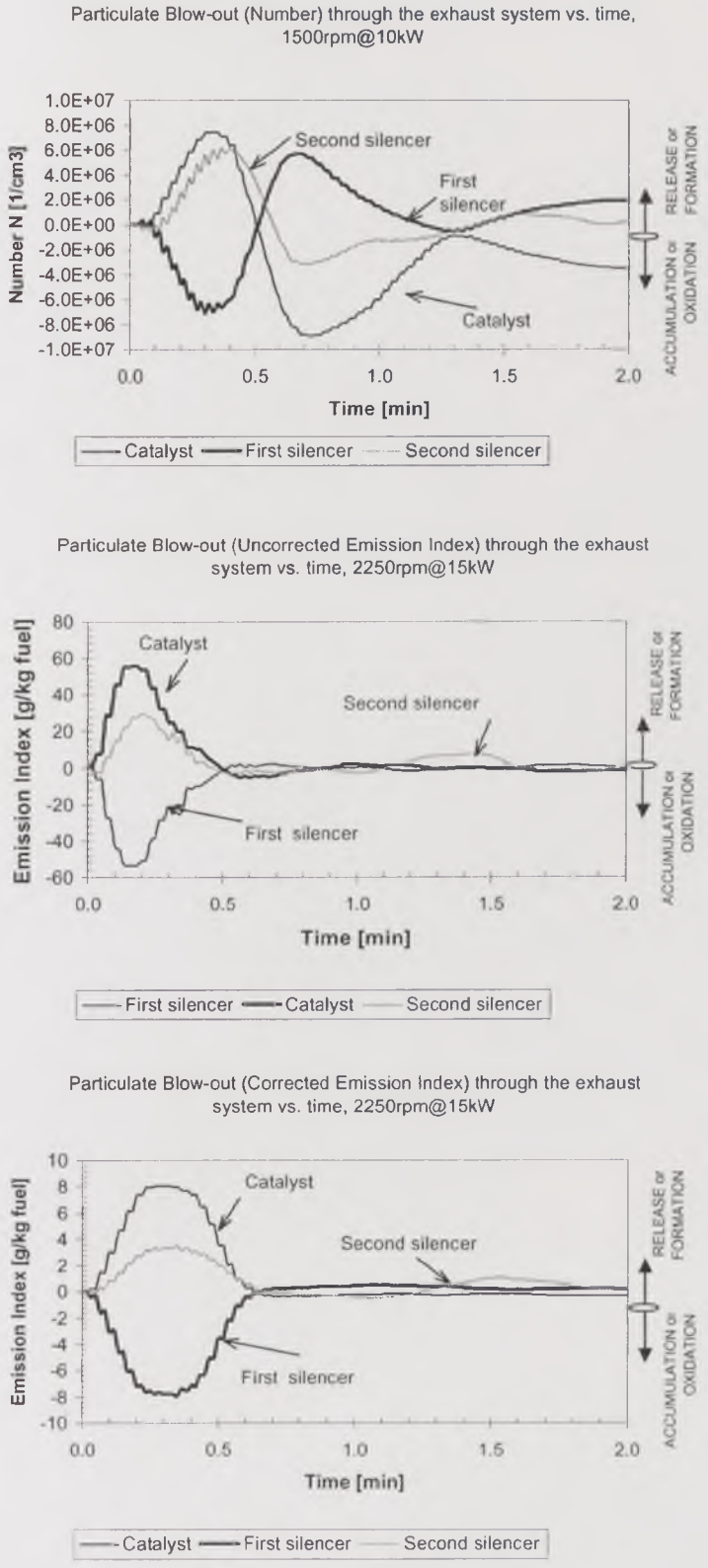

Figure 3.34. Total number and mass concentrations through the exhaust system against time during cold start at 2250rpm – 15kW. b) Blow out.

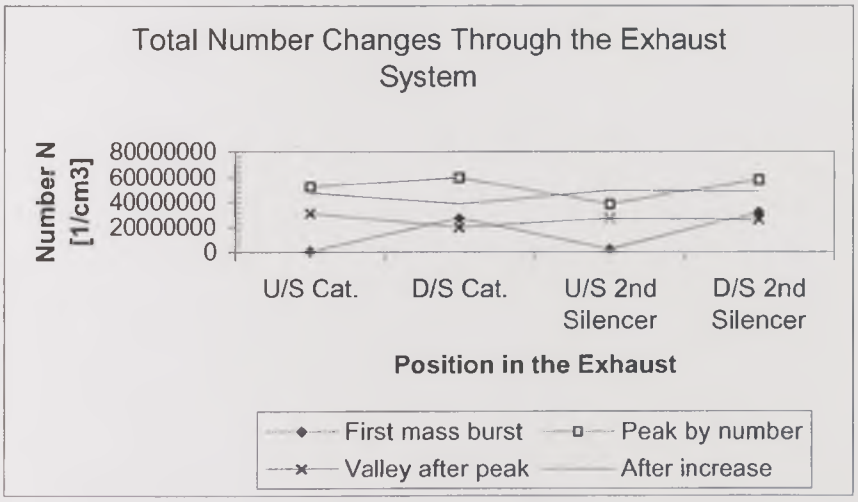

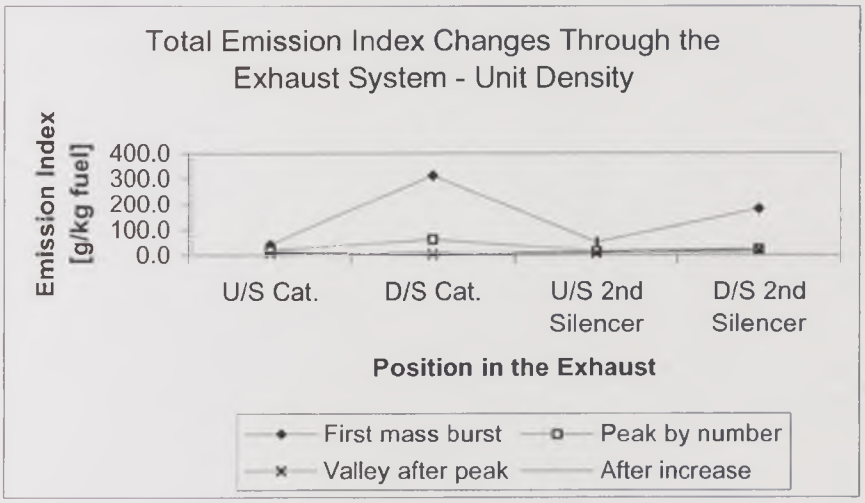

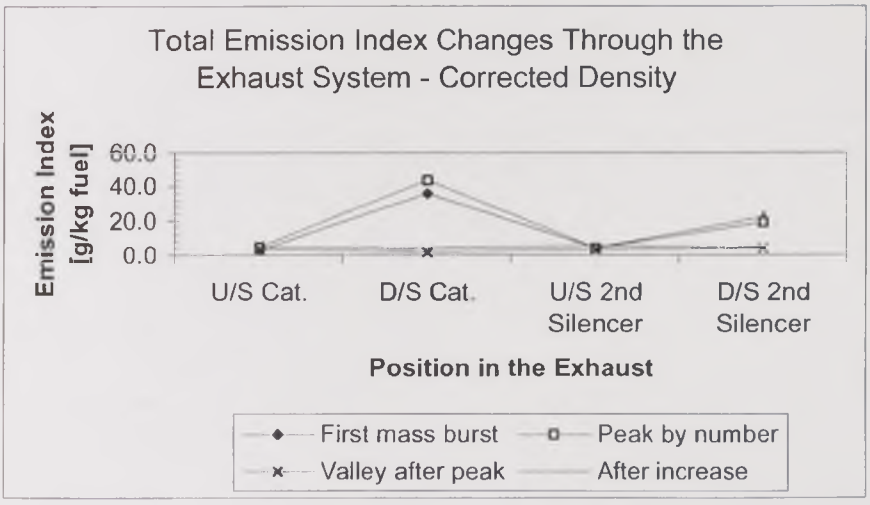

Figure 3.35. Total number and mass concentrations for the main events during cold start at 2250rpm – 15kW against the position in the exhaust.

The increase in particle concentration occurred for all particle sizes, being more significant in number for particles around 0.2μm and in mass for those around

8μm. The results indicate that oxidation catalysts may play a significant role in the blow-out phenomenon.

Through the first silencer, the total particle number and mass concentration decreased to very low levels, similar to those leaving the turbocharger. The decrease was as significant as 91%, 83% and 88% in total number concentration, uncorrected and corrected Emission Index respectively, the resulting levels being $4.8x10^5$ cm^{-3}, 10.2 g/kg fuel and 0.9 g/kg fuel, also respectively. Particles of all size ranges deposited through the silencer. Again, particles around 0.2μm and 8μm contributed more significantly to these changes.

As it occurred through the catalyst, the total particle number concentration increased considerably through the second silencer, emitting $6.2x10^6$ cm^{-3} at the tailpipe, 12-fold as many particles as upstream of the second silencer. The Emission Index more than doubled (quadrupled, if using the corrected mass conversion) through the silencer. These changes occurred for all particle sizes, in the same fashion as through the catalyst (Figure 3.36. and 3.37).

In summary, exhaust particles over all the size range measured suffered deposition through the catalyst and the second silencer, in an exactly opposed behaviour to that through the first silencer, consisting of blow-out. A very similar behaviour was observed during the first-mass-burst event of the 1500rpm 10kW cold-start test, which differed only in the change through the first silencer for particles smaller than 1.0μm. The difference in behaviour of the two silencers may be associated with the temperature differences, the second silencer being colder.

3.6.3.2. Peak by number

As in the test at 1500rpm 10kW, the total particle number concentration increased considerably at all sampling points until reaching a peak. Upstream of the catalyst the peak was $1.3x10^7$ cm^{-3}. The corresponding Emission Index was 4.0 g/kg fuel (uncorrected) or 0.9 g/kg fuel (corrected). The total number concentration decreased to $1.2x10^7$ cm^{-3} (12% decrease) through the catalyst. The Emission Index, on the contrary, increased to 12.8 g/kg fuel (a two-fold increase) or 8.6 g/kg fuel (an 8-fold increase), uncorrected and corrected, respectively. Particle deposition and coagulation accounted for the decrease in particle number concentration mainly below 0.3μm. Particles between 0.3μm and 2.0μm were formed and blown out and particles larger than 2.0μm deposited, although to a lower extent than the deposited middle-sized particles.

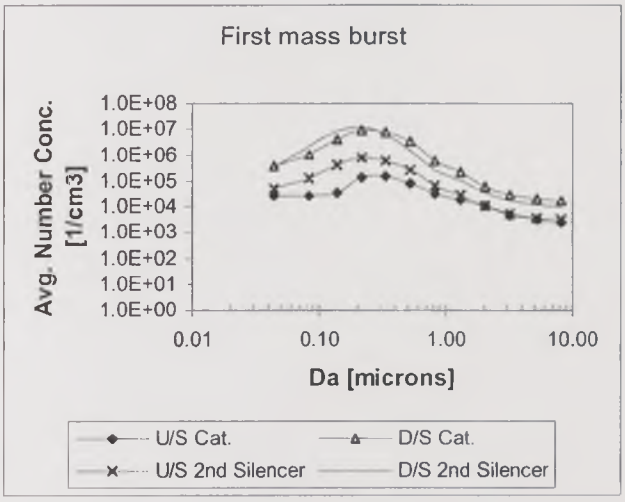

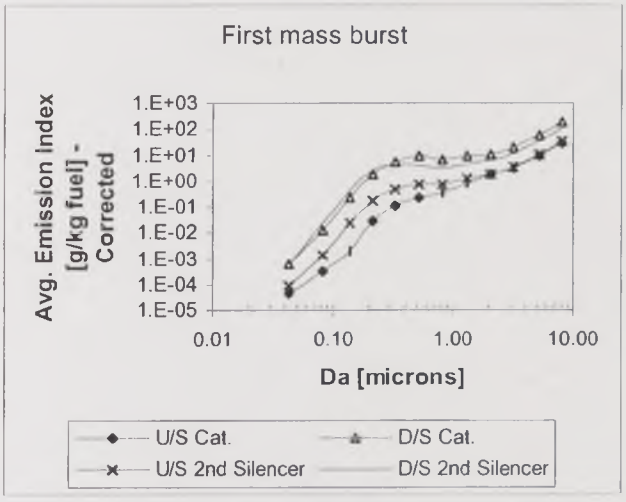

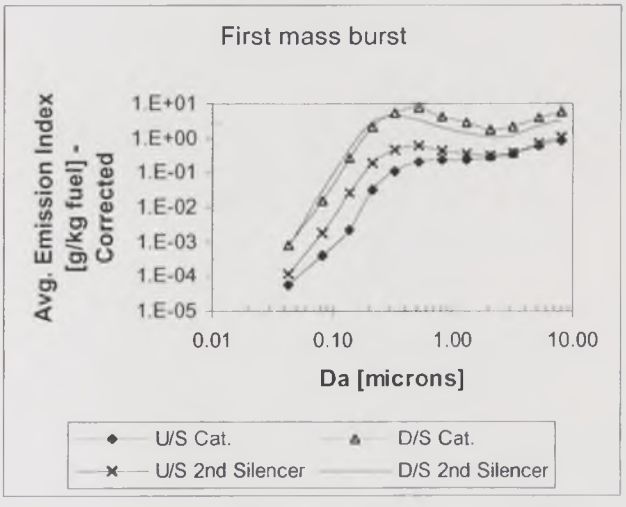

Figure 3.36. Particle size distributions for the first mass burst at various points through the exhaust system (2250rpm – 15kW).

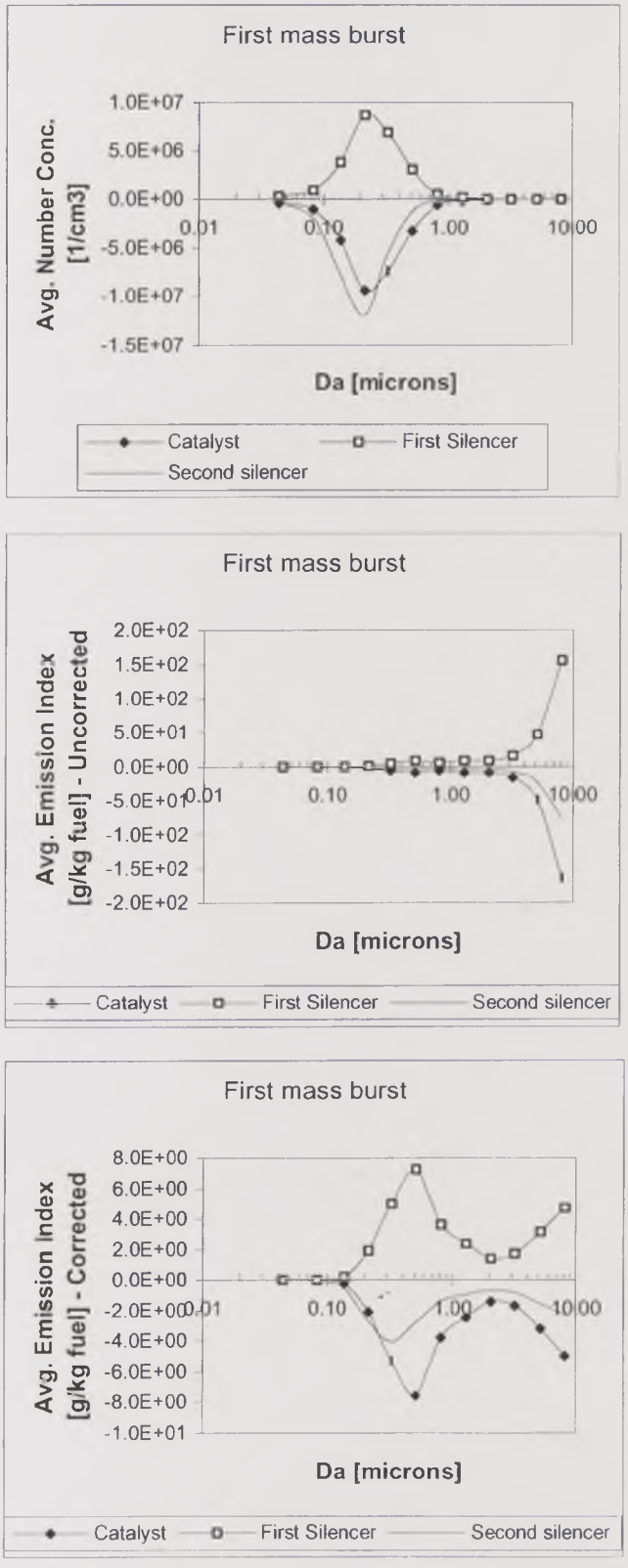

Figure 3.37. Particle blow-out through three sections of the exhaust system, for different size ranges, during the first mass burst event of the cold start (2250rpm – 15kW).

Through the first silencer, total number concentration decreased by 19%, to $9.4x10^6$ cm^{-3}. The Emission Index also decreased in both uncorrected and corrected conversion; by 77%, to 2.3 g/kg fuel, uncorrected; by 91%, to 0.7 g/kg fuel, corrected. The decrease in number concentration, and in Emission Index, was due to the deposition of particles between 0.2μm and 3.0μm. Particles below 0.2μm an larger than 5μm were blown out, as observed in Figures 3.38. and 3.39.

The total particle number concentration increased by 24%, to $1.2x10^7$ cm^{-3}, through the second silencer. The Emission Index also increased by 46%, to 4.4 g/kg fuel when uncorrected, and by 4 times, to 3.7 g/kg fuel when corrected. The changes by size were entirely parallel to those through the catalyst: deposition of particles below 0.2μm and larger than 4μm, and blow out of particles in the middle size range.

In summary, the behaviour of the aerosol through the catalyst and the second silencer has shown to be similar and opposite to that through the first silencer. Fine and coarse particles were deposited through the catalyst and the second silencer, and were blown out from the first silencer, whereas middle-sized particles were deposited through the first silencer and increased their concentration through the catalyst and the second silencer. As a result of combined processes, the particle size distribution shifted towards larger sizes through the catalyst, back to finer sizes through the first silencer, and once again towards larger sizes through the second silencer.

3.6.3.3. Valley after peak

The peak particle number concentration was followed by a decrease to a temporary stabilisation level or valley for all sampling points. Upstream of the catalyst, the valley number concentration was $7.32x10^6$ cm^{-3}, which converted to an Emission Index of 1.6 g/kg fuel (uncorrected) or 0.68 g/kg fuel (corrected). These levels decreased, owing to coagulation, deposition and oxidation through the catalyst, to $4.67x10^6$ cm^{-3}, 1.01 g/kg fuel and 0.37 g/kg fuel respectively, which corresponds to 36%, 34% and 45%, respectively. The number of particles of all size ranges was reduced.

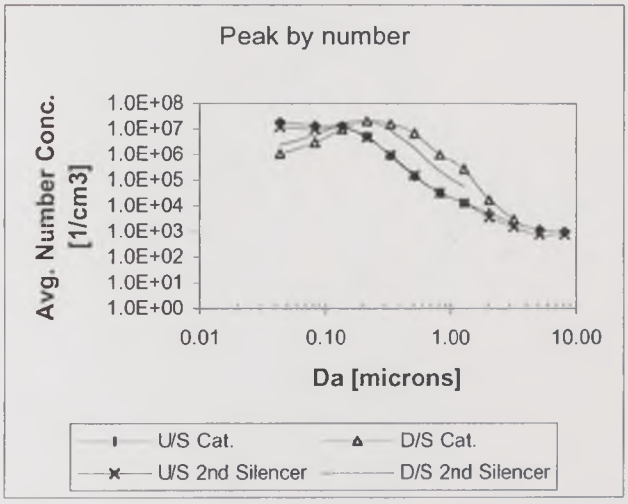

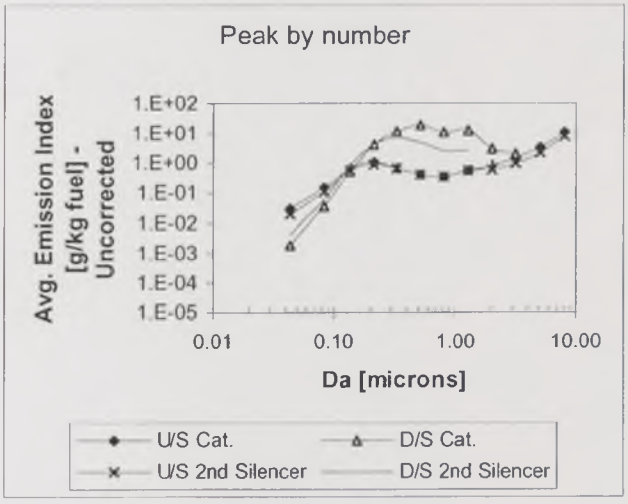

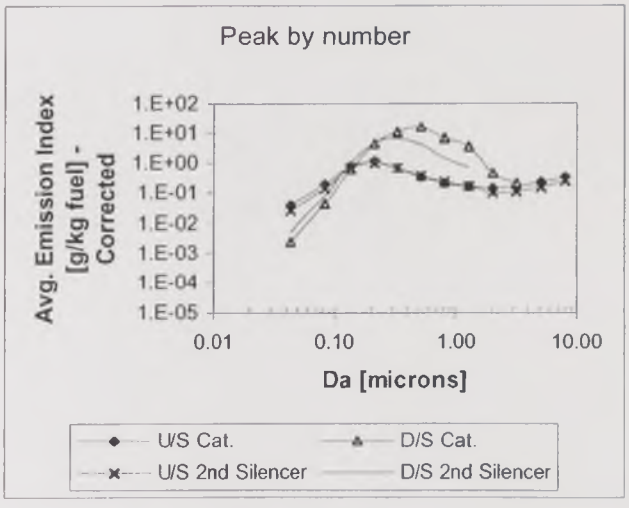

Figure 3.38. Particle size distributions for the peak number at various points through the exhaust system (2250rpm – 15kW).

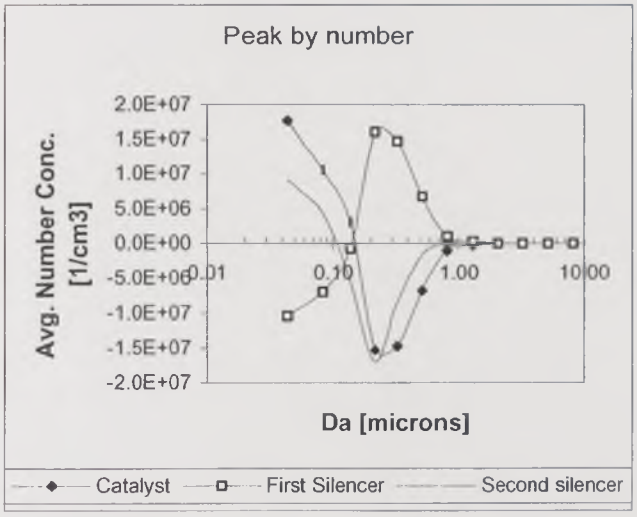

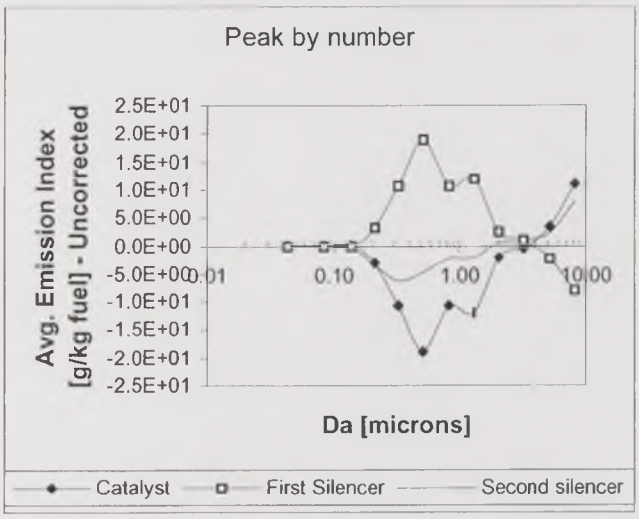

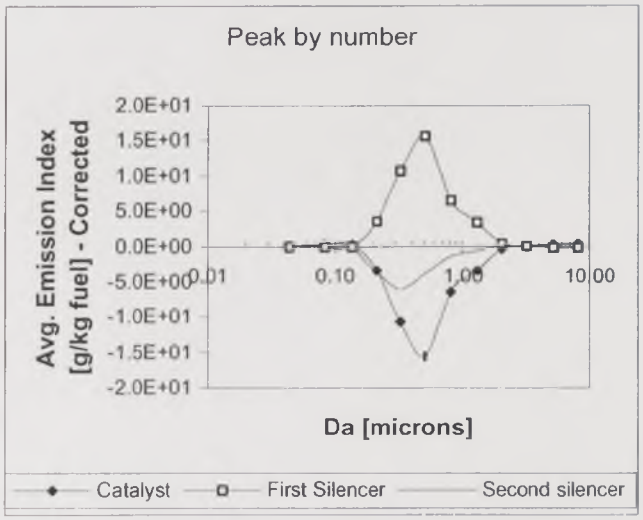

Figure 3.39. Particle blow-out through three sections of the exhaust system, for different size ranges, during the peak number event of the cold start (2250rpm – 15kW).

Through the first silencer, particle number concentration and Emission Index increased by 30% and 42% (uncorrected) or 88% (corrected) respectively, so 6.06×10^6 cm^{-3} were measured downstream of the silencer. This converted to 1.51 g/kg fuel without the number-to-mass correction and 0.37 g/kg fuel with the correction. Only particles in the particle size range 0.1μm to 0.3μm deposited through the silencer, whereas particles smaller than 0.1μm and larger than 0.3μm were blown out from it. Middle-size particle deposition was insignificant either by mass or by number, so the overall effect in total mass was always particle blow-out.

The total particle number concentration did not change through the second silencer during the valley event, so it remained at 6.07×10^6 cm^{-3}. The calculated mass, however, increased by 142%, when no correction was applied, or 12%, when corrected, owing to a change in the particle size distribution. The number of particles around 0.035μm was reduced through the silencer by coagulation and deposition, particles between 0.08μm and 0.5μm were blown out, and those larger than 0.5μm hardly experienced any change in mass concentration, as shown in Figures 3.40. and 3.41. The downstream Emission Index was, therefore, 3.67 g/kg fuel or 0.93 g/kg fuel, for uncorrected and uncorrected conversions respectively.

The valley-after-peak event at 2250rpm – 15kW showed once more that, when passing through the catalyst and the second silencer, the aerosol showed opposite deposition and/or blow-out trends from those observed when passing through the first silencer. The catalyst showed again a good capacity to reduce the particle number and mass by deposition and oxidation. Very fine and large particles showed parallel deposition/blow-out trends, opposite to those of middle-sized particles. No significant change in particle size distribution was observed.

3.6.3.4. Increase after EGR

As mentioned above, the EGR valve opening caused an increase in particle number concentration after the temporary stabilisation described in the valley-after-peak event. In most cases this caused an increase in Emission Index, with some exceptions, as described below.

Particle number concentration upstream of the silencer reached $1.10 \times 10^7 cm^{-3}$ and 2.26 g/kg fuel (or 0.96 g/kg fuel with the corrected conversion) after increasing as a result of the EGR valve opening. Through the catalyst, these values decreased to 8.78×10^6 cm^{-3} and 2.10 g/kg fuel (0.86 g/kg fuel, corrected), which corresponds to a 20% and 6% (10%, corrected) decrease by coagulation, deposition and oxidation. Figures 3.42. and 3.43. show that no large particles were blown-out from the catalyst walls for any size range, they all were deposited.

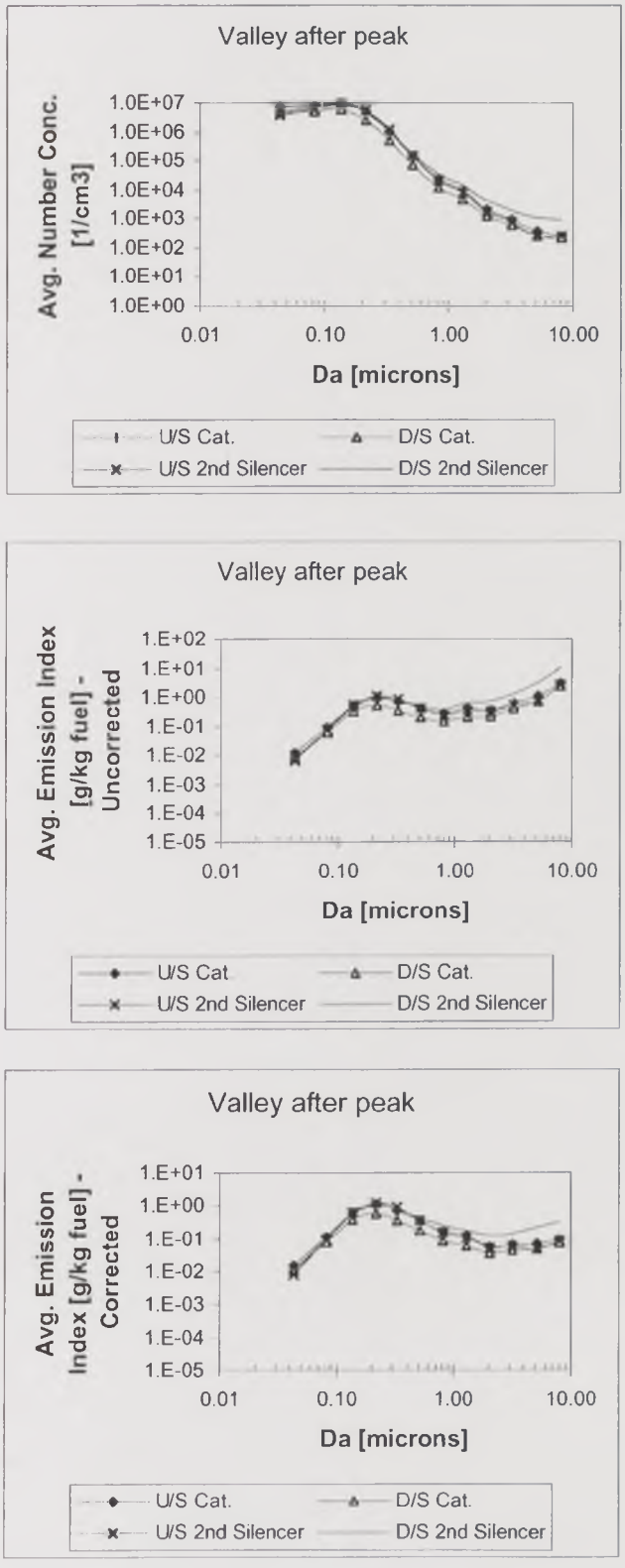

Figure 3.40. Particle size distributions for the valley-after-peak event at various points through the exhaust system (2250rpm – 15kW).

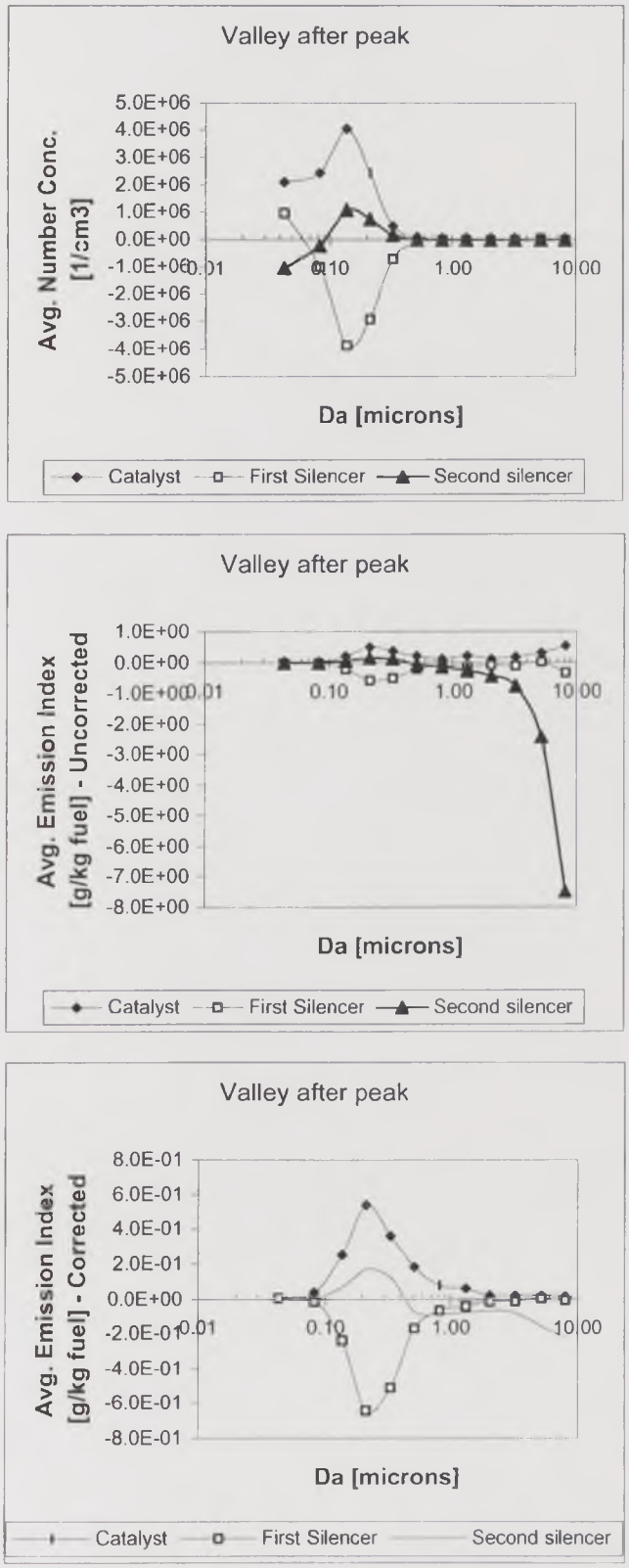

Figure 3.41. Particle blow-out through three sections of the exhaust system, for different size ranges, during the valley-after-peak event of the cold start (2250rpm – 15kW).

Through the first silencer, particle number concentration increased by 28%, reaching $1.13x10^6$ cm^{-3}. The Emission Index increased by 10% (uncorrected) or 24% (corrected), reaching 2.33 g/kg fuel or 1.06 g/kg fuel respectively. The increase was due to the formation of fine particles and the blow-out of large particles from the silencer walls. Only particles around 0.5μm deposited, but the extent of this deposition was negligible.

Particle number concentration decreased due to deposition through the second silencer by just 1% during this event, to $1.12x10^6$ cm^{-3}. Emission Index decreased to 1.96 g/kg fuel (uncorrected) or 0.93 g/kg fuel (corrected), that is, by 16% or 12 %, respectively. The deposition occurred for particles larger than 0.1μm. Particles below that size were formed by nucleation-condensation-coagulation processes, although not significantly.

In summary, after the number concentration increase due to the EGR valve opening, the catalyst continued showing a good retention and conversion capacity for particles of all sizes. Particles were blown-out from the first silencer and deposited through the second silencer. These trends were observed in previous events of this test. No important change in particle size distribution was observed.

3.7. Key points from this chapter

3.7.1. Filter measurements

- The oxidation catalytic converter acted as a particulate trap during cold start at initial ambient temperature, with an efficiency that was higher at idle and low-speed conditions than at high-speed conditions. It acted as an efficient particle trap at idle.
- The previous operational history of the engine had a greater influence on the catalyst performance than did the initial temperature.
- Particulate mass deposits were released from the section of the exhaust located downstream of the catalyst at all conditions studied, as an overall result of accumulation and release through the two silencers.
- Particulate mass was released from the first silencer of the exhaust system and deposited in the second silencer in all cold-start tests for the three conditions studied. Mass accumulation and release rates at idle were more important than those at low and high speed.
- The net release of particulates downstream of the catalyst was a very large fraction of the tailpipe particulate emissions at all test conditions.

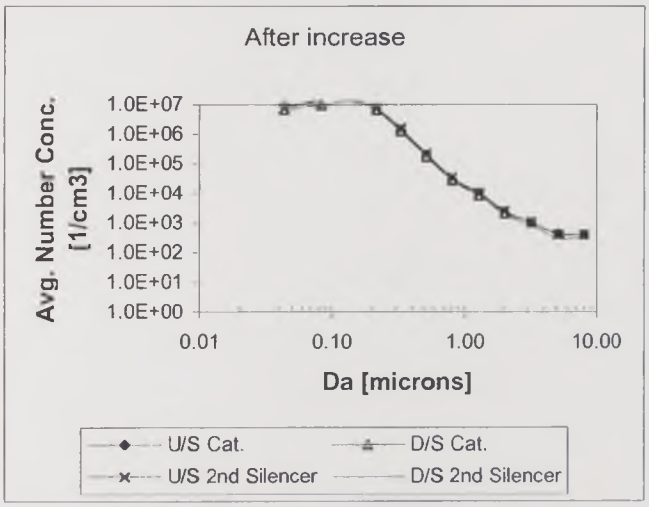

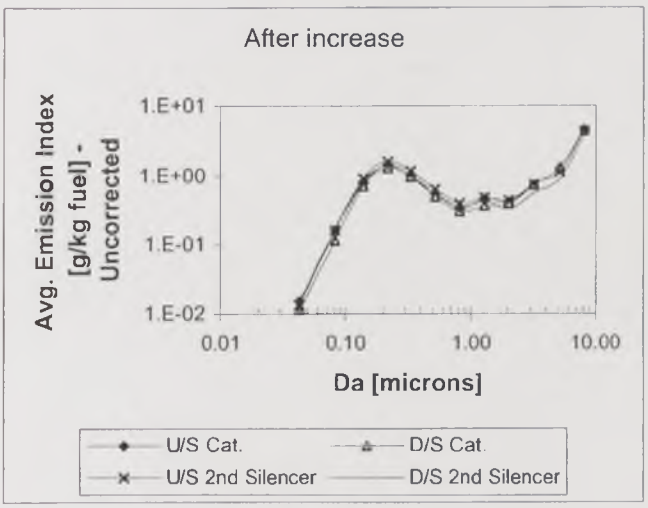

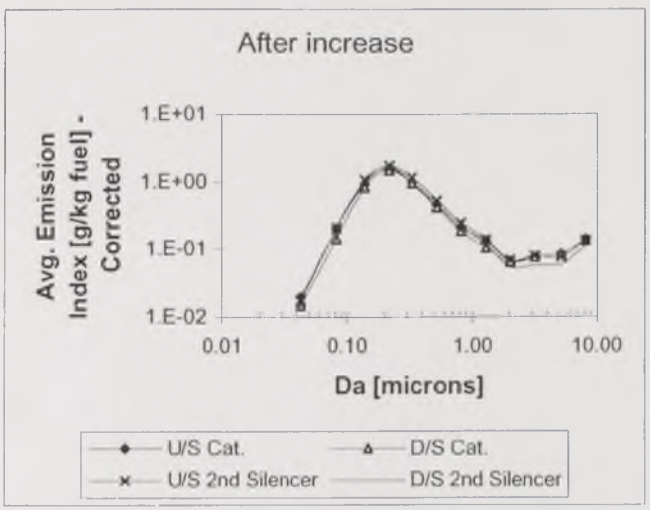

Figure 3.42. Particle size distributions for the increase-after-EGR event at various points through the exhaust system (2250rpm – 15kW).

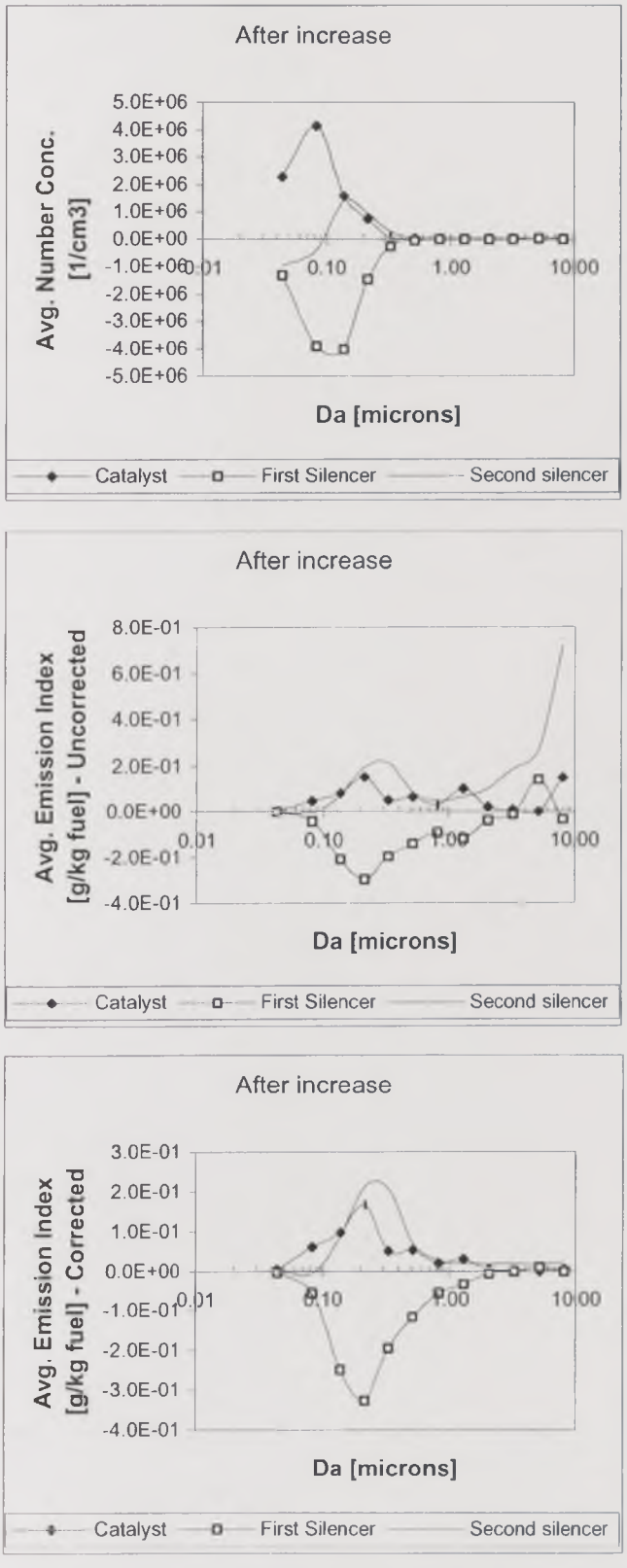

Figure 3.43. Particle blow-out through three sections of the exhaust system, for different size ranges, during the increase-after-EGR event of the cold start (2250rpm – 15kW).

- The deposition in the exhaust section downstream of the catalyst was greater than the tailpipe emissions at all test conditions.
- The tailpipe emissions were greater than those downstream of the catalyst at all test conditions. Consequently, exhaust system particulate deposition played an important role in tailpipe emissions and the transient emissions depended on the previous operational history of the engine.
- For the three test conditions of idle, 10 and 15kW all showed particulate deposition in parts of the exhaust. All three test conditions showed a net blow out from the exhaust, downstream of the catalyst. These low power test conditions are typical of urban driving in dense traffic conditions. It was considered that a net blow from all parts of the exhaust required a higher flow rate condition. This was investigated, and the results are shown in Chapter 4.

3.7.2. Size distribution measurements

- Particle number concentrations at 1500rpm and 10 kW were between twice and ten times as high as those at 2250 rpm and 15 kW and idle.
- The occurrence of processes increasing the particle number concentration and Emission Index was demonstrated. These were gas-to-particle conversion in the ultrafine size range, condensation and coagulation in the mid-size range, and resuspension of large particles stored on the catalyst and in both silencers. Fast accelerations promoted to a certain extent these processes throughout the exhaust. Resuspended particles had been accumulated from previous conditioning at idle.
- At Idle, the catalyst and the second silencer accumulated particles during cold start. The first silencer promoted particle formation and resuspension in the same period.
- At low and high speed, the catalyst promoted ultrafine particle formation during the first seconds of the cold start.
- Particles through the first silencer showed a symmetrically opposite behaviour to that through the catalyst at low speed, being accumulated during the first minute and released afterwards. At high speed, particle growth was the predominant process that occurred inside the silencer.
- These opposite trends in the mass and number of particles emitted were due to differences in the particle size involved in the events. The

engine-out mass emissions were dominated by particle sizes of 3μm - 8μm, which had a negligible contribution to the total particle number. The peak particle number concentration was due to ultrafine (~0.040μm – 0.080μm) particles.

Further analysis of the effect of engine conditions, main events during transient and exhaust devices on particulate emissions and size distribution changes is given in Chapter 4, after describing the results from cold-start high engine speed and high engine load tests.

Chapter 4.
Cold Start Particulate Mass Emission and Particle Size Distribution Changes Through a Practical Exhaust System – High Speed and High Power Tests

Particulate mass concentration, total particle number concentration and particle size distribution were measured during cold start at 2250rpm –35kW and 3500rpm – 15kW. Particulate mass tests were carried out using the gravimetric filter mass measurement technique; the number concentration and the number-weighed particle size distribution were measured with an ELPI, using an ejector-type, double dilution system for a 100:1 dilution ratio. Temperatures along the exhaust system were monitored and gas analysis downstream of the catalyst was carried out continuously. Two preconditioning procedures were used the day before for comparison, namely Idle for four hours, and high speed for ten minutes. The aim of the first procedure was to produce an important particulate deposition in the exhaust system in a short time, an amount of mass equivalent to that deposited under urban driving conditions for about a week. The second procedure aimed to quickly clean the exhaust system of fluffy particulate deposits. In this way, the influence of the previous history of the engine was investigated through a comparison between "dirty" and "clean" exhaust conditions at the moment of running cold-start tests.

4.1. Exhaust Temperature Changes During Cold Start: Catalyst light-off temperature and aerosol - metal temperature differences

As in the previous tests, gas and exhaust system wall temperatures were monitored during cold start at the new conditions tested, with the aim of detecting the catalyst light-off temperature and determining the thermophoretic deposition potential (Figures 4.1. and 4.2.).

Catalyst temperatures show the moment at which the catalyst lights off, indicated at the first moment at which the temperature downstream of the catalyst was higher than upstream of it as a consequence of the heat release by the oxidation of CO and UHC once the catalyst is active. This occurred around 110 seconds from cold start at 3500rpm – 15kW and 30 seconds later at 2250rpm – 35kW, at a temperature around 240°C and 300°C respectively.

At high-load conditions, 2250rpm - 35kW, the exhaust gas temperature increased from ambient to 650°C in 4 to 5 minutes, with a maximum gas-metal difference of about 300°C after the first two minutes. At the tailpipe, the gas

temperature decreased to 350°C and its difference with the metal temperature was around 100°C. The temperature difference between gas and metal was less than 200°C in the first silencer and 100°C in the second during the same period.

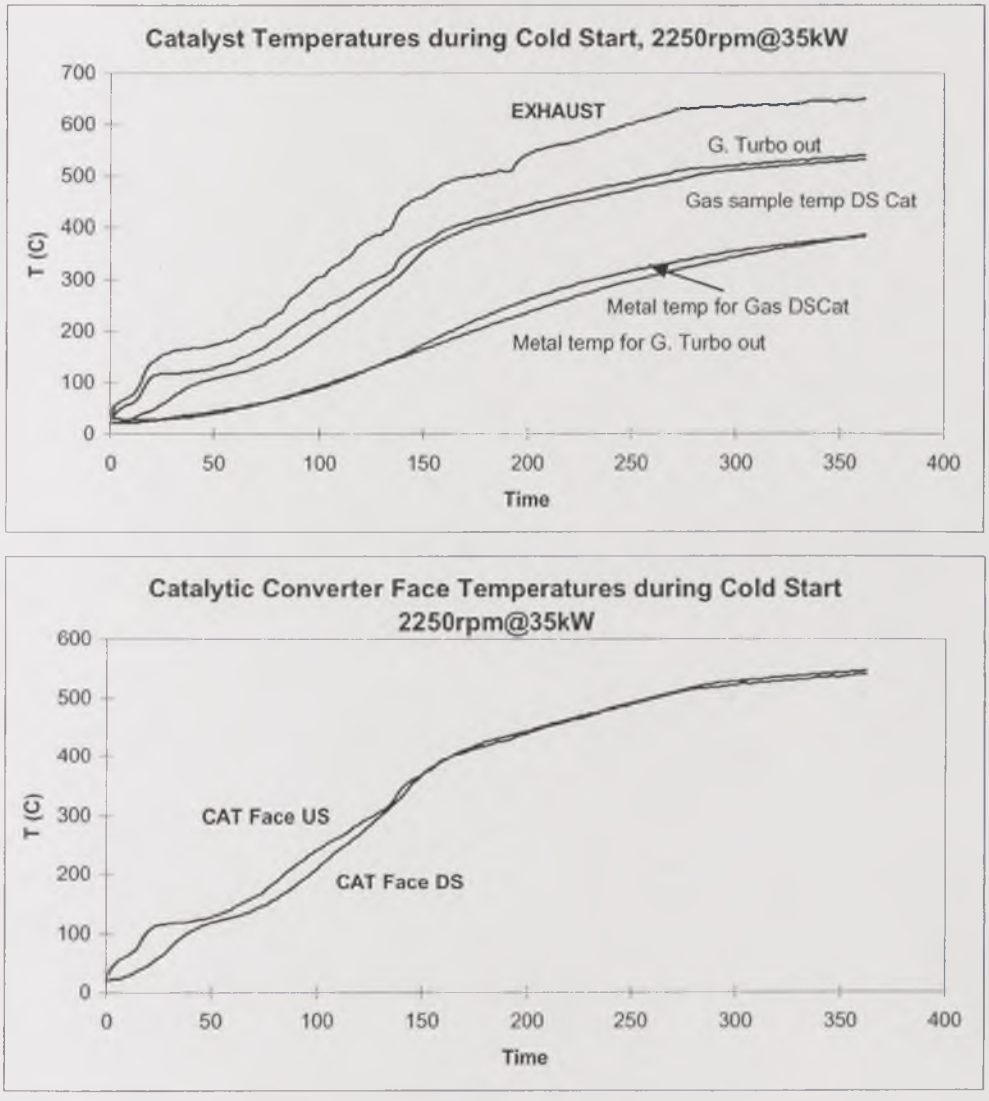

Figure 4.1. Catalyst temperatures during cold start at various operation conditions. a) 2250rpm - 35kW.

In contrast, the gas temperature at the exhaust during the test at high speed and medium load conditions, 3500rpm 15kW, increased only up to 350°C in 4 minutes, with a maximum gas-metal difference of 150°C after the first 2 minutes. This difference was just over 50°C in the first silencer and lower in the second silencer and at the tailpipe, where the gas temperature has decreased to just above 200°C.

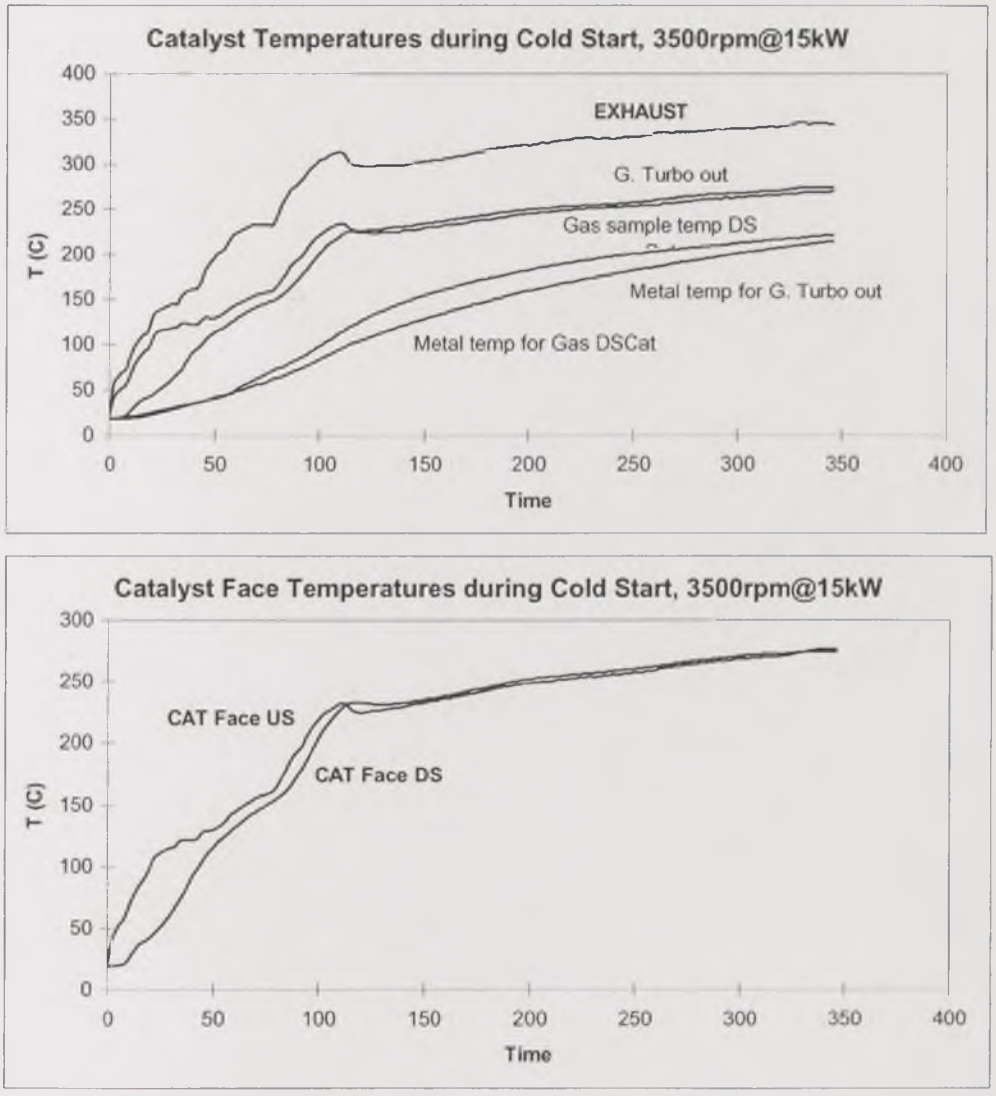

Figure 4.1. Catalyst temperatures during cold start at various operation conditions.
b) 3500rpm - 15kW.

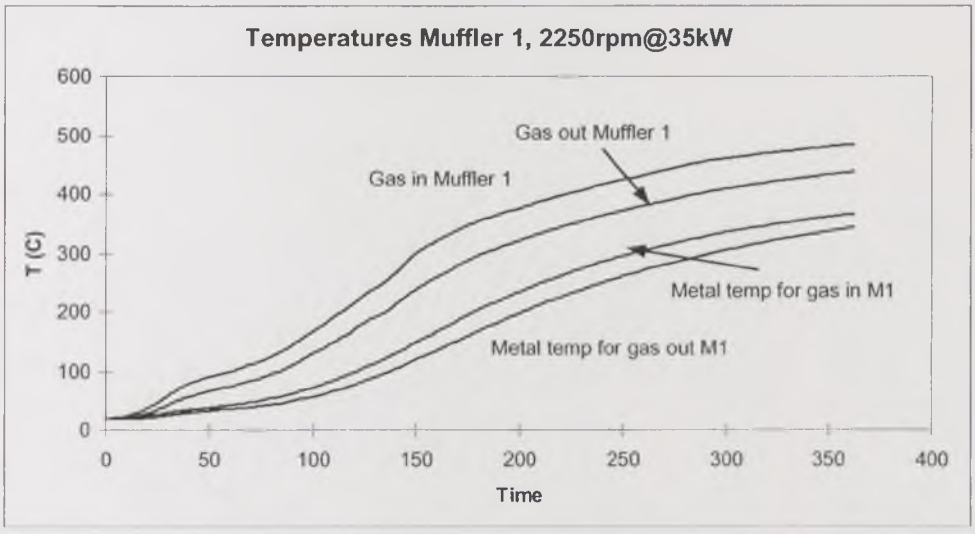

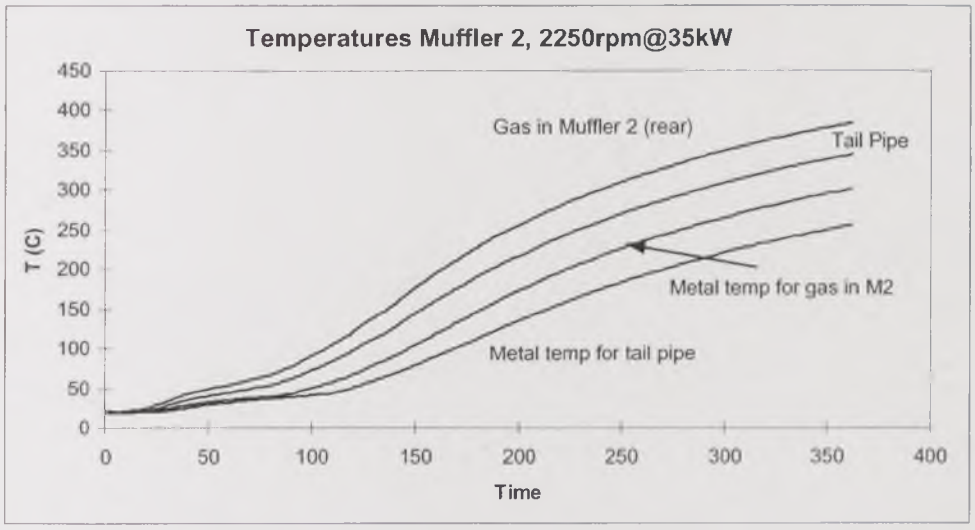

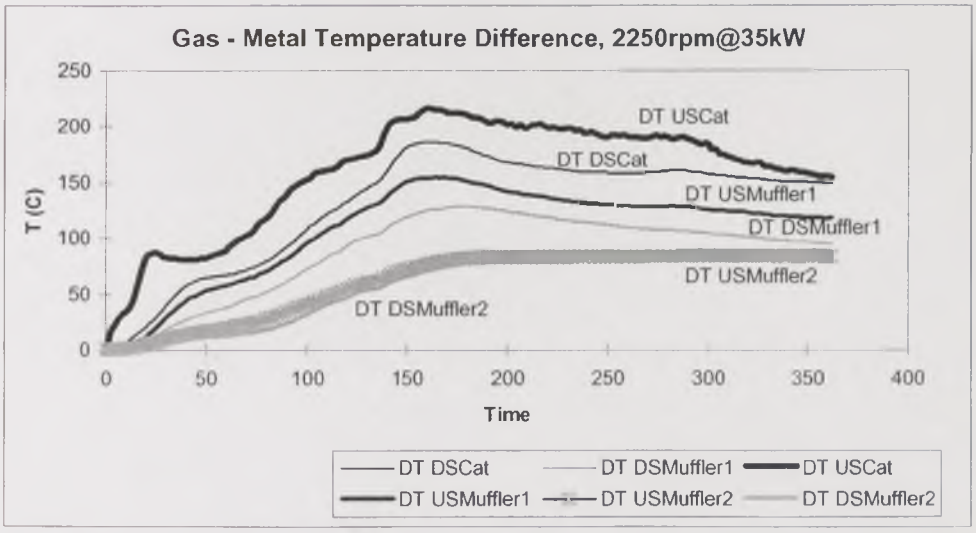

Figure 4.2. Exhaust gas and wall temperatures and temperature differences through the exhaust system. a) 2250rpm - 15kW.

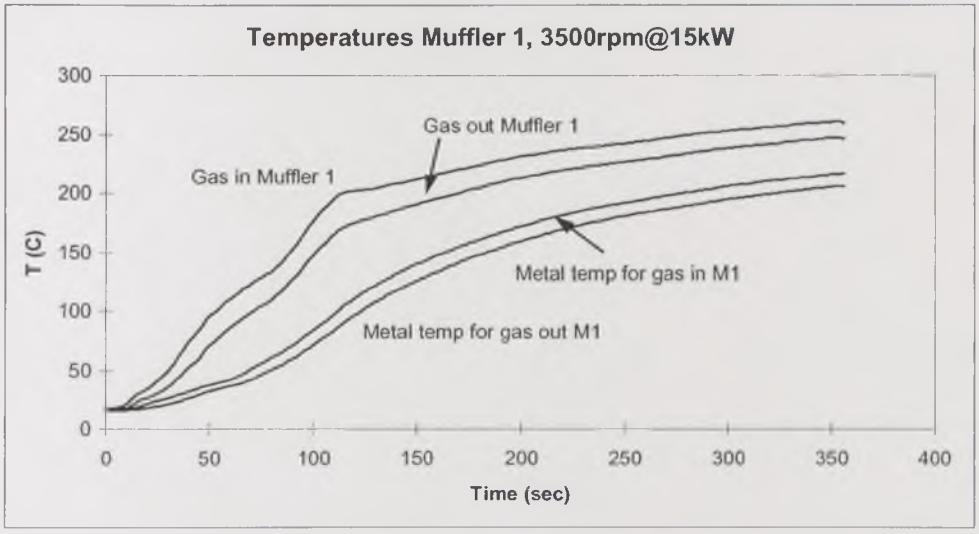

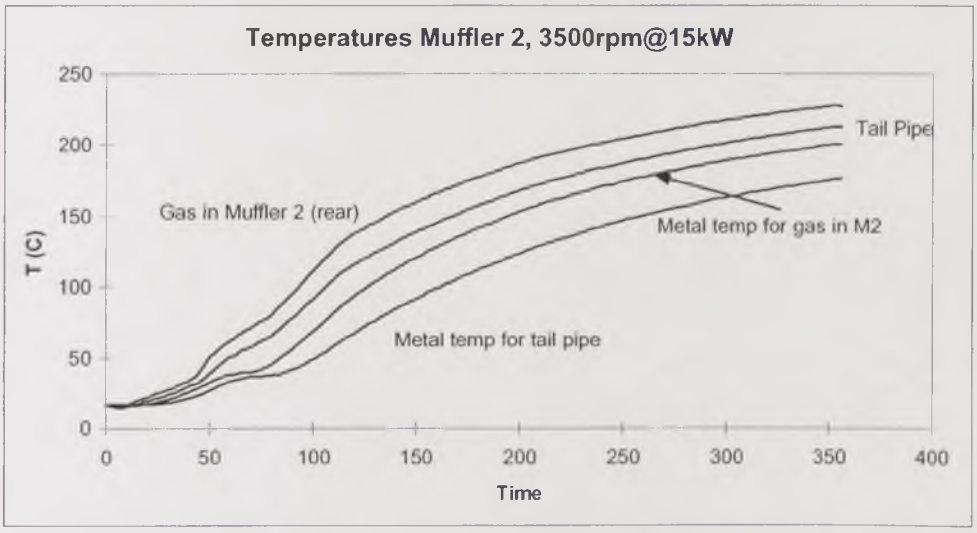

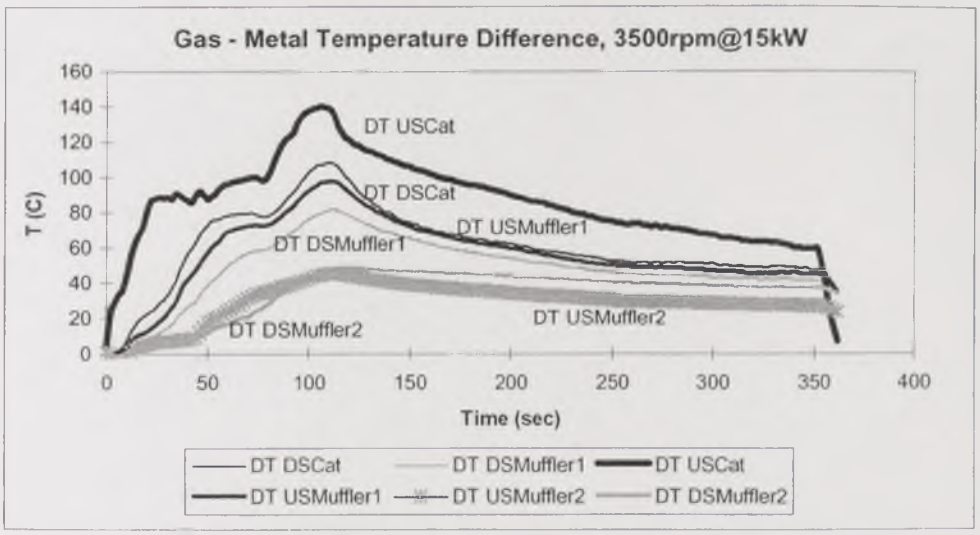

Figure 4.2. Exhaust gas and wall temperatures and temperature differences through the exhaust system. b) 3500rpm - 15kW.

4.2. Hydrocarbon Emissions During Cold Start

Different hydrocarbon profiles were observed at the various conditions tested. Hot-FID UHC analysis downstream of the catalyst shows in Figure 4.3. how, during the cold start at 3500rpm – 15kW with idle preconditioning, the hydrocarbon adsorber worked properly during the first twenty seconds, impeding a stronger increase in UHC to levels over 200ppm. However, the increase in temperatures over 100°C caused thermal desorption of previously adsorbed hydrocarbons and a new increase occurred to nearly 350ppm UHC downstream of the catalyst between 40 and 90 seconds. After the desorption, and helped by the catalyst light-off, a decrease in UHC levels to 100ppm in half a minute and just a few ppm in the following three to four minutes occurred.

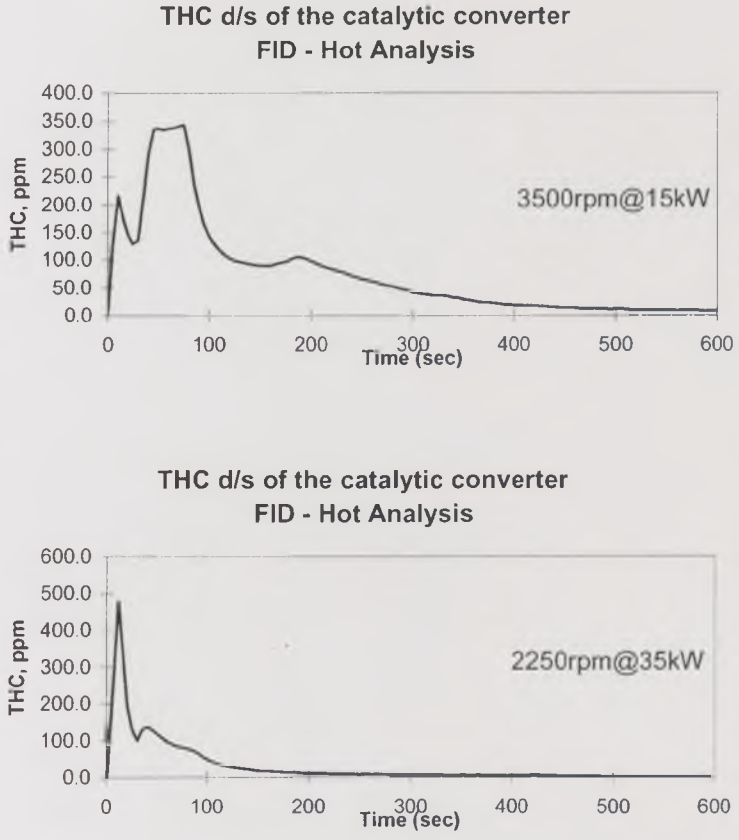

Figure 4.3. Hydrocarbon emissions during cold start measured downstream of the catalyst.

On the other hand, at 2250rpm – 35kW with high-speed preconditioning a higher initial peak in UHC occurred owing to a heavier acceleration, which was

controlled by the hydrocarbon adsorber in a few seconds. Despite the higher increase in temperature caused by high-load conditions, the increase in UHC levels observed in the conditions explained above did not occur, since there were no deposited particles from which HC could be desorbed. Instead, a continuous decrease in HC levels under 100ppm was achieved before 100 seconds from cold start, with a further decrease in the following minutes.

4.3. Filter Mass Concentration Changes Through the Exhaust System During Cold Start

4.3.1. Particulate concentration changes at different positions in the Exhaust System

The particulate mass emissions, as g/kg-fuel (Emission Index), are shown at the four simultaneous sampling positions in the exhaust in Figure 4.4. Both high-speed and high-load conditions, with idle and high-speed preconditioning, are shown as a function of the time from the cold start. The data points are shown for the middle of the time period for which the filter papers were sampled over. Similarly, Figure 4.5. shows the Emission Index as a function of time for high-speed preconditioning, but in this occasion the sampling time was extended to 2400 seconds, approximately one sample every 600 seconds.

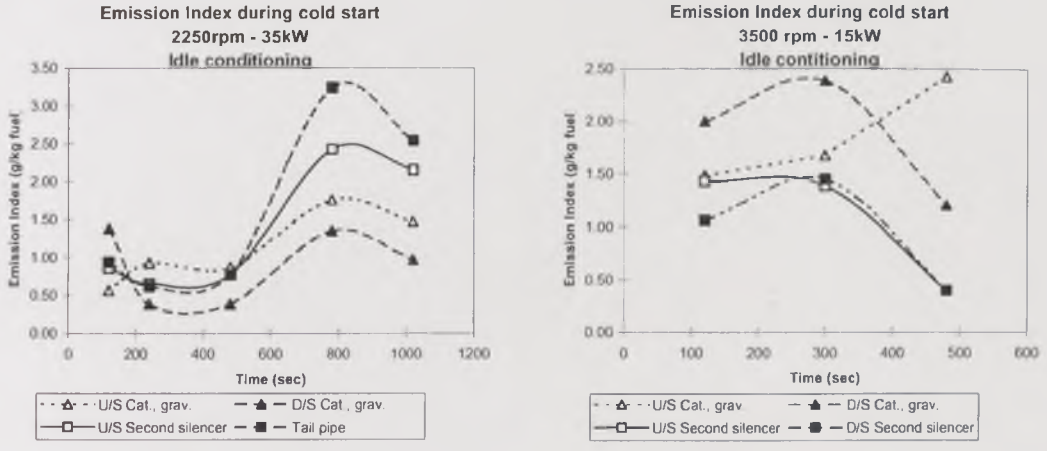

Figure 4.4. Emission Index during cold start through the exhaust system after Idle preconditioning.

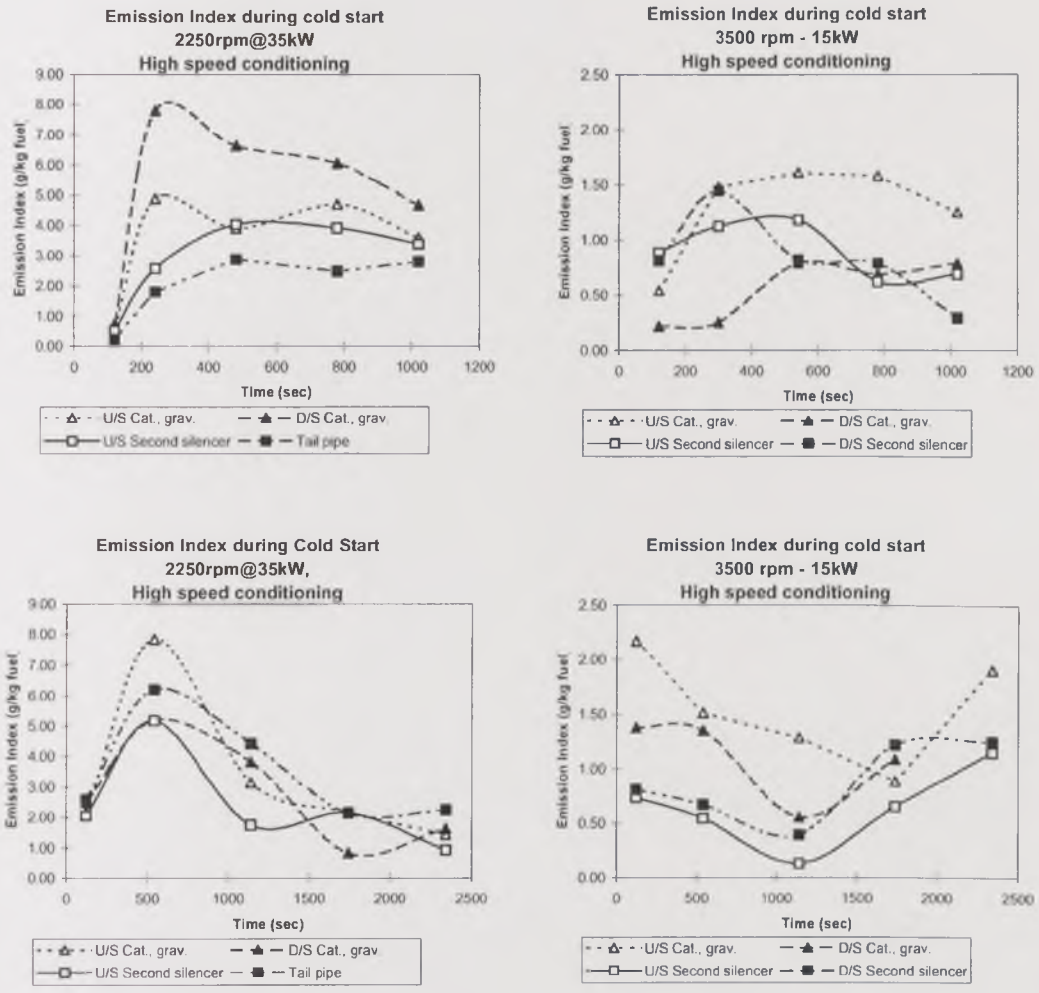

Figure 4.5. Emission Index during cold start through the exhaust system after high-speed preconditioning.

As it was seen in the previous stage of the work, the present results show that for all of the tests there was considerable difference in the particulate emissions between the four sample positions during cold start. However, for the new conditions tested, there was more complexity in the Emission Index profiles against time. A first overview reveals similar profiles when running at 2250rpm – 35kW; Emission Index increased or decreased at the same time at different points and definite trends could be depicted. This similarity occurred for both Idle and high-speed tests, though there were key differences between both tests that will be analysed below. In contrast, similar profiles were observed only for a short period of the tests at 3500rpm – 15kW and there were no clear increases or decreases of the Emission Index against time.

As a general rule, Emission Index profiles at high-load conditions showed an initial low level followed by an increase to a maximum level and a further decrease

to levels where a trend towards stabilisation was observed. The initial increase occurred between 10 and 15 minutes from cold start in the test with idle preconditioning, and between 5 and 10 minutes from cold start when running the test with high-speed preconditioning. The levels reached were also different: a maximum below 3.5 g/kg-fuel and an average around 1.75 g/kg-fuel for the test with Idle preconditioning; and a maximum of 8.0 g/kg-fuel and an average around 3.0 g/kg-fuel for the test with high-speed preconditioning. These results were surprising, since a higher Emission Index was expected at all points downstream of the catalyst in the test with Idle preconditioning, when deposits had been built on the system walls. However, looking at the Emission Index upstream of the catalyst, which corresponds to the raw emissions from the engine, the same situation was observed, so there might have been a different factor affecting the particulate emission before they enter the exhaust system, and apparently, the EGR valve and EGR system in general were playing a role. A comparison of tailpipe emissions at the stabilisation period (2.0 g/kg-fuel) with legislated levels indicated that emissions at these conditions greatly exceeded the limit of 0.32 g/kg-fuel.

Emission Index profiles at 3500rpm – 15kW fell into a lower and narrower range than those described for 2250rpm – 35kW. An average between 1.0 g/kg fuel and 1.5 g/kg-fuel was observed in all tests, with some minimum values around 0.2 g/kg-fuel and maximum around 2.4 g/kg-fuel. Tailpipe emissions fell normally around 0.5 g/kg-fuel, which still exceeded the legislated limit, though not so dramatically as in the high-speed conditions. In summary, emissions showed that both of the high-speed and high-load conditions selected were unfavourable to the compliance of legislated limits.

Cold start with a step change to high-speed and high-load conditions showed differences in Emission Index along the exhaust system, which indicated that deposition and blow-out processes were occurring at these conditions, as well as the low-speed and low-load conditions tested in the previous stage of this work.

4.3.2. Particulate Storage and Blow-out in the Exhaust Section Downstream of the Catalyst

Figure 4.6. shows the particulate blow out from different exhaust sections downstream of the catalyst, expressed in g/kg-fuel, for both high-speed and high-load conditions, and for both Idle and high-speed preconditioning procedures. Positive values indicate that particulate blow out from the walls at the designated section occurred. Negative values, in contrast, indicate particulate deposition.

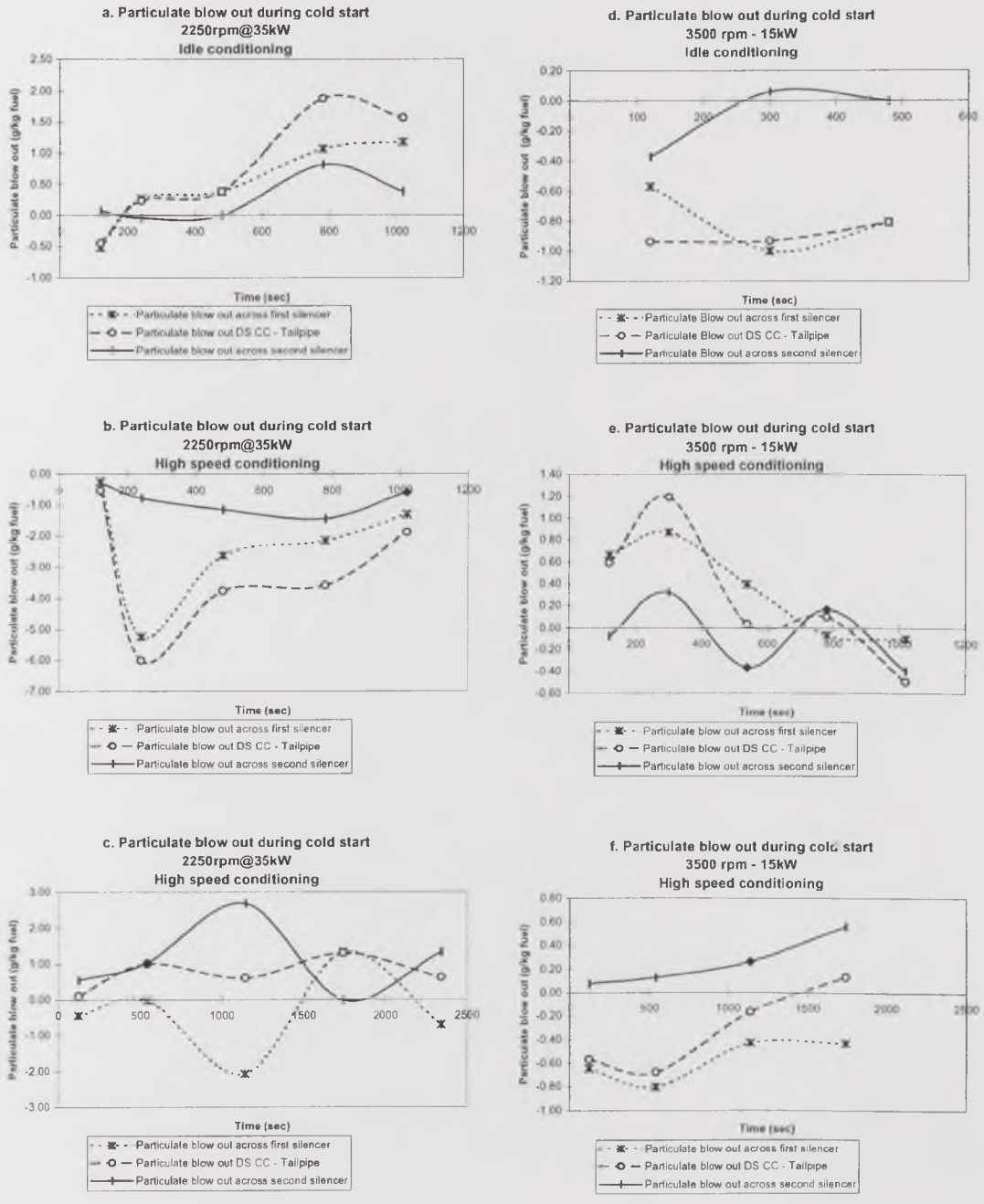

Figure 4.6. Particulate mass blow-out loss through the section downstream of the catalyst at the high load and high-speed conditions, with idle and high-speed preconditioning.

During the test at 2250rpm – 35kW with Idle preconditioning, initial particulate deposition was observed, followed by blow out from the first silencer with increasing levels with time, with a maximum around 1.0 g/kg-fuel from 13 minutes onwards. At the same conditions, virtually no deposition or blow out was observed through the second silencer for the first ten minutes, after which Particulate Matter was blown out at nearly 1.0 g/kg-fuel. The overall result was a clear blow out

of particulates at these conditions. Results of the first test with high-speed preconditioning showed the opposite behaviour. Particulate Matter was deposited through both silencers at all times during the test, at a higher rate for around five minutes from the cold start, decreasing gradually with time. A bigger mass was deposited through the first silencer than through the second. The extended test with high-speed preconditioning showed particulate deposition through the first silencer alternating with some blow-out at 30 minutes. Particulate Matter was blown out from the second silencer at all times, except for a situations with no deposition and no blow out at 30 minutes mark, the same moment at which the opposite change in trend occurred for the first silencer.

The results from both tests suggested:

- that the first silencer had a stronger trend to accumulate particles when it had been cleaned by high-speed operation;
- that the deposition and blow out of particles from each silencer tended to occur out-of-phase, as was observed in an earlier stage of the work;
- that the test-to-test repeatability at these conditions was still limited, owing to the manual operation of the dynamometer and the engine and sampling from only one point per test.

Results from the cold-start step to high-speed conditions after Idle preconditioning showed an opposite deposition and blow out pattern from that observed for the step change to high-load conditions in the corresponding tests. At 3500rpm – 15kW with Idle preconditioning, deposition of particulates through the first silencer occurred throughout the test at a rate of 0.6 to 1.0 g/kg-fuel. This accounted for most of the deposition downstream of the catalyst during the first two minutes and nearly all the deposition after the first five minutes, since there was little deposition at the beginning and virtually no deposition or blow-out over the late period through the second silencer.

This result was surprising since particulate matter was expected to be blown out during the cold start reaching high-speed conditions after an Idle preconditioning. However, this apparently contradicting result was reinforced when observing that during the test with high-speed preconditioning, which was run with a presumably clean exhaust system, particulate matter was blown out in the level of 0.6 g/kg fuel to 1.2 g/kg-fuel from the first silencer during the first ten minutes, and deposited only from the 15 minute mark. Alternating particulate deposition and blow-out processes were observed through the second silencer. The longer test with high-speed preconditioning showed deposition through the first silencer and

deposition through the second silencer at all times, with an overall deposition in the section downstream of the catalyst of the order of 0.2 g/kg fuel to 0.6 g/kg-fuel. The off-phase trend in the deposition/blow out patterns through the silencers was also observed once more.

Particulate blow-out results are shown also in Figure 4.7. expressed as a percentage of the tailpipe emissions, which underlines the significance of the role played by particulate deposition and blow out in the emissions. Deposition through the first silencer at the beginning of the cold-start test, at 2250rpm – 35kW after Idle preconditioning, represented 50% of the tailpipe emissions, and the blow-out from the same device in the following minutes accounted for up to 60% of the total particulate emitted to the atmosphere. For the first test with high-speed preconditioning, the deposition through the first silencer was more than three times as high as the tailpipe emissions. The second tests showed less dramatic changes, with deposition or blow out through the first silencer around 40% to 60% of the tailpipe emissions. The off-phase phenomena through the second silencer accounted for up to 60% of the tailpipe emissions, thus reducing the overall effect through the section downstream of the catalyst to levels around 25%, with some excursions to higher values.

Particulate deposition and blow out during cold start at 3500rpm – 15kW were, in general, more significant than at high-load conditions when expressed as a percentage of tailpipe emissions. An amount of particulate between 50% and 200% of particulate tailpipe emissions deposited through the first silencer in the test with idle preconditioning. Similar deposition levels through this device were observed in the test with high-speed preconditioning. Blow out occurred, but only accounted for only 25% of tailpipe emissions. Similar percentages were observed through the second silencer. In the second test after high-speed preconditioning, blow out from the second silencer represented between 5% and 60% of tailpipe emissions, whereas deposition through the first was between 25% and 125% of the total emissions to the atmosphere.

4.3.3. Catalytic converter efficiency

During the first minutes of cold start, particles could be deposited on or blown out from the walls of the catalytic converter without being oxidised, since the catalyst had not lit off. Afterwards, not only this physical process but also catalytic oxidation of the hydrocarbons adsorbed on the particles took place. In this work, catalytic converter efficiency is defined as the fraction of particulate matter that is lost (deposited and converted) when passing through the catalyst. Figure 4.8. shows the catalytic converter efficiency at both conditions and preconditioning procedures.

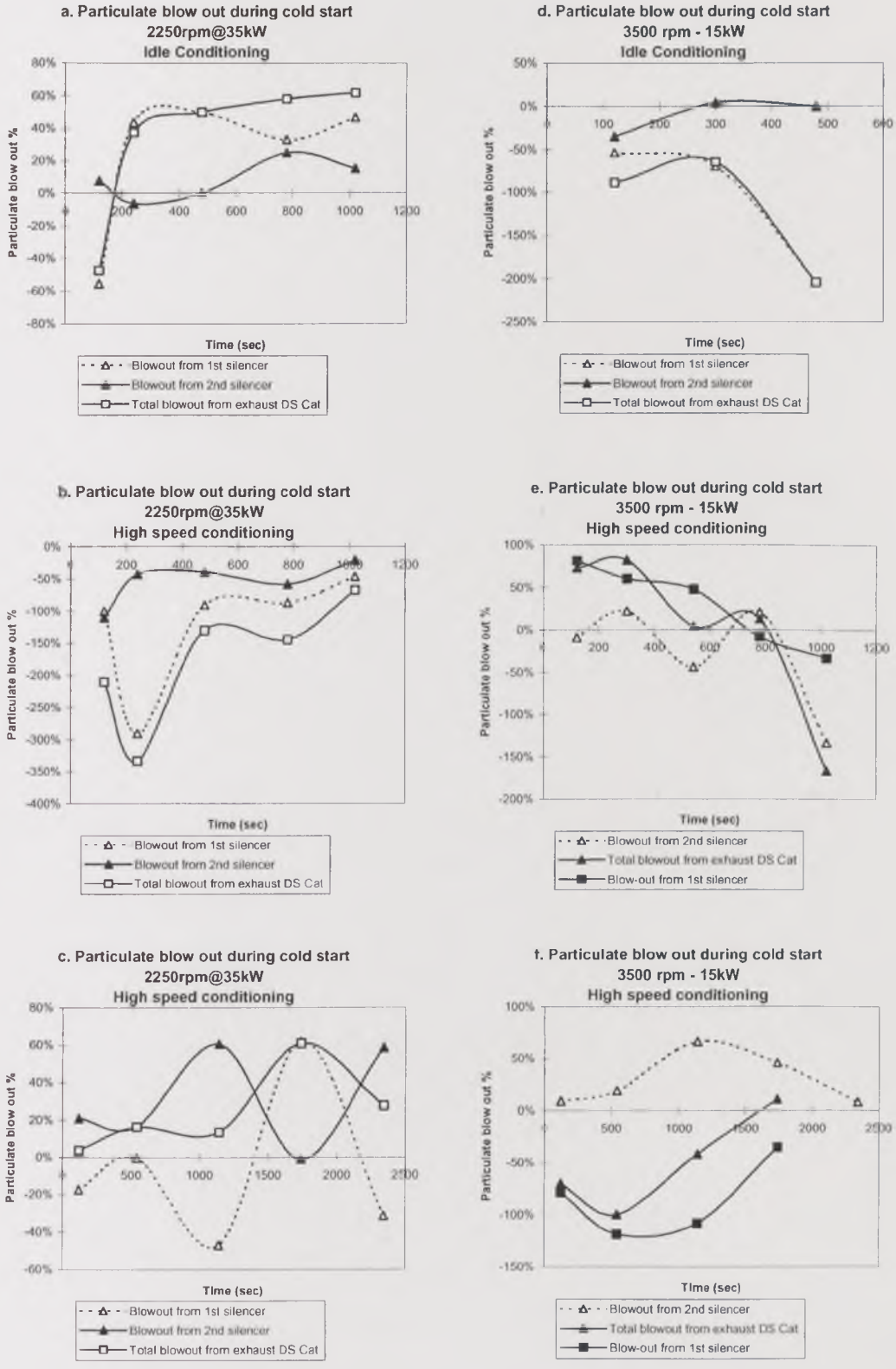

Figure 4.7. Particulate mass blow-out loss through the section downstream of the catalyst at the high load and high-speed conditions, with idle and high-speed preconditioning.

Particulate matter was blown out from the catalyst during the first two minutes of the cold start at 2250rpm – 35kW with idle preconditioning, in the order of 1.5 times as much particulate mass as entering the catalyst. In the following minutes the catalyst stored and converted particulate with an efficiency between 25% and 50%. This was an expected trend with Idle preconditioning. Unexpected were the results from the first high-load test after high-speed preconditioning, which showed a negative efficiency at all times, 20% in the first two minutes, 70% after ten minutes and 30% from 13 minute mark onwards. The second test with high-speed preconditioning produced an oscillating efficiency with positive values between 30% and 60% and negative values between 10% and 20%. This was closer to what was expected from a test with high-speed preconditioning.

The test at 3500rpm – 15kW after Idle preconditioning had a similar result to the corresponding test at 2250rpm – 35kW. Particulates were blown out from the catalyst and then deposited and converted. However, in the high-speed test, the converter efficiency was positive just after 10 minutes from cold start, later than in the high-load test, even though the catalyst light-off temperature was reached at about the same time in both tests. The first high-speed test with high-speed preconditioning caused deposition of particulate at all times, as expected for a previously cleaned catalyst, with efficiencies between 40% and 80%. The second test showed a similar trend, though a negative efficiency of 20% was observed at 30 minutes.

4.4. Chemical composition by TGA during cold start

The samples collected with the Oliver filter mass measurement instrument during cold start at 2250rpm - 35kW and 3500rpm - 15kW were analysed by TGA, following the procedures described in Chapter 2. The results are presented here as carbon content in relation to the (Carbon + SOF) fractions, against time and location in the exhaust system. Unfortunately, the ash content was not accurately determined owing to operational errors in the laboratory, so changes in the ash fraction were not detected. However, the Carbon and SOF variations were observed. The ash fraction was estimated to be between at most 14% in some cases and less than 10% in most of them, which is supported by Ahamed (Ahamed, 1999). It is possible, however, that this fraction can be as high as 50% at idle conditions.

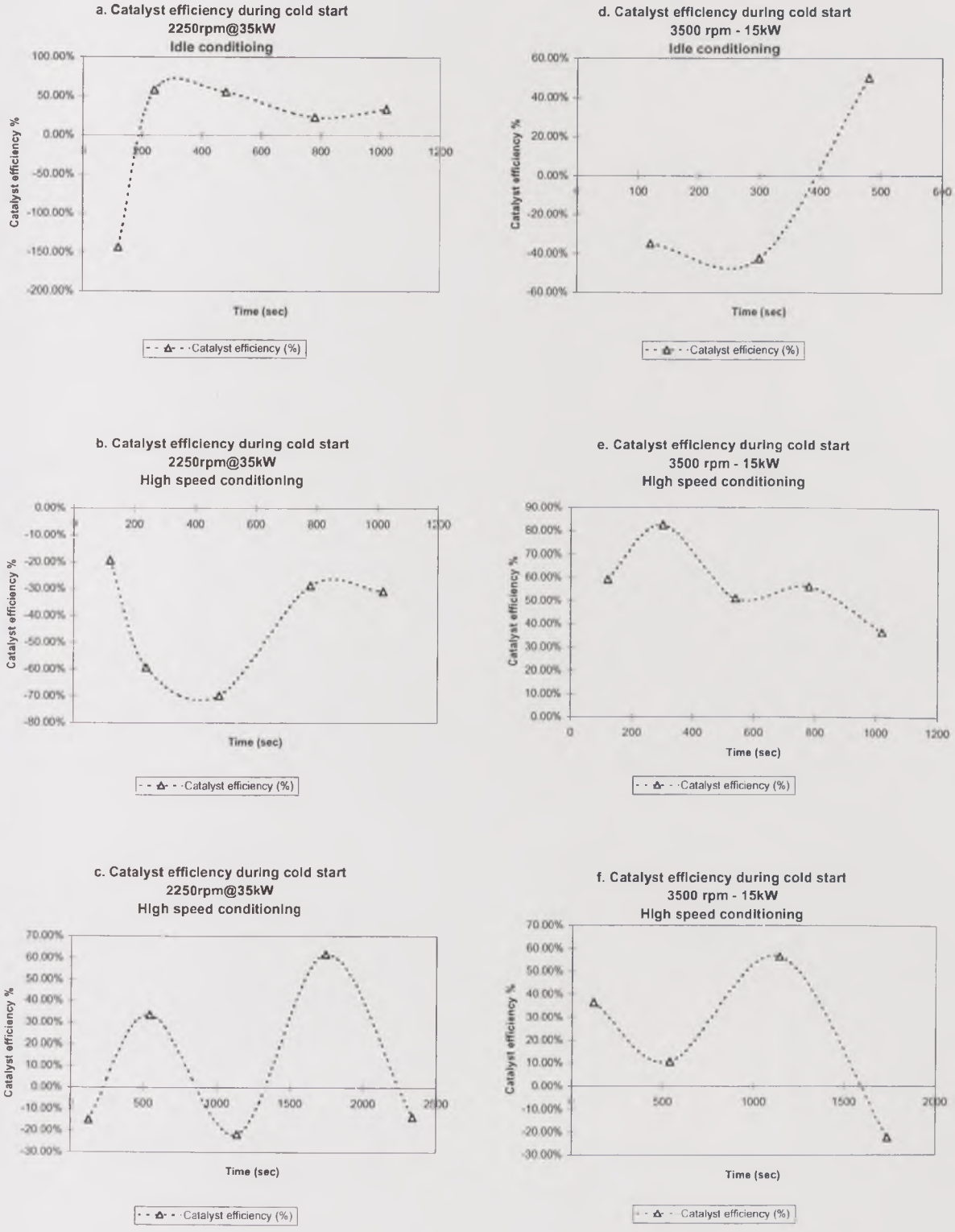

Figure 4.8. Catalyst efficiency during cold start at various operation conditions.

4.4.1. Cold start and stabilisation at 2250rpm - 35kW

In contrast with the low power conditions analysed in Chapter 3, the carbon content of the particulate emitted at high power conditions, 2250rpm - 35kW, was higher than 50% at all times during cold start, and reached levels as high as 81.4% in the process. In the first two minutes, the carbon content of the particulate entering the system was 50% average through the exhaust system, increasing with time until reaching an average 78% at 9 minutes from start, when the highest carbon levels at all sampling points were reached. Afterwards, the carbon content decreased to an average 67.1% at 19 minutes from start, 62% at 29 minutes from start, and 60% minutes at 39 minutes from start, when a trend was towards stabilisation around that value was observed. The low carbon content during the first five minutes were presumably due to a more significant condensation of species from the gas phase, since temperatures in the exhaust are the lowest during this period.

Regarding the changes through the exhaust system, only in the first two-minute sample did the carbon content decrease through the catalyst, from 55.2% to 44.4%, to increase again through the silencers reaching 54.1% at the tailpipe. Later, there was a continuous increase in carbon content through the exhaust system, more significant through the catalyst and the second silencer than through the first silencer. Then, the difference between the carbon content upstream of the catalyst and downstream of the second silencer was typically 10%, from which not more than 1.6% was due to the first silencer. These changes are more difficult to explain than time-related changes, since they are caused by several opposite processes. Condensation would decrease the carbon fraction through the exhaust system. However, the resuspension of particles would increase it.

4.4.2. Cold start at 3500rpm - 15kW

The particulate carbon content at high-speed conditions, 3500rpm - 15kW, were between 13% and 26% at all times and for all exhaust sampling points, much lower than at high power conditions. The carbon content did not change much with time from start, being 20% average practically at all times, excepting only a decrease to 17% average around 5 minutes from start.

At all times, the carbon content decreased through the catalyst, increased again through the first silencer and decreased through the second silencer. The carbon content upstream of the catalyst was between 19.6% and 25.7%. Downstream of the catalyst, about 7% lower, between 12.8% and 17.1%. Upstream of the second silencer, it was between 18.7% and 22.1%, about 5% higher than the previous point. And downstream of the second silencer, just 1% lower than upstream, between 17.2% and 20.6%.

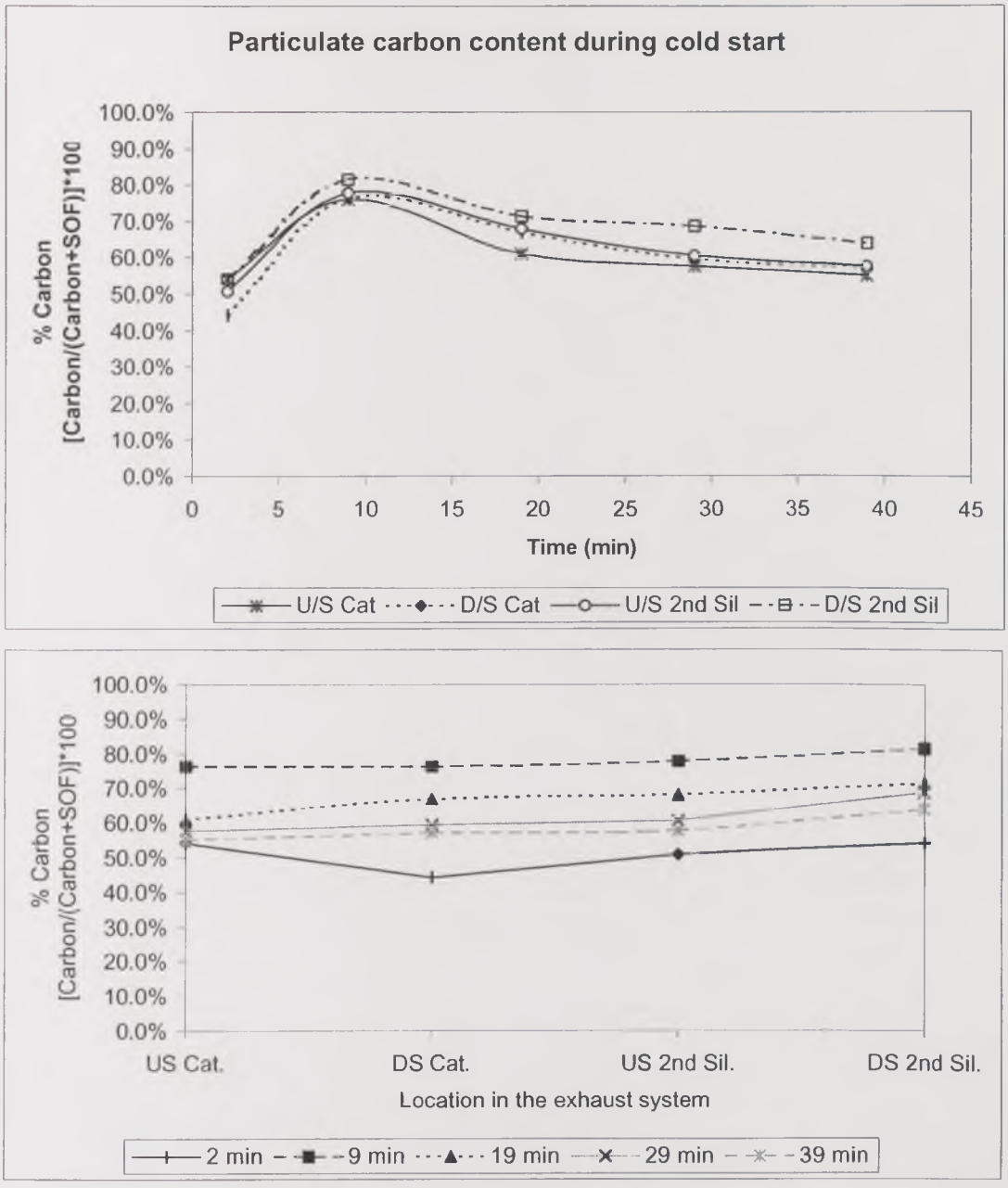

Figure 4.9. TGA particulate carbon content during cold start at 2250rpm - 35kW.

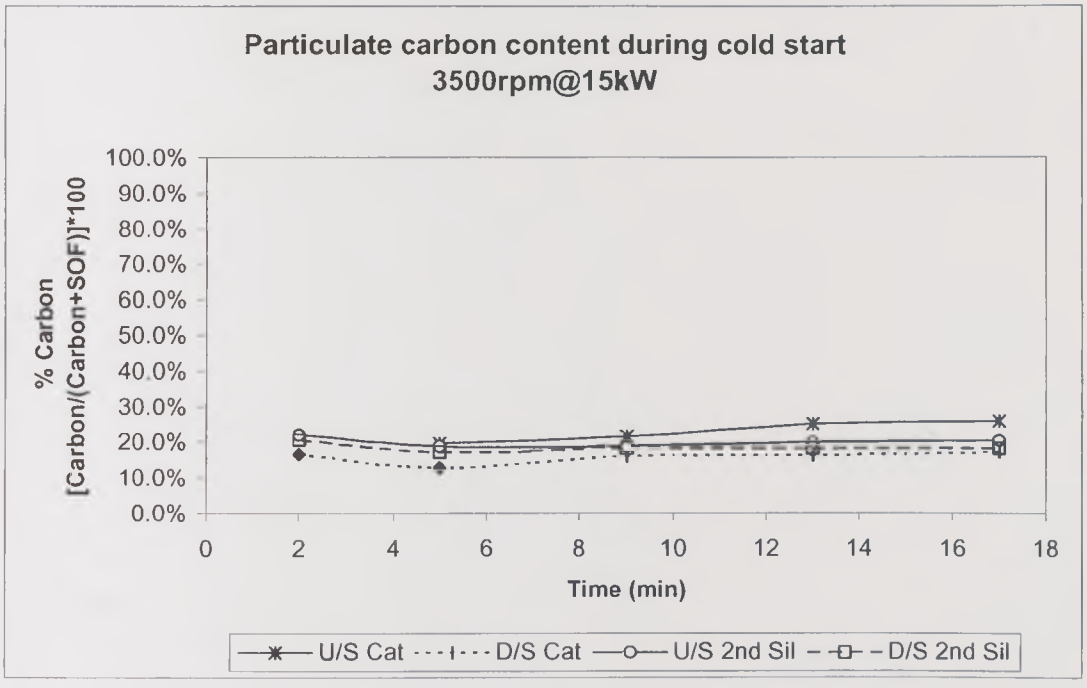

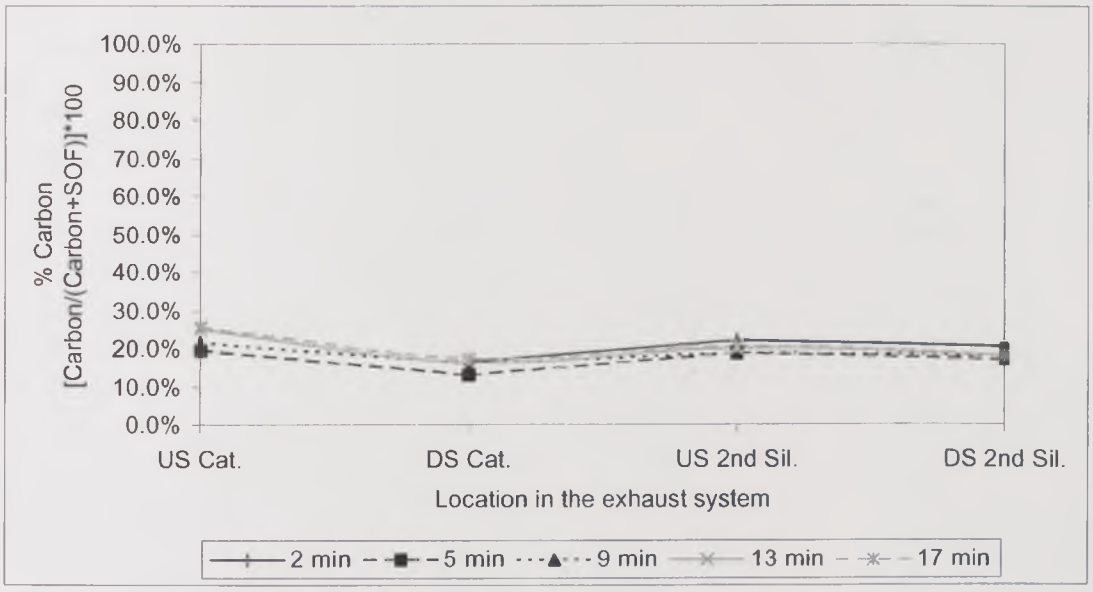

Figure 4.10. TGA particulate carbon content during cold start at 3500rpm - 15kW.

4.5. Total Number, Mass Concentration and Particle Size Distribution Changes Through the Exhaust System During Cold Start

Data from the ELPI were converted into number and mass distribution and total concentration. Mass data, expressed as Emission Index, were calculated by assuming that the particles were spherical, although it is well known that diesel particles are long-branched fractal-like agglomerates [Brasil, 1999; Skillas, 1998;

Gorbunov, 1999]. The conversion from particle number to Emission Index included the same correction used in the previous cold-start tests and described in Chapter 6. The implications of the assumption for the density values are of great importance for this study, since the particle blow-out events were essentially a mass related issue.

The EGR control strategy does not open the EGR valve during the cold-start tests for the high-speed condition, whereas it does open the valve when for the high-load condition, as shown in Figure 4.11, where the parameter on the right-hand side (EGR desired density or EGR_desddty) indicates the extent to which the EGR is used, given by the control strategy of the engine.

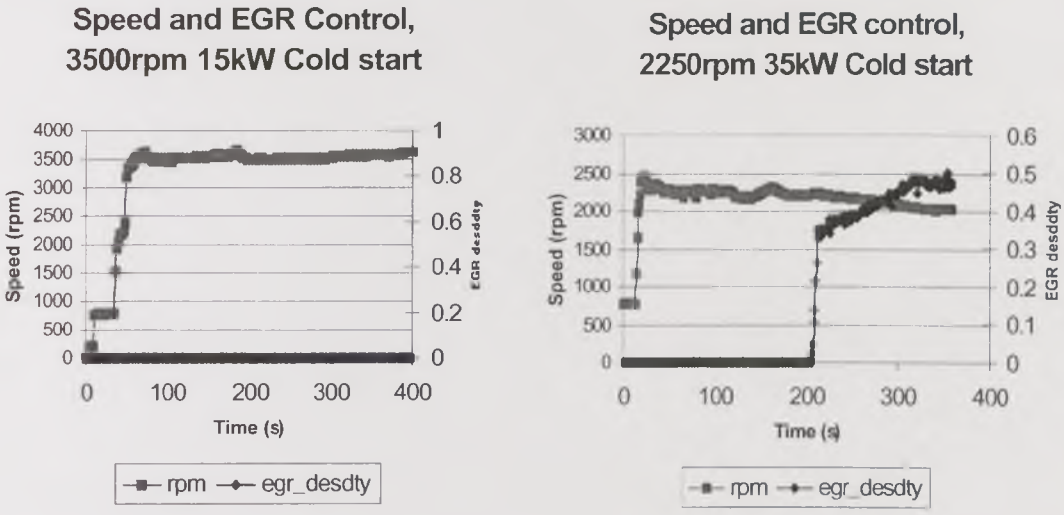

Figure 4.11. EGR valve opening during cold start at high-speed and high-load conditions.

Compared to previous results [12-14], the number concentration emissions at 2250rpm - 35kW upstream of the catalyst were comparable to those at the same speed but 15kW power. However, during the first three minutes of cold start, the number concentration was much higher, between two and fourfold the concentration at 2250rpm, when the speed increased to 3500rpm and 15kW. Downstream of the catalyst, the number concentration levels at both high-speed and high-load conditions were comparable to those at 2250rpm - 15kW (Figure 4.12.).

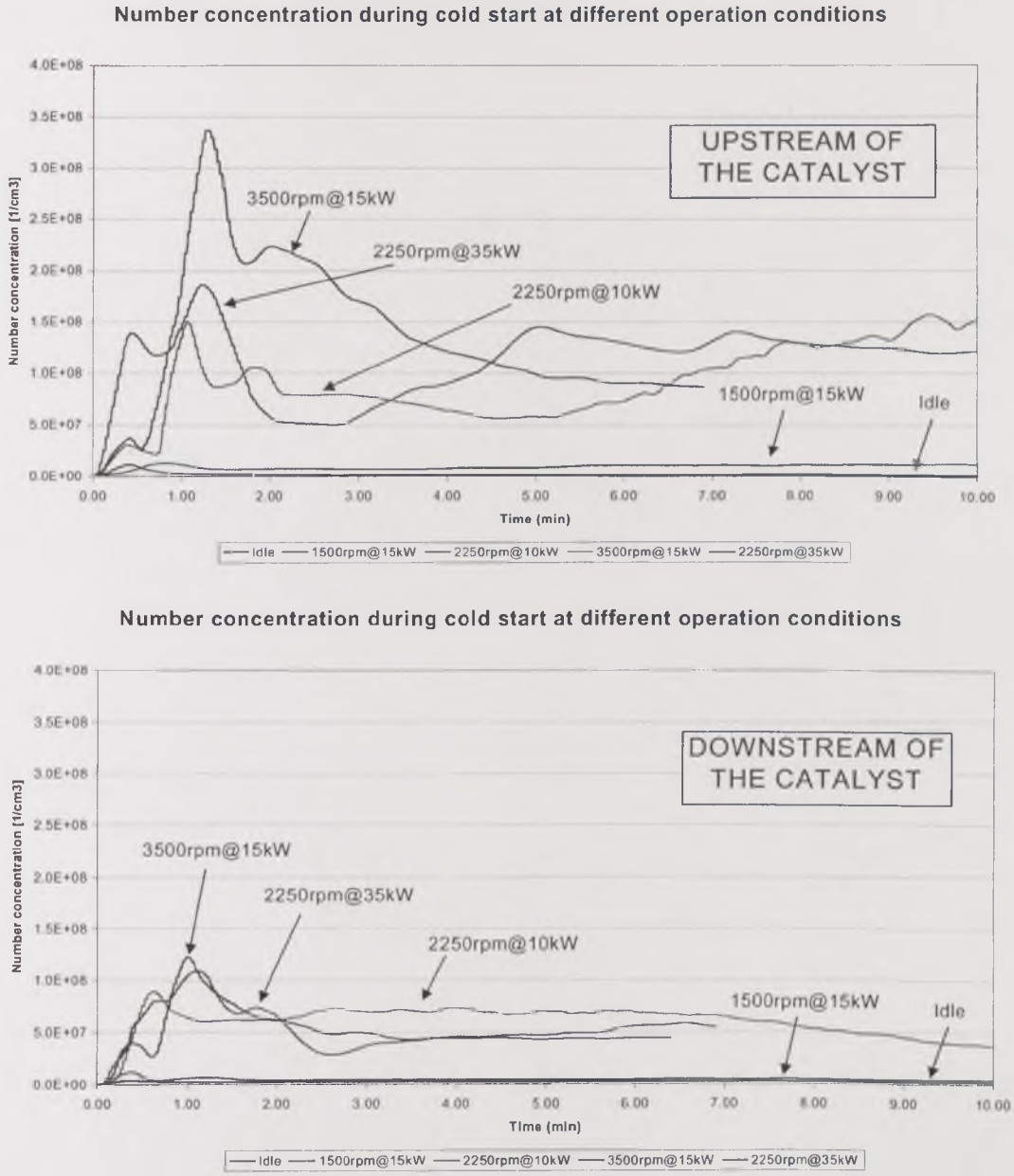

Figure 4.12. Total number concentration upstream and downstream of the catalyst during cold start at various conditions. a) Catalyst

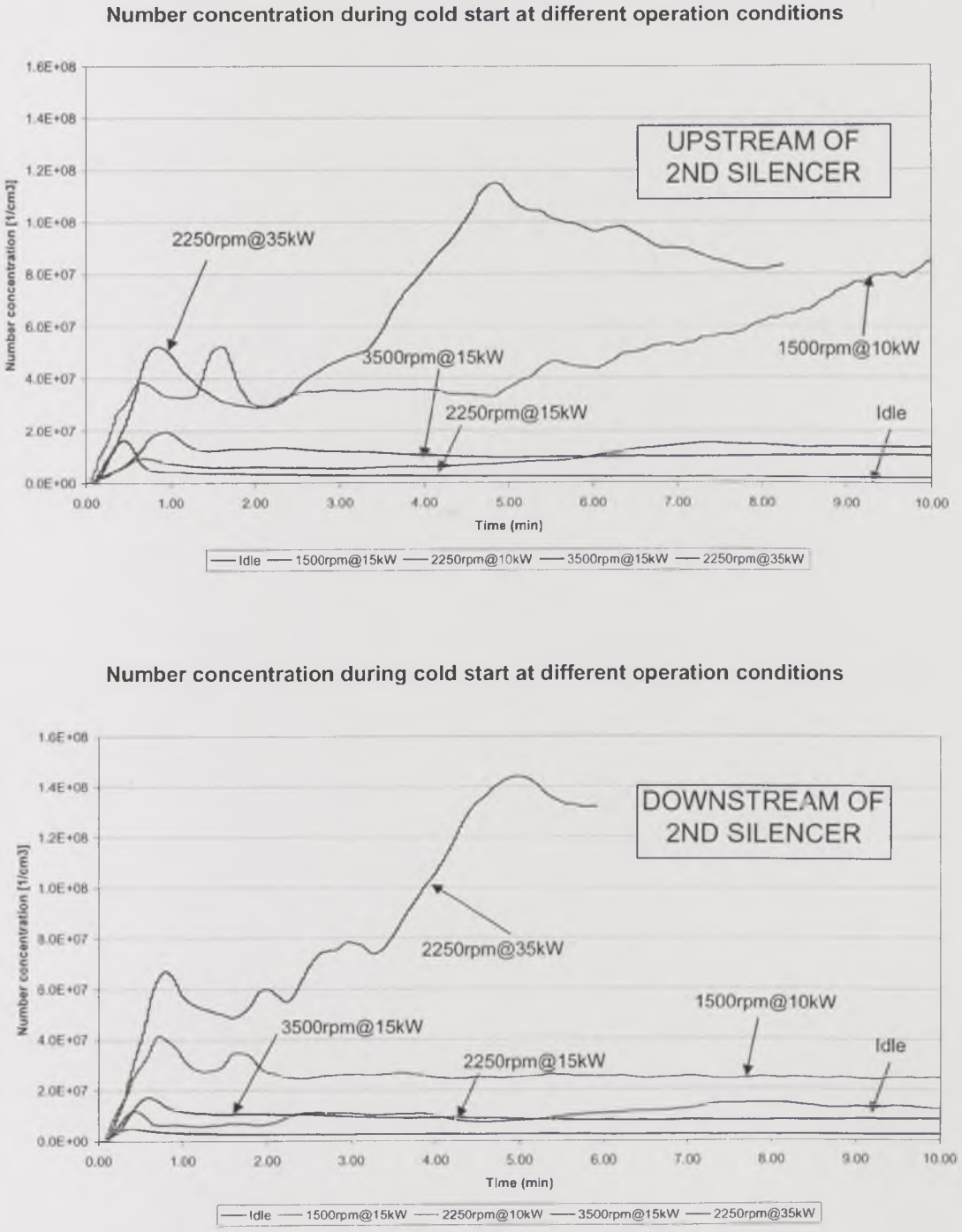

Figure 4.12. Total number concentration upstream and downstream of the catalyst during cold start at various conditions. b) Second Silencer

Upstream of the second silencer, number concentrations during the test at 2250rpm - 35kW were about fivefold those at the same speed but lower power, 10 kW, at all times. Number concentrations at this sort of power level but higher speed, namely 3500rpm - 15kW, were about twofold those at 2250rpm - 10kW during the first three minutes of cold start, but after minute 4 the situation changed, and the

number concentration at the latter conditions were higher than at the former. Number concentrations at 1500rpm - 10kW upstream of the second silencer were at the same sort of level of those at 2250rpm - 15kW. Downstream of the catalyst, the situation was the opposite, suggesting that the 1500rpm - 10kW condition promoted the blow-out of particulate from the first silencer.

Downstream of the second silencer, the number concentration comparison among different operating conditions showed a very similar situation to that upstream of the silencer: high levels at 2250rpm - 35kW and 1500rpm - 10kW, lower levels at 2250rpm - 15kW, 3500rpm - 15kW and Idle. This means that the second silencer had a lesser effect on particulate emissions than the first silencer.

Cold-start total particle number concentration and Emission Index at the two conditions tested are shown in Figures 4.13. and 4.14. for high-speed tests, and Figures 4.29. and 4.30. for high-load tests. The following general characteristics at all sampling points are shown:

1. A mass burst occurred in the first 30 seconds, when the acceleration was not yet completely developed, followed by;

2. A peak in number between one and two minutes from cold start, as a product of the acceleration and;

3. A decrease in particle number concentration and Emission Index;

4. For the tests at high load, an increase in number as well as in Emission Index, which was not seen in the high-speed tests, occurred around three minutes from cold start.

The events of mass burst and peak number showed some variations among tests, such as oscillations during the same period, as observed for the 1500rpm - 10kW and the 2250rpm - 15kW tests. This was mainly due to the manual acceleration manoeuvre. The dynamometer used in the tests used a water break, which was very slow for automatic control of a step change. For this reason, manual operation of the throttle was chosen to produce a fast acceleration, with the inconvenience of affecting the synchronised repeatability of the events. Hence, two successive peaks were the result of an irregular rather than a smooth acceleration.

The difference in the number concentration and Emission Index profiles against time after the first three minutes of cold start appeared as a consequence of the EGR system operation. Opening the valve showed a strong effect on particle number and mass emissions, which increased to levels even higher than those of the peak number observed during the first minute of cold start. This increase occurred

for all four sampling points, indicating that the catalyst action was not strong enough to cope with the effect of the EGR valve opening.

4.6. Deposition And Reentrainment Through The Exhaust System At High Speed and Load Conditions

4.6.1. 3500rpm – 15kW, Idle preconditioning

As explained above, the cold-start test at 3500rpm - 15kW after Idle preconditioning showed three characteristic events, namely an initial mass burst, a peak number concentration and stabilisation. The number concentration and Emission Index changes through the exhaust system during these events are described below.

4.6.1.1. First mass burst

During the initial seconds of cold start, when the first mass-burst event was observed, the total particle number concentration of the exhaust aerosol at the manifold was $6.2x10^6$ cm^{-3}, which converted to an Emission Index of 74.8 g/kg fuel (uncorrected) or 6.4g/kg fuel (corrected). Through the catalyst, the number concentration increased to $3.8x10^7$ cm^{-3} (fivefold increase), indicating particle blow-out from the catalyst walls. The uncorrected Emission Index, in contrast, decreased to 25.3 g/kg fuel, which corresponds to a 66% decrease, but applying the correction the Emission Index increased to 13.8 g/kg fuel, that is, a 115% increase. This discrepancy arose from the difference in changes by size, as observed in the particle size distribution charts, Figure 4.15. Whereas particles below 1.0μm were formed, increasing the number concentration but not contributing significantly to the Emission Index, larger particles deposited through the catalyst. Therefore, when the correction was not applied, the large particle effect on the total Emission Index was very significant, producing a decrease. The correction, in contrast, gave more importance to the contribution of the ultrafine particle to the total Emission Index, hence increasing its value.

Through the first silencer, the total particle number concentration decreased to $4.2x10^6$ cm^{-3}, just below the original concentration upstream of the catalyst. This was equivalent to a decrease by 89%, due to particulate deposition. The Emission Index decreased by 81% (uncorrected) or 95% (corrected), to 4.7 g/kg fuel or 0.75 g/kg fuel, respectively. Deposition occurred for particles at all size ranges.

The total particle number concentration increased by 70% through the second silencer, to $7.0x10^6$ cm^{-3}. The Emission Index also increased, either uncorrected and corrected, by 1.9 times or 87%, to 13.6 g/kg fuel or 1.4 g/kg fuel, respectively. All

this indicates that ultrafine particles formed and coagulated, and large particles were blown out from the silencer. Comparatively, however, the change was not significant, with respect to those occurred through the catalyst or the first silencer.

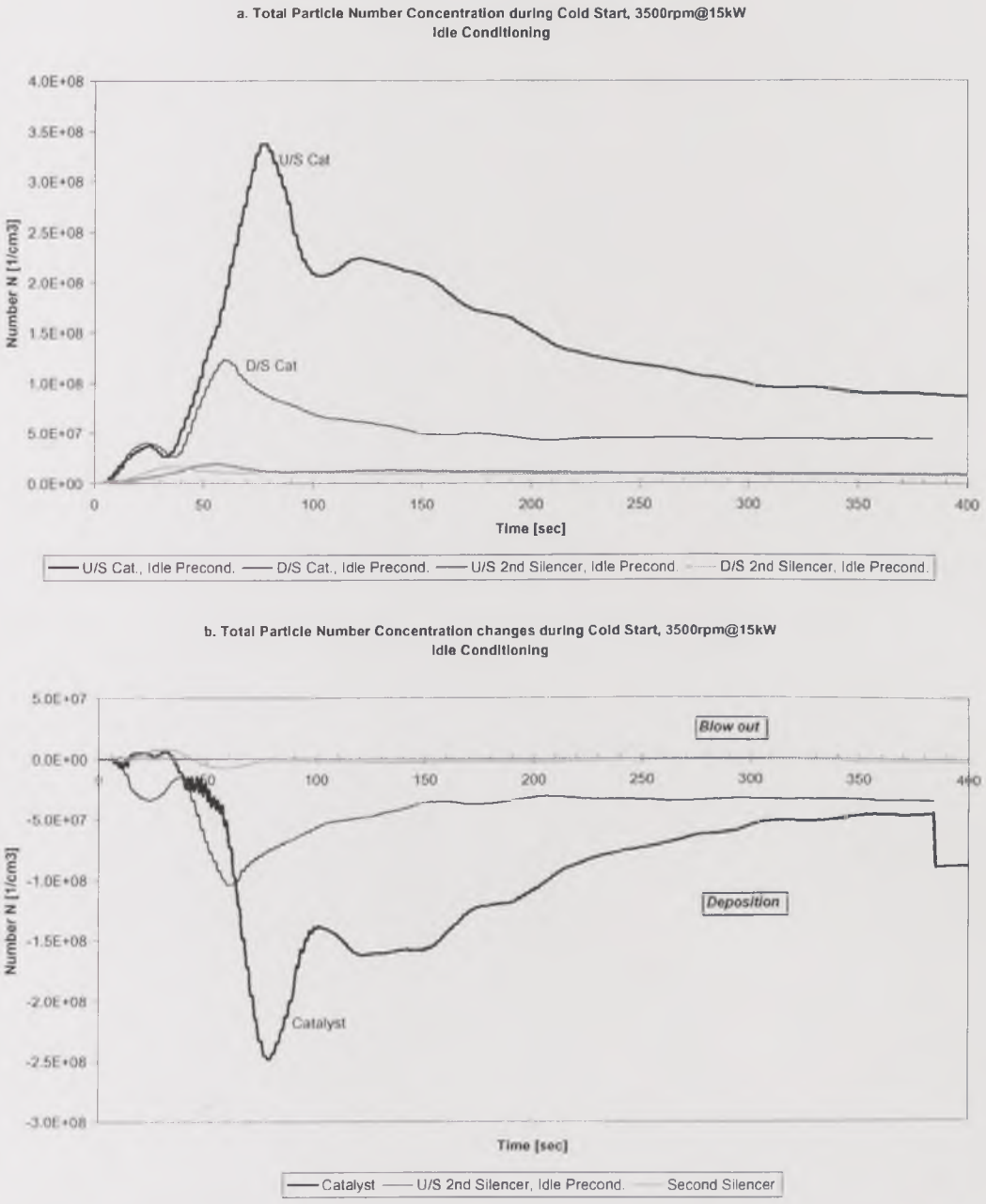

Figure 4.13. Total number and mass concentrations vs. time during cold start at high-speed conditions after Idle preconditioning at various points through the exhaust system. a) Particle number concentration

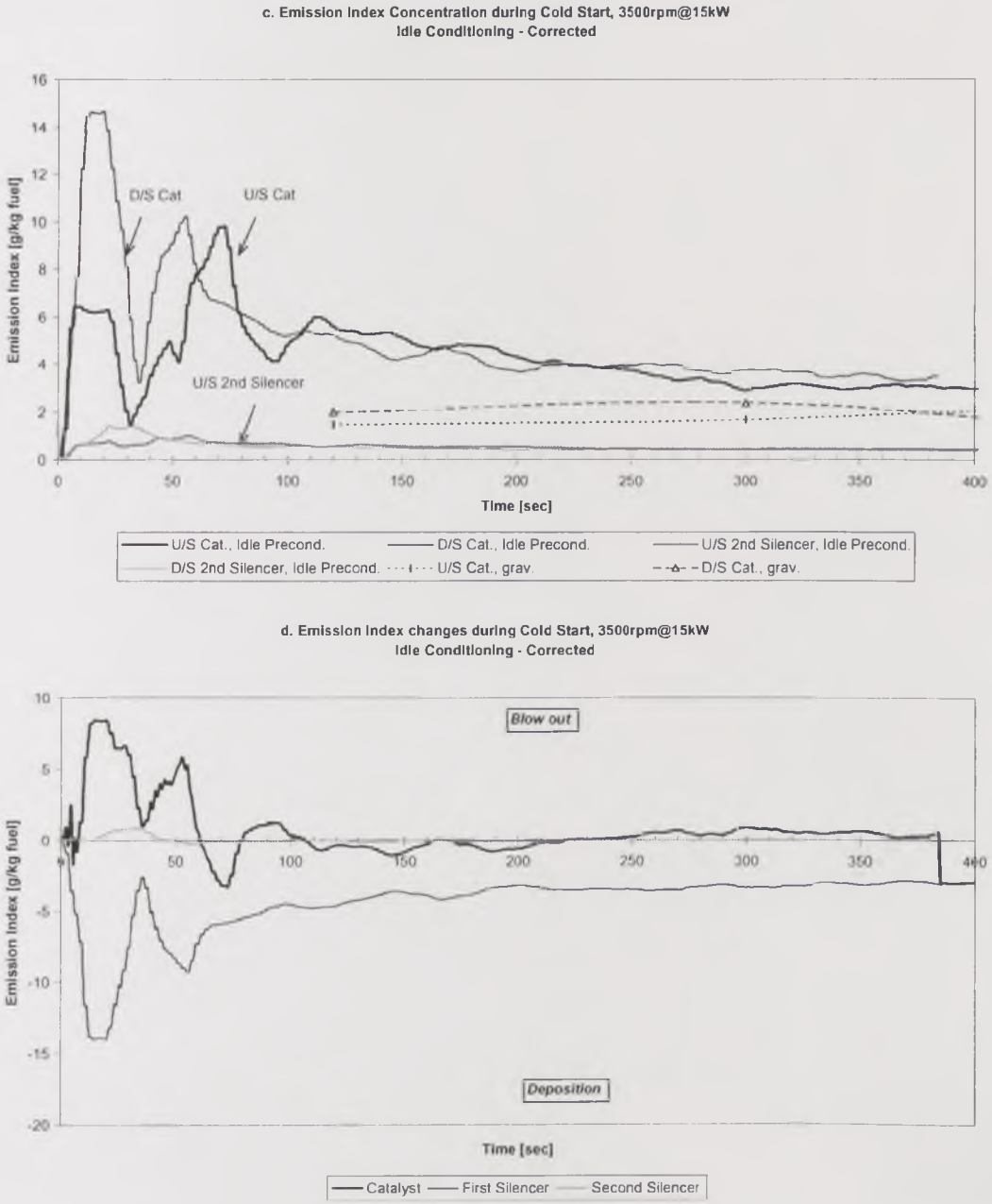

Figure 4.13. Total number and mass concentrations vs. time during cold start at high-speed conditions after Idle preconditioning at various points through the exhaust system. b) Corrected Emission Index

In summary, the first mass-burst event of the cold start at 3500rpm - 15kW after Idle preconditioning showed a very significant particulate blow-out from the catalyst and a less important blow-out from the second silencer. Deposition occurred from the first silencer.

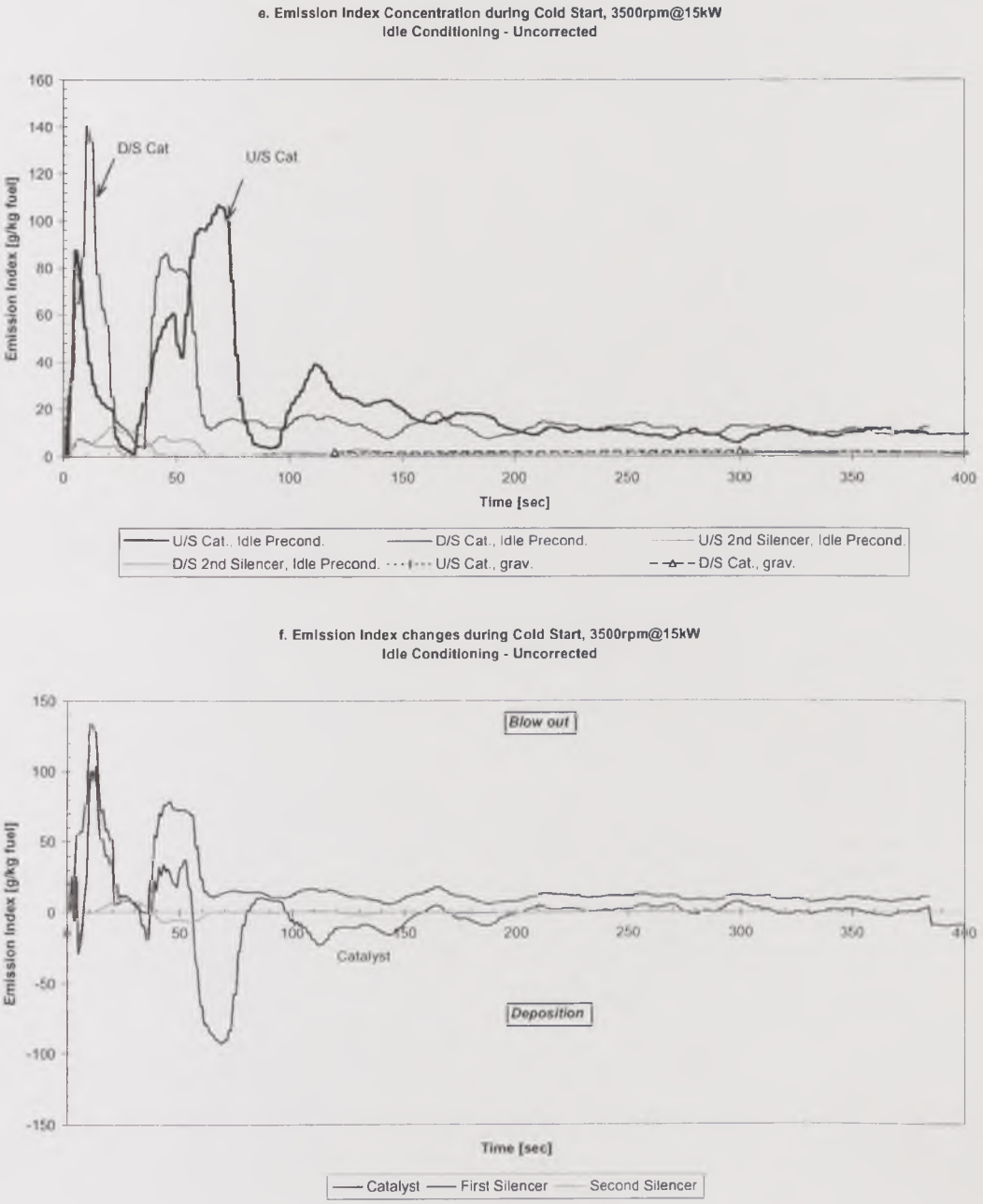

Figure 4.13. Total number and mass concentrations vs. time during cold start at high-speed conditions after Idle preconditioning at various points through the exhaust system. c) Uncorrected Emission Index

Again, the opposite trends in the particulate deposition/blow-out behaviour between the Catalyst/Second silencer and the First silencer were observed. Ultrafine particles, below 1.0μm, were formed through the catalyst and first silencer. The result of various processes caused a shift towards smaller sizes in the particle size distribution through the first silencer.

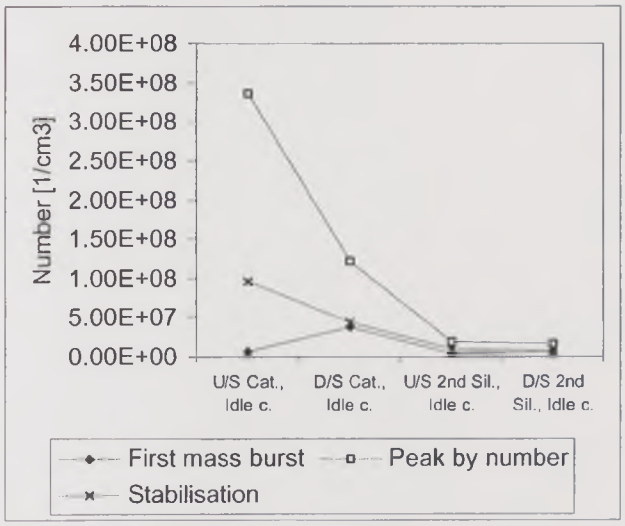

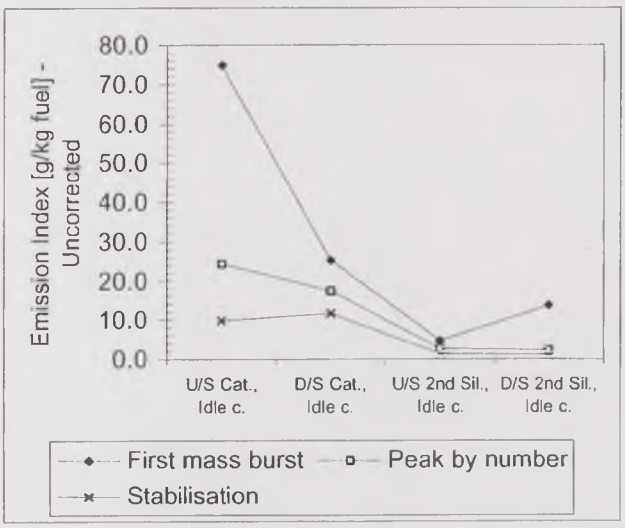

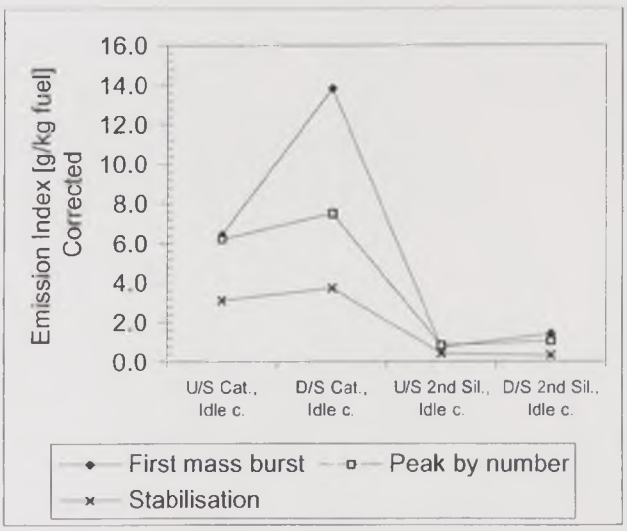

Figure 4.14. Total number and mass concentrations vs. position in the exhaust system for the main events of the cold start at high-speed condition after Idle preconditioning.

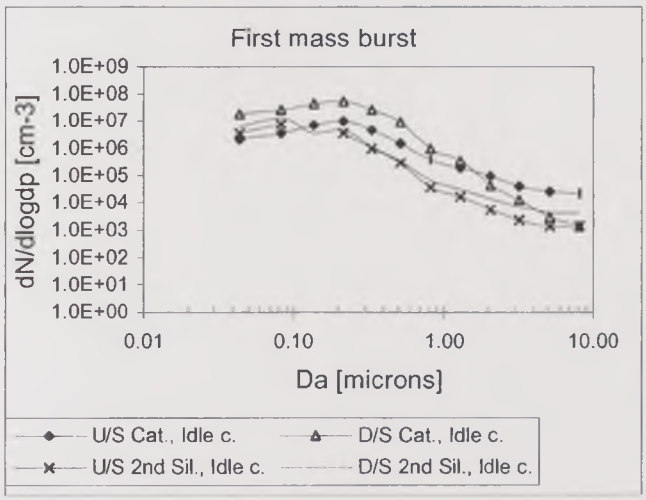

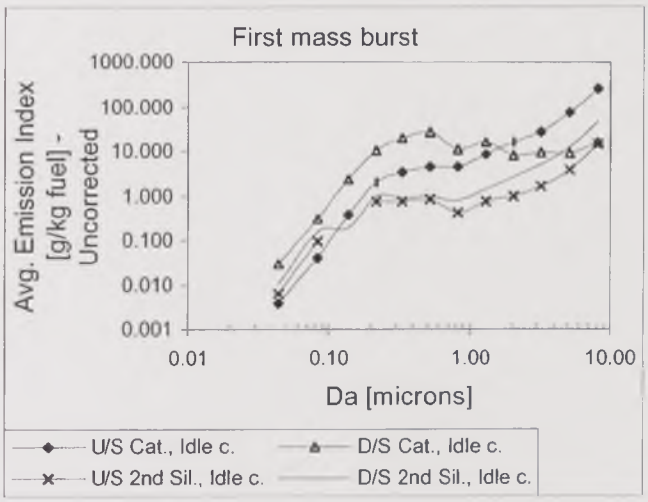

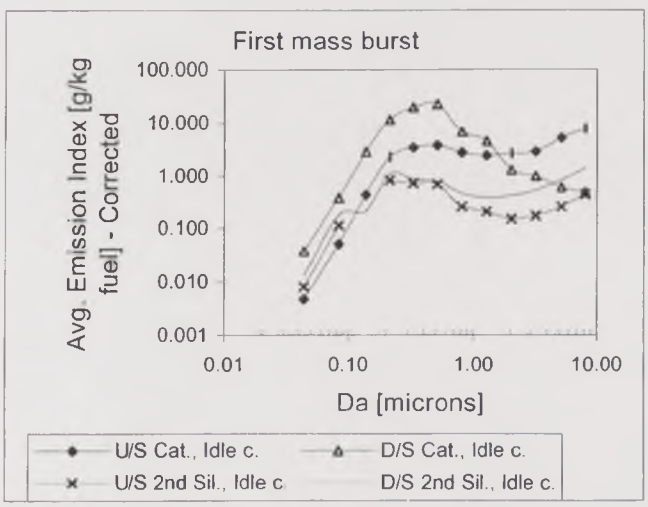

Figure 4.15. Particle size distribution during the first mass-burst event of the cold start at 3500rpm – 15kW after Idle preconditioning.

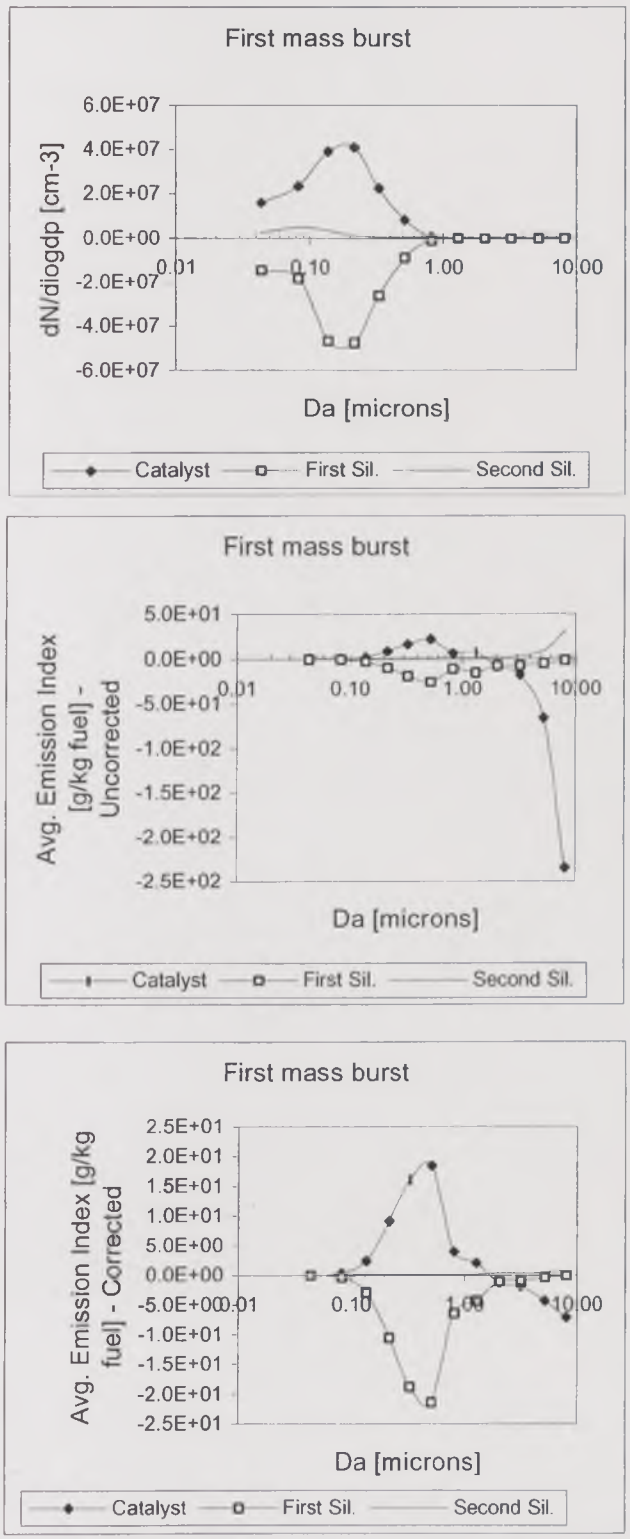

Figure 4.16. Particulate blow-out in various size ranges during the first mass-burst event of the cold start at 3500rpm – 15kW after Idle preconditioning.

4.6.1.2. Peak by number

The total particle number concentration of the exhaust aerosol leaving the engine during the peak-number event was $3.4x10^8$ cm^{-3}, two orders of magnitude higher than the concentration at the same point during the first-mass-burst event. The corresponding Emission Index was 24.35 g/kg fuel or 6.22 g/kg fuel, when using the uncorrected or corrected conversion, respectively. Through the catalyst, the total particle number concentration decreased to $1.2x10^8$ cm^{-3} (64% decrease) and the uncorrected Emission Index, to 17.5 g/kg fuel (28% decrease). The corrected Emission Index, on the contrary, increased to 7.5 g/kg fuel (21% increase). The difference was due to the opposite behaviour of particles in different size ranges. Particles smaller than 0.2μm were oxidised, and coagulated to form larger particles; particles larger than 2μm were deposited through the catalyst, and the number of those within that interval increased by coagulation. A shift towards larger particles occurred through the catalyst, as a result of particle coagulation.

Through the first silencer, the total particle number concentration decreased by 84%, to $2.0x10^7$ cm^{-3}. The Emission Index also decreased significantly, both uncorrected and corrected: by 85% and 89%, to 2.71 g/kg fuel and 0.85 g/kg fuel, respectively. Particles at all size ranges were deposited.

Through the second silencer, the total particle number concentration decreased to $1.7x10^7$ cm^{-3} (by 12%) and the uncorrected Emission Index, to 2.25 g/kg fuel (by 17%). The corrected Emission Index, in contrast, increased to 1.08 g/kg fuel (by 26%). Through this silencer, very fine particles, below 0.1μm, deposited and coagulated; large particles, above 2μm, deposited; and the number of middle-sized particles within those limits increased by coagulation, and perhaps some resuspension from the silencer walls in the large particle end of the range. This was very similar to what occurred through the catalyst in the same period, although the shift in particle size distribution did not occur.

The parallel behaviour of the exhaust aerosol through the catalyst and the second silencer, opposite to that through the first silencer, was observed once more in the peak-number event. Blown-out particles from the catalyst and the second silencer were in the middle-size range only. Very fine particles were oxidised, deposited or coagulated, and large particles deposited through those devices. Particles of all sizes deposited through the first silencer.

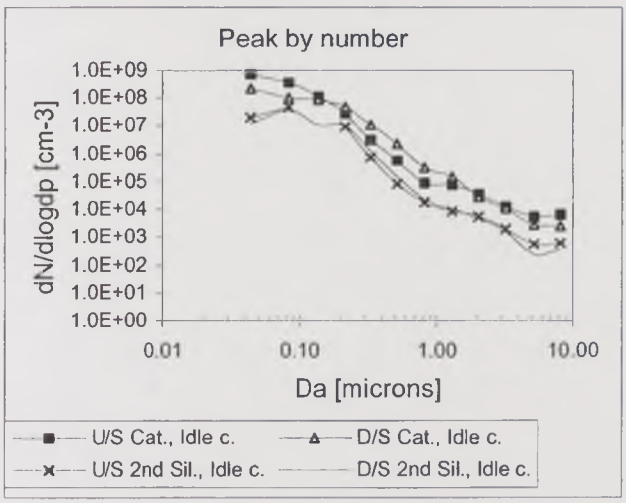

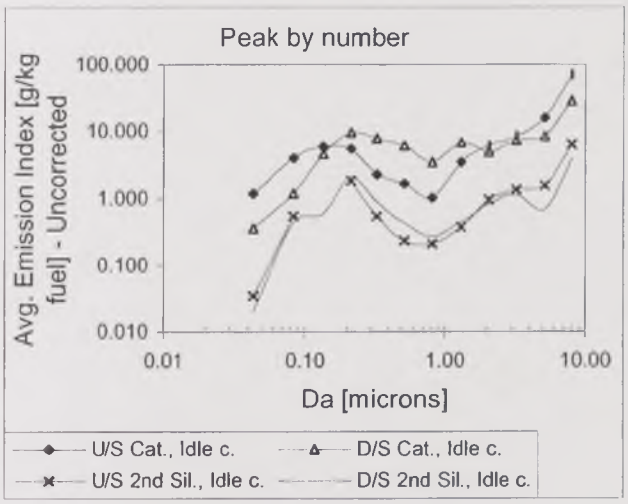

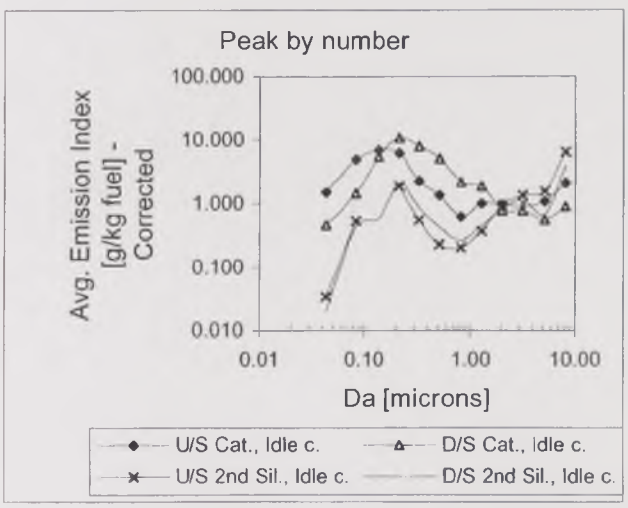

Figure 4.17. Particle size distribution during the peak-number event of the cold start at 3500rpm – 15kW after Idle preconditioning.

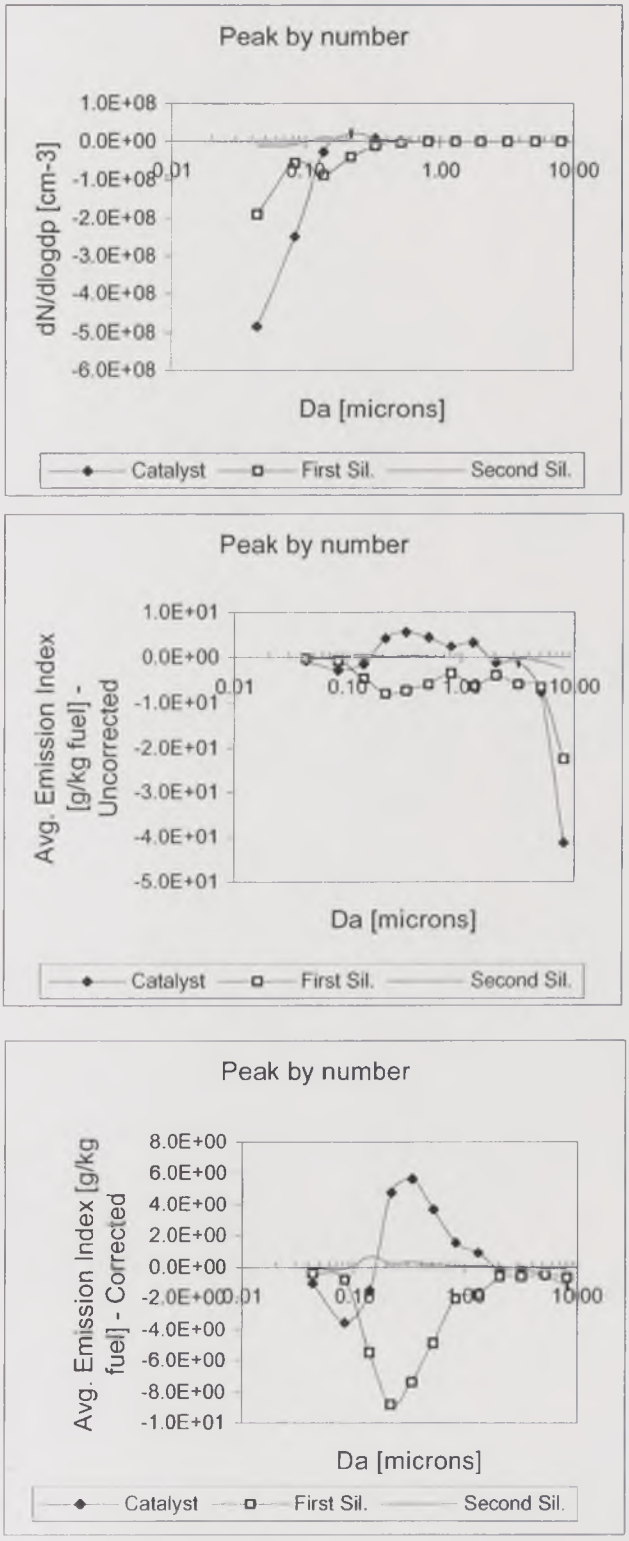

Figure 4.18. Particulate blow-out for various size ranges during the peak-number event of the cold start at 3500rpm – 15kW after Idle preconditioning.

4.6.1.3. Stabilisation

Once the stabilisation in the readings with the ELPI was reached, around 5 minutes after the peak-number event, the total particle number concentration of the exhaust aerosol leaving the engine was $9.6x10^7$ cm^{-3} (28% of the maximum level reached in the peak-number event), with a corresponding Emission Index of 9.76 g/kg fuel (uncorrected) or 3.11 g/kg fuel (corrected). The total number concentration decreased by 54% through the catalyst, to $4.4x10^7$ cm^{-3}. The uncorrected and corrected Emission Index, on the contrary, increased by 18% or 20%, to 11.6 g/kg fuel or 3.72 g/kg fuel, respectively. The decrease in particle number concentration was due to coagulation, deposition and oxidation of very fine particles, below 0.1 μm, and the increase in Emission Index, to the blow-out of particles larger than that size.

Through the first silencer, the total particle number concentration decreased to $1.0x10^7$ cm^{-3}, one fourth of the value downstream of the catalyst. The uncorrected and corrected Emission Index decreased by nearly 90%, to 1.42 g/kg fuel (uncorrected) or 0.43 g/kg fuel (corrected). Particles of all sizes deposited through the silencer.

The second silencer had a lower effect on the aerosol than the first silencer. Through it, the total number concentration decreased to $8.3x10^6$ cm^{-3} and the Emission Index to 1.12 g/kg fuel (uncorrected) or 0.36 g/kg fuel (corrected), the decrease for all cases being around 20%. Particles of all sizes deposited through the silencer, with the only exception of particles around 0.14μm, which increased in number concentration, presumably by coagulation.

In summary, once the stabilisation was observed, particle coagulation increased mid-sized particle number concentration through the catalyst, and large particles were blown out from it. Particles of all sizes deposited through both silencers, more significantly through the first silencer.

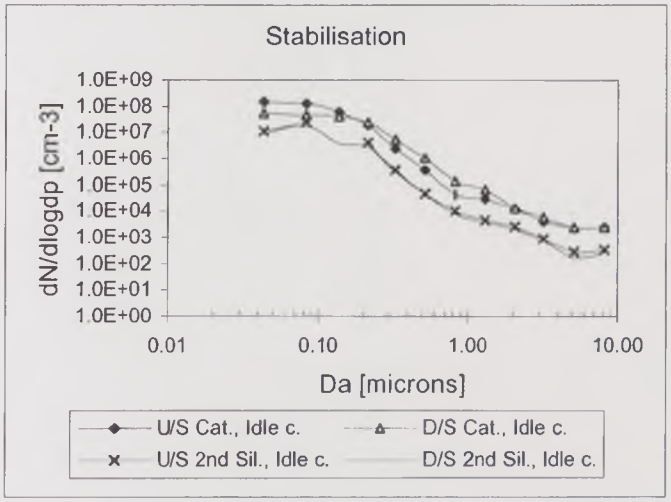

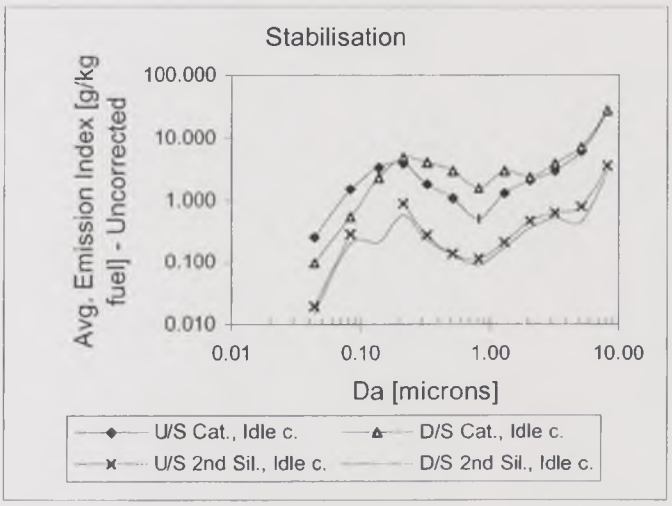

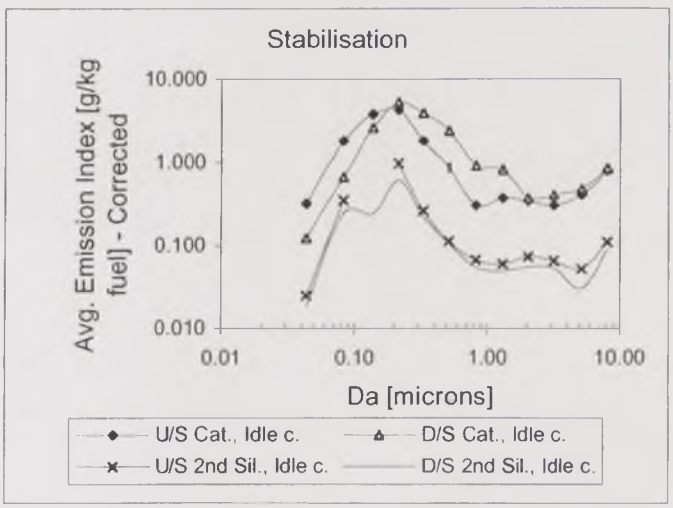

Figure 4.19. Particle size distribution during the stabilisation of the cold start at 3500rpm – 15kW after Idle preconditioning.

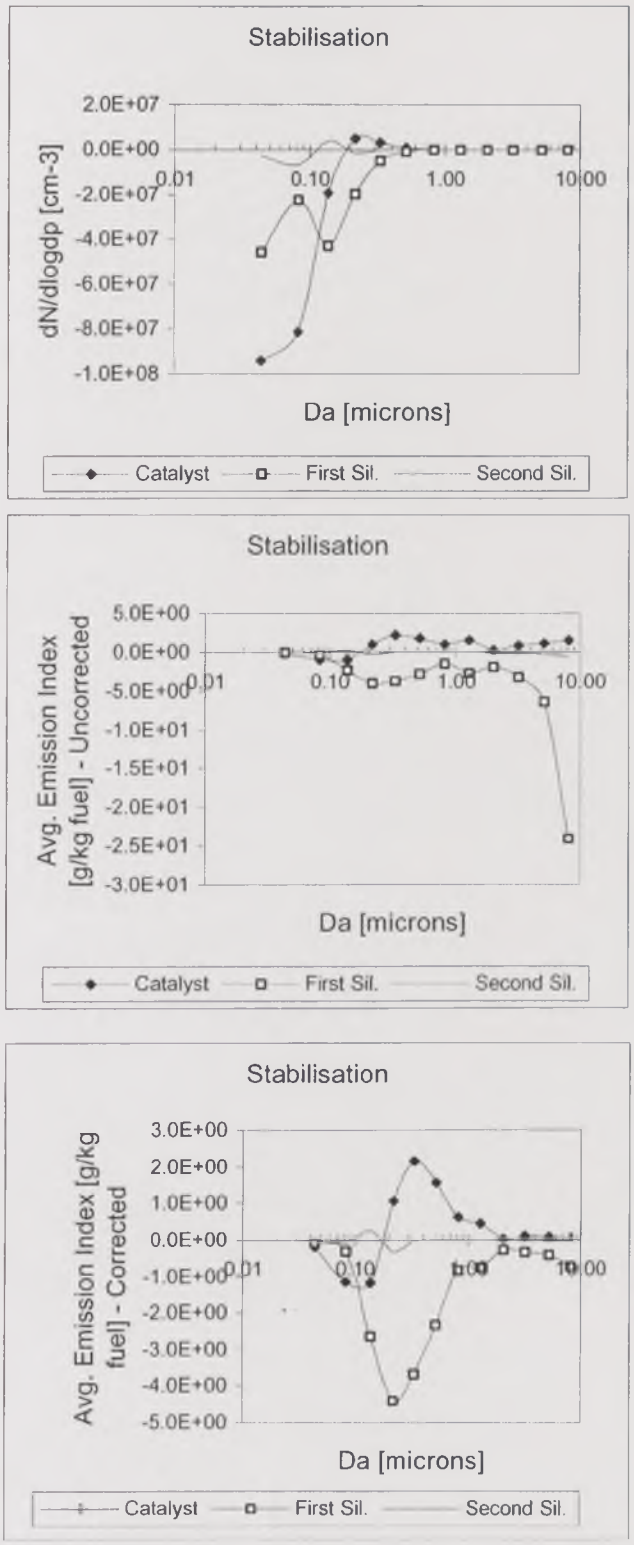

Figure 4.20. Particulate blow-out for various size ranges during the stabilisation event of the cold start at 3500rpm – 15kW after Idle preconditioning.

4.6.2. 3500rpm – 15kW, High-speed preconditioning

The high-speed preconditioning procedure consisted of ten minutes running at 3500rpm - 15kW with the aim of blowing out fluffy deposits from the walls of the exhaust system, in contrast with the idle preconditioning procedure, which was designed to produce those deposits. After this, the engine was soaked overnight and a cold-start test at 3500rpm - 15kW was run, with the results described in this section.

The general characteristics of the particulate emissions at the conditions tested were the same as those observed during the test after idle preconditioning, showing a first mass burst, followed by a peak number concentration in the first minute of cold start, and a stabilisation in particle number concentrations and Emission Index four to five minutes later.

4.6.2.1. First mass burst

During the first seconds of cold start, when the first mass burst occurred, the total particle number concentration of the exhaust aerosol leaving the engine was 1.4×10^7 cm^{-3}, converting to an Emission Index of 327 g/kg fuel (uncorrected) or 24 g/kg fuel (corrected). Through the catalyst, the number concentration increased to 2.0×10^7 cm^{-3} (by 38%). However, the Emission Index, uncorrected and corrected, decreased significantly, by 91 and 82%, to 29 g/kg fuel and 4 g/kg fuel, respectively. Ultrafine particles, below 0.1μm, were formed and larger particles deposited through the catalyst. As a result, the trend of the number concentration was opposite to that of the Emission Index, and the particle size distribution shifted towards lower sizes.

Through the first silencer, the total particle number concentration decreased by 70%, to 5.9×10^6 cm^{-3}. The uncorrected and corrected Emission Index decreased by 81% and 74%, to 5.43 g/kg fuel and 1.14 g/kg fuel, respectively. Particles of all sizes deposited through the silencer, and there was no significant change in the particle size distribution.

Through the second silencer, the total particle number concentration decreased by 31%, to 4.1×10^6 cm^{-3}, and the uncorrected Emission Index, by a similar percentage, to 3.76 g/kg fuel. The corrected Emission Index decreased by 41%, to 0.67 g/kg fuel. Particles of all sizes deposited through the second silencer, as occurred through the first silencer, and no significant change in size distribution was observed.

In summary, particle deposition occurred throughout the exhaust system during the first mass-burst event of the cold-start test at 3500rpm - 15kW after high-speed

preconditioning, and the only increase in number concentration was due to the formation of ultrafine particles through the catalyst.

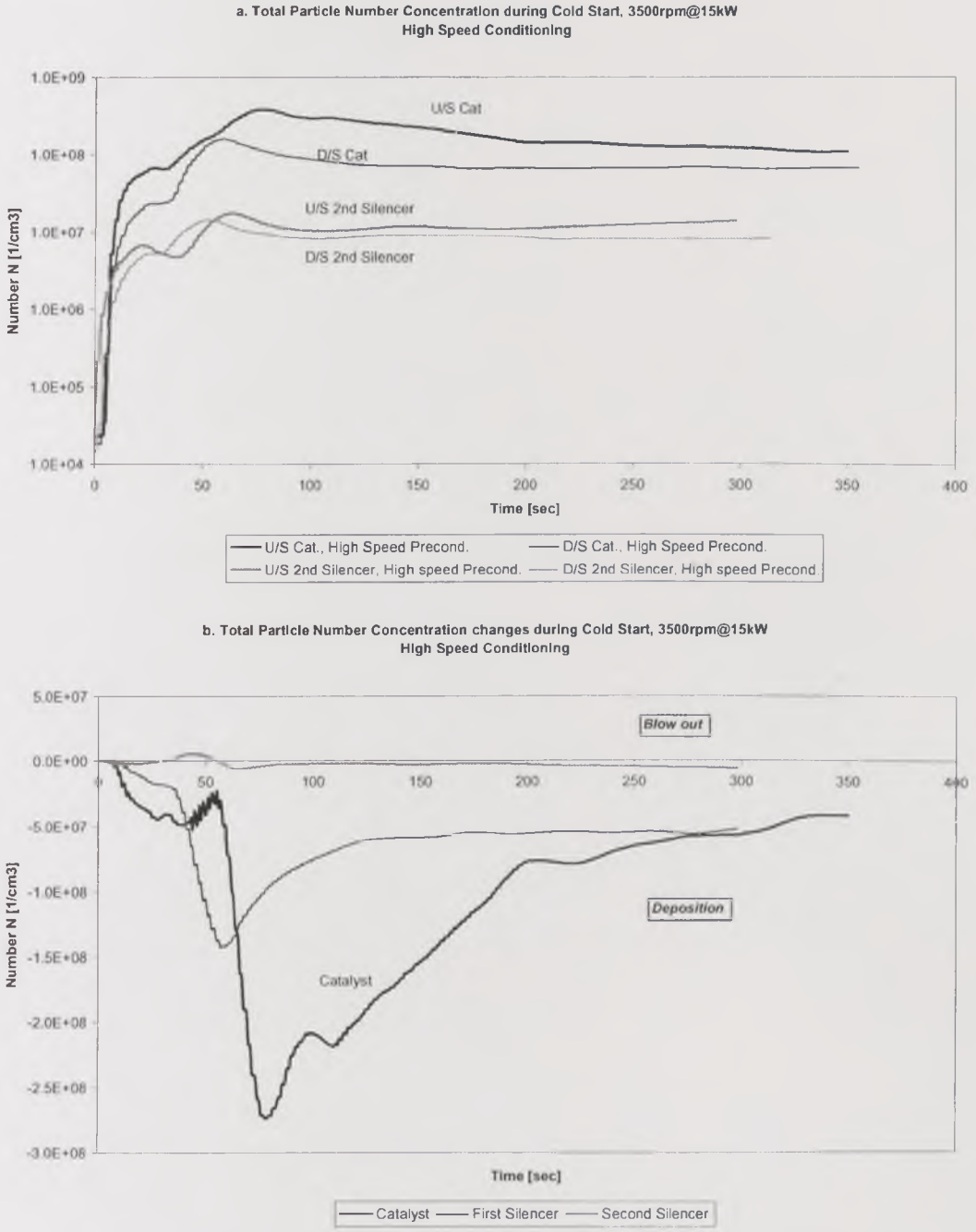

Figure 4.21. Total number and mass concentrations vs. time during cold start at high-speed conditions after high-speed preconditioning, at various exhaust points. a) Particle number concentration.

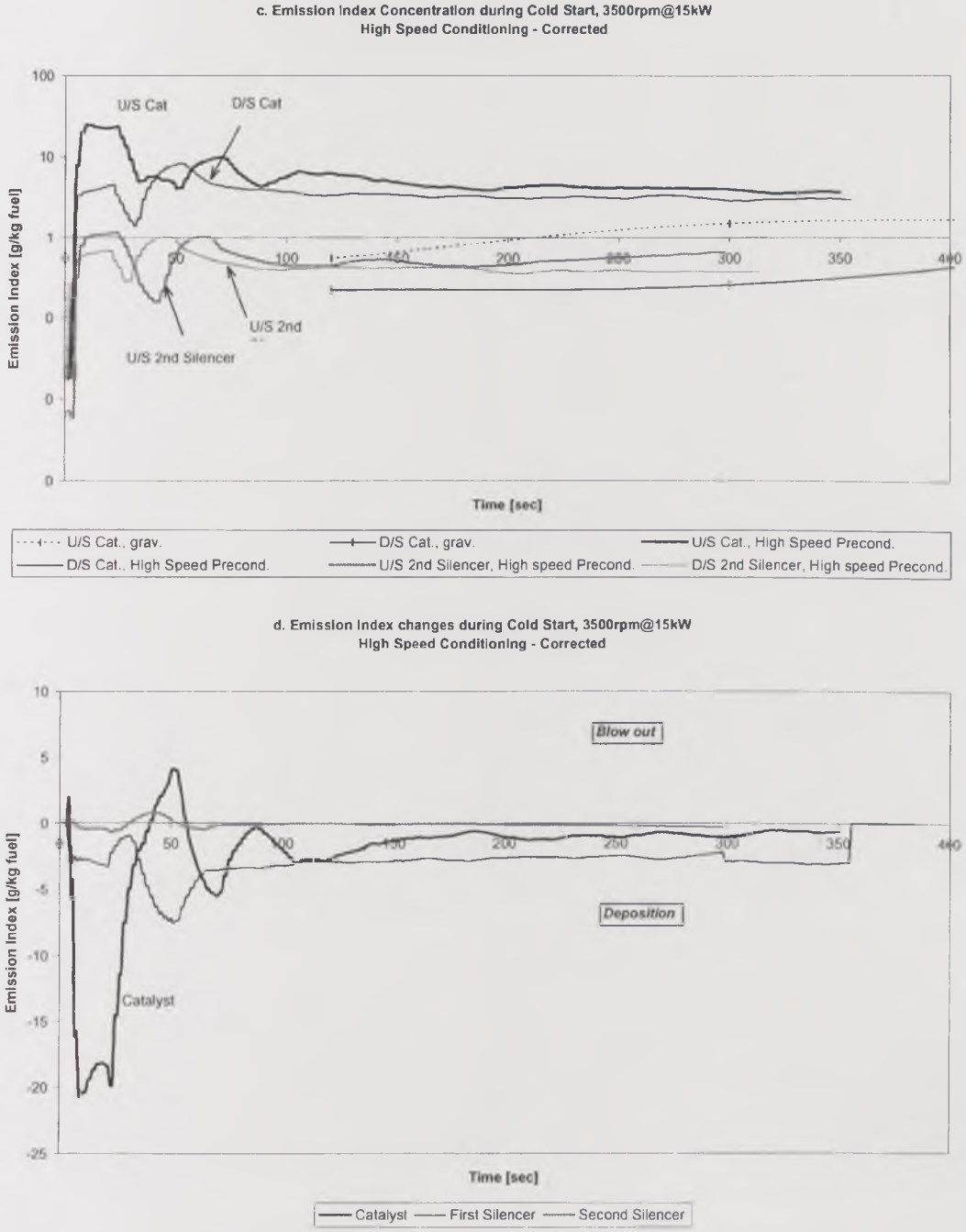

Figure 4.21. Total number and mass concentrations vs. time during cold start at high-speed conditions after high-speed preconditioning, at various exhaust points. b) Corrected Emission Index.

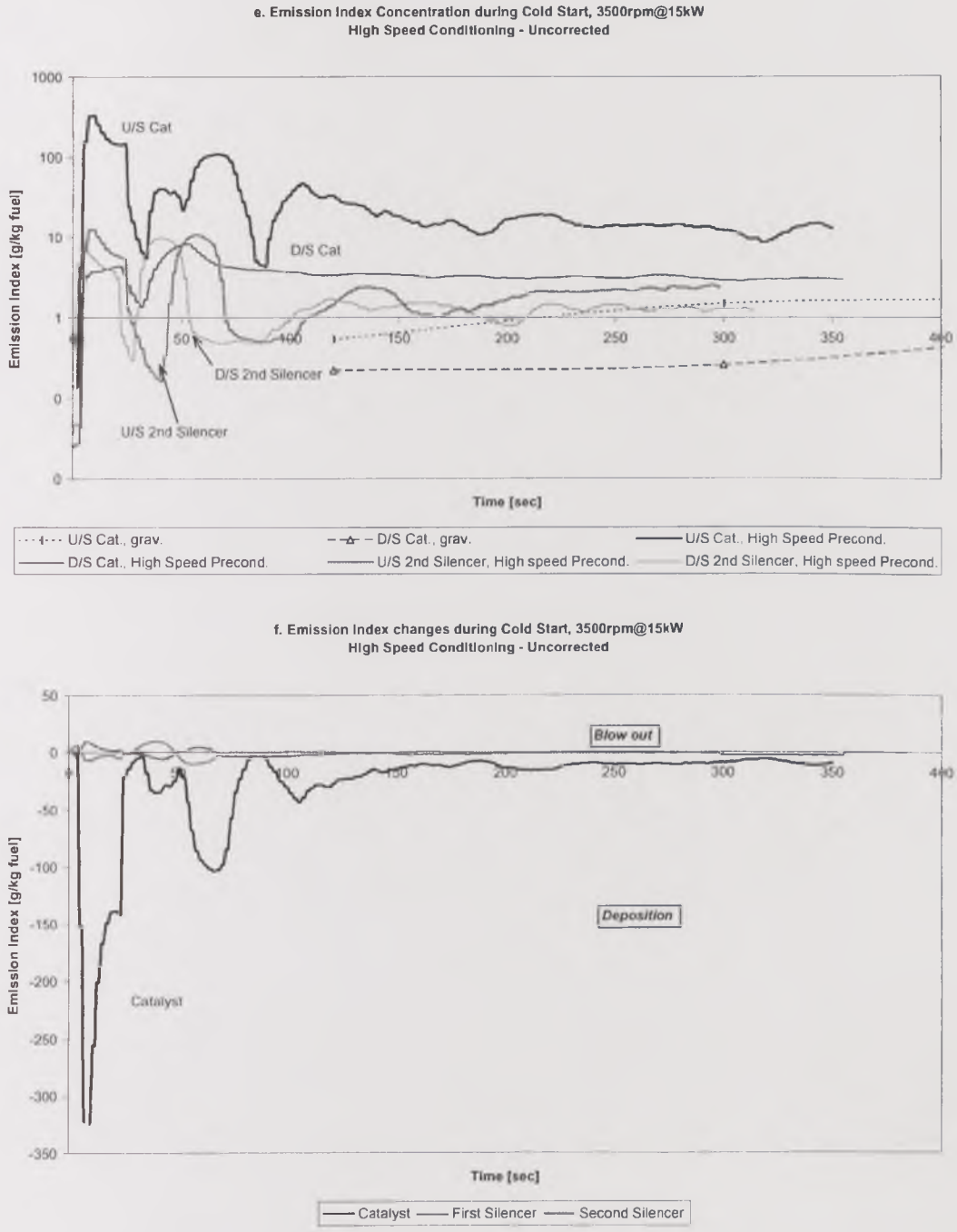

Figure 4.21. Total number and mass concentrations vs. time during cold start at high-speed conditions after high-speed preconditioning, at various exhaust points. c) Uncorrected Emission Index.

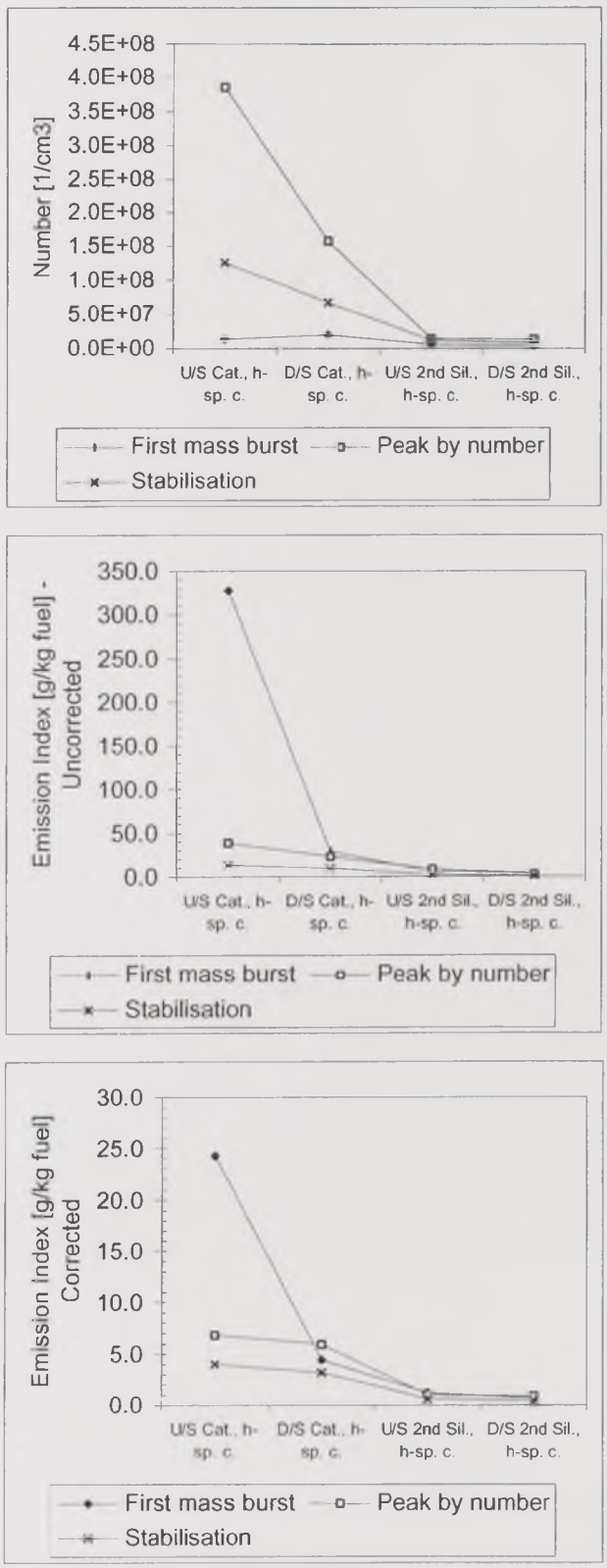

Figure 4.22. Total number and mass concentrations vs. location in the exhaust for various events during cold start at high-speed conditions after high-speed preconditioning.

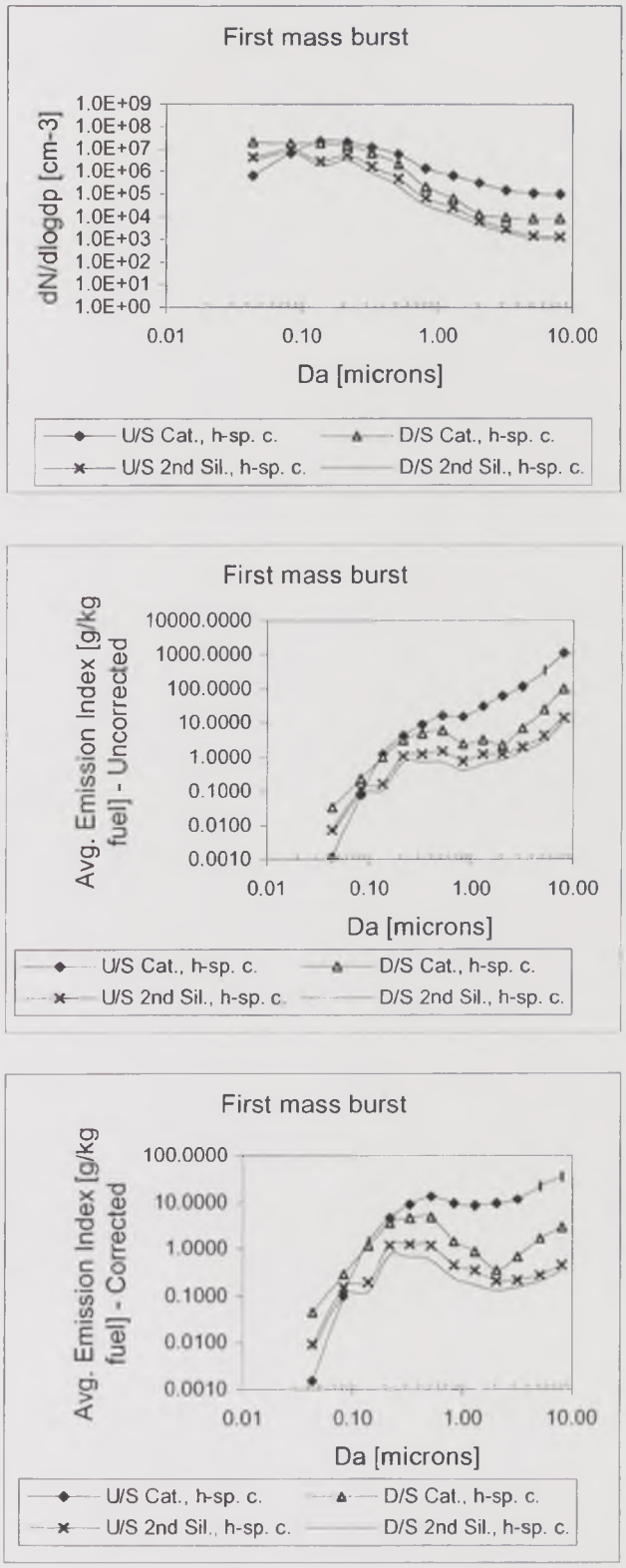

Figure 4.23. Particle size distribution during the first mass-burst event of the cold start at 3500rpm – 15kW after high-speed preconditioning.

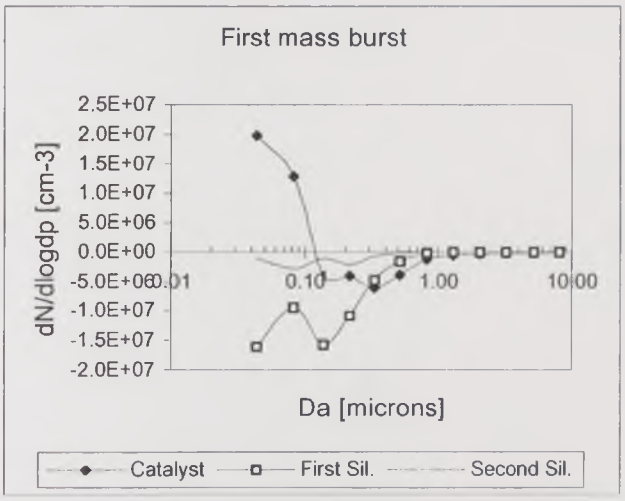

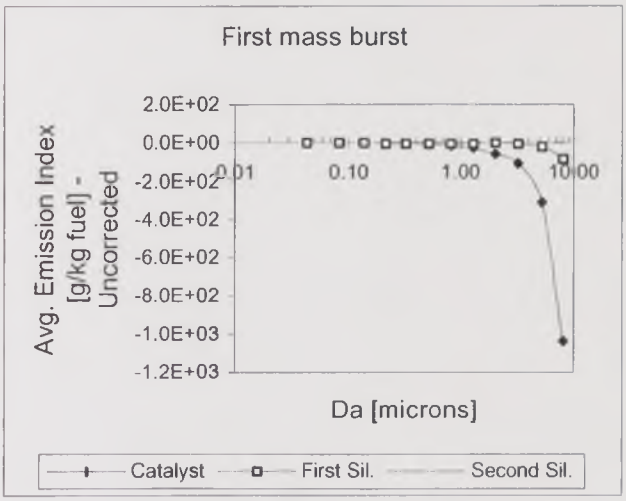

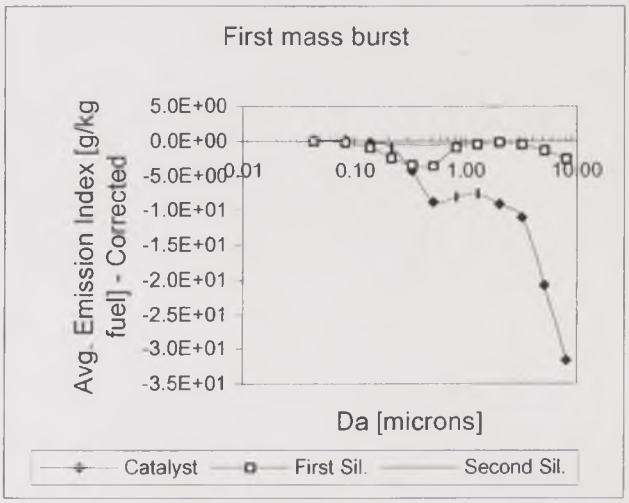

Figure 4.24. Particulate blow-out for various size ranges during the first mass-burst event of the cold start at 3500rpm – 15kW after high-speed preconditioning.

4.6.2.2. Peak by number

After the first mass-burst event, the total particle number concentration peaked at $3.9x10^8$ cm^{-3}, the corresponding Emission Index being 38.76 g/kg fuel (uncorrected) or 6.84 g/kg fuel (corrected). Through the catalyst, the particle number concentration decreased to $1.6x10^8$ cm^{-3} (59% decrease). The Emission Index, uncorrected and corrected, also decreased, by 40% and 14%, to 23.1 g/kg fuel and 5.89 g/kg fuel, respectively. Particles below 0.2μm were oxidised, coagulated and deposited, whereas particles larger than 1.0μm deposited and particles within those limits were formed by coagulation through the catalyst. As a result, the particle size distribution shifted towards larger sizes.

Through the first silencer, the total particle number concentration decreased to $1.2x10^7$ cm^{-3}, which was a 90% decrease. The uncorrected and corrected Emission Index decreased to 8.58 g/kg fuel and 1.02 g/kg fuel, by 63% and 83%, respectively. Particles of all sizes deposited through the silencer.

Through the second silencer, the decrease in total particle number concentration was just by 7%, so the concentration at the tailpipe was $1.4x10^7$ cm^{-3}. The decrease in uncorrected Emission Index was more significant, by 65%, so 3.05 g/kg fuel of particulate were emitted at the tailpipe. The corrected Emission Index, however, decreased by just 19% through the second silencer, to 0.83 g/kg fuel. The deposition occurred for particles at nearly all size ranges, with the exception of particles between 0.1μm and 0.4μm, whose number concentration increased slightly as a result of coagulation.

In summary, the general trends in the behaviour of the exhaust aerosol during the peak-number event at 3500rpm - 15kW after high-speed preconditioning were identical to those observed for the same event at the 3500rpm - 15kW test after Idle preconditioning, showing parallel size-dependent changes through the catalyst and the second silencer, and deposition for all particle sizes through the first silencer. Through the catalyst, the formation of ultrafine particles made the particle size distribution shift towards larger sizes.

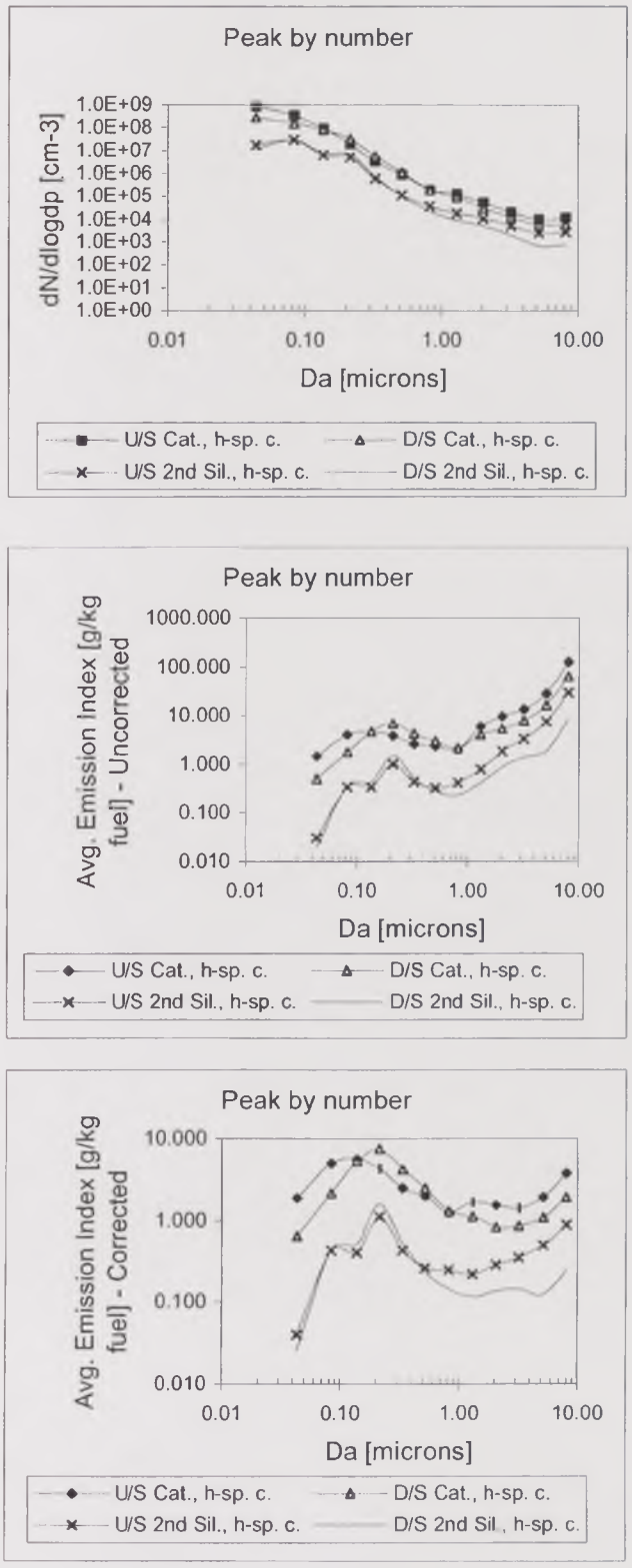

Figure 4.25. Particle size distribution during the peak-number event of the cold start at 3500rpm – 15kW after high-speed preconditioning.

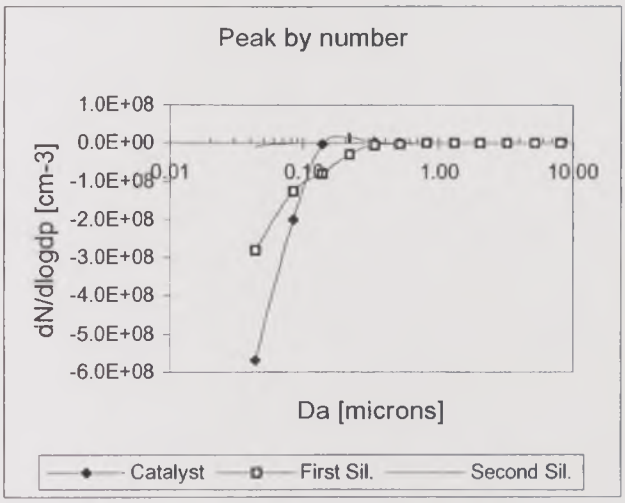

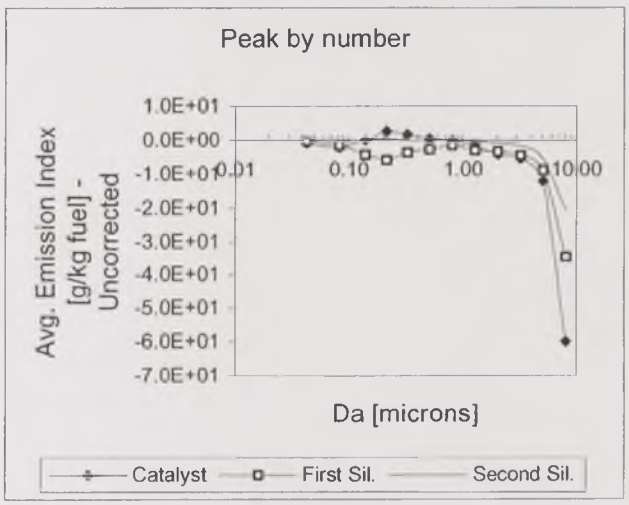

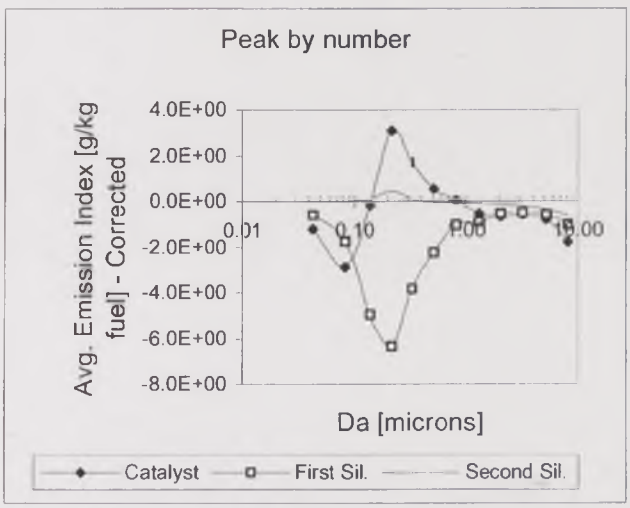

Figure 4.26. Particulate blow-out for various size ranges during the peak-number event of the cold start at 3500rpm – 15kW after high-speed preconditioning.

4.6.2.3. Stabilisation

The total particle number concentration of the exhaust aerosol leaving the engine decreased with time after the number peak and reached a stabilisation level at $1.3x10^8$ cm^{-3} after 5 minutes. The uncorrected Emission Index during this period was 13.74 g/kg fuel, and the corrected, 3.98 g/kg fuel. The catalyst produced a decrease by 47% in particle number concentration and by 28% (uncorrected) or 22% (corrected) in Emission Index, so the levels downstream of the catalyst were $6.7x10^7$ cm^{-3} and 9.83 g/kg fuel or 3.12 g/kg fuel, respectively. Particles were deposited through the catalyst at most sizes, except those between 0.3μm and 1.0μm, whose concentration increased as a result of coagulation, making the size distribution shift slightly towards larger sizes.

Through the first silencer, the total particle number concentration decreased to $1.2x10^7$ cm^{-3}, and the Emission Index, to 2.10 g/kg fuel (uncorrected) and 0.55 g/kg fuel (corrected). The decrease in both particle number concentration and Emission Index was by around 80%, due to particle deposition for all size ranges.

Particles at all size ranges deposited through the second silencer, although less significantly than through the first silencer. Total particle number concentration decreased by 31%, and Emission Index, by 39% (uncorrected) or 28% (corrected), so an $8.4x10^6$ cm^{-3} aerosol was emitted at the tailpipe. This converted to a tailpipe Emission Index of 1.28 g/kg fuel (uncorrected) or 0.39 g/kg fuel (corrected).

In summary, the stabilisation period of the cold-start test at 3500rpm - 15kW after high-speed preconditioning showed similar features to those observed for the test at the same conditions after idle preconditioning, showing deposition throughout the exhaust system, and the formation by coagulation of middle-sized particles through the catalyst. These results indicate that preconditioning has a lesser influence for high-speed cold start compared with low-speed cold start. This may be due to the higher exhaust temperatures as well as the high exhaust flow rates. The greater temperature gradient had lead to more thermophoretic deposition on the wall followed by 'baking' of the deposits at the higher temperatures.

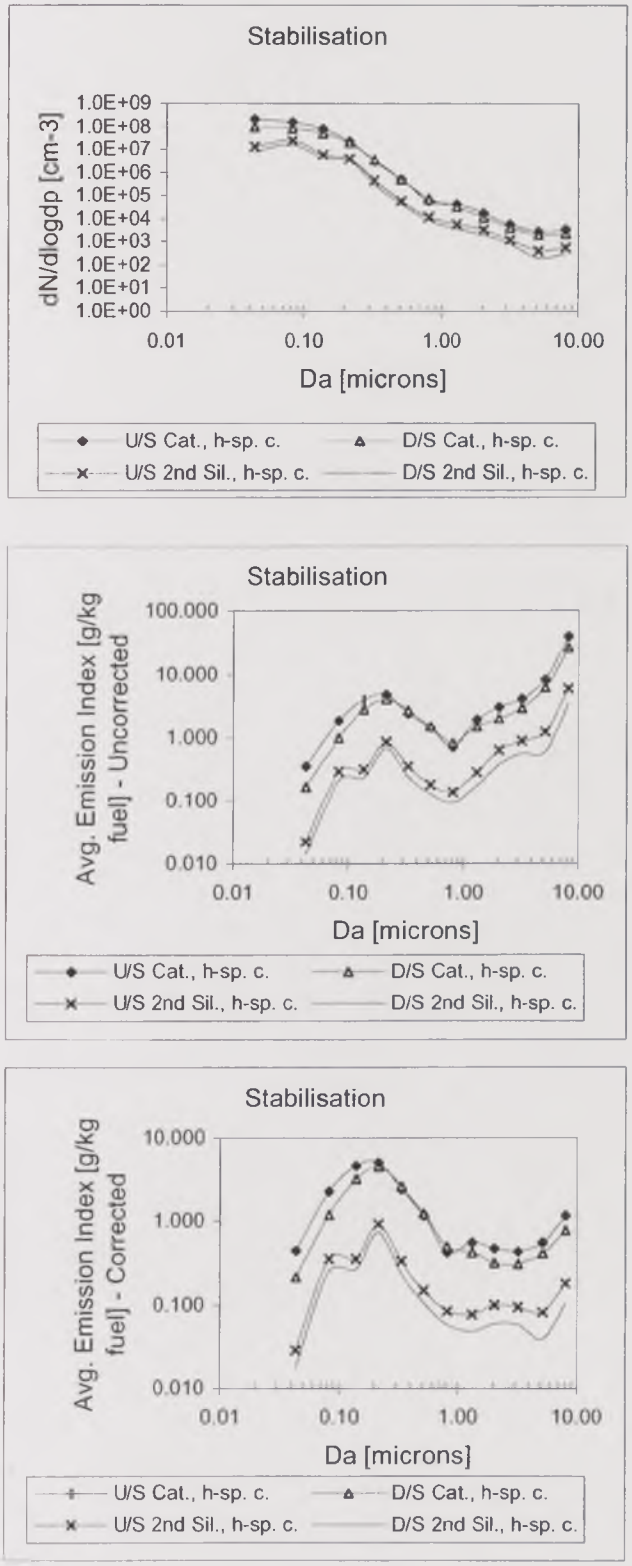

Figure 4.27. Particle size distribution during the first mass-burst event of the cold start at 3500rpm – 15kW after high-speed preconditioning.

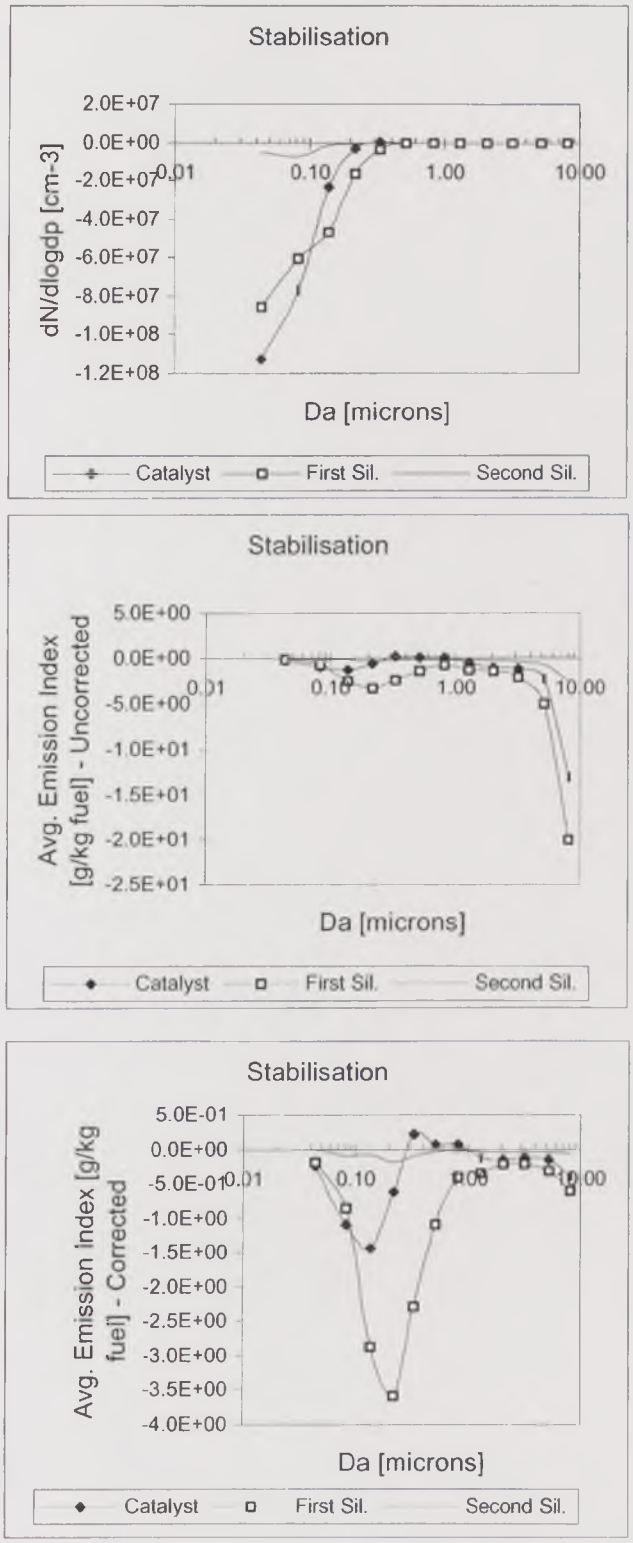

Figure 4.28. Particulate blow-out for various size ranges during the stabilisation event of the cold start at 3500rpm – 15kW after high-speed preconditioning.

4.6.3. 2250rpm - 35kW, Idle preconditioning

High power step-change cold-start tests, at 2250rpm - 35kW, were run after both idle and high-speed preconditioning, as in the case of high-speed tests described in the previous section. After idle preconditioning, the exhaust system was expected to have a considerable amount of fluffy particulate aggregates onto the deposition layer. Results from the high-power cold-start test are presented here.

In contrast with the high-speed cold-start tests, the high-power tests showed the effect of the EGR-valve opening after 150 seconds from cold start. The total particle number concentration and Emission Index increased as a result of the event, as shown in Figure 4.29 and 4.30. The details of the changes in the exhaust aerosol throughout the exhaust system during this and other events are shown below.

4.6.3.1. First mass burst

During the first seconds from cold start, during the first mass-burst event, the total particle number concentration of the exhaust aerosol upstream of the catalyst was 1.1×10^{8} cm^{-3}. The equivalent uncorrected Emission Index was 37.42 g/kg fuel, and the corrected, 3.08 g/kg fuel. Through the catalyst, the number concentration was reduced to 4.7×10^{7} cm^{-3}, a 59% decrease. The Emission Index, however, increased by 21% when uncorrected and 192% when corrected, to 45.2 g/kg fuel and 8.97 g/kg fuel, respectively. As in other cases, the opposite changes were due to size-dependent increase or decrease in particulate number. Very fine particles, below 0.1μm, accounted for the decrease in particulate number, as they oxidised, coagulated and deposited by diffusion through the catalyst. Middle-sized and large particles were blown-out of the catalyst, with the only exception of particles around 8μm, which deposited through it. The particle size distribution shifted towards larger particles, as shown in Figure 4.31.

Through the first silencer, the total particle number concentration decreased by 69%, to 1.7×10^{7} cm^{-3}. The Emission Index also decreased, to 18.25 g/kg fuel (uncorrected) and 2.84 g/kg fuel (corrected), that is, a 60% and 68% decrease, respectively. Particles at all size ranges deposited through this silencer.

Through the second silencer, the total particle number concentration increased by 68%, so it was 2.4×10^{7} cm^{-3} when emitted at the tailpipe. Only very fine particles, below 0.2μm, were formed, accounting for the increase in number concentration. Middle-sized and large particles deposited and, therefore, the Emission Index decreased. It reached 16.15 g/kg fuel (uncorrected) or 2.31 g/kg fuel (corrected), for a 12% or 19% decrease from the Emission Index upstream of the silencer. The particle size distribution shifted slightly towards smaller particles, owing to the

formation of ultrafine particles by outgassing, nucleation, condensation and coagulation processes.

Figure 4.29. Total number and mass concentrations vs. time during cold start at high-load conditions after Idle preconditioning at various exhaust points. a) Particle number concentration.

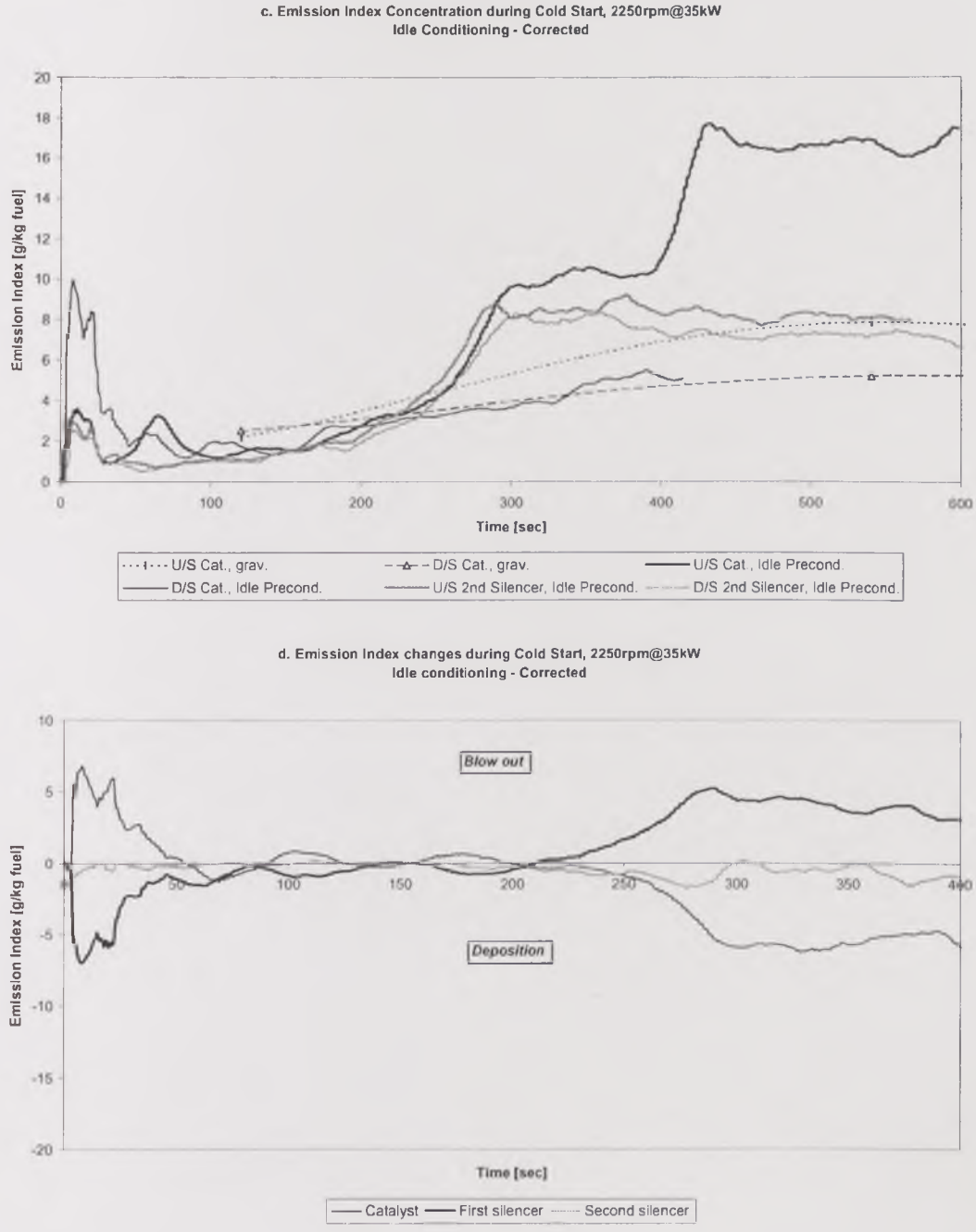

Figure 4.29. Total number and mass concentrations vs. time during cold start at high-load conditions after Idle preconditioning at various exhaust points. b) Corrected Emission Index.

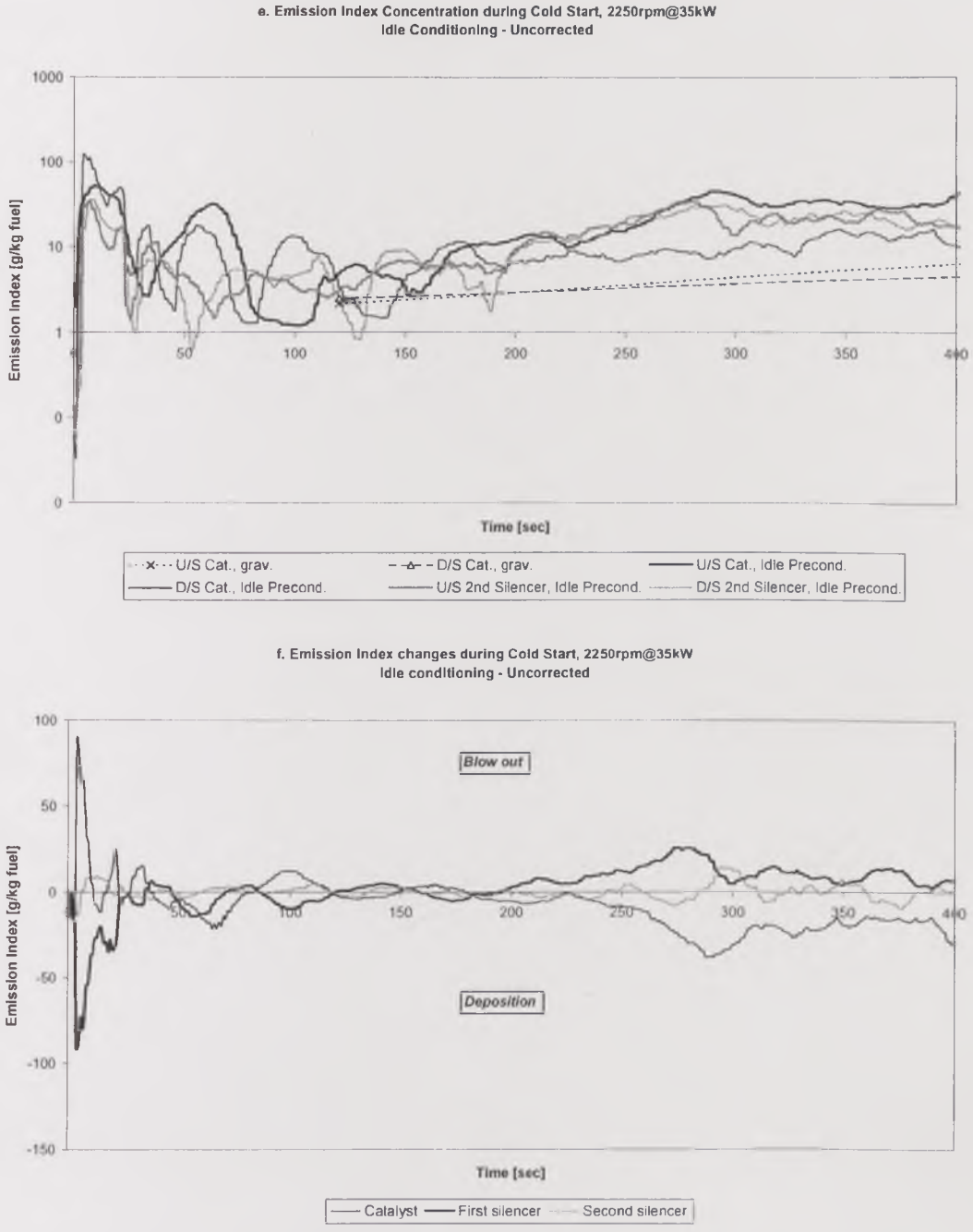

Figure 4.29. Total number and mass concentrations vs. time during cold start at high-load conditions after Idle preconditioning at various exhaust points. c) Uncorrected Emission Index.

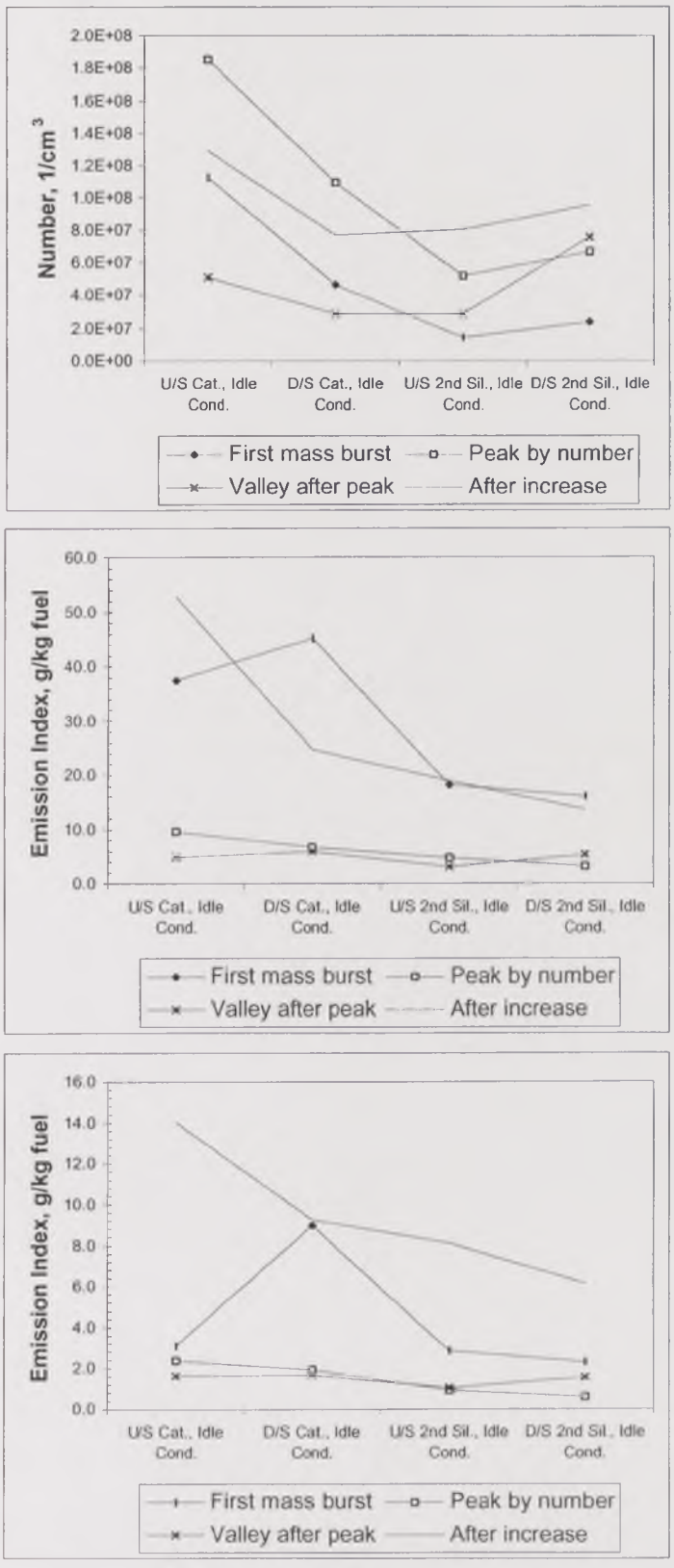

Figure 4.30. Total number and mass concentrations for the main events of the cold start at high-load conditions after Idle preconditioning vs. location in the exhaust system.

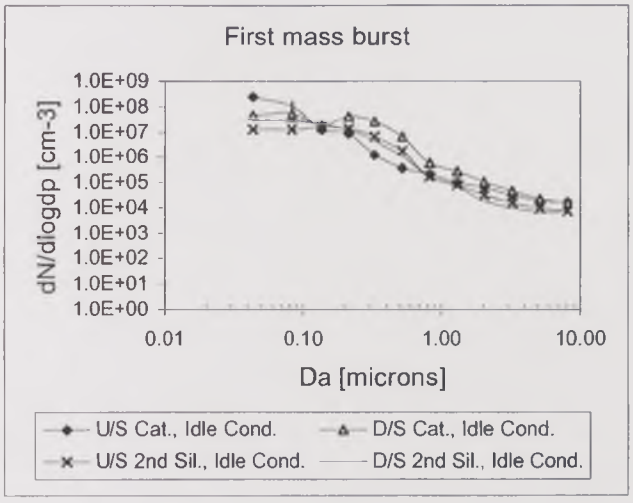

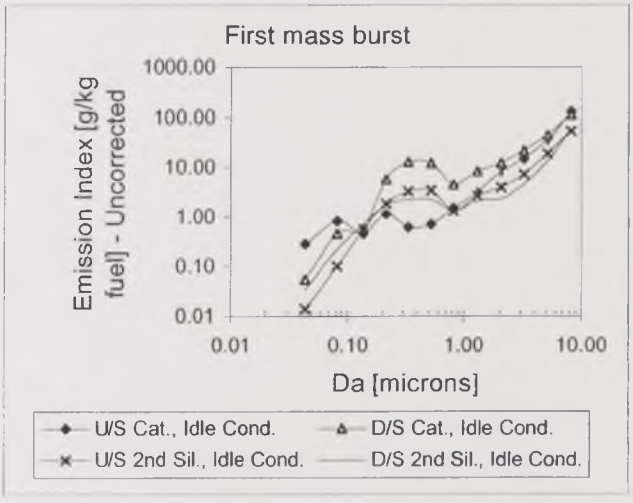

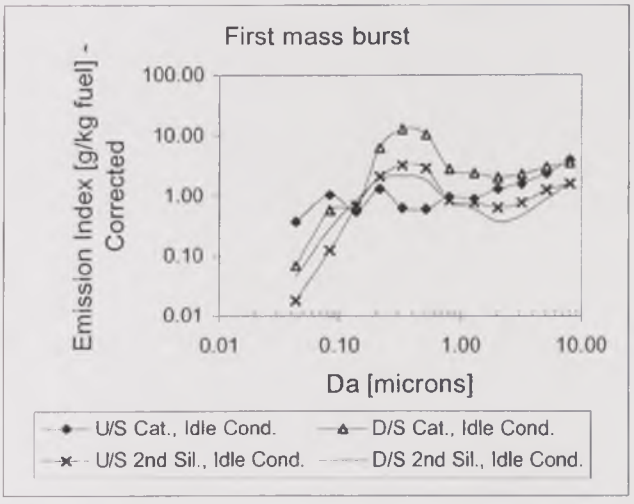

Figure 4.31. Particle size distribution during the first mass-burst event of the cold start at 2250rpm – 35kW after Idle preconditioning.

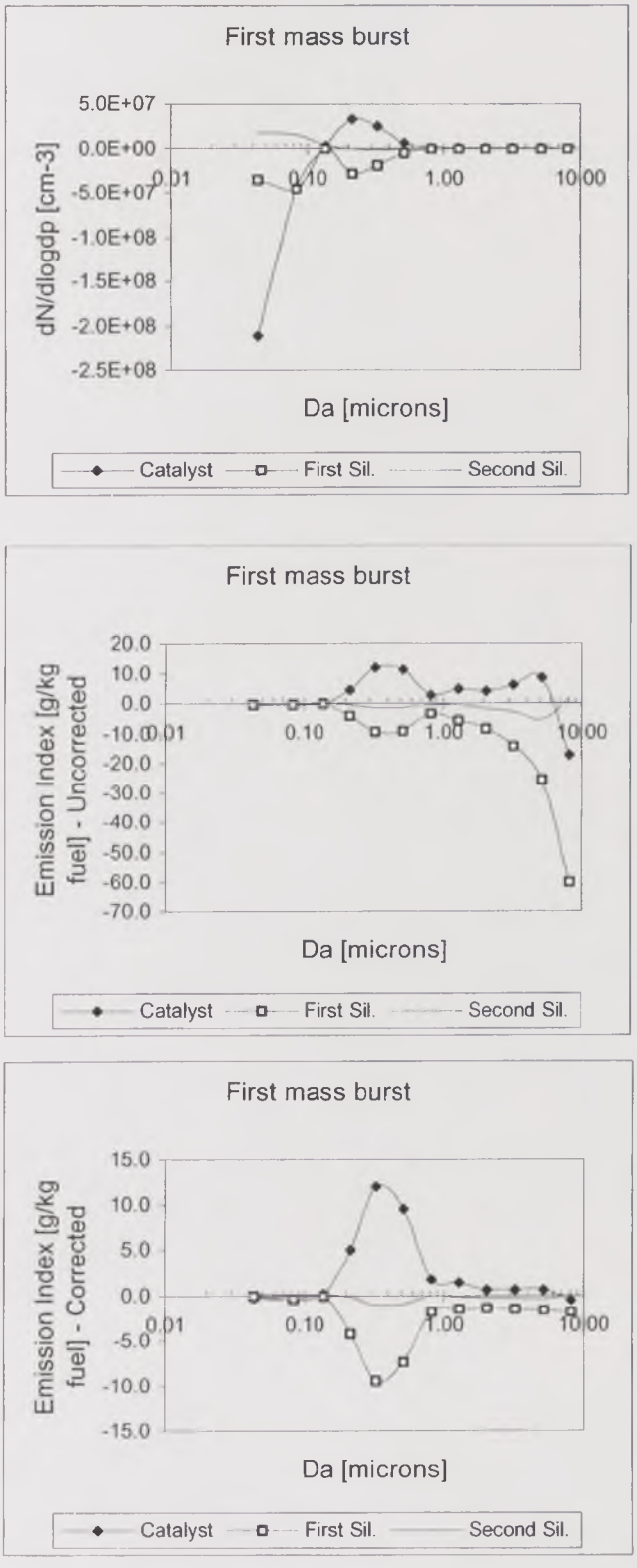

Figure 4.32. Particulate blow-out for various size ranges during the first-mass-burst event of the cold start at 2250rpm - 35kW after Idle preconditioning.

The first mass burst was the first observation of an opposite behaviour of the exhaust aerosol through the catalyst and the second silencer, which had shown

parallel changes in previous tests. The general trend throughout the exhaust system in this event was particle deposition. As exceptions, the number concentration of middle-sized particles increased by coagulation and large particle were blown out from the catalyst; also, very fine particles were formed through the second silencer.

4.6.3.2. Peak by number

The total particle number concentration of the exhaust aerosol leaving the engine peaked at $1.9x10^{8}$ cm^{-3} just before the first minute from cold start. The corresponding Emission Index was 9.65 g/kg fuel (uncorrected) or 2.38 g/kg fuel (corrected). Through the catalyst, the number concentration decreased by 41%, to $1.1x10^{8}$ cm^{-3}, and the Emission Index, by 31% or 19%, to 6.70 g/kg fuel or 1.93 g/kg fuel, uncorrected or corrected, respectively. Most of the particles deposited through the catalyst, with the exception of particles between 0.3μm and 0.5μm, the number of which increased, presumably by coagulation, with the corresponding loss of finer particles.

The total particle number concentration decreased by 53% through the first silencer, reaching $5.2x10^{7}$ cm^{-3} downstream of it. The Emission Index decreased to 3.17 g/kg fuel (uncorrected) or 0.92 g/kg fuel (corrected), which was a 29% or 52% decrease, respectively. Particles of all size ranges deposited, with the exception of particles around 0.14μm, whose concentration increased by coagulation, and those around 5μm, which were blown out.

In a similar way to the first mass burst, ultrafine particles were formed through the second silencer, and particles larger than 1.0μm, which deposited. This caused an opposite change in total particle number concentration in the Emission Index. The number concentration, dominated by ultrafine particles, increased by 29%, reaching $6.7x10^{7}$ cm^{-3}. In contrast, the Emission Index decreased by 30% or 32%, to 3.30 g/kg fuel or 0.60 g/kg fuel, uncorrected and corrected, respectively.

Again, the exhaust aerosol passing through the second silencer showed opposite trends from those observed through the catalyst, which was an important difference from previous tests at different operating conditions. Apparently, the temperature drop in the second silencer triggered a marked ultrafine particle formation mechanism through the second silencer. As a result, it was the first silencer that was in phase with the catalyst in terms of the effects on the exhaust particles. The most likely cause for these changes was the increased temperature of the exhaust gas, which created a wider temperature drop through the exhaust system.

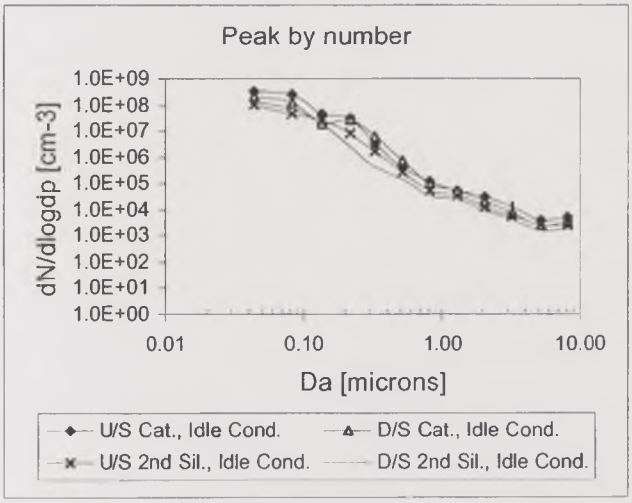

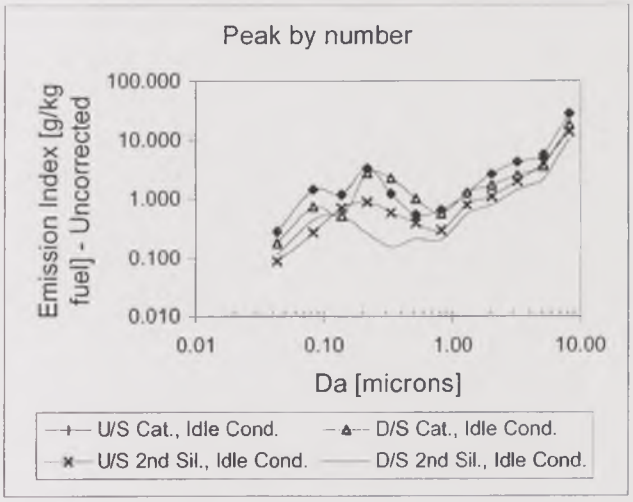

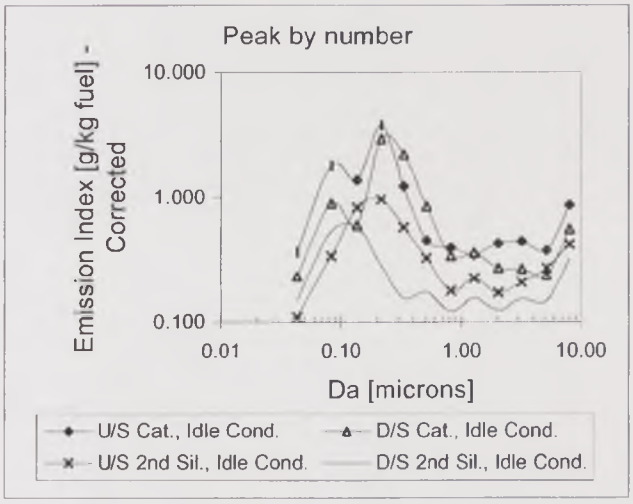

Figure 4.33. Particle size distribution during the peak-number event of the cold start at 2250rpm – 35kW after Idle preconditioning.

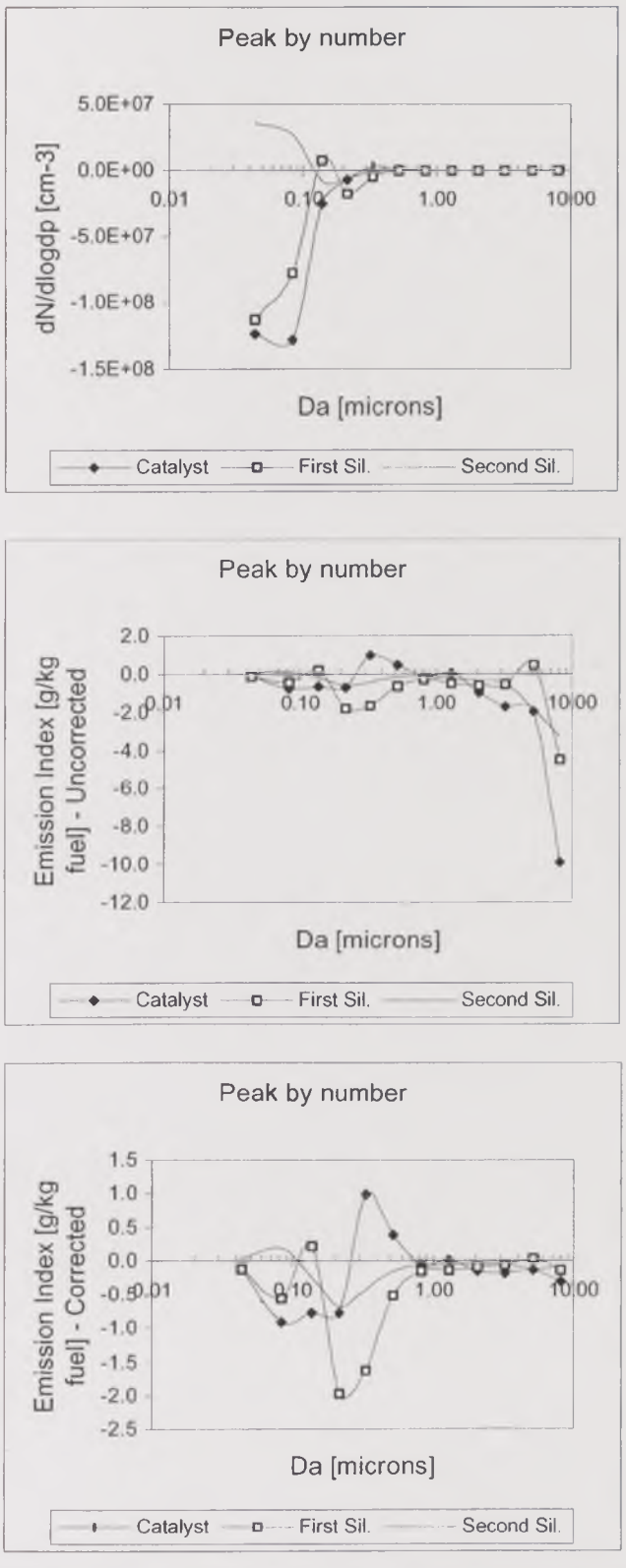

Figure 4.34. Particulate blow-out for various size ranges during the peak-number event of the cold start at 2250rpm - 35kW after Idle preconditioning.

4.6.3.3. Valley after peak

The total particle number concentration decreased after the peak of the first minute from cold start at all points, except the tailpipe, to a comparatively low value or "valley" event. This could have been due to a re-deposition period after the initial blow out. There are internal engine deposition in the water cooled exhaust port walls as well as in the piston and cylinder crown areas. These can cause the transient in engine-out particulate. Upstream of the catalyst, the number concentration for the valley was $5.1x10^7$ cm^{-3}, which was 26% of the peak value. The corresponding Emission Index was 4.96 g/kg fuel (uncorrected) and 1.63 g/kg fuel (corrected), a 51% or 68% of the Emission Index during the number peak. Through the catalyst, the total particle number concentration decreased to $2.9x10^7$ cm^{-3} (44% decrease), and the Emission Index increased to 5.99 g/kg fuel (21% increase) and 1.66 g/kg fuel (2% increase). Particles below 0.3μm were oxidised, coagulated or deposited through the catalyst, but larger particles increased in number concentration by coagulation and were blown out from it. The particle size distribution shifted slightly towards larger sizes through the catalyst.

Through the first silencer, the total particle number concentration increased just by 1%, remaining around $2.9x10^7$ cm^{-3}. The uncorrected Emission Index decreased by 47%, to 3.17 g/kg fuel, and the corrected Emission Index, by 37%, to 1.04 g/kg fuel. Most of the particles deposited through the silencer, with the exception of those around 0.04 and 0.14μm, which were formed through it, increasing their number concentration. As a result, the particle size distribution shifted towards smaller sizes.

Through the second silencer, the total particle number concentration increased very significantly, reaching $7.6x10^7$ cm^{-3}, 162% higher than upstream of the catalyst. The Emission Index also increased, to 5.40 g/kg fuel, uncorrected, or 1.53 g/kg fuel, corrected, 70% or 47% higher than upstream of the catalyst, respectively. The number of particles of all sizes increased, by coagulation of ultrafine particles as well as blow out of large particles from the silencer walls. The particle size distribution shifted slightly towards smaller sizes.

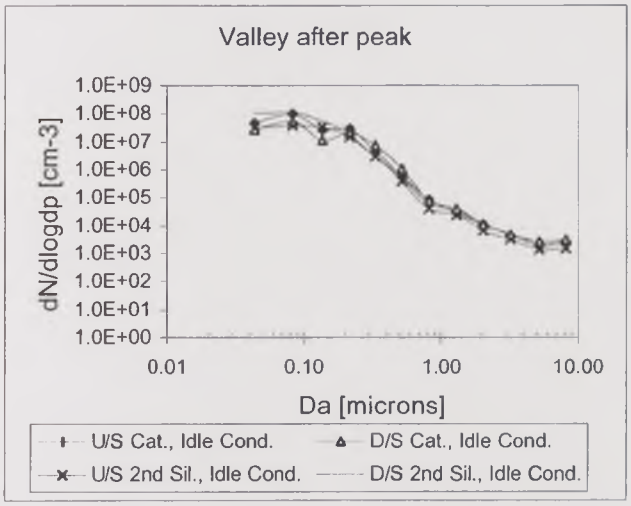

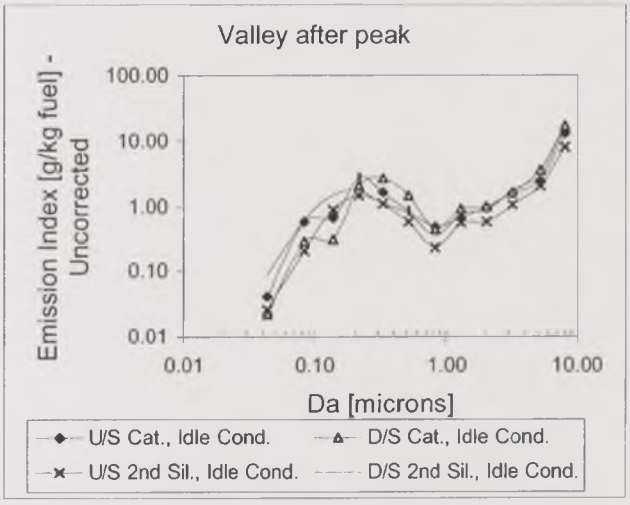

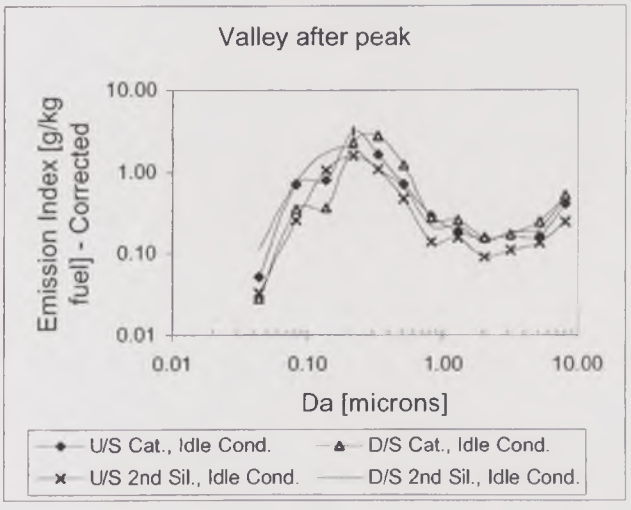

Figure 4.35. Particle size distribution during the valley-after-peak event of the cold start at 2250rpm – 35kW after Idle preconditioning.

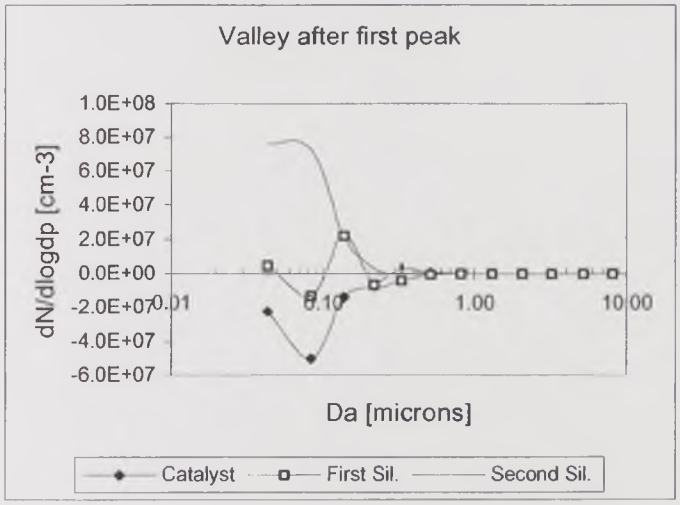

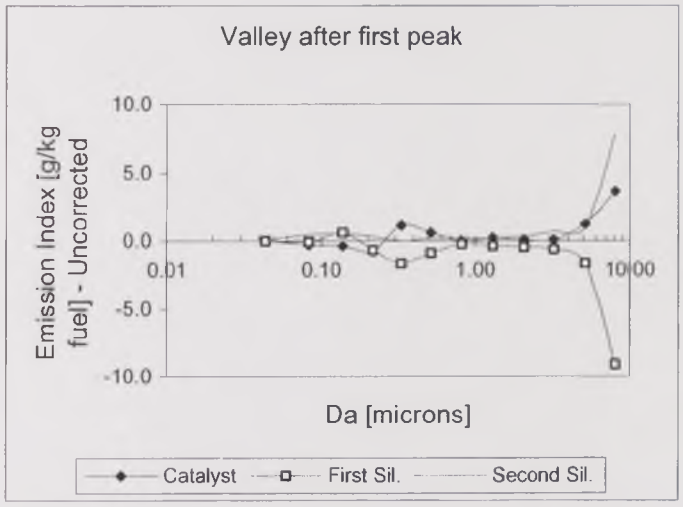

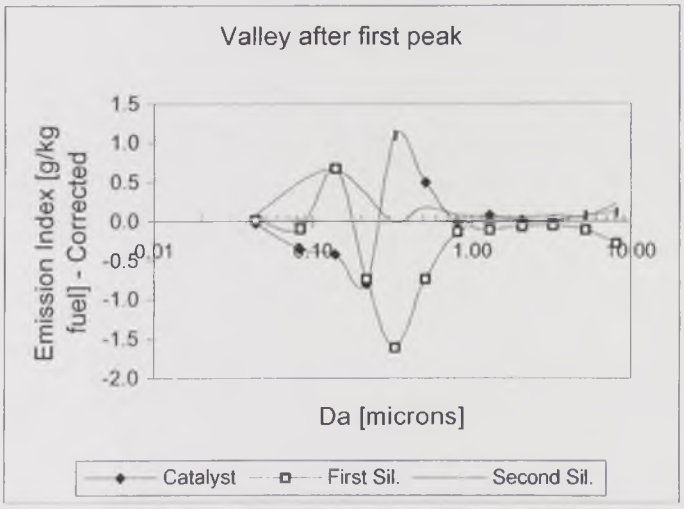

Figure 4.36. Particulate blow-out for various size ranges during the valley-after-peak event of the cold start at 2250rpm - 35kW after Idle preconditioning.

4.6.3.4. Increase after EGR-valve opening

The exhaust total particle number concentration at the inlet of the exhaust system during the test period after the EGR-valve opening was $1.3x10^8$ cm^{-3}, which was nearly 70% of the total number concentration during the number peak, and 2.5 times as high as that during the valley. The corresponding Emission Index was very high, 52.74 g/kg fuel when uncorrected and 14.02 g/kg fuel when corrected. The uncorrected Emission Index at this point was higher than tenfold -and the corrected, more than eightfold- higher than the Emission Index during the valley event.

Through the catalyst, the total particle number concentration decreased to $7.7x10^7$ cm^{-3} and the Emission Index to 24.67 g/kg fuel (uncorrected) or 9.25 g/kg fuel (corrected), which was a 40%, 53% and 34% decrease, respectively. Very fine particles were oxidised, coagulated or deposited, and the rest of the particles deposited through the catalyst. No significant change in particle size distribution was observed.

Through the first silencer, the total particle number concentration increased to $8.0x10^7$ cm^{-3}, for a 4% increase. The Emission Index decreased by 23% or 13%, to 18.99 g/kg fuel or 8.08 g/kg fuel, uncorrected or corrected, respectively. Changes through this silencer were very similar to those occurred during the valley event, most of the particles deposited through the silencer, except those around 0.04μm and 0.14μm.

Through the second silencer, the total particle number concentration increased by 19%, to $9.6x10^7$ cm^{-3}, as a result of the formation of ultrafine particles, those below 0.2μm increased. Larger particles, however, deposited through the silencer, causing an Emission Index decrease by 28% or 24%, to 13.58 g/kg fuel or 6.13 g/kg fuel, uncorrected or corrected, respectively.

In summary, particulate matter deposited throughout the exhaust system during the stabilisation period following the EGR valve opening, with the exception of particles below 0.3μm, which were formed, increasing their concentration through the second silencer. No significant change in particle size distribution was observed.

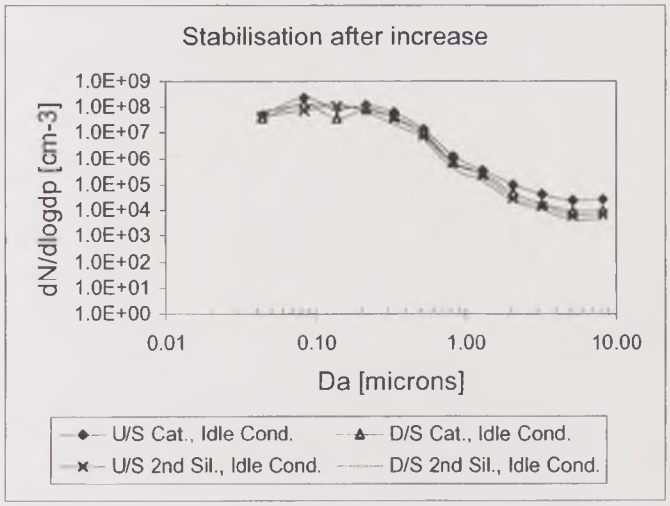

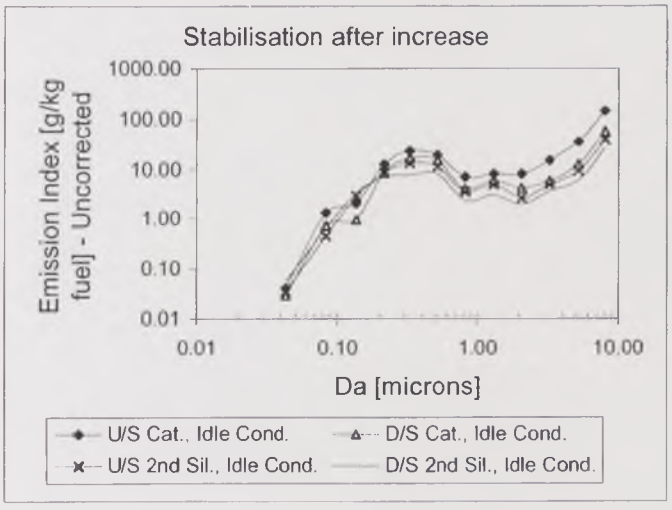

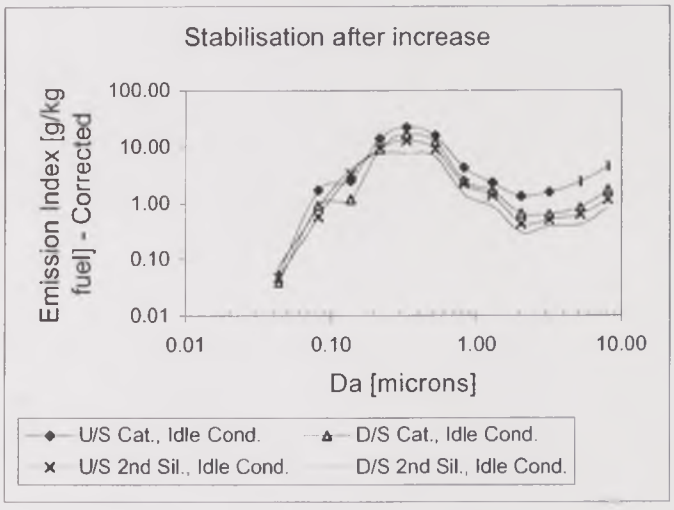

Figure 4.37. Particle size distribution during the increase-after-EGR event of the cold start at 2250rpm – 35kW after Idle preconditioning.

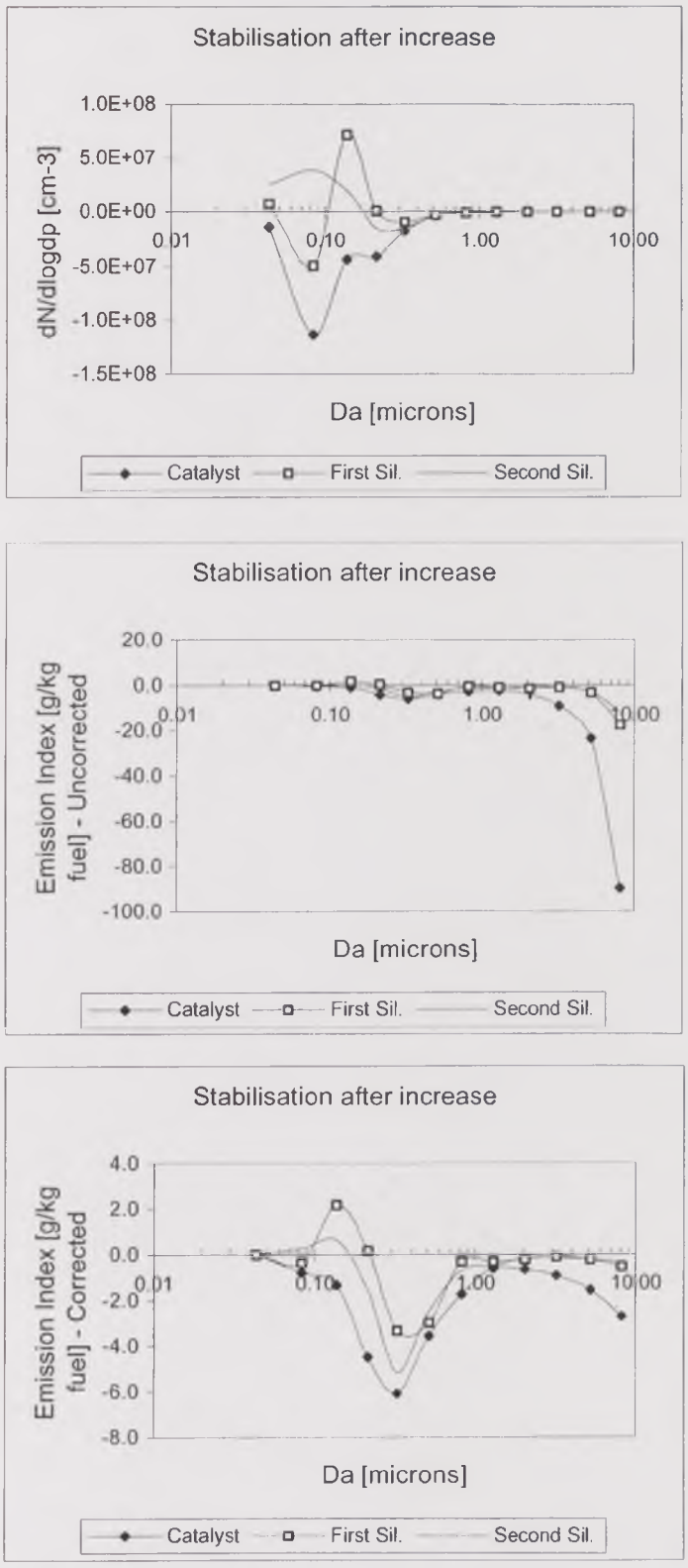

Figure 4.38. Particulate blow-out for various size ranges during the increase-after-EGR event of the cold start at 2250rpm - 35kW after Idle preconditioning.

4.6.4. 2250rpm - 35kW, High-speed preconditioning

High-power step-change cold-start tests were also run after high-speed preconditioning, to provide a comparison basis to the Idle-preconditioning tests. High-speed preconditioning consisted of a ten-minute run at 3500rpm - 15kW, that had the objective of blowing out fluffy deposits from the exhaust system walls, in contrast to the idle preconditioning, which aimed to produce such deposits. The general features of the particulate emissions with time during the cold start were similar to those previously observed. There was a first mass burst during the first few seconds, followed by a peak and a decrease to a flat "valley" in total particle number concentration, and a new increase both in number concentration and Emission Index, due to the EGR-valve opening.

4.6.4.1. First mass burst

The initial particle number concentration during the step-change cold-start test at 2250rpm - 35kW after high-speed preconditioning, in the first mass-burst event, was 3.7×10^7 cm^{-3} at the sampling point upstream of the catalyst. The Emission Index was 28.97 g/kg fuel (uncorrected) or 6.05 g/kg fuel (corrected), about 30% lower than the Emission Index at the same point and same event in the test after idle preconditioning. Through the catalyst, the aerosol particle number concentration decreased to 1.6×10^7 cm^{-3} and the Emission Index, to 2.68 g/kg fuel (uncorrected) or 1.55 g/kg fuel (corrected). This represented a 56% decrease in total particle number concentration; 90% and 74% in uncorrected and corrected Emission Index, respectively, which suggests that the catalyst was very effective in particulate adsorption at low temperatures if following a high-speed preconditioning. Particles coagulated were oxidised, or deposited to the catalyst walls. Hence particles of all sizes accounted for the significant total number and mass reduction.

Through the first silencer, the total particle number concentration decreased through the silencer by only 2%, staying around 1.6×10^7 cm^{-3}. The Emission Index, in contrast, increased very significantly, as much as fivefold, uncorrected, or by 103%, corrected. The resulting Emission Index downstream of this silencer was 17.21 g/kg fuel, uncorrected, or 3.14 g/kg fuel, corrected. As in previous cases, size-dependent changes caused the different trends in number concentration and Emission Index. Particles below 0.2µm accounted for the reduction in number concentration as they deposited or coagulated from the silencer, whereas the number of mid-sized particles increased by the effect of the coagulation and large particles were blown out, accounting for the increase in Emission Index. A very slight shift of the particle size distribution towards smaller sizes was observed.

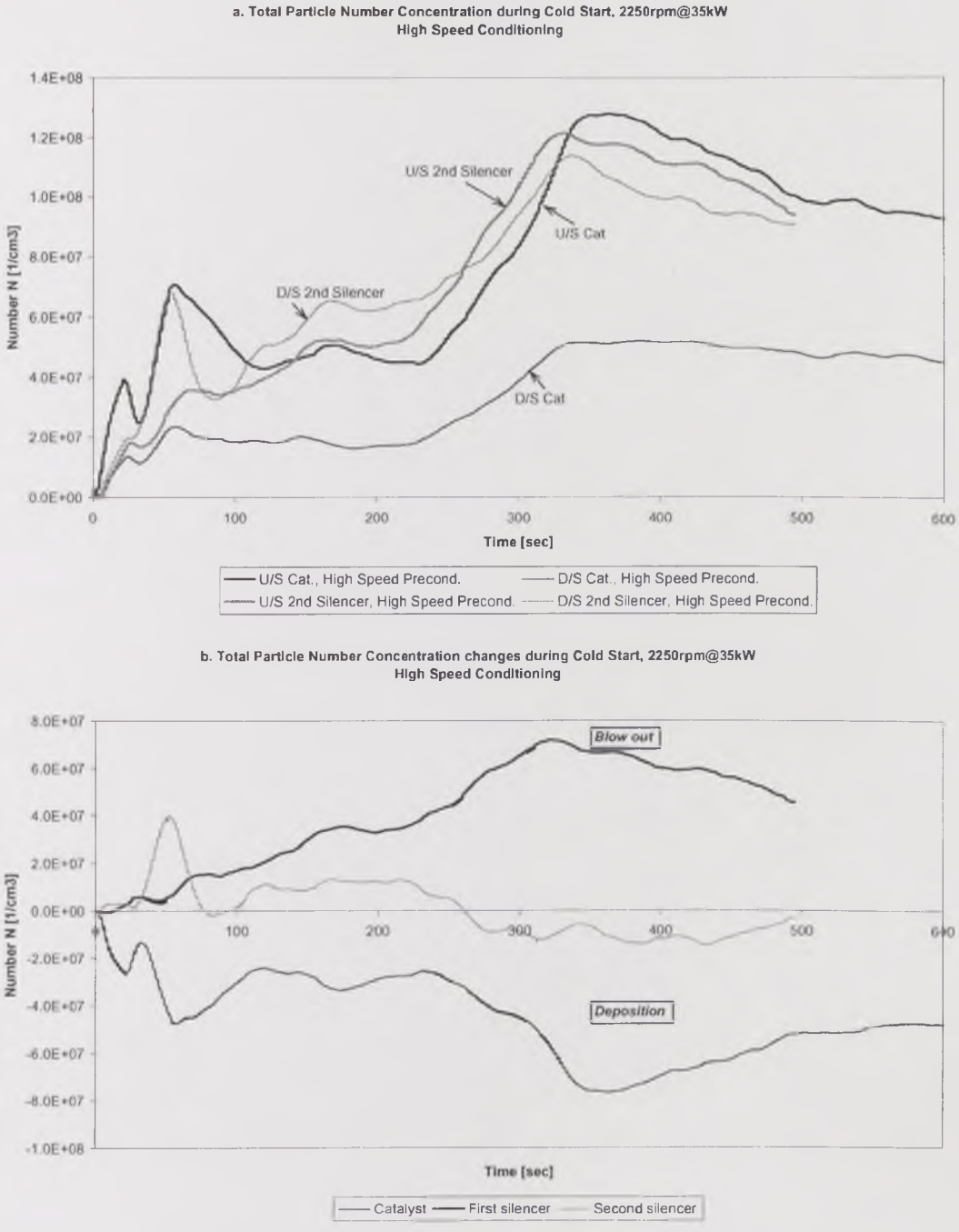

Figure 4.39. Total number and mass concentrations vs. time during cold start at high-load conditions after high-speed preconditioning at various points of the exhaust system. a) Particle number concentration.

The second silencer's effect on exhaust particulate was opposite to that of the first silencer. Through it, the total particle number concentration increased by 8% and the Emission Index decreased by 23%, corrected, or 4%, uncorrected. At the tailpipe, as a result, the total particle number concentration was 1.7×10^7 cm^{-3}, and the Emission Index, 13.27 g/kg fuel and 3.02 g/kg fuel, uncorrected and corrected, respectively.

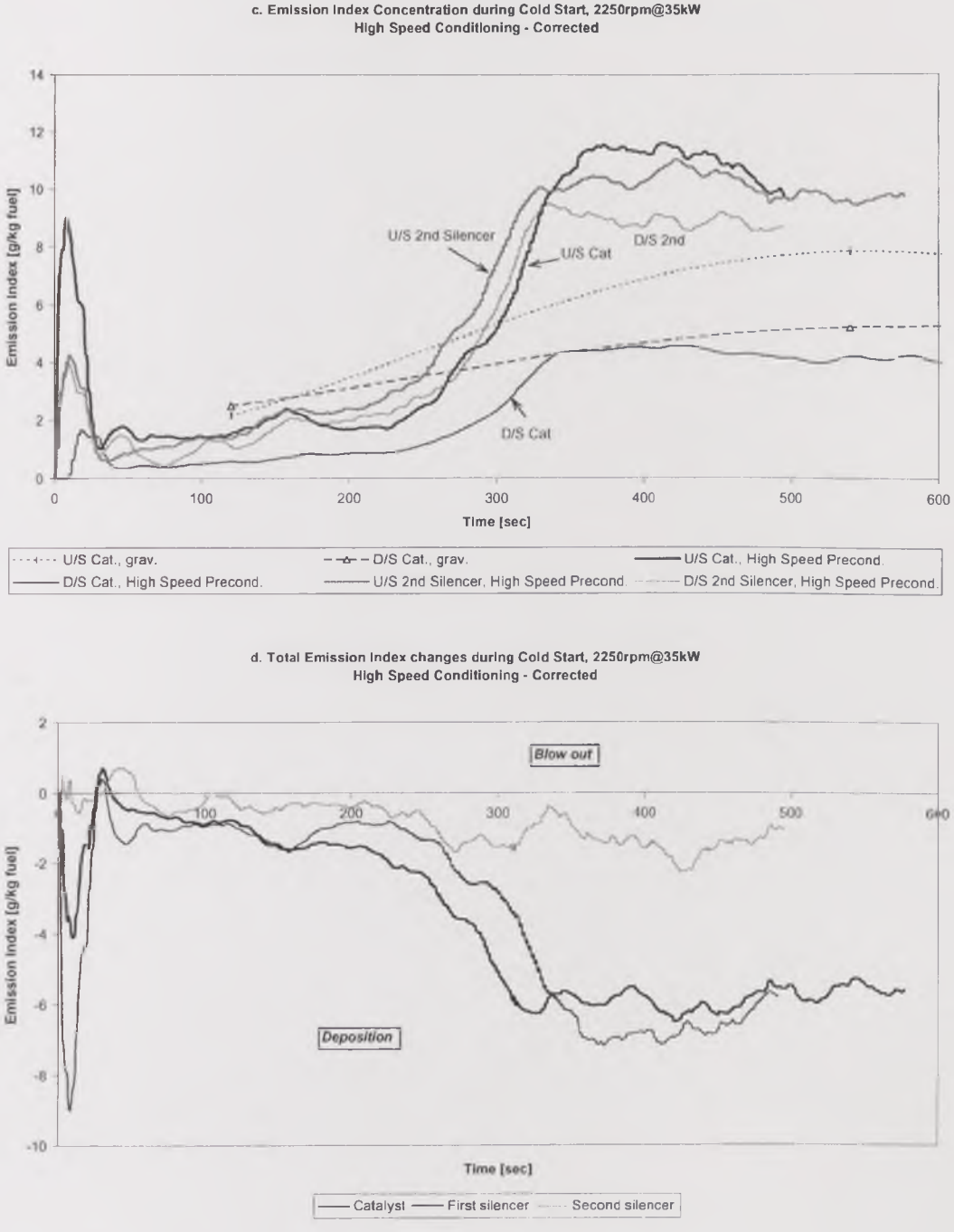

Figure 4.39. Total number and mass concentrations vs. time during cold start at high-load conditions after high-speed preconditioning at various points of the exhaust system. b) Corrected Emission Index.

The changes in different size ranges varied, and were very small. The number of particles below 0.2μm and a few between 0.5μm and 2μm increased through the silencer, the former accounting for the increase in number concentration. Particles between 0.2μm and 0.5μm, and those larger than 2μm deposited through it, the latter accounting for the main decrease in Emission Index.

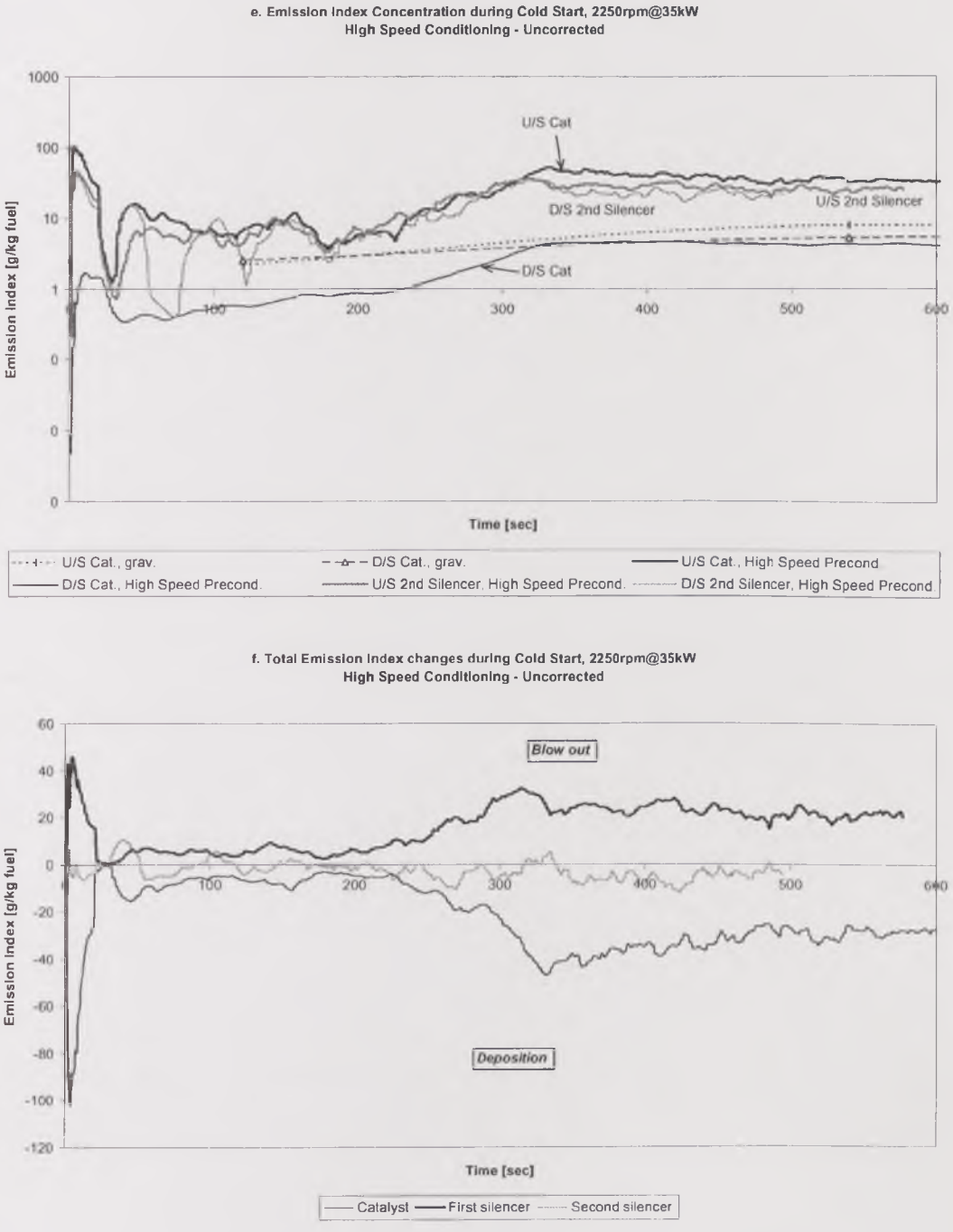

Figure 4.39. Total number and mass concentrations vs. time during cold start at high-load conditions after high-speed preconditioning at various points of the exhaust system. c) Uncorrected Emission Index.

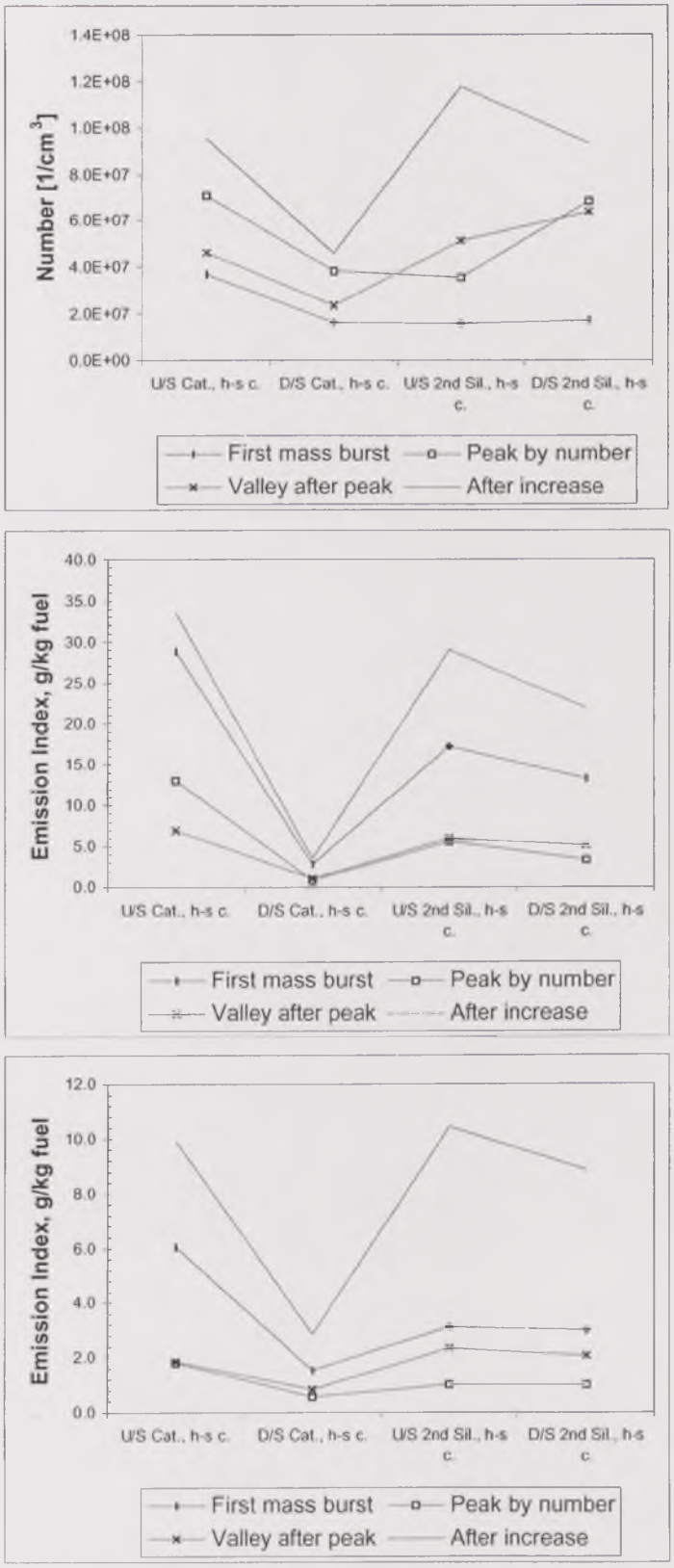

Figure 4.40. Total number and mass concentrations for the main events of the cold start at 2250rpm - 35kW after high-speed preconditioning vs. location in the exhaust.

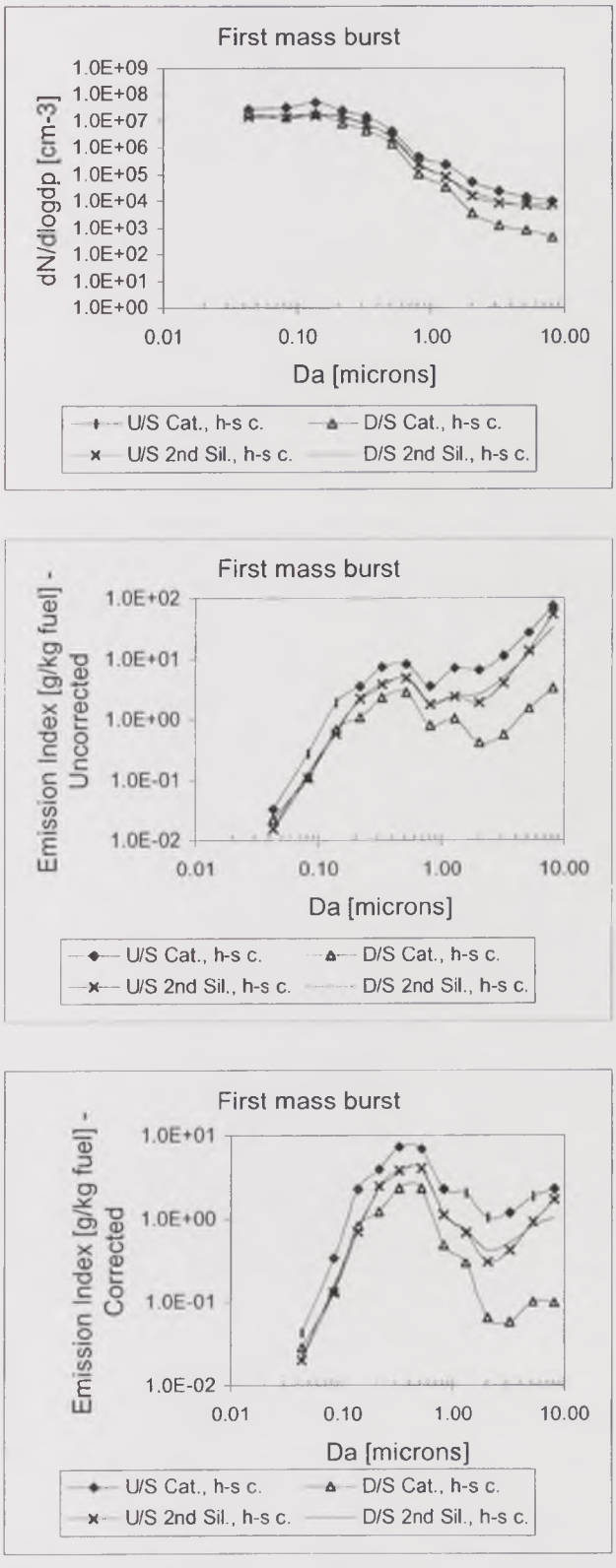

Figure 4.41. Particle size distribution during the first mass-burst event of the cold start at 2250rpm – 35kW after high-speed preconditioning

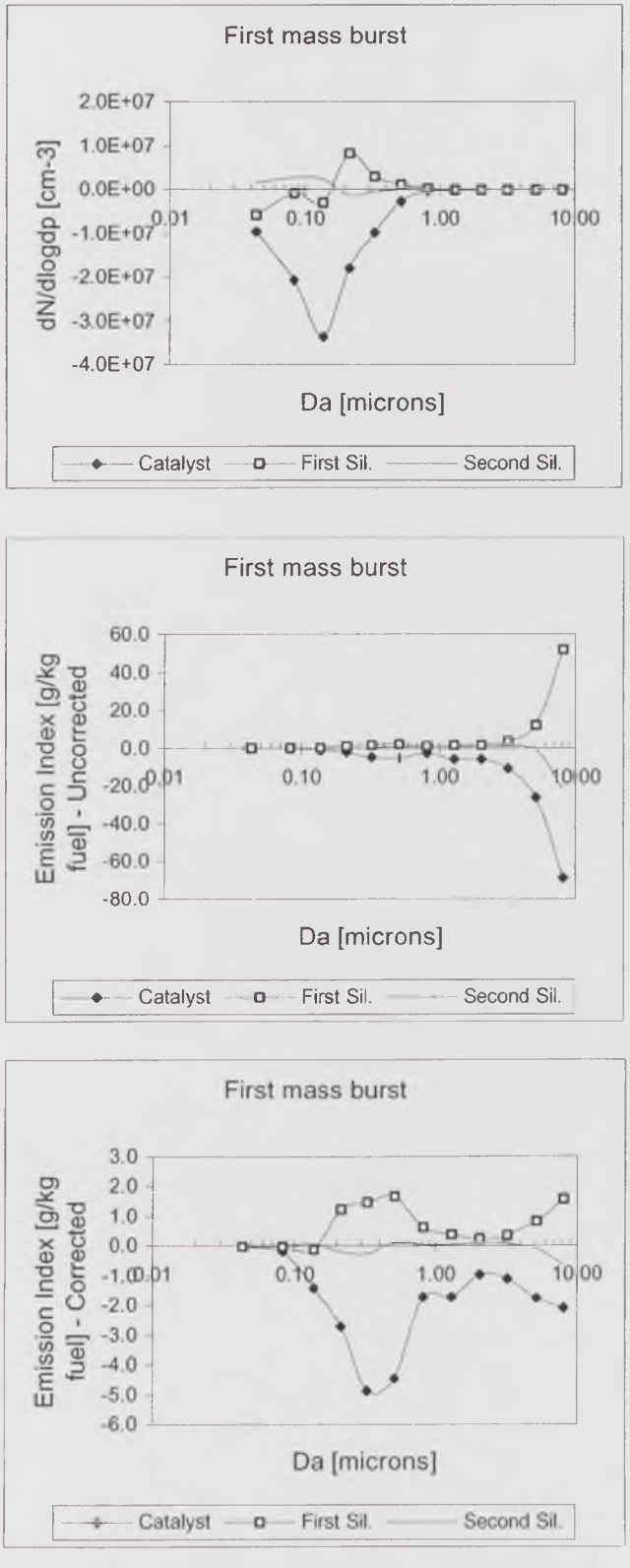

Figure 4.42. Particulate blow-out for various size ranges during the first-mass-burst event of the cold start at 2250rpm - 35kW after high-speed preconditioning.

In summary, the first mass-burst event of the step-change cold-start at 2250rpm - 35kW after high-speed preconditioning showed the effective deposition

at particles at all size ranges through the catalyst. This trend continued for middle-sized and large particles, but not for very fine particles, through the silencers. Many particles below 0.1μm were formed through the silencers mainly by coagulation.

4.6.4.2. Peak by number

The total particle number concentration increased after the first seconds of cold start, peaking by the end of the first minute at all sampling points. Upstream of the catalyst, the number peaked at $7.1x10^7$ cm^{-3}, converting to an Emission Index of 13.07 g/kg fuel, uncorrected, or 1.80 g/kg fuel, corrected. Through the catalyst, the particle number concentration decreased to $3.8x10^7$ cm^{-3}, and the Emission Index, to 0.88 g/kg fuel, uncorrected, or 0.56 g/kg fuel, corrected. This corresponded to a 46% decrease in particle number concentration, and 93% or 69% in uncorrected and corrected Emission Index, respectively. Particles at all size ranges contributed to these changes, no particulate formation or blow-out was recorded at any size.

The total particle number concentration decreased through the first silencer by 7%, to $3.6x10^7$ cm^{-3}. The Emission Index, in contrast, increased by as much as fivefold, uncorrected, or 81%, corrected, to 5.6 g/kg fuel or 1.02 g/kg fuel, respectively. The reduction in particle number concentration was due to the oxidation, coagulation or deposition of very fine particles, whereas the increase in Emission Index was caused by the blow-out of particles larger than 0.1μm.

Through the second silencer, as occurred during the first mass burst, the particle number concentration increased and the Emission Index decreased. The particle number concentration increase was as high as by 92%, reaching $6.8x10^7$ cm^{-3} at the tailpipe, and the Emission Index decreased by 40% or 2%, to 5.6 g/kg fuel or 1.00 g/kg fuel, uncorrected or corrected, respectively. Particles below 0.2μm were formed through the silencer, larger particles deposited through it, with the exception of very few particles around 0.5μm, whose number concentration increased by coagulation.

In summary, the peak-number event of the step-change cold-start at 2250rpm - 35kW after high-speed preconditioning, the catalyst retained and transformed particles at all size ranges, large particles were blown out from the first silencer and deposited through the second, and the number of ultrafine particles increased as a result of outgassing, nucleation, condensation and coagulation from the second silencer.

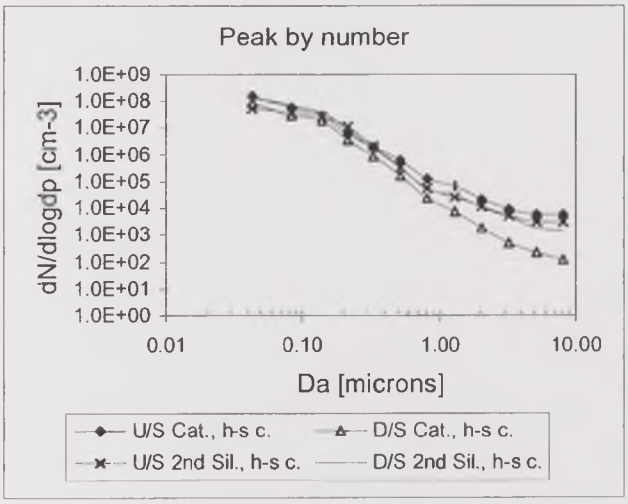

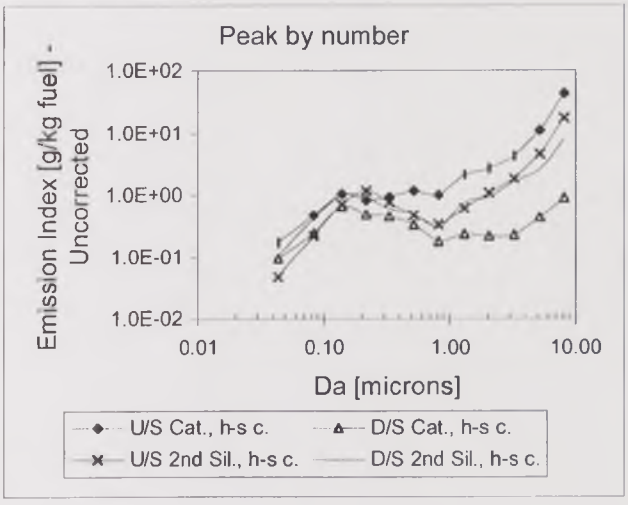

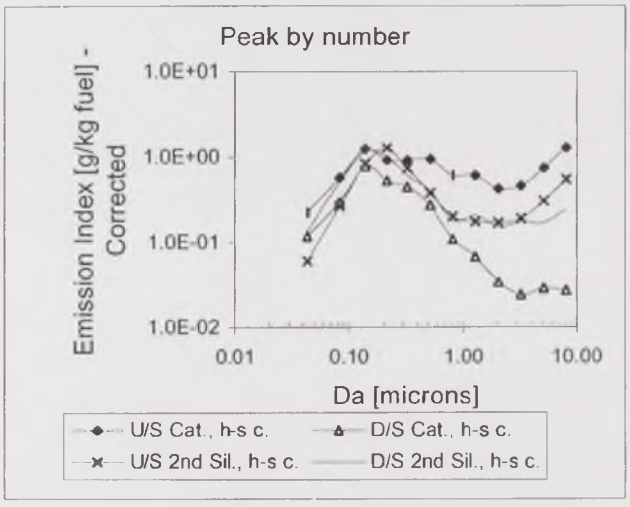

Figure 4.43. Particle size distribution during the peak-number event of the cold start at 2250rpm – 35kW after high-speed preconditioning.

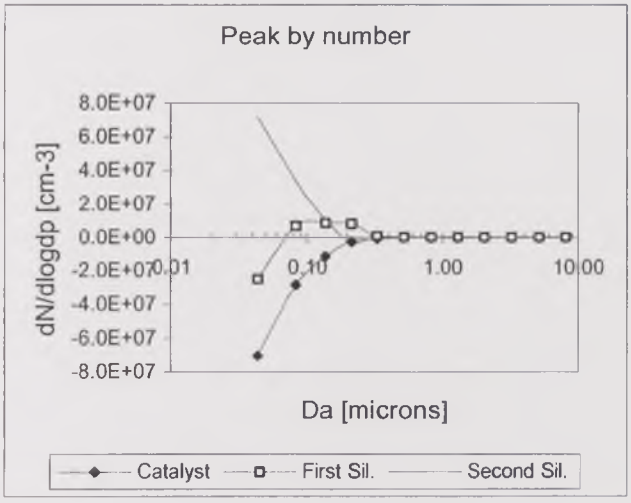

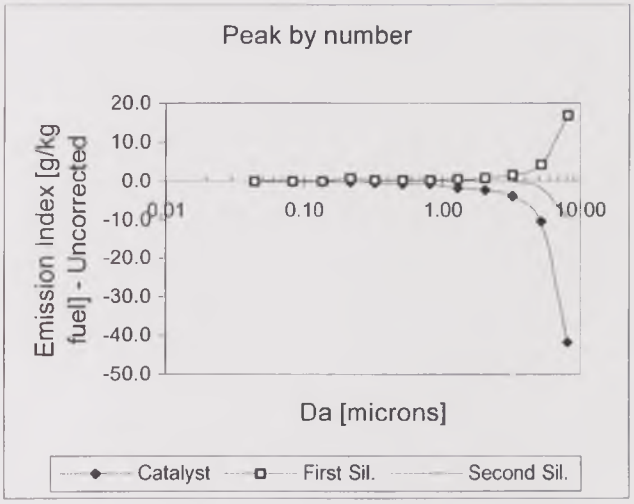

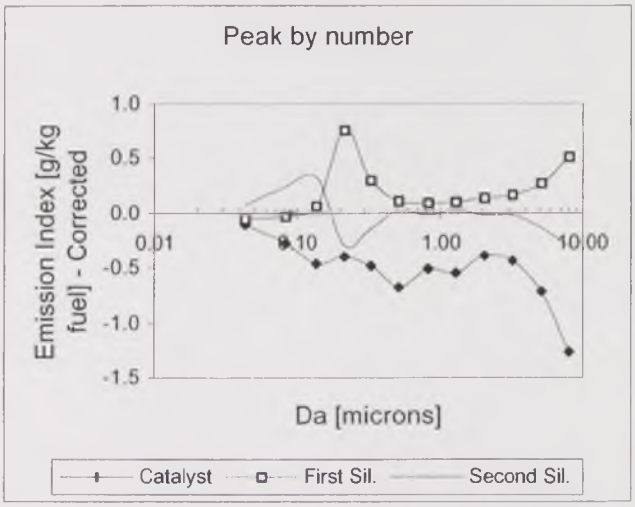

Figure 4.44. Particulate blow-out for various size ranges during the peak-number event of the cold start at 2250rpm - 35kW after high-speed preconditioning.

4.6.4.3. Valley after peak

During the valley-after-peak event, the total particle number concentration upstream of the catalyst decreased to $4.6x10^7$ cm^{-3}, 33% lower than the concentration at the same point during the number peak event. On the other hand, the Emission Index decreased to 6.8 g/kg fuel, uncorrected, and 1.85 g/kg fuel, corrected. The latter was practically equal to that during the peak-number event.

Through the catalyst, the number concentration decreased to $2.4x10^7$ cm^{-3}, and the Emission Index, to 1.07 g/kg fuel and 0.83 g/kg fuel, uncorrected and corrected, respectively. This corresponded to a 49% decrease in particle number and an 85% or 55% decrease in Emission Index, uncorrected or corrected, respectively. Particles were oxidised, deposited and coagulated so that their number and mass decreased for all size ranges.

Through the first silencer, the total particle number concentration and the Emission Index increased very significantly, to $5.1x10^7$ cm^{-3}, and 6.00 g/kg fuel, uncorrected or 2.34 g/kg fuel, corrected. This was 118%, and 461% or 181% higher than upstream of the silencer, respectively. The increase occurred for particles of all size ranges, by coagulation for ultrafine and mid-sized particles, and large particle resuspension from the silencer walls.

The second silencer produced a 24% increase in particle number concentration and a 14% or 12% decrease in Emission Index, uncorrected or corrected, respectively. The downstream aerosol, as a result, was $6.4x10^7$ cm^{-3}, and 5.15 g/kg fuel or 2.05 g/kg fuel. The increase in particle number concentration was due to the formation of particles below 0.2μm by nucleation, condensation and coagulation, and the decrease in Emission Index, to deposition of larger particles.

From these observations, the second silencer affected the fine particles in a similar way to the first silencer, and large particles in a similar way to the catalyst. Through the first silencer and the catalyst, the aerosol showed opposite changes. No significant change in the particle size distribution was observed.

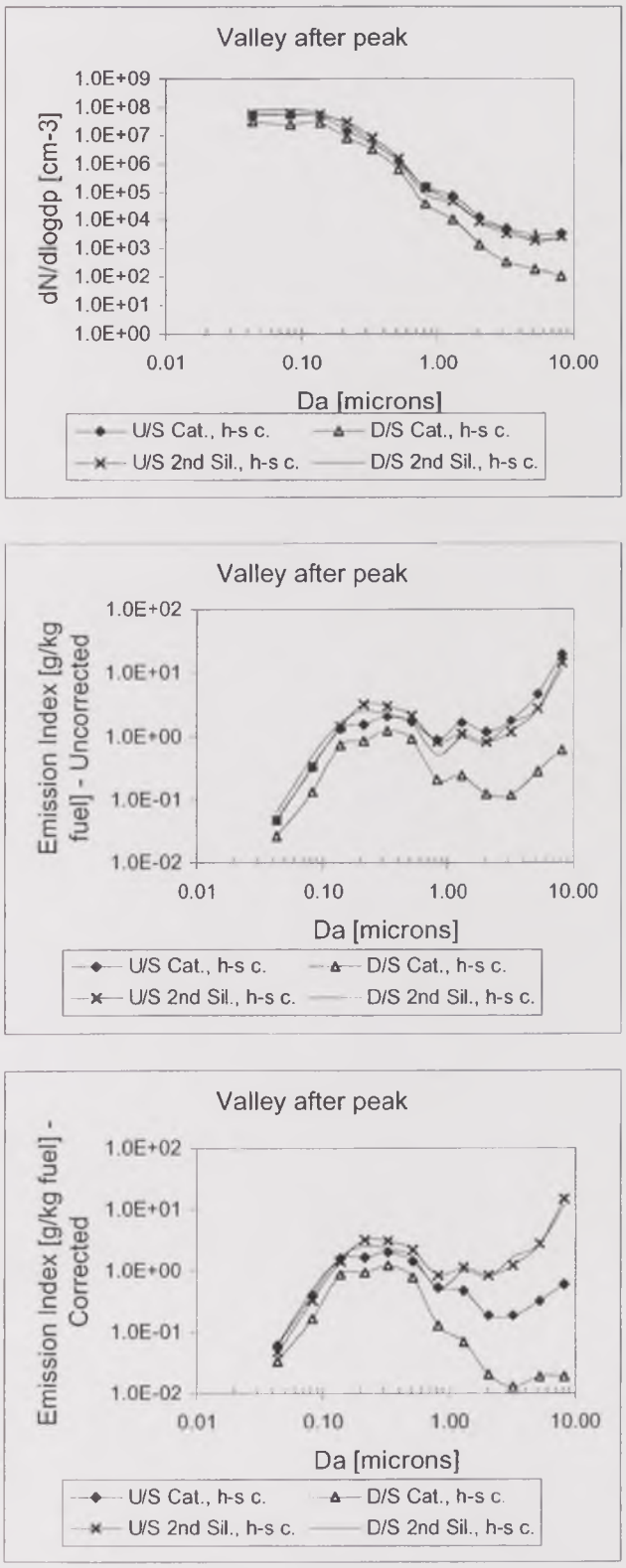

Figure 4.45. Particle size distribution during the valley-after-peak event of the cold start at 2250rpm – 35kW after high-speed preconditioning.

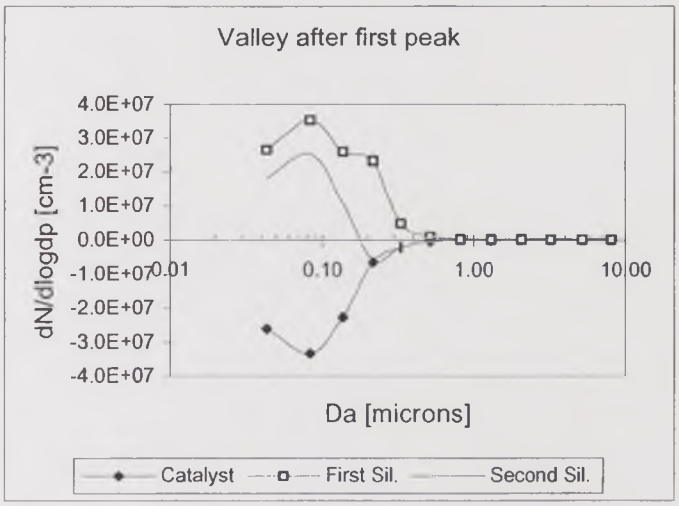

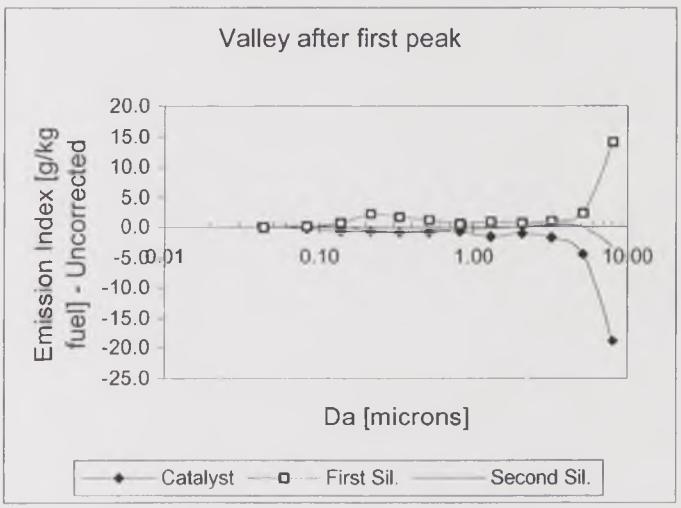

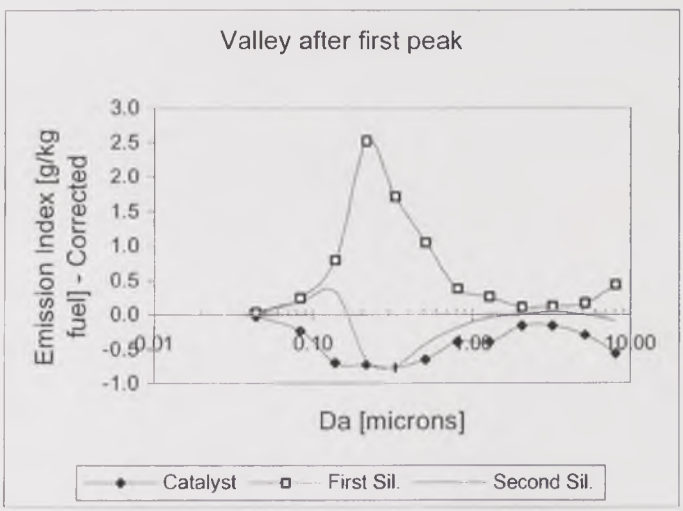

Figure 4.46. Particulate blow-out for various size ranges during the valley-after-peak event of the cold start at 2250rpm - 35kW after high-speed preconditioning.

4.6.4.4. Increase after EGR-valve opening

The total particle number concentration of the exhaust aerosol leaving the engine, after the EGR-valve opened, stabilised around $9.5x10^7$ cm^{-3}, nearly 34% higher than the peak number of the first minute from cold start. The corresponding Emission Index was 33.54 g/kg fuel, uncorrected, or 9.92 g/kg fuel, corrected, 17% or 64% higher than the Emission Index during the first mass burst at the same sampling point. Through the catalyst, the total particle number concentration decreased to $4.6x10^7$ cm^{-3}, for a 48% decrease. The Emission Index decreased to 3.56 g/kg fuel, uncorrected, or 2.86 g/kg fuel, corrected, for an 89% or 71% decrease, respectively. The decrease occurred for all particle size ranges, and the particle size distribution did not changed significantly.

The first silencer released particles after the EGR valve opened. Through it, the total particle number concentration increased by 155%, to $1.2x10^8$ cm^{-3}. The increase in Emission Index was even more significant, a sevenfold increase, uncorrected, or 265%, corrected, or to 28.99 g/kg fuel or 10.45 g/kg fuel, respectively. The increase in particle concentration occurred as a result of ultrafine particle formation and coagulation, as well as large particle resuspension.

Through the second silencer, the changes were opposite to those through the first silencer during the same period. The particle number concentration decreased to $9.3x10^7$ cm^{-3}, and the Emission Index, to 21.91 g/kg fuel, uncorrected, or 8.85 g/kg fuel, corrected. This represented a 21% decrease in particle number concentration and 24% or 15% decrease in uncorrected or corrected Emission Index, respectively. The decrease occurred for particles of all size ranges.

In summary, the stabilisation period after the increase in number concentration and Emission Index at 2250rpm - 35kW was characterised by a parallel behaviour of the exhaust aerosol through the catalyst and the second silencer, and an opposite behaviour in the first silencer. The particle size distribution underwent only a slight swift towards smaller sizes, owing to the formation of ultrafine particles by nucleation, condensation and coagulation.

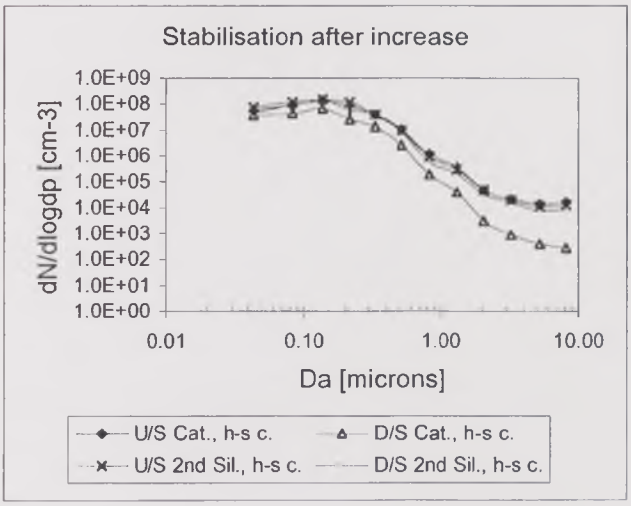

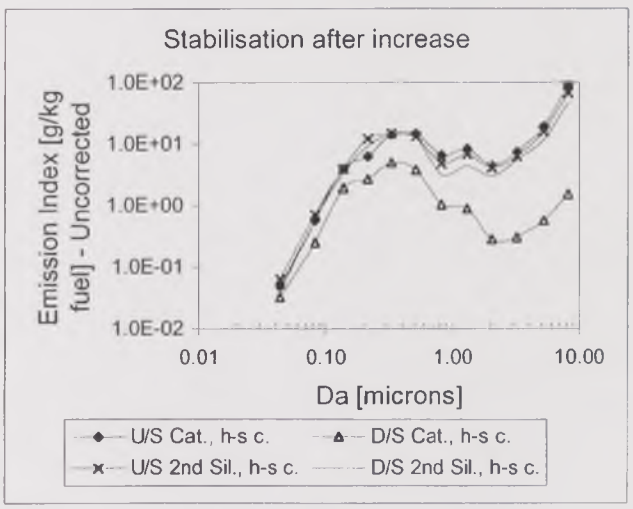

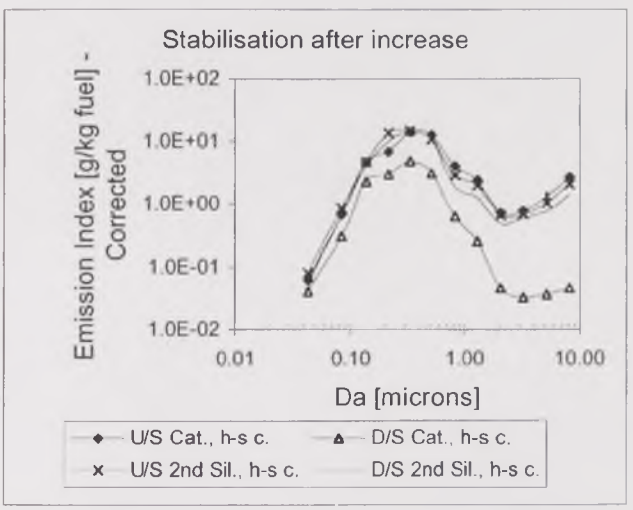

Figure 4.47. Particle size distribution during the increase-after-EGR event of the cold start at 2250rpm – 35kW after high-speed preconditioning.

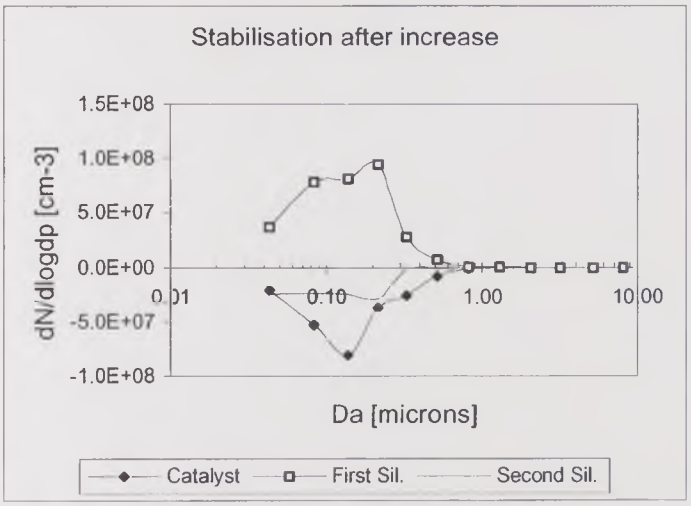

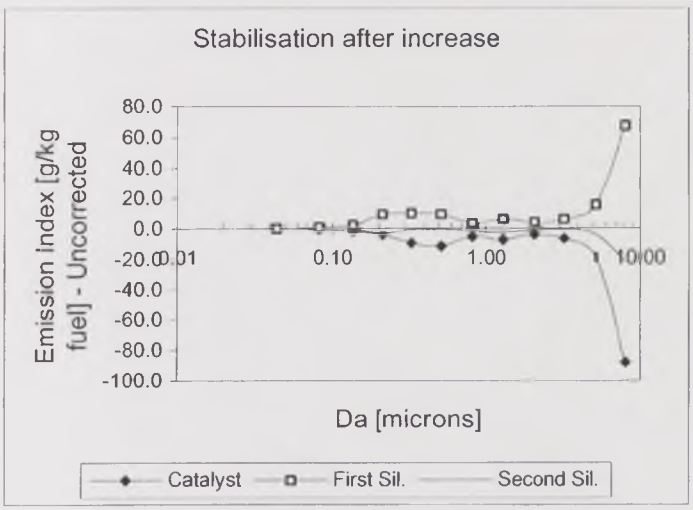

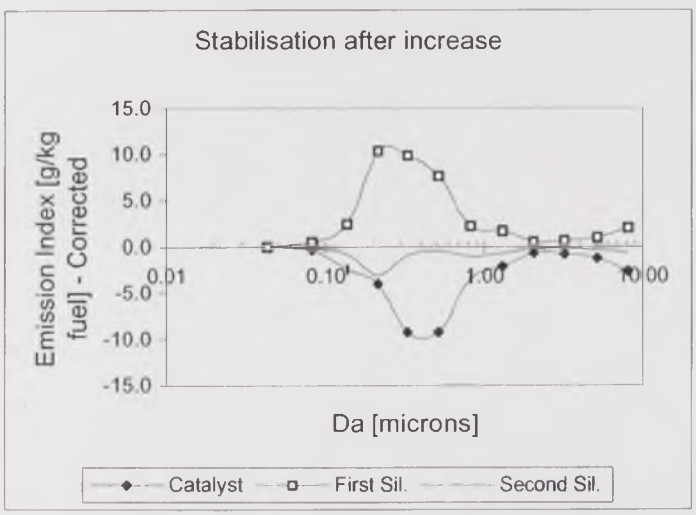

Figure 4.48. Particulate blow-out for various size ranges during the increase-after-EGR event of the cold start at 2250rpm - 35kW after high-speed preconditioning.

4.7. Comparative summary of the cold start results

4.7.1. Direct deposition/blow out comparison

The results from the cold-start tests were shown in detail and the complexity of the particulate deposition/resuspension issue, combined with particle formation and growth by condensation and coagulation, became evident. Direct conclusions were very difficult to draw from the results, since no simple trends were observed and there were many factors involved. In this section, an attempt to find more common aspects between some of such factors is made.

Figure 4.49 shows a summary of the blow out and deposition through each one of the exhaust system devices, expressed as the changes in number concentration and Emission Index vs. time during cold start.

For the catalyst, Figure 4.49. a) shows that in both number concentration and Emission Index, particle deposition and conversion was greatly predominant over particle blow out, and it occurred at significantly higher levels than blow out at 3500rpm - 15kW after both idle and high-speed conditioning. This was presumably due to higher temperatures, reached in shorter times at high-power and high-speed conditions than at other conditions, enhancing the catalyst performance to retain and oxidise particles. Particle number blow-out occurred only during the first 30 seconds of cold start at 3500rpm - 15kW after Idle preconditioning and during the first 50 seconds of the cold start tests at 2250rpm - 15kW. Particle mass blow out (expressed as Emission Index –corrected-) occurred only during the first 30 seconds of the cold start tests at 2250rpm - 15kW, 3500rpm - 15kW after Idle preconditioning, 1500rpm - 10kW and 2250rpm - 35kW after Idle preconditioning. Mass blow out was very significant at 2250rpm - 15kW. On the other hand, deposition was more significant at 3500rpm - 15kW than at any other engine operation condition.

For the first silencer, Figure 4.49. b) shows a very similar situation to that observed for the catalyst. Particle deposition (in number) predominated over particle blow-out for most conditions during the first 150 seconds of the cold start tests, and was particularly significant in the tests at 3500rpm - 15kW (after both idle and high-speed preconditioning) and 2250rpm - 35kW after Idle preconditioning. However, particle number blow-out was observed after 150 seconds from cold start for most conditions, more significantly at 2250rpm - 35kW, 2250rpm - 15kW, 1500rpm - 10kW. Particle deposition after 150 seconds from cold start occurred only in the tests at 3500rpm - 15kW. Regarding particle mass, as Emission Index –corrected-, the situation was very similar to that observed in particle number concentration. The only major difference was that the most significant particle mass deposition during

the first 150 seconds occurred at 2250rpm - 15kW, for which the deposition in number was not important.

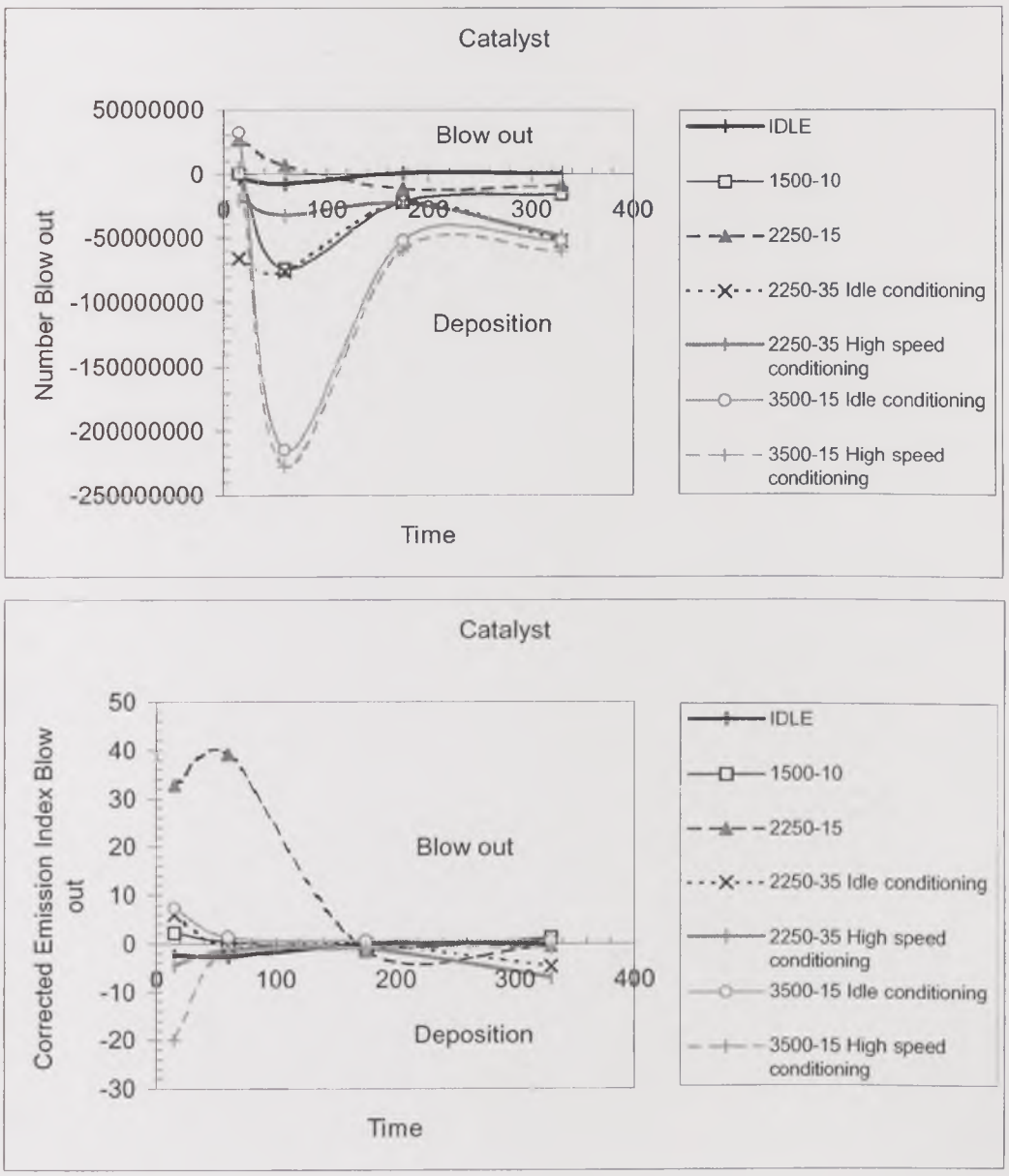

Figure 4.49. Summary of the particulate blow-out during cold start for all the engine operation conditions studied, expressed as number concentration and Emission Index blow out vs. time. a) Catalyst.

For the second silencer, Figure 4.49. c) shows that particle blow out, expressed as number concentration, occurred in important levels for the tests at 2250rpm - 35kW after both idle and high-speed preconditioning. It was also important in the test at 2250rpm - 15kW for the first 150 seconds. Deposition was significant during the first 150 seconds of the test at idle during the whole test at 1500rpm - 10kW. In particle mass, expressed as Emission Index, blow out occurred significantly during

the first 150 seconds of the test at 2250rpm - 15kW. Deposition was predominant for all other conditions, and was significant at Idle and 1500rpm - 10kW during the first 150 seconds, and also at 2250rpm - 35kW afterwards.

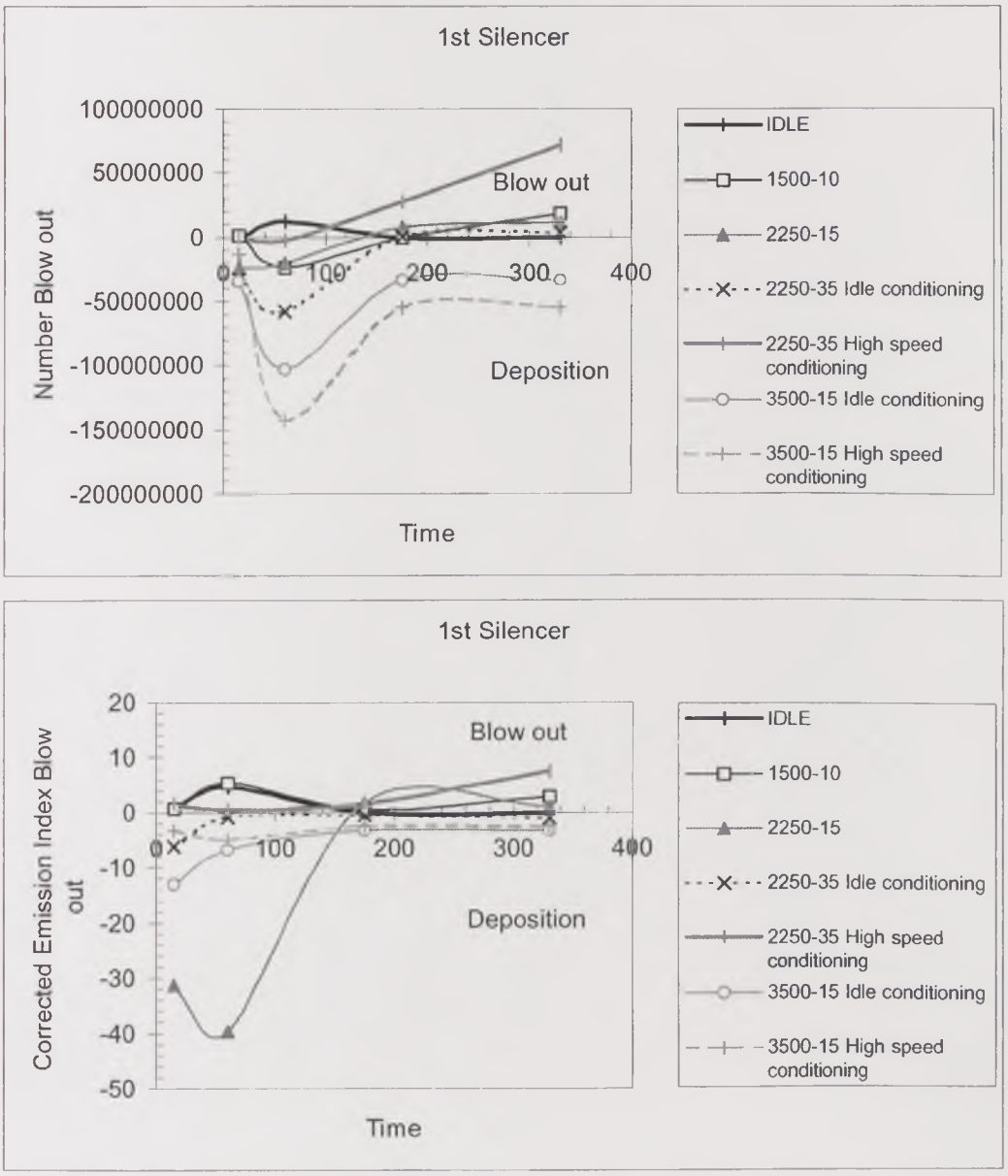

Figure 4.49. Summary of the particulate blow-out during cold start for all the engine operation conditions studied, expressed as number concentration and Emission Index blow out vs. time. b) First silencer.

From this general picture, there is clear evidence that the catalyst reduced the particle number concentration and Emission Index for most conditions during cold start. However, this trend does not discard the possibility of particles occasionally being blown out of the catalyst at important concentrations, as in the case of the 2250rpm - 15kW test. There is also evidence that the changes in particle

concentration through the first silencer are opposite to those occurring through the second silencer in most cases. This indicates that deposition and reentrainment mechanisms, as well as other parallel processes such as condensation and coagulation are affected in an opposite manner through each silencer.

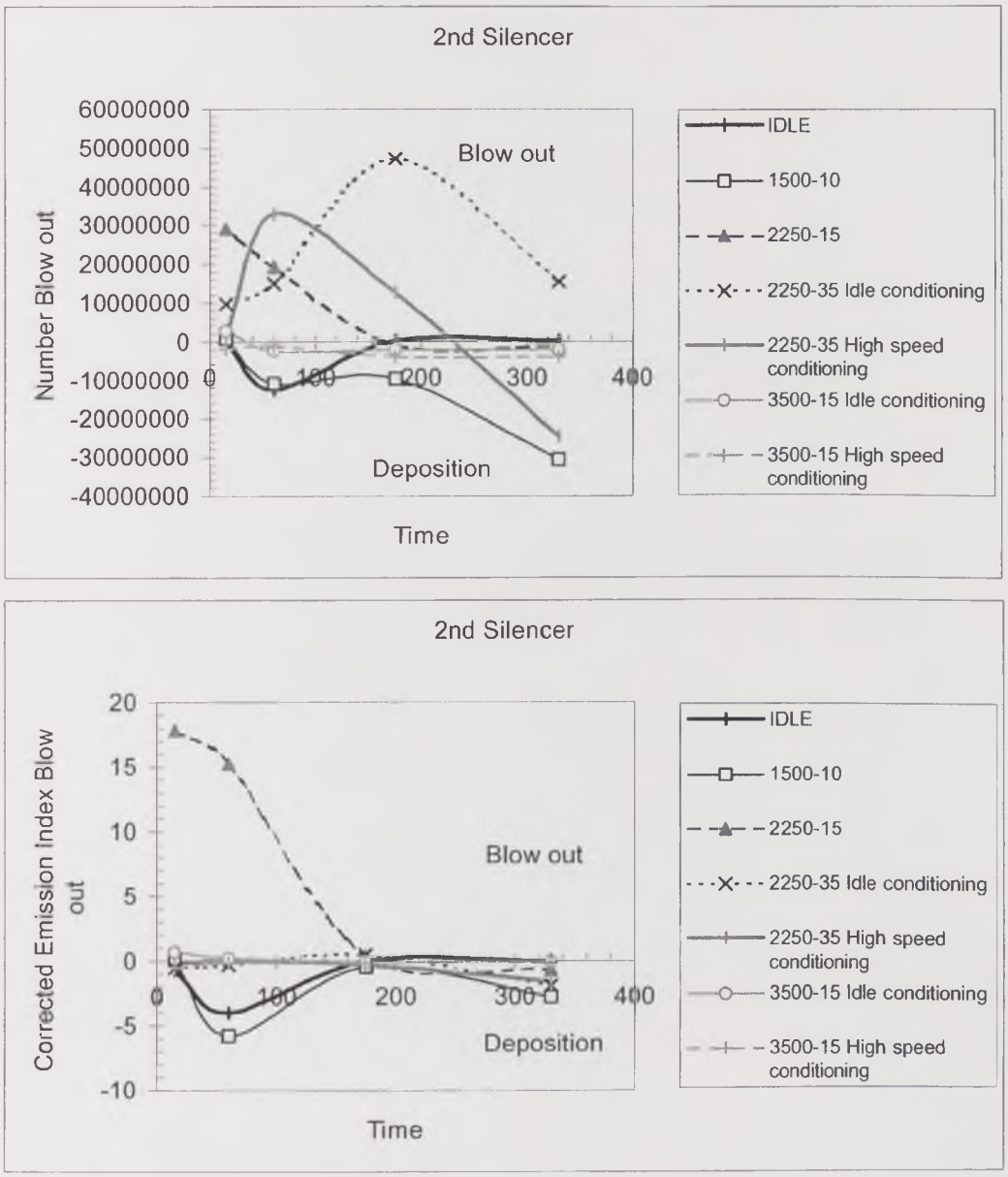

Figure 4.49. Summary of the particulate blow-out during cold start for all the engine operation conditions studied, expressed as number concentration and Emission Index blow out vs. time. c) Second silencer.

4.7.2. Analysis based on the number of deposition/blow out cases

Table 4.1. shows a summary of the most likely processes observed during the cold-start tests, based on the particulate number and mass differences between consecutive sampling points along the exhaust system. Each cell of the table was

considered as a 'case' for the analysis, and corresponded to one of the particle size ranges that showed common behaviour in the vast majority of the tests, namely, particles smaller than 0.1μm, particles between 0.1μm and 1.0μm, and particles larger than 1.0μm. Processes that contributed to reduce the particle number cases appear in *italic* characters, and those that increased the particle number cases, in underlined characters. For the cases in which particles within these ranges showed both increase and decrease, the cells are shown in dotted-underlined characters. In some cases, the change was not measured by the ELPI, as a result of correction warnings that are explained elsewhere in this work. The cases were counted for each process related to the effect of the various devices in the exhaust, transient events and engine conditions. The counts were compared in Figures 4.49. to 4.51., which illustrate the differences in the contribution of each factor. Each figure has two components, the first for the ultrafine particles (<0.1μm) and the other for medium (0.1μm to 1.0μm) and large (1.0μm to 10μm) particles.

The analysis of these cases will be made with the aim of identifying those conditions that showed evidence of promoting the increase in particulate concentration through the exhaust system. For the ultrafine particles, this implies the formation of finer particles by nucleation and their growth by condensation or coagulation. However, the coagulation can imply also the reduction in their number concentration, if they form medium size particles. On the other hand, in the large size range, the increase in particle number concentration is directly related to resuspension processes.

From the cold-start tests, Figure 4.50. shows that ultrafine particle deposition and coagulation to form larger particles overwhelmed the formation processes in virtually all conditions, except 1500rpm - 10kW and 2250rpm - 15kW. No direct relationship was found to explain this, but a high saturation ratio of condensable species when running the tests at these conditions, which was unfortunately not measured, might have been the determining factor. For medium and large particles, the number of deposition cases overwhelmed the number of cases for which processes increased the number of particles, such as coagulation of finer particles to form mid-sized particles, and reentrainment of large particles, in most cases, for all test conditions. This would indicate that significant levels of particle resuspension are rather unusual, but may be critical when they occur.

The formation of ultrafine particles occurred mainly at 1500rpm - 10kW, 2250rpm - 15kW and Idle, when low temperatures favoured the condensation processes. Also the 2250rpm - 35kW test after high-speed preconditioning

contributed with a number of cases of ultrafine particle formation, but in this case this was more likely due to enhanced coagulation than condensation.

The conditions under which the number of both mid-sized and large particles increased most significantly, which would indicate a clear trend towards particulate blow-out from the exhaust system, were, unexpectedly, 1500rpm - 10kW and 2250rpm - 15kW. The high-speed test after Idle preconditioning contributed to a number of cases increasing the concentration of mid-sized particles, but not very significantly to the number of resuspension cases, in opposition to what was expected. This was presumably due to enhanced coagulation of fine particles owing to the increased turbulence, and the lack of significance of resuspension forces even at high engine speeds. High power conditions showed a small contribution to both particle concentration-increasing processes through the exhaust system.

		Size range			Size range		
		Small	Middle	Large	Small	Middle	Large
Event	Device	0.01-0.1μm	0.1-1.0μm	1.0-10.0μm	0.01-0.1μm	0.1-1.0μm	1.0-10.0μm
		Idle			1500rpm - 10kW		
First mass burst	Catalyst	*Coagulation & Deposition*	*Deposition*	*Deposition*	Formation	Coagulation	Blow-out
	First Silencer	*Coagulation & Deposition*	Coagulation	Blow-out	Formation	Coagulation	*Deposition*
	Second Silencer	Formation	*Deposition*/Coagulation	*Deposition*	Formation	Coagulation	Blow-out & *Deposition*
Number peak	Catalyst	*Coagulation & Deposition*	*Deposition*	Not measured	*Coagulation & Deposition*	Coagulation	Blow-out
	First Silencer	Formation	Coagulation	Not measured	*Coagulation & Deposition*	Coagulation	*Deposition*
	Second Silencer	*Coagulation & Deposition*	*Deposition*	Not measured	Formation	*Deposition*	Blow-out
Valley after peak	Catalyst				*Coagulation & Deposition*	*Deposition*	*Deposition*
	First Silencer				*Coagulation & Deposition*	Coagulation	Blow-out
	Second Silencer				*Coagulation & Deposition*	*Deposition*	*Deposition*
Stabilisation	Catalyst	Formation	Coagulation	Blow-out	*Coagulation & Deposition*	Coagulation	Blow-out
	First Silencer	*Coagulation & Deposition*	*Deposition*	*Deposition*	Formation	Coagulation	Blow-out
	Second Silencer	Formation	Coagulation	Blow-out	*Coagulation & Deposition*	*Deposition*	*Deposition*

Table 4.1. a) Summary of deposition and blow-out cases for the cold-start tests, including the exhaust devices, three size ranges - idle and low speed conditions.

Event	Device	Size range Small 0.01-0.1μm	Middle 0.1-1.0μm	Large 1.0-10.0μm
		2250rpm - 15kW		
First mass burst	Catalyst	Formation	Coagulation	Blow-out
	First Silencer	*Coagulation & Deposition*	*Deposition*	*Deposition*
	Second Silencer	Formation	Coagulation	Blow-out
Number peak	Catalyst	*Coagulation & Deposition*	Coagulation	*Deposition*
	First Silencer	Formation	*Deposition*	Blow-out
	Second Silencer	*Coagulation & Deposition*	Coagulation	*Deposition*
Valley after peak	Catalyst	*Coagulation & Deposition*	*Deposition*	*Deposition*
	First Silencer	Formation	*Deposition*	Blow-out
	Second Silencer	*Coagulation & Deposition*	Coagulation	*Deposition*
Stabilisation	Catalyst	*Coagulation & Deposition*	*Deposition*	*Deposition*
	First Silencer	Formation	Coagulation	Blow-out
	Second Silencer	Formation	*Deposition*	*Deposition*

Table 4.1. b) Summary of deposition and blow-out cases for the cold-start tests, including the exhaust devices, three size ranges - medium speed, low-power conditions.

Event	Device	Size range Small 0.01-0.1μm	Middle 0.1-1.0μm	Large 1.0-10.0μm	Size range Small 0.01-0.1μm	Middle 0.1-1.0μm	Large 1.0-10.0μm
		3500rpm@15kW, Idle preconditioning			3500rpm@15kW, High-speed preconditioning		
First mass burst	Catalyst	Formation	Coagulation	*Deposition*	Formation	*Deposition*	*Deposition*
	First Silencer	*Coagulation & Deposition*	*Deposition*	*Deposition*	*Coagulation & Deposition*	*Deposition*	*Deposition*
	Second Silencer	Formation	Coagulation	Blow-out	*Coagulation & Deposition*	*Deposition*	*Deposition*
Number peak	Catalyst	*Coagulation & Deposition*	Coagulation	*Deposition*	*Coagulation & Deposition*	Coagulation	*Deposition*
	First Silencer	*Coagulation & Deposition*	*Deposition*	*Deposition*	*Coagulation & Deposition*	*Deposition*	*Deposition*
	Second Silencer	*Coagulation & Deposition*	Coagulation	*Deposition*	*Coagulation & Deposition*	Coagulation	*Deposition*
Valley after peak	Catalyst						
	First Silencer						
	Second Silencer						
Stabilisation	Catalyst	*Coagulation & Deposition*	Coagulation	Blow-out	*Coagulation & Deposition*	Coagulation	*Deposition*
	First Silencer	*Coagulation & Deposition*	*Deposition*	*Deposition*	*Coagulation & Deposition*	*Deposition*	*Deposition*
	Second Silencer	*Coagulation & Deposition*	*Deposition*	*Deposition*	*Coagulation & Deposition*	*Deposition*	*Deposition*

Table 4.1. c) Summary of deposition and blow-out cases for the cold-start tests, including the exhaust devices, three size ranges - high-speed conditions.

		Size range			Size range		
		Small	Middle	Large	Small	Middle	Large
Event	Device	0.01-0.1μm	0.1-1.0μm	1.0-10.0μm	0.01-0.1μm	0.1-1.0μm	1.0-10.0μm
		2250rpm@35kW, Idle preconditioning			2250rpm@35kW, High-speed preconditioning		
First mass burst	Catalyst	*Coagulation & Deposition*	Coagulation	Blow-out	*Coagulation & Deposition*	*Deposition*	*Deposition*
	First Silencer	*Coagulation & Deposition*	*Deposition*	*Deposition*	Formation	*Deposition*	*Deposition*
	Second Silencer	Formation	*Deposition*	*Deposition*	Formation	*Deposition & Coagulation*	*Deposition*
Number peak	Catalyst	*Coagulation & Deposition*	Coagulation	*Deposition*	*Coagulation & Deposition*	*Deposition*	*Deposition*
	First Silencer	*Coagulation & Deposition*	*Deposition*	*Deposition*	*Coagulation & Deposition*	Coagulation	Blow-out
	Second Silencer	Formation	*Deposition*	*Deposition*	Formation	*Deposition*	*Deposition*
Valley after peak	Catalyst	*Coagulation & Deposition*	*Deposition & Coagulation*	Blow-out	*Coagulation & Deposition*	*Deposition*	*Deposition*
	First Silencer	*Coagulation & Deposition*	*Deposition*	*Deposition*	Formation	Coagulation	Blow-out
	Second Silencer	Formation	*Deposition*	*Deposition*	Formation	*Deposition & Coagulation*	*Deposition*
Stabilisation	Catalyst	*Coagulation & Deposition*	*Deposition*	*Deposition*	*Coagulation & Deposition*	*Deposition*	*Deposition*
	First Silencer	*Coagulation & Deposition*	*Deposition*	*Deposition*	Formation	Coagulation	Blow-out
	Second Silencer	Formation	*Deposition & Coagulation*	*Deposition*	*Coagulation & Deposition*	*Deposition*	*Deposition*

Table 4.1. d) Summary of deposition and blow-out cases for the cold-start tests, including the exhaust devices, three size ranges - high-power conditions.

Although the analysis above appears to contradict the expected results, this does not mean that the deposition was absolutely more significant during high-speed conditions or that blow-out was absolutely more significant during low-speed conditions, since the number concentration and Emission Index levels were significantly higher at high-speed and high-power conditions. What this means is that the natural trend of the particles at high-speed and high-power conditions was to deposit through the system, but when blow-out occurred, it did at high levels. At low-speed conditions, in contrast, there were more particulate blow-out cases, but in low concentrations compared to those observed at higher speeds.

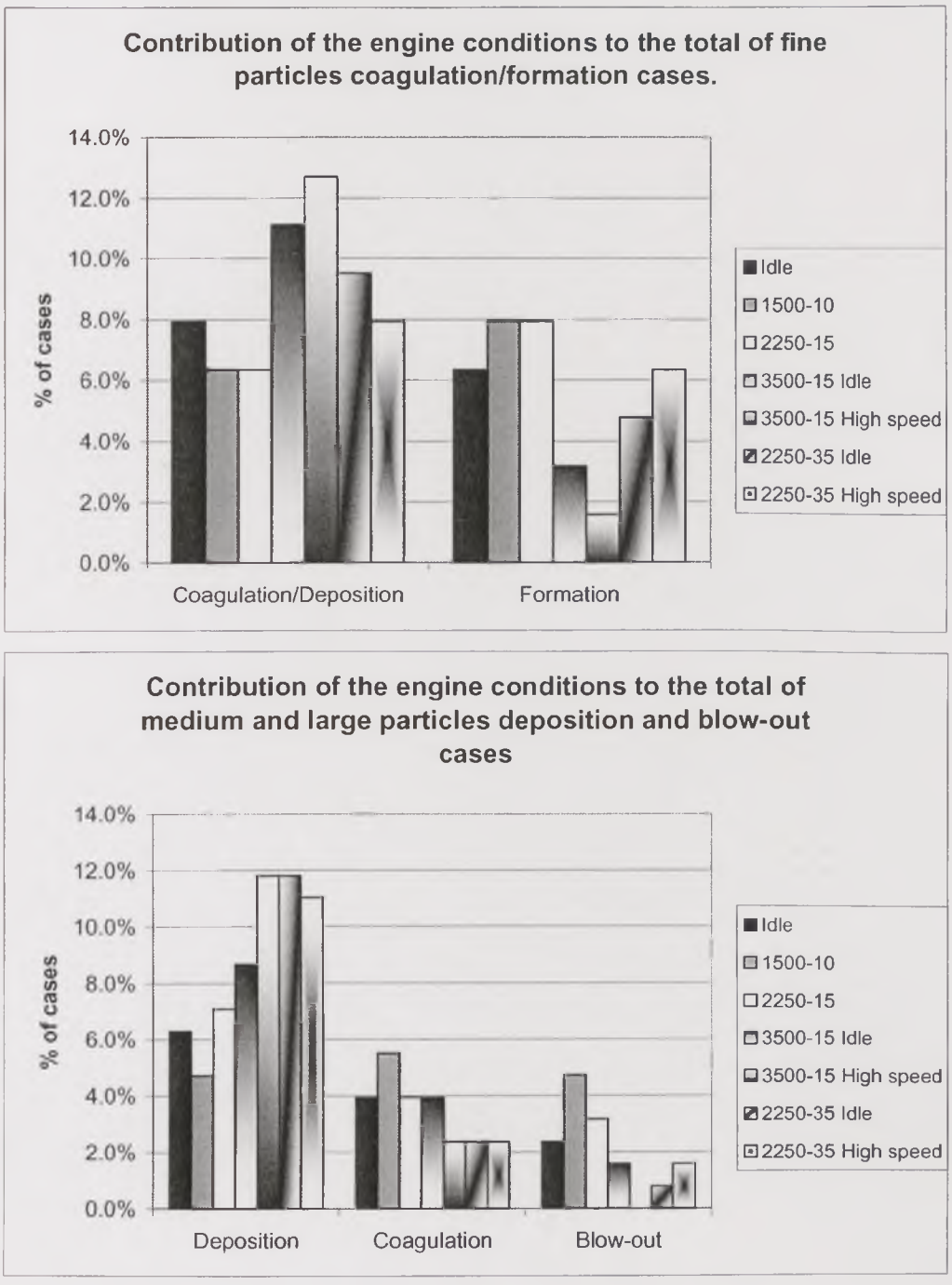

Figure 4.50. Contribution of the engine conditions to the total of increase and decrease in particle number during cold-start tests.

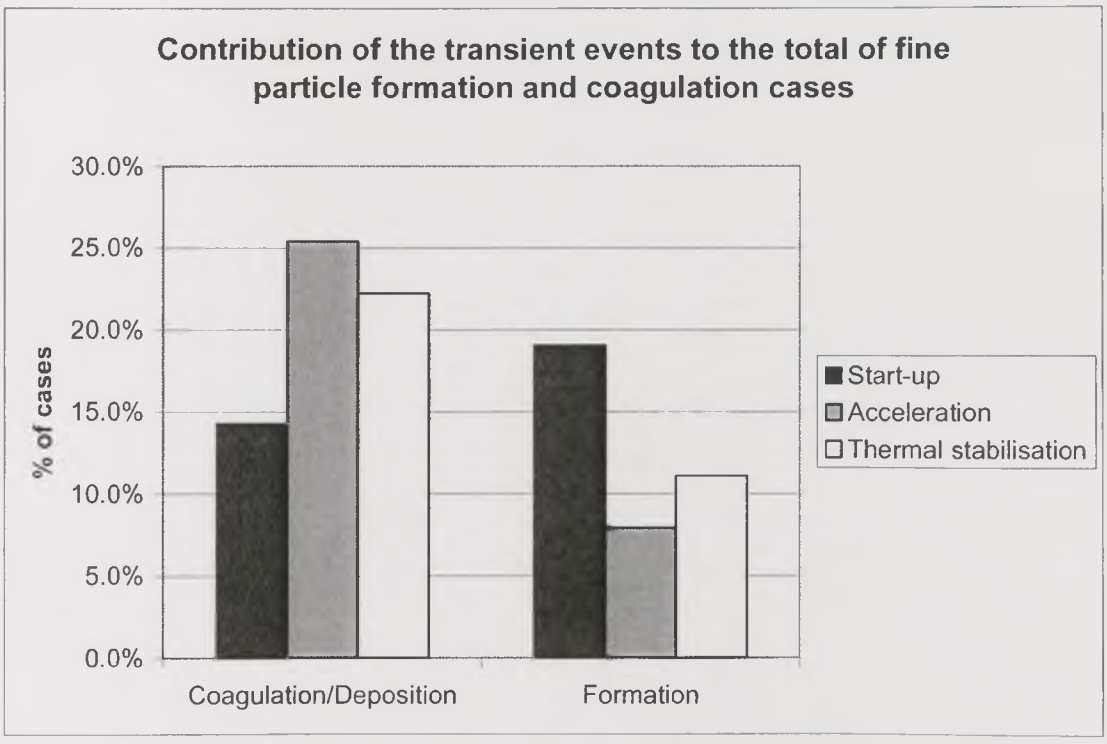

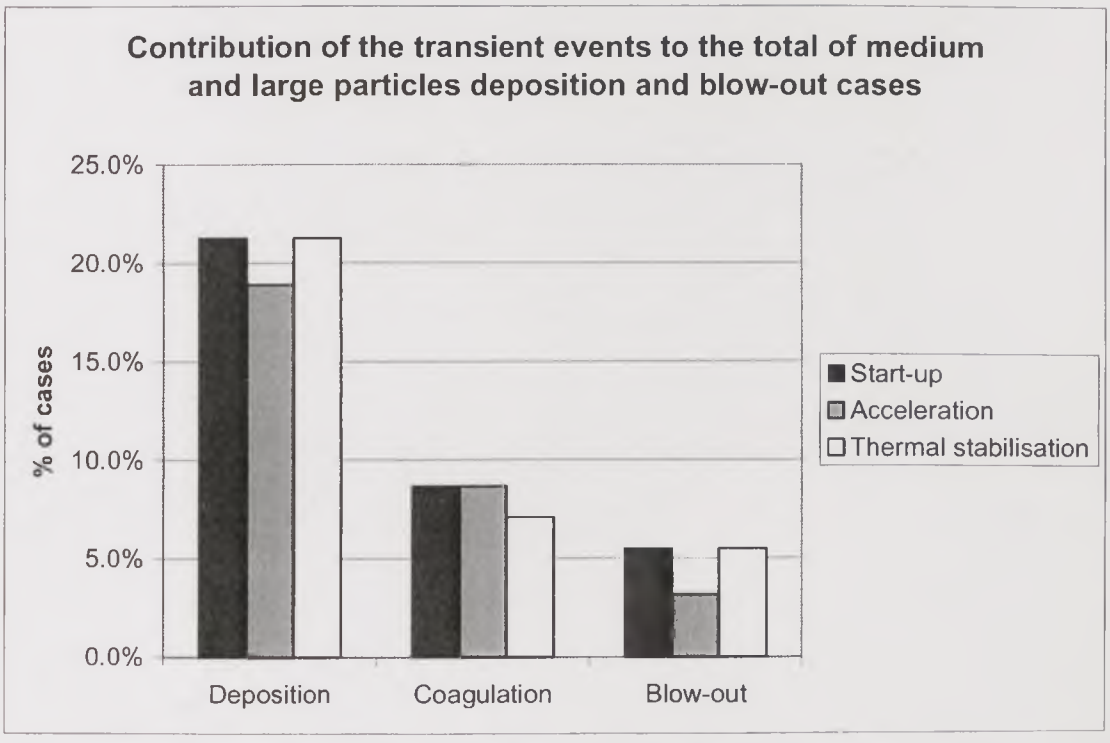

Figure 4.51. Contribution of transient events to the total of blow-out and deposition cases during cold-start tests.

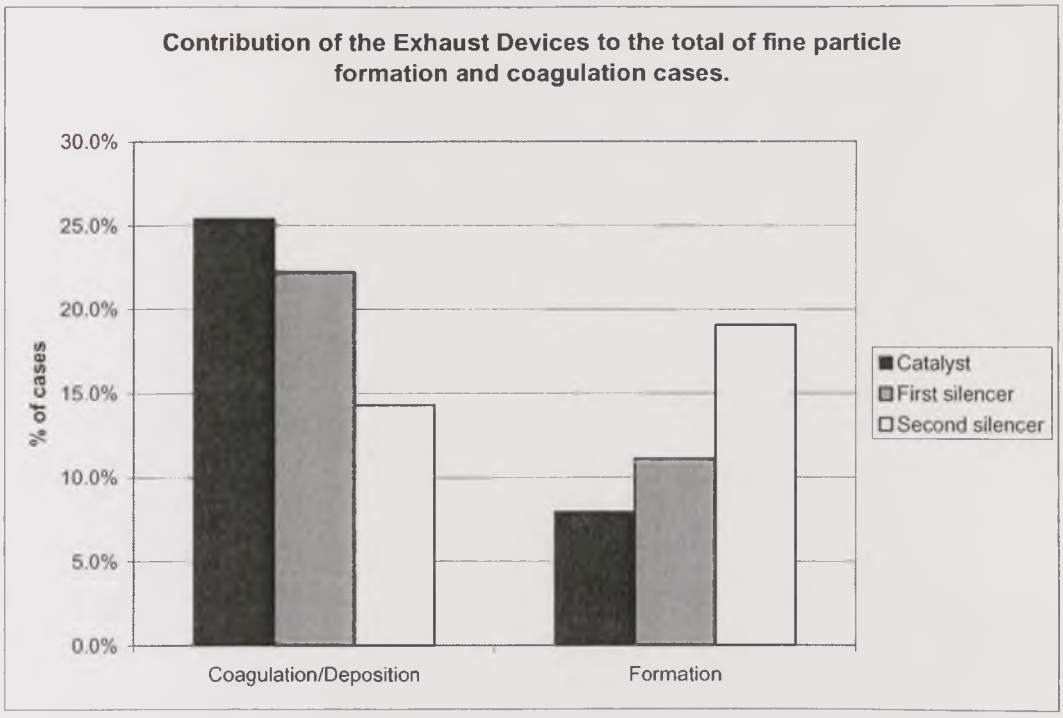

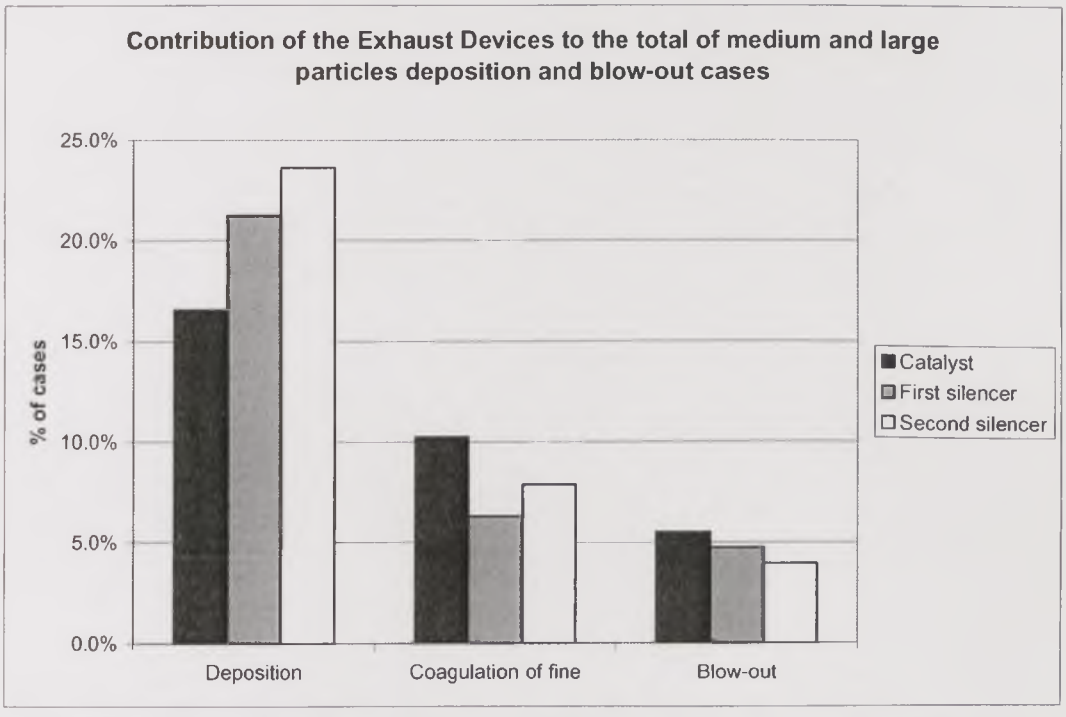

Figure 4.52. Contribution of exhaust devices to the total of blow-out and deposition cases during cold-start tests.

The comparison of the contribution of the main events during cold start, Figure 4.51., shows that the engine start-up (mass burst), which was the first disturbance over the system, contributed more to the number of cases of ultrafine and mid-sized particle formation, as well as large particle resuspension, than the acceleration (peak-number) and the thermal stabilisation. The particle size distribution during

start-up was found to have larger size modes, and therefore a higher Emission Index, so it is this event where visible clouds would be more likely. The acceleration contributed to as many cases of mid-sized particle formation as the start-up, but less cases of large particle resuspension, in contrast with what was expected for visible particulate clouds to be likely.

Finally, Figure 4.52. shows that the catalyst contributed to the highest number of fine particle deposition or reduction cases compared to the silencers. This was expected from its channel geometry, high surface area and also catalytic activity. However, the number of cases of deposition of mid-sized and large particles was the highest through the second silencer. The second silencer contributed to an increase in the number of ultrafine particles in more cases than the other devices, owing to its cooler condition and therefore enhanced condensation. Something similar occurred through the catalyst for mid-sized particles and the resuspension of large particles.

The analysis of number of cases was useful in identifying the natural trends in the particulate behaviour through the exhaust system. The results did not agree with the expected effects, in the sense that there was no statistical evidence that the acceleration to a high-speed or high-load condition during cold start would unmistakably cause particulate blow-out.

It was observed that the changes through the exhaust system did not follow single condition-dependent trends, but they were the result of opposing processes of particulate formation, growth, deposition and resuspension. The preponderance of one process over others opposing to it apparently depends on very subtle differences in the aerosol flow and temperature conditions but this can make a significant difference in the overall results.

4.8. Key points from this chapter

4.8.1. Filter measurements

- Tests at high-speed and high-load conditions resulted in a preconditioning-dependent performance of the catalyst. Negative efficiencies were observed during the first minutes of cold start in most of the tests, excepting that at high-speed cold start with high-speed preconditioning. The efficiency recovered after the catalyst lit off, though it was lowered owing to the high particulate emission by the engine at high-load conditions.
- Particulate deposition and blowout processes during the cold start through the silencers downstream of the catalyst resulted in very

complex trends that were dependent on the preconditioning of the exhaust system.

- High mass concentrations at high load produced levels of particulate deposition and blowout about fourfold the level of high-speed conditions during cold start, with a maximum at 6.0g/kg-fuel and 1.2g/kg-fuel respectively. In terms of percentage of tailpipe emissions, deposition and blowout reached significant levels at both conditions, with both preconditioning modes. Deposition reached levels as high as 300% of the tailpipe emissions at high-load and 150% at high-speed conditions, whereas maximum blowout remained under 60% at high-load and under 80% at high-speed conditions.
- Higher deposition and blow out levels occurred through the first silencer compared to those through the second, in most cases. This may be explained by their different geometry and temperatures. Higher temperatures of the exhaust gas through the first silencer may have promoted either thermophoresis or thermal outgassing, whose effect is reduced for the cooler exhaust gas through the second silencer.
- During cold start at high-load conditions, particulate blowout predominated after idle preconditioning whereas deposition did when the exhaust system had been cleaned up during high-speed preconditioning. High-speed cold-start produced opposite effects, since the exhaust flow effect became more important than temperature gradient effects that are predominant at high-load conditions.

4.8.2. Particle size distribution measurements

- For the conditions tested, net particulate mass release from the catalyst predominated only during the first thirty seconds of cold start, after a preconditioning procedure of 4 hours at idle the day prior to the test and an overnight cold soak.
- Tests after the preconditioning procedure at high speed and overnight cold soak showed no net mass release from the catalyst. Little release of particles between 0.1μm and 1μm was observed in the test reaching 3500rpm – 15kW, and no release at any particle size was observed during the whole test at 2250rpm – 35kW.
- The catalyst reduced the number and the mass of diesel particles during cold start, although its efficiency was affected by the preconditioning procedure. High-speed preconditioning enhanced the capacity of the

catalyst to retain particulates during the first seconds of cold start. Only in the tests after high-speed preconditioning, did particles smaller than 0.1μm penetrate the catalyst. Idle preconditioning, in contrast, not only reduced this capacity, but also slightly promoted the mass release of particles between 0.1μm and 10μm.

- Particle growth, according to Fujiwara and Fukazawa (35), is very significant for particles with a mean particle size by volume between 0.030μm and 0.045μm when the exhaust cools down, especially in the 200°C- 50°C temperature region. In these tests, the gas temperature was under 200°C during the first 100 seconds. Therefore, particle growth is an important mechanism causing a decrease in number and mass of very fine particles in this period. Although ultrafine particle formation would counteract this effect, it is less likely when the saturation ratio is not very high, so coagulation becomes the predominant process.
- Larger particles, between 1μm and 10μm, deposit by inertial separation when the temperature gradient is not significant, and this occurred to a greater extent at 2250rpm – 35kW than at 3500rpm – 15kW. The gas flow rate at 2250 rpm was too low, in comparison to the 3500rpm condition, to keep these large particles suspended, so the particles deposited.
- The particles that were released, especially during high-speed operation, were considered to be particles that deposited on the catalyst walls during the 4-hour idle preconditioning period. To be easily removed by the gas flow at high speed indicates that they were fluffy deposits.
- The combined hydrocarbon adsorber and oxidation catalyst was shown to be effective at retaining particulate matter during cold start, with 60% to 70% of the total emissions number and 10% to 60% in corrected mass. Inertial separation was the main process for the reduction of large particles, and the particle growth that occurred in the middle size range.
- Particulate deposit formation during city driving conditions, simulated by a 4-hour idle preconditioning procedure, reduced the capacity of the catalyst to retain particles larger than 1.0μm. Instead, these were released from the catalyst walls, especially at high-speed conditions. They appeared to have formed easy-to-remove catalyst deposits during

idle operation. In addition, the number of mid-size particles increased through the catalyst as a consequence of coagulation processes.

- The particle number-to-mass correction for the measurements by the ELPI reduced the large overestimation in particle mass that the original conversion algorithm of this instrument produced. However, this inaccuracy in the measurement of particle number concentrations in the 1.0μm - 10μm size range was still significant in some cases, indicating that more work on this kind of correction is necessary.
- Fine particle coagulation and deposition were the predominant processes taking place through the exhaust system at all times and for all engine conditions. The engine start-up was the main process that made the particle gas-to-particle conversion and resuspension processes predominate over coagulation and deposition.
- The catalyst acted in many cases as a fine particle agglomerator and promoted fine particle deposition, but did not retain very effectively large particles. Through the second silencer, ultrafine particles formation by gas-to-particle conversion was promoted.
- There was not enough evidence in these tests that the acceleration to a high-speed or high-load condition during cold start would always cause particulate blow-out. No single condition-dependent trends occurred through the exhaust system, since opposing gas-to-particle conversion and resuspension processes acted over particles in a very complex fashion. The preponderance of one process over others opposing to it apparently depended on very subtle differences in the aerosol flow and temperature conditions.
- Transient cold-start emissions in step-change cycle tests such as those carried in this work may be used to estimate changes in emissions due to transients, with respect to multi-mode steady-state legislative cycles such as the R49 and the ESC. This is explained and illustrated in Chapter 7.

Chapter 5.
Rapid Acceleration Particulate Mass Emission and Particle Size Distribution Changes Through a Practical Exhaust System in Place

5.1. Total Exhaust Outlet Measurements: Total Particulate Number and Mass Emissions during free Accelerations from Idle

Prior to the use of an ejector-type dilution system, a dilution tunnel was used to allow the measurement of the total number concentration and size distribution of diesel exhaust. The air flow was controlled to give an approximately constant 180:1 dilution ratio during the acceleration periods of the engine, in two dilution stages, the dilution ratio of the first stage being 2:1. The overall dilution ratio is within the range used by most laboratory engine-emissions studies. It is much lower than the atmospheric dilution ratio, which is around 1000:1 after just 1s from the moment of emission at the tailpipe and much higher afterwards.

The use of the low dilution ratio in the primary stage, 2:1, can produce artifices in the total number measurement owing to gas-to-particle conversion processes, which are extensively explained by Kittelson et al. (Kittelson, 1999; Abdul-Khalek, 1999). However, most of these changes fall between 7nm and 30nm, well below the cut-off point of the ELPI's particle size range, 35nm. The low primary dilution was due to installation difficulties of supplying clean air total dilution of the total exhaust. This pre-dilution air was extracted from the main filtered air to the dilution tunnel.

The total particle number concentrations and Emission Index vs. time during acceleration tests using the double-stage dilution tunnel are shown in Figures 5.1., 5.4. and 5.5. for the three acceleration targets from Idle, namely 4100rpm (two tests), 3000rpm and 2000rpm. Once again, the total Emission Index was calculated from the sum of number concentrations converted into Emission Index for each of the twelve size ranges classified by the ELPI, for both unit and corrected densities, as explained in chapters 3 and 4, and derived in Chapter 6. The resulting profiles for each acceleration cycle showed very similar characteristics to the cold start transients, and consisted of an increase in both number concentration and Emission Index, causing a mass burst peak followed by a number concentration peak. Subsequently, particle and number concentration decreased to stabilisation levels. Deceleration to Idle caused a consequent reduction in particle number concentration and Emission Index. The second acceleration cycle (and a third acceleration in some

tests) showed similar characteristics, but the first peak in number had much lower values than that of the first cycle. This was the first indication of a cleared exhaust after the first acceleration cycle. In most cases, however, the Emission Index calculated with unit densities did not show this difference between the peaks of first and second cycles, indicating that the difference in numbers were related to the formation and coagulation of very fine particles during the first acceleration, when temperatures are colder. These particles do not contribute much to the total mass. The effect was not observed when using the correction for Emission Index.

Particle size distribution for the most significant events are shown in Figures 5.2., 5.3., 5.4. and 5.5. These illustrate the changes in particle size for the main events of the transients and show the difference between the Emission Index calculations with and without the correction.

5.1.1. Acceleration to 4100rpm (2 tests)

The number concentration peak for the first cycle of the acceleration tests from idle to 4100rpm were $1.94x10^{8}$ cm^{-3} (test 1) and $1.62\ x10^{8}$ cm^{-3} (test 2), as can be observed in Figure 5.1. The uncorrected Emission Index peaks were 80.6 g/kg fuel and 105.0 g/kg fuel, respectively, and the corrected Emission Index, 6.7 g/kg fuel and 7.4 g/kg fuel, also respectively. This was the order of variability that can be expected from these peak events, which might have depended on the variability in the manual operation of the throttle and the dilution air flow.

For the stabilisation period, the number decreased to $1.47x10^{8}$ cm^{-3} in the first test and $1.35x10^{8}$ cm^{-3} in the second, still somewhat different to the same event at the same conditions in the first cycle. The uncorrected Emission Index was 6.7 g/kg fuel in the first test and 3.8 g/kg fuel in the second, which converted to 5.9 g/kg fuel and 2.9 g/kg fuel when applying the corrected density.

The second cycle of the first test showed a less evident peak in number concentration than that in the first cycle, which was expected as a result of the first acceleration. The maximum number concentration was $1.67x10^{8}$ cm^{-3}, 14% lower than the peak of the first cycle. The maximum uncorrected Emission Index was 44.7 g/kg fuel, practically half the value of the peak in the first cycle, and the corrected Emission Index also halved with respect to the first cycle, being 2.7 g/kg fuel. All this showed that the particle release caused by the second acceleration cycle was lower than that of the first cycle, presumably because of the much shorter Idle period previous to the second cycle, 10 min., compared to the 4h conditioning before the first acceleration. The third acceleration cycle of the same test mirrored perfectly the second cycle, showing that the short idle period between cycles had the same effect on the system.

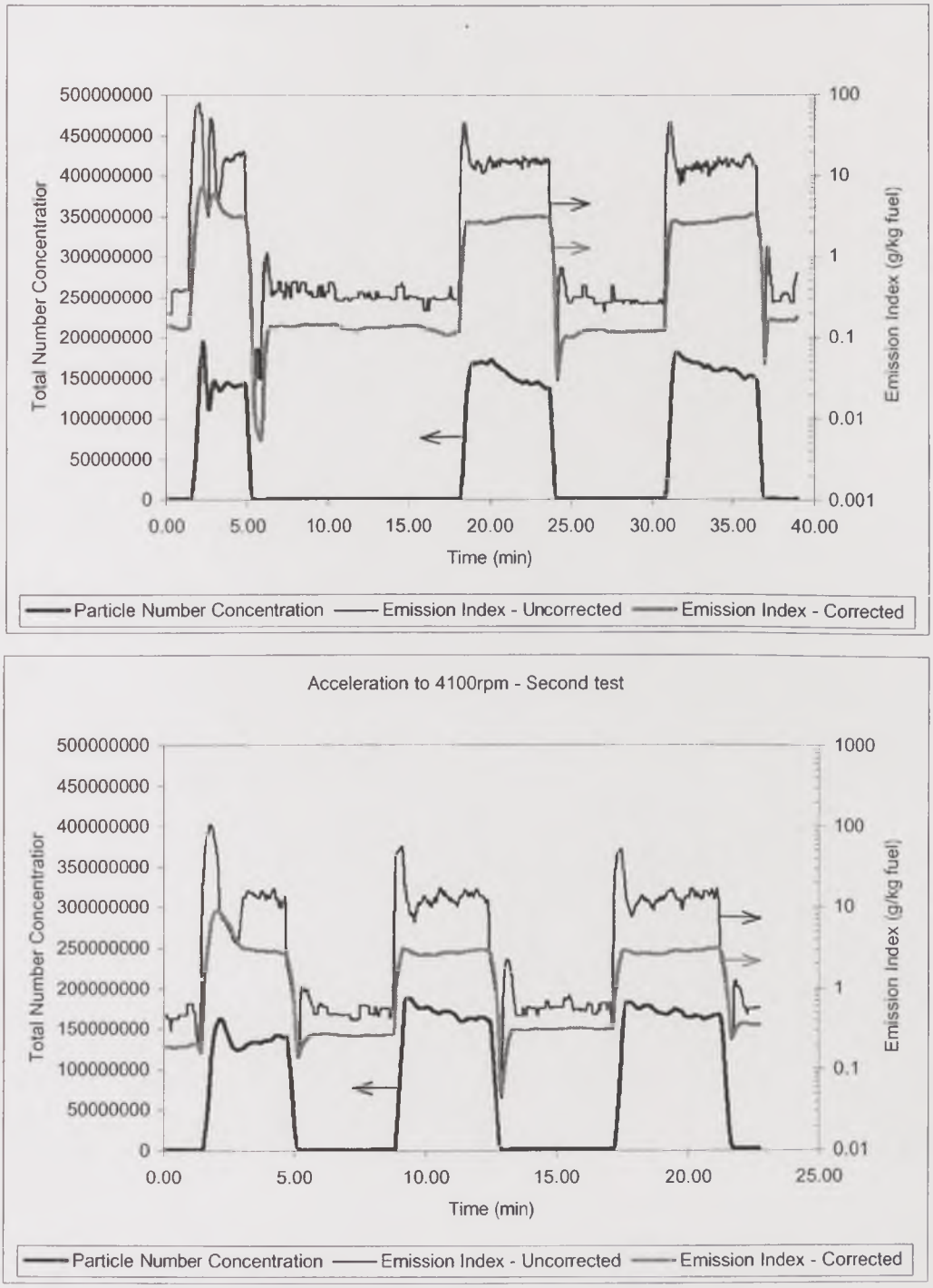

Figure 5.1. Total particle number concentration during acceleration tests from idle to 4100rpm using the ELPI with total-exhaust dilution.

The same comparison applied to the second test at the same conditions, which was somewhat contradictory with the previous observations. The second and third acceleration cycles, which perfectly matched each other, showed higher number

concentrations than those of the first acceleration cycle, so there was no clear evidence of a larger deposition in the system left by the long preconditioning period.

The Emission Index, however, showed exactly the same kind of behaviour as in the first test, with a high peak in the first acceleration cycle and lower peaks in the second and third cycles. The stabilisation periods of the second and third cycles showed very similar number concentrations to those of the second and third cycles of the first test, suggesting that the difference was only in the first cycle and that the main systematic error in the measurement was the manual operation of the throttle and air flow controls. The most likely error was a higher dilution in the first cycle of the second test, which affected the total particle number, but did not affect significantly the Emission Index.

The particle size distributions by number and Emission Index plotted in Figure 5.2. for the first test and Figure 5.3. for the second test, do not show major differences for the corresponding periods of consecutive acceleration cycles, with the exception of the number peak events. In the first peak number, the particle size distribution showed a larger mode than in the subsequent acceleration events. Two curves for idle periods were coincident, with a slight difference in the particles below 0.1μm; and stabilisation curves also matched each other very closely, with the exception of particles between 0.1μm to 0.3μm, which were slightly higher in the first cycle. The particle size distribution of the exhaust aerosol showed a shift towards finer particle sizes for the acceleration events when compared to Idle conditions: the accumulation mode decreased from 0.3μm to 0.20μm in the first peak-number event and 0.15μm in the subsequent events.

Particles associated with the number peak of the first event showed a trend towards larger sizes than the same event of the second cycle, particularly in the range between 0.1μm and 0.6μm. Considering that the key difference between both acceleration cycles was the duration of the Idle period previous to each cycle, the larger particle size was due to outgassing and recondensation of the higher mass of volatile components deposited on the walls during the Idle preconditioning. Enhanced coagulation process, owing to lower temperatures in the first cycle, also contributed to the formation of more particles between 0.1μm to 2.0μm than in the second cycle. Apparently, no significant large particle resuspension occurred.

5.1.2. Acceleration to 3000 rpm

Total particle number concentration showed a peak at 4.7×10^7 cm^{-3} in the first acceleration cycle to 3000rpm and 5.2×10^7 cm^{-3} in the second cycle. The corresponding stabilisation periods averaged 4.0×10^7 cm^{-3} and 4.3×10^7 cm^{-3}. These measurements were practically in the same order and suggested that there was no

clear difference in the particulate changes through the system walls after the significantly different durations of the Idle preconditioning before each cycle.

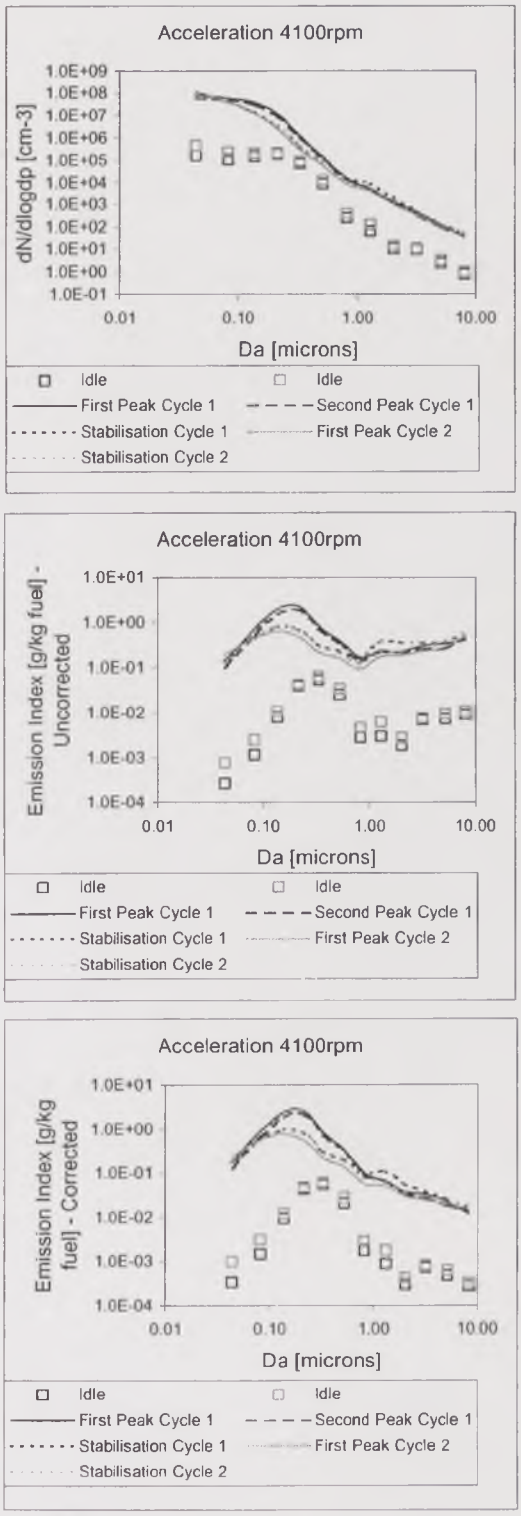

Figure 5.2. Particle size distribution during the first acceleration test from idle to 4100rpm using the ELPI with total-exhaust dilution.

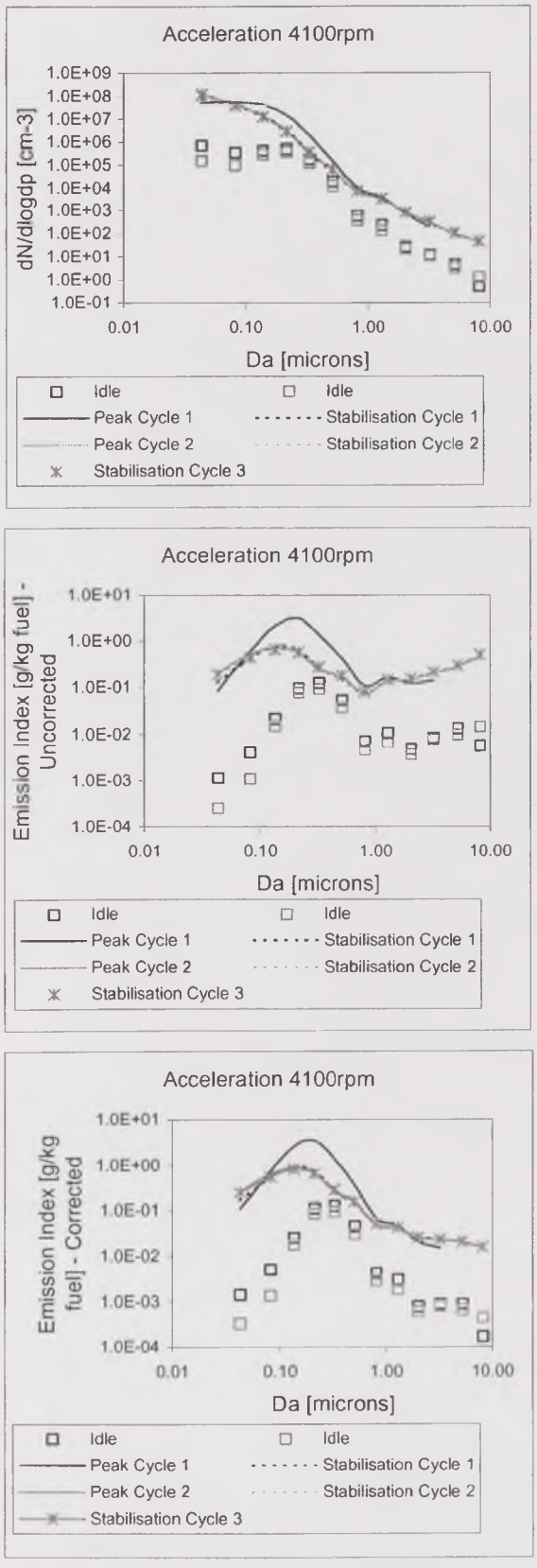

Figure 5.3. Particle size distribution during the second acceleration test from idle to 4100rpm using the ELPI with total-exhaust dilution.

A similar conclusion was inferred from the observation of the uncorrected Emission Index profiles with time. For both acceleration cycles, the peak Emission Index was also very similar, 30.5 g/kg fuel and 29.2 g/kg fuel. Likewise, during the stabilisation period, the Emission Index averaged 6.1 g/kg fuel and 6.3 g/kg fuel for the first and second cycles, respectively.

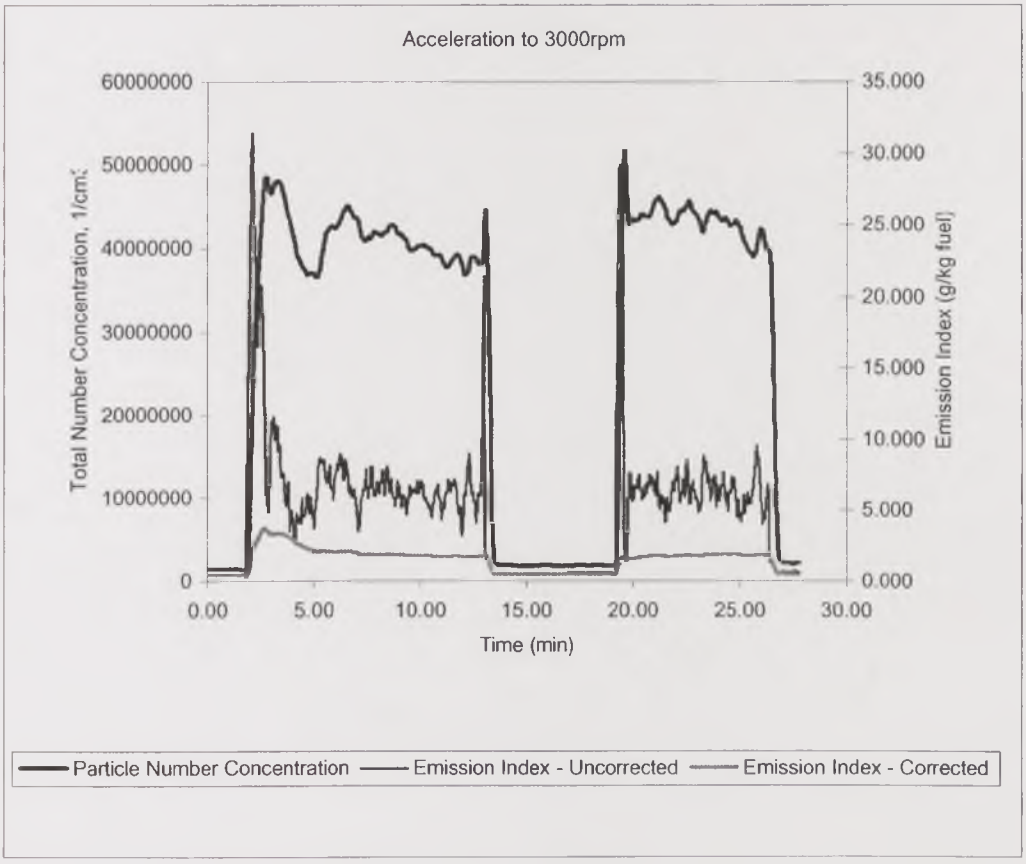

Figure 5.4. Total particle number concentration during acceleration tests from idle to 3000rpm using the ELPI with total-exhaust dilution.

Nevertheless, the corrected Emission Index did show some differences between the acceleration cycles: the first cycle had a number peak of 3.6 g/kg fuel followed by a stabilisation period at 1.9 g/kg fuel, whereas the second cycle did not show a peak, but only increased to a stable 1.9 g/kg fuel. If the assumptions about the corrections for the particle number concentrations measured by the ELPI were correct, this would indicate that a longer Idle preconditioning period contributed to a higher deposition of particles on the system walls with higher mass release during the first acceleration cycle.

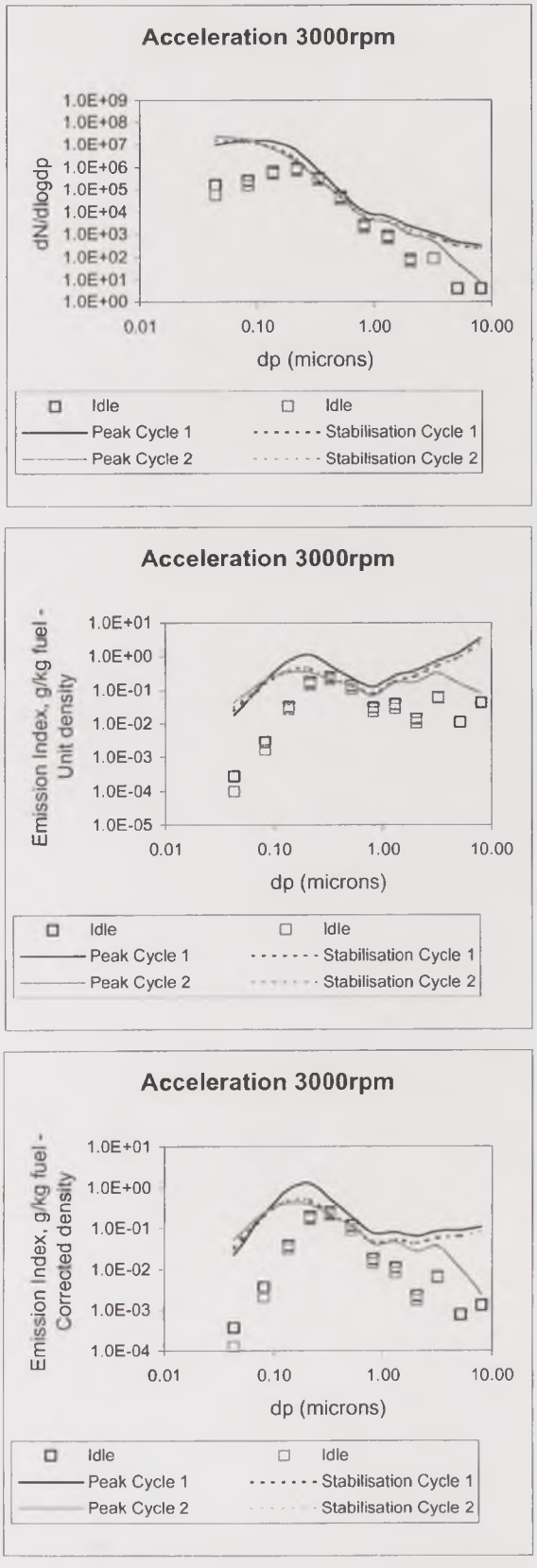

Figure 5.5. Particle size distribution during the second acceleration test from idle to 3000rpm using the ELPI with total-exhaust dilution.

Figure 5.5. shows that there were no significant differences between the particle size distributions of the various corresponding events of the acceleration cycles. As in the test at 4100rpm, the distributions for two separated idle periods were coincident, and so were the distributions for stabilisation events, and they showed larger particle size distribution modes than the events during acceleration. During peak number events, which showed that a larger number of particles between 0.1μm and 1.0μm was measured in the number peak the first cycle than in the second cycle. This contributed also to a higher Emission Index, both uncorrected and corrected. Also, a smaller number of particles between 1.0μm and 10.0μm was measured in the peak number of the second cycle. These observations supported the evidence given by the corrected Emission Index above, that enhanced coagulation processes, outgassing, nucleation and condensation of volatile material from the deposition layer occurred to a greater extent during the first acceleration cycle than the second.

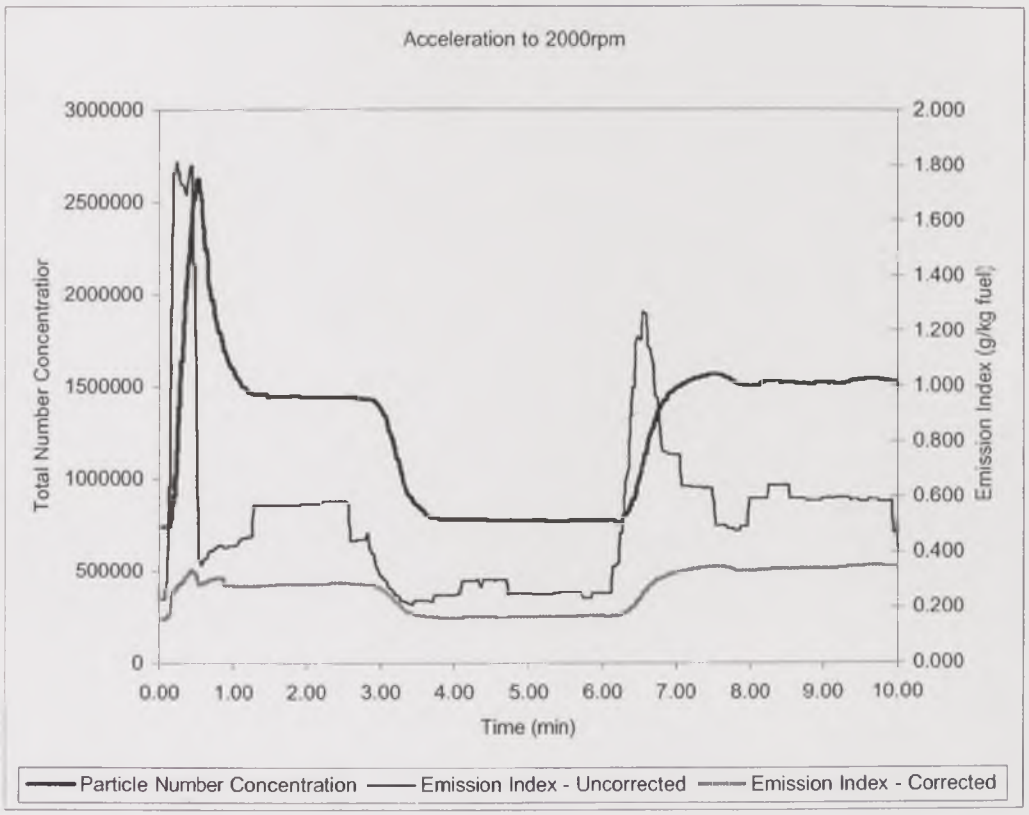

Figure 5.6. Total particle number concentration during acceleration tests from idle to 2000rpm using the ELPI with total-exhaust dilution.

5.1.3. Acceleration to 2000rpm

Total particle number concentration vs. time is shown for two consecutive acceleration cycles from idle to 2000rpm in Figure 5.6. The first cycle showed a

peak number concentration of $2.6x10^7$ cm^{-3}, followed by a quick stabilisation at $1.4x10^7$ cm^{-3}. The second cycle did not show the peak in number concentration, indicating that the duration of the Idle preconditioning prior to acceleration affected the particulate formation and reentrainment during acceleration in particle number terms. Mass release during the second acceleration period did occur, according to the uncorrected Emission Index profile vs. time that showed a peak at 1.3 g/kg fuel, slightly lower than the 1.8 g/kg fuel peak in the first acceleration cycle. The stabilisation Emission Index for both cycles averaged 0.55 g/kg fuel. The significance of the Emission Index peaks during the acceleration was, however, diminished with the correction: the corrected Emission Index did not show such peaks, but step changes to a stable value around 0.35 g/kg fuel for both cycles.

The particle size distribution charts in Figure 5.7. shows the differences between the number peak of the first acceleration cycle and the stabilisation levels. Fine particles, between 0.035μm and 0.1μm had the most significant contribution to the number concentration peak, whereas the distributions were coincident for larger particles.

5.2. Changes Through the Exhaust System During Fast acceleration

Fast acceleration tests to the same conditions used during cold-start tests were run after exhaust preconditioning using the ELPI at various points along the exhaust system, to determine which of both transient processes was more significant for the deposition or blow-out of particulate. This comparison also aimed to define whether the difference in the performance of the engine when cold or warm produced differences in the particulate emissions during transient.

The preconditioning procedure for these tests consisted, as in the day-before preconditioning for cold start tests, in running the engine at idle for four hours. Immediately after this, a step-change in the engine speed and power conditions was applied. After 10 minutes running at the target conditions, stabilisation was achieved and the engine was taken back to idle conditions, where it was kept for ten minutes. A second step-change/idle cycle with the same characteristics was then applied, to determine whether a short period at idle could have a significant effect on the system in terms of particulate deposition.

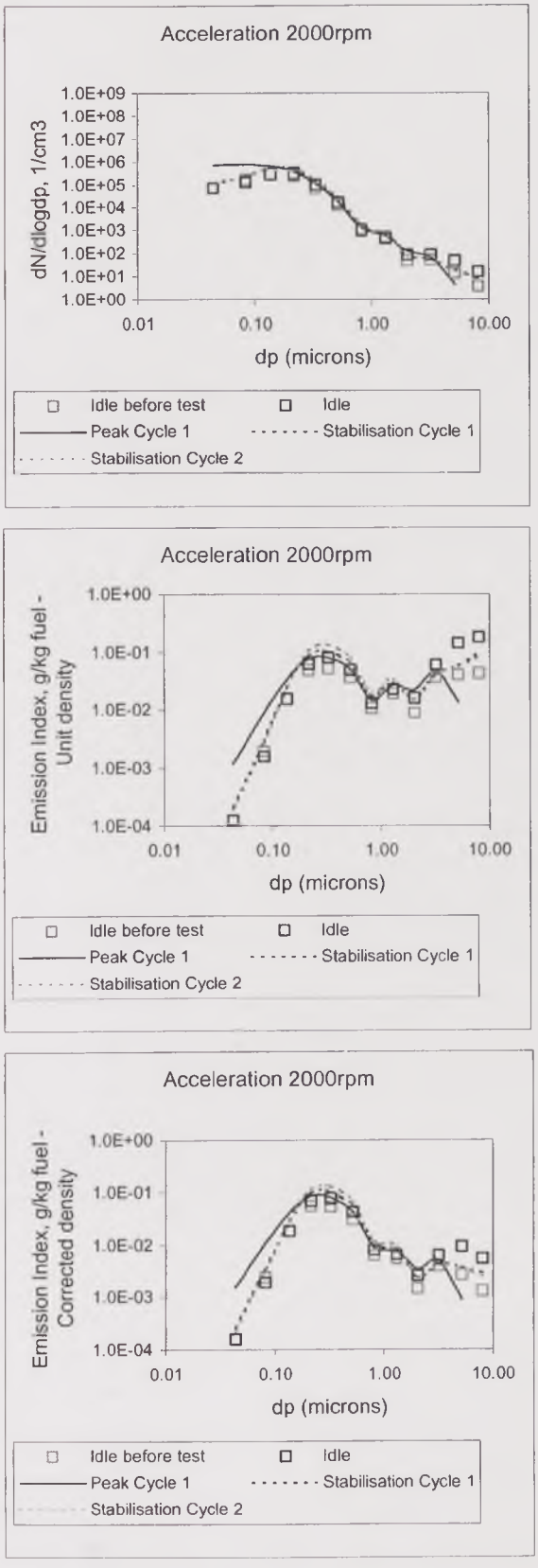

Figure 5.7. Particle size distribution during the second acceleration test from idle to 3000rpm using the ELPI with total-exhaust dilution.

The target conditions of the acceleration tests were 2250rpm – 15kW and 3500rpm - 15kW, which were taken from the cold-start tests' targets as a reference. Unfortunately, the intended acceleration test to high power conditions, namely 2250rpm - 35kW, was not possible to run owing to problems in the delivery of fuel to the combustion cylinders, presumably related to a failure in the fuel pump or in the engine control strategy.

5.3. Exhaust Temperature Changes

Temperature profiles against time at various points along the exhaust system, as well as the corresponding temperature differences between the exhaust gas and metal for the points downstream of the catalyst, are shown in Figure 5.8., for the acceleration cycles to 3500rpm - 15kW, and Figure 5.9., for those to 2250rpm - 15kW.

From temperatures between 50°C and 100°C and gas-metal temperature differences around 20°C in the exhaust system at idle conditions, the acceleration in the 3500rpm - 15kW first cycle caused a rapid and steady increase during the first 150 to 180 seconds, to temperatures between 250°C and 350°C. At the end of this period, when the target conditions were reached, gas-metal temperature differences peaked, being 142°C at the entrance of the first silencer, 110°C at the entrance of the second silencer and 59°C at the tailpipe. As a result of the stabilisation at the target condition, the temperatures increased more slowly in the following minutes of the cycle, and seemed to stabilise at 360°C upstream of the catalyst, 355°C at the entrance of the first silencer, 345°C at the entrance of the second silencer and 300°C at the tailpipe. The gas-metal temperature differences stabilised very quickly, around 66°C at the entrance of the first silencer, 58°C at the entrance of the second silencer and 40°C at the tailpipe.

The temperature profiles during the second acceleration cycle had virtually identical characteristics as those during the first cycle, differing only in the starting temperature around 30°C higher before the second cycle than before the first cycle. The corresponding gas-metal temperature differences, however, were virtually identical for both cycles.

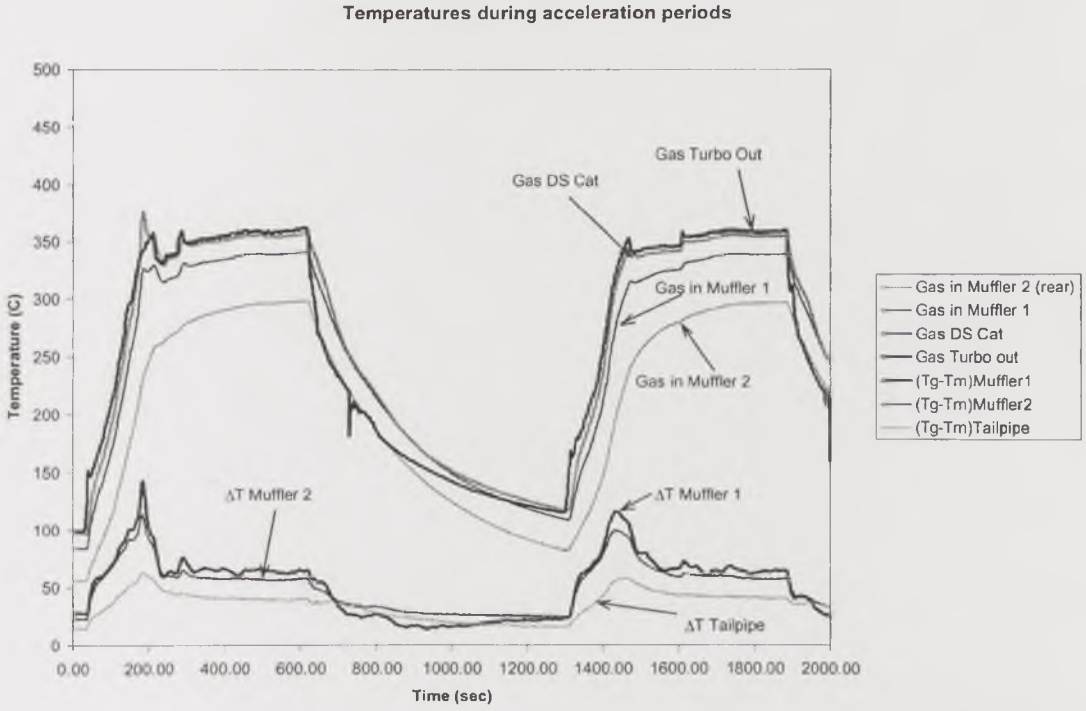

Figure 5.8. Exhaust Temperature Changes and gas-metal temperature differences during acceleration to 3500rpm - 15kW after idle preconditioning.

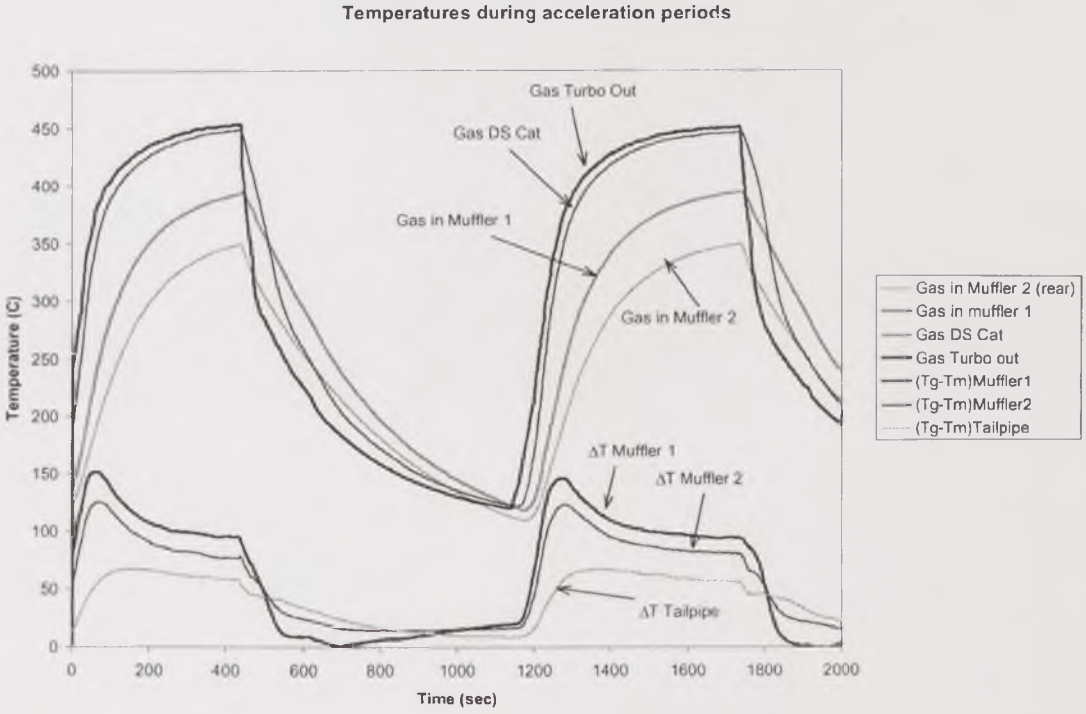

Figure 5.9. Exhaust temperature changes and gas-metal temperature differences during acceleration to 2250rpm - 15kW after idle preconditioning.

During the acceleration cycles to 2250rpm - 15kW, exhaust temperature profiles against time showed very similar general characteristics to those at high-speed conditions, characterised by a rapid, steady increase during the first 150 to 180 seconds, and a slower increase afterwards, reaching stable temperatures by the end of the cycles. Stabilisation temperatures were higher than those reached during fast-speed cycles: 453°C upstream of the catalyst, 450°C upstream of the first silencer, 395°C downstream of the second silencer and 350°C at the tailpipe. Gas-metal temperature differences also increased quickly at the beginning of the acceleration cycles and reached a maximum once the target condition was reached, around 150°C upstream of the first silencer, 130°C upstream of the second silencer and 75°C at the tailpipe. Afterwards, the differences decrease until stabilising around 95°C, 81°C and 56°, respectively. Both exhaust gas temperatures and gas-metal temperature differences were higher than at high-speed conditions.

5.3.1. Hydrocarbon Emissions

Total Hydrocarbon Emissions measured by FID at 190°C upstream and downstream of the catalyst during the acceleration cycles at high-speed and high-load conditions are shown in Figure 5.10. The diagrams show a quick increase in THC concentration peaking in the first 5 to 20 seconds after starting the test. Upstream of the catalyst, the peaks were around 2500ppm and 1000ppm for the tests at high-speed and high-load conditions, respectively. Downstream of the catalyst, the corresponding THC concentrations were 216ppm and 82ppm, also respectively. After peaking, THC concentrations decreased very quickly. In the tests at high power, THC stabilised around 17ppm and 15ppm, upstream and downstream of the catalyst, respectively. High-speed cycles showed a second peak at 1000ppm upstream of the catalyst and 340 downstream of the catalyst, after one minute from cold start. Afterwards, THC decreased and stabilised at 40ppm upstream of the catalyst and 10ppm downstream of the catalyst.

The sharp decrease in THC levels indicated that the catalyst activity was very good during acceleration. However, when very low UHC levels were emitted from the exhaust during the thermal stabilisation of the engine, the catalyst efficiency value was markedly reduced, and the THC levels upstream and downstream of the catalyst were very similar.

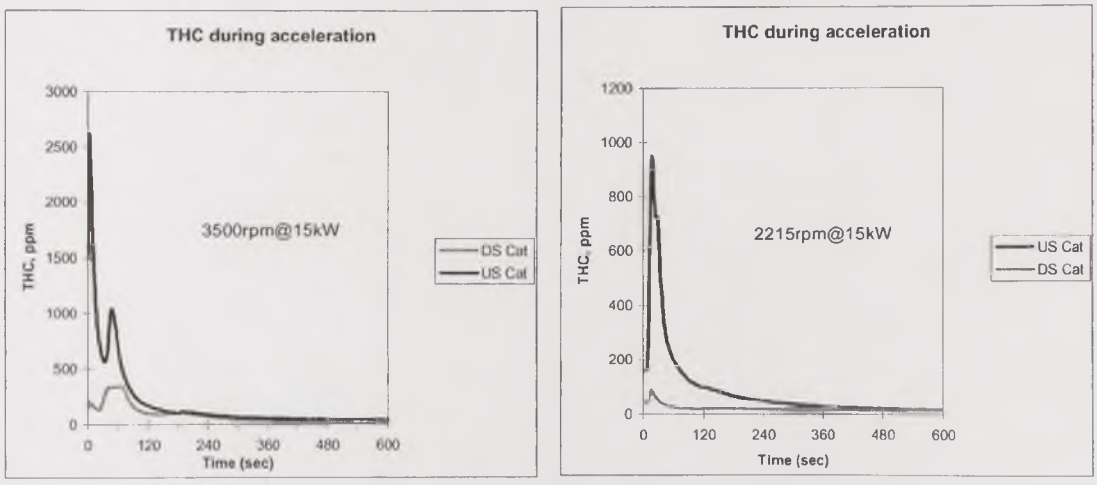

Figure 5.10. Hydrocarbon emissions during acceleration to 3500rpm - 15kW (left) and 2250rpm - 15kW (right) after idle preconditioning.

5.3.2. Total Number Concentration, Emission Index and Size Distribution Changes

5.3.2.1. Acceleration from Idle to 3500rpm – 15kW

Total particle number concentration vs. time profiles during acceleration for the four sampling points along the exhaust system are shown in Figure 5.11. Similarly to the cold start profiles performed with this target condition, the acceleration profiles showed an increase in total number concentration during the first two minutes, until reaching a peak, followed by a decrease to a stabilisation level. This profile was observed in both acceleration cycles.

As general observations, the number peak and the mass burst of the first acceleration cycle were much higher than the corresponding events of the second cycle for all sampling points, and the stabilisation levels were about the same for both cycles. This indicated that the increase in number concentration was an effect of the transient only, and that the previous history of the engine, represented by the duration of the idle period, was an important factor in the transient emissions.

Another characteristic that can be observed from the profiles was that the increase in number concentration was not monotonous, but had two or three stages that included temporary peaks other than the maximum. These stages are related to the manual acceleration of the engine and the slow response of the hydraulic dynamometer. Although the manual operation was executed most carefully, this control mode made the speed profiles not as smooth as desirable, clearly affecting the appearance of the number concentration profiles.

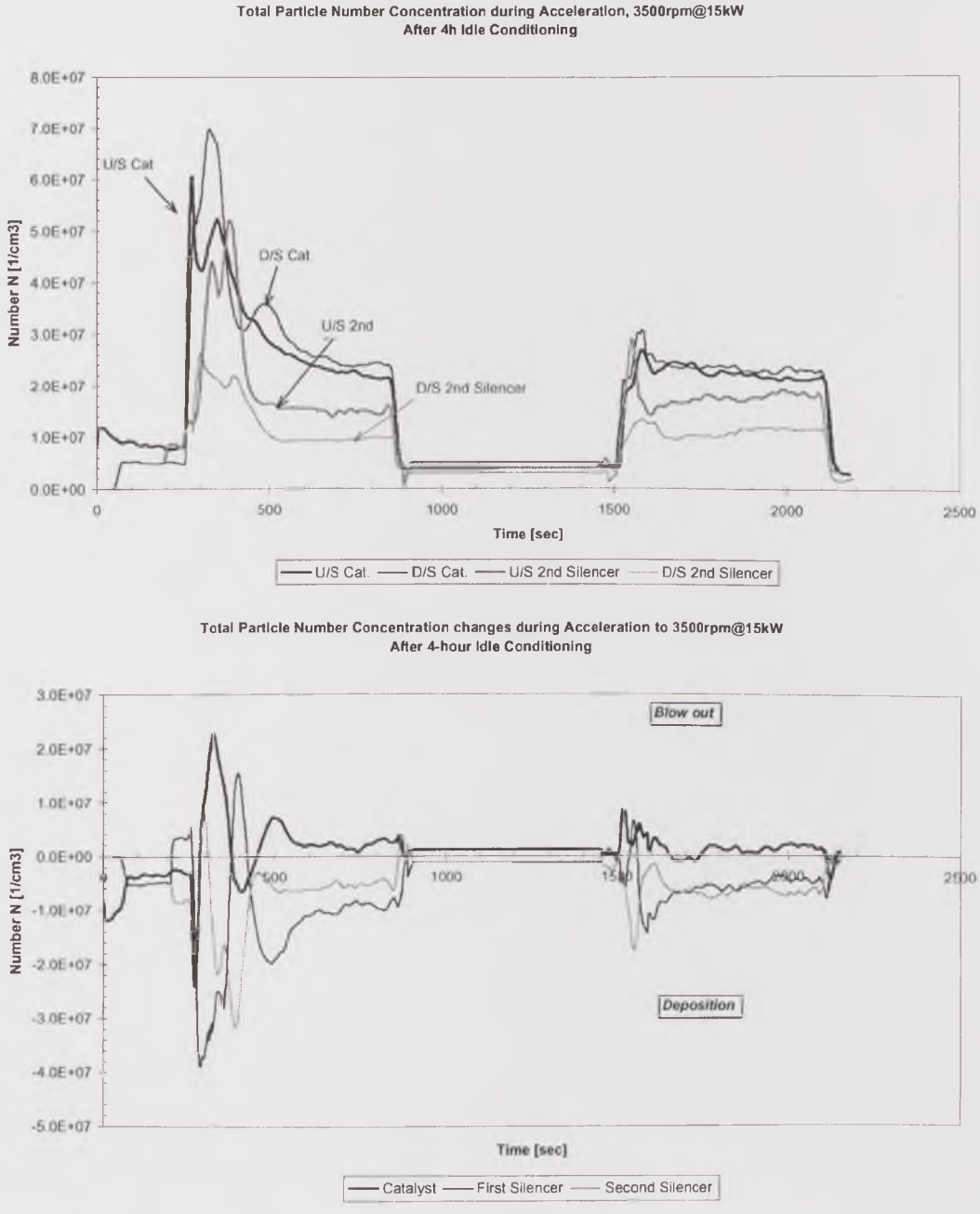

Figure 5.11. Total number and mass concentrations vs. time during acceleration to high-speed conditions, 3500rpm – 15kW, after a 4-hour Idle preconditioning at various points through the exhaust system. a) Particle number concentration.

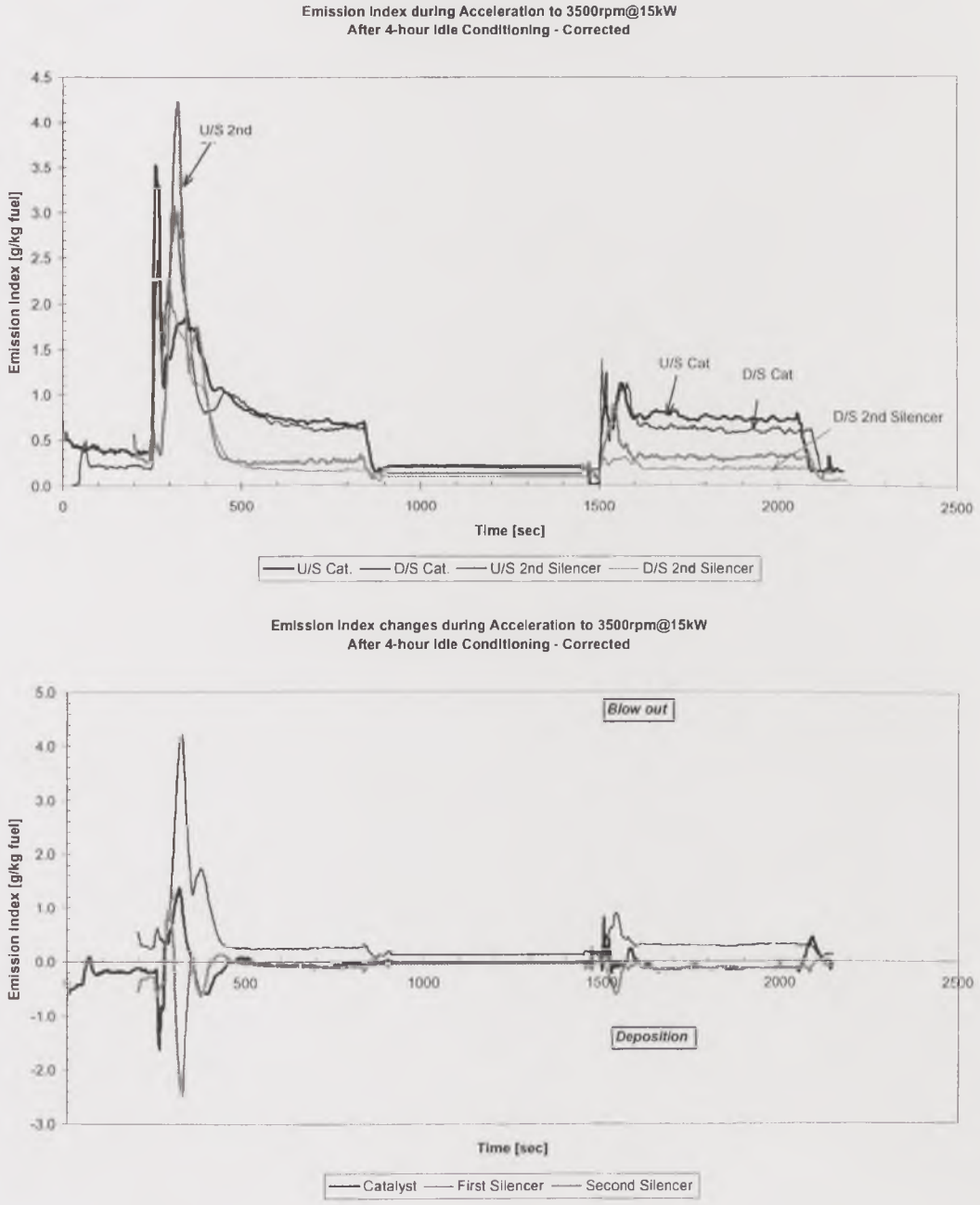

Figure 5.11. Total number and mass concentrations vs. time during acceleration to high-speed conditions, 3500rpm – 15kW, after a 4-hour Idle preconditioning at various points through the exhaust system. b) Corrected Emission Index.

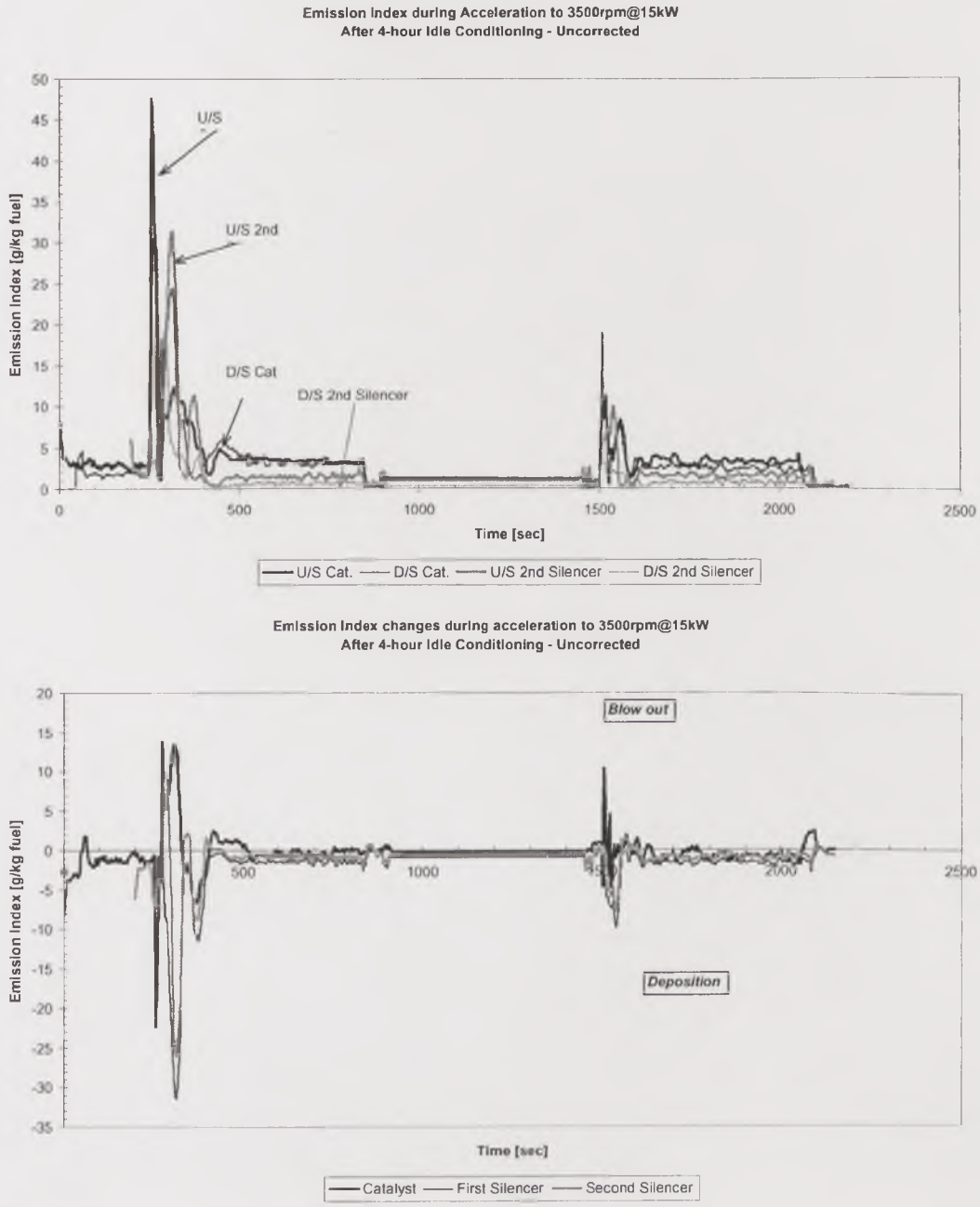

Figure 5.11. Total number and mass concentrations vs. time during acceleration to high-speed conditions, 3500rpm – 15kW, after a 4-hour Idle preconditioning at various points through the exhaust system. c) Uncorrected Emission Index.

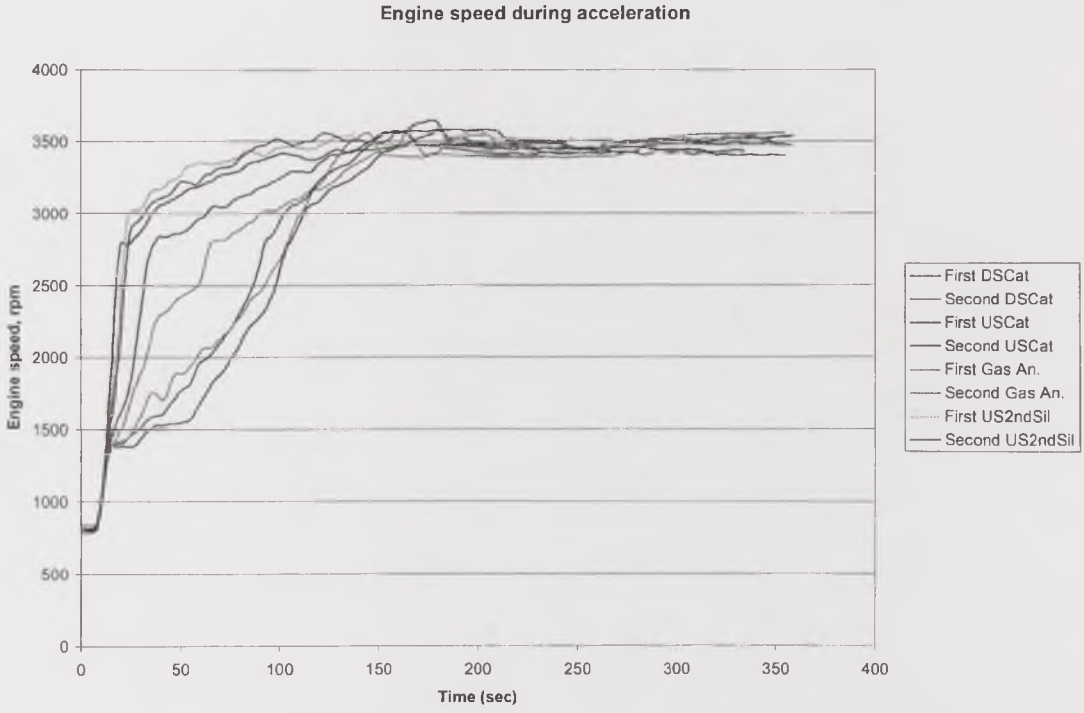

Figure 5.12. Speed vs. time profiles for several acceleration cycles to 3500rpm - 15kW.

Figure 5.12. shows the speed profiles vs. time for 8 acceleration cycles in different tests (2 tests per sampling point), illustrating the variability in the manual operation. This certainly reflects to a certain extent what occurs in real life. However, this was a serious inconvenience for the analysis of the results owing to the reduced repeatability. The target speed being 3500rpm, an intermediate speed of 2500rpm was achieved in a period as short as 15 seconds for a couple of cycles, and as long as 80 seconds for other two cycles, with intermediate periods for the remaining cycles. The stabilisation at the target speed was reached in 90 to 150 seconds. It was observed that the number-peak event appeared during acceleration and not when a constant speed was reached.

From the previous observations, it was considered that a second-by-second comparison of the number concentration and the associated Emission Index would be significantly affected by the variability in the manual operation. Therefore, an event-to-event comparison, similar to that performed for cold-start tests, will be used to simplify the analysis. This is shown in Figure5.13., where the total particle number concentration and Emission Index are plotted against the location in the exhaust for the main events of the acceleration cycles.

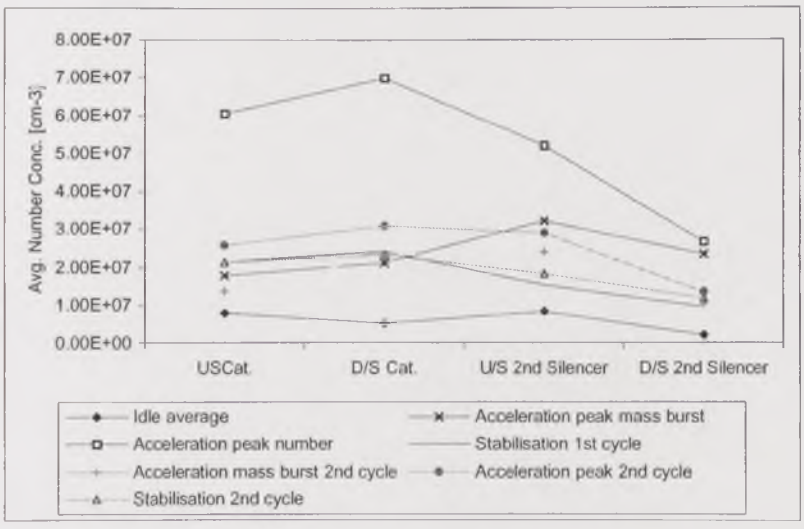

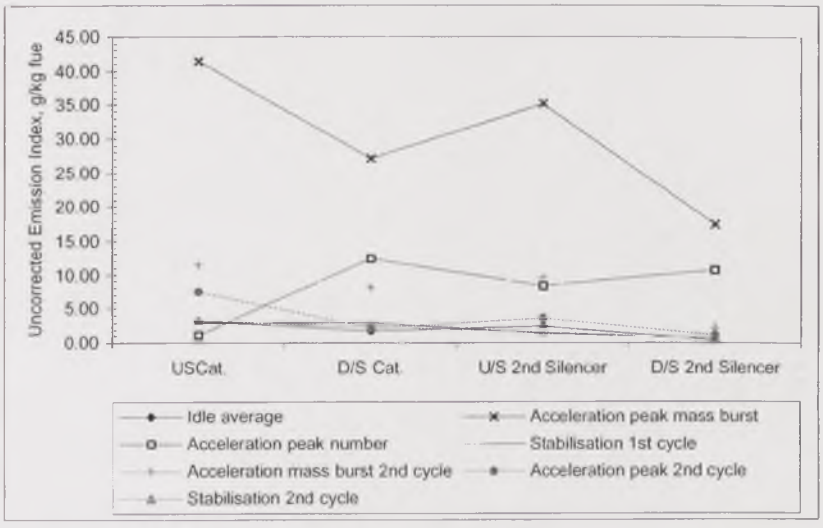

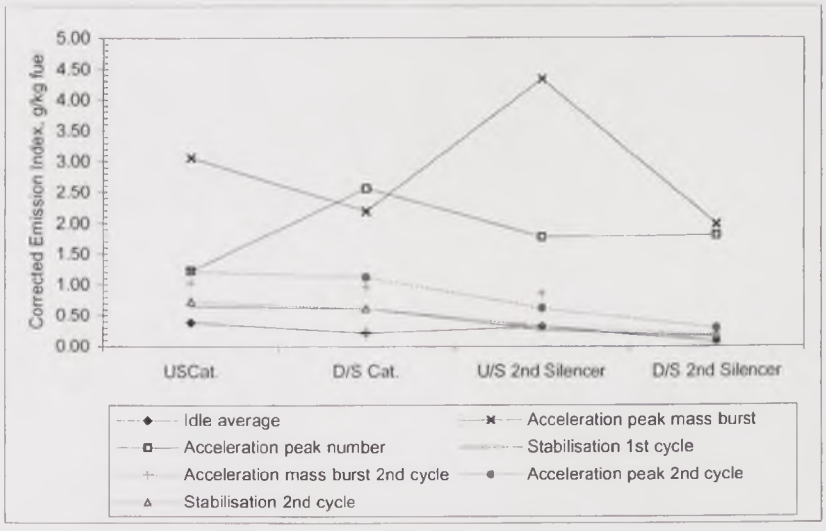

Figure 5.13. Total number and mass concentrations vs. location in the exhaust system for the main events of the acceleration to high-speed conditions, 3500rpm – 15kW, after a 4-hour Idle preconditioning.

5.3.2.1.1. Idle preconditioning scenario

The exhaust aerosol was sampled during idle periods in order to obtain a baseline for the subsequent acceleration cycles. The total particle number concentration of the exhaust aerosol leaving the engine at these conditions was 7.88×10^6 cm^{-3}, which converted to an Emission Index of 3.22 g/kg fuel or 0.38 g/kg fuel, uncorrected or corrected, respectively.

Through the catalyst, the number concentration decreased to 5.08×10^6 cm^{-3} (by 36%) and the Emission Index, to 1.85 g/kg fuel (by 43%) or 0.21 g/kg fuel (by 45%). This decrease occurred for all size ranges, as shown in Figure 5.15., and was presumably due to different processes, depending on the particle size. Very fine particles, below 0.1μm, mainly tend to diffuse and undergo thermophoretic deposition onto the walls and those larger than 1.0μm experience mostly gravimetric and inertial deposition. Particles in the mid-size range have higher transport efficiency, and no significant deposition was thus expected. There was no evidence of coagulation through the catalyst in the size range measured.

The total particle number concentration increased through the first silencer to 8.40×10^6 cm^{-3} (a 65% increase). The Emission Index also increased, to 2.39 g/kg fuel (by 29%), uncorrected; or 0.31 g/kg fuel (by 48%), corrected. The important increase in mass indicated that particulate was formed by nucleation and condensation, and also reentrained from the silencer walls. Ultrafine particle formation took place, and large particles were reentrained. The concentration of mid-sized particles did not change significantly.

Through the second silencer, there was a significant decrease, by 75%, in the total particle number concentration, to 2.05×10^6 cm^{-3}, and in Emission Index, to 0.43 g/kg fuel or 0.07 g/kg fuel (by 82% or 77%, in uncorrected or corrected Emission Index, respectively). This indicated that even after a 4-hour conditioning period, the second silencer still preserved a large capacity for particulate deposition on its walls. The deposition occurred for all size ranges and it was more significant for particles below 0.1μm and above 1.0μm than for middle-sized particles.

In summary, the baseline idle scenario from which the acceleration cycles were run showed a reduction in particle number and Emission Index for all particle sizes through the catalyst and the second silencer. Through the first silencer, ultrafine particle formation occurred. The combined processes affected the particle size distribution modes only through the catalyst, where it shifted slightly towards finer sizes.

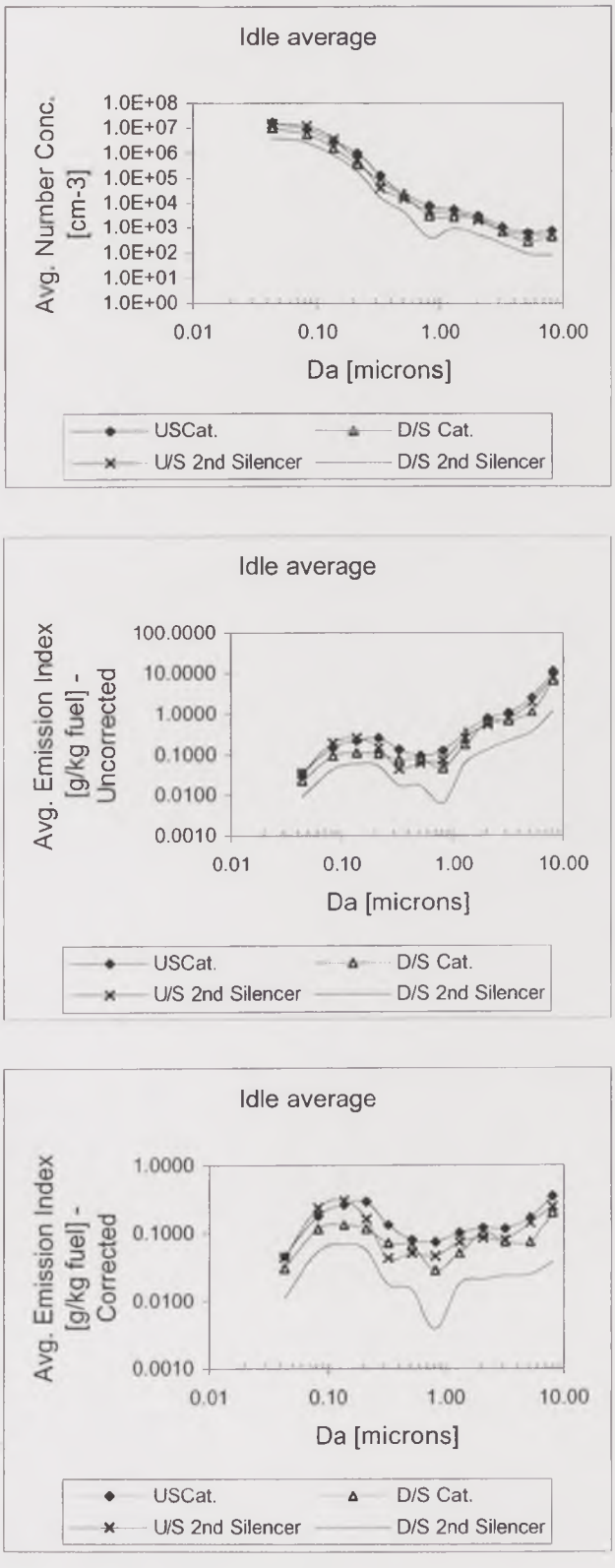

Figure 5.14. Particle size distribution at idle

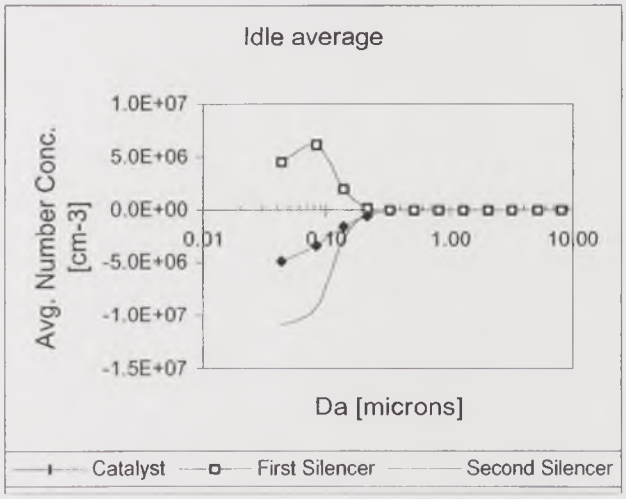

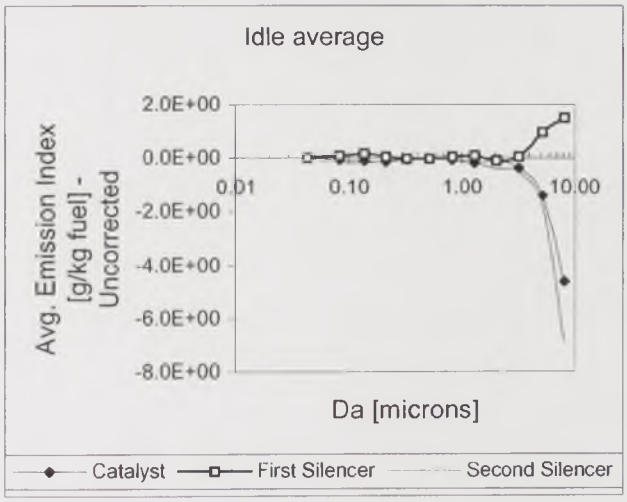

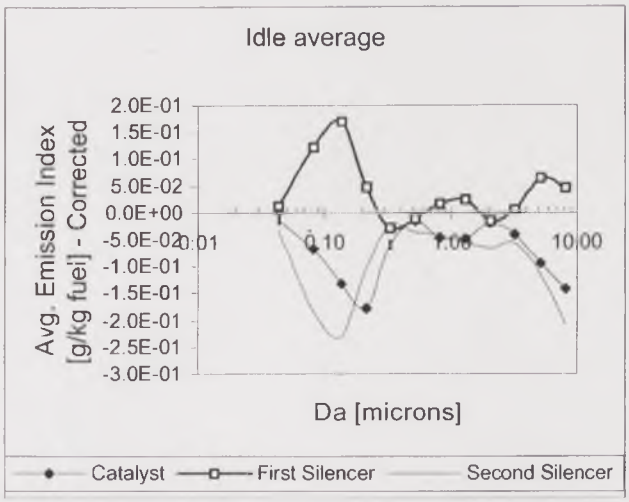

Figure 5.15. Particulate blow-out for various size ranges at Idle.

The opposite behaviour of the particulate matter through the devices was observed very often in different events during previous cold start tests, indicating

that this was the natural trend of particulate matter through the system. The changes indicated that the situation was quite dynamic, and the deposition and release processes, together with particulate formation by gas-to-particle processes and coagulation, represented a significant fraction of the emissions.

5.3.2.1.2. Acceleration mass burst, both cycles

The disturbance introduced to the engine and the exhaust system at the start of an acceleration cycle causes a particulate mass (Emission Index) increase that reaches a local maximum in time, even before the speed and power condition had not been reached by the engine. This is previous to the peak in particle number concentration and, as it will be seen, the significance of the first mass burst, relative to the Emission Index at the number peak event varied. Sometimes the Emission Index was significantly higher in the first mass burst than in the peak number, sometimes it was much lower, and sometimes they were nearly at the same level. Perhaps the relationship between the Emission Index values in both events was given by the aggressiveness of the acceleration. These results indicate that mass emissions were controlled by the blow out of large particles from wall agglomerates and the peak number was controlled by fine (<0.1μm) particles.

At the entrance to the exhaust system, the total particle number concentration was 1.79×10^7 cm^{-3}, 2.2 times as high as the idle concentration at that sampling point. The corresponding Emission Index was 41.43 g/kg fuel, uncorrected, or 3.06 g/kg fuel, corrected, nearly 13 and 8 times as high as the respective Emission Index at idle. At this point it is interesting to make a comparison with the corresponding event in the second cycle. In it, the total particle number concentration was 1.36 $\times 10^7$ cm^{-3}, 76% of that of the same event in the first cycle. On the other hand, the Emission Index was 28% or 34% of that of the first cycle. These figures show that the duration of the idle preconditioning did affect the deposition layer of the system upstream of the catalyst (including the combustion chamber, exhaust valves, the turbocharger and the EGR system), and this layer was affected by the acceleration.

In the first cycle, the catalyst did not reduce the particle number concentration but, in contrast, this increased to 2.11×10^7 cm^{-3}, by 18%. However, this did not imply an increase in the Emission Index, which on the contrary decreased to 27.12 g/kg fuel, uncorrected, or 2.19 g/kg fuel, corrected (by 35% and 28%, respectively). The contrasting trends between particle number concentration and Emission Index was due to the distinct behaviour of particles of different sizes, as seen in Figures 5.16. and 5.17. Only ultrafine particles, smaller than 0.2μm, left the catalyst in higher numbers than those entering, presumably because of nucleation, so particles in this size range dominated the increase in total particle number concentration. In

contrast, the number of larger particles decreased, owing mainly to deposition of very large particles (~8μm) and mid-sized particles, causing the decrease in Emission Index.

		USCat.	D/S Cat.	U/S 2nd Silencer	D/S 2nd Silencer
Avg. Number Conc. [cm-3]	Acceleration peak mass burst	1.79E+07	2.11E+07	3.22E+07	2.34E+07
	Acceleration mass burst 2nd cycle	1.36E+07	2.32E+07	2.38E+07	1.04E+07
Avg. Emission Index [g/kg fuel]	Acceleration peak mass burst	41.43	27.12	35.16	17.49
- Unit density	Acceleration mass burst 2nd cycle	11.48	8.21	9.55	2.22
Avg. Emission Index [g/kg fuel]	Acceleration peak mass burst	3.06	2.19	4.33	1.98
- Corrected density	Acceleration mass burst 2nd cycle	1.03	0.96	0.86	0.29

Table 5.1. Comparison between the first and second acceleration cycles regarding the acceleration mass burst event, 3500rpm – 15kW.

In the second cycle, the catalyst also caused an increase in particle number concentration, this time to 2.32×10^7 cm^{-3}, by 71%, which was much higher than the increase in the first cycle. The Emission Index increased by a similar fraction to that in the first cycle, when uncorrected, by 29%, to 8.21 g/kg fuel. However, the corrected Emission Index decreased just by 7%, to 0.96 g/kg fuel, much lower than the decrease by 18% in the first cycle. This disagreement was due to the distinct behaviour of particles according to their size. In the first mass burst of the second acceleration cycle, particles between 0.2μm and 0.4μm were emitted from the catalyst in higher numbers than those entering, which did not occur in the first cycle, making the total number concentration increase more significantly and the corrected Emission Index decrease less significantly than in the first cycle.

Through the first silencer, the total particle number concentration increased to 3.22×10^7 cm^{-3} in the first cycle, and to 2.38×10^7 cm^{-3} in the second silencer, which represented an increase by 53% and 3%, respectively. The uncorrected Emission Index also increased, by 30% and 16% in the first and second cycles respectively, to 35.16 g/kg fuel and 9.55 g/kg fuel, also respectively. The corrected Emission Index increased in the first cycle by 98%, to 4.33 g/kg fuel, but decreased in the second cycle by 11%, to 0.86 g/kg fuel. The changes through the first silencer were more significant in the first cycle than in the second, and the size dependent behaviour of the particles also differed between both cycles. In the first cycle, particles of all sizes, only excepting those around 0.035μm, were emitted in higher numbers than those entering the silencer, as a result of nucleation, condensation and resuspension processes. In the second cycle, in contrast, only particles around 0.04μm and those

higher than 4.0μm were emitted in slightly higher numbers than those entering, whereas the number of mid-sized particles was slightly reduced through the silencer. Comparatively, the changes through the silencer in the second cycle were much less significant in net mass change (not in mass percentage) than in the first cycle in this event.

Through the second silencer, the total particle number concentration decreased by 27% in the first cycle, to 2.34×10^7 cm^{-3}, nearly the same value as that upstream of the first silencer. In the second cycle, it decreased to an even lower value, 1.04×10^7 cm^{-3}, which is a decrease by more than 50%. The uncorrected Emission Index decreased by 50% in the first cycle, to 17.49 g/kg fuel, and by 77%, to 2.22 g/kg fuel, in the second cycle. When corrected, the decrease showed similar significance, by 54% in the first cycle, to 1.98 g/kg fuel, and by 66% in the second cycle, to 0.29 g/kg fuel. This is evidence that through the second silencer the particles tended to be deposited very effectively on the walls, in contrast to the more significant particle formation and resuspension characteristics from the first silencer. In both cycles, the number of particles and therefore the Emission Index decreased for all size ranges.

In summary, the behaviour of the particles through the second silencer was a nearly perfect mirror of that described through the first silencer. The deposition and formation/resuspension processes occurred off-phase between both silencers, as seen in many occasions during cold start tests. The increase in particle number concentration and Emission Index through the first silencer occurred at the same time as the decrease through the second silencer and changes in both devices were exactly opposite to each other even by size, as can be seen in the particulate blow-out vs. particle size profiles in Figure 5.17. In the first cycle, the particle size distribution shifted towards smaller sizes through the first silencer, but did not change significantly through the catalyst and the second silencer. In the second cycle, no significant change in particle size distribution was observed through the exhaust system.

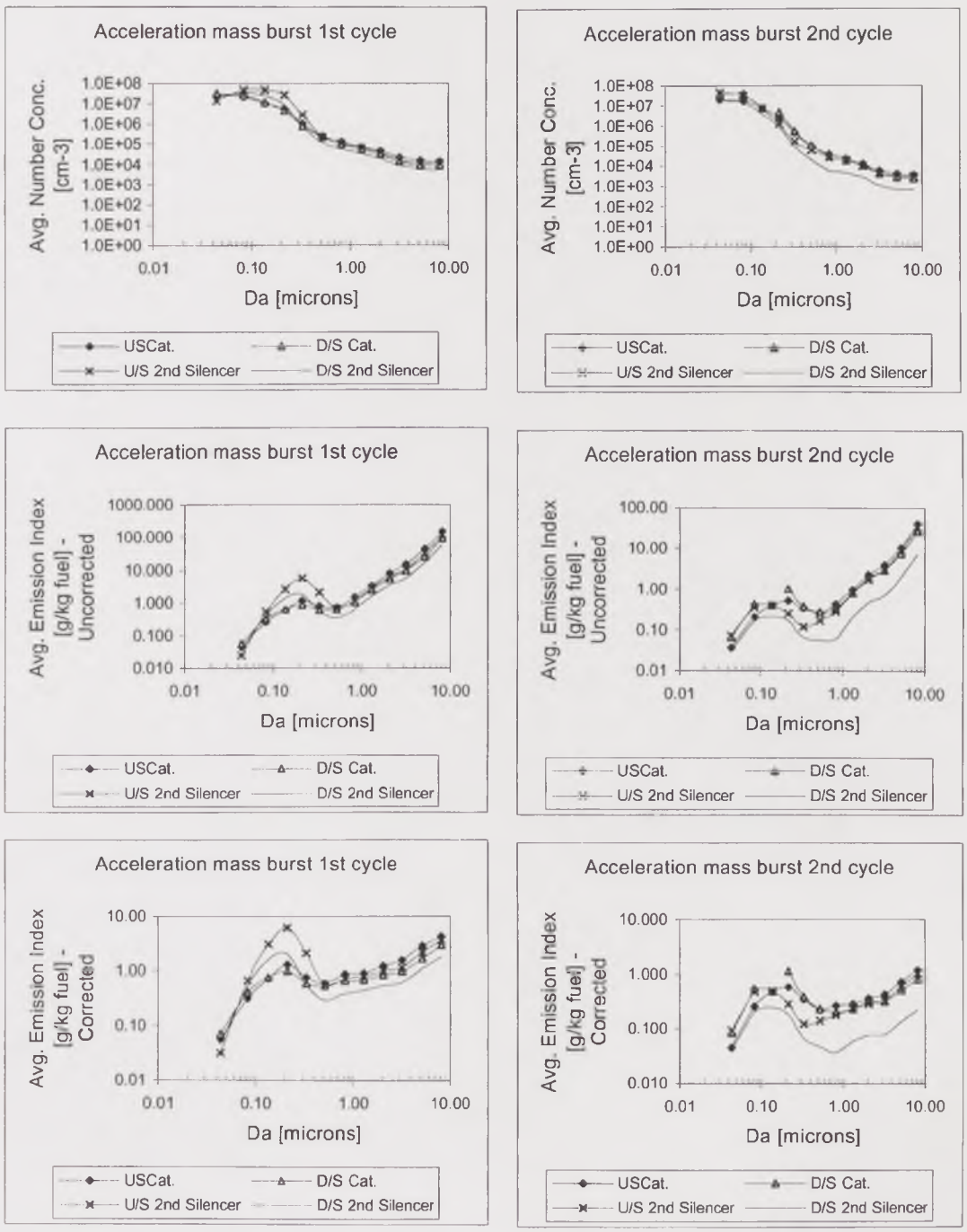

Figure 5.16. Particle size distribution for the mass burst event of the acceleration cycles, 3500rpm – 15kW.

5.3.2.1.3. Acceleration number peak, both cycles

The acceleration number peak occurred once the target speed/power condition was reached. The increase in number with respect to the mass burst event was very significant in the first acceleration cycle and only slightly significant in the second cycle, for all sampling points. At the entrance to the exhaust system, the number

concentration peak was 6.06×10^7 cm^{-3} in the first cycle and just 2.57×10^7 cm^{-3} in the second cycle.

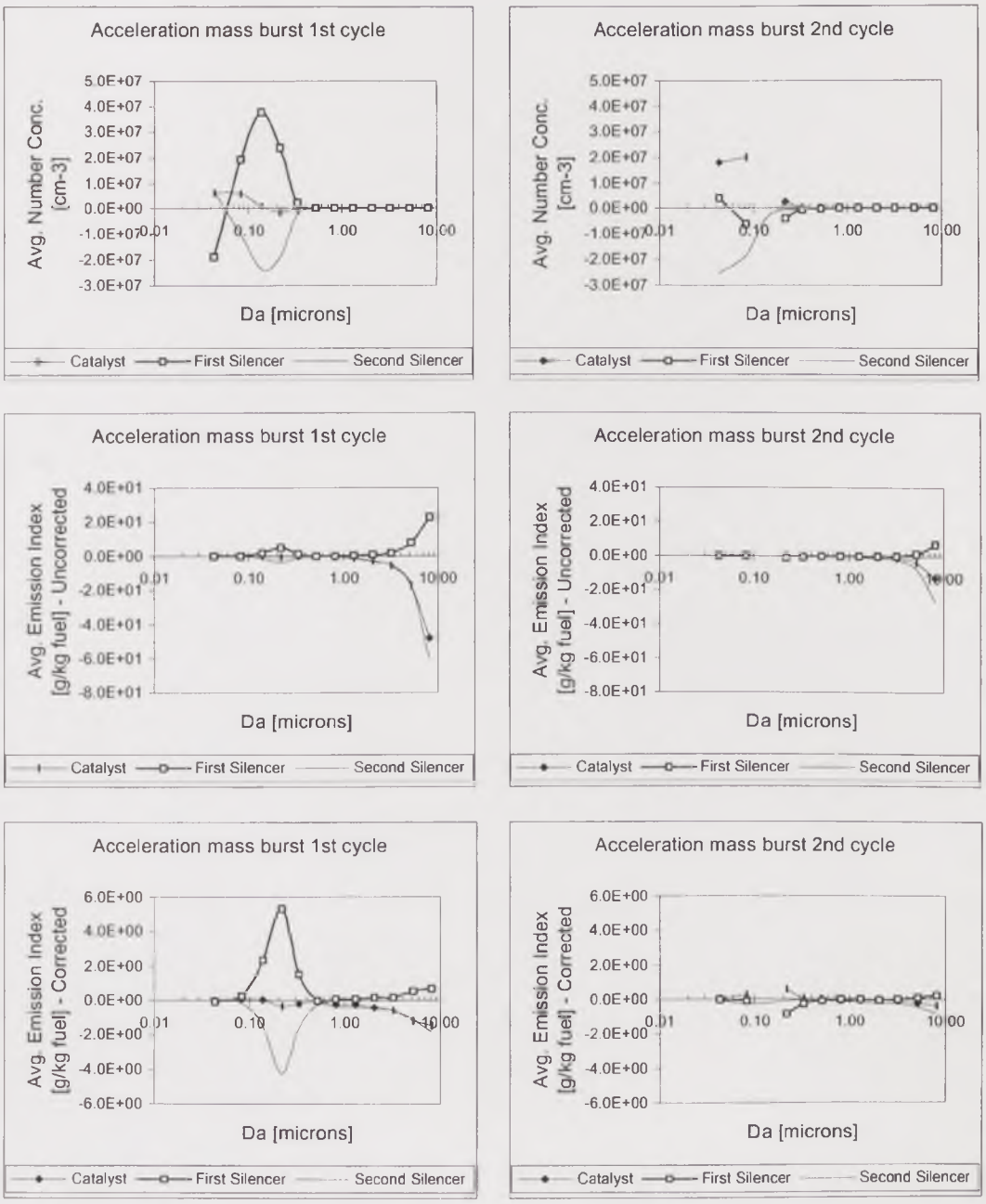

Figure 5.17. Particulate blow-out for various size ranges at the mass burst events for both acceleration cycles, 3500rpm – 15kW.

The uncorrected Emission Index was 1.14 g/kg fuel in the first cycle and 7.55 g/kg fuel in the second. The corrected Emission Index was 1.23 g/kg fuel in the first cycle and 1.22 g/kg fuel in the second. The size distribution in the number peak was characterised by a smaller size distribution mode than that measured at idle condition and in the mass-burst event for all sampling points, although this is not

easy to see in the number size distribution charts, but is seen when the Emission Index is calculated.

		USCat.	D/S Cat.	U/S 2nd Silencer	D/S 2nd Silencer
Avg. Number Conc. [cm-3]	Acceleration peak number	6.06E+07	6.99E+07	5.20E+07	2.65E+07
	Acceleration peak 2nd cycle	2.57E+07	3.07E+07	2.90E+07	1.33E+07
Avg. Emission Index [g/kg fuel]	Acceleration peak number	1.14	12.38	8.34	10.69
- Unit density	Acceleration peak 2nd cycle	7.55	2.22	3.59	1.14
Avg. Emission Index [g/kg fuel]	Acceleration peak number	1.23	2.55	1.77	1.80
- Corrected density	Acceleration peak 2nd cycle	1.22	1.11	0.61	0.28

Table 5.2. Comparison between the first and second acceleration cycles regarding the peak number event.

The total number concentration increased through the catalyst, by 15% in the first cycle, to 6.99×10^7 cm^{-3}, and by 20% in the second cycle, to 3.07×10^7 cm^{-3}. However, the Emission Index showed different trends from one cycle to the other. In the first cycle, the uncorrected Emission Index increased to 12.38 g/kg fuel, nearly 11 times the value upstream of the catalyst, although it was just more than twice that value for the corrected Emission Index, 2.55 g/kg fuel. In the second cycle, in contrast, the Emission Index decreased by 71% when uncorrected and by 9% when corrected, reaching 2.22 g/kg fuel or 1.11 g/kg fuel, respectively. The change in trends between total number and total Emission Index in the second cycle was due to the relative contributions of the various size ranges. Particles larger than 1.0μm deposited through the catalyst in the peak number event of the second cycle, whereas in the first cycle the evidence indicated that they had been blown out from the catalyst. Particles below 1.0μm increased in Emission Index through the catalyst in both cycles, more significantly in the second than in the first cycle, as shown in Figure 5.18. The increase was related to gas-to-particle formation and coagulation processes.

Through the first silencer, the total number concentration decreased by 26%, to 5.20×10^7 cm^{-3} in the first cycle, and by 5%, to 3.07×10^7 cm^{-3} in the second cycle. The uncorrected Emission Index decreased by 33%, to 8.34 g/kg fuel in the first cycle, but decreased in the second cycle by 62%, to 3.59 g/kg fuel. And the corrected Emission Index decreased by 31%, to 1.77 g/kg fuel in the first cycle, and by 45%, to 0.61 g/kg fuel, in the second cycle. Hence, the only increase through the first silencer occurred for the Emission Index in the second cycle, as a consequence of the blow-out of large particles, i.e. larger than 1.0μm, which dominated the total Emission Index, giving an overall increase as a result. For the total number

concentration and the corrected Emission Index, this blow-out of large particles became unimportant. Particles smaller than 1.0μm deposited through the first silencer in both cycles.

The total particle number concentration decreased through the second silencer by 49% in the first cycle, to $2.65x10^7$ cm^{-3}, and by 54%, to $1.33x10^7$ cm^{-3}, in the second cycle. The uncorrected Emission Index, however, increased by 28% in the first cycle, to 10.69 g/kg fuel, but decreased by 68%, to 1.14 g/kg fuel, in the second cycle. When corrected, the Emission Index increased just by 2% in the first cycle, to 1.80 g/kg fuel, and decreased by 53% in the second cycle, to 0.28 g/kg fuel. The main difference between cycles was that particles larger than 1.0μm deposited through the silencer in the event during first cycle and were blown out from it in the corresponding event of the second cycle. Particles smaller than 1.0μm deposited through the silencer in both cycles, with the only exception of some particles around 0.2μm – 0.3μm, which increased in number concentration by coagulation in the first cycle.

In summary, the acceleration peak number event showed mid-sized particle numbers increasing through the catalyst, presumably because of coagulation of ultrafine particles (those not measured by the ELPI), and decreasing through both silencers. Large particles, larger than 1.0μm, deposited through the second silencer when blown out from the first silencer and vice versa, showing that the dominant deposition and resuspension mechanisms are very different through these two devices. In the second cycle, the particle size distribution shifted towards smaller sizes as a result of combined processes.

5.3.2.1.4. Stabilisation, both cycles

The stabilisation event gave very similar results for both cycles throughout the catalyst, as summarised in Table 5.3. The particle number concentration upstream of the catalyst, starting point for this analysis, was identical for both cycles, $2.14x10^7$ cm^{-3}. The uncorrected Emission Index was 3.00 g/kg fuel for the first cycle and 3.19 g/kg fuel for the second cycle, which diverged because of slight differences in the particle size distributions. Likewise, the corrected Emission Index was 0.65 g/kg fuel for the first cycle and 0.72 g/kg fuel for the second silencer.

Through the catalyst, the particle number concentration increased by 12% in the first cycle and by 9% in the second cycle, reaching $2.40x10^7$ cm^{-3} and $2.32x10^7$ cm^{-3}, respectively. Despite this increase, the uncorrected Emission Index actually decreased, by just 1% in the first cycle and by 21% in the second cycle, to 2.99 g/kg fuel and 2.52 g/kg fuel, respectively, because of deposition of very large particles.

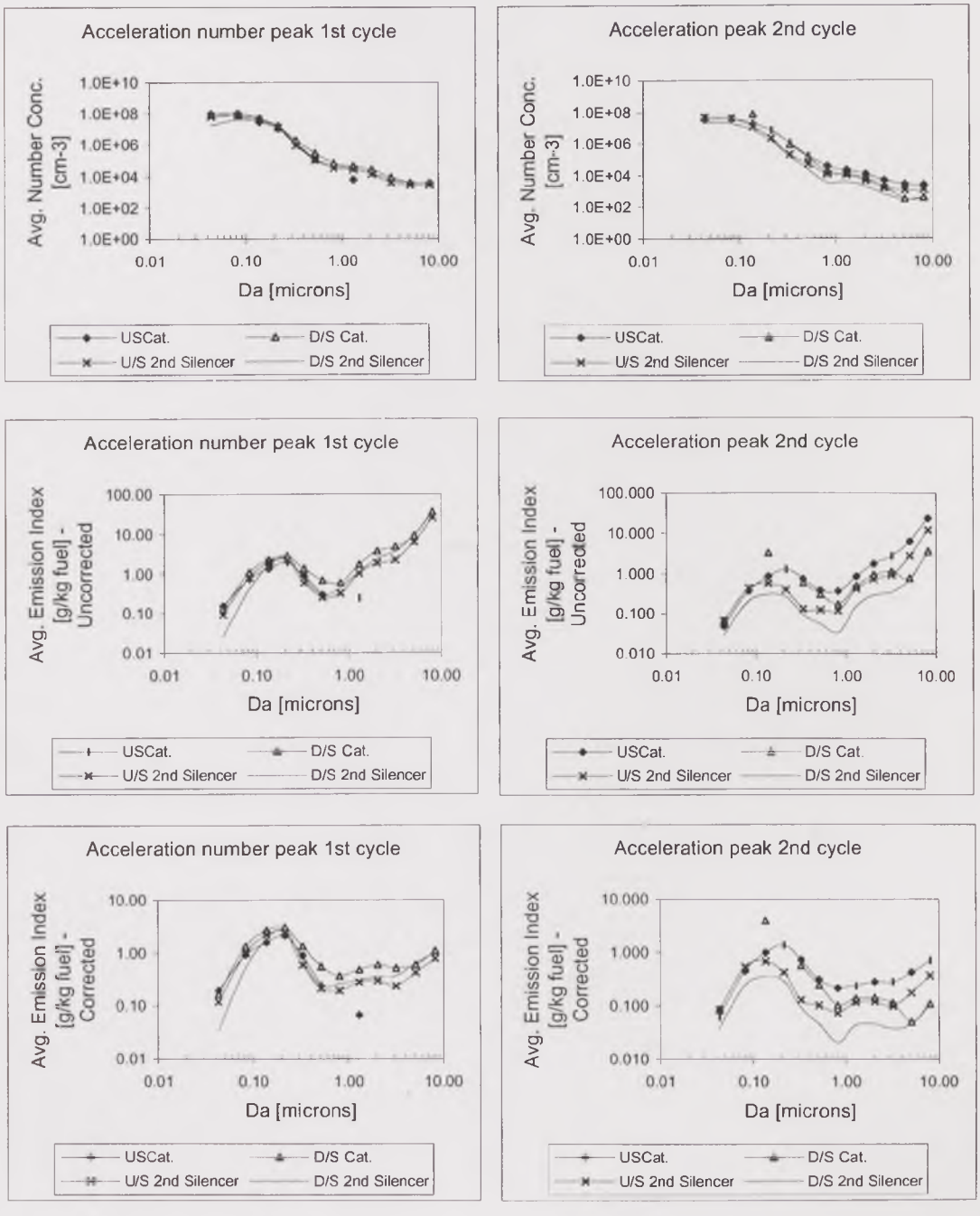

Figure 5.18. Particle size distribution for the peak number events of the acceleration cycles, 3500rpm – 15kW.

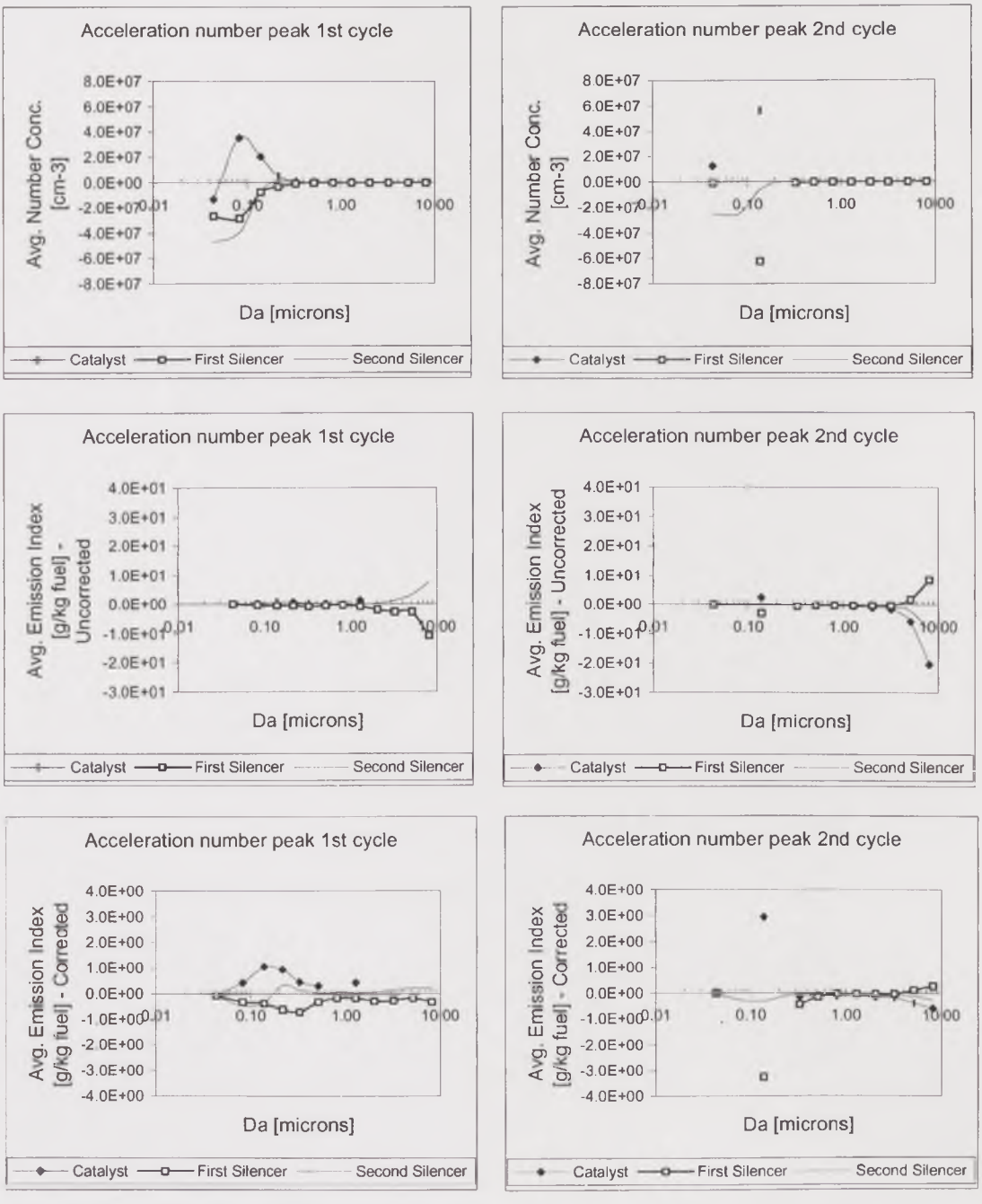

Figure 5.19. Particulate blow-out for various size ranges at the peak number events for both acceleration cycles, 3500rpm – 15kW.

When corrected, the decrease in Emission Index was by 6% and 15%, to 0.61 g/kg fuel and 0.62 g/kg fuel, for the first and second cycles, respectively. The changes occurred nearly in an identical manner for both cycles; particles below 0.1μm increased their number concentration, presumably by gas-to-particle conversion and coagulation, whereas those between 0.1μm and 1.0μm deposited through the catalyst. Larger particles were blown out from the catalyst, except those around 10μm, which deposited. These very large particles originated the largest

difference observed, since they deposited more effectively during the second cycle than during the first cycle.

		USCat.	D/S Cat.	U/S 2nd Silencer	D/S 2nd Silencer
Avg. Number Conc. [cm-3]	Stabilisation	2.14E+07	2.40E+07	1.53E+07	9.51E+06
	Stabilisation 2nd cycle	2.14E+07	2.32E+07	1.83E+07	1.17E+07
Avg. Emission Index [g/kg fuel]	Stabilisation	3.00	2.99	1.43	0.64
- Unit density	Stabilisation 2nd cycle	3.19	2.52	1.56	0.68
Avg. Emission Index [g/kg fuel]	Stabilisation	0.65	0.61	0.26	0.16
- Corrected density	Stabilisation 2nd cycle	0.72	0.62	0.32	0.19

Table 5.3. Comparison between the first and second acceleration cycles regarding the stabilisation event.

The particle number concentration decreased through the first silencer by 36% in the first cycle and by 21% in the second cycle, to 1.53×10^7 cm^{-3} and to 1.83×10^7 cm^{-3}, respectively. This also caused a decrease in the uncorrected Emission Index by 52% in the first cycle and by 38% in the second cycle, to 1.43 g/kg fuel and 1.56 g/kg fuel, respectively. The decrease in the corresponding corrected Emission Index was somewhat higher, by 57% in the first cycle and 49% in the second cycle, to 0.26 g/kg fuel and 0.32 g/kg fuel, respectively. The higher decrease in the first cycle was dominated by particles smaller than 0.1μm. Larger particles had practically identical changes in both cycles, with the only exception of particles around 8μm, the concentration of which decreased more significantly in the first cycle than in the second.

Finally, through the second silencer, the particle number concentration decreased by 38% in the first cycle, to 9.56×10^6 cm^{-3}, and by 36% in the second cycle, to 1.17×10^7 cm^{-3}. The decrease in the uncorrected Emission Index was nearly identical in both cycles, by 55% and 56%, to 0.64 g/kg fuel and 0.68 g/kg fuel. The corrected Emission Index decreased by 38% and 34%, to 0.16 g/kg fuel and 0.19 g/kg fuel, in the first and second cycles, respectively.

In summary, particle deposition throughout the exhaust system was the main feature during the stabilisation event in both cycles. Only through the catalyst, particles smaller than 0.1μm and those between 1.0μm and 8.0μm increased in number, presumably by the coagulation of newly formed particles, which were originated from outgassed components. The particle size distribution shifted slightly towards smaller sizes through the first silencer.

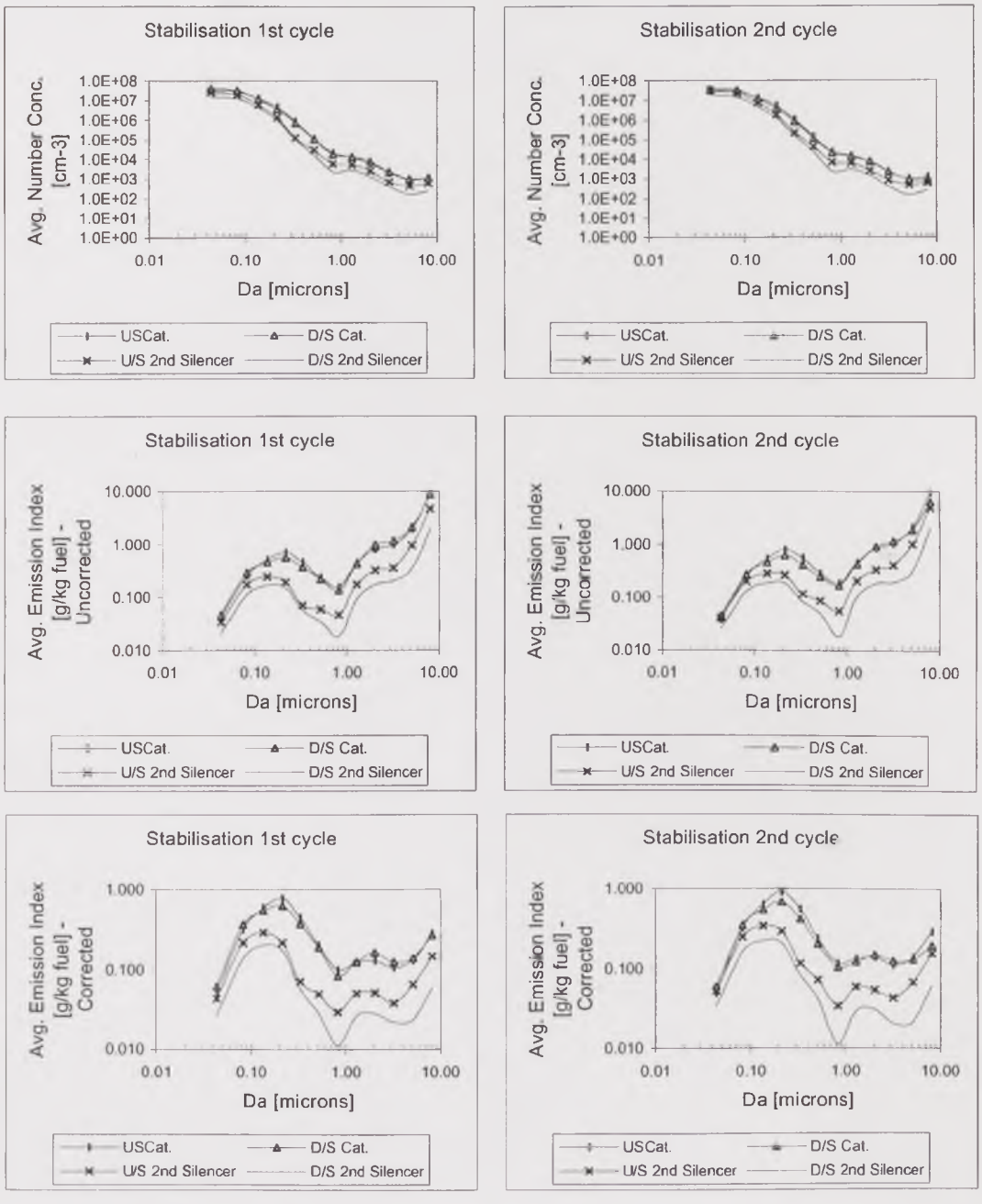

Figure 5.20. Particle size distribution for the stabilisation events of the acceleration cycles, 3500rpm – 15kW.

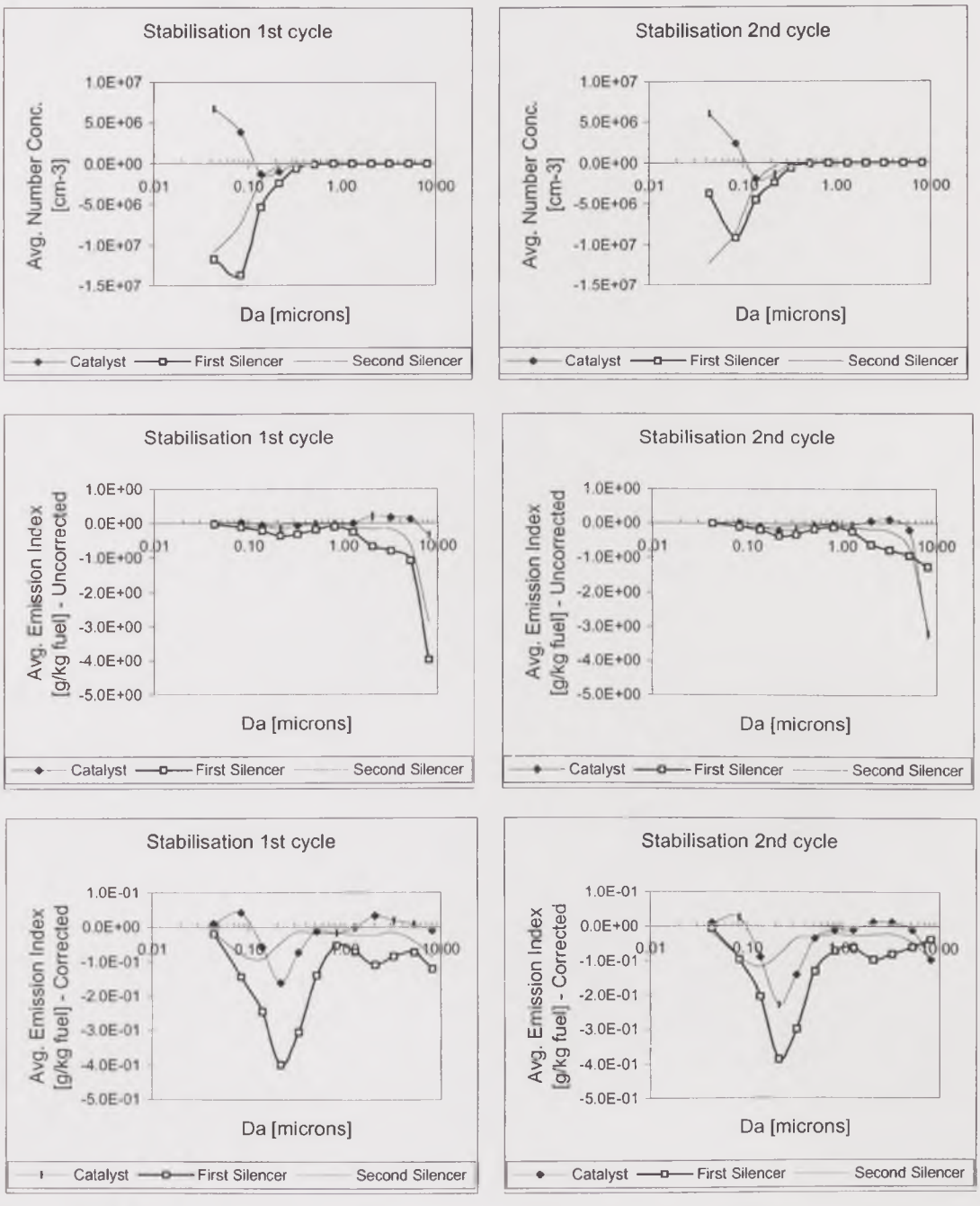

Figure 5.21. Particulate blow-out for various size ranges at the stabilisation events for both acceleration cycles, 3500rpm – 15kW.

5.3.2.2. Acceleration from Idle to 2250rpm – 15kW

The total particle number concentration and Emission Index for the acceleration tests to 2250rpm - 15kW after a 4-hour conditioning period are plotted against time in Figure 5.22., where each line corresponds to one of the four sampling points. Also, the changes through the three sections, namely catalyst, first silencer and second silencer, are plotted as a particulate blow-out, so that positive values

represent an increase in the corresponding parameter through the device, and negative values, a decrease, or deposition.

The profiles against time showed the same basic characteristics as those observed during acceleration to 3500rpm - 15kW, namely a mass burst at the beginning of each acceleration cycle, followed by a peak number and then a stabilisation in both total number concentration and Emission Index. The stabilisation event, however, took more time to be reached in this low-speed condition than at high-speed condition, mainly because of the influence of the EGR system and the instabilities created by the higher breaking effort in the dynamometer. This was reflected by fluctuations in the emissions after the peak number event.

As in the acceleration tests to 3500rpm - 15kW, the number peak and mass burst events of the acceleration to 2250rpm - 15kW showed higher levels in the first cycle than in the second, although the difference was less significant for the latter condition in most cases. Nevertheless, in the case of the second silencer the number concentration in the peak number event of the first cycle was lower than that of the second cycle, but the Emission Index showed the opposite result.

A new interesting feature was observed in two of the profiles shown in Figure 5.22., namely downstream of the catalyst and downstream of the second silencer. There was a significant increase in both particle number concentration and Emission Index when starting the deceleration, at the end of the first cycle. This occurred when the speed was taken down significantly more quickly than the load from the engine by the manual control of the dynamometer.

In the same way as the acceleration tests to 3500rpm - 15kW, the speed profiles are plotted against time in Figure 5.23., for the acceleration to 2250rpm - 15kW, showing the variability in the manual control of the speed during transient tests when using the hydraulic dynamometer. Also, the particle number concentration and Emission Index for the main events of both cycles against the position in the exhaust system are shown in Figure 5.24.

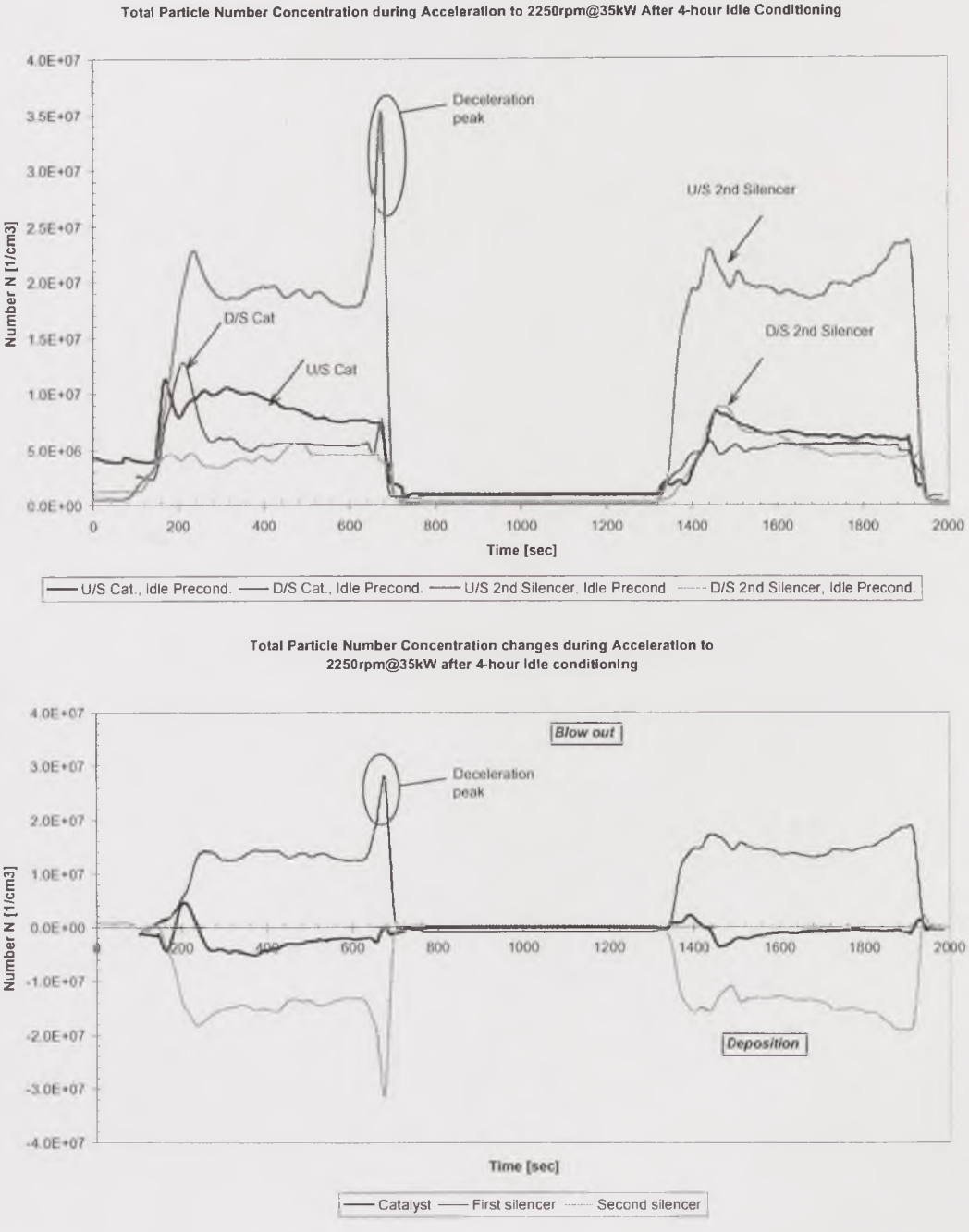

Figure 5.22. Total number and mass concentrations vs. time during acceleration to low-speed conditions, 2250rpm – 15kW, after a 4-hour Idle preconditioning at various points through the exhaust system. a) Particle number concentration.

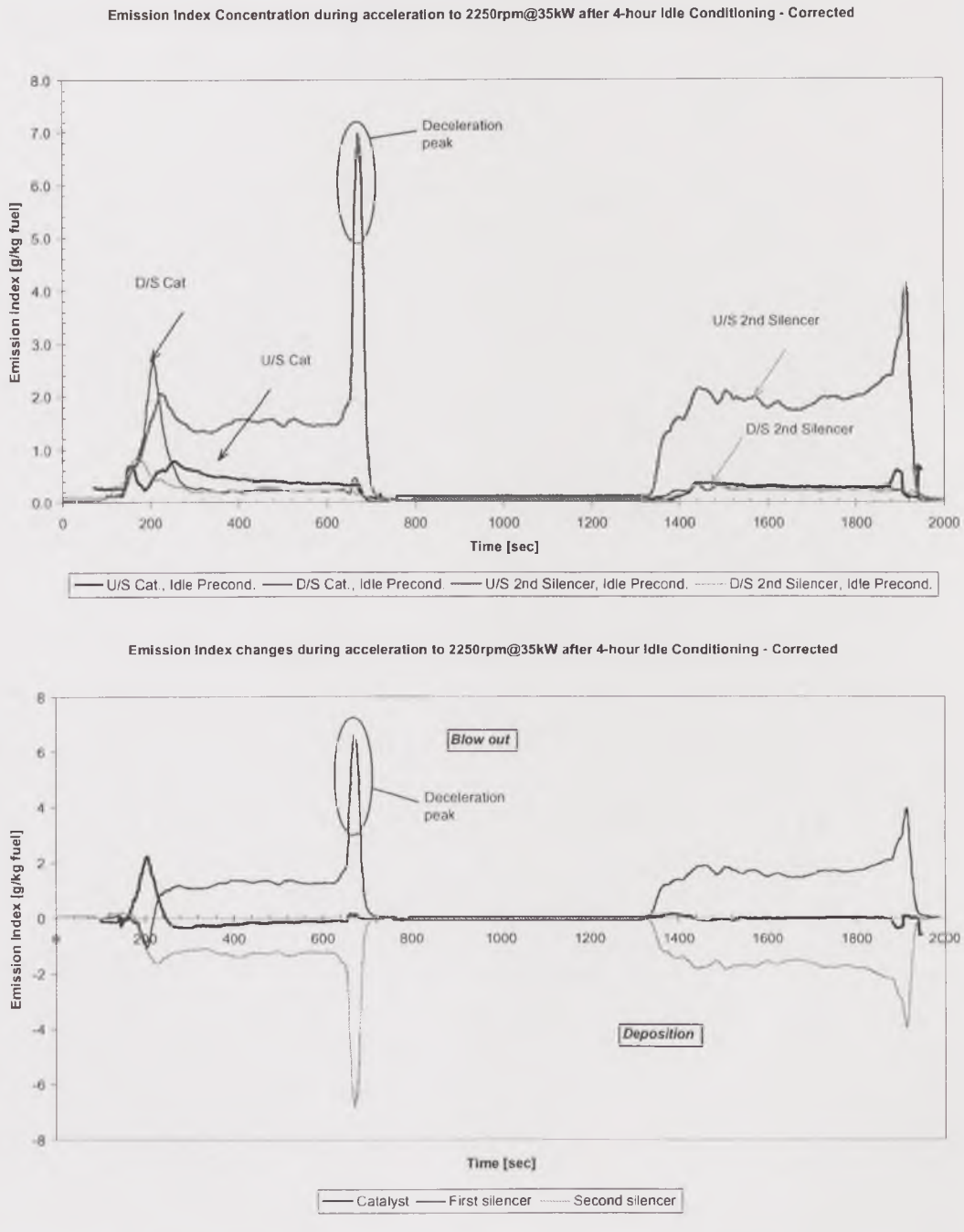

Figure 5.22. Total number and mass concentrations vs. time during acceleration to low-speed conditions, 2250rpm – 15kW, after a 4-hour Idle preconditioning at various points through the exhaust system. b) Corrected Emission Index.

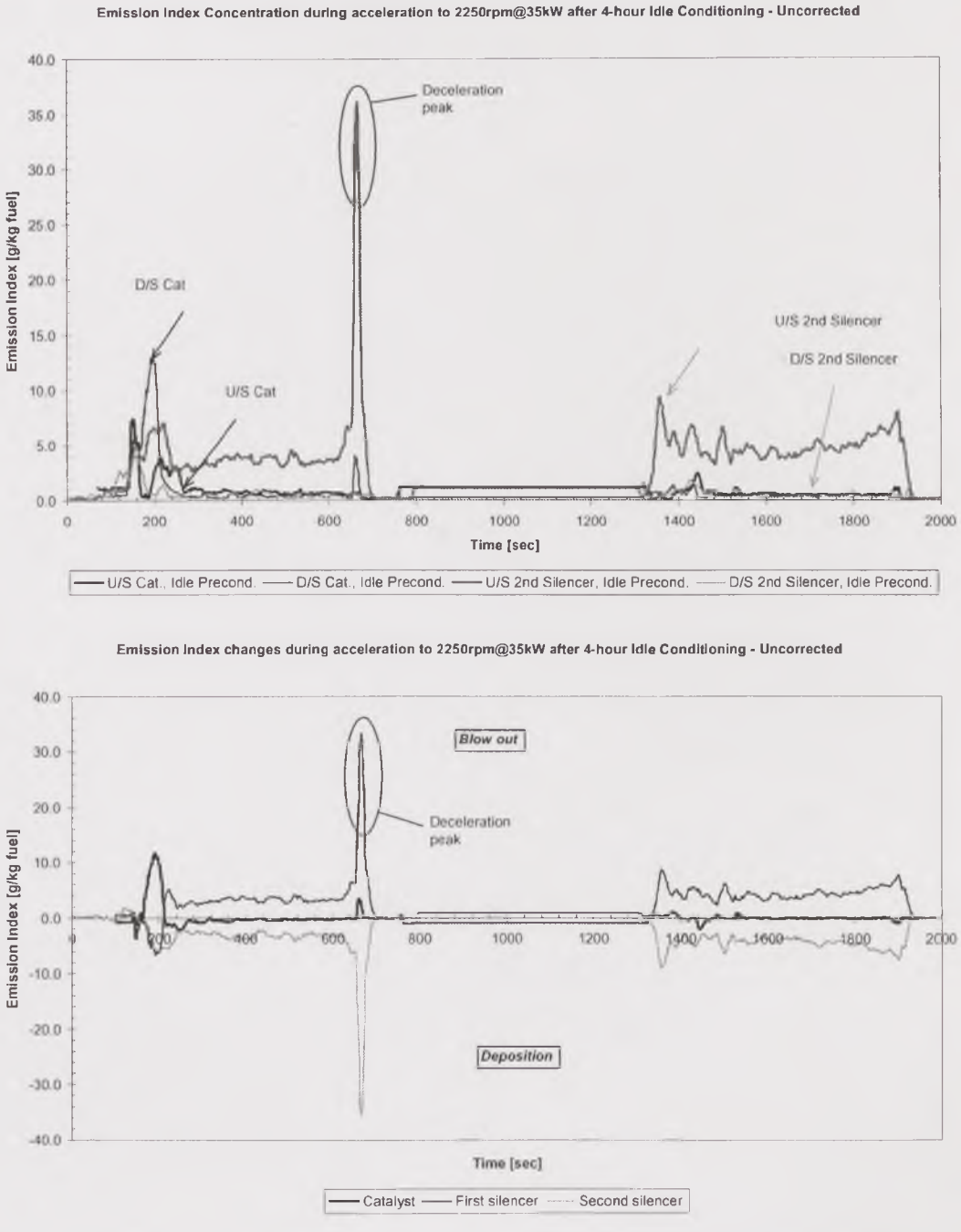

Figure 5.22. Total number and mass concentrations vs. time during acceleration to low-speed conditions, 2250rpm – 15kW, after a 4-hour Idle preconditioning at various points through the exhaust system. c) Uncorrected Emission Index.

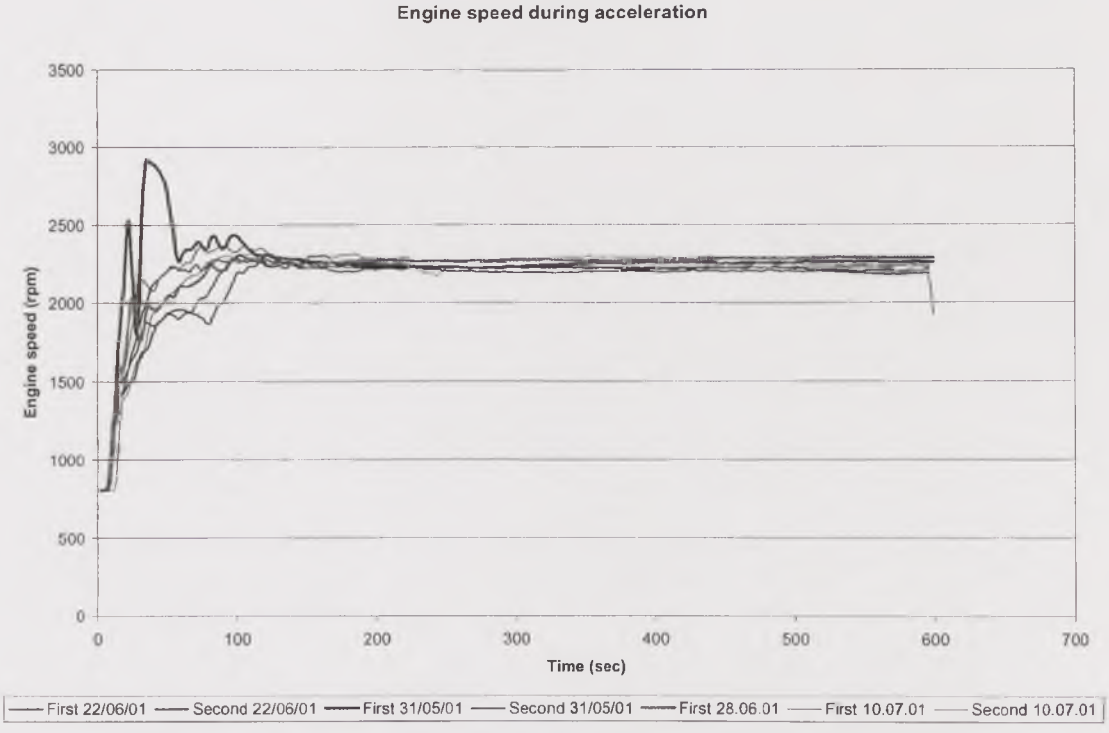

Figure 5.22. Speed vs. time profiles for several acceleration cycles to 2250rpm - 15kW. The deceleration was not recorded.

5.3.2.2.1. Preconditioning at idle

The starting point of the test, idle condition, showed an aerosol entering the exhaust system with a total particle number concentration of $2.0x10^6$ cm^{-3}, an uncorrected Emission Index of 0.77 g/kg fuel and a corrected Emission Index of 0.14 g/kg fuel. Through the catalyst, the particle number concentration increased to $5.5x10^6$ cm^{-3} (nearly three-fold) and the Emission Index, to 1.18 g/kg fuel (53% increase) when uncorrected and to 0.65 g/kg fuel (more than three-fold) when corrected. The increase occurred for all size ranges, with the exception of those between 3.0μm and 5.0μm, which underwent not a very significant decrease in number concentration and Emission Index. The increase was presumably due to nucleation and coagulation of particles, since the temperature along the system at idle was low.

Through the first silencer, the particle number concentration decreased dramatically, by one order of magnitude, to $5.4 x10^5$ cm^{-3}. The uncorrected Emission Index decreased to 0.18 g/kg fuel (a decrease by 85%) and the corrected Emission Index, to 0.04 g/kg fuel (a decrease by 94%). The changes were exactly the opposite of those through the catalyst and occurred by deposition for all size ranges.

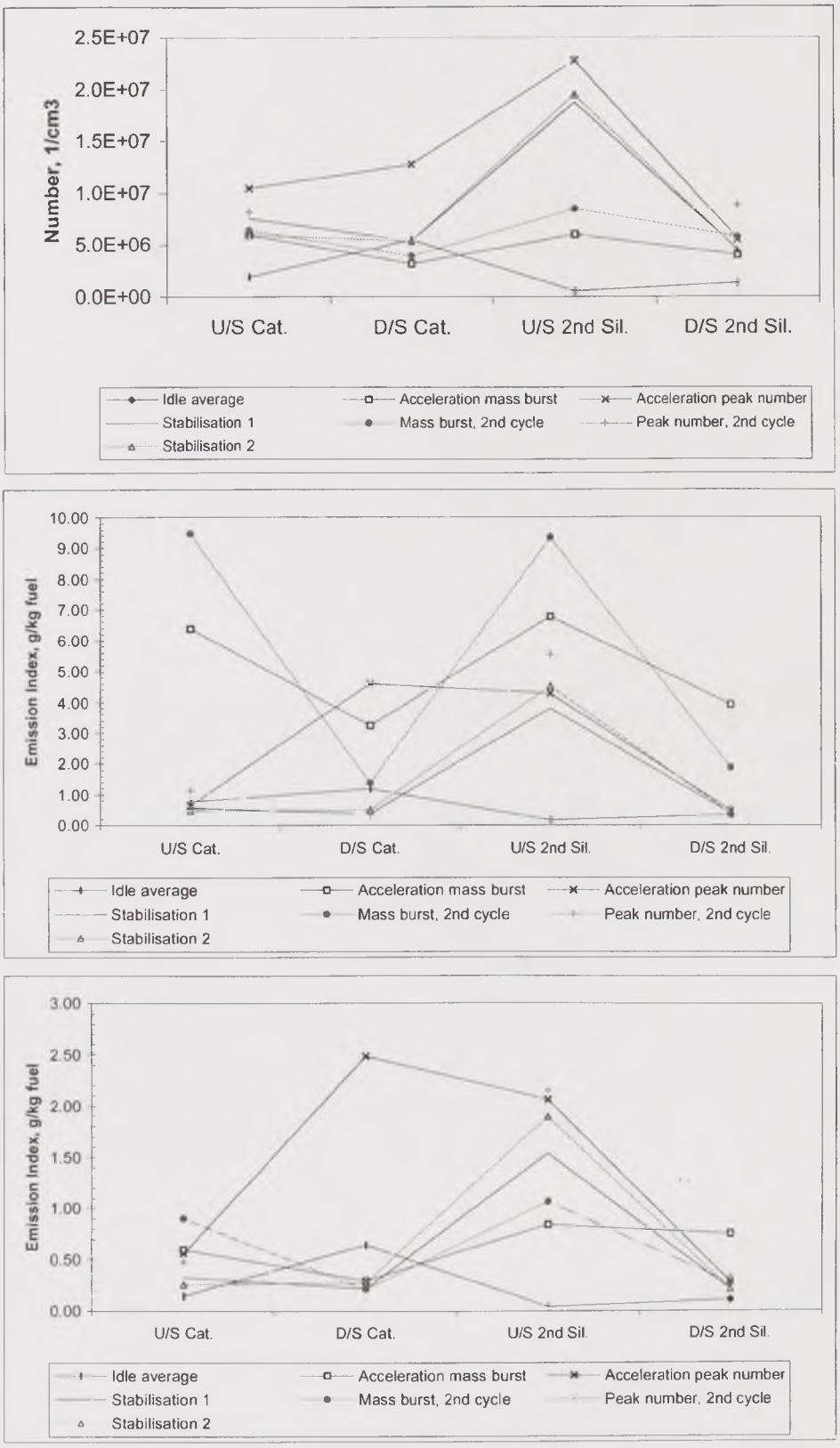

Figure 5.23. Total number and mass concentrations vs. location in the exhaust system for the main events of the acceleration to low-speed conditions, 2250rpm – 15kW, after a 4-hour Idle preconditioning.

Finally, through the second silencer, the particle number concentration increased again, to $1.3x10^6$ cm^{-3}; the uncorrected Emission Index nearly doubled, reaching 0.34 g/kg fuel, and the corrected Emission Index increased even more significantly, to 0.11 g/kg fuel. These changes, however, were less important in absolute terms when compared to those through the catalyst and the first silencer. In the second silencer, the most likely process was particle resuspension from the silencer walls, and coagulation may have played also an important role.

The tailpipe emission was very close to that entering the exhaust system, as a result of significant, opposite changes through the different devices. However, the particles coming out of the exhaust were not wholly those that entered it, but those previously deposited in the second silencer. The particle size distribution remained virtually unchanged through the exhaust system, and only through the catalyst did it shift slightly toward larger sizes.

5.3.2.2.2. Acceleration mass burst (both cycles)

The mass burst event occurred in the first few seconds of the acceleration cycles, and had a very short duration, two to four seconds. Table 5.4. shows a comparison between both acceleration cycles in terms of total particle number concentration and Emission Index. The aerosol entering the system showed, in the first cycle, a number concentration of $6.0x10^6$ cm^{-3} and an Emission Index of 6.39 g/kg fuel (uncorrected) and 0.59 g/kg fuel (corrected). In the second cycle, the number concentration was slightly higher, 6.4 $x10^6$ cm^{-3}, and more significantly higher was the Emission Index: 9.47 g/kg fuel (uncorrected) and 0.90 g/kg fuel (corrected).

The particle number concentration decreased through the catalyst in both cycles during this event; by 47% in the first cycle, to $3.2x10^6$ cm^{-3}, and by 38% in the second cycle, to $4.0x10^6$ cm^{-3}. The uncorrected Emission Index also decreased, by 49% in the first cycle, to 3.25 g/kg fuel, and by 85% in the second cycle, to 1.37 g/kg fuel. A similar reduction was observed for the corrected Emission Index, which decreased by 50% in the first cycle, to 0.30 g/kg fuel, and by 77% in the second cycle, to 0.21 g/kg fuel. The reduction occurred for all size ranges, presumably by deposition and adsorption, in similar absolute terms for both cycles.

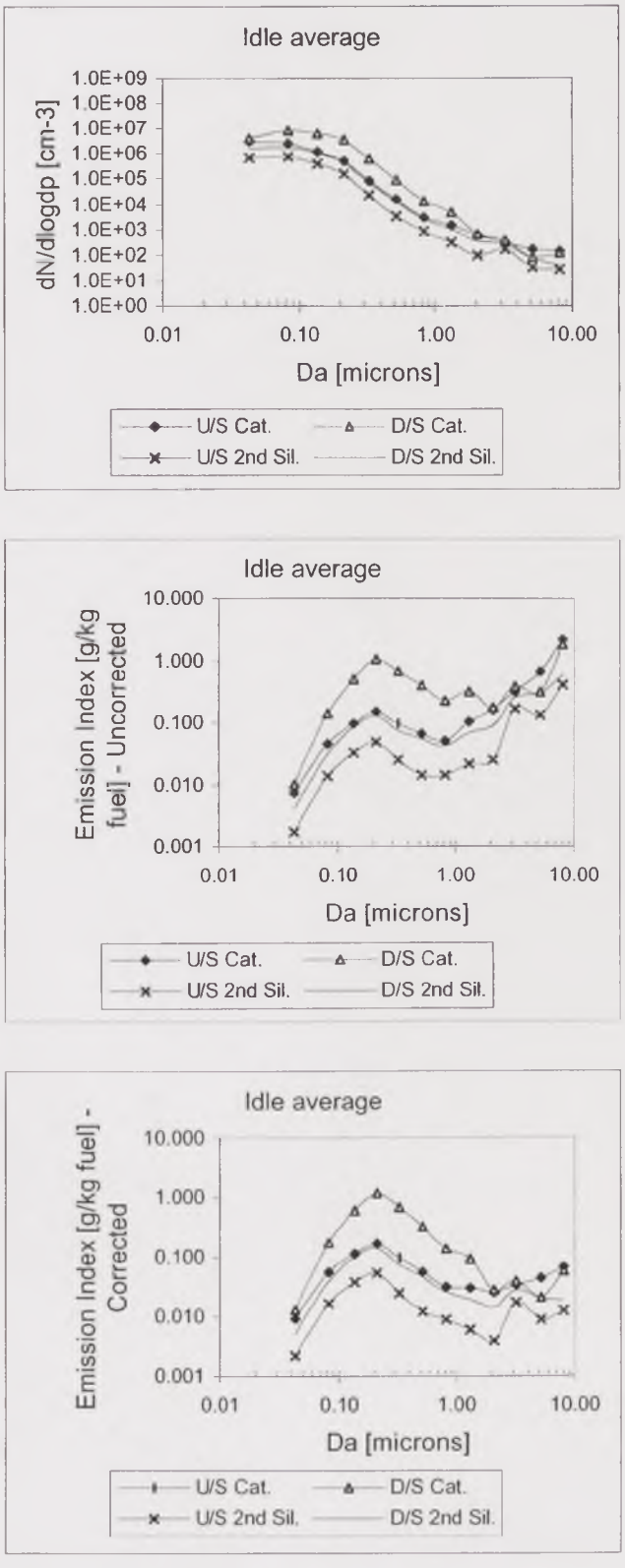

Figure 5.24. Particle size distribution at idle

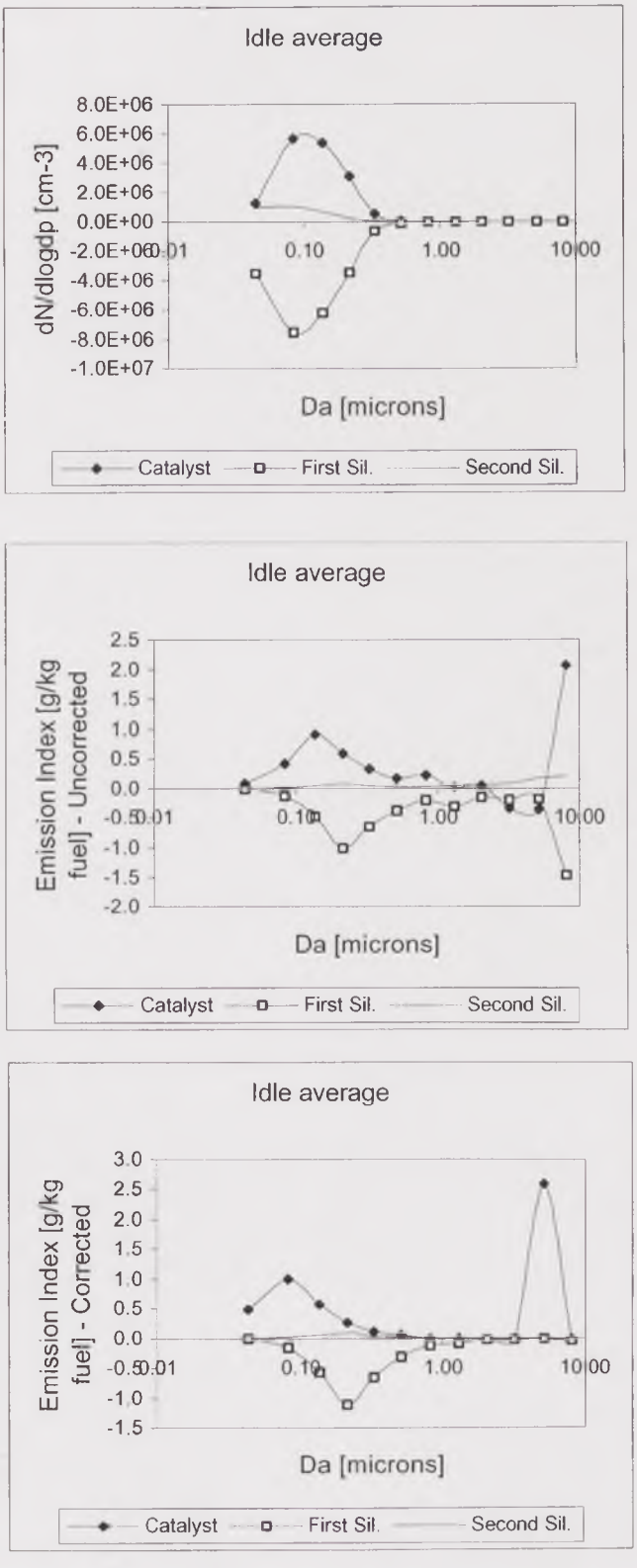

Figure 5.25. Particulate blow-out for various size ranges at Idle.

		USCat.	D/S Cat.	U/S 2nd Silencer	D/S 2nd Silencer
Avg. Number Conc. [cm-3]	Acceleration peak mass burst	6.0E+06	3.2E+06	6.0E+06	4.0E+06
	Acceleration mass burst 2nd cycle	6.4E+06	4.0E+06	8.5E+06	5.7E+06
Avg. Emission Index [g/kg fuel]	Acceleration peak mass burst	6.39	3.25	6.77	3.93
- Unit density	Acceleration mass burst 2nd cycle	9.47	1.37	9.34	1.86
Avg. Emission Index [g/kg fuel]	Acceleration peak mass burst	0.59	0.30	0.84	0.76
- Corrected density	Acceleration mass burst 2nd cycle	0.90	0.21	1.07	0.28

Table 5.4. Comparison between the first and second acceleration cycles regarding the acceleration mass burst event, 2250rpm – 15kW.

Through the first silencer, the particle number concentration increased again, to $6.0x10^6$ cm^{-3} in the first cycle and $8.5x10^6$ cm^{-3} in the second cycle, which was equivalent to an increase by 88% and 115%, respectively. The uncorrected Emission Index increased even more dramatically, to 6.77 g/kg fuel in the first cycle and 9.34 g/kg fuel in the second cycle, that is, by a factor of 1.1 and 5.8 times the incoming concentration. Similarly, the corrected Emission Index increased to 0.84 g/kg fuel in the first cycle and 1.07 g/kg fuel in the second cycle, by 1.8-fold and 4.1-fold the incoming concentration, respectively. This clear increase showed once again that the deposition layer in the first silencer was severely affected by transients such as acceleration, particularly in this case when the vibration of the system was significant. As a result, a large amount of particulate was released from the silencer walls. The release or resuspension occurred for all size ranges, and was nearly as significant in both cycles, as shown in Figure 5.28. Also, new particles were formed from outgassed components, and then coagulated to form larger particles, thus contributing to the increase in total number and Emission Index. Evidence of this was the increase in the mode of the particle size distribution through the first silencer, which can be observed in Figure 5.27.

Through the second silencer, a new increase in total particle number concentration occurred, by 33% in the first cycle, to $4.0x10^6$ cm^{-3}, and by the same percentage in the second cycle, to $5.7x10^6$ cm^{-3}. The uncorrected Emission Index decreased by 42% in the first cycle, to 3.93 g/kg fuel, and by 80% in the second cycle, to 1.86 g/kg fuel. When corrected, it decreased by 10% in the first cycle, to 0.76 g/kg fuel, and by 74% in the second cycle, to 0.28 g/kg fuel. The difference between cycles was due to the contrasting behaviour of the mid-sized particles: in the first cycle, their concentration increased through the silencer, presumably by

condensation; in the second cycle, in contrast, these deposited, together with fine and large particles.

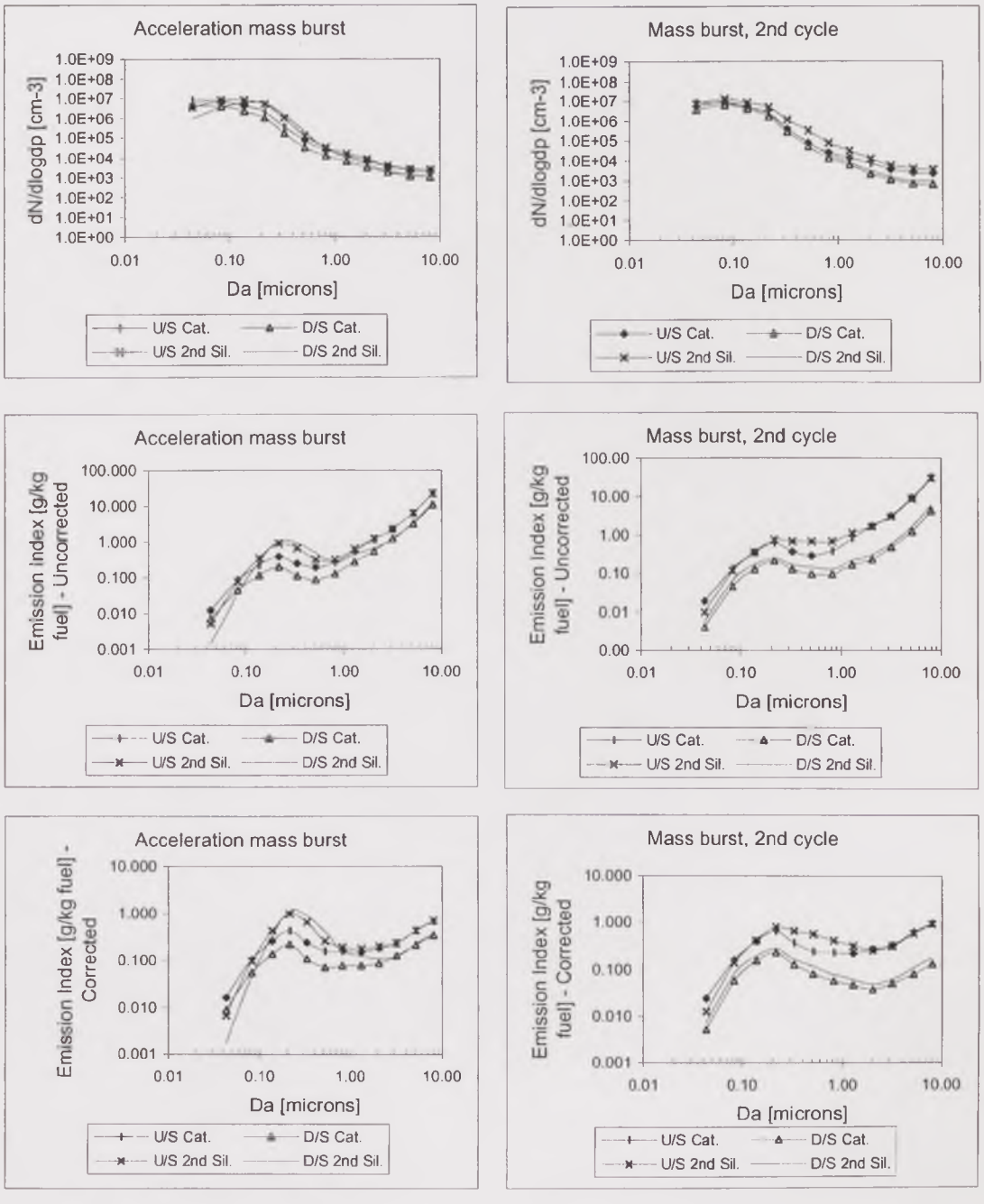

Figure 5.26. Particle size distribution for the mass burst event of the acceleration cycles, 2250rpm – 15kW.

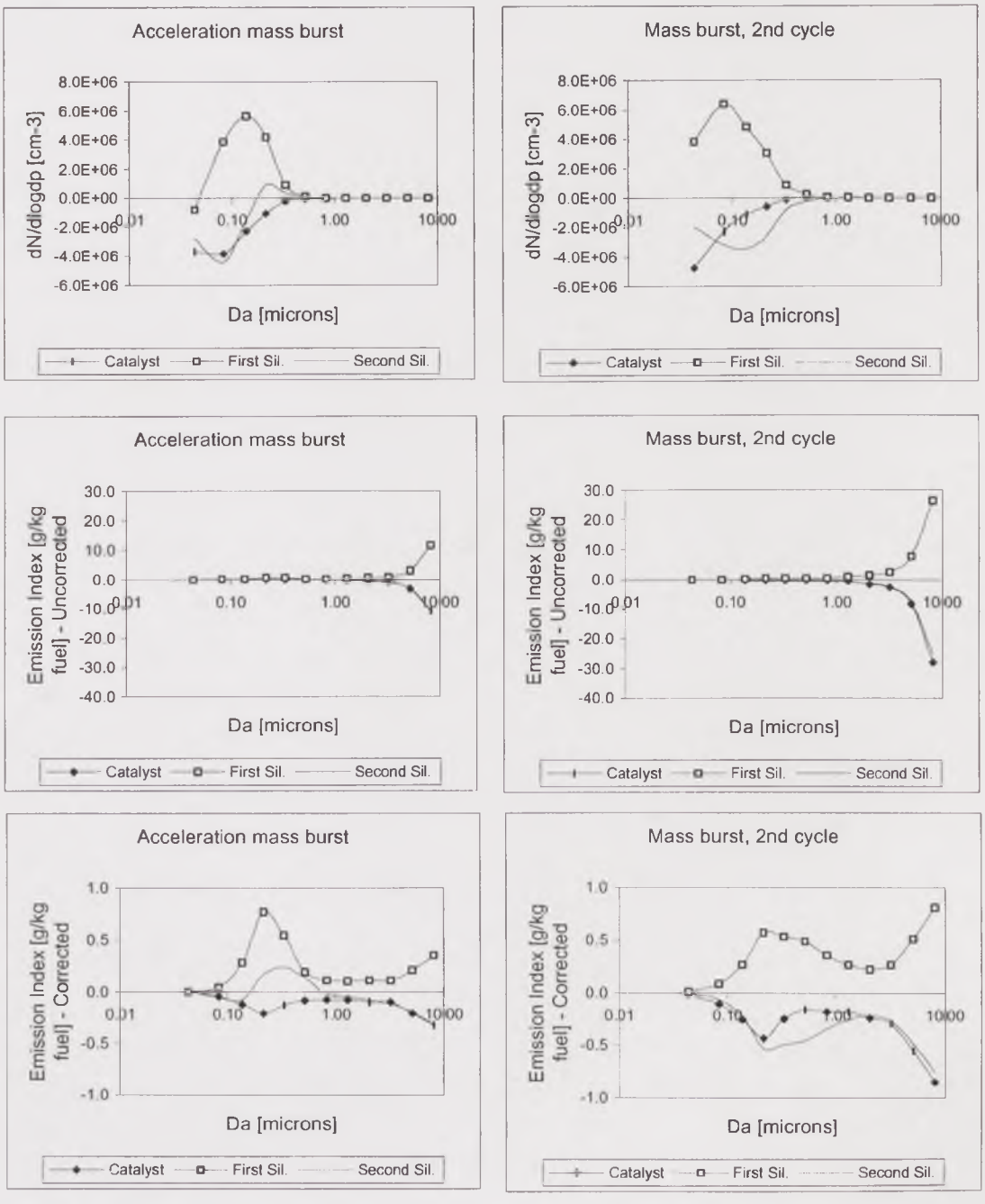

Figure 5.27. Particulate blow-out for various size ranges at the mass burst events for both acceleration cycles, 2250rpm – 15kW.

5.3.2.2.3. Acceleration number peak (both cycles)

The number peak event occurred between 30 seconds and one minute after the start of the acceleration cycles and, as the mass burst event, it was very short. In this event, the aerosol entering the system had a total particle number concentration of 1.1×10^{7} cm^{-3} in the first cycle and somewhat lower, 8.2×10^{6} cm^{-3}, in the second cycle. The corresponding uncorrected Emission Index was 0.66 g/kg fuel in the first cycle and nearly twice as high, 1.15 g/kg fuel, in the second cycle. The corrected

Emission Index was 0.56 g/kg fuel in the first cycle and slightly lower, 0.48 g/kg fuel, in the second cycle. Through the catalyst, the particle number concentration increased by 22% in the first cycle, to $1.3x10^7$ cm^{-3}, but decreased in the second cycle by 34%, to $5.4x10^6$ cm^{-3}. This divergence was reflected also in the uncorrected Emission Index, which increased by more than 6-fold in the first cycle, to 4.61 g/kg fuel, and decreased by 68% in the second cycle, to 0.37 g/kg fuel. The increase in the corrected Emission Index in the first cycle was by 3.5-fold, to 2.48 g/kg fuel, and the decrease in the second cycle was by 40%, to 0.29 g/kg fuel. The difference between both cycles was due to mid-sized and large particles, larger than 0.1μm, which were either formed by coagulation and condensation or blown out from the catalyst in the first cycle. In the second cycle, in contrast, particles deposited and were adsorbed through the catalyst regardless of their size.

Through the first silencer, the particle number concentration increased by 78% in the first cycle, reaching $2.3x10^7$ cm^{-3}, and by more than 3-fold in the second cycle, reaching the same value than in the first cycle, $2.3x10^7$ cm^{-3}. Despite the increase in number concentration, the uncorrected Emission Index decreased by 7% in the first cycle, to 4.28 g/kg fuel. In the second cycle, it increased significantly, by 14-fold, to 5.55 g/kg fuel. The corresponding changes in the corrected Emission Index were a decrease by 17% in the first cycle, to 2.06 g/kg fuel, and an increase by 6.5-fold in the second cycle, to 2.15 g/kg fuel. In the first cycle, particles smaller than 0.2μm and those between 0.5μm and 2.0μm were blown out from the silencer, but the remaining particles, between 0.2μm and 0.5μm, as well as those larger than 2.0μm, deposited through it. On the other hand, in the second cycle, the concentration of ultrafine and mid-sized particles increased by gas-to-particle and coagulation processes, and large particles were blown out from the silencer. This difference accounted for the divergence in the overall changes in number concentration and Emission Index.

Finally, through the second silencer, the particle number concentration decreased by 76% in the first cycle, to $5.5x10^6$ cm^{-3}, and by 61% in the second cycle, to $8.8x10^7$ cm^{-3}. The uncorrected Emission Index decreased by 89% in the first cycle, to 0.46 g/kg fuel, and by 90% in the second cycle, to 0.56%. When corrected, it decreased by 86% in the first cycle, to 0.28 g/kg fuel, and by 84% in the second cycle, to 0.33 g/kg fuel. These changes were very similar, and occurred in the same manner for all size ranges in both cycles: all particles deposited through the silencer.

In summary, differential behaviour of particles of different sizes determined contrasting overall trends in the first and the second acceleration cycles through the

catalyst and the first silencer. Mid-sized increased concentrations by coagulation and condensation occurred, and large particles were easily resuspended from the catalyst in the first cycle, just after the long idle preconditioning period. The first silencer accumulated these particles. Afterwards, in the second cycle, the behaviour was exactly the opposite. The catalyst had recovered its accumulating capacity and the particles previously accumulated in the first silencer were resuspended by the second disturbance. The behaviour of the particle deposits in the second silencer was practically unaffected by the duration of the conditioning period, being equivalent for both cycles. The particle size distribution mode did not change significantly through the exhaust system.

		USCat.	D/S Cat.	U/S 2nd Silencer	D/S 2nd Silencer
Avg. Number Conc. [cm-3]	Acceleration peak number	1.1E+07	1.3E+07	2.3E+07	5.5E+06
	Acceleration peak number 2nd cycle	8.2E+06	5.4E+06	2.3E+07	8.8E+06
Avg. Emission Index [g/kg fuel]	Acceleration peak number	0.66	4.61	4.28	0.46
- Unit density	Acceleration peak number 2nd cycle	1.15	0.37	5.55	0.56
Avg. Emission Index [g/kg fuel]	Acceleration peak number	0.56	2.48	2.06	0.28
- Corrected density	Acceleration peak number 2nd cycle	0.48	0.29	2.15	0.33

Table 5.5. Comparison between the first and second acceleration cycles regarding the acceleration peak number event, 2250rpm – 15kW.

5.3.2.2.4. Stabilisation (both cycles)

Once the disturbance introduced in the system by the acceleration was over, there was a stabilisation in particle number concentration and Emission Index at a level lower than the acceleration peak. The particle number concentration of the aerosol system during this event was $7.6x10^6$ cm^{-3} in the first cycle and $6.0x10^6$ cm^{-3} in the second cycle. The uncorrected Emission Index was 0.58 g/kg fuel in the first cycle and 0.47 g/kg fuel in the second cycle, and the corresponding corrected Emission Index, 0.32 g/kg fuel in the first cycle and 0.26 g/kg fuel in the second cycle. Through the catalyst, the particle number concentration decreased to $5.4x10^6$ cm^{-3} in both cycles, a decrease by 29% and 10% in the first and second cycles, respectively. The uncorrected Emission Index decreased by 31% in the first cycle and increased by just 5% in the second cycle, reaching similar levels of 0.40 g/kg fuel and 0.50 g/kg fuel, respectively. Similarly, the corrected Emission Index decreased by 33% in the first cycle and increased by 8% in the second cycle, reaching 0.22 g/kg fuel and 0.28 g/kg fuel, respectively. Particles of all sizes deposited through the catalyst in both cycles.

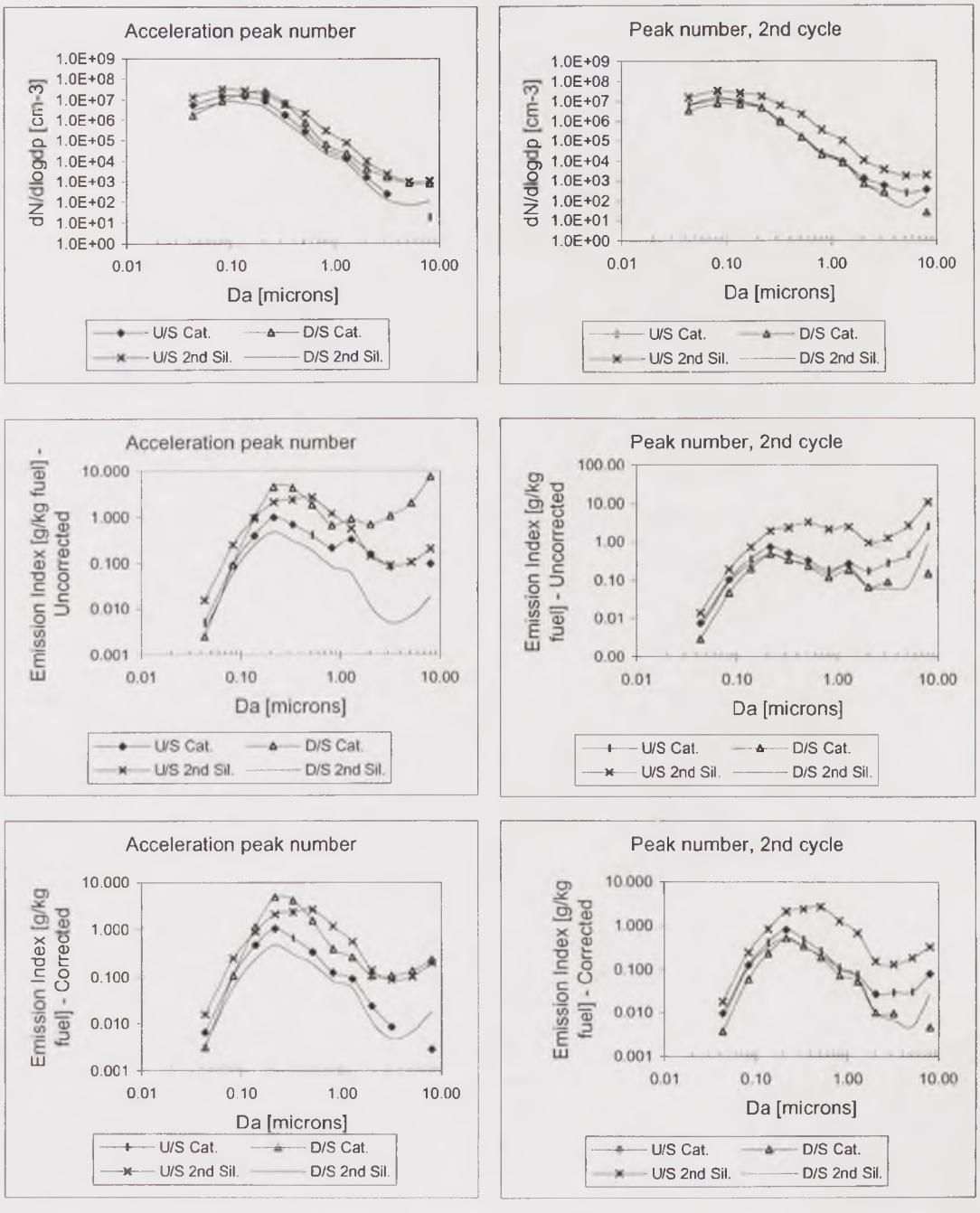

Figure 5.28. Particle size distribution for the peak number events of the acceleration cycles, 2250rpm – 15kW.

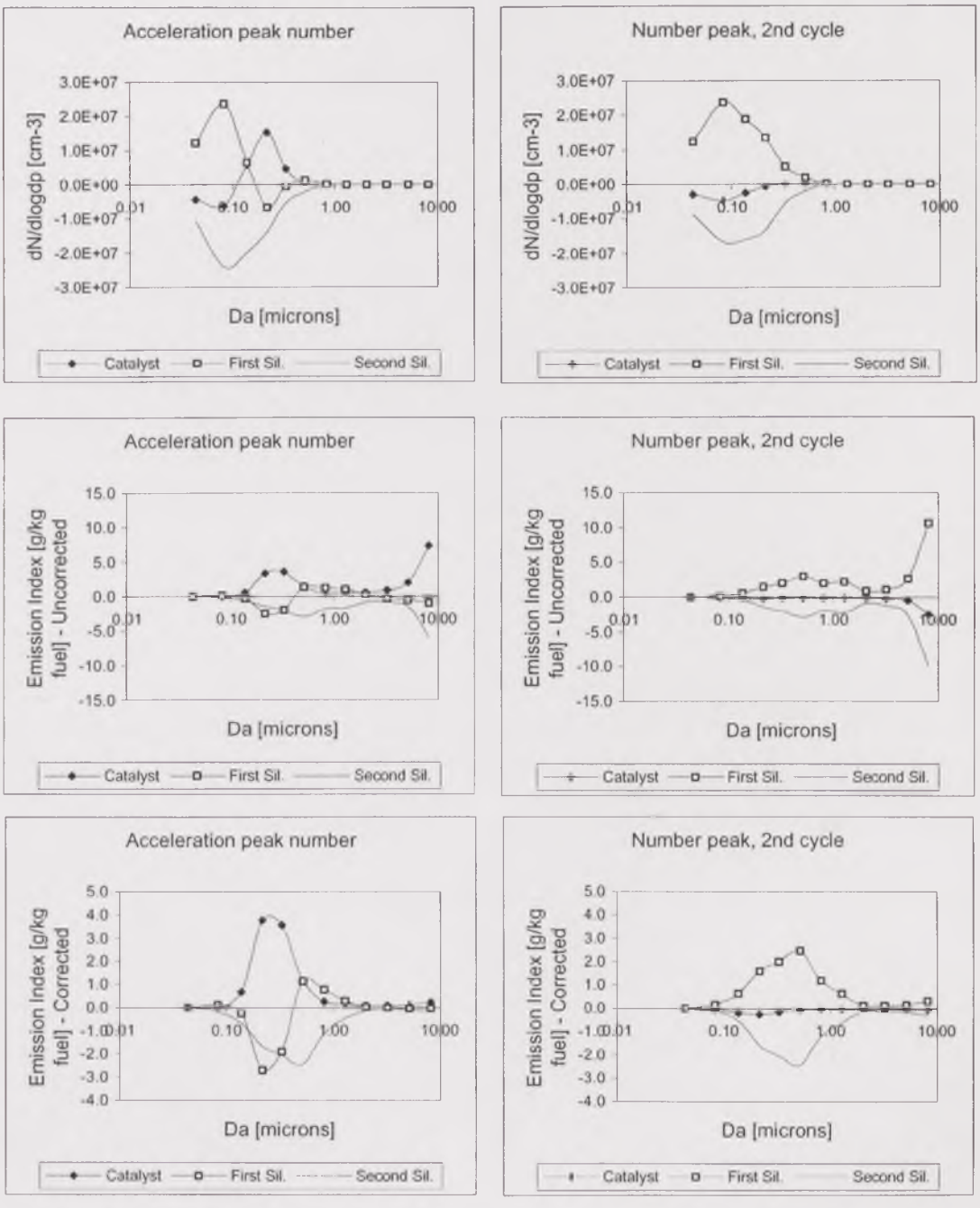

Figure 5.29. Particulate blow-out for various size ranges at the peak number events for both acceleration cycles, 2250rpm – 15kW.

Through the first silencer, the particle number concentration increased to 1.9×10^6 cm^{-3} in both cycles, an increase by 250%. The uncorrected Emission Index increased by 8.5-fold in the first cycle, to 3.81 g/kg fuel, and by 8.1-fold in the second cycle, to 4.54 g/kg fuel. The corrected Emission Index increased to 1.54 g/kg fuel in the first cycle, and to 1.90 g/kg fuel in the second cycle, which was an increase by 6.1-fold and 5.9-fold, respectively. These changes were nearly identical for both cycles through this silencer, consisting of increase in particle concentration

by gas-to-particle and coagulation processes for fine particles, and blow-out of large particles, as can be observed in Figure 5.31.

		USCat.	D/S Cat.	U/S 2nd Silencer	D/S 2nd Silencer
Avg. Number Conc. [cm-3]	Acceleration peak mass burst	7.6E+06	5.4E+06	1.9E+07	4.5E+06
	Acceleration mass burst 2nd cycle	6.0E+06	5.4E+06	1.9E+07	4.5E+06
Avg. Emission Index [g/kg fuel]	Acceleration peak mass burst	0.58	0.40	3.81	0.39
- Unit density	Acceleration mass burst 2nd cycle	0.47	0.50	4.54	0.37
Avg. Emission Index [g/kg fuel]	Acceleration peak mass burst	0.32	0.22	1.54	0.21
- Corrected density	Acceleration mass burst 2nd cycle	0.26	0.28	1.90	0.21

Table 5.6. Comparison between the first and second acceleration cycles regarding the stabilisation event, 2250rpm – 15kW.

Through the second silencer, the particle number concentration decreased to $4.5x10^6$ cm^{-3} in both cycles, which corresponded to a 76% and 77% decrease, for the first and second cycles, respectively. The decrease in uncorrected Emission Index was by 90% and 92%, to 0.39 g/kg fuel and 0.37 g/kg fuel in the first and second cycles, respectively. The corrected Emission Index decreased to 0.21 g/kg fuel in both cycles, a decrease by 86% and 89% in the first and second cycles, respectively. As through the first silencer, the changes were nearly identical for both cycles, and consisted of deposition of particles of all sizes.

In summary, the stabilisation events were shown to be identical in both cycles, which indicated that the disturbance and the duration of the conditioning period caused only transient effects and that differences in deposition/resuspension occurred only for the mass burst and number peak events, but their effect was small after the end of the transient acceleration.

5.4. Comparative analysis of the acceleration results

In the same way as the cold start tests, a comparative analysis of the acceleration results was made as an attempt to find behavioural trends through the system at different conditions. The summary of processes is shown in Table 5.7., using the same convention as that in Chapter 4, namely *italic* characters for an increase in number concentration, underlined characters for deposition or reduction in number concentration, and dotted-underlined characters for mixed processes within the three previously defined particle size ranges. Again, the main aim of the

analysis was to identify the conditions at which the particle concentration increases (formation and resuspension, or blow-out events).

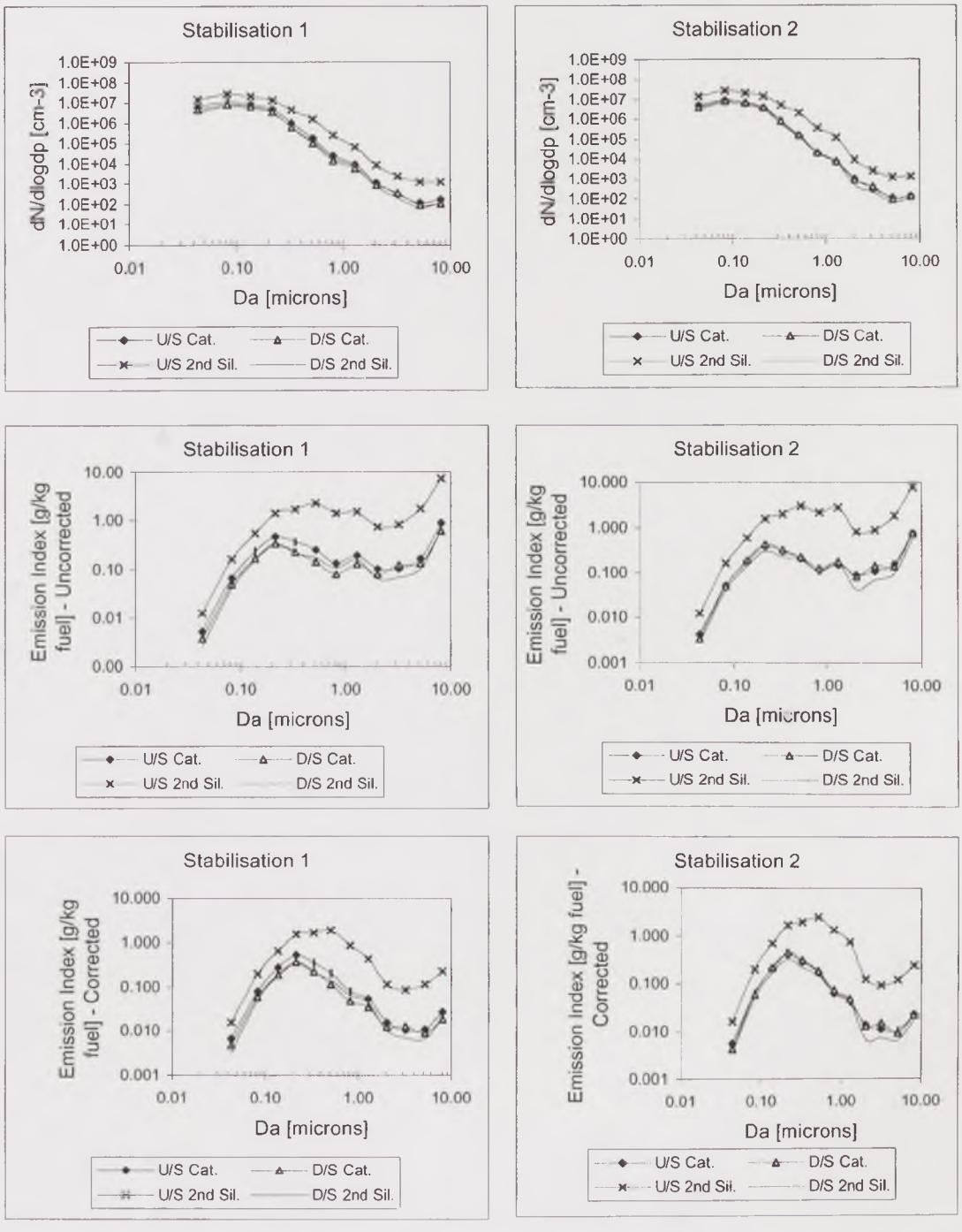

Figure 5.30. Particle size distribution for the stabilisation events of the acceleration cycles, 2250rpm – 15kW.

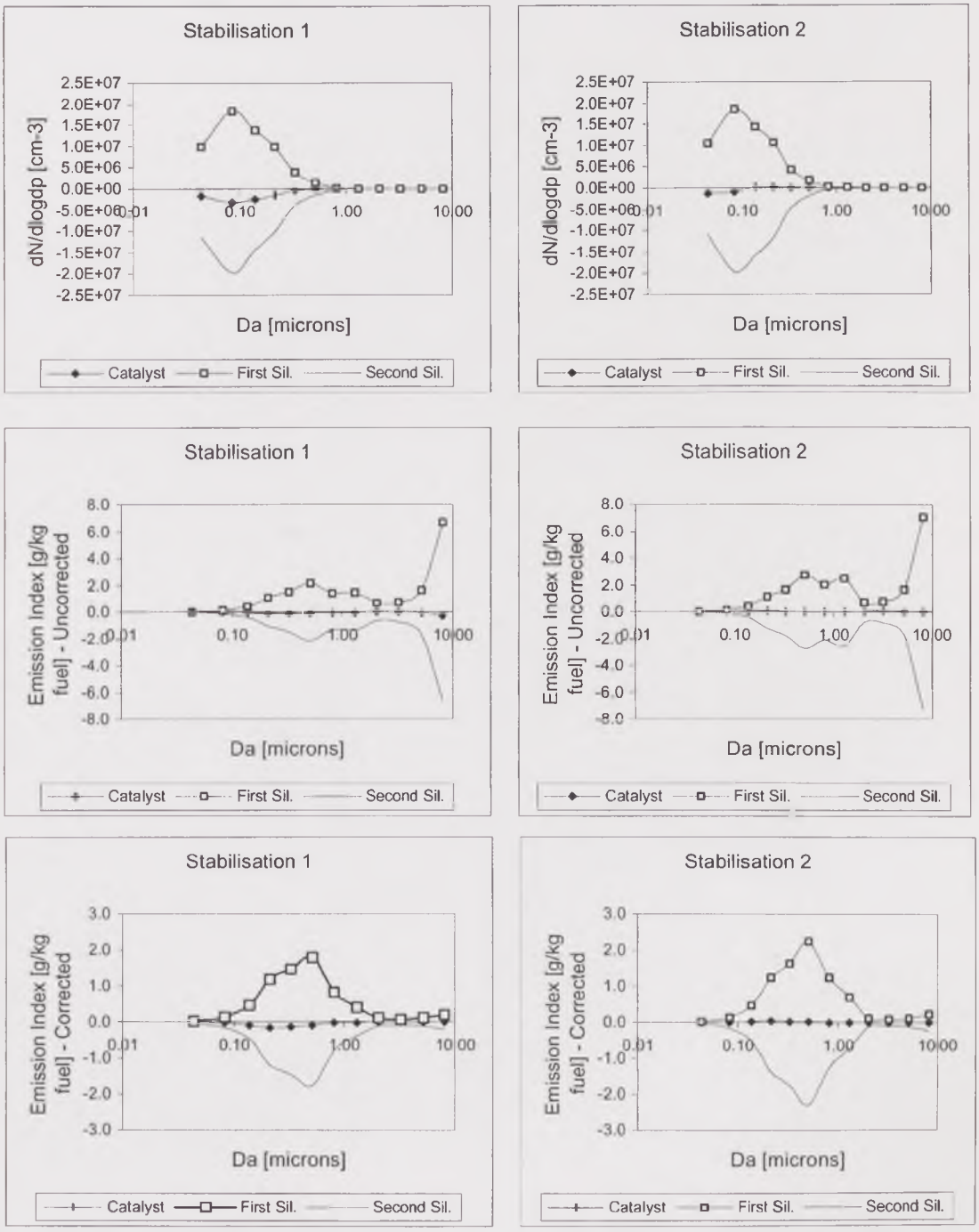

Figure 5.31. Particulate blow-out for various size ranges at the stabilisation events for both acceleration cycles, 2250rpm – 15kW.

The number of deposition cases overwhelmed the number of particle formation and resuspension at all conditions. Figure 5.33. shows that the high-speed conditions, 3500rpm - 15kW, contributed to more cases of formation of ultrafine particles than its low speed counterpart, 2250rpm – 15kW, but the opposite occurred for larger particles: the high-load condition contributed to more cases of mid-size particle formation and large particle resuspension, presumably by enhanced

coagulation and thermal effects on the deposition layer at the higher temperatures. To a certain extent, a higher speed was expected to produce more blow-out cases. However, the higher turbulence at high speeds can actually enhance deposition. As it was said for the cold start tests, the higher contribution to the number of deposition cases does not necessarily mean that, when blow-out occurs, it is less significant. The blow-out events during acceleration tests to high-speed produced higher changes Emission Index than those during acceleration to low-speed.

		Size range			Size range		
		Small	Middle	Large	Small	Middle	Large
Event	Device	0.01-0.1mm	0.1-1.0mm	1.0-10.0mm	0.01-0.1mm	0.1-1.0mm	1.0-10.0mm
		3500rpm - 15kW			2500rpm - 15kW		
Idle	Catalyst	Coagulation & Deposition	Deposition	Deposition	Formation	Coagulation	Blow-out
	First Silencer	Formation	Coagulation	Blow-out	Coagulation & Deposition	Deposition	Deposition
	Second Silencer	Coagulation & Deposition	Deposition	Deposition	Formation	Coagulation	Blow-out
First mass burst 1st cycle	Catalyst	Formation	Deposition	Deposition	Coagulation & Deposition	Deposition	Deposition
	First Silencer	Formation	Coagulation	Blow-out	Formation	Coagulation	Blow-out
	Second Silencer	Coagulation & Deposition	Deposition	Deposition	Coagulation & Deposition	Coagulation	Deposition
First mass burst 2nd cycle	Catalyst	Formation	Deposition & Coagulation	Deposition	Coagulation & Deposition	Deposition	Deposition
	First Silencer	Coagulation & Deposition	Deposition	Deposition	Formation	Coagulation	Blow-out
	Second Silencer	Coagulation & Deposition	Deposition	Deposition	Coagulation & Deposition	Deposition	Deposition
Number peak	Catalyst	Formation	Coagulation	Blow-out	Coagulation & Deposition	Coagulation	Blow-out
	First Silencer	Coagulation & Deposition	Deposition	Deposition	Formation	Deposition & Coagulation	Blow-out/Deposition
	Second Silencer	Coagulation & Deposition	Deposition	Blow-out	Coagulation & Deposition	Deposition	Deposition
Number peak 2nd cycle	Catalyst	Formation	Coagulation	Deposition	Coagulation & Deposition	Deposition	Deposition
	First Silencer	Coagulation & Deposition	Deposition	Blow-out	Formation	Coagulation	Blow-out
	Second Silencer	Coagulation & Deposition	Deposition	Deposition	Coagulation & Deposition	Deposition	Deposition
Stabilisation	Catalyst	Formation	Deposition	Blow-out/Deposition	Coagulation & Deposition	Deposition	Deposition
	First Silencer	Coagulation & Deposition	Deposition	Deposition	Formation	Coagulation	Blow-out
	Second Silencer	Coagulation & Deposition	Deposition	Deposition	Coagulation & Deposition	Deposition	Deposition
Stabilisation 2nd cycle	Catalyst	Formation	Deposition	Blow-out/Deposition	Coagulation & Deposition	Coagulation	Deposition
	First Silencer	Coagulation & Deposition	Deposition	Deposition	Formation	Coagulation	Blow-out
	Second Silencer	Coagulation & Deposition	Deposition	Deposition	Coagulation & Deposition	Deposition	Deposition

Table 5.7. Summary of deposition and blow-out cases for the acceleration tests, including the exhaust devices, three size ranges, target conditions and acceleration cycle.

From the comparison between cycles, Figure 5.33. shows that more blow-out cases were observed during the first cycle than during the second cycle. This was an expected result, since the idle preconditioning before the first cycle was significantly much longer than the idling period before the second cycle, so there was much more particulate matter likely to be blown-out during the first cycle.

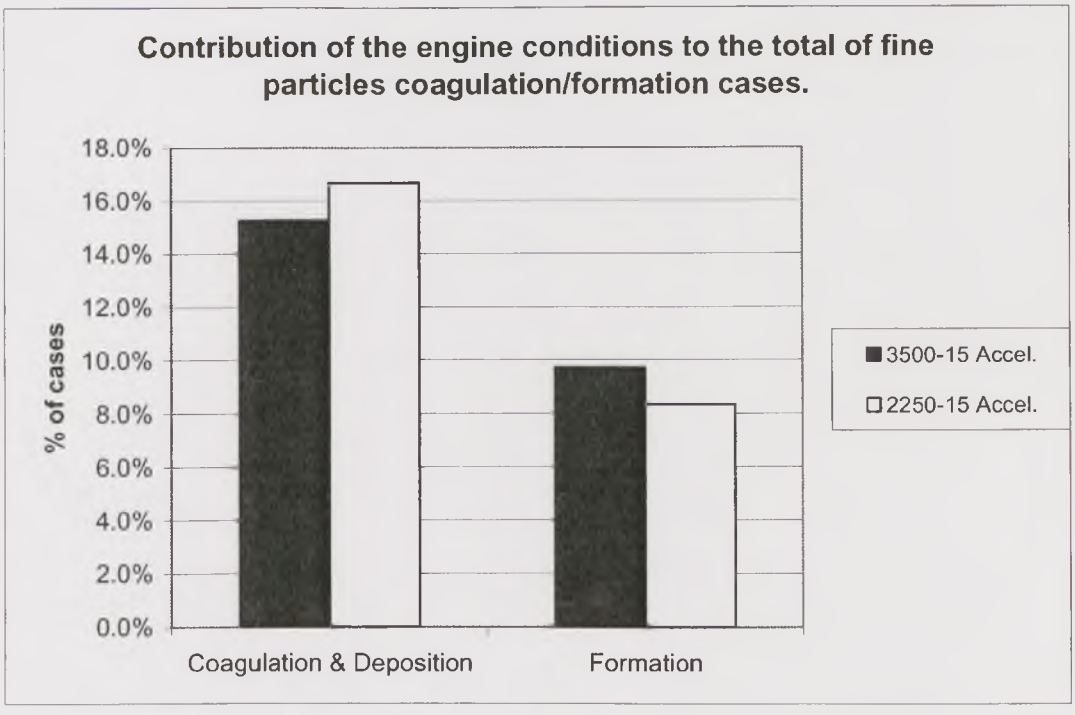

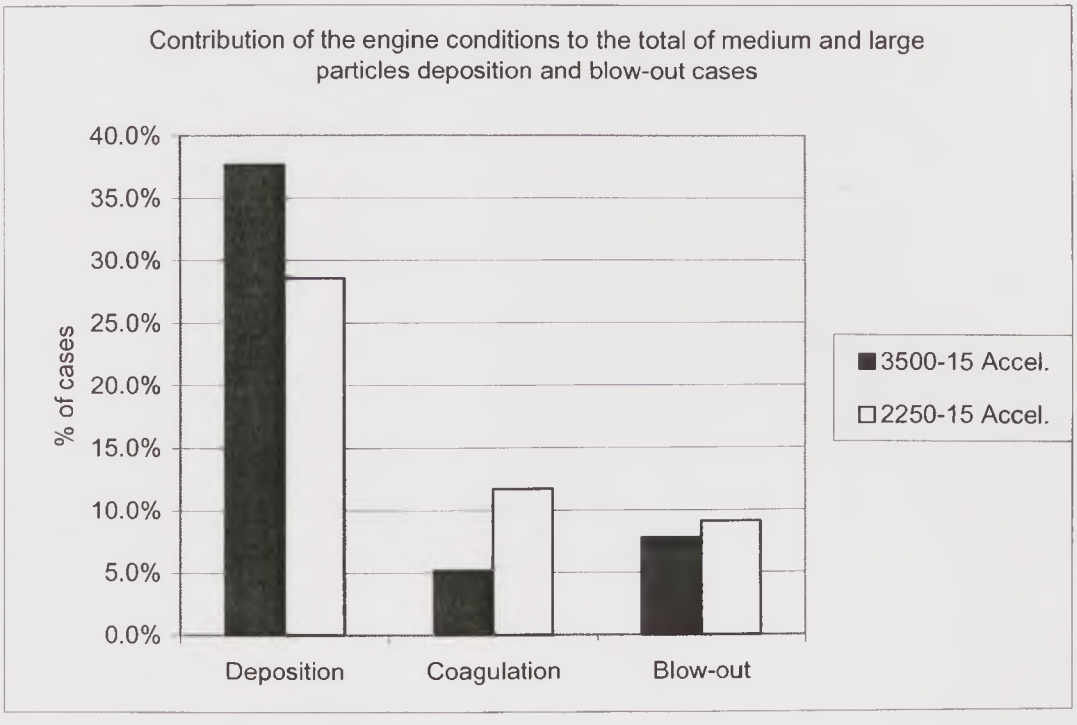

Figure 5.32. Contribution of engine target conditions to the total of blow-out and deposition cases during acceleration tests.

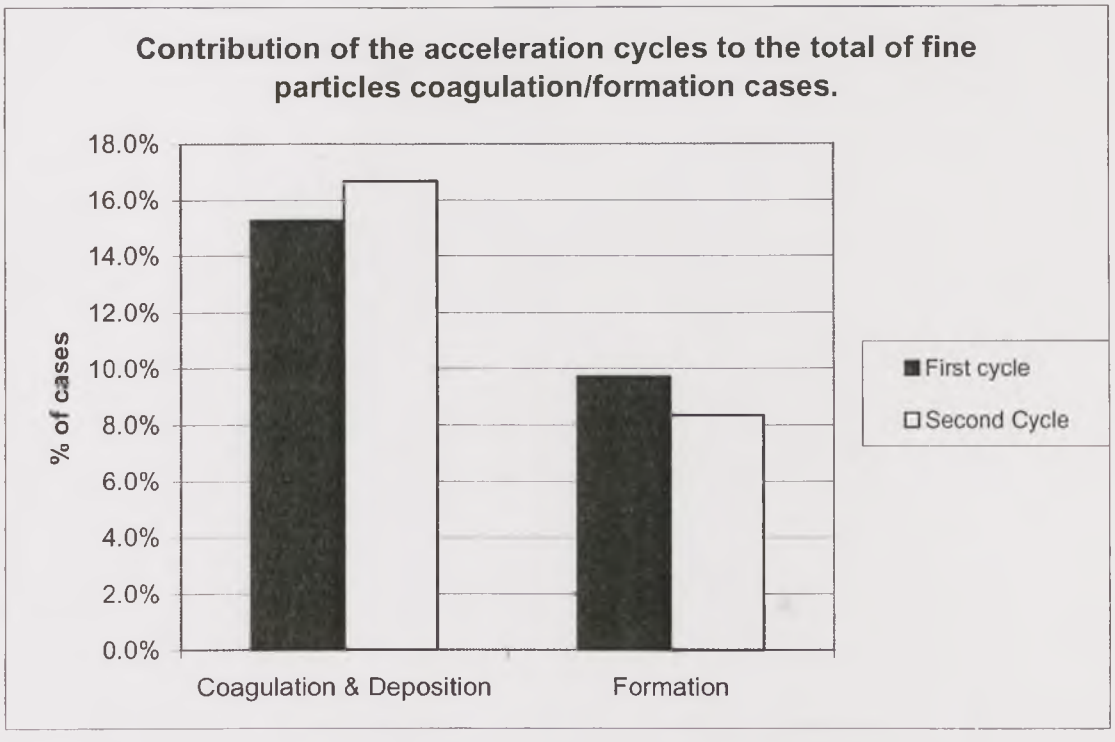

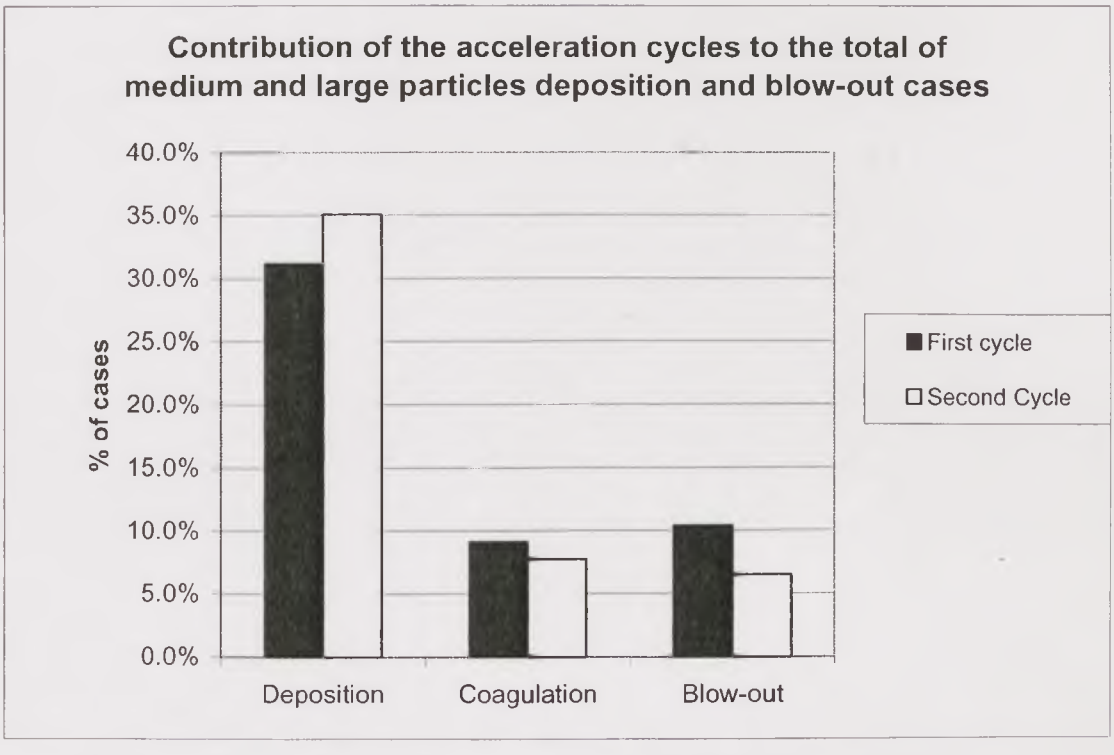

Figure 5.33. Contribution of acceleration cycles to the total of blow-out and deposition cases during acceleration tests.

Figure 5.34. shows that the start-up contributed to more ultrafine particle formation cases than the acceleration and the thermal stabilisation. For mid-sized particles, start-up and acceleration contributed to the same number of particle

formation cases, higher than during stabilisation, and it was the acceleration the main contributor to large particle blow-out or resuspension cases. Once thermal stabilisation was reached, particle deposition was the main trend observed.

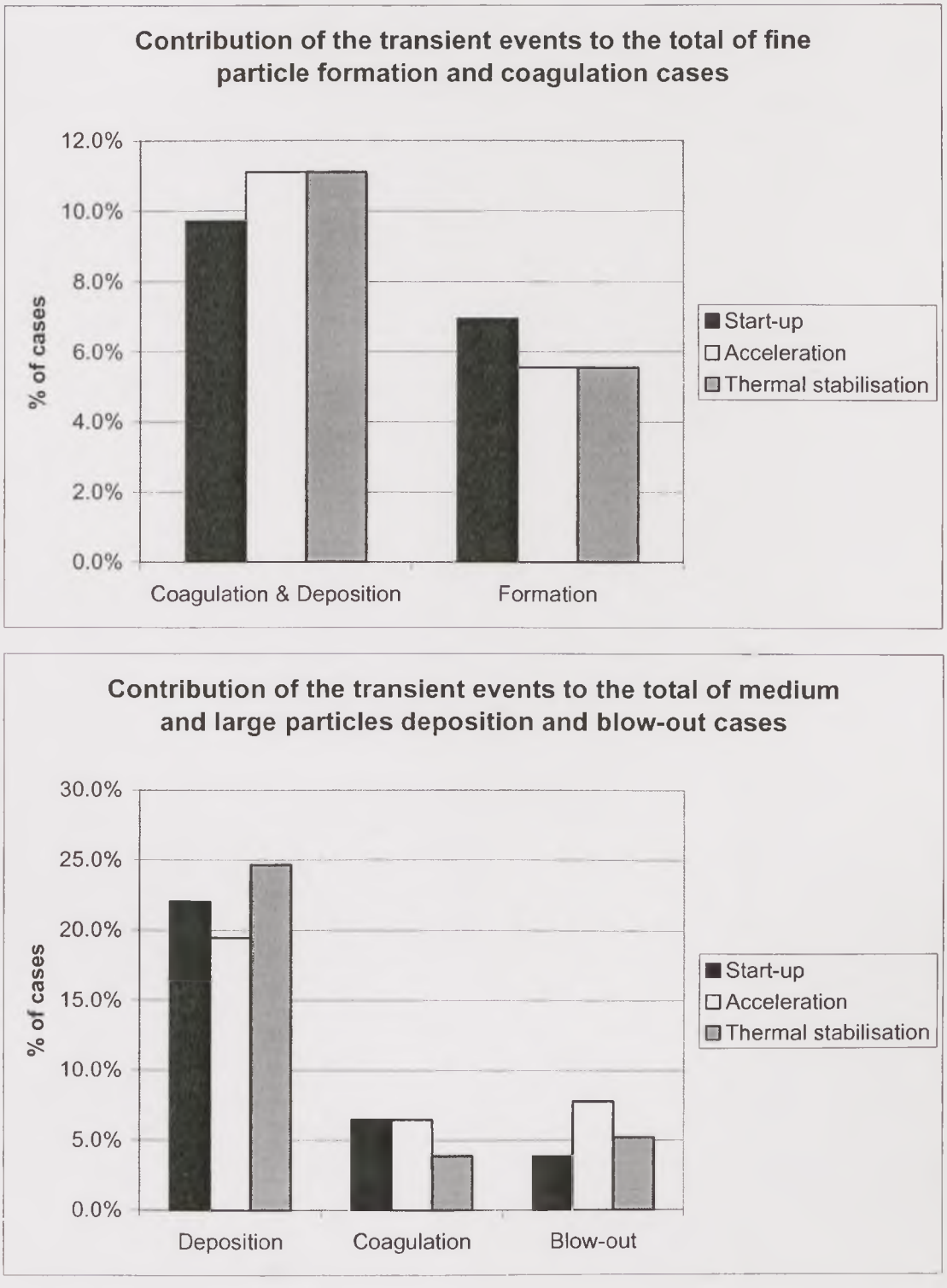

Figure 5.34. Contribution of transient events to the total of blow-out and deposition cases during acceleration tests.

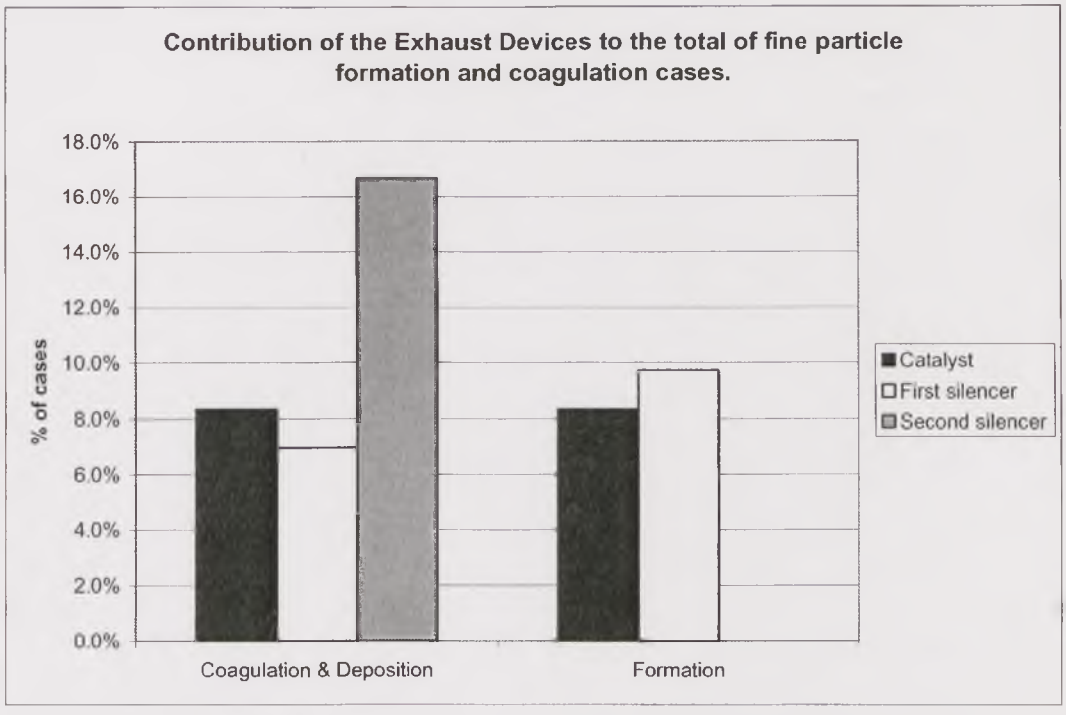

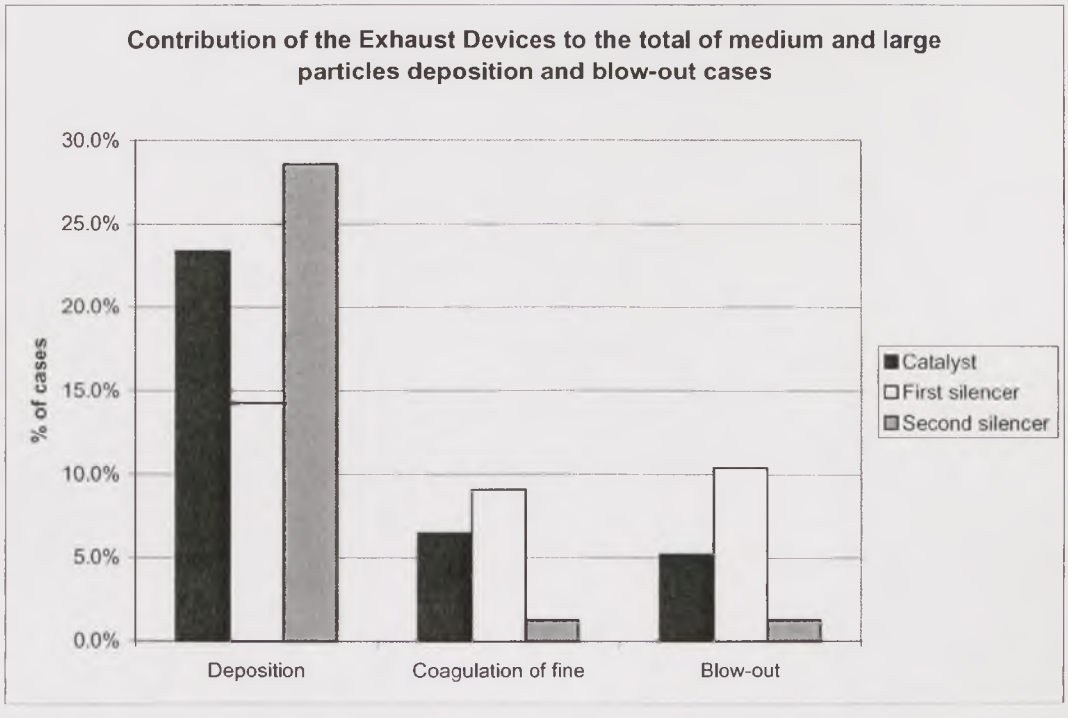

Figure 5.35. Contribution of exhaust devices to the total of blow-out and deposition cases during acceleration tests.

Finally, Figure 5.35. shows that, in the acceleration tests, the first silencer contributed significantly to the number of particle formation and resuspension cases. The catalyst contribution to the number of such cases was less important than the first silencer, but still significant. In contrast, the second silencer showed no case of ultrafine particle formation predominating over particle deposition and only very

few cases of particle resuspension. Perhaps the initial temperature of the catalyst in the acceleration tests, which was higher than in the cold start tests, deteriorated the adsorption capacity of the catalyst when the disturbance appeared, relegating the catalyst to be less effective a particulate accumulator than the second silencer.

5.5. Key points from this Chapter

Cold start tests allowed determining that important levels of particle formation and resuspension through the exhaust system were likely to occur at high-speed and high-load conditions, but were inconclusive regarding the frequency at which these events take place. The results from this Chapter, after the analysis of the number of particle concentration-change cases during the acceleration tests, identified the following factors to favour fine particle formation and large particle resuspension:

- Relatively high loads and therefore high exhaust temperatures, rather than high speed but low temperatures.
- Long preconditioning at Idle (or low speeds), rather than short periods under the same conditions, represented by the differences between first and second acceleration cycles.
- The start and the whole duration of the acceleration, rather than the stabilisation at the target condition.
- The flow through the first silencer and the catalyst, rather than through the second silencer.
- Nevertheless, the number of cases for which deposition was predominant over particle formation and resuspension overwhelmed the number of cases for which the opposite situation occurred, even in the most likely conditions to promote particle formation, growth and resuspension.
- Transient acceleration emissions in step-change cycle tests such as those carried in this work may be used to estimate changes in emissions due to transients, with respect to multi-mode steady-state legislative cycles such as the R49 and the ESC. This is explained and illustrated in Chapter 7.

Chapter 6.
New Exhaust Tests

In the last stage of this research, the exhaust system downstream of the catalyst was replaced with a new section with identical configuration. Cold-start tests were performed without any prior use of the exhaust. The aim was to study wall deposition losses when there was no prior wall deposits. There was no exhaust preconditioning in the tests, the aim being to undertake tests with no presence of particles in the exhaust. The emissions were monitored continuously with the ELPI at four sampling points, so that the changes through the exhaust system with clean walls could be observed. Total number concentration and number-weighted size distribution were recorded every second and converted into total Emission Index and mass-weighted size distribution. The same correction applied to previous tests was used here, reducing the contribution of large particles in the mass-weighted size distribution and thus reducing the total Emission Index by about one order of magnitude. No filter measurements were carried out with the new exhaust to compare with the mass estimations from the ELPI, so it was assumed that the correction was still valid. The discussion on this issue can be found in section 2.11.

Since it was not possible to have several instruments to perform simultaneous measurements, which would have been the ideal situation to observe the real time effects of the clean walls, each test was kept very short, so as not to produce important alterations to the system. The sampling time for each test was 10 minutes from cold start. After each test, the engine was shut down and allowed to cool down to ambient temperature to perform the following test. In the first test, the sample was taken at the tailpipe. For subsequent tests, the sampling point was moved backwards in the exhaust system, finishing upstream of the catalyst.

The Emission Index profiles vs. time in Figure 6.1. showed that, during the first seconds of cold start, a mass-burst event occurred, as was observed in all previous cold-start tests. This lasted around 15s, during which the number concentration also increased. After reaching a maximum, the Emission Index decreased quickly, but the number concentration kept increasing for another 10 seconds to reach a maximum and then decrease slightly. From this point on, there were several oscillations in the particle number concentration at levels increasingly higher than the first temporary maximum. Oscillations occurred also in the Emission Index profiles, but at lower levels than the mass burst at the start of the test. This

was the first indication that these changes were produced in the fine-particle size range.

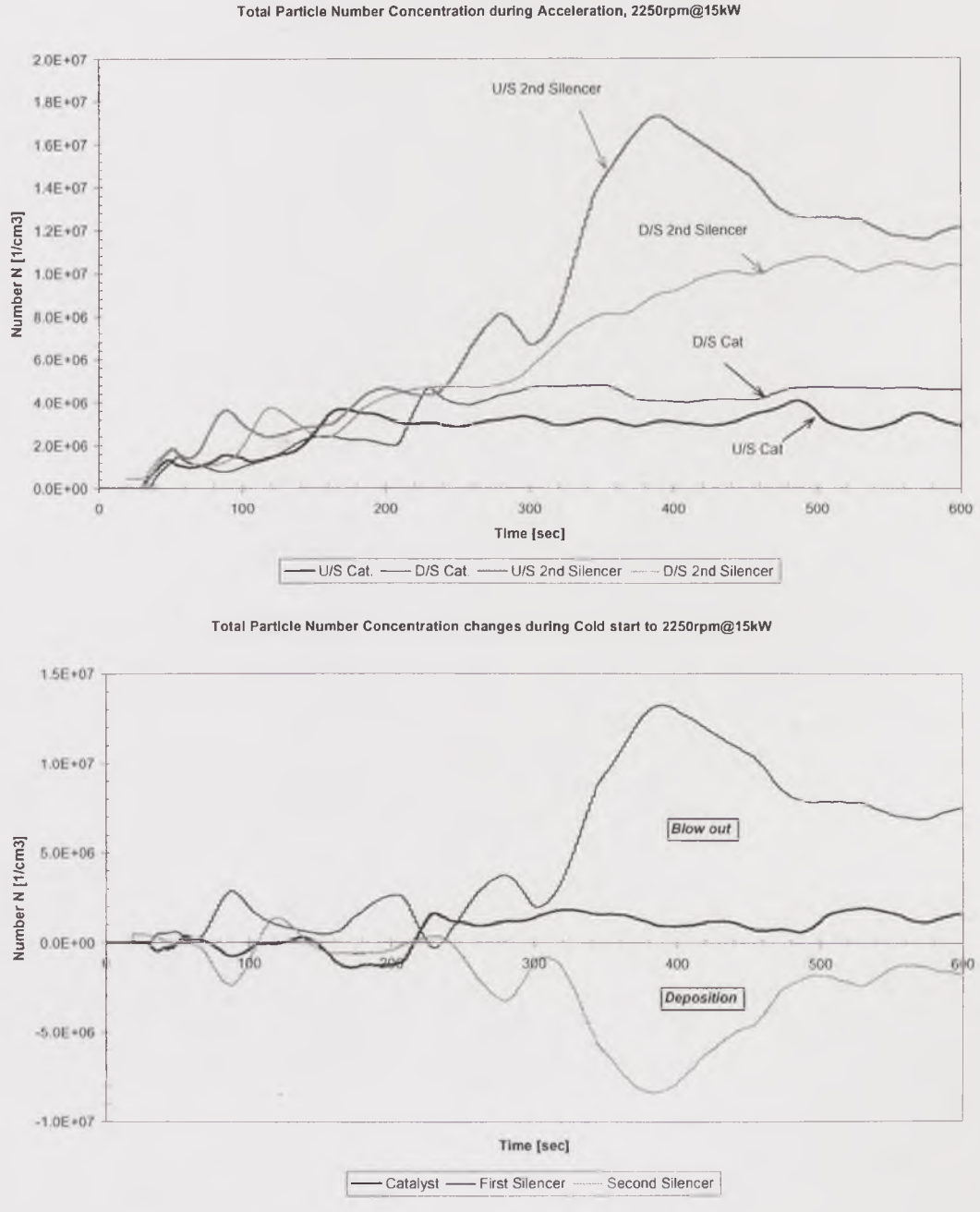

Figure 6.1. Total number concentration and Emission Index vs. time during cold start at 2250rpm - 15kW for various points through the brand new exhaust system.

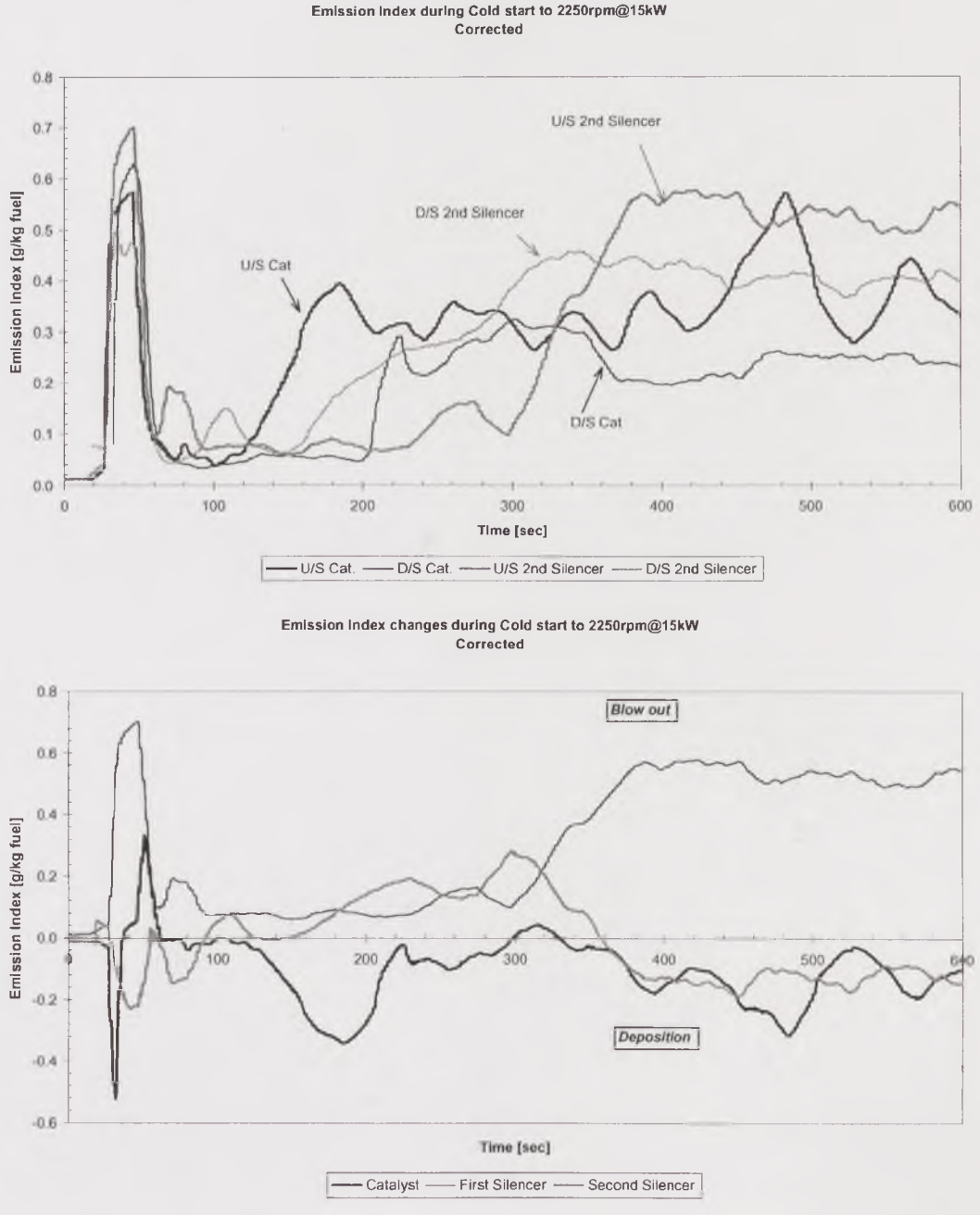

Figure 6.1. Total number concentration and Emission Index vs. time during cold start at 2250rpm - 15kW for various points through the brand new exhaust system. b) Corrected Emission Index.

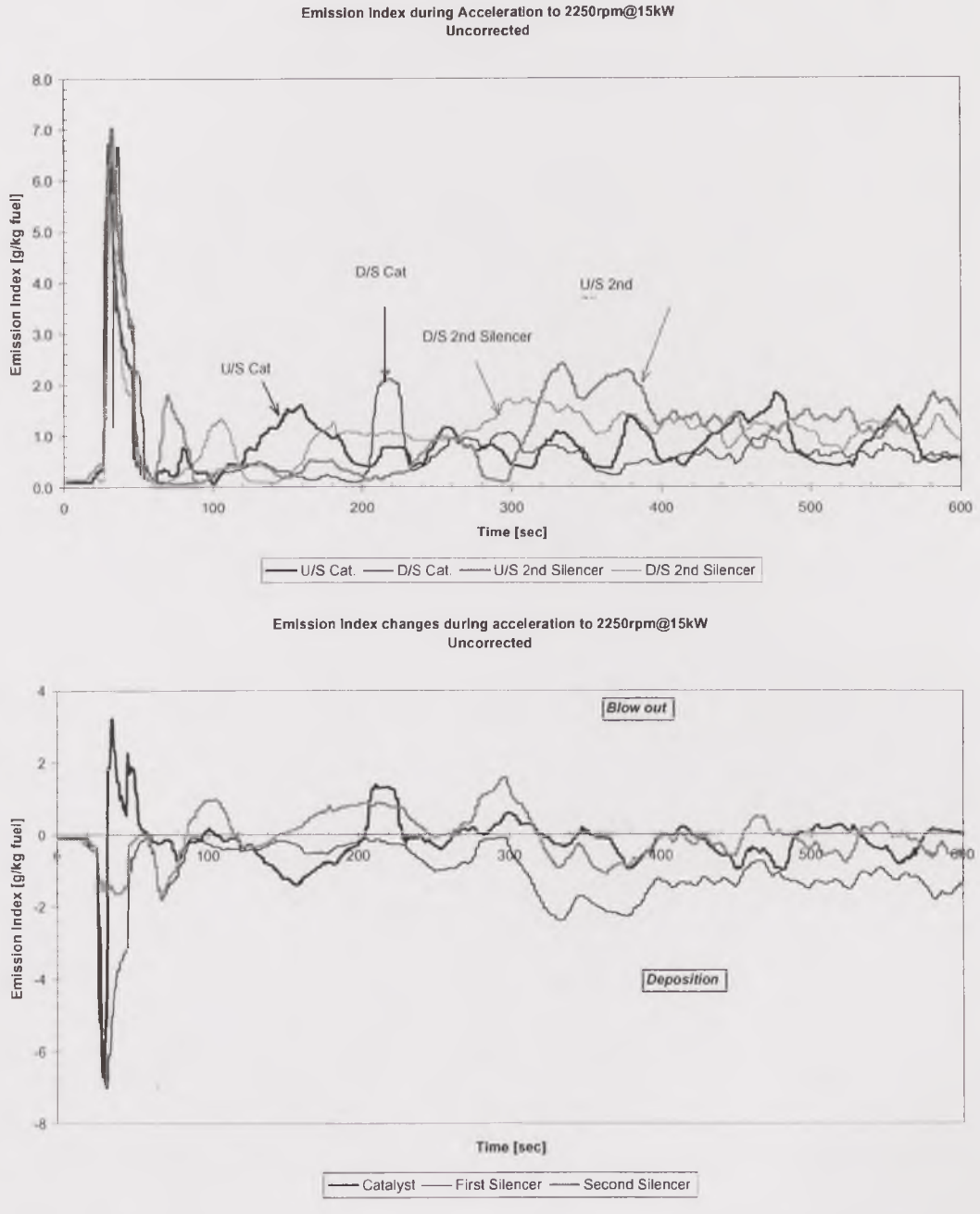

Figure 6.1. Total number concentration and Emission Index vs. time during cold start at 2250rpm - 15kW for various points through the brand new exhaust system. b) Uncorrected Emission Index.

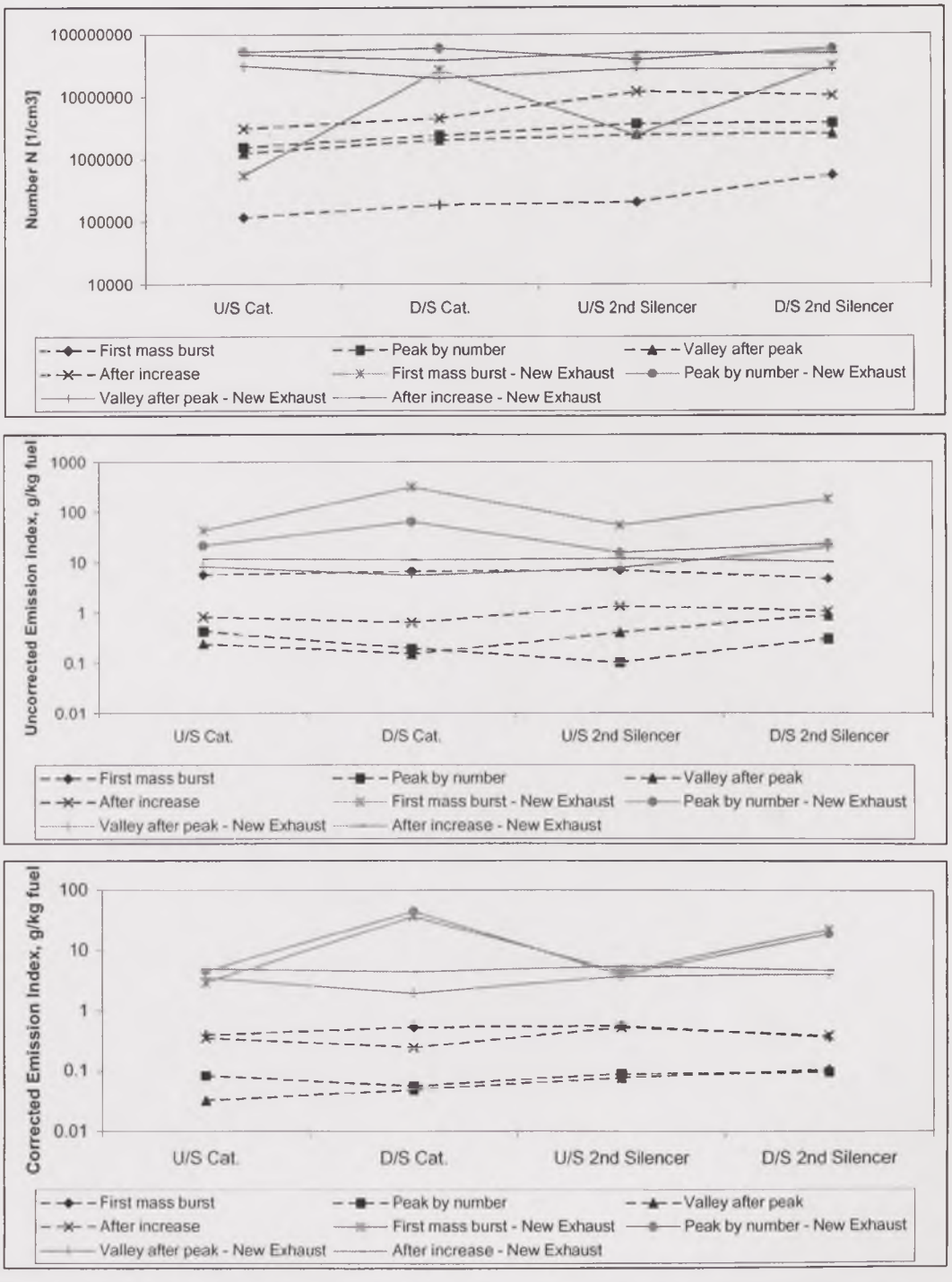

Figure 6.2. Total number concentration and Emission Index vs. position in the new exhaust for the main events during cold start at 2250rpm - 15kW.

One of the cycles was particularly significant in the increase of both particle number concentration and Emission Index, and was related to the EGR valve opening, as observed in previous tests. After 300s, the particle number concentration and Emission Index tended to stabilise for most of the tests, except when sampling

downstream of the second silencer, which took around 100s more to reach a stable condition.

As in previous tests, the particle number concentration and Emission Index variations with time were summarised in a set of the most significant events, to determine the changes through the exhaust system. This is shown in Figure 6.2. Before starting the description of the changes in particulate emissions during the main events of the cold start test, it is worthwhile noticing that the particle number and mass concentrations in Figures 6.1. and 6.2. are between one and two orders of magnitude higher in the tests with the new exhaust system than in the corresponding tests with the old exhaust system at the same conditions. This occurs for both number and mass emissions, as shown in Figure 6.2., and for all sampling points, including upstream and downstream of the catalyst, which were not supposed to change, or at least not to this extent. The reasons for which the emissions were so different are not clear, but the following factors may have played an important role in this change:

- The tests were performed with a two-year and a half difference, period over which a major maintenance and several minor changes were performed to the engine. During the major maintenance period, the engine was totally dismantled and then rebuilt with new spare parts such as the gasket sealing plates. Also, cooling-system hoses and the fuel pump were replaced, but it is not well understood why this increased particulate emissions.
- The fuel was always bought from the same retailer and under the same specifications. However, it is likely that some of its characteristics changed, so that the fuel used for the new exhaust tests may have had different combustion characteristics, mainly regarding particulate formation. The main parameter in this respect may be the fuel sulphur content.
- There was a change in the technician performing the engine maintenance and operation around the middle of the testing period for this work. Different practices and maintenance procedures may have been important in the engine overall performance and, therefore, emissions. The author, however, was not aware of these changes.

From these considerations, the results from the tests with the new exhaust were not really comparable to those from the previous tests. Therefore, the new exhausts results were considered rather independently, in terms of emission levels, although the trends in deposition or reentrainment processes were taken into account to make as many contributions as possible to the conclusions of this work.

The following sections describe the changes through the system for the different events.

6.1. First mass burst

During the first mass-burst event, analysed for particle size distribution changes in Figure 6.3., the exhaust aerosol entering the exhaust system had a particle number concentration of 1.15×10^5 cm^3, an uncorrected Emission Index of 5.70 g/kg fuel and a corrected Emission Index of 0.40 g/kg fuel. Through the catalyst, an increase by 61% took the particle number concentration to 2.06×10^5 cm^3, and the Emission Index increased by 17% and 34%, to 6.67 g/kg fuel and 0.54 g/kg fuel, uncorrected and corrected, respectively. Particle coagulation and reentrainment occurred through the catalyst.

Through the second silencer, the particle number concentration increased by 11%, to 2.06×10^6 cm^{-3}. The uncorrected Emission Index increased by 5%, to 7.0 g/kg fuel, and the corrected Emission Index, by 4%, to 0.559 g/kg fuel. The increase in number occurred for particles smaller than 0.08μm, and the increase in Emission Index, for particles larger than 2.0μm. Particles between 0.08μm and 2.0μm were deposited through the silencer. Since the test sampling from the points involved, namely upstream and downstream of the first silencer, was carried out after running the engine for some time, the blown-out particles larger than 2.0 were, presumably, part of the first deposition layer formed on the clean walls during the first test, which sampled the exhaust aerosol from the point downstream of the catalyst. The increase in the number and Emission Index of particles finer than 0.08μm was presumably due to very fast condensation and coagulation processes.

Through the second silencer, the particle number concentration nearly doubled, to 5.58×10^6 $cm\text{-}^3$. However, the Emission Index decreased by 34%, to 4.59 g/kg fuel when uncorrected, and 0.37 g/kg fuel when corrected. The increase in number occurred for particles between 0.035μm and 0.3μm and was presumably due to condensation and agglomeration processes, whereas the decrease in Emission Index occurred for particles larger than 0.3μm, which deposited on the second silencer walls.

In summary, the analysis of changes through the exhaust system in the mass-burst event gave evidence that there was a new deposition layer developing on the walls of the new exhaust, formed mainly by mid-sized and large particles, and that increases in particle number through the exhaust system was due to condensation and coagulation processes.

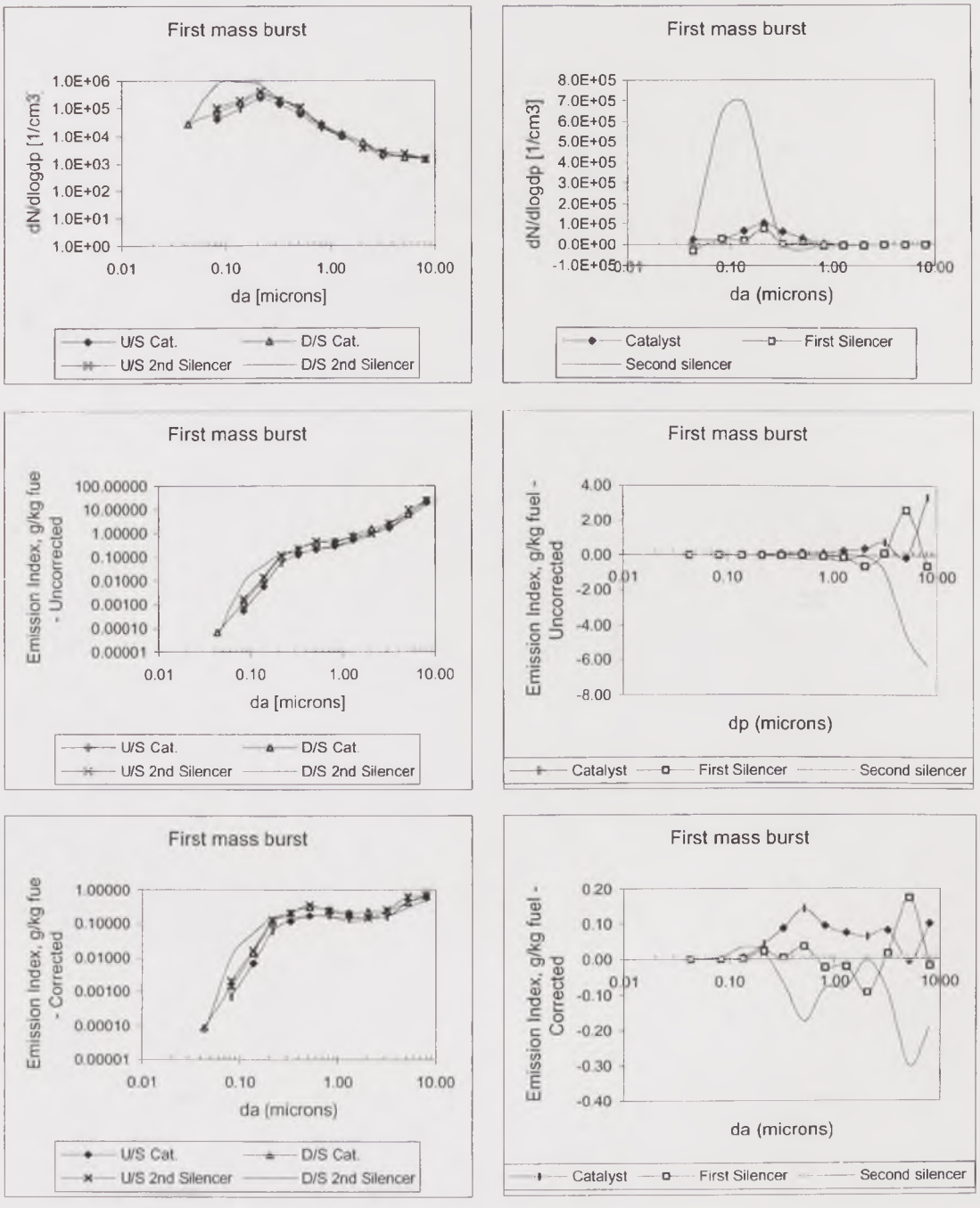

Figure 6.3. Particle number and Emission Index size distributions (left), and particulate changes vs. particle size, expressed as blow-out (right), for various points through the exhaust system during the first mass-burst event of the cold start at 2250rpm - 15kW.

6.2. First temporary peak-number event

Together with the mass-burst event, the first peak-number event, shown in Figure 6.4., was considered in this analysis to represent the transient -acceleration- effects on the deposition/resuspension processes through the exhaust system. Further changes introduce the thermal equilibration processes in the engine and exhaust system once the target conditions have been reached.

The particle number concentration of the exhaust aerosol leaving the turbocharger during the peak-number event was 1.54×10^6 cm^{-3}, one order of magnitude higher than during the mass-burst event. The corresponding Emission Index was, in contrast, one order of magnitude lower, 0.43 g/kg fuel when uncorrected, and 0.083 g/kg fuel when corrected. Through the catalyst, the particle number concentration increased by 56%, to 2.40×10^6 cm^{-3}, but the Emission Index decreased by 56% or 33%, to 0.19 g/kg fuel or 0.056 g/kg fuel, when uncorrected or corrected, respectively. The increase in number occurred for particles smaller than 0.1μm and was mainly due to agglomeration, whereas the decrease in Emission Index occurred for particles larger than 0.1μm, which deposited through the catalyst. Some of these large particles around 4.0μm actually were blown out as a result of the partial contribution of particle reentrainment processes, but their contribution to the overall change in Emission Index was negligible.

Through the first silencer, the particle number concentration increased by 51%, to 3.62×10^6 cm^{-3} owing to the formation of fine particles by condensation. The Emission Index decreased by 48%, to 0.099 g/kg fuel when uncorrected, and by 58%, to 0.077 g/kg fuel, when corrected, owing to deposition of large particles. This contradictory trend between number concentration and Emission Index was due to the size-dependent differences. There was evidence that large particles tended to deposit through the silencer, even at the higher exhaust gas speeds during this event.

Through the second silencer, the particle number concentration increased by only 3%, to 3.72×10^6 cm^{-3}. The uncorrected Emission Index nearly tripled, to 0.295 g/kg fuel, and the corrected Emission Index increased by just 10%, to 0.099. Particles smaller than 0.4μm tended to deposit by thermophoresis, although the number of those around 0.1μm actually increased, presumably by coagulation of finer particles. The number of particles larger than 0.4μm increased and caused a marked increase in the overall uncorrected Emission Index, but this effect was reduced with the correction.

In summary, there was evidence that coagulation of fine particles occurred throughout the exhaust system and that larger particles tended to form a stable

deposition layer on the new walls. However, this layer was unstable owing to the change in speed and temperature, which caused the resuspension of large particles in the section downstream of the first silencer. Changes in the deposition layer were extremely fast.

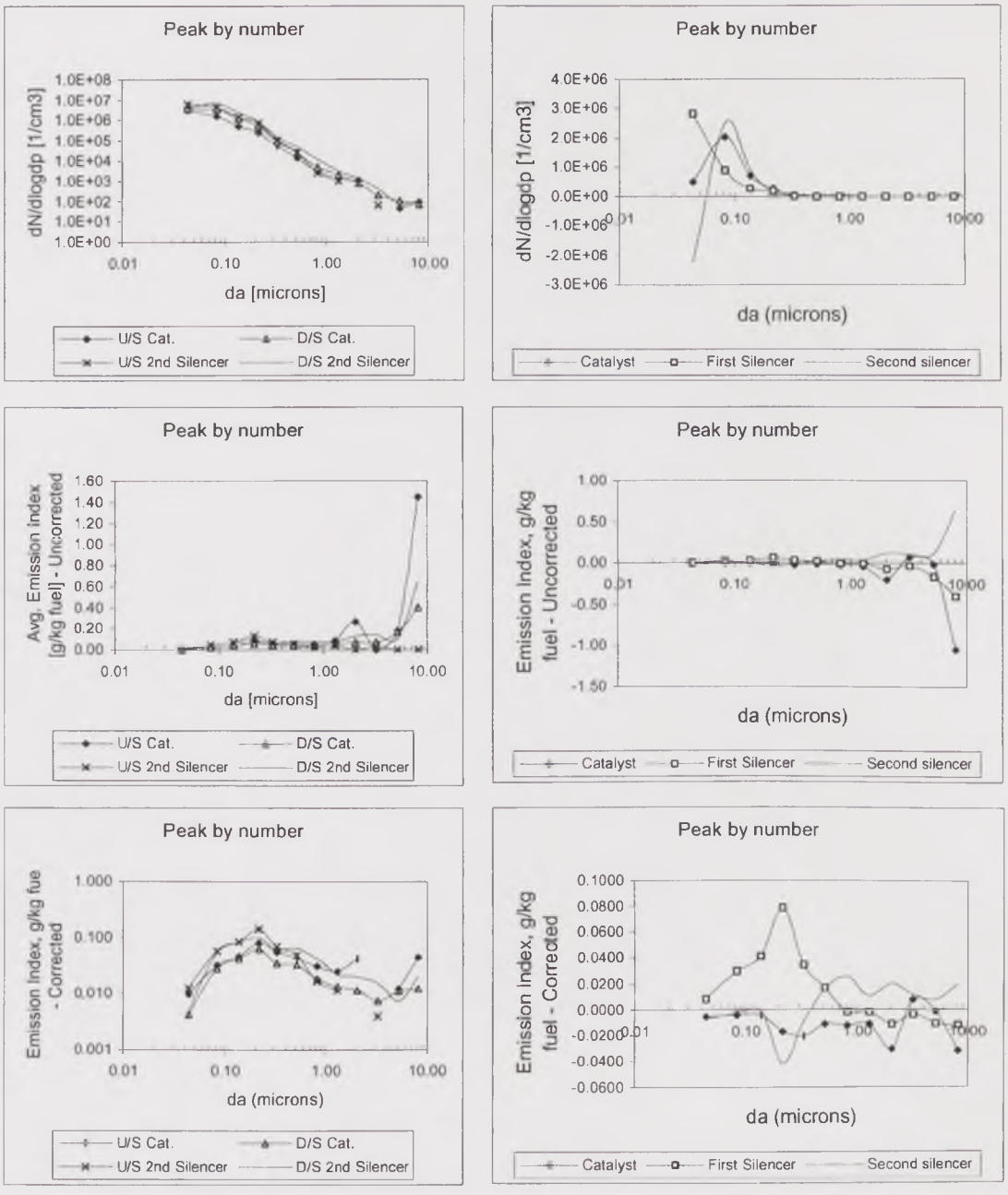

Figure 6.4. Particle number and Emission Index size distributions (left), and particulate changes vs. particle size, expressed as blow-out (right), for various points through the exhaust system during the peak-number event of the cold start at 2250rpm - 15kW.

6.3. Valley after peak

The valley after the temporary peak-number event, Figure 6.5. represented an intermediate point between the disturbance caused by the main acceleration towards target conditions and the thermal-stabilisation of the engine and the exhaust system. The valley event would have been nearly equivalent to a stabilisation condition should the EGR valve have not opened. But the action of the EGR control interrupted this trend towards stabilisation just a few seconds after the low level was reached. During this short period, the total particle number concentration at the entrance to the system was 1.25×10^6 cm^{-3}, 19% lower than in the peak-number event. The corresponding uncorrected and corrected Emission Index values were 0.24 g/kg fuel and 0.033 g/kg fuel, respectively, 44% and 60% lower than during the peak-number, also respectively.

Through the catalyst, the particle number concentration increased by 63%, to 2.03×10^6 cm^{-3}, unlike the uncorrected Emission Index, which decreased by 38%, to 0.148 g/kg fuel. The corrected Emission Index, however, did increase by 49%, to 0.049 g/kg fuel. As in other similar cases, the difference in trends was due to size-dependent opposite changes through the system: the number of particles smaller than 1.0μm increased through the catalyst by condensation and coagulation of finer particles, whereas the majority of larger particles actually deposited.

Through the first silencer, the particle number concentration increased by 20%, to 2.44×10^6 cm^{-3}; the uncorrected Emission Index, by 1.7 times, to 0.399 g/kg fuel; and the corrected Emission Index, by 58%, to 0.077 g/kg fuel. The number of particles increased for virtually all size ranges, with the only exception of those around 0.3μm, which underwent a very slight decrease. The increase in the number of particles smaller than 1.0μm was presumably due to condensation and coagulation of finer particles, and larger particles were presumably released from the newly formed deposition layer.

Through the second silencer, the particle number concentration increased by only 3%, to 2.51×10^6 cm^{-3}; the uncorrected Emission Index, by 1.2 times, to 0.865 g/kg fuel; and the corrected Emission Index, by 42%, to 0.110 g/kg fuel. The increase in number of particles occurred at virtually all size ranges, except just the smallest measured by the ELPI, around 0.035μm. Particles smaller than 1.0μm formed presumably by outgassing, condensation and coagulation processes, increasing the number concentration in this size range. Particles larger than 1.0μm were reentrained as a result of the equilibration processes in the deposition layer at the target condition reached.

In summary, there was evidence that the equilibration processes in the deposition layer on the walls of the exhaust system section downstream of the catalyst originated the reentrainment of particles during the valley-after-peak event and an increment in the number concentration of fine particles by outgassing of semi-volatile components. The increase in number of particles occurred also through the catalyst, but larger particles deposited on it walls.

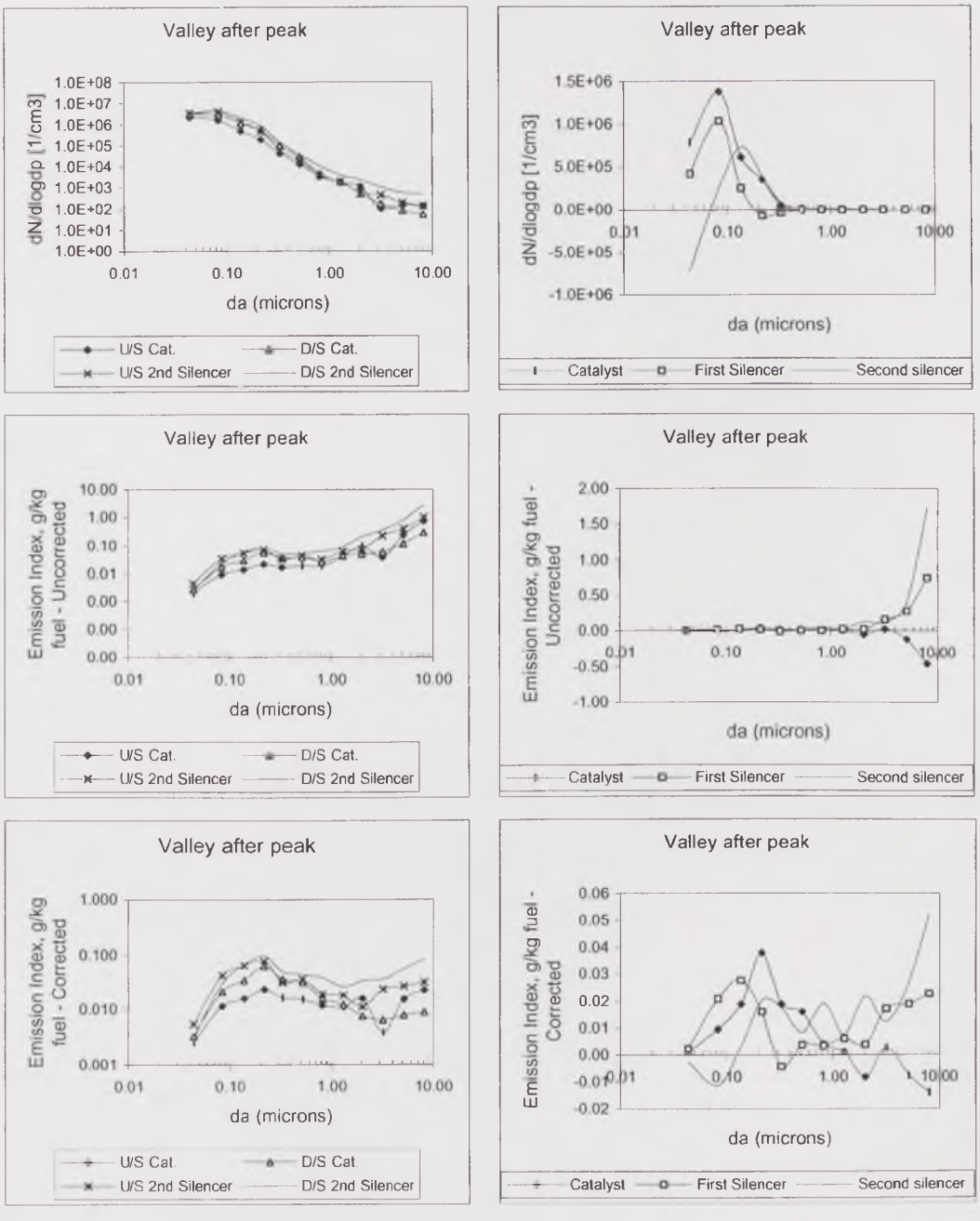

Figure 6.5. Particle number and Emission Index size distributions (left), and particulate changes vs. particle size, expressed as blow-out (right), for various points through the exhaust system during the valley-after-peak event of the cold start at 2250rpm - 15kW.

6.4. Stabilisation after increase

The particle number concentration underwent a number of oscillations to increasingly higher levels until reaching a stabilisation after a rather long period, about 300s. Both particle number concentration levels reached were significantly higher than those observed during the peak number event. Similarly, Emission Index levels were similar to those during the mass burst event. This was a consequence of the increased particulate emission levels originated after the EGR valve opened.

Once stabilised, the particle number concentration upstream of the catalyst was $3.15x10^{6}$ cm^{-3}, and the Emission Index was 0.810 g/kg fuel and 0.351 g/kg fuel, uncorrected and corrected, respectively. Through the catalyst, the particle number concentration increased by 42%, to $4.46x10^{6}$ cm^{-3}. In contrast, the uncorrected Emission Index decreased by 22%, to 0.632 g/kg fuel, and the corrected Emission Index also decreased, by 30%, to 0.245 g/kg fuel. The increase in number occurred for particles smaller than 0.3µm, as shown in Figure 6.6., presumably by outgassing, condensation and coagulation of finer particles, and the decrease in Emission Index was dominated by the reduction in emissions of larger particles due to deposition.

Through the first silencer, the particle number concentration increased by 1.7 times, to $1.20x10^{7}$ cm^{-3}; the uncorrected Emission Index more than doubled, reaching 1.315 g/kg fuel, and the corrected Emission Index underwent even a higher change, to 0.526 g/kg fuel. This considerable increase in number and Emission Index occurred for all size ranges, and was the result of outgassing, condensation and coagulation processes, for fine particles, and reentrainment of large particles. As observed in previous tests this kind of changes are not rare through this section, including the first silencer, in which the characteristics of the flow may be not favourable for the formation of a stable deposition layer.

Through the second silencer, the particle number concentration decreased by 15%, to $1.01x10^{7}$ cm^{-3}; the Emission Index decreased by 21% or 25%, to 1.039 g/kg fuel or 0.392 g/kg fuel, uncorrected or corrected, respectively. The decrease occurred for all size ranges, by thermophoretic, gravitational and inertial deposition, presumably enhanced by turbulence.

In summary, the mirrored behaviour of the particles through the first and second silencers observed in previous tests occurred again for the clean walls of the brand new exhaust system once the stabilisation conditions were reached after the first cold start set of tests. This indicated that the flow characteristics through the system plays a more significant role than the roughness of the new or old systems in

the behaviour of the deposition layer and, therefore, in the particle deposition and reentrainment processes.

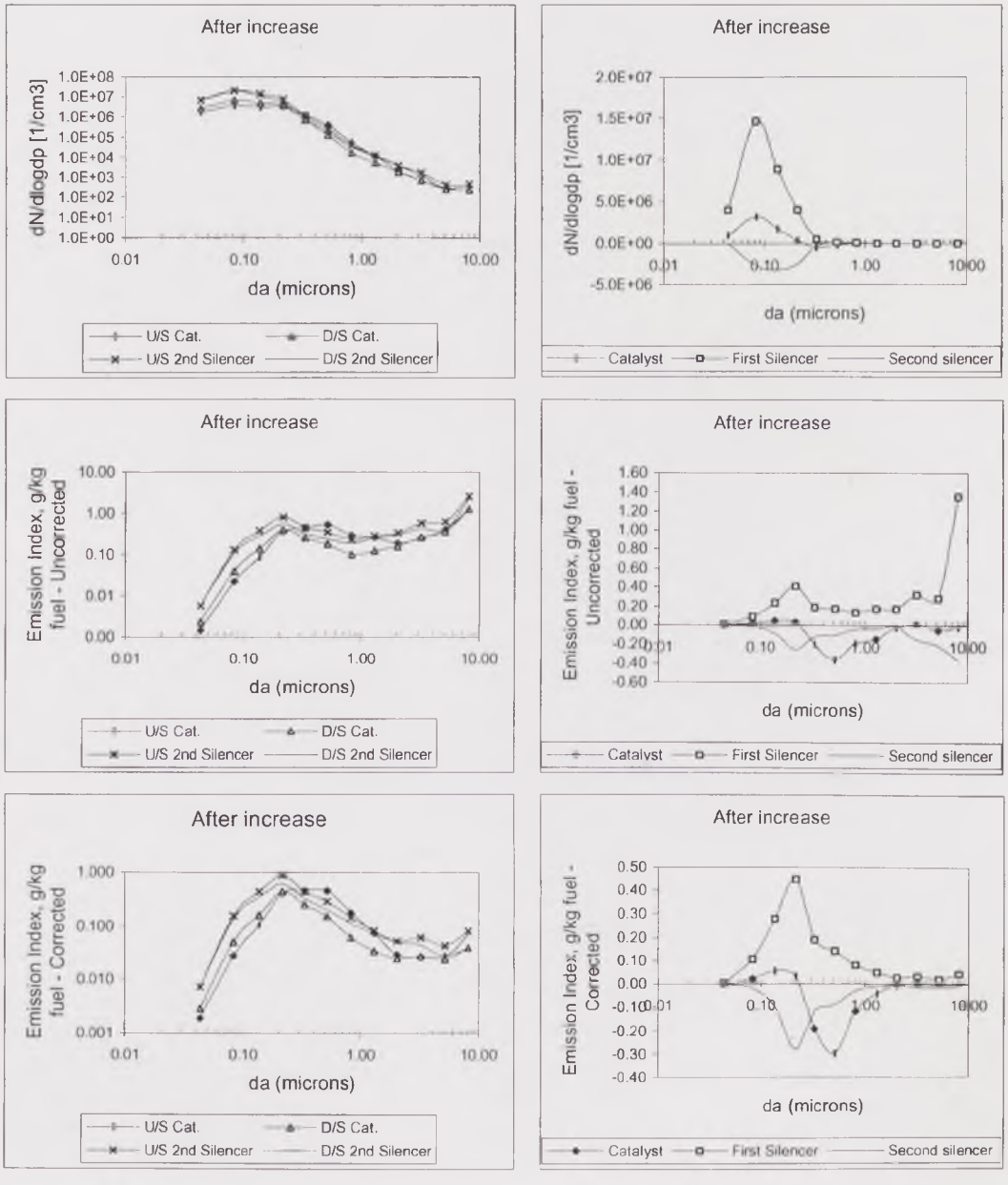

Figure 6.6. Particle number and Emission Index size distributions, and particulate changes vs. particle size, expressed as blow-out, for various points through the exhaust system during the stabilisation event of the cold start at 2250rpm - 15kW.

6.5. Summary of the cold-start with the new exhaust

With the new exhaust section downstream of the catalyst (the catalyst was not changed), the deposition of ultrafine particles through the catalyst and the first silencer was nil, as shown in Figure 6.7. Ultrafine particles were formed through

these devices in most cases, by gas-to-particle conversion processes. Ultrafine particles deposition occurred only through the second silencer, although in fewer cases than ultrafine particle formation.

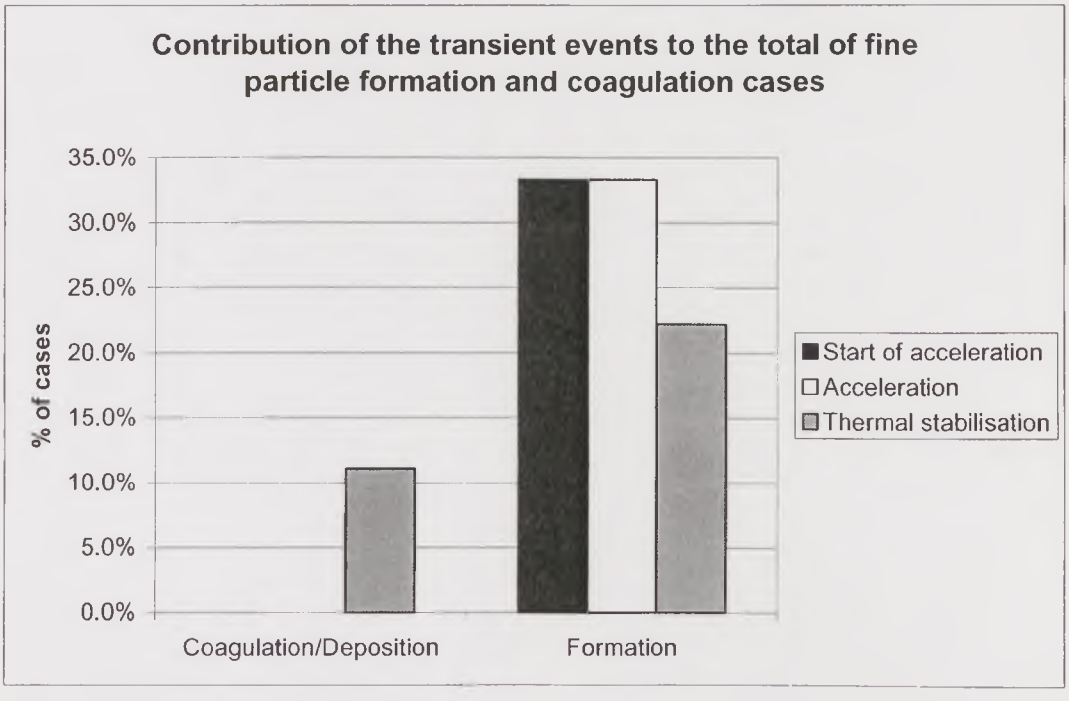

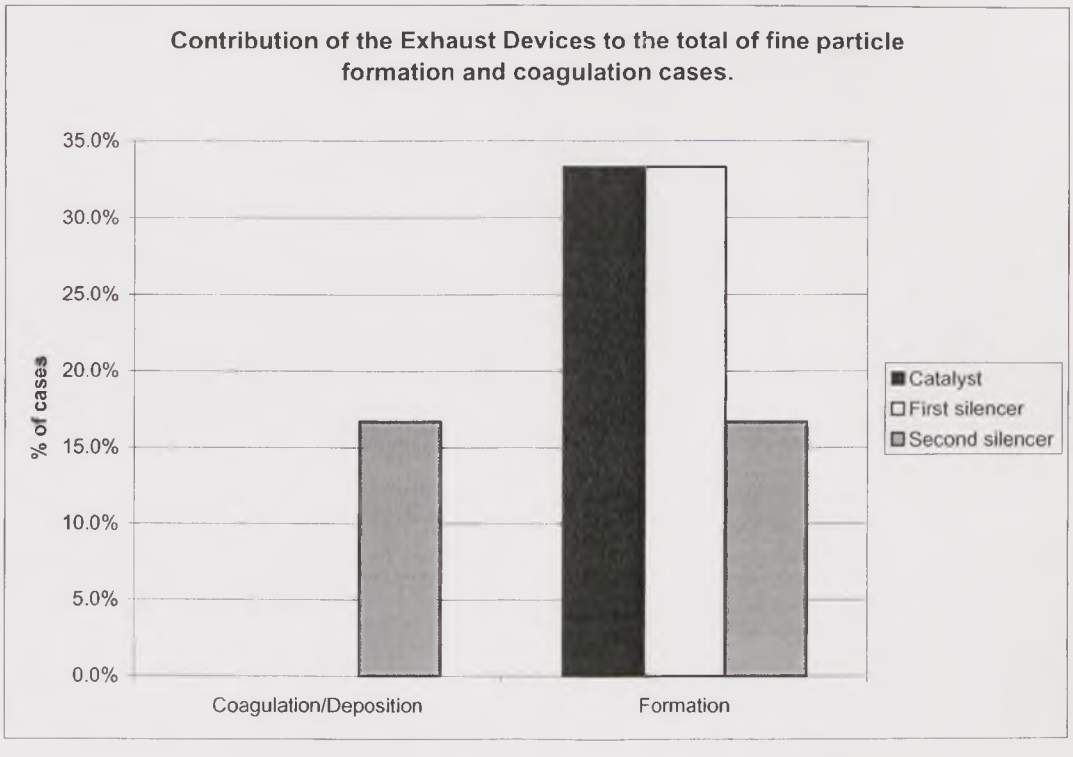

Figure 6.7. Contribution of particle size, transient events and exhaust devices to the total of deposition and blow-out cases during cold start at 2250rpm - 15kW with the brand new exhaust. a) Fine particles.

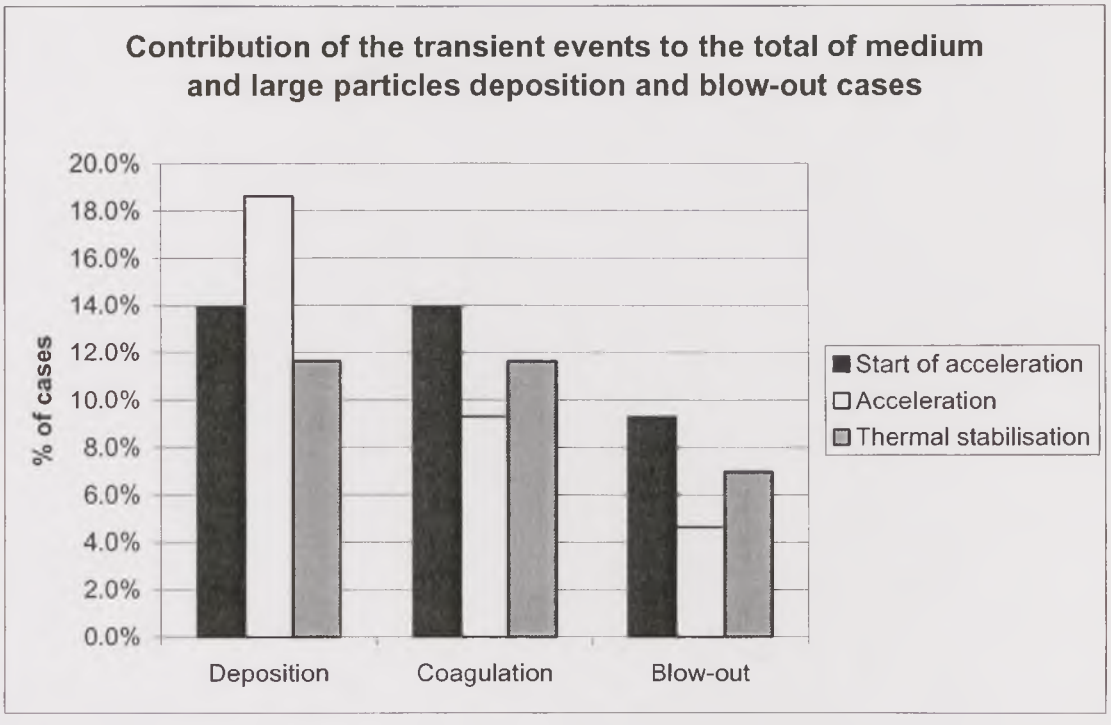

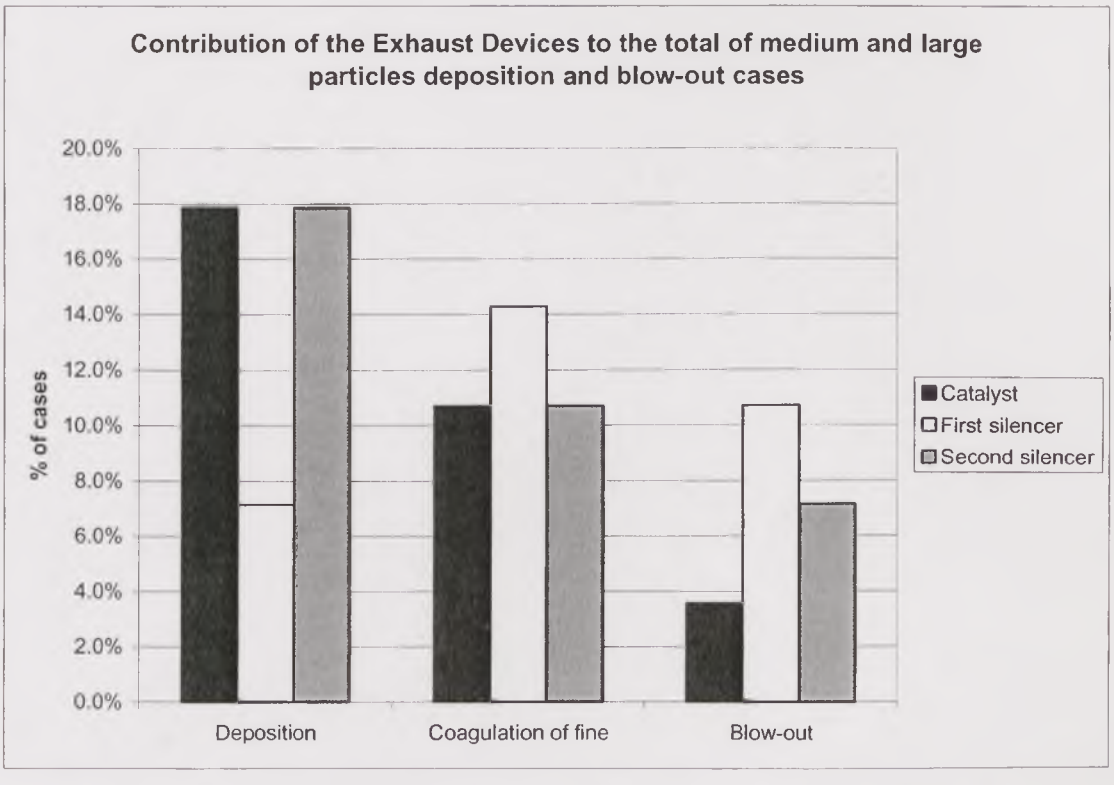

Figure 6.7. Contribution of particle size, transient events and exhaust devices to the total of deposition and blow-out cases during cold start at 2250rpm - 15kW with the brand new exhaust. b) Mid-sized and large particles.

Large particles were deposited mainly through the catalyst and the second silencer, and resuspended from the newly formed deposition layer on the first

silencer walls. The first silencer also promoted condensation and ultrafine particle coagulation in more cases than the catalyst and the second silencer.

Ultrafine particle formation by gas-to-particle formation occurred mainly during acceleration, when virtually no deposition of these particles occurred through the exhaust system. Fine particle coagulation and large particle resuspension were predominant during the start of the acceleration, but not during the whole acceleration period. After the first few seconds of acceleration, particle deposition through the system was the prevalent process.

6.6. Idle steady-state with the new exhaust

The engine was run at idle for 4 hours to observe the changes in particulate emissions through the brand new exhaust system. Figure 6.8. shows the average particulate number concentration and Emission Index vs. location in the exhaust system, including the error bars given by the standard deviation of the measurements at each point, and Figure 6.9., the size distribution changes.

The particle number concentration at the entrance of the exhaust system was 1.73×10^6 cm^{-3}; the uncorrected Emission Index, 0.626 g/kg fuel; and the corrected Emission Index, 0.100 g/kg fuel. Through the catalyst, the particle number concentration decreased by 42%, to 9.96×10^5 cm^{-3}; the Emission Index decreased by 35% and 42%, to 0.407 g/kg fuel and 0.058 g/kg fuel, uncorrected and corrected, respectively. The decrease occurred for all size ranges by thermophoretic and gravitational deposition processes, as well as catalytic oxidation. There were no significant changes in the size distribution through the exhaust system.

Through the first silencer, the particle number concentration increased by 11%, to 1.11×10^6 cm^{-3}; the Emission Index increased by 24%, to 0.510 g/kg fuel and 0.072 g/kg fuel, uncorrected and corrected, respectively. The change occurred for all size ranges, by condensation and coagulation of very fine particles, and by resuspension of large particles.

Through the second silencer, a new decrease in particle number concentration occurred, by 10%, to 9.92×10^5 cm^{-3}; the uncorrected Emission Index decreased by 7%, to 0.473 g/kg fuel; and the corrected Emission Index, by 4%, to 0.069 g/kg fuel. The decrease in number concentration occurred for all size ranges, although it was negligible for particles between 0.3μm and 3.0μm. The decrease in particle number concentration was mainly due to deposition and coagulation of particles below 0.1μm, and the decrease in Emission Index was the result of the deposition of large particles, with some contribution of the coagulation of particles around 0.2μm.

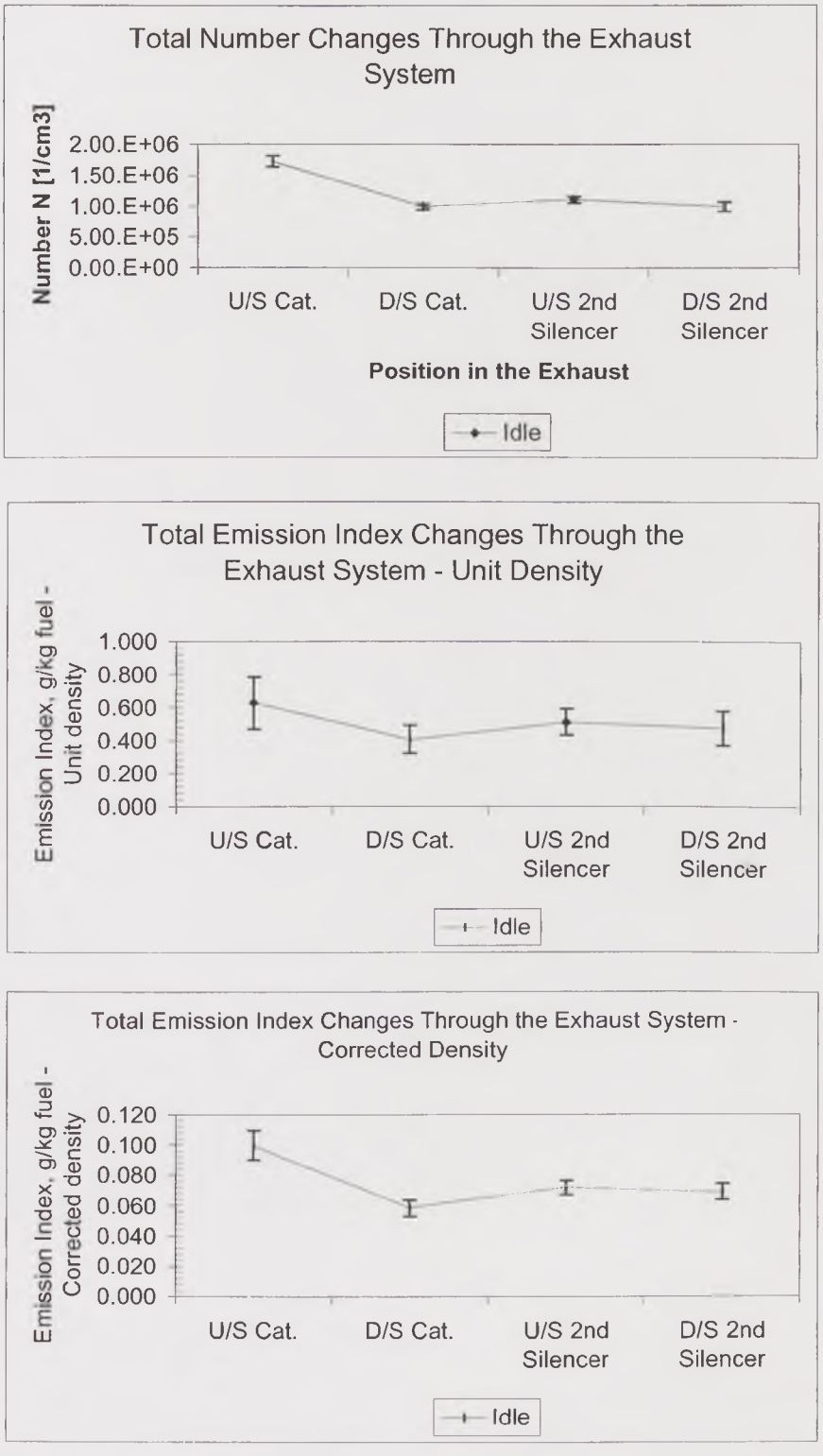

Figure 6.8. Total number concentration and Emission Index through the new exhaust system at idle steady-state conditions.

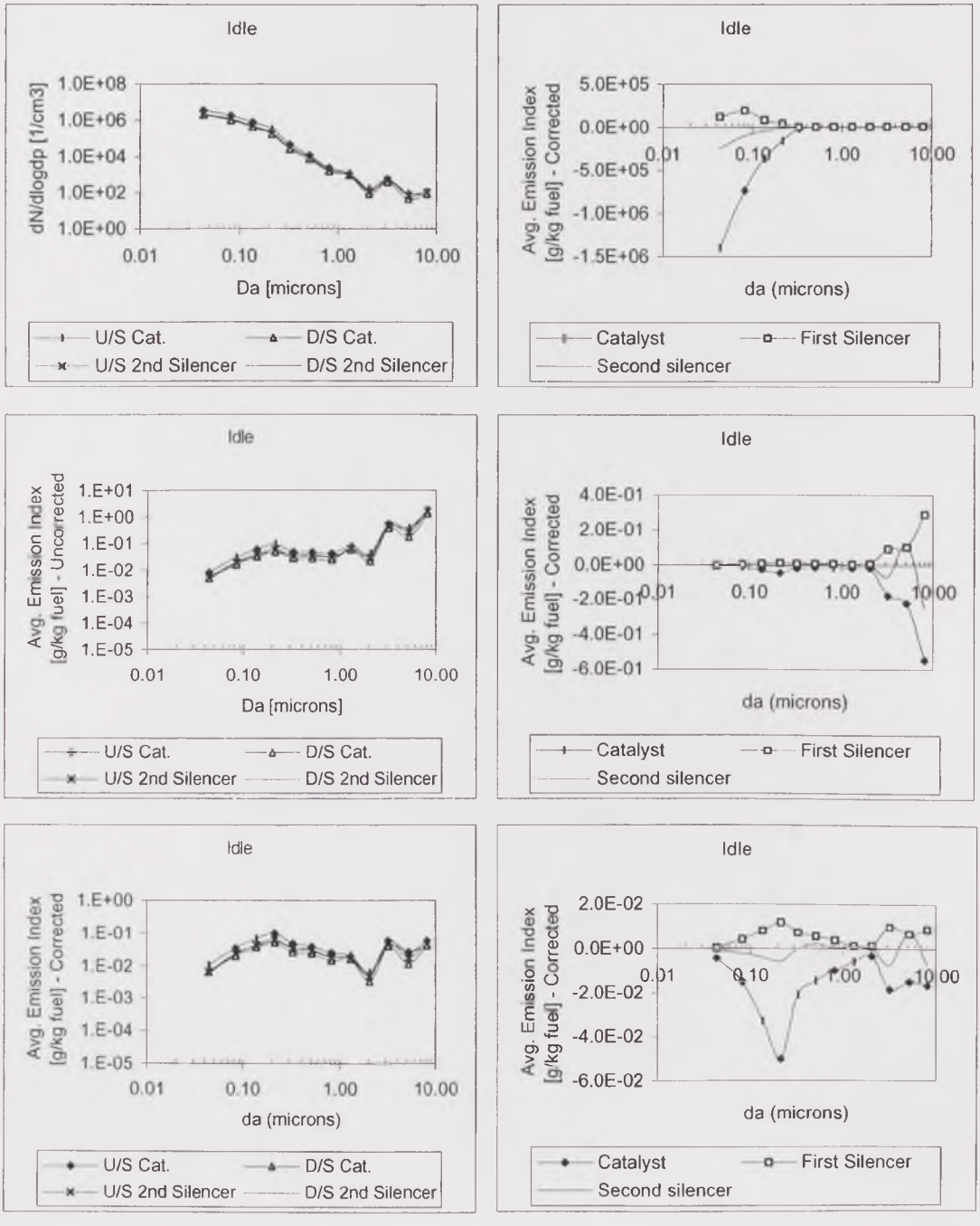

Figure 6.9.Particle Number and Emission Index size distributions and blow-out vs. size at Idle steady state conditions through the new exhaust system.

6.7. Key points from this chapter

The cold-start and idle tests with the new exhaust were performed with the aim of investigating the influence of a new exhaust system on the particulate deposition processes and comparing the resulting emission levels with previous results. This objective, however, was not thoroughly fulfilled owing to reasons that are not totally

understood. The main influencing factors were identified as the most likely contributors to this:

- a major maintenance that included the total dismantling and rebuilding of the engine
- several maintenance inspections and replacement of spare parts, some of them as important as the fuel pump
- variability in the fuel quality, despite buying it from the same retailer
- variability in the maintenance performed by different technicians

The measurements from the new exhaust tests showed evidence that:

- the particulate deposition layer was formed very quickly on the walls of the exhaust system, mainly by deposition of mid-sized and large particles;
- processes of reentrainment were present whenever deposition takes place, and there was evidence that both processes were simultaneous even with an incipient deposition layer;
- ultrafine particles were not deposited throughout the new exhaust, but formed by gas-to-particle processes.

Chapter 7.
Discussion

7.1. Analytical summary of the results

7.1.1. Comparison of ELPI measurements vs. engine conditions throughout this work

Continuous monitoring of a diesel engine's cold-start and acceleration transients throughout this work showed recurring characteristics that have been identified as an initial mass burst followed by a peak in number concentration and subsequent changes leading to a stabilisation in particle number concentration and Emission Index, which may include an increase in these parameters if the EGR valve opens in the process.

The summary of the exhaust-system-average total particle number concentration and Emission Index from ELPI measurements for the peak-number and stabilisation events of the various tests is shown in Table 7.1. and Figure 7.1. Table 7.2. and Figure 7.2. show the corresponding Emission Index measurements with total mass filters for cold-start tests.

The lowest average particle number concentration during the peak-number event occurred at idle, at 9.0×10^6 cm^{-3}. For the same event, the acceleration cycles to 2250rpm - 15kW showed the second lowest average number concentrations, 1.3×10^7 cm^{-3} and 1.1×10^7 cm^{-3}. Higher concentrations were measured for the second cycle of the acceleration to 3500rpm - 15kW, 2.5×10^7 cm^{-3}, and the first cycle of the same test, 5.2×10^7 cm^{-3}. The latter level was very close to the concentration in the cold-start tests at 2250rpm - 15kW and 2250rpm - 35kW after high-speed conditioning, 5.2×10^7 cm^{-3} and 5.3×10^7 cm^{-3}, respectively. The cold-start test at 1500rpm - 10kW showed a peak number concentration at 8.0×10^7 cm^{-3}. The remaining tests, namely the cold-start test at 2250rpm - 35kW after idle conditioning, and both cold-start tests at 3500rpm - 15kW, showed the highest peak number concentrations: 1.0×10^8 cm^{-3}; $1.2 \times 10^8 cm^{-3}$ and 1.4×10^8 cm^{-3}, respectively. Overall, the number concentration during the peak-number event showed a factor-of-15 difference among the various tests.

The particle number concentration during the stabilisation event showed a similar relative relationship to the test conditions as that during the peak-number event. The lowest concentrations occurred in the cold-start test at idle and acceleration tests to 2250rpm - 15kW, 2.1×10^6 cm^{-3}, 9.0×10^7 cm^{-3} and 8.8×10^7 cm^{-3},

respectively; and the highest in the cold-start tests at 2250rpm - 35kW, $9.5x10^7$ cm^{-3} and $8.8x10^7$ cm^{-3}. The acceleration tests to 3500rpm - 15kW showed intermediate concentrations, around $1.8x10^7$ cm^{-3}, and the cold-start tests to the same conditions, $4.0x10^7$ cm^{-3}, and $5.4x10^7$ cm^{-3}. Similar values were observed for the cold-start tests at 1500rpm - 10kW and 2250rpm - 15kW, $6.0x10^7$ cm^{-3} and $4.6x10^7$ cm^{-3}, respectively. The variation between the lowest and highest average number concentrations in this event was a factor of 38 higher than that in the peak-number event.

	Number concentration, cm^{-3}		Uncorrected Emission Index, g/kg fuel			Corrected Emission Index		
Condition	Peak number	Stabilisation	Mass burst	Peak number	Stabilisation	Mass burst	Peak number	Stabilisation
Idle	9.01E+06	2.05E+06	20.01	4.66	0.50	1.69	2.77	0.16
1500-10	8.00E+07	6.03E+07	54.73	13.96	15.12	4.04	4.49	5.84
2250-15	5.20E+07	4.57E+07	147.80	30.85	11.26	16.34	17.81	4.88
2250-35 Idle conditioning	1.04E+08	9.55E+07	29.26	6.09	27.50	4.30	1.46	9.37
2250-35 High-speed conditioning	5.33E+07	8.81E+07	15.53	5.73	22.00	3.44	1.09	8.02
3500-15 Idle conditioning	1.24E+08	3.96E+07	29.59	11.70	5.96	5.60	3.92	1.90
3500-15 High-speed conditioning	1.44E+08	5.36E+07	91.32	18.37	6.74	7.63	3.65	2.01
2250-15 Acceleration 1	1.29E+07	9.05E+06	5.09	2.50	1.30	0.62	1.35	0.57
2250-15 Acceleration 2	1.13E+07	8.84E+06	5.51	1.91	1.47	0.61	0.81	0.66
3500-15 Acceleration 1	5.22E+07	1.75E+07	30.30	8.14	2.01	2.89	1.84	0.42
3500-15 Acceleration 2	2.47E+07	1.86E+07	7.87	3.63	1.99	0.78	0.80	0.46

Table 7.1. Average Particle Number Concentration and Emission Index from ELPI measurements throughout this work.

The Emission Index calculated from the ELPI particle size distributions showed also great changes among the various tests. In the initial mass burst event, the Uncorrected Emission Index showed an average as high as 147 g/kg fuel during the cold-start test at 2250rpm - 15kW. This, which appears to be an unrealistic value when compared to filter measurements, converted to 16.34 g/kg fuel when corrected. Other high Emission Index in this event occurred in the cold-start test at 3500rpm - 15kW after high-speed conditioning, at 1500rpm - 10kW, and at 2250rpm - 35kW after Idle conditioning, as well as in the first cycle of the acceleration test to 3500rpm - 15kW: 91.3 g/kg fuel (7.63 g/kg fuel corrected), 54.7 g/kg fuel (4.0 g/kg fuel corrected), 29.3 g/kg fuel (4.3 g/kg fuel corrected) and 30.3 g/kg fuel (2.9 g/kg

fuel corrected), respectively. The lowest values were measured in the acceleration cycles to 2250rpm - 15kW and the second acceleration cycle to 3500rpm - 15kW: 5.1 g/kg fuel (0.6 g/kg fuel corrected), 5.5 g/kg fuel (0.61 g/kg fuel corrected) and 7.9 g/kg fuel (0.8 g/kg fuel corrected). Overall, in the mass-burst event, the uncorrected Emission Index was between 5 g/kg fuel and 50 g/kg fuel, and the corrected Emission Index, between 0.6 g/kg fuel and 7.0 g/kg fuel.

Condition	Emission Index first 2 min. (Cold start), g/kg fuel	Emission Index after 2 min. (Stabilisation), g/kg fuel
Idle	19.31	22.15
1500 rpm, 10 kW	13.98	5.72
2250 rpm, 15 kW	2.25	4.29
2235-15, Idle conditioning	1.15	1.68
2235-15, High-speed conditioning	2.33	3.27
3500-15, Idle conditioning	1.49	1.41
3500-15, High-speed conditioning	1.10	0.54

Table 7.2. Average Emission Index from total mass filter measurements in cold-start tests.

The stabilisation event was equivalent to steady-state operation after the effect of the transient changes in engine speed and load had ceased. However, some differences in Emission Index were observed during the stabilisation event at the same conditions, depending on the type of test performed. The stabilisation Emission Index was the lowest at Idle, 0.5 g/kg fuel (0.2 g/kg fuel corrected). The second lowest level occurred at 3500rpm - 15kW in the acceleration tests, 1.4 g/kg fuel (0.6 g/kg fuel corrected) and at 2250rpm - 15kW also in the acceleration tests, 2.0 g/kg fuel (0.4 g/kg fuel corrected). At 3500rpm - 15kW, in the cold-start tests, the Emission Index was around 6.3 g/kg fuel (2.0 g/kg fuel corrected). The highest levels were measured in the cold-start test at 2250rpm - 15kW, 1500rpm - 10kW and 2250rpm - 35kW: 11.3 g/kg fuel (4.9 g/kg fuel corrected), 15.1 g/kg fuel (5.8 g/kg fuel corrected) and 24 g/kg fuel (9.0 g/kg fuel corrected).

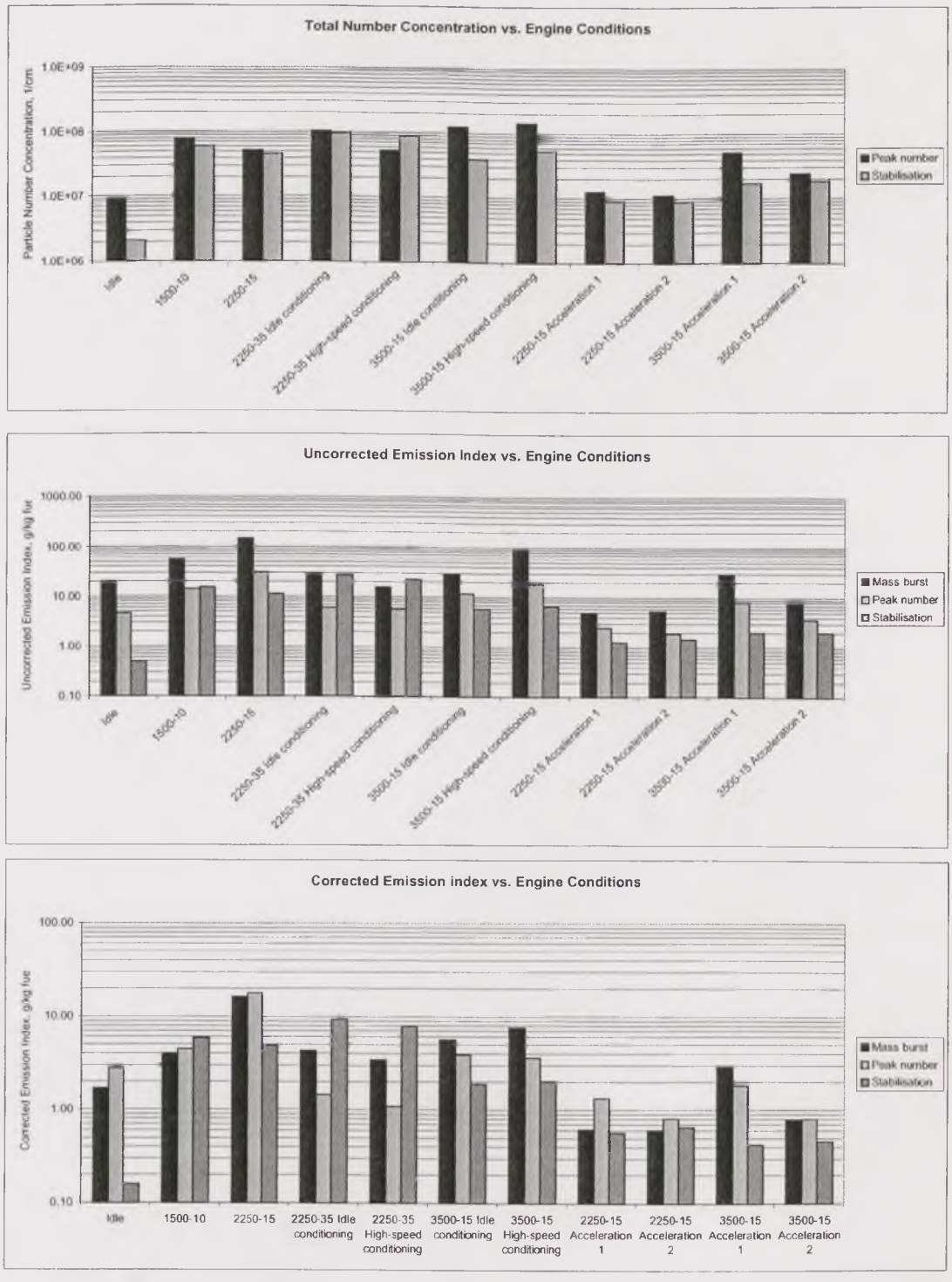

Figure 7.1. Average Particle Number Concentration and Emission Index from ELPI during the main events of cold start and acceleration tests.

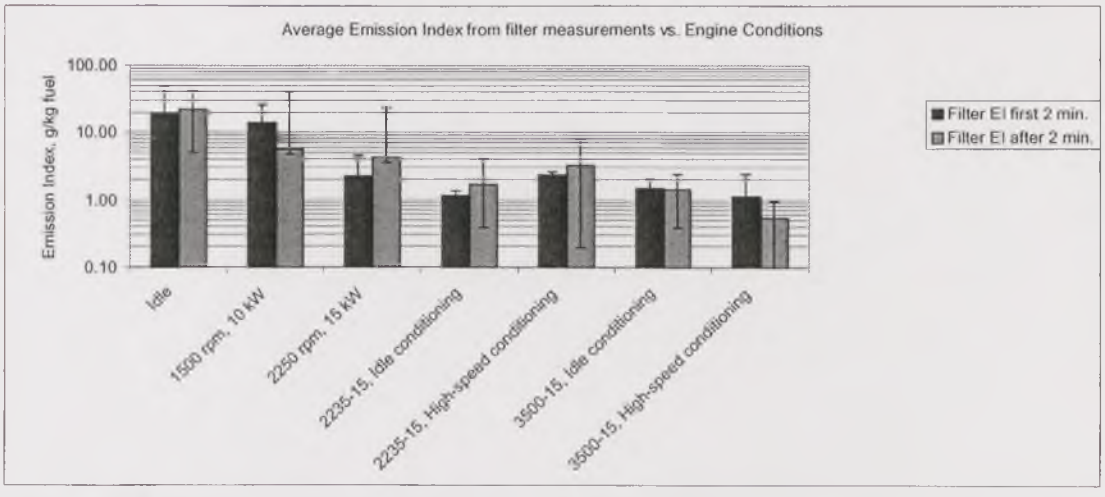

Figure 7.2. Average Emission Index from total mass filter measurements during cold start tests.

The particle size distribution had a great impact on the calculation of Emission Index from particle number concentrations, especially for particles larger than 1.0μm, since it was assumed, for this calculation, that particles were spherical. From the bimodal lognormal distribution fit, the accumulation and coarse modes revealed this impact, as differences between number-weighed and mass-weighed size distribution modes. The modes and standard deviations of the distributions were calculated as the geometric median diameters in the appropriate size range (accumulation and coarse ranges), using equations 1.6., 1.7. and 1.8.

Operation conditions, as well as the various transient events during cold-start and acceleration tests, also affected the distribution modes. These effects are shown in Figure 7.3., for the accumulation mode (particles between 0.1μm and 1μm, and Figure 7.4., for the coarse mode (particles larger than 1μm). The number-weighed accumulation mode had a maximum range between 0.06μm and 0.24μm. During the cold start tests, the accumulation mode in the mass-burst event was higher than in the number-peak event. At idle, 1500rpm - 10kW and 2250rpm - 15kW, the accumulation mode in the mass-burst event was in the high edge of the range, around 0.2μm, indicating the preferential emission of mid-size particles in this event. For the high-speed and high-power conditions, the aerosol emissions in the mass-burst event had a smaller accumulation mode, around 0.12μm. Only in the cold-start test at 2250rpm - 35kW did the aerosol show a mass-burst accumulation mode at 0.07μm. This was the most recurring mode for the number-peak event of cold start tests instead. The only tests showing a peak-number accumulation mode larger than 0.1μm were those at Idle and 2250rpm - 15kW. In the stabilisation event, most cold-start tests showed an accumulation mode around 0.1μm, with the exceptions of idle (0.08μm), and 3500rpm - 15kW (0.07μm). The acceleration tests

showed a lesser influence of the transient events: in the acceleration tests to 3500rpm - 15kW, the accumulation mode tended to the lower end of the range, between 0.07μm and 0.08μm for all events, whereas at 2250rpm - 15kW, the accumulation mode was closer to 0.1μm. This indicated that larger particles were emitted at high-power conditions, presumably owing to the higher carbon content of the particles, which acted as a promoter of heterogeneous condensation.

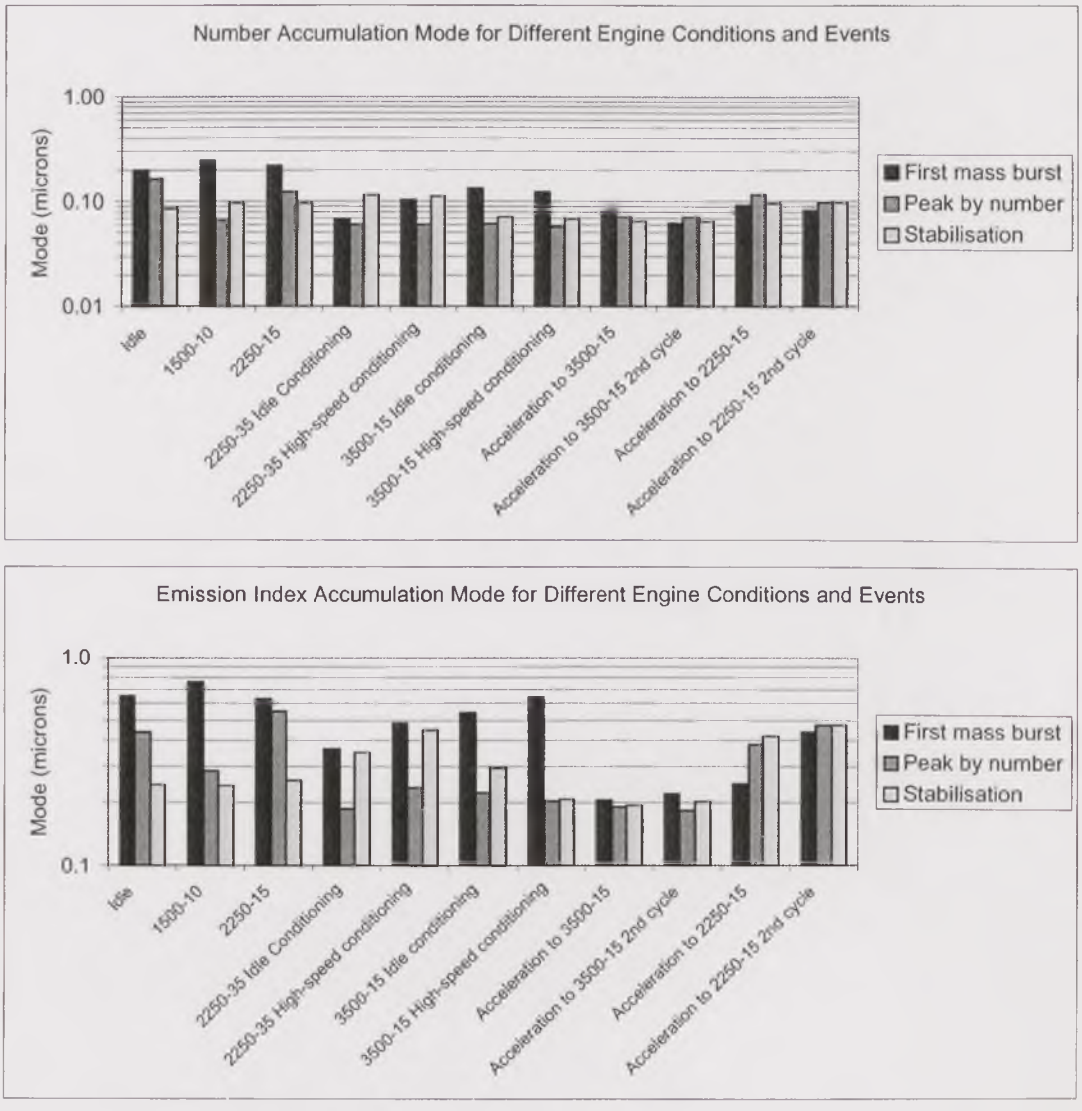

Figure 7.3. Accumulation mode diameter (calculated as the geometric mean diameter in the accumulation size range) based on Number and Corrected Emission Index Size Distributions for the main events of cold start and acceleration tests.

The Emission-Index based accumulation mode diameter did not keep an apparent relationship with its number-based counterpart. It varied between 0.18μm and 0.76μm, being one order of magnitude larger than the number-based Emission Index accumulation mode. The highest values were around 0.7μm, corresponding to

the mass-burst events of the cold-start tests at 1500rpm - 10kW, Idle, 3500rpm - 15kW after high-speed conditioning and 2250rpm - 15kW. The lowest values occurred in the peak-number event of the acceleration cycles to 3500rpm - 15kW and the cold-start at 2250rpm - 35kW after Idle preconditioning.

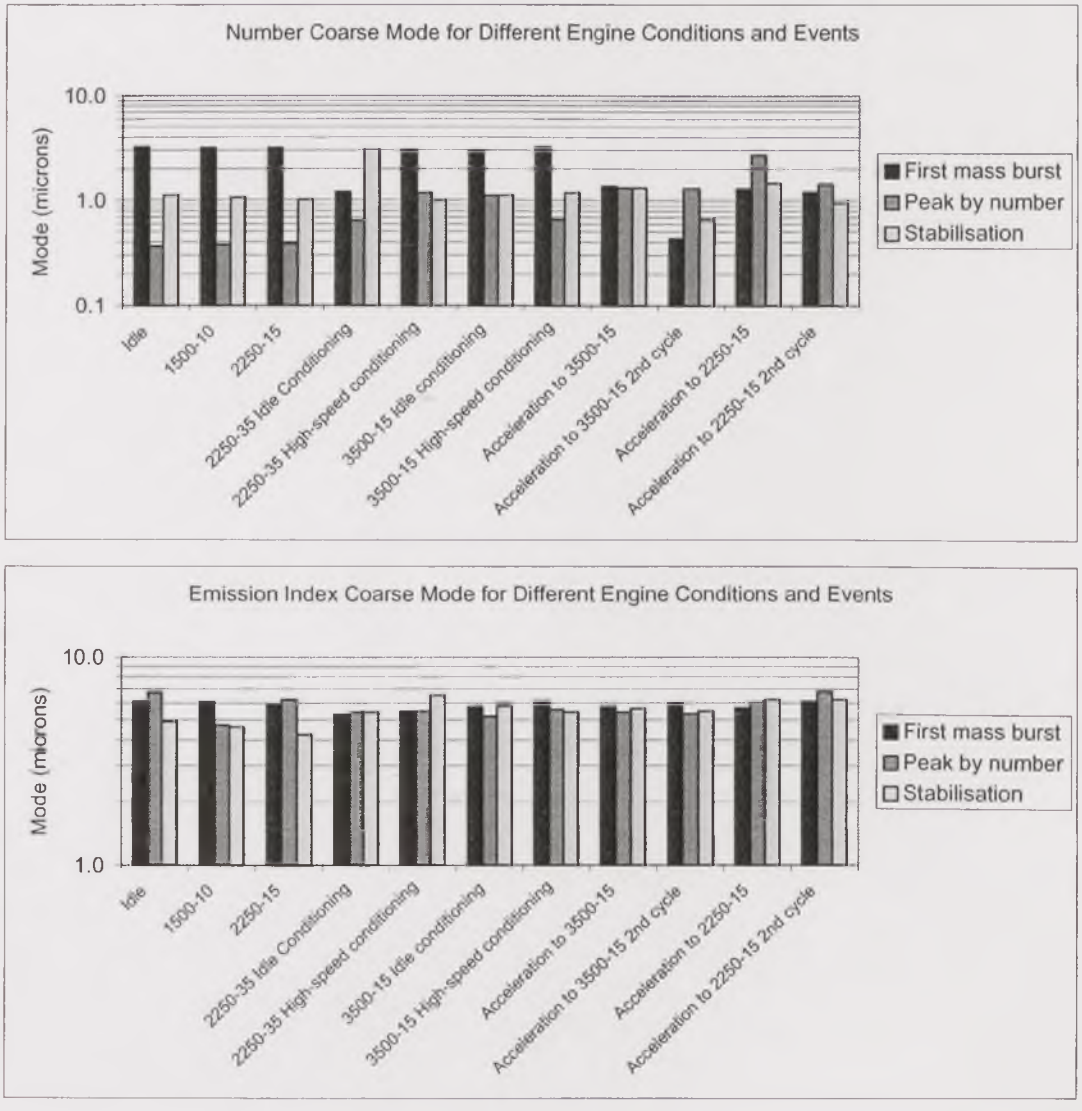

Figure 7.4. Coarse mode diameter (calculated as the geometric mean diameter in the coarse size range) based on Number and Emission Index Size Distributions for the main events of cold start and acceleration tests.

Similarities were found between the cold-start tests at Idle, 1500rpm - 10kW and 2250rpm - 15kW, for which the Emission Index accumulation mode in the mass-burst event was over 0.6µm, decreasing in the number-peak event and settling around 0.25µm in the stabilisation event. For the cold-start tests at 2250rpm - 15kW, the test after idle preconditioning had lower mode values in the mass-burst and stabilisation events, 0.35µm, compared to 0.46µm for the test after high-speed

preconditioning. The peak-number accumulation mode in both cases was around 0.2μm. For the cold-start tests at 3500rpm - 15kW, the stabilisation accumulation mode was higher in the test after idle preconditioning (0.3μm) than after high-speed preconditioning (0.2μm). Around this latter value were measured all the accumulation modes during the acceleration cycles to the same high-speed conditions. Thus, 3500rpm - 15kW emerged as a fine-particle-emitting operating condition for the engine in question. The opposite can be said for the 2250rpm - 15kW conditions, which showed a large Emission-Index accumulation mode during the peak-number and stabilisation events, around 0.4μm.

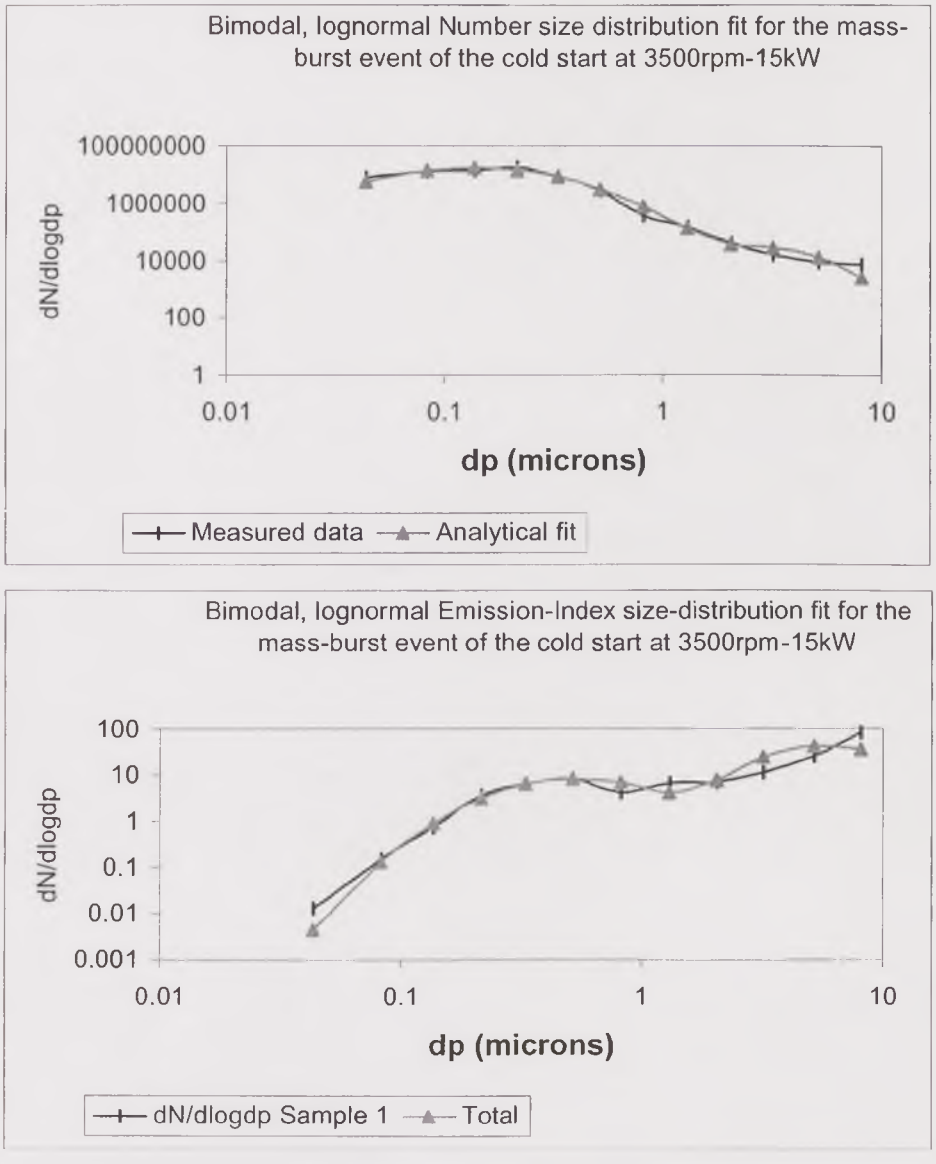

Figure 7.5. Example of analytical fit of a bimodal, lognormal size distribution to ELPI data, from which the accumulation and coarse modes were estimated.

The number coarse mode showed an interesting difference between the cold-start tests and the acceleration tests. For most of the cold-start tests, with the only exception of the test at 2250rpm - 35kW after idle preconditioning, the number coarse mode in the mass-burst event was around 3.0μm, decreasing to 1.0μm in the stabilisation event. The number coarse mode was lower for the mass-burst event of the acceleration cycles, around 1.3μm for three of the four cycles, 0.4μm for the remaining, the second acceleration cycle to 3500rpm - 15kW. From here, the engine appeared to emit larger particles in the mass-burst event of the cold start cycles. In the peak-number event the number coarse mode was similar to that of the cold-start tests at high-speed and high-power conditions in the corresponding event.

The Emission Index coarse mode did not show any discernible trend related to the engine operation conditions. Its value was between 4.2μm and 6.8μm, but this was precisely the range with the poorest fit between the measured data and the analytical bimodal, lognormal size distribution. An example of such fit is shown in Figure 7.5.

7.1.2. Impact of cold-start and acceleration on total emissions for legislative purposes

The integration of number and mass emissions allowed determining the net percentage of emissions during transients, namely cold start and acceleration. Emission values at the tailpipe are shown in Figure 7.6. For most of the tests, particulate mass emissions during cold start or acceleration accounted for more than 20% of the total emissions at the tailpipe, with the exceptions of the cold-start tests with the high-power target condition, 2250rpm - 35kW, and the second cycle of the 2250rpm - 15kW acceleration test. The most dramatic cases were the first cycle of the acceleration test to 3500rpm - 15kW, with 46% of the emissions produced during the transient period, and the first cycle of the acceleration test to 2250rpm - 15kW, with 36%. This is a very significant fraction of the emissions, considering that during the transient period the engine delivered only 7% to 10% of the total work delivered by the engine throughout each test, as shown in Figure 7.7 (the work delivered by the engine is the area under the curve power vs. time). The work-specific particulate mass emissions in Figure 7.8., show clearly that emissions during transients are much higher than those running at steady conditions in most cases, with the exception of the cold start tests at 2250rpm - 35kW and the second cycle of the acceleration test to 2250rpm - 15kW. Despite this, the transient emissions do not dominate the total work-specific emissions for these tests, which are indicated by the dots between the bars showing transient and steady emissions in Figure 7.8., owing to the low ratio between transient and steady engine work.

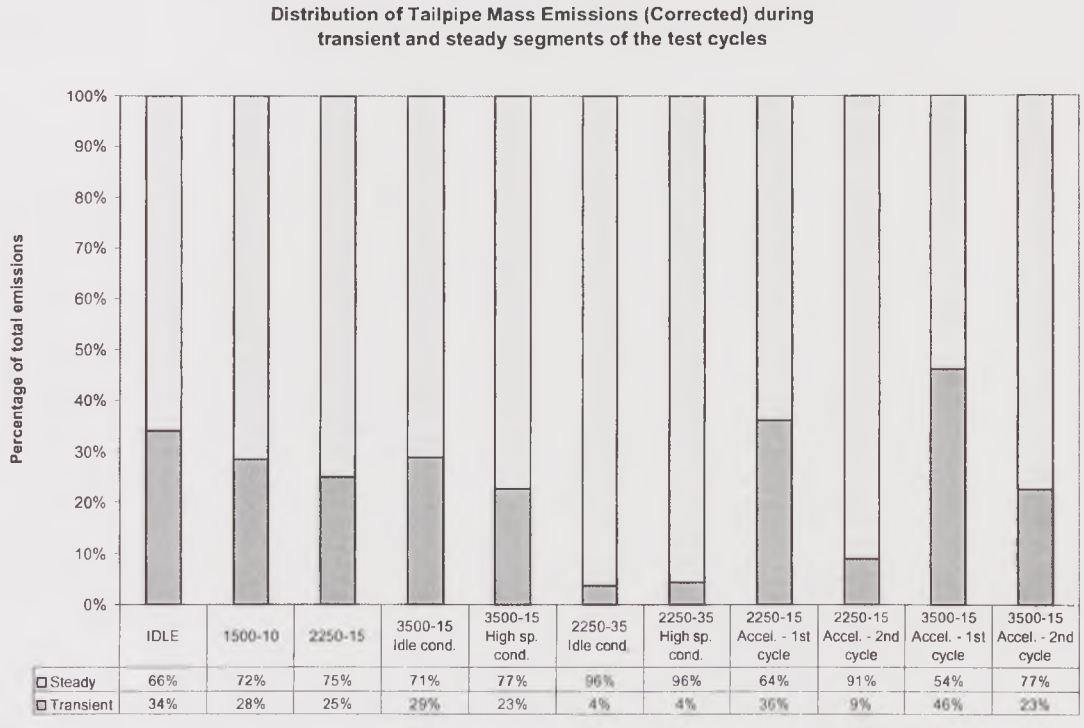

Figure 7.6. Percentage of corrected mass emissions during transient and steady segments of the tests.

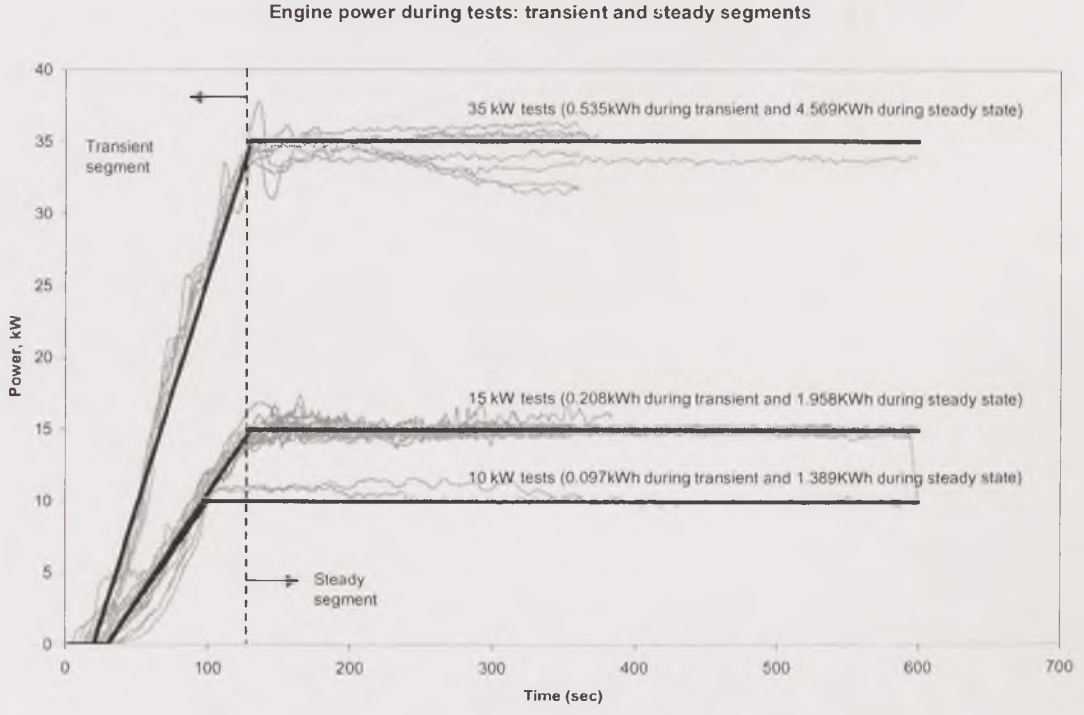

Figure 7.7. Work delivered by the engine during the step-change tests.

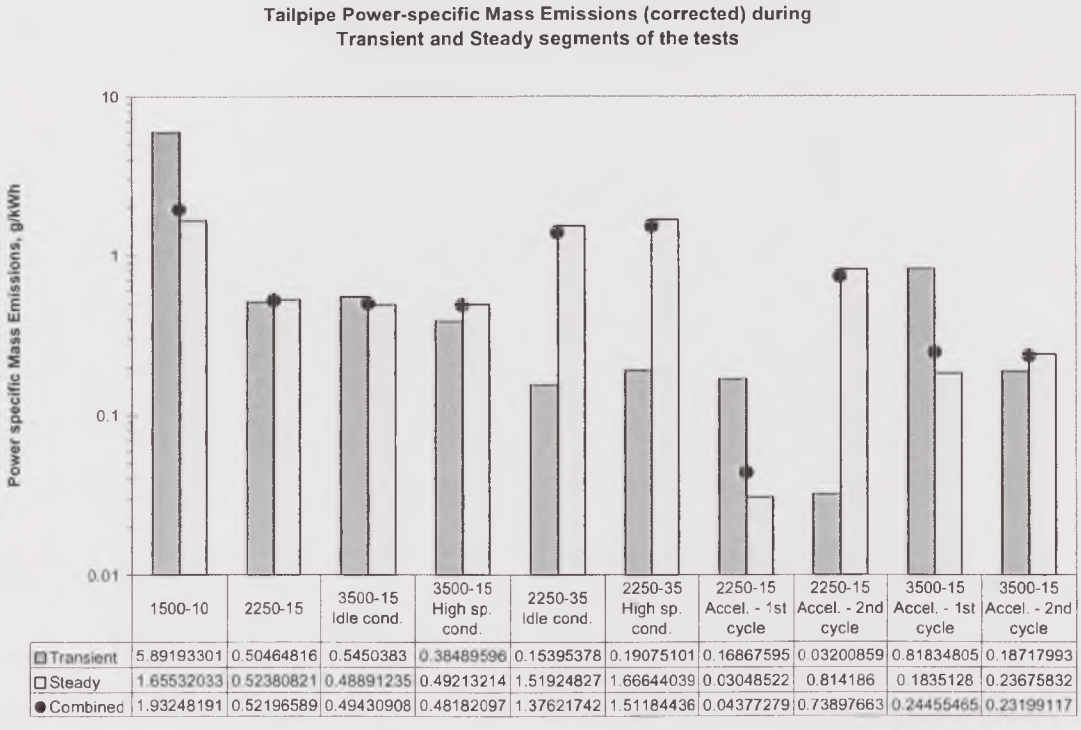

	1500-10	2250-15	3500-15 Idle cond.	3500-15 High sp. cond.	2250-35 Idle cond.	2250-35 High sp. cond.	2250-15 Accel. - 1st cycle	2250-15 Accel. - 2nd cycle	3500-15 Accel. - 1st cycle	3500-15 Accel. - 2nd cycle
Transient	5.89193301	0.50464816	0.5450383	0.38489596	0.15395378	0.19075101	0.16867595	0.03200859	0.81834805	0.18717993
Steady	1.65532033	0.52380821	0.48891235	0.49213214	1.51924827	1.66644039	0.03048522	0.814186	0.1835128	0.23675832
Combined	1.93248191	0.52196589	0.49430908	0.48182097	1.37621742	1.51184436	0.04377279	0.73897663	0.24455465	0.23199117

Figure 7.8. Work-specific corrected mass emissions during the tests.

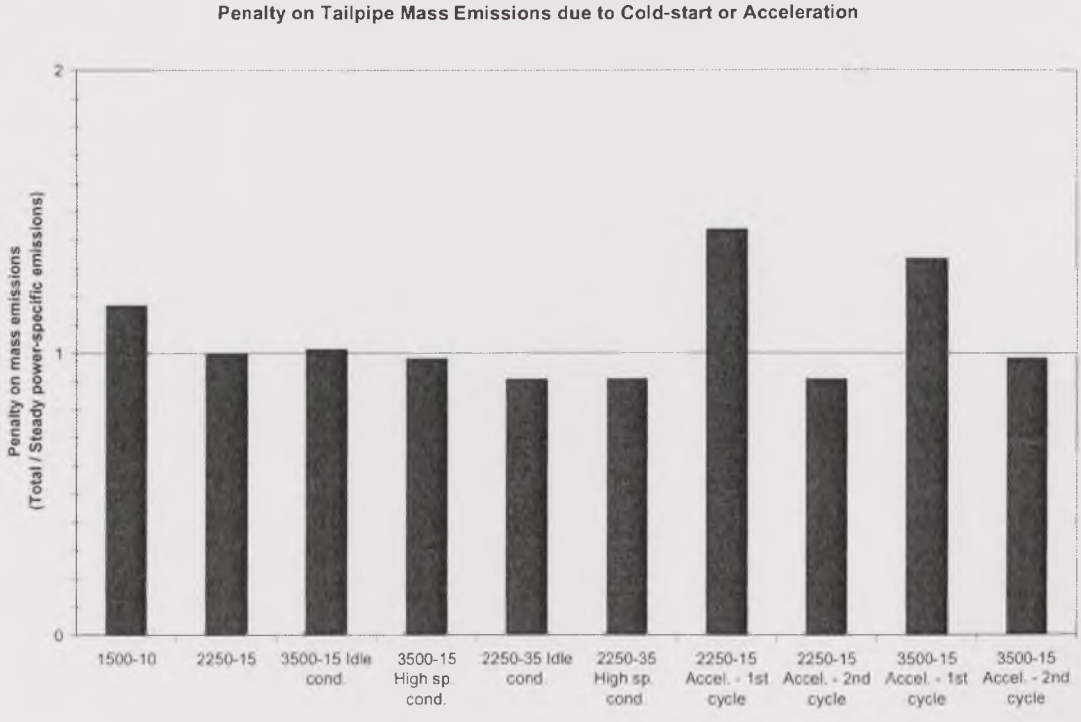

Figure 7.9. Change in mass emissions due to cold-start or acceleration during the test cycles.

The change introduced by a transient period on the total work-specific test emissions was calculated as the ratio between total work-specific emissions and

steady-state work-specific emissions. The result is shown in Figure 7.9., which indicates the change in emissions due to a single step-change transient period, either cold-start or acceleration. It is interesting to see that transient emissions actually decreased the value of total work-specific emissions in a number of tests.

The change introduced by a single step-change in emissions may be used to estimate the total emissions in different cycles that involve not only one but several acceleration/deceleration changes. Taking the steady-state emissions as a basis, the change introduced by a transient period was defined as:

$$I_c = \frac{\overline{m_{wc}}}{\overline{m_{ws}}}, \qquad \text{(Equation 7.1.)}$$

where

I_c is the emissions change for the step-change cycle (dimensionless)

$\overline{m_{wc}}$ is the work-specific particulate mass emissions for the step-change cycle, in g/kWh, and

$\overline{m_{ws}}$ is the work-specific particulate mass emissions for the steady segment of the cycle, in g/kWh.

$$\overline{m_{wc}} = \frac{\overline{m_{ws}} w_s + \overline{m_{wt}} w_t}{w_t + w_s}, \qquad \text{(Equation 7.2.)}$$

where

$\overline{m_{wt}}$ is the work-specific particulate mass emissions for the transient segment of the cycle, in g/kWh.

w_s is the engine work during the steady segment of the cycle, and

w_t is the engine work during the transient segment of the cycle.

Including Equation 7.2. in Equation 7.1., and defining $c_{ts}=w_t/w_s$, the change introduced by the transient becomes:

$$I_c = \frac{\overline{m_{ws}} + \overline{m_{wt}} c_{ts}}{\overline{m_{ws}}(1 + c_{ts})}. \qquad \text{(Equation 7.3.)}$$

This equation is useful to calculate the change introduced by, for example, one cold start and several acceleration periods, if transient and steady work-specific emissions are considered constant values (emission factors) for a given condition and the ratio between the power delivered by the engine in each segment of the cycle

is known. As an illustrative example, let us estimate the total emissions in a cycle with the following characteristics:

- Cold start with a step change to 1500rpm - 10kW.
- Short steady segment for the cold start, so c_{ts} for the cold start subcycle equals 0.2.
- Acceleration to 3500rpm - 15kW.
- cts for the acceleration subcycle: 0.16.
- The power delivered by the engine during the cold-start subcycle is 40% of the total power throughout the cycle.

From Figure 7.8., the work-specific particulate emissions for the cold start with a step change to 1500rpm - 10kW are: $(\overline{m_{wt}})_{\text{cold-start}}$ = 5.89g/kWh and $(\overline{m_{ws}})_{\text{cold-start}}$= 1.66g/kWh. For the acceleration to 3500rpm - 15kW (taken as a second cycle), $(\overline{m_{wt}})_{\text{accel}}$= 0.19g/kWh and $(\overline{m_{ws}})_{\text{accel.}}$ =0.24g/kWh. The change in emissions, as given by the Equation 7.3. for each subcycle, is:

$$(I_c)_{cold-start} = \frac{1.66 + 5.89 \times 0.2}{1.66 \times (1 + 0.2)} = 1.42$$

$$(I_c)_{accel.} = \frac{0.24 + 0.19 \times 0.16}{0.24 \times (1 + 0.16)} = 0.97$$

Then the total work-specific emissions are:

$$\overline{m_{wc}} = 0.4 \times (1.42 \times 1.66) + 0.6 \times (0.97 \times 0.24) = 1.08 \text{ g/kWh}$$

The emissions of the whole cycle in this example were 4.5 fold the steady-state emissions at 3500rpm - 15kW and 65% of the steady-state emissions at 1500rpm - 10kW. Without taking into account the transient effect, the emissions would have been:

$$(\overline{m_{wc}})_{no-transients} = (0.4 \times 1.66) + (0.6 \times 0.24) = 0.81 \text{ g/kWh}$$

Therefore, the transients contributed to an increase by 33% with respect to the emissions estimated with only steady-state emission factors in this example. This is relevant to the multi-mode legislative test cycles such as the R49 and the ESC, where only steady-state emissions are measured and then weighted to estimate total emissions during the cycle. Steady-state based factors for these cycles would underestimate real emissions, and many vehicles that may be high emitters during transients would be considered as low emitters as a result.

The main difficulty of this approach is that transient emissions have been shown to be highly variable, and therefore cannot be considered constant.

Furthermore, they can be strongly affected by the previous history of the engine, as has been shown in this work. However, as the example above has shown, measuring transient emissions and applying the resulting factors to the estimation of total emissions during cycles is useful and can help to prevent the underestimation of emissions in multi-mode legislative cycles.

7.1.3. ELPI vs. Total-Mass Filters Emission Index

The average Emission Index values, both uncorrected and corrected, were compared for various engine conditions during cold start, and the results were expressed as ELPI/Filter Emission Index ratio in Figures 7.10. and 7.11., for the first, or 'cold-start', filter and an average of subsequent, or 'stabilisation' filters. The cold-start filter (First two minutes of test) was compared to both mass-burst and peak-number events identified with the ELPI, to determine which of the events from the ELPI was closer to representing the gravimetric value. The stabilisation filters collected afterwards were compared to the stabilisation event from ELPI measurements.

For the cold-start filter, taking the mass-burst as a reference for comparison, the ELPI uncorrected Emission Index in Figure 7.10. a) overestimated the gravimetric Emission Index by as much as 83 fold at 3500rpm - 15kW after high-speed preconditioning, and other high values for medium speed conditions. The only exact agreement in this case occurred at idle, and at 1500rpm - 10kW the overestimation was the lowest among other conditions, 3.9 fold. The correction in the ELPI reduced these values by 5 to 14 times, and even so, the ELPI overestimated the Emission Index for most of the tests by as much as seven fold. At idle and 1500rpm - 10kW, the ELPI actually underestimated the Emission Index, reaching only a 10% to 30% of the gravimetric value. The closest agreement occurred at 2250rpm - 35kW, where an overestimation of 1.5 took place.

The ELPI overestimation of the Emission Index decreased significantly for the cold-start filter when using the peak-number event as a reference. When uncorrected, the maximum ELPI/filter ratios were 16.7 and 13.7, for 3500rpm - 15kW after high-speed preconditioning and 2250rpm - 15kW, respectively, and below 10 for other conditions. Exact agreement occurred at 1500rpm - 10kW. The correction reduced all ratio values by 1.7 to 5.2 times, to below 10 in all cases, and the maximum overestimation occurred at 2250rpm - 15kW, 7.9. Once again, idle and 1500rpm - 10kW values were underestimated with the correction.

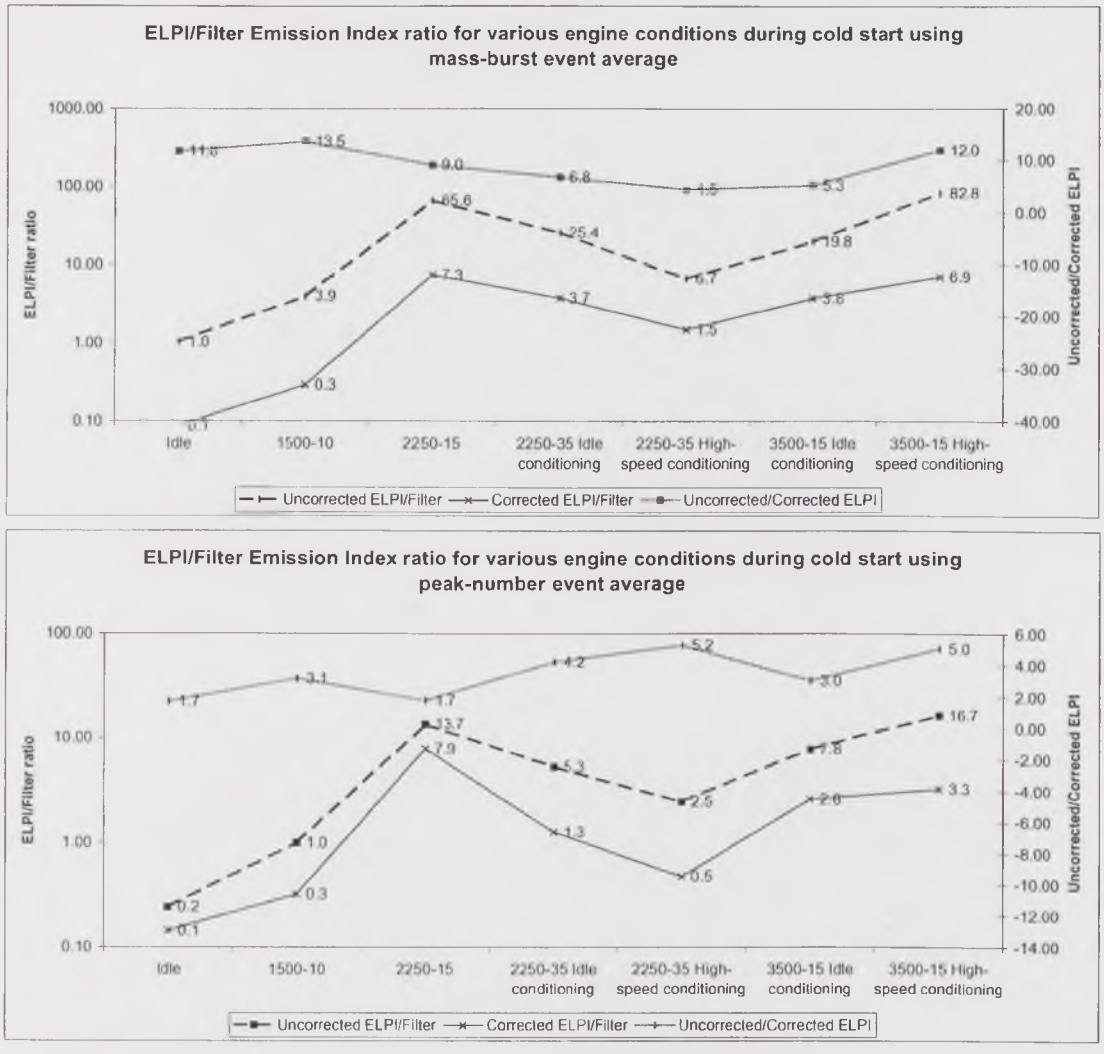

Figure 7.10. ELPI / Filter Emission Index ratio during cold start using mass-burst and peak-number event as references. a) Mass burst; b) Number peak.

For the stabilisation filter, the maximum overestimations by the ELPI, when uncorrected, occurred at 2250rpm - 35kW after Idle preconditioning, when the ELPI/filter ratio was 16.4, and at 3500rpm - 15kW after high-speed preconditioning, with a 12.5 ratio. The correction ratio was between 2.3 and 3.3, so the maximum corrected ELPI/filter ratios were 5.6 at 2250rpm - 35kW and 3.7 at 3500rpm - 15kW after high-speed preconditioning. Corrected ELPI and filters Emission Index agreed exactly at 1500rpm - 10kW and 2250rpm - 15kW, and the ELPI/filter ratio was just 1.3 at 3500rpm - 15kW after idle preconditioning. As expected, there was an increased agreement during the stabilisation period.

The fact that the ELPI overestimated the total particulate mass in a different fashion for the various conditions tested may be due to the changes in particulate structure (expressed by the fractal dimension) and composition with those conditions. According to Skillas et. al., 1998, as much as one order of magnitude more primary particles are produced under high load conditions, which also have higher temperatures. The resulting aggregates are more compact than those produced under low load conditions, and therefore their correction in the ELPI would be less significant than that needed for particles produced under low load conditions. This is reflected by the lower Uncorrected/Corrected Emission Index ratio for the 1500rpm - 10kW (2.6:1), 2250rpm - 15kW (2.3:1) and 2250rpm - 35kW (2.7:1, 2.9:1) conditions, for which the load is relatively higher than for other conditions. Unfortunately, it was not possible to corroborate this argument because the fractal dimension was measured only for high load conditions.

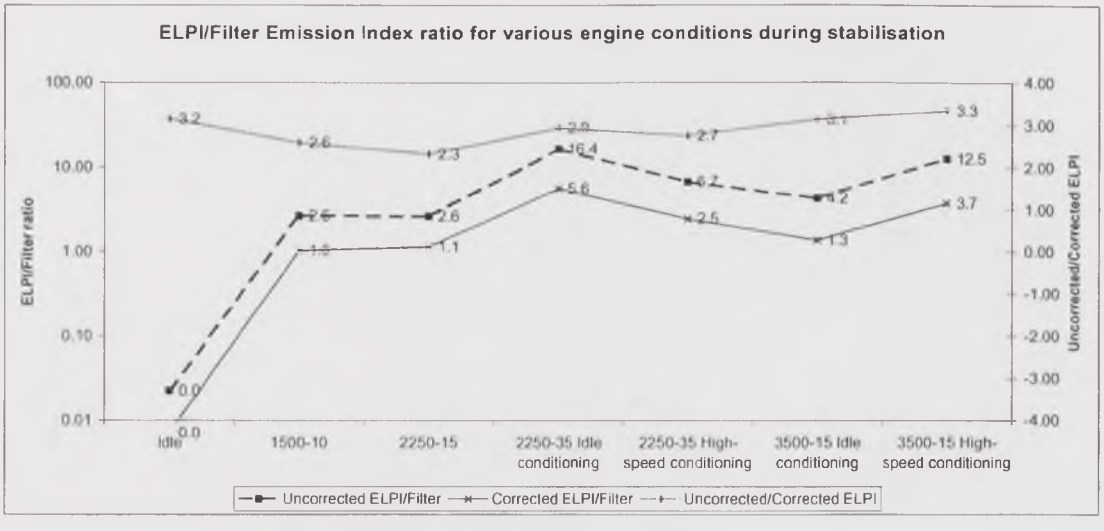

Figure 7.11. ELPI / Filter Emission Index ratio during stabilisation.

7.1.4. Comparisons with results from other studies

A number of researchers have carried out particle number and size distribution measurements, mostly over legislated cycles, expressing the results in km^{-1} rather than cm^{-3}. This makes the comparisons with the present results difficult, apart from having the same sort of difficulties and limitations that legislators have foreseen in the definition of an emission standard based on total particle number concentration, owing to the great sensitivity of this parameter. Number concentration, unlike total mass, 'is not conserved and it may change dramatically by nucleation and coagulation during dilution and sampling' (Kittelson, 1998).

Any comparison is also affected by the measurement techniques, which are based on different principles and therefore show different measurement ranges and sensitivity. Previous evaluations, such as a study by CONCAWE involving seven light-duty diesel vehicles, have shown the SMPS to have the best repeatability among other instruments such as the EAA and DMA (CONCAWE, 1998). For total mass measurements in the same study, the legislated gravimetric technique and the BLPI showed very good repeatability, and the QCM was considered unreliable. In respect of this, a report by Donald et al. remarked that there were conflicting results between the number-mode and mass-mode of the ELPI, which may have been the result of the original conversion from current signals to number concentration. However, the ELPI, the TEOM and the Andersen impactor gave similar mass particle flux measurements for the different engines and loads tested (Donald, 1997). This work has shown that corrections in such conversions are needed for the calculated mass concentrations to agree with gravimetric measurements.

	Particle Number concentration, km^{-1}		Uncorrected Emission rate, g/km			Corrected Emission rate, g/km		
Condition	Peak number	Stabilisation	Mass burst	Peak number	Stabilisation	Mass burst	Peak number	Stabilisation
Idle	4.04E+13	9.21E+12	1.58	0.37	0.04	0.13	0.22	0.01
1500-10	1.87E+14	1.41E+14	4.32	1.10	1.19	0.32	0.35	0.46
2250-15	9.05E+13	7.95E+13	11.68	2.44	0.89	1.29	1.41	0.39
2250-35 Idle conditioning	1.67E+14	1.53E+14	2.31	0.48	2.17	0.34	0.12	0.74
2250-35 High-speed conditioning	8.56E+13	1.42E+14	1.23	0.45	1.74	0.27	0.09	0.63
3500-15 Idle conditioning	1.91E+14	6.10E+13	2.34	0.92	0.47	0.44	0.31	0.15
3500-15 High-speed conditioning	2.21E+14	8.26E+13	7.21	1.45	0.53	0.60	0.29	0.16
2250-15 Acceleration 1	1.99E+13	1.39E+13	0.40	0.20	0.10	0.05	0.11	0.05
2250-15 Acceleration 2	1.74E+13	1.36E+13	0.44	0.15	0.12	0.05	0.06	0.05
3500-15 Acceleration 1	8.04E+13	2.70E+13	2.39	0.64	0.16	0.23	0.15	0.03
3500-15 Acceleration 2	3.80E+13	2.87E+13	0.62	0.29	0.16	0.06	0.06	0.04

Table 7.3. Summary of particle number and mass emission rates in particles/km and g/km in the present work.

Number concentration and Emission Index results from Table 7.1. were converted to emission rates, expressed in particles/km and g/km, using a standard diesel fuel consumption factor of 79 g/km, equivalent to 12.7 km/kg fuel. This allowed establishing an approximate comparison with results from other studies in such units. The converted figures are shown in Table 7.3.

7.1.4.1. Particulate Mass and Number levels

In the CONCAWE study (Hall, 1998), mass emission rates from diesel passenger car engines during the cold-start ECE + EUDC cycle averaged 0.040 g/km for a 1.9L IDI engine equipped with a DOC (V1) and 0.168 g/km for a 1.9L TC DI engine (V2). In this work, the average emissions over the first ten minutes from cold start, as measured with the ELPI and total mass filters with the Ford XLD 418T diesel engine were around 0.250 g/km. It would not be sensible to compare directly these figures, but apparently this indicates that the Ford XLD 418T was a more polluting engine in terms of mass emissions. Total number emissions, however, were very similar in both studies, being between $1x10^{14}$ km^{-1} and $2x10^{14}$ km^{-1} for V1 and V2, respectively – the average from the Ford engine was $1.57x10^{14}$ km^{-1} for the first minutes of cold start and $1.1x10^{14}$ km^{-1} for the stabilisation period. Regarding the size distribution, the number modes were 0.085μm for V1 engine and 0.150μm for V2, both within the range of modes found in this work. The Ford XLD 418T engine, however, tended to emit aerosols with lower modes, around 0.060μm, during peak number events, indicating a higher emission of ultrafine and very fine particle during acceleration periods.

Pattas et al. (Pattas, 1998) used the ELPI size analyser on a Renault T1100D 2.5 litre passenger car fitted with a Corning EX47 particle trap, running at three steady-state conditions within the UDC and EUDC cycles. The total number of particles at idle was $5x10^{6}/cm^{3}$, at 30 km/hr (similar to 1500rpm - 10kW or 2250rpm - 15kW in this work) it was $1.8x10^{7}/cm^{3}$ and at 120km/hr (similar to 3500rpm - 15kW in this work) it was $3.2x10^{7}/cm^{3}$. The mode of the number size distribution was between 60nm and 110 nm for the UDC and EUDC cycles, similar to the modes found in this work. The number concentration results were in the same order of magnitude of stabilisation events of various conditions in this work. On the other hand, number concentrations were up to one order of magnitude lower than number-peak events in this work.

A number of tests at the University of Minnesota reviewed by Kittelson (Kittelson, 1998) have shown diesel particle number concentrations in emissions from various models (1984 to 1995) to vary by as much as three orders of magnitude when measured with an EAA. A 1995 DI diesel engine emitted between $3x10^{6}$ cm^{-3} and $1x10^{7}$ at 1600rpm and around $2x10^{7}$ at 2600rpm, and at the same level of a 1984 IDI diesel engine. These were lower than those at similar conditions in this work (a 1995 IDI diesel engine) for the cold-start tests, although somewhat higher than this work for the acceleration tests. Much higher number concentrations were measured in the exhaust aerosol of older engines, around 10^{8} cm^{-3} for the 1988 DI diesel

engine and $1x10^9$ for a 1991 DI diesel engine. Such high concentrations, although not higher than $1.5x10^8$ cm^{-3}, were measured in this work only in the first minute of some cold start tests at high-power and high-speed conditions. Regarding the number size distribution modes, Kittelson reported a nuclei mode between 0.011μm and 0.020μm for the 1991 IDI and the 1995 DI engines, and an accumulation mode around 0.070μm. Mass size distributions showed an accumulation mode around 0.125μm. No mass coarse mode was reported, since this was out of the range measured by the EAA. These results are in good agreement with those from the present work.

Abdul-Khalek et al (Abdul-Khalek, 1998) used an SMPS instrument to determine the particle size distribution on a number basis for a Perkins T4.40 DI TCIC engine. At idle the total number of particles was $7x10^6/cm^3$ ($4 x10^6/cm^3$ in this work). For the other modes in the 13-mode tests the particle total number varied between $2x10^7$ cm^{-3} and $9x10^7$ cm^{-3}. This instrument, however, is not appropriate for transient cycles. Then the same author characterised the emissions from a 1991 Detroit Diesel Corporation Series 60, 12.7L TC/IC DI diesel engine with an ELPI during the FTP transient cycle. He observed monomodal distributions with number distribution modes between 0.085μm and 0.14μm, the smallest mode corresponding to idle conditions and the highest to acceleration events. Mass distribution modes were higher, around 0.15μm to 0.2μm. The total number emissions were between $1x10^8$ cm^{-3} and $7x10^{10}$ cm^{-3}, being higher during the Los Angeles modes of the test than during the New York modes. The ELPI overestimated particulate mass emissions by 50% with respect to the total mass filter determination, in agreement with findings by other authors. Overestimation in this work was much greater. This may indicate either a real overestimation due to the structure of the particles produced by the Ford XLD 418T or, more likely, a failure in the calibration of the piece of equipment used.

Tsakumoto et al. evaluated the mass emissions for a Nissan 13.3L N/A DI Diesel PG6, showing an ELPI/filter ratio of 1.5 to 2 for 25%+ loads at 1050rpm and 1680rpm (Tsakumoto, 2000). The reasons for the much higher ratios in this work are not clear, but presumably they have to do with the assumptions of constant charger efficiency and constant density. Particle properties may vary with the engine technology, and with them, the charger efficiency and particle density, which are involved in the number and mass concentration calculations, respectively. However, a failure in the calibration of the piece of equipment used appears to be a more likely explanation.

Rickeard et al. (Rickeard, 1996) compared particulate emissions from both Spark Ignition and Diesel engines. They found that, at high-speed cruising conditions, emissions from spark-ignition engines, around $1.0x10^{14}$ km^{-1}, were very close to the diesel $1.5x10^{14}$ km^{-1} emissions. The number distribution mode was around 60nm for Spark Ignition engines and 110nm for diesel engines. The number emission rates in the present work were lower than those from the diesel engine tested by Rickeard. The size distribution mode was similar for a number of events, but in general, this work showed lower values for the number accumulation mode during the stabilisation events.

Ji Ping Shi et al. (ETH, 2000) carried out particle number concentration measurements of the emissions from vehicles passing the sampling point on the road with a condensation particle counter, CPC. Dilution ratio was estimated measuring CO_2 and using it as a tracer, resulting in a 1000:1 dilution ratio in the plume. They showed reductions when using a diesel oxidation catalyst, from $1x10^6$ cm^{-3} to $3x10^5$ cm^{-3} during cruising conditions, and from $4x10^6$ cm^{-3} to $7x10^5$ cm^{-3} during acceleration conditions. Although the number concentrations were lower than those measured in this work, the reductions through the catalyst were similar, and the evidence that the particle number concentration increases with the vehicle acceleration is in agreement with the present results.

In the summary report of the results from the DETR/SMMT/CONCAWE Particulate Research Programme 1998-2001 (Andersson, 2001; Wedekind, 2000) the particulate mass emissions from a diesel passenger car were around 0.02 g/km over the EDC. For the same cycle, a light-duty diesel engine emitted between 0.05 g/km and 0.07 g/km. In both cases, the particulate emissions were much lower than those from the Ford passenger car diesel engine in the cold-start tests in this work. As in other comparisons, the results from cold-start tests this work exceeded cycle emissions as a consequence of the performance of the engine during cold conditions. However, results from the stabilisation events of the acceleration tests, which started with a warm engine, showed emission rates around 0.04 g/km, which agreed with the results reported by Andersson for the light-duty diesel engine. The integrated particle number emissions were between $2x10^{13}$ km^{-1} and $2x10^{14}$ km^{-1} for the passenger car engine and between $6x10^{13}$ km^{-1} and $4x10^{14}$ km^{-1} for the light-duty engine. The number emission rates from this work were within this range. Andersson reported number accumulation modes between 70nm and 100nm in the emissions from diesel engines, and also a nuclei mode between 11nm and 25nm when high-sulphur fuel was used. At high-speed conditions, they showed high emissions from Spark Ignition engines, comparable to those from diesel engines,

although much more particles were in the nano-size range, showing a nucleation mode around 11nm.

An evaluation of diesel aftertreatment technologies by Khair et al. (Khair, 1999) showed that diesel oxidation catalysts (DOC) reduced particulate matter by 30% when the EGR system is present in the vehicle over the 13-mode FTP cycle. The reduction, however, was not observed for all cycle modes. They observed that particulate matter increased through the catalyst by nearly 15% in mode 3 and was unaffected in mode 5.

Tanaka et al. (Tanaka, 1999) analysed the particle composition for the different fractions of diesel particulate collected by the ELPI. They found that adsorbed SOF increased the size of particles. Large particles have in general a higher SOF content than fine particles, although SOF-only particles are finer than 0.050μm themselves. This was in some agreement with the results from this work, which showed 90% SOF in large particles and 10% SOF in fine particles. The higher SOF content in the present work may be attributable to the cold engine conditions, which promote condensation and adsorption of volatile material on the particle surface. Their mass-weighed size distribution data showed three apparent modes: one below 0.032μm, corresponding to nuclei mode; 0.20μm, accumulation mode; and 1.5μm to 2.0μm, coarse mode. The mass accumulation and coarse modes were observed in this work, but the nucleation mode was not shown by the ELPI, and presumably did not occur because of the low sulphur content of the fuel used in this work compared to that used by Tanaka: 50ppm vs. 500ppm and 2000ppm, respectively.

7.1.4.2. Particulate resuspension

Explanations to the various changes observed through the exhaust system during transients are directly related to particle deposition and reentrainment processes, and also with chemisorption, in the case of the catalyst. Particle deposition on exhaust walls, as shown in the calculations in Chapter 3, was promoted mainly by thermophoresis and gravitational forces, the former being more significant for very fine particles, below 0.1μm, and the latter, for large particles, those larger than 1.0μm. Reentrainment processes still require much more detail on basic research to be applicable in real world conditions, since the exact mechanism of particle detachment is not well understood. However, practical contributions to this work come from the study by Adhiwidjaja et al (Adhiwidjaja, 2000), briefly described in Chapter 1.

	Exhaust mass flow (kg/s)	Exhaust volumetric flow (m^3/s)	Exhaust gas velocity (m/s)
Idle	0.034	0.039	24
1500rpm - 10kW	0.042	0.081	51
2250rpm - 15kW	0.050	0.114	72
3500rpm - 15kW	0.082	0.127	80
2250rpm - 35kW	0.115	0.265	167

Table 7.4. Exhaust mass and volumetric flow and exhaust gas velocity for steady state conditions.

As observed in the theoretical deposition calculations in Chapter 2, the engine produces a certain exhaust mass flow for each given operation condition, and therefore a certain gas velocity through the exhaust pipe. These parameters are summarised for steady state conditions in Table 7.4. For steady state conditions (equivalent to the stabilisation period of the cold start tests), the average particle number concentration and Emission Index are related to the Exhaust mass and volumetric flow, and hence to the exhaust gas velocity as observed in Figure 7.12.

Under equilibrium conditions such as the stabilisation period of the cold start tests, for which the parameters shown above are valid, a striped pattern forms on the walls and moves at constant velocity, provided that the material has a low roughness, e.g. the collision/adhesion-moment ratio is higher than 1 (Adhiwidjaja, 2000). During transients, however, such behaviour is not expected. From the cold start tests, Figures 7.13. to 7.14. show the particulate blow out, expressed as number concentration and Emission Index, plotted against various exhaust aerosol parameters, namely exhaust mass flow, exhaust volumetric flow, and exhaust gas velocity. The particulate blow out is also plotted against two factors from the engine operation, the Air/Fuel ratio (AFR) and Fuel consumption, as well as against the particle load, expressed as number of particles per second and particle mass per second. The data were very scattered, indicating the great complexity of the processes affecting particle deposition and reentrainment. As observed earlier, deposition was preponderant over particulate blow out for most of the conditions, which complicates the analysis of reentrainment causes from the experimental evidence.

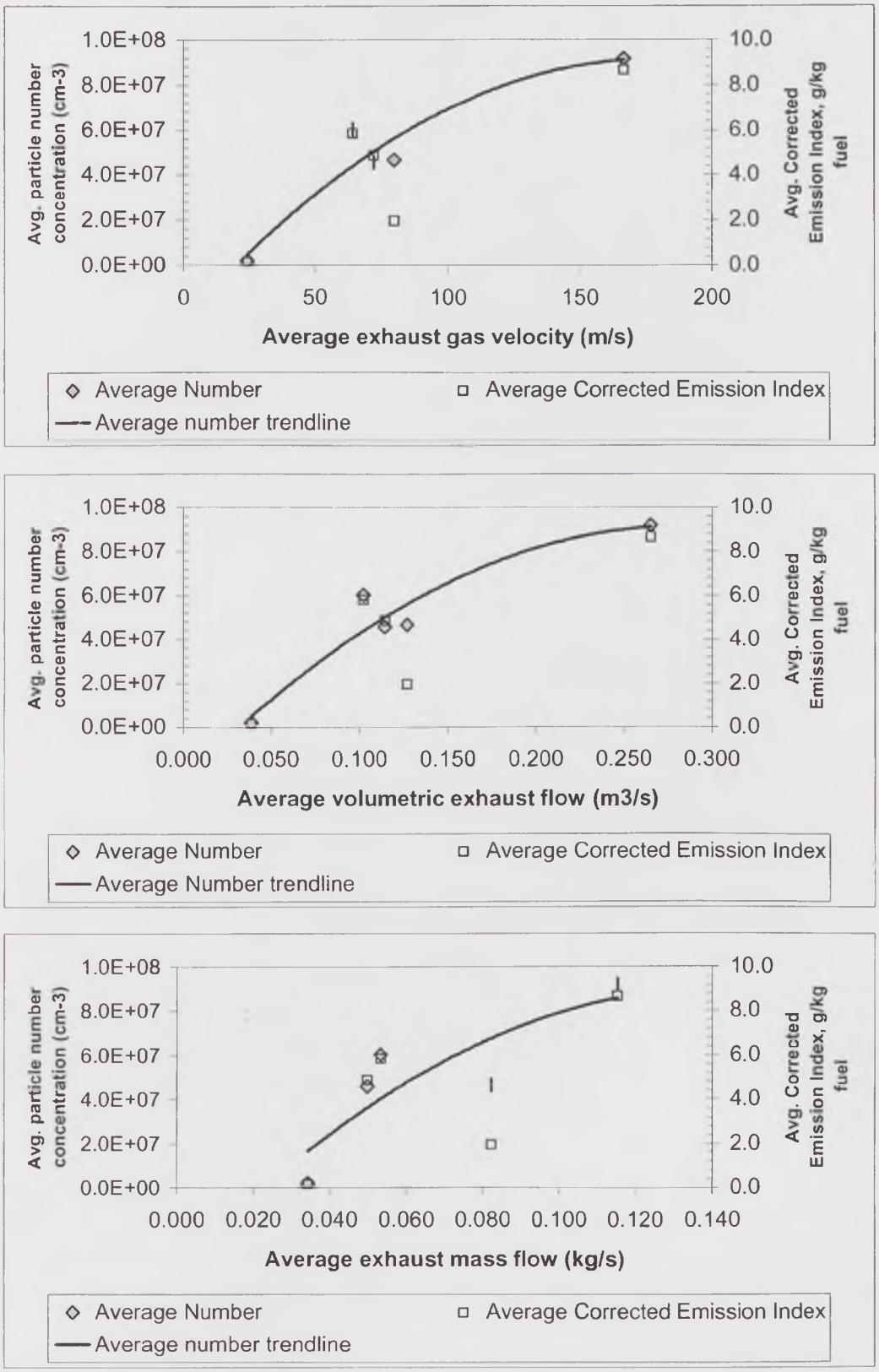

Figure 7.12. Average particle number concentration and Emission Index vs. Average exhaust gas velocity, exhaust mass flow and exhaust volumetric flow at steady state.

An acceleration disturbance to the equilibrium state implies: an increase in the gas velocity through the exhaust pipe; an increase in the temperature of the gas; a change (either increase or decrease) in the particle *concentration* in the aerosol and, probably, some changes in the size distribution; a decrease in the particulate mass concentration per unit area in the deposition layer, towards a new equilibrium.

The possible consequences of these changes are described below.

- The increase in velocity may increase the collision velocity of particles in the aerosol against particles in the deposition layer and, therefore, the collision/adhesion-moments ratio. As a result, the motion velocity of the deposition layer downstream of the exhaust pipe would also increase. However, higher gas velocities produce higher turbulence, and changes in the collision angles of impinging particles, which may become unfavourable for the collision forces to act over the particles in the deposition layer. This would actually decrease the collision/adhesion-moments ratio.
- The increase in the aerosol temperature increases the deposition flux by thermophoresis and hence the collision moment, promoting the motion of the deposition layer. It causes also an increase in the metal temperature, causing outgassing of volatile compounds. This may affect the properties of the particles in the deposition layer, reducing the particulate concentration by unit area. In response, particle deposition would be promoted to keep the layer equilibrium. The net effect would depend on the relative magnitude of the deposition and resuspension fluxes.
- The aerosol particle concentration may either increase or decrease with the gas velocity, as a result of combined, opposite effects of combustion time, mixing and temperature: the higher the engine speed, the shorter the mixing and reaction times, to the detriment of the efficiency and in favour of the particulate formation, but also the higher the temperature and the turbulence, which produce the opposite effect. If the particle concentration increases, so does the deposition flux, and the deposition layer may increase its velocity, blowing out more particles.

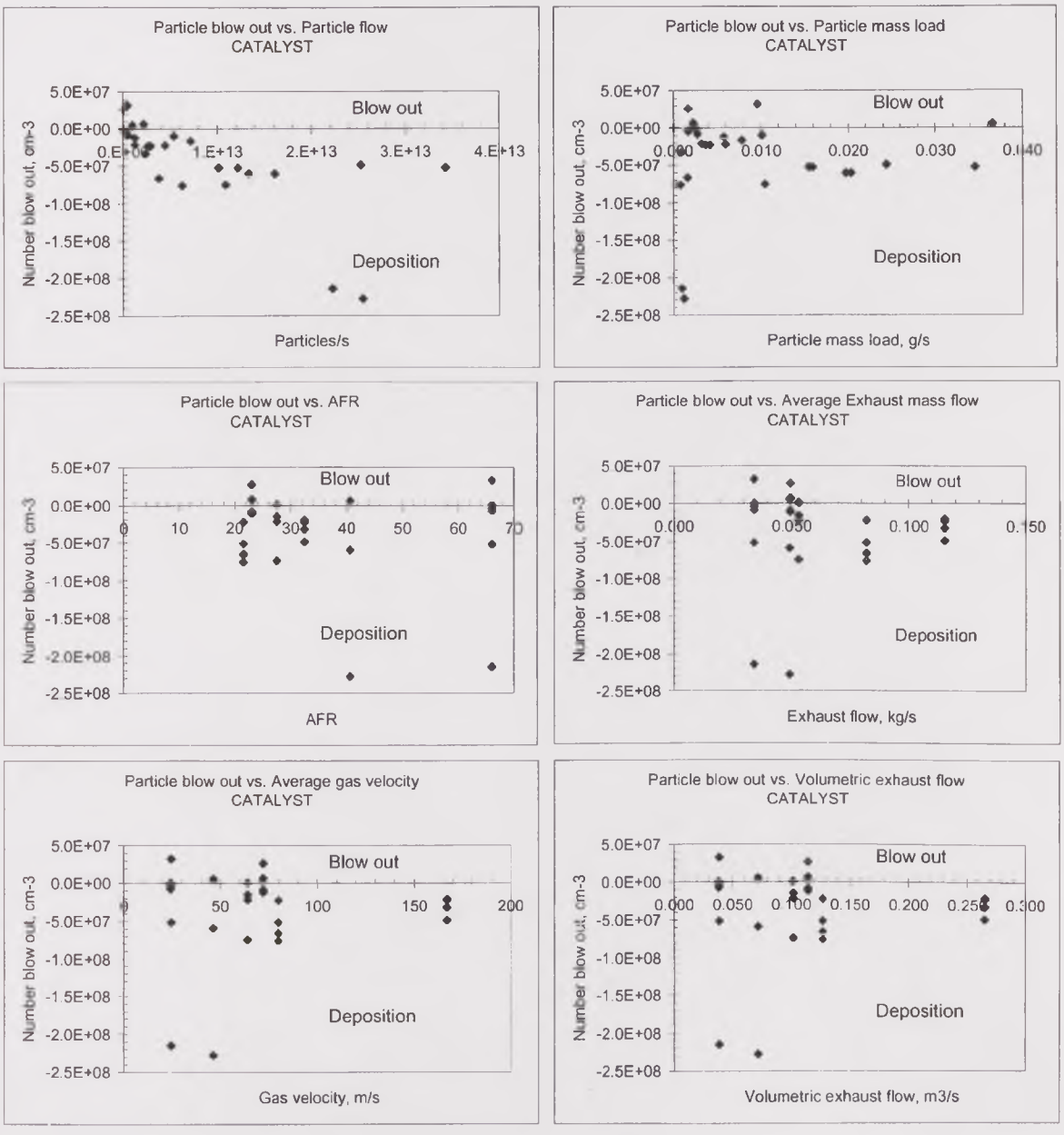

Figure 7.13. Particulate blow out from the Catalyst (a) as Number concentration vs. various exhaust aerosol parameters.

- If, in contrast, it decreases, the deposition layer decreases its velocity and it may even stop moving, despite of the increased gas velocity. Particle concentration, however, is not a good enough parameter to determine the deposition or reentrainment fluxes, and particle size distribution becomes a very important factor here. Approximately, the force of adhesion is proportional to the diameter of the particles, whereas the force of collision is proportional to the $(1/5)^{th}$ power of the particle diameter. Therefore, if the particle size distribution during the transition has a lower mode than that at the previous condition, it

becomes less likely that the collision momentum increases and, therefore, that the particulate blow out occurs.

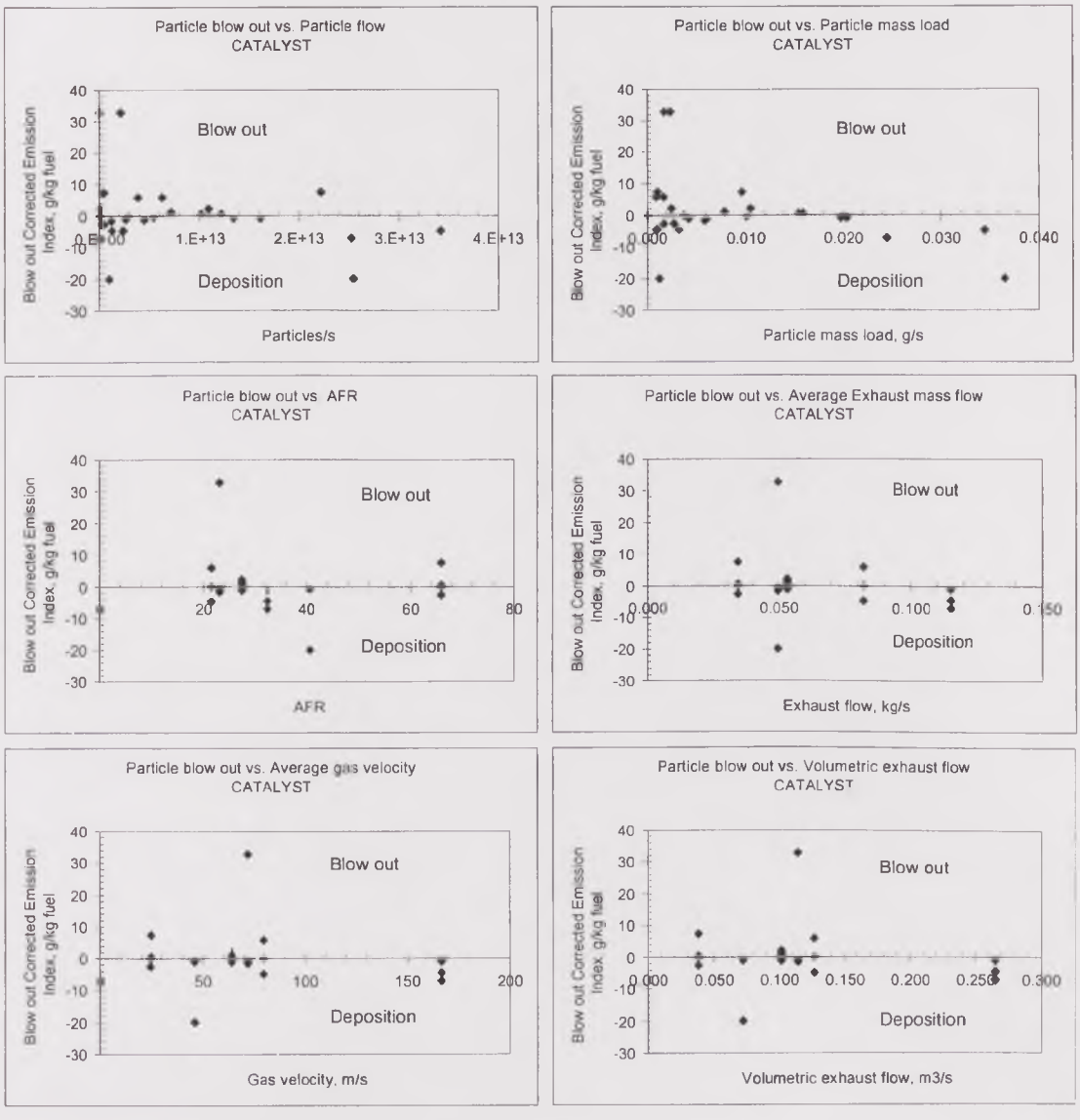

Figure 7.13. Particulate blow out from the Catalyst (b) as Emission Index vs. various exhaust aerosol parameters.

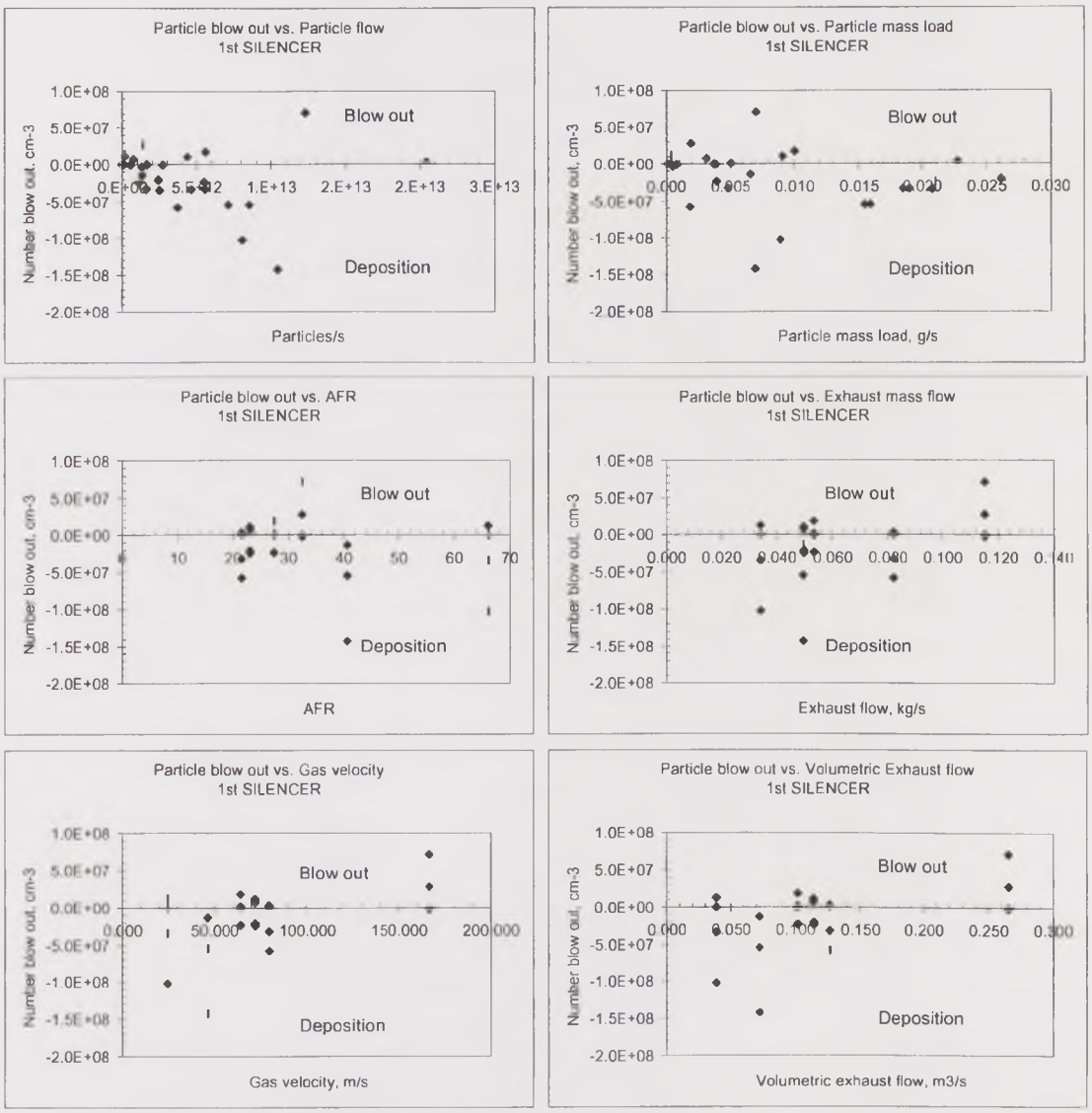

Figure 7.14. Particulate blow out from the First silencer (a) as Number concentration) vs. various exhaust aerosol parameters.

- The equilibrium particle concentration per surface area for the increased gas velocity is lower than at a lower velocity. This suggests that, as long as the particle concentration in the aerosol is constant or lower during the transition between low and high gas velocity (acceleration), many more particles would be resuspended than deposited, causing a noticeable particulate blow-out.

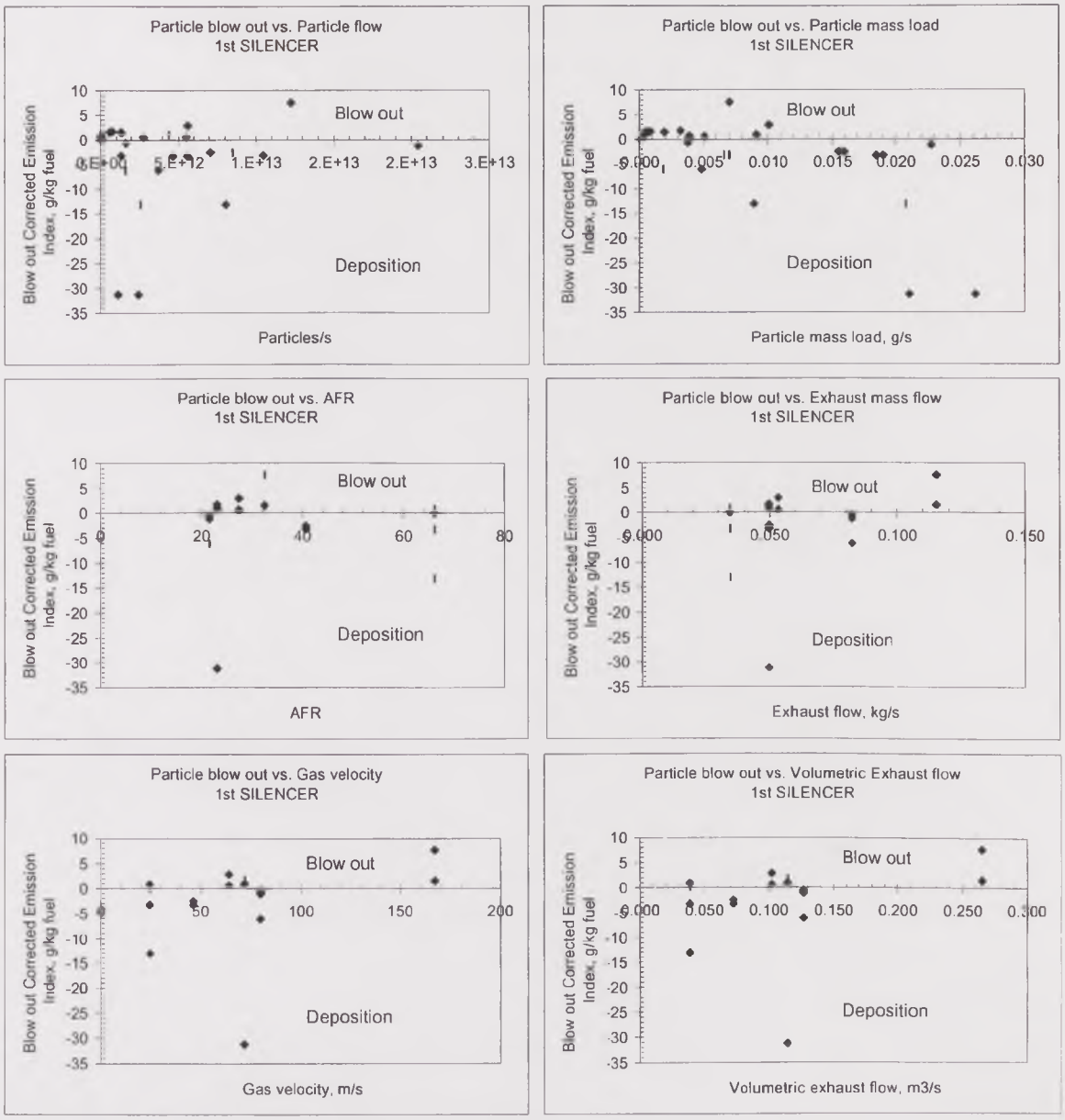

Figure 7.14. Particulate blow out from the First silencer (b) as Emission Index vs. various exhaust aerosol parameters.

As it is shown, the effects of the acceleration depend on a complex set of opposite conditions around a delicate equilibrium between particulate deposition and reentrainment occurring simultaneously. This would explain the difficulty in finding single trends in the particle motion for the various test conditions.

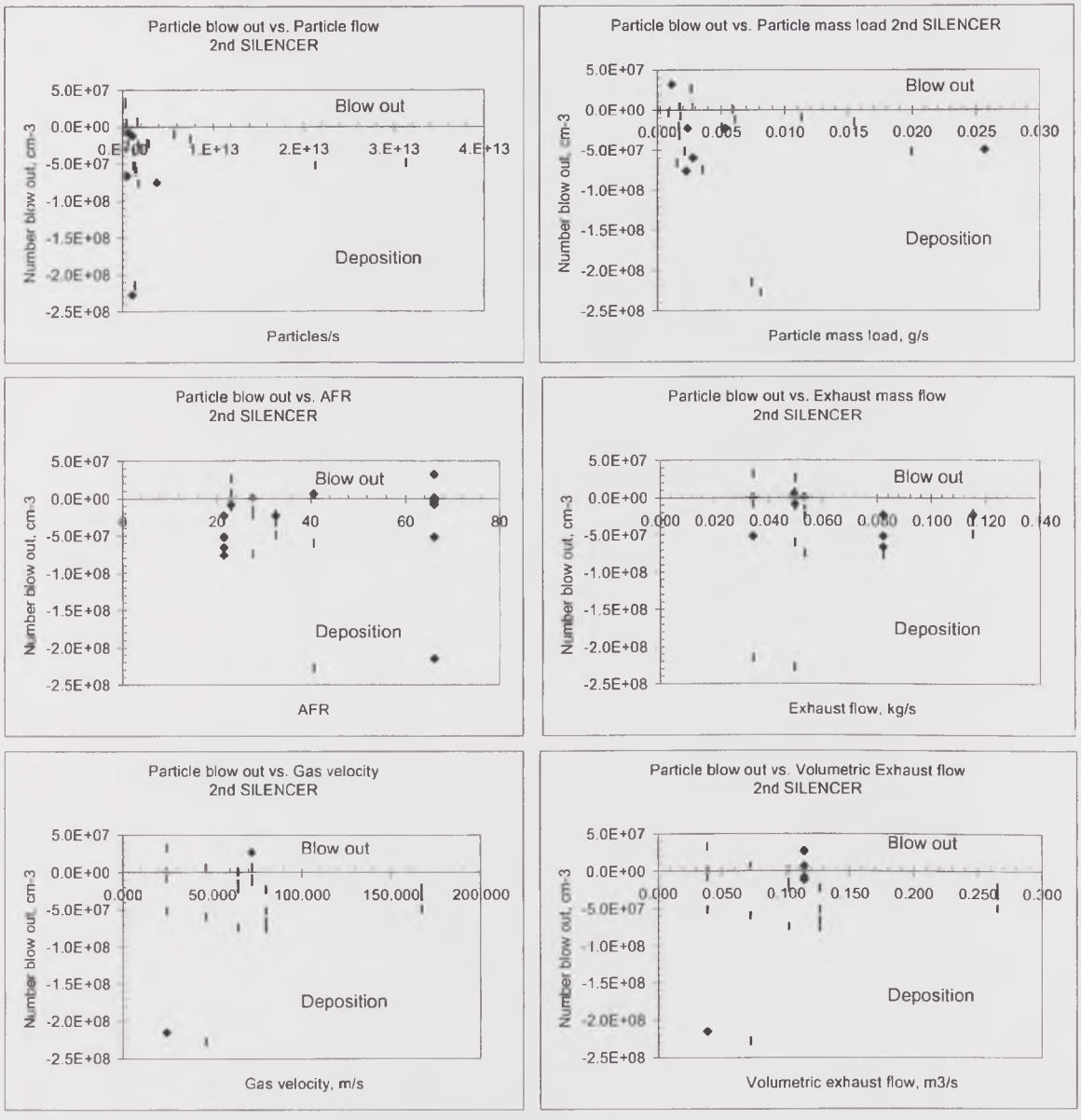

Figure 7.15. Particulate blow out from the Second silencer (a) as Number concentration vs. various exhaust aerosol parameters.

The clearest evidence on the reentrainment of particles as a consequence of transient cold-start and acceleration emissions was the significant contribution of the mass-burst and peak-number events to the number of blow out cases: they accounted for 53% of the total of blow-out cases. These were the events that really show the effect of the transients, since they were associated with short-term responses, in the time range reported by Adhiwidjaja et al. (Adhiwidjaja, 2000) to be needed by the deposition layer to be fully developed, less than 100s.

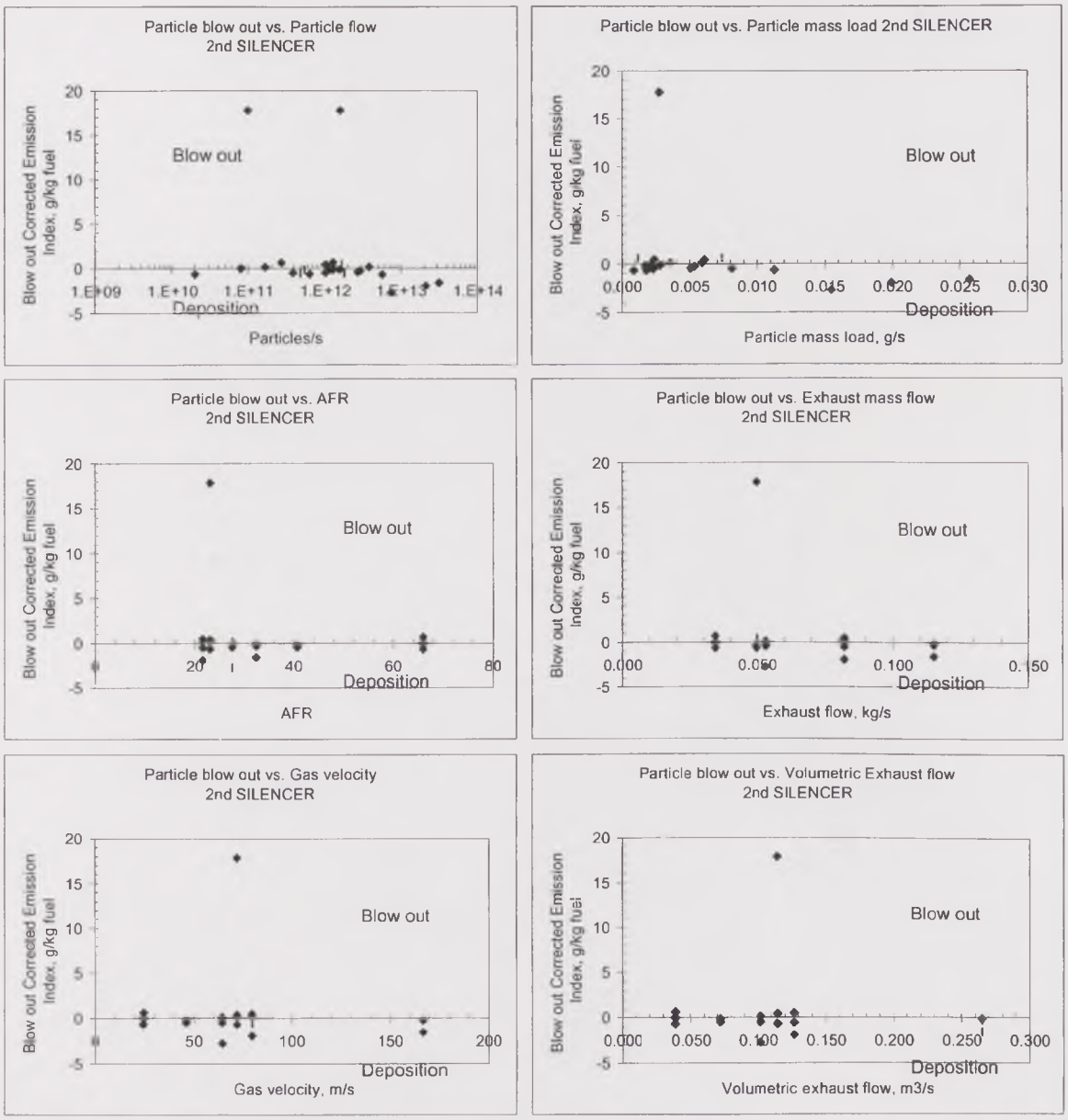

Figure 7.15. Particulate blow out from the Second silencer (b) as Emission Index vs. various exhaust aerosol parameters.

Changes in further events were due to the subsequent thermal equilibration in the engine and exhaust pipe systems. In their study on Spark Ignition engine emissions during start-up and transient operation, Kayes et al. (Kayes, 1999) showed very similar transient responses in the particulate matter emissions (e.g. reentrainment) to those resulting from this work, described as an increase with a peak concentration during start-up followed by a level concentration. They also showed an additional increase during the engine shutdown. The mode of the number size distribution increased between the number peak and the stabilisation as a result of the transient, which also agreed with the findings in this work. The causes of this

were mainly particle resuspension and particle formation from vapours outgassed from the deposition layer followed by their coagulation.

In the study on Spark Ignition emissions during transients by Hall et al. (Hall, 2000), the release of previously stored particles from the exhaust and dilution system walls was found to be related to the engine operation temperature: after prolonged operation of both vehicle and tunnel at high-speed and temperature, low particulate emissions were measured, suggesting that the system and the dilution tunnel was 'cleaned' during high temperature operation and then the actual, low emissions from the engine were measured. This was partially true, although the authors did not include part of the argument: the emissions measured after the high-temperature operation may have been reduced by deposition through the system, since the deposition layer structure may have started recovering for new low temperature conditions.

This work showed that the exhaust system was partially 'cleaned' by the engine operation at high load conditions, which produce high temperatures in the exhaust system. On the other hand, the high-speed, low load tests, for which the temperatures were not as high as in the high-load tests, this "cleaning" effect was not observed. Also, the results from the multiple acceleration tests showed that the deposition layer formed during a long conditioning period accumulated more particles than that formed in the 10-minute conditioning period (much higher number of particles released in the first acceleration cycle), but this did not produce a large difference in the mass released by the transient operation (slightly higher Emission Index in the first acceleration cycle), meaning that the recovery of the deposition layer was a very fast process.

Chapter 8. Conclusions and final remarks

8.1. Conclusions

The Ford XLD 418T, 1.8L TC/IC IDI diesel engine used in this work was shown to emit high particulate emissions during cold-start and acceleration transients, but once it was hot and running at steady state conditions, these emissions decreased to comparable levels to those produced by similar engines in studies by other authors. Transient particulate emissions were strongly influenced in both number concentration and Emission Index by changes through the various components of the exhaust system, including pipes, the oxidation catalyst and silencers. These changes were dependent themselves on various conditions related to the time from the start of the transient events, such as exhaust aerosol and system walls temperatures, engine speed and acceleration regime.

The dependence relationships between the particulate changes and the conditions of the exhaust system were not easy to discern, because of the great sensitivity and complexity of the physical processes that produce such changes. Particles of all sizes were shown to be deposited by the action of thermophoresis, gravitational and inertial forces. The number of ultrafine and mid-sized particles increased as a consequence of gas-to-particle conversion and coagulation processes;. Particles larger than 1.0μm were resuspended from the exhaust walls by the action of shear and lift forces and by the impact of particles in the aerosol. Some of these processes oppose each other, and they all occur simultaneously. The prevalence of one process, or a set of processes, over the others occurred at very different conditions, which suggested that very subtle differences in the conditions of the system were sufficient to produce significant changes in the processes and hence in the resultant emissions.

Simultaneous measurements with total mass filters at various points along the exhaust system showed that the amount of particulate deposited, or resuspended and formed, through the exhaust system constituted a significant fraction of, the tailpipe emissions, or even exceeded them by more than one order of magnitude. Thus, a single transient event may have the capacity to produce a highly visible tailpipe particulate emission, even when the engine does not produce it itself.

Total mass filter measurements showed also that the particulate mass changes through the system were dependent on the immediately previous operational history of the engine. Idle operation was selected and proved to reproduce a good condition

for particle deposition, so this was adopted as a fast preconditioning period that would reproduce the deposition of an amount of particulate mass similar to that deposited in a driving period of a week under urban conditions, following a pattern of 1-2 hours drive per day. In contrast, a high-speed operation for ten minutes was used to reproduce an exhaust-system cleaning condition. These were adopted as preconditioning procedures for cold start tests with filters and the ELPI. The acceleration tests showed that high transient number concentrations and Emission Index were emitted after a long idle preconditioning, but was much lower after a short idle period.

Total mass measurements gave evidence that particulate matter tended to be easily resuspended from the first silencer and then deposited through the second silencer. This trend was also observed in the measurements with the ELPI during the cold-start tests and confirmed during the acceleration tests. This was not a permanent situation, but was observed in several cases. In addition, the changes in particulate concentration through the second silencer tended to be parallel to those observed through the catalyst, and opposite to those through the first silencer, in a number of cases. This was even size related: when ultrafine particles, for example, were being formed through the catalyst and the second silencer, they deposited or coagulated through the first silencer. Likewise, when particles larger than 10.0μm were being deposited through the catalyst and the second silencer, they were resuspended from the first silencer walls. Again, such behaviour was not a permanent situation, but it was observed in a good number of events, which indicated that the trend was real and recurrent.

In the cold-start tests, the catalyst was shown to promote fine particle coagulation and large particles were resuspended from its walls. The second silencer promoted fine particle formation and large particle deposition, and through the first silencer there was significant particle growth and large particles were resuspended in many cases. In the acceleration cycles, which only tested high-speed and medium-load conditions, the catalyst and the second silencer promoted particle deposition, ultrafine particles formed and coagulated through the catalyst and the first silencer, and large particles were reentrained mainly from the second silencer walls and to a certain extent from the catalyst.

Real-time tests with the ELPI showed that the relationship of deposition and resuspension processes with the target conditions reached during cold-start tests was not simple, given the large differences in particle number and mass emissions in one condition or another. Some results even apparently contradicted the expected effects of the target conditions on the changes through the system. Low-speed tests showed

many more cases of large particle resuspension and fine particle formation, and fewer cases of large particle deposition, than high-speed and high-load tests. However, the particle number concentration and Emission Index emitted during high-speed and high-load conditions were one or two orders of magnitude higher than at low-speed and low-load conditions. The former contributed much more significantly to the total particle formation, deposition and resuspension when comparing the total particle number and mass emissions.

The most significant emissions, and therefore the most significant absolute changes through the exhaust system, occurred in the first few seconds after the engine start up. Great numbers of ultrafine particles were formed and large particles were resuspended during this short period. The subsequent acceleration contributed mostly to the coagulation of ultrafine particles to form mid-sized particles, but it did not actually contribute significantly to large particle resuspension. Once the system was stabilised at the target condition, particle resuspension still occurred in many cases.

The acceleration tests showed that large particles were reentrained from the exhaust system walls mainly during acceleration. However, they also made clear that all processes predominated over their opposite in a similar number of cases, confirming that very subtle differences were sufficient to change the particulate behaviour through the system.

Acceleration tests also showed that the higher temperatures found during high-load operation promoted ultrafine particle coagulation and large particle resuspension at a higher extent than high-speeds. High-speed operation, in contrast, promoted ultrafine particle formation and large particle deposition in more cases than high-load operation.

Regarding the chemical composition, particles emitted during high-load operation had a much lower SOF than those emitted at high-speeds, with 40% and 80%, respectively. The high SOF content may explain the higher significance of ultrafine particle formation at high-speed conditions. On the other hand, the lower SOF content at high-load conditions may be related to the observed trend towards large particle resuspension. The SOF content did not change significantly through the exhaust system. A slight increase through the catalyst at high speed was related to gas-to-particle conversion processes, and the decrease in SOF, mainly through the first silencer, was presumably due to large particle resuspension from the walls, mostly formed by particles with high carbon content.

A correction function was derived in this work in an attempt to reduce the effect of the ELPI's original over-correction in the calculation of large particle

number concentration from measured current values. The correction was based on comparison of ELPI mass concentration data with filter mass data at steady-state conditions. The use of the derived correction reduced significantly, and in some cases eliminated, the overestimation produced by the ELPI. The correction was limited, and not applicable for all cases, since the particle structural and physical-chemical characteristics, and therefore their impaction behaviour, change with operational conditions.

Transient and steady-state emissions from the tests were used to estimate the effect of transients on driving cycles different from the step-change cycles used in this work. The methodology to do this, using work-specific emisisons in transient and steady-state segments of the cycles, was shown. In some step-change cycles run in this work, transient emissions may reduce and not increase total cycle emissions under certain operational conditions such as a cold-start with a target high-power steady-state condition.

Transients have the potential to affect (in many cases, increase) significantly the emissions from a driving cycle that originally takes into account only steady-state modes, such as the R49 and the ESC. An illustrative example of this, using the emission factors from this work, was shown.

Cold-start tests with the new exhaust were not comparable to those at the same conditions with the old exhaust, owing presumably to a major maintenance of the engine and changes that may have reduced the particulate emissions to values one to two orders of magnitude lower than those in previous tests. These tests, however, were useful to show that the incipient deposition layer was formed very quickly over the walls of the new exhaust and that particulate resuspension processes started being important since the very beginning of the life of the new exhaust.

Particle images from TEM and SEM allowed measuring the fractal dimension of particulate matter collected during high-load engine operation. Fractal dimension was 1.82 with a correlation factor R^2=0.88.

8.2. Remarks and recommendations for future work

This work gave useful evidence about the changes undergone by diesel particulate matter through a practical exhaust system under laboratory cold-start and acceleration test conditions. The main limitations inherent to the equipment for the planned objectives were:

- The low response speed of the hydraulic dynamometer in automatic mode. This did not allow reproducing the real-world transient acceleration more closely.
- The manual operation of the throttle during transient step changes. This caused variability in the time needed to reach the target conditions, and may have affected the number concentration and Emission Index levels in the various transient events.
- The lack of a real-time mass measurement technique, e.g. TEOM. The filter mass measurements only suggested the particle mass changes with time, but its time resolution was too poor.
- The use of only one ELPI instrument per test, per sampling point. The great sensitivity of the particulate changes through the exhaust system shown in this work justifies the use of at least two ELPI instruments simultaneously in different sampling points.

From these limitations, the following recommendations were derived, to enhance the understanding of the particulate changes through the exhaust systems:

- The use of a fast-response totally automated electrical dynamometer.
- The use of at least two TEOM instruments for simultaneous real-time total particulate mass measurements and the comparison of these mass values with the ELPI derived values. This will allow finding a better correction strategy for the mass calculation from ELPI number concentrations.
- The simultaneous use of two particle-size-distribution measurement instruments, either two ELPIs or one ELPI and one SMPS, in different sampling points along the exhaust system. The SMPS is not a real time measurement instrument, but it can be used to track near real-time changes in a narrow particle size range. In addition, the use of both ELPI and SMPS is an useful combination to understand more thoroughly the particle characteristics.

Additionally, the following recommendations should be considered:

- Further work is required on the effect of the catalyst initial temperature on particulate deposition and reentrainment.
- The use a real-time technique to determine the particulate chemical composition, such as laser-based techniques (Schraml, 1999) or charge diffusion/photoelectric techniques (ETH, 2000) is recommended.

- The development of a comprehensive CFD model that takes into account the majority of factors and processes involved in the complex changes of the exhaust aerosol through the exhaust system is necessary. The Fluent® code has been used for turbulent deposition with thermophoresis, including the Saffman lift force (Chunghong, 1998), but not a more accurate model for resuspension as that suggested by Adhiwidjaja et al (Adhiwidjaja, 2000).

References

Abbass, 1989	M.K. Abbass, G.E. Andrews, P.T. Williams, K.D. and Bartle. Diesel Particulate Composition Changes along an Air Cooled Exhaust Pipe and Dilution Tunnel. SAE Technical Paper 890789, 1989.
Abbass, 1991	M.K. Abbass, Y. Shen, S. Abdulhalim, G.E. Andrews and P.T. Williams. Comparison of the methods for the determination of SOF of diesel particulates and development of a rapid TGA method for the estimation of the unburnt fuel and lubricating oil fractions, IMechE Seminar on Experimental Methods in Engine R&D, pp. 109-114, MEP, 1991.
Abdul-Khalek, 1995	I.S. Abdul-Khalek, D.B. Kittelson. Real time measurement of volatile and solid exhaust particles using a catalytic stripper. SAE Technical Paper 950236, 1995.
Abdul-Khalek, 1998	I.S. Abdul-Khalek, Kittleson, D.B. and F. Brear. Diesel Trap Performance: Particle Size Measurements and Trends, SAE Paper 982599, 1998.
Abdul-Khalek, 1998 (2)	I.S. Abdul-Khalek, Kittleson, D.B., B.R. Graskow, Q. Wei and F. Brear. Diesel exhaust particle size: measurement issues and trends, SAE Paper 980525, 1998.
Abdul-Khalek, 1999	I.S. Abdul-Khalek, Kittleson, D.B. and F. Brear. The influence of dilution conditions on diesel exhaust particle size distribution measurements, SAE Paper 1999-01-1142, 1999.
Abdul-Khalek, 2000	I.S. Abdul-Khalek. Characterisation of Particle Size Distribution of a Heavy-Duty Diesel Engine During FTP Transient Cycle Using ELPI. SAE Technical Paper 2000-01-2001, 2000.
Abdul-Khalek, 2000	I.S. Abdul-Khalek, D.B. Kittelson and F. Brear. Nanoparticle Growth During Dilution and Cooling of Diesel Exhaust: Experimental Investigation and Theoretical Assessment. SAE Technical Paper 2000-01-0515, 2000.
Abraham, 1996	J. Abraham. Thermophoretic Effects on Soot Distribution in a Direct Injection Diesel Engine, SAE Technical Paper 960320, 1996.
Adams, 1996	K. Adams, J.V. Cavataio, T. Sale, W.A. Rimkus and R.H. Hammerle. Laboratory Screening of Diesel Oxidation Catalysts and Validation with Vehicle Testing: The Importance of Hydrocarbon Storage. SAE Technical Paper 962049, 1996.

Adhiwidjaja, 2000	I. Adhiwidjaja, S. Matsusaka, H. Tanaka and H. Masuda. Simultaneous Phenomenon of Particle Deposition and Reentrainment: Effects of Surface Roughness on Deposition Layer of Striped Pattern. Aerosol Science and Technology, Vol. 33, pp. 323-333, 2000.
Adhiwidjaja, 2000	I. Adhiwidjaja, S. Matsusaka, S. Yabe and H. Masuda. Simultaneous Phenomenon of Particle Deposition and Reentrainment in Charged Aerosol Flow - Effects of Particle Charge and External Electric Field on the Deposition Layer. Advanced Powder Technology, Vol. 11, pp. 221-233, 2000.
Ahamed, 1999	F. Ahamed. PhD Thesis. Particulate emissions from Spark Ignition engines. University of Leeds. Leeds, October 1997.
Ahlvik, 1998	P. Ahlvik, L. Ntziachristos, J. Keskinen and A. Virtanen. Real time measurements of diesel particle size distribution with an ELPI, SAE Paper 980410, 1998.
Alander,1999	T. Alander, A. Leskinen, I. Ruotsalainen and T. Raunemaa. The Effects of Operation Parameters on Spark Ignition Engine Particle Size and Volatility. J. Aerosol Sci., Vol 30, Suppl. 1, pp. S583-S584, 1999
Anderson, 2000	H.R. Anderson. Differential Epidemiology of Ambient Aerosols. Phylosophical Transactions of The Royal Society of London, Series A, vol. 358, No. 1775, pp. 2771-2785. 15 Octobre 2000.
Andersson, 2001	J. Andersson and B. Wedekind. DETR/SMMT/CONCAWE Particulate Research Programme 1998-2001. Summary report, Ricardo Consulting Engineering, DP01/0515. www.ricardo.com. UK, May 2001.
Andrews, 2000	G.E. Andrews, A.G. Clarke, N.Y. Rojas, D. Gregory and T. Sale. Particulate mass accumulation and release in practical diesel engine exhaust systems under cold start conditions, SAE Paper 2000-01-0508.
Andrews, 2000 (2)	G.E. Andrews, A.G. Clarke, N.Y. Rojas, D. Gregory and T. Sale. Diesel particle size distribution changes at the exhaust pipe outlet during cold start in a passenger car IDI diesel with a practical exhaust system in place, SAE Paper 2000-01-0511.

Andrews, 2000 (3)	G.E. Andrews, A.G. Clarke, N.Y. Rojas, D. Gregory and T. Sale. Diesel Particle Size Distribution Changes Along a Practical Exhaust System During Cold Start in a Passenger Car IDI Diesel, SAE Paper 2000-01-0514.
Andrews, 2001	G.E. Andrews, A.G. Clarke, N.Y. Rojas, D. Gregory and T. Sale. The Transient Storage And Blow-Out Of Diesel Particulate In Practical Exhaust Systems. SAE Paper 2001-01-0204, 2001.
Andrews, 2001 (2)	G.E. Andrews, A.G. Clarke, N.Y. Rojas, D. Gregory and T. Sale. Diesel Particle Size Distribution:The Conversion Of Particle Number Size Distribution To Mass Distribution. SAE Paper 2001-01-1946, 2001.
Andrews, 2001 (3)	G.E. Andrews, A.G. Clarke, N.Y. Rojas, D. Gregory and T. Sale. The Transient Deposition and Particle Changes Across a Combined Oxidation and Hydrocarbon Storage Catalyst under Diesel Cold Start Conditions. SAE Paper 2001-01-1951.
Baert, 1999	R. S. G. Baert, D. E. Beckman, A. Veen. Efficient EGR technology for future HD diesel engine emission targets. SAE Technical Paper 1999-01-0837, 1999.
Bagley, 1998	S.T. Bagley, D.G. Leddy, A.M. Kreso, J.H. Johnson, L.D. Gratz. A study of the effects of exhaust gas recirculation on heavy-duty diesel engine emissions. SAE Technical Paper 981422, 1998.
Bagley, 1998 (2)	S.T. Bagley, D.G. Leddy, A.M. Kreso, J.H. Johnson, L.D. Gratz. A study of the vapor- and particle-phase sulfur species in the heavy-duty diesel engine EGR cooler. SAE Technical Paper 981423, 1998.
Baker, 1998	J.A. Baker. Particulate Matter Regulation and Implications for the Diesel Engine. SAE Technical Paper 981174, 1998.
Ball, 1983	D.J. Ball and R. Caswell. Smoke from Diesel-Engined Road Vehicles – An Investigation into the Basis of British and European Emission Standards. Atmos. Environ. 17, pp. 169-181. 1983.
Banse, 2001	D. F. Banse, K. Esfeld, M. Hermann, B. Sierau, A. Wiedensohler. Particle counting effiency of the TSI CPC 3762 for different operating parameters. Aerosol Science 32, pp. 157-161, 2000.
Baumgard, 1991	K.J. Baumgard, J.H. Johnson, D.G. Leddy, L.D. Grazt, and S.T. Bagley. The effect of a ceramic particulate trap on the particulate and vapor-phase emissions from a heavy duty diesel engine, SAE Paper 910609, 1991.

Baumgard, 1992	K.J. Baumgard and J.H. Johnson. The effect of low sulphur fuel and a ceramic particle filter on diesel exhaust particle size distributions, SAE Paper 920566, 1992.
Baumgard, 1996	K.J. Baumgard and J.H. Johnson. The Effect of Fuel and Engine Design on Diesel Exhaust Particle Size Distributions, SAE Paper 960131, 1996.
Begsteiger, 1999	I. Begsteiger, K. Richter, E. Jacob and G. Emmerling. Hydrocarbon Sorption and Oxidation Catalyst for Heavy Duty Engines. SAE Technical Paper 1999-01-3560, 1999.
Berger,1995	C. Berger, H. Horvat and W. Schindler. The Deposition of Soot Particles from Hot Gas Streams Through Pipes. Journal of Aerosol Science, Vol 26, No. 2, 1995.
Black, 1991	F. Black. An Overview of the Technical Implications of Methanol and Ethanol as Highway Motor Vehicle Fuels. SAE Technical Paper 912413, 1991.
Bockhorn, 2000	H. Bockhorn. Ultrafine Particles from Combustion Sources: Approaches to what we want to know. Phylosophical Transactions of The Royal Society of London, Series A, vol. 358, No. 1775, pp. 2659-2673. 15 October 2000.
Booker, 1995	D.R. Booker and T.M. Merrifield. Development of a Real-Time Mass Weighted Aerodynamic Particle Sizer, 9th Annual Conference Aerosol Society, 1995.
Boulaud, 1996	D. Boulaud, M. Pourprix, R. Gougeon, E. Le Bronec and A. Renoux. A New Method for the Determination of Aerosol Particle Density and Mass. AAAR 15th Annual Conference. pp. 275. 1996.
Brace, 1999	C. J. Brace, A. Cox, J. G. Hawley, N. D. Vaughan and F. W. Wallace, R. W. Horrocks and G. L. Bird. Transient Investigation of Two Variable Geometry Turbochargers for Passenger Vehicle Diesel Engines. SAE Technical Paper 1999-01-1241, 1999.
Brasil, 1999	A.M. Brasil, T.L. Farias and M.G. Carvalho. A for Image Characterisation of Fractal-like Aggregates. J. Aerosol Sci. Vol 30 No.10, pp 1379-1389, 1999.
Brown, 1997	R.C. Brown. Tutorial review: Simultaneous measurement of particle size and particle charge. Journal of Aerosol Science Vol 28 No. 8, pp. 1373-1391, 1997.

Brown, 2000	L.M. Brown, N. Collings, A.D. Harrison, A.D. Maynyard and R.L. Maynyard. Ultrafine Particles in the Atmosphere: Introduction. Phylosophical Transactions of The Royal Society of London, Series A, vol. 358, No. 1775, pp. 2563. 15 October 2000.
Burtscher, 2000	H. Burtscher. Characterization of Ultrafine Particle Emissions from Combustion Systems. SAE Technical Paper 2000-01-1997, 2000.
Burtscher, 2001	H. Burtscher, U. Baltensperger, N. Bukowiecki, P. Cohn, C. HuKglin, M. Mohr, U. Matter, S. Nyeki, V. Schmatloch, N. Streit, E. Weingartner. Separation of volatile and non-volatile aerosol fractions by thermodesorption: instrumental development and applications. Journal of Aerosol Science Vol. 32, pp. 427-442, 2001.
Cadle, 1997	S.H. Cadle, P.J. Groblicki, R.A. Gorse, J. Hood, D. Korduba-Sawicky, M. Sherman. A dynamometer study of off-cycle exhaust emissions—The auto/oil air quality improvement research program. SAE Technical Paper 971655, 1997.
Cadle, 1999	S.H. Cadle, P.A. Mulawa, E.C. Hunsanger, K. Nelson, R.A. Ragazzi, R. Barrett , G.L. Gallagher, D.R. Lawson, K.T. Knapp and R. Snow. Composition of Light-Duty Motor Vehicle Exhaust Particulate Matter in the Denver, Colorado Area. Environmental Science and Technology. Vol. 33. pp 2328-2339. 1999.
Campbell, 1981.	J. Campbell, J. Scholl, F. Hibbler, S.T. Bagley, D.G. Leddy, D. Abata and J. H. Johnson. The Effect of Fuel Injection Rate and Timing on the Physical, Chemical and Biological Character of Particulate Emissions from a Direct Injection Diesel. SAE Technical Paper 810996, 1981.
Cass, 2000	G.R. Cass, L.A. Hughes, P. Bhave, M.J. Kleeman, J.O. Allen and L.G. Salmon. The Chemical Composition of Atmospheric Ultrafine Particles. Phylosophical Transactions of The Royal Society of London, Series A, vol. 358, No. 1775, pp 2581-2592. 15 October 2000.
Chan, 2000	T.W. Chan, M. Mozurkewich. Measurement of the coagulation rate constant for sulfuric acid particles as a function of particle size using tandem differential mobility analysis. Aerosol Science 32, 321-339, 2001.
Chell, 1993	M. Chell, D. Hutchinson. London Energy Study, Energy Use and the Environment. London Research Centre, 1993.

Chen, 1995	M. Chen, K. Kontomaris and J.B. McLaughlin. Dispersion, Growth and Deposition of Coalescing Aerosols in a Direct Numerical Simulation of Turbulent Channel Flow. ASME Publications - FED. Vol. 228, pp. 27-32, 1995.
Chen, 1998	D.R. Chen, D.Y.H. Pui, D. Hummes, H. Fissan, F.R. Quant and G.J. Sem. Design and evaluation of a nanometer aerosol differential mobility analyser, NanoDMA. Journal of Aerosol Science Vol. 29, No. 5/6, pp. 497-509, 1998.
Cheng, 1999	C. Y. R. Cheng and T. W. Wu. Exhaust Muffler Design and Analysis Using A Boundary Element Method Based Computer Program. SAE Technical Paper 1999-01-1661, 1999.
Chiou, 1996	M.C. Chiou and J.W. Cleaver. Effect of Thermophoresis on submicron particle deposition from a laminar forced convection boundary layer flow onto an isothermal cylinder. Journal of Aerosol Science Vol 27, No. 8, pp. 1155-1167, 1996.
Cho, 2000	J. Cho and M. Choi. Determination of number density, size, and morphology of silica aggregate particles in coflow diffusion flames using light scattering and local sampling. Journal of Aerosol Science Vol. 31, No. 9, pp. 1077-1095, 2000.
Choi, 1995	M.Y. Choi, G.W. Mulholland, A. Hamins and T. Kashiwagi. Comparisons of the soot Volume Fraction Using Gravimetric and Light Extinction Techniques. Combustion and Flame 102, pp. 161-169, 1995.
Choi, 1995	C.Y. Choi and D.E. Foster. In cylinder augmented mixing through controlled gaseous jet injection. SAE Technical Paper 952358, 1995.
Chunhong, 1998	H. Chunhong and G. Ahmadi. Particle Deposition with Thermophoresis in Laminar and Turbulent Duct Flows. Aerosol Science and Technology, Vol. 29, pp. 525-546, 1998.
Clarke, 2001	A.G. Clarke. Personal communication.
Clement, 1999	C.F. Clement, I.J. Ford. Gas-to-particle conversion in the atmosphere: II. Analytical models of nucleation bursts. Atmospheric Environment 33, 489-499, 1999
Collings, 2000	N. Collings and B.R. Graskow. Particles from Internal Combustion Engines - what we need to know. Phylosophical Transactions of The Royal Society of London, Series A, vol. 358, No. 1775, pp. 2611-2622. 15 October 2000.
COMEAP, 1995	COMEAP, Annual Report 1995

CONCAWE, 1999	CONCAWE, Ultra Low Sulphur Fuel. CONCAWE Review, Vol. 8, No. 1, April 1999.
CONCAWE, 1999 (2)	CONCAWE, Automotive Particulate Matter, CONCAWE Review, Vol. 8, No. 1, April 1999.
CONCAWE, 1999 (3)	CONCAWE, The Challenges in Automotive Engineering, CONCAWE Review, Vol. 8, No. 1, April 1999.
CONCAWE, 1999 (4)	CONCAWE, Understanding EPEFE, CONCAWE Review, Vol. 8, No. 1, April 1999.
CONCAWE, 1999 (5)	CONCAWE, Automotive Polycyclic Aromatic Hydrocarbons (PAH), CONCAWE Review, Vol. 8, No. 1, April 1999.
De Vlieger, 2000	I. De Vlieger, D. De Keukeleere, J.G. Kretzschmar. Environmental effects of driving behaviour and congestion related to passenger cars. Atmospheric Environment 34, pp. 4649-4655, 2000.
Dekati, 1999	Dekati web page, ELPI Frequently Asked Questions. http://www.dekati.fi, 1999.
Dementhon, 1997	J.B. Dementhon and B. Martin. Influence Of Various Diesel Traps On Particle Size Distribution, SAE Technical Paper 972999, 1997.
Derwent, 2000	R.G. Derwent and A.L. Malcolm. Photochemical Generation of Secondary Particles in the United Kingdom. Phylosophical Transactions of The Royal Society of London, Series A, vol. 358, No. 1775, pp. 2643-2656. 15 October 2000.
di Stasio, 2001	S. di Stasio. Observation of restructuring of nanoparticle soot aggregates in a diffusion flame by static light scattering. Journal of Aerosol Science Vol. 32 pp. 509-524, 2001.
di Stasio, 2001 (2)	S. di Stasio. Electron microscopy evidence of aggregation under three different size scales for soot nanoparticles in flame. Carbon, Vol. 39, pp. 109-118, 2001.
Dick, 2000	C.A.J. Dick, V. Stone, D.M. Brown, M. Watt, J.W. Cherrie, S. Howarth, A. Seaton and K. Donaldson. Toxic and Inflammatory Effects of Filters Frequently Used for the Collection of Airborne Particulate Matter. Atmospheric Environment. Vol 34, pp. 2587-2592, 2000.
Dickey, 1998	D.W. Dickey, T.W. Ryan and A.C. Matheaus. NOx control in heavy-duty diesel engines—What is the limit? SAE Technical Paper 980174, 1998.

Dockery, 1993	D.W. Dockery. An Association between Air Pollution and Mortality in Six U.S. Cities. The New England Journal of Medicine, December 9, 1993.
Dockery, 1994	D.W. Dockery and C.A. Pope. Acute Respiratory Effects of Particulate Pollution. Annu. Rev. Public Health, 15. Pp. 107-132. 1994.
Donald, 1997	J. R. Donald and D.P. Moon. 1997. UK Research Program on the Characterization of Vehicle Particulate Emissions. (Contract Report for the Department of the Environment, Transport and the Regions and the Society of Motor Manufacturers and Traders by ETSU – a group within AEA). ETSU-R98.
Donaldson, 1998	K. Donaldson. Ultrafine (nanometric) particle mediated lung injury. Journal of Aerosol Science, 29 No. 5/6: 553-560, 1998.
Donaldson, 2000	K. Donaldson, V. Stone, P.S. Gilmour, D.M. Brown and W. MacNee. Ultrafine Particles: Mechanisms of Lung Injury. Phylosophical Transactions of The Royal Society of London, Series A, vol. 358, No. 1775, pp. 2741-2748. 15 October 2000.
Durbin, 2000	T.D. Durbin, J.R. Collins, J.M. Norbeck and M.R. Smith. Effects of Biodiesel, Biodiesel Blends , and a Synthetic Diesel on Emissions from Light Heavy Duty Diesel Vehicles. Environmental Science and Technology. Vol. 34, No. 3, 2000.
Dye, 1999	A.L. Dye, M.M. Rhead and C.J. Trier. The Quantitative Morphology of Roadside and Background Urban Aerosol in Plymouth, UK. Atmospheric Environment 34, pp. 3139-3148, 2000.
EEA, 2000	European Environment Agency. Indicators on transport and environment integration in the EU. Environmental issues series No 12. Copenhagen, February 2000.
Engler, 1993	B.H. Engler, D. Lynder, E.S. Lox, K. Ostgathe, Schäfer-Sindlinger and W. Müller. Reduction of Exhaust Gas Emissions by Using Hydrocarbon Adsorber Systems. SAE Technical Paper 930738, 1993.
ETH, 2000	Proceedings of the 4th ETH International Conference on Nanoparticle Measurement, Zurich, August 7-9 2000.
Fanick, 1996	E. Robert Fanick, Kevin A. Whitney, Brent K. Bailey. Particulate characterization using five fuels. SAE Technical Paper 961089, 1996.

Farias, 2001	T. L. Farias, A. M. Brasil, M. G. Carvalho, U. O. Koylu. Numerical characterization of the morphology of aggregated particles. Journal of Aerosol Science Vol. 32, pp. 489-508, 2001.
Farrow, 1993 (1)	I.K. Farrow, J.M. Kisenyi, R.S. Cudworth, C.A. Savage and A.C. Simmonds. Legislated Emissions from the Seven Diesel Vehicles from the Large Scale Survey. Report No. LR 931, Warren Spring Laboratory. Stevenage, 1993.
Farrow, 1993 (2)	I.K. Farrow, R.S. Cudworth, C.A. Savage and A.C. Simmonds. Regulated Emissions from the Three Gasoline Vehicles with Catalysts from the Large Scale Survey. Report No. LR 932, Warren Spring Laboratory. Stevenage, 1993.
Farrow, 1993 (3)	I.K. Farrow, R.S. Cudworth, C.A. Savage and A.C. Simmonds. Regulated Emissions from the Forty Gasoline Vehicles without Catalysts from the Large Scale Survey. Report No. LR 933, Warren Spring Laboratory. Stevenage, 1993.
Ferion, 1996	J. Ferion, G. Oberdörster and D.P. Penney. Pulmonary retention of ultrafine and fine particles in rats, American J. Respiratory Cell Molecular Biology, Vol. 6, pp.535-542, 1992.
Fernández de la Mora, 1998	J. Fernández de la Mora, L. de Juan. Sizing nanoparticles with a focusing impactor: effect of the collector size. Journal of Aerosol Science Vol. 29, no. 5/6, pp. 589-599, 1998.
Flagan, 2000	R.C. Flagan, D.R. Collins, A. Nenes and J.H. Seinfeld. The scanning flow DMA. Journal of Aerosol Science Vol. 31, No. 10, pp. 1129-1144, 2000
Fraser, 1998.	Gas-Phase and Particle-Phase Organic Compounds Emitted from Motor Vehicle Traffic in a Los Angeles Roadway Tunnel. Environmental Science and Technology. Vol. 32, pp. 2051-2060, 1998.
Friedlander, 2000	S.K. Friedlander. Smoke, dust and haze. Second Edition. Oxford University Press. Oxford, 2000.
Friedlander, 2000	S.K. Friedlander and C. Xiong. Measurements of Fractal-like Atmospheric Particles. J. Aerosol Sci. Vol 31, Suppl. 1, pp. S226-S227, 2000.
Fujiwara, 1980	Y. Fujiwara and S. Fukazawa. Growth and combustion of soot particulates in the exhaust of diesel engines, SAE Paper 800984, 1980.

Furutani, 1992	H. Furutani, S. Tsuge and S. Goto. The Dependence of Carbon/Hydrogen Ratio on Soot Particle Size. SAE Technical Paper 920689, 1992.
Garg, 2000	B.D. Garg, S.H. Cadle, P.A. Mulawa, P.J. Groblicki, C. Laroo and G.A. Parr. Brake Wear Particulate Matter Emissions. Environmental Science and Technology Vol. 34. No. 21, 2000.
Gartner, 1952	Gartner, Architectural and industrial hygiene, 6: 339, 1952.
Gehr, 2000	P. Gehr, M. Geiser, V. Im Hof and S. Schürch. Surfactant-Ultrafine Particle Interactions: What We Can Learn from PM10 Studies. Phylosophical Transactions of The Royal Society of London, Series A, vol. 358, No. 1775, pp. 2707-2717. 15 October 2000.
Girard, 1999	J.W. Girard, L.D. Gratz, J.H. Johnson, S.T. Bagley, D.G. Leddy. A study of the character and deposition rates of sulfur species in the EGR cooling system of a heavy-duty diesel engine. SAE Technical Paper 1999-01-3566, 1999.
Gorbunov, 1999	B. Gorbunov, A.G. Clarke and R.S. Hamilton. Coagulation of soot particles and fractal dimension, J. Aerosol Sci., Suppl. 1 pp. S455-s446, 1999.
Graskow, 1999	B.R. Graskow, D.B. Kittelson, M.R. Ahmadi and J.E. Morris. Exhaust Particulate Emissions from Two Port Fuel Injected Spark Ignition Engines. SAE Technical Paper 1999-01-1144, 1999.
Graskow, 2000	B.R. Graskow, D.B. Kittelson, M.R. Ahmadi and J.E. Morris. Exhaust Particulate Emissions from a Direct Injection Spark Ignition Engine. SAE Technical Paper 1999-01-1145, 1999.
Greenwood, 1996	S.J. Greenwood, J.E. Coxon, T. Biddulph and J. Bennett. An investigation to determine the exhaust particulate size distributions for diesel, petrol, and compressed natural gas fueled vehicles. SAE Technical Paper 961085, 1996.
Gregory, 1999	D. Gregory. "Artifice in particle size distribution measurement" lecture in the ENGINES EMISSIONS MEASUREMENT Short Course, 28 June –2 July 1999.
Groblicki	Particle Size Variation in Diesel Car Exhaust
Grosjean, 1998	E. Grosjean , D. Grosjean and R.A. Rasmussen. Ambient Concentrations, Sources, Emission Rates, and Photochemical Reactivity of C2-C10 Hydrocarbons in Porto Alegre, Brazil. Environmental Science and Technology. Vol. 32, pp. 2061-2069, 1998.

Guillham, 1992	C.A. Guillham, P.K. Leech and H.S. Egleston. UK Emissions of Air Pollutants. Warren Spring Laboratory, Report LR 887. Stevenage, 1992.
Hall, 1998	D.E. Hall, CONCAWE. Automotive emissions management group, Special task force AE/STF-10. A Study on the Number, Size and Mass of Exhaust Particles Emitted by Diesel and Gasoline Engines under Steady State and European Driving Cycle Conditions, Report No. 98/51. Brussels, Feb. 1998.
Hall, 1998	D.E. Hall, CONCAWE. Automotive emissions management group, Special task force AE/STF-10. Polycyclic Aromatic Hydrocarbons in Automotive Exhaust Emissions and Fuels, Report No. 98/55. Brussels, Feb. 1998.
Hall, 1998	D.E. Hall, C.L. Goodfellow, P. Heinze, D.J. Rickeard, G. Nancekevill, G. Martini, J. Hevesi, L. Rantanen, M.P. Merino, T.D.B. Morgan and P.J. Zemroch. A Study on the Size, Number and Mass Distribution of the Automotive Particulate Emissions from European Light Duty Vehicles. SAE Technical Paper 982600, 1998.
Hall, 1998 (2)	D.E. Hall, D.J. King, T.D.B. Morgan, S.J. Baverstock, P. Heinze and B.J. Simpson. A review of recent literature investigating the measurement of automotive particulates: the relationship with environmental aerosol, air quality and health effects, SAE Paper 982602, 1998.
Hall, 1999	D.E. Hall, C.J. Dickens. Measurement of the Number and Size Distribution of Particles Emitted from a Gasoline Direct Injection Vehicle. SAE Technical Paper 1999-01-3530, 1999.
Hall, 2000	D.E. Hall, R.J. Stradling, P.J. Zemroch, D.J. Rickeard, N. Mann, P. Heinze, G. Martini, R. Hagemann, L. Rantanen, J. Szendefi. Measurement of the Number and Size Distribution of Particle Emissions from Heavy Duty Engines. SAE Technical Paper 2000-01-2000.
Hall, 2000	D.E. Hall, C.J. Dickens. Measurement of the Numbers Of Emitted Gasoline Particles: Genuine Or Artefact?. SAE Technical Paper 2000-01-2957, 2000.
Hammerle, 1994	R.H. Hammerle, D.A. Ketcher, R.W. Horrocks, G. Lepperhoff, G. Hüthwohl, B. Lüers. Emissions from current diesel vehicles. SAE Technical Paper 942043, 1994.

Harris, 1998	D.B. Harris. Development of Fine Particulate Emission Factors from In-Use Heavy-Duty Diesel Trucks: Installation and Operation of Near-Real Time Particle Sizing Devices. AAAR 17th Annual Conference. pp. 118. 1998.
Harrison, 1993	R.M. Harrison, P. Brimblecombe, R.G. Derwent, G.J. Dollard, R.S. Hamilton, A.J. Hickman, C. Holman, D.P.H. Laxen, M.J. Pilling and F.B. Smith. Diesel Vehicle Emissions and Urban Quality, Second Report of the Air Quality of Urban Air Review Group. December, 1993.
Harrison, 1996	R.M. Harrison, P. Brimblecombe, R.G. Derwent, G.J. Dollard, S. Egleston, R.S. Hamilton, A.J. Hickman, C. Holman, D.P.H. Laxen and S. Moorcroft. Airborne Particulate Matter in the United Kingdom, Third Report of the Air Quality of Urban Air Review Group. May, 1996.
Harrison, 1998	R.M. Harrison, R. van Grieken. Atmospheric Particles. IUPAC Series on Analytical and Physical Chemistry of Environmental Systems, Vol. 5. John Wiley & Sons, Chichester, 1998.
Harrison, 1999	R.M. Harrison, Ji Ping Shi, M.R. Jones. Continuous measurements of aerosol physical properties in the urban atmosphere. Atmospheric Environment 33, pp. 1037-1047, 1999.
Harrison, 2000	R.M. Harrison, Shi J.P., Xi S., Khan A., Mark D., Kinnersley R. and Yin J. Measurement of Number, Mass and Size Distribution of Particles in the Atmosphere. Phylosophical Transactions of The Royal Society of London, Series A, vol. 358, No. 1775, pp. 2567-2579. 15 October 2000.
Harrison, 2000	R.M. Harrison, J. Yin. Particulate matter in the atmosphere: which particle properties are important for its effects on health?. . The Science of the Total Environment 249, pp. 85-101, 2000.
Hawker, 1996	P. Hawker, G. Huthwohl, J. Henn, W. Koxh, H. Luders, B. Luers and P. Stommel. Effect of a continuously regenerating diesel particulate filter on non-regulated emissions and particle size distribution, SAE Paper 980189, 1998.
HEI, 1995	Health Effects Institute (HEI), Diesel Exhaust: A Critical Analysis of Emissions, Exposure and Health Effects. Cambridge, 1995.

HEI, 1999 — Health Effects Institute (HEI), Diesel Emissions and Lung Cancer: Epidemiology and Quantitative Risk Assessment. A Special Report of the Institute's Diesel Epidemiology Expert Panel. Cambridge, MA. June, 1999.

Hill, 1999 — L. Hill. "CVS systems for light duty vehicle emissions measurement" lecture in the ENGINES EMISSIONS MEASUREMENT Short Course, U. of Leeds, 28 June – 2 July 1999.

Hoard, 2000 — J. Hoard, R.L. Bretz, S. Kaberline, L.P. Haack, E. Kalashnikov. Composition of Clusters Formed by Plasma Discharge in Simulated Engine Exhaust. SAE Technical Paper 2000-01-2967, 2000.

Hontañón, 2000 — E. Hontañón, A. de los Reyes and J. A. Capitao.The Caesar code for aerosol resuspension in turbulent flows assessment against the storm experiments. Journal of Aerosol Science, Vol. 31, No. 9, pp. 1061-1076, 2000.

Horn,1993 — H.G. Horn. A New Technique for Automatic Phantom and Coincidence Count Reduction in the Aerodynamic Particle Sizer APS 3310. Report Series in Aerosol Science, No. 23, pp 185-190, 1993.

Howard, 2000 — J.B. Howard and H. Richter. Formation of polycyclic aromatic hydrocarbons and their growth to soot—a review of chemical reaction pathways. Progress in Energy and Combustion Science Vol. 26, pp. 565–608, 2000.

Hummel, 2000 — R. Hummel, A. Krasenbrink and G. de Santi. Characterisation of Vehicle Emissions. J. Aerosol Sci. Vol 31, Suppl. 1, pp. S246-S247, 2000.

Hunter, 1981 — G. Hunter, F. Scholl, F. Hibbler, S.T. Bagley, D.G. Leddy, D. Abata and J.H. Johnson. The effect of fuels on diesel oxidation catalyst performance and the physical, chemical and biological character of diesel particulate emissions, SAE Paper 811192, 1981.

IEA, 1993 — International Energy Agency (IEA), Organisation for Economic Cooperation and Development (OECD). Cars and Climate Change. OECD. Paris, 1993.

Jaeger, 1999 — L.W. Jaeger, K. Boulouchos and M. Mohr. Analysis of Factors Influencing Particulate Matter Emissions of a Compression-Ignition Direct-Injection Engine. SAE Technical Paper 1999-01-3492, 1999.

Jefferson, 2000	D.A. Jefferson. The Surface Activity of Ultrafine Particles. Phylosophical Transactions of The Royal Society of London, Series A, vol. 358, No. 1775, pp. 2683-2692. 15 October 2000.
Johnson, 1994	J.H. Johnson, S.T. Bagley, L.D., D.G. Gratz and D.G. Leddy. A review of diesel particulate control technology and emission effects. SAE Technical Paper 940233, 1994.
Kakoi, 1998.	Y. Kakoi, Y. Tsutsui, N. Ono, U. Katsunori and N. Kondo. Emission Reduction Technologies Applied to High-Speed Direct Injection Diesel Engine. SAE Technical Paper 980173, 1998.
Kales, 1994	S.N. Kales and D.C. Christiani. Progression of chronic obstructive pulmonary disease after multiple episode of an occupational inhalation fever. Journal of occupational medicine, 36. pp. 75-78, 1994.
Kamm, 2000	S. Kamm, M. Koyro, D. Mihelcic, O. Möhler, K.-H. Naumann and U. Schurath. Volatilisation and surface oxidation processes of soot aerosol with high NO_2 concentrations. Proceedings of the EUROTRAC Symposium 2000, Garmisch-Partenkirchen, March 27-31, 2000.
Katoh, 1998	K. Katoh, Y. Kosaki, T. Watanabe and M. Funabiki. Compatibility of NOx and PM abatement in diesel catalysts. SAE Technical Paper 980931, 1998.
Katoshevski, 2001	D. Katoshevski, B. Zhao, G. Ziskind, E. Bar-Ziv. Experimental study of the drag force acting on a heated particle. Journal of Aerosol Science Vol. 32, pp. 73-86, 2001.
Kawamani, 1998	M. Kawamani, M. Horiuchi, H. Klein and M. Jenkins. Development of Oxidation and de-NOx Catalyst for High Temperature Exhaust Diesel Trucks. SAE Technical Paper 981196, 1998.
Kayes, 1999	D. Kayes, H. Liu and S. Hochgreb. Particulate Matter Emission during Start-up and Transient Operation of a Spark Ignition Engine. SAE Technical Paper 1999-01-3529, 1999.
Kazuhisa, 1999	K. Inagaki, S. Takasu and K. Nakakita. In-cylinder Quantitative Soot Concentration Measurement By Laser-Induced Incandescence, SAE Technical Paper 1999-01-0508, 1999.
Kerminen, 1999	V.M. Kerminen, T. Makela, R. Hillamo and L. Rantanen, Relation between particle and mass size distribution in the diesel car exhaust, J. Aerosol Sc. Vol. 30, Suppl. 1, pp. S777-S778, 1999.

Keskinen, 1992	J. Keskinen, K. Pietarinen, and M. Lehtimaki. Electrical low pressure impactors, J. Aerosol Sci., Vol.23 No. 4, 1992.
Keskinen, 2001	J. Keskinen, A. Virtanen, M Marjamäki and J. Ristimäki. Fine Particle Losses in Electrical Low-Pressure Impactor. Journal of Aerosol Science Vol. 32, pp 389-401, 2001.
Khair, 1999	M. Khair and D.L. McKinnon. Performance evaluation of advanced emission control technologies for diesel heavy-duty engines. SAE Technical Paper 1999-01-3564, 1999.
Khatri, 1978	N.J. Khatri and J.H. Johnson. Physical Size Distribution Characterisation of Diesel Particulate Matter and the Study of the Coagulation Process, SAE Technical Paper 780788, 1978.
Kim, 2000	C.S. Kim and P.A. Jaques. Respiratory Dose of Inhaled Ultrafine Particles in Healthy Adults. Phylosophical Transactions of The Royal Society of London, Series A, vol. 358, No. 1775, pp. 2693-2706. 15 October 2000.
Kittelson, 1977	D.B. Kittelson and J. Verrant. Sampling and Physical Characterisation of Diesel Exhaust Aerosols, SAE Technical Paper 770720, 1977.
Kittelson, 1978	D.B. Kittelson, D.F. Dolan, R.B. Diveer and E. Aufderheide. Diesel Exhaust particle Size Distributions - Fuel and Additive Effects. SAE Technical Paper 780787, 1978.
Kittelson, 1990	D.B. Kittelson, J.L. Ambs and H. Hadjkacem. Particulate Emissions from Diesel Engines: Influence of In-Cylinder Surface. SAE Technical Paper 900645, 1990.
Kittelson, 1991	D.B. Kittelson and J.H. Johnson, Variability in particle emission measurements in the heavy-duty transient test, . SAE Technical Paper 910738, 1991.
Kittelson, 1994	D.B. Kittelson SAE Technical Paper 941015, 1994.
Kittelson, 1998	D.B. Kittelson. Engines and Nanoparticles: A Review. Journal of Aerosol Science, Vol. 25, No. 5/6, pp 575-588, 1998.
Kittelson, 1998	D.B Kittelson, W.F. Watts and M. Arnold. Review of Diesel Experimental Sampling Methods. Aerosol dynamics, laboratory and on-road studies. University of Minnesota, Minneapolis, MN July 31, 1998.

Kittelson, 1999	D.B. Kittelson, W. Watts, U. Baltensperger, E. Weingartner, U. Matter, S. Pandis, N. Clark and M. Gautum. Diesel Aerosol Sampling Methodology, University of Minnesota Center for Diesel Research, January 19, 1999.
Kleeman, 1998	M.J. Kleeman and G.R. Cass. Source Contributions to the Size and Composition of Urban Particulate Air Pollution. Atmospheric Environment Vol. 32, No. 16, pp. 2803-2816, 1998.
Kleeman, 2000	M.J. Kleeman, J.J. Schauer and G.R. Cass. Size and Composition of Fine Particulate Matter Emitted from Motor Vehicles. Environmental Science and Technology. Vol. 34, No. 7, 2000.
Klein, 1998	H. Klein, E. Lox, T. Kreuzer, M. Kawanami, T. Reid and K. Bachman. Diesel particulate emissions of passenger cars - new insights into structural changes during the process of exhaust aftertreatment using diesel oxidation catalysts, SAE Paper 980196, 1998.
Kostandopoulos, 2000	A.G. Kostandopoulos, M. Kostogiou, E. Skaperdas, E. Papaioannou, D. Zarvalis and E. Klapadopoulou. Fundamental Studies of Diesel Particulate Filters: Transient Loading, Regeneration and Aging. SAE Technical Paper 2000-01-1016, 2000.
Kostoglou, 2000	M. Kostoglou and A.G. Kostandopoulos. Brownian Coagulation of Fractal Aggregates. J. Aerosol Sci., Vol. 31, Suppl. 1, pp. S574-S575, 2000.
Krestinin, 2000	A. V. Krestinin. Detailed Modeling of Soot Formation in Hydrocarbon Pyrolysis. Combustion and Flame Vol. 121 pp. 513–524 2000.
Krüger, 1998	Krüger, Lüders, Stommel and Lüers. The role of sampling conditions in particle size distribution measurements, SAE Paper 981374, 1998.
Kühlwein, 2000	J. Kühlwein, R. Friedrich. Uncertainties of modelling emissions from road transport. Atmospheric Environment Vol. 34, pp. 4603-4610, 2000.
Kuo-Liang, 1998	L. Kuo-Liang Shih. Study of the Relationship between Diesel Engine Emissions and the Formation and Contents of Deposit. SAE Technical Paper 981425, 1994.
Lai, 2000	A.C. K. Lai, M.A. Byrne, A.J.H. Goddard. Aerosol deposition in turbulent channel flow on a regular array of three-dimensional roughness elements. Aerosol Science 32, 121-137, 2001.

Laitinen, 1997	A. Laitinen, J. Hautanen, M. Moisio, M. Marjamäki, A. Elsilä, K. Nieminen and J. Keskinen. Real Time Measurement of the Size Distribution Urban Aerosols with Electrical Low Pressure Impactor. J. Aerosol Sci. Vol. 27 Suppl. 1, pp. S299 - S300, 1996.
Lanning, 2000	L A. Lanning, K. W. Smith and C.J. Tennant. A New Method for Diesel HC Collection and Speciation. SAE Technical Paper 2000-01-2951, 2000.
Le Bronec, 1999	E. Le Bronec, A. Renoux, D. Boulaud and M Pourprix. Effect of Gravity in Differential Mobility Analysers - A New Method to Determine the Mass and Density of Aerosol Particles. Journal of Aerosol Science Vol 30, No. 1, pp. 89-103, 1999.
Lee, 2001	K.O. Lee, R. Cole, R. Sekar, J. Zhu, M.Y. Choi. Morphology, Microstructure and Dimensions of Diesel Engine Particulates. Presented at the 2nd Joint Meeting of the U.S. Sections of the Combustion Institute. Oklahoma, March 2001.
Lee, 2001(2)	J.W. Lee, M.Shin. Memory effect in the Eulerian particle deposition in a fully developed turbulent channel. Journal of Aerosol Science, Vol. 32 pp. 675-693, 2001.
Leet, 1998	J.A. Leet, A. Matheaus, D. Dickey. EGR system integration on a pump-line-nozzle engine. SAE Technical Paper 980181, 1998.
Leppenhoff, 1994	G. Lepperhoff, G. Hüthwohl, B. Lüers-Jongen. Methods to Analyse Non-Regulated Emissions from Diesel Engines. SAE Technical Paper 941952, 1994.
Leyrer, 1996	J. Leyrer, E. S. Lox, K. Ostgathe, W. Strehlau, T. Kreuzer, G. Garr. Advanced studies on diesel aftertreatment catalysts for passenger cars. SAE Technical Paper 960133, 1996.
Lindi, 1999	B. Lindi and G. Schmitz. Cold Start Equipment for Diesel Direct Injection Engines. SAE Technical Paper 1999-01-1244, 1999.
Lipkea, 1978	W.H. Lipkea, J.H. Johnson and C.T. Vuk. The Physical and Chemical Character of Diesel Particulate Emissions - Measurement Techniques and Fundamental Considerations. SAE Technical Paper 780108, 1978.
Lippmann, 2000	M. Lippmann and K. Ito. Contributions that Epidemiological Studies Can Make to the Search for a Mechanistic Basis for the Health Effects of Ultrafine and Larger Particles. Phylosophical Transactions of The Royal Society of London, Series A, vol. 358, No. 1775, pp. 2787-2797. 15 Octobre 2000.

Loscertales, 2000	I.G. Loscertales and F.J. Gómez. Calibration of a Nano-DMA Using High-Mobility Non-Diffusional Particles. J. Aerosol Sci., Vol. 31, Suppl. 1, pp. S402-S403, 2000.
Loscertales, 2000	I.G. Loscertales. Mass Diameter versus Aerodynamic Diameter of Nanoparticles. Implications on the Calibration Curve of an Inertial Impactor. J. Aerosol Sci. Vol 31, No. 8, pp. 923-932, 2000.
Ludykar, 1999	D. Ludykar, R. Westerholm and J. Almén. Cold Start Emissions at +22, -7 and -20oC Ambient Temperatures from a Three-Way Catalyst (TWC) Car: Regulated and Unregulated Exhaust Components. The Science of the Total Environment 235, pp. 65-69, 1999.
Lyyränen,1999	J. Lyyränen, J. Jokiniemi, E. Kauppinen and J. Joutsensaari. Aerosol Characterisation in Medium Speed Diesel Engines Operating with Heavy Fuel Oils. Journal of Aerosol Science, Vol. 30 No. 6, 1999.
MacLean, 2000	H.M. MacLean and L.B. Lave. Environmental Implications of Alternative-Fueled Automobiles: Air Quality and Greenhouse Gas Tradeoffs. Environmental Science and Technology, Vol. 34, No. 2, 2000.
Makkee, 2000	M. Makkee, B.A.A.L. van Setten, J.M. Schouten, J.A. Moulijn. Realistic contact for soot with an oxidation catalyst for laboratory studies. Applied Catalysis B: Environmental 28 pp. 253–257, 2000.
Maricq, 1999	M.M. Maricq, D.H. Podsiadlik, D.D. Brehob and M. Haghgoole. Particulate Emissions from a Direct-Injection Spark Ignition (DISI) Engine. SAE Technical Paper 1999-01-1530, 1999.
Maricq, 1999	M.M. Maricq, R.E. Chase, D. Podsiadlik and R. Vogt. Vehicle Exhaust Particle Size Distributions: A Comparison of Tailpipe and Dilution Tunnel Measurements. SAE Technical Paper 1999-01-1461, 1999.
Maricq, 1999	M.M. Maricq, R.E. Chase and D. Podsiadlik. Comparing ELPI and SMPS Measurements of Motor Vehicle Exhaust PM, 3rd. International ETH Workshop on Nanoparticle Measurement, Zürich, 9 - 10 August 1999.
Maricq, 1999	M.M. Maricq, D.H. Podsiadlik and R.E. Chase Examination of the Size Resolved and Transient Nature of Motor Vehicle Particle Emissions. Environmental Science and Technology. Vol. 33, pp. 1618-1626, 1999.

Maricq, 1999	M.M. Maricq, D.H. Podsiadlik and R.E. Chase Gasoline Vehicle Particle Size Distributions: Comparison of Steady State, FTP and US06 Measurements. Environmental Science and Technology. Vol. 33, No. 12, 1999.
Maricq, 2001	M.M. Maricq and S.J. Harris. Signature size distributions for diesel and gasoline engine exhaust particulate matter. Journal of Aerosol Science Vol. 32, pp. 749-764, 2001.
Marjamäki, 1998	M. Marjamäki, A. Virtanen, and J. Keskinen. Fine Particle Losses in Cascade Impactors. J. Aerosol Sci. Vol. 29 Suppl. 1, pp. S441 - S442, 1998.
Marjamäki, 2000	M. Marjamäki, J. Keskinen, D.R. Chen, D.Y.H. Pui. Performance Evaluation of the Electrical Low-Pressure Impactor (ELPI). J. Aerosol Sci. Vol 31 No. 2, pp. 249-261, 2000.
Marjamäki, 2000	M. Marjamäki, J. Ristimäki, A. Virtanen, M. Moisio, R. Luoma and J. Keskinen. Testing Porous Metal as a Collection Substrate in ELPI. J. Aerosol Sci. Vol 31, Suppl. 1, pp. S76-S77, 2000.
Martonen, 2000	T.B. Martonen, J.D. Schroeter, D. Hwang, J.S. Fleming and J.H. Conway. Human Lung Morphology Models for Particle Deposition Studies. Inhalation Toxicology, 12 (Supplement 4), pp 109-121, 2000.
Matsusaka, 1993	S. Matsusaka, M. Shimizu and H. Masuda. Formation of Wall Particle Layers by Simultaneous Deposition and Reentrainment. Kagaku Kogaku Ronbunshu. Vol. 19, No. 2, pp. 251-257, 1993.
Matter, 1999	U. Matter, H.C. Siegmann, M. Kasper and H. Burtscher. Distinction of Volatile and Nonvolatile Particles in Exhaust of Diesel Engines with Particle Traps. Journal of Aerosol Science Vol. 30 Suppl. 1 pp S471-S472, 1999.
Mauderly, 1994	J.L. Mauderly. Pulmonary Toxicity of Inhaled Diesel Exhaust and Carbon Black in Chronically Exposed Rats. Health Effects Institute Research Report No. 68, October, 1994.
Mayer, 1995	A.H. Mayer, H. Egli, J. Burtscher, D. Gehrig and J. Czerwinski. Particle size distributions downstream of traps of different designs, SAE Paper 950373, 1995.
Mayer, 1996	A.H. Mayer. Trapping Efficiency Depending on Particulate Size, SAE Technical Paper 960472, 1996.

Mayer, 1998	A.H. Mayer, U. Matter, Scheidegger, J. Czerwinski, M. Wyser, D. Kieser and Weidhofer. VERT: Diesel Nano-Particulate Emissions: Properties and Reduction Strategies. SAE Technical Paper 980539, 1998.
Maynard, 2000	A.D. Maynard. Overview of Methods for Analysing Ultrafine Particles. Phylosophical Transactions of The Royal Society of London, Series A, vol. 358, No. 1775, pp. 2593-2610. 15 October 2000.
McAughey, 1998	J. McAughey. Regional Lung Deposition and Dose of Ambient Particulate in Humans by Particle Mass and Number. Air and Waste Management Association Publications - VIP No. 80, pp. 499-507, 1998.
McMurry, 1996	P.H. McMurry, M. Litchy, P.F. Huang, X. Cai, B.J. Turpin, W.D. Dick and A. Hanson. Elemental composition and morphology of individual particles separated by size and hygroscopicity with the TDMA. Atmospheric Environment Vol. 30, No.1, pp. 101-108, 1996.
McMurry, 2000	P.H. McMurry, K.S. Woo, R. Weber, D.R. Chen and D.Y.H. Pui. Size Distributions of 3-10nm Atmospheric Particles: Implications for Nucleation Mechanisms. Phylosophical Transactions of The Royal Society of London, Series A, vol. 358, No. 1775, pp. 2625-2642. 15 October 2000.
McMurry, 2000	P.H. McMurry. A review of atmospheric aerosol measurements. Atmospheric Environment Vol. 34, pp. 1959-1999, 2000.
Micallef, 1999	A. Micallef and J. Colls. Measuring and modelling the airborne particulate matter mass concentration field in the street environment: model overview and evaluation. The Science of the Total Environment Vol. 235 pp. 199-210, 1999.
Miguel, 1998	A.H. Miguel, T.W. Kirchstetter and R. Harley. Environmental Science and Technology. Vol. 32, pp. 450-455. 1998.
Mogi, 1999	H. Mogi, K. Tajima, M. Hosoya and M. Shimoda. The Reduction of Diesel Engine Emissions by Using the Oxydation Catalysts on Japan Diesel 13 Mode Cycle. SAE Technical Paper 1999-01-0471, 1999.
Mohr, 2000	M. Mohr, A. Forss and D. Steffen. Particulate Emissions of Gasoline Vehicles and Influence of the Sampling Procedure. SAE Technical Paper 2000-01-1137, 2000.

Moisio, 1995	M. Moisio, M. Marjamäki and J. Keskinen Real Time Size Distribution Monitoring of Power Plant Particle Emissions. J. Aerosol Sci. Vol. 26 Suppl. 1, pp. S675 - S676, 1995.
Moisio, 1997	M. Moisio, Hautanen J., A. Virtanen, M. Marjamäki and J. Keskinen Electrical Low Pressure Impactor Data Processing - Effect of Particle Density. J. Aerosol Sci. Vol. 28 Suppl. 1, pp. S143 - S144, 1997.
Moisio, 1999	M. Moisio. PhD Thesis. Real Time Size Distribution Measurement of Combustion Aerosols. Tampere University of Technology Publications 279. Tampere, Finland, 1999.
Morawska, 1998	L. Morawska, N.D. Bofinger, L. Kocis and A. Nwankwoala. Submicrometer and Supermicrometer Particles from Diesel Vehicle Emissions. Environmental Science and Technology. Vol. 32, No. 14, 1998.
Morawska, 1999	L. Morawska, G. Johnson, Z.D. Ristovski and V. Agranovski. Relation between particle mass and number for submicrometer airborne particles, Atmospheric Environment 33, pp. 1983-1990, 1999.
Morgan, 1999	R. E. Morgan, S. P. Edwards, A. J. Nicol, I. D. Johnston, J. R. Needham. A premium heavy-duty engine concept for 2005 and beyond. SAE Technical Paper 1999-01-0831, 1999.
Mori, 1997	K. Mori. Worldwide trends in heavy-duty diesel engine exhaust emission legislation and compliance technologies. SAE Technical Paper 970753, 1997.
Murphy, 1998	Murphy, Life Science, 62 (19): 1789, 1998.
Neumann, 1999	K.H. Neumann, D. Schürmann, P. Kohoutek P., Beyersdorf J., Hartung A., Nagel C. and Schulze J. Unregulated Exhaust Gas Components of Modern Diesel Passenger Cars. SAE Technical Paper 1999-01-0514, 1999.
Nieki, 1994	S.A.P. Nyeki and I. Colbeck. Measurement of the Fractal Dimension of Individual Soot Agglomerates in Two and Three Dimensions. International Aerosol Conference 1994. Vol. 1 pp. 32-33. 1994.
Niessner, 2001	R. Niessner, E.F.Mikhailov, S.S.Vlasenko, Lutz Krämer. Interaction of soot aerosol particles with water droplets: influence of surface hydrophilicity. Journal of Aerosol Science Vol. 32. pp. 697-711, 2001.

Nikula, 1999	K.J. Nikula, G.L. Finch, R.A. Westhouse, J.C. Seagrave, J.L. Mauderly, D.R. Lawson and M. Gurevich. Progress in Understanding the Toxicity of Gasoline and Diesel Engine Exhaust Emissions. SAE Technical Paper 1999-01-2250, 1999.
Ntziachristos, 2000	L. Ntziachristos and Z. Samaras. Sampling Conditions Effects on Real-Time Particle Measurements from a Light Duty Vehicle. SAE Technical Paper 2000-01-2049, 2000.
Oberdörster, 1994	G. Oberdörster, Environmental Health Perspectives, 102 (5): 173, 1994.
Oberdörster, 2000	G. Oberdörster, Toxicology of Ultrafme Particles: In Vivo Studies. Phylosophical Transactions of The Royal Society of London, Series A, vol. 358, No. 1775, pp. 2719-2740. 15 October 2000.
OECD, 1988	Organisation for Economic Cooperation and Development (OECD). The State of the Environment. OECD. Paris, 1988.
Offenberg, 1999	J.H. Offenberg and J.E. Baker. Aerosol Size distributions of Polycyclic Aromatic Hydrocarbons in Urban and Over-Water Atmospheres. Environmental Science and Technology. Vol 33, No. 19, 1999.
Oh, 1996	E.K. Oh and S.G. Kim. Modelling and measurement of aerosol deposition on a heated substrate. Journal of Aerosol Science Vol. 27, No. 8, pp. 1143-1154, 1996.
Pagán, 1999	J. Pagán. Study of particle size distributions emitted by a diesel engine, SAE Paper 1999-01-1141.
Park, 2000	S.H. Park F.E. Kruis, K.W. Lee and H. Fissan. Evolution of Particle Size Distribution due to Turbulent Coagulation. J. Aerosol Sci., Vol. 31, Suppl. 1, pp. S572-S573, 2000.
Pattas, 1998	K. Pattas, N. Kyriakis, Z. Samaras, Z., P. Pistikopoulos and P. Ntziachristos. Effect of DPF on particulate size distribution using and Electrical Low Pressure Impactor, SAE Paper 980544, 1998.
Perkins, 1999	Perkins, SAE Technical Paper 1999-01-0842.
Peters, 1997	Peters, American Journal of respiratory critical case medicine, 155: 1376, 1997.
Phares, 2000	D.J. Phares, G.T. Smedley and R.C. Flagan. Effect of Particle Size and Material Properties on Aerodynamic Resuspension from Surfaces. Journal of Aerosol Science, Vol. 31, No. 11, pp. 1335-1353, 2000.

Ping, 1998	J. Ping, R.M. Harrison and F. Brear. Ultrafine particle formation during diesel exhaust dilution. Second international ETH workshop on nanoparticle measurement, August 1998.
Ping, 1999	J. Ping, R.M. Harrison and F. Brear. Investigation of Ultrafine Particle Formation during Diesel Exhaust Dilution. Environmental Science and Technology. Vol 33. No. 21. 1999.
Ping, 1999	J. Ping, R.M. Harrison and F. Brear. Particle Size Distribution from a modern Heavy-Duty Diesel Engine, The Science of the Total Environment 235, pp. 305-317, 1999.
Ping, 1999	J. Ping, R.M. Harrison and A.A. Khan. Measurements of Ultrafine Particle Concentration and Size Distribution in the Urban Atmosphere, The Science of the Total Environment 235, pp. 51-64, 1999.
Ping, 2000	J. Ping, R.M. Harrison and D. Mark. Characterisation of Particles from a Current Technology Heavy-Duty Diesel Engine. Environmental Science and Technology, Vol. 34. No. 5, 2000.
Ping, 2001	J. Ping, R.M. Harrison and D. Mark. Sources and concentration of nanoparticles (<10nm diameter) in the urban atmosphere. Atmospheric Environment, Vol. 35. No. 1193, 1202, 2001.
Pope, 1992	C.A. Pope. Architecture environmental health, 47: 211-217, 1992.
Pratsinis, 1995	S.E. Pratsinis and S. Vemury. Self-preserving size distributions of agglomerates. Journal of Aerosol Science Vol. 26, No. 2. pp. 175-185 and No. 4. p. 701 (erratum), 1995.
Preining, 1998	O. Preining. The physical nature of very, very small particles and its impact on their behaviour. Journal of Aerosol Science Vol. 29, No. 5/6 pp. 481-495, 1998.
Pui, 1988	D.Y.H. Pui, Physica Scripta Vol. 37, 252-269, 1988.
Pungs, 2000	A. Pungs, S. Pischinger, H. Bäcker, G. Lepperhoff. Analysis of the Particle Size Distribution in the Cylinder of a Common Rail DI Diesel Engine During Combustion and Expansion. SAE Technical Paper 2000-01-1999, 2000.
Querol, 2001	X. Querol, A. Alastuey, S. Rodriguez, F. Plana, E. Mantilla, C.R. Ruiz. Monitoring of PM10 and PM2.5 around primary particulate anthropogenic emission sources. Atmospheric Environment Vol. 35, pp. 845-858, 2001.

Reeks, 2001	M.W. Reeks and D. Hall. Kinetic models for particle resuspension in turbulent flows: theory and measurement. Journal of Aerosol Science 32 pp. 1-31, 2001.
Reilly, 1998	P.T. Reilly, R.A. Gieray, W.B. Whitten and J.M. Ramsey. Real-Time Characterisation of the Organic Composition and Size of Individual Diesel Engine Smoke Particles. Environmental Science and Technology, Vol. 32, No. 18, 1998.
Reist, 1993	P.C. Reist. Aerosol Science and Technology. 2nd Edition. Mc. Graw-Hill, Inc. Singapore, 1993.
Riera, 2000	E. Riera, J.A. Gallego, G. Rodríguez, V.M. Acosta, J.J. Rodríguez, J.L. Dorronsoro, D. Sanz, F.J. Gómez and M. Martín. Acoustic Agglomeration of Submicron Particles in Diesel Exhausts: First Results of the Influence of Humidity at Two Acoustic Frequencies. J. Aerosol Sci., Vol. 31, Suppl. 1, pp. S827-S828, 2000.
Ristovski, 1998	Z. Ristovski, L. Morawska and G. Johnson. A Real Time Particulate Matter Mass Distribution Monitor. J. Aerosol Sci. Vol. 29 Suppl. 1, pp. S401 - S402, 1998.
Ristovski, 1998	Z. Ristovski, L. Morawska, N.D. Bofinger and J. Hitchins. Submicrometer and Supermicrometer Particulate Emissions from Spark Ignition Vehicles. Environmental Science and Technology. Vol. 32, No. 24, 1998.
Ristovski, 2000	Z. Ristovski, L. Morawska, J. Hitchins, S. Thomas, C. Greenaway and D. Gilbert. Particle emissions from compressed natural gas engines. Journal of Aerosol Science. Vol. 31, No. 4, pp. 403-413, 2000.
Rockne, 2000	K.J. Rockne, G.L. Taghon, D.S. Kosson Pore structure of soot deposits from several combustion sources. Chemosphere Vol. 41 pp. 1125-1135, 2000.
Romay, 1998	F.J. Romay. Thermophoretic Deposition of Aerosol Particles in Turblent Pipe Flow. Journal of Aerosol Science, Vol 29, No. 8, 1998.
Ruellan, 2001	S. Ruellan, H. Cachier. Characterisation of fresh particulate vehicular exhausts near a Paris high flow road. Atmospheric Environment Vol. 35, pp. 453-468, 2001.

Russell, 1997	M.F. Russell. "Recent developments in conventional fuel injection equipment" lecture notes, 1997. Presented in the DIESEL PARTICULATES AND NOx EMISSIONS Short Course, U. of Leeds, 12-16 April 1999.
Saathoff, 2000	H. Saathoff, S. Kamm, O. Möhler, K.-H. Naumann, and U. Schurath. Trace-gas interaction with spark-generated and diesel soot. Proceedings of the EUROTRAC Symposium 2000, Garmisch-Partenkirchen, March 27-31, 2000.
Sale, 1998	T. Sale. Personal communication, 1998.
Salvat, 2000	O. Salvat, P. Marez and G. Belot. Passenger Car Serial Application of a Particulate Filter System on a Common Rail Direct Injection Diesel Engine. SAE Technical Paper 2000-01-0473, 2000.
Sanger, 1995	R.P. Sanger. CONCAWE. Automotive emissions management group, Special task force AE/STF-3. Motor Vehicle Emission Regulations and Fuel Specifications in Europe and the United States, 1995 Update. Brussels, Dec. 1995.
Saracco, 2000	G. Saracco , N. Russo, M. Ambrogio, C. Badini, V. Specchia. Diesel particulate abatement via catalytic traps. Catalysis Today 60 pp. 33–41, 2000.
Schauer, 1999.	J.J. Shauer, M.J. Kleeman, G.R. Cass, B.R.T. Simoneit. Measurement of Emissions from Air Pollution Sources. 2. C1 Through C30 Organic Compounds from Medium Duty Diesel Trucks. Environmental Science and Technology. Vol. 33, pp. 1578-1587, 1999.
Schmidt, 2000	F. Schmidt and C. Sager. Deposition of Particles in Turbulent Pipe Flows. J. Aerosol Sci., Vol. 31, Suppl. 1, pp. S847-S848, 2000.
Schraml, 1999	S. Schraml, S. Will and A. Leipertz. Simultaneous Measurement of Soot Mass Concentration and Primary Particle Size in the Exhaust of a DI Diesel Engine by Time-Resolved Laser Induced Incandescence (TIRE-LII). SAE Technical Paper 1999-01-0146, 1999.
Schraml, 1999	S. Schraml, S. Will and A. Leipertz. Simultaneous Soot Mass Concentration and Primary Particle Size Measurements in the Exhaust Gas of Diesel Engines Based on Laser Induced Incandescence (LII). ISATA Proceedings 1999, 32nd, pp 167-174. 99CPE022, 1999.

Schröder, 1999	O. Schröder, J. Krahl, A. Munack and J. Bünger. Environmental and Health Effects Caused by the use of Biodiesel. SAE Technical paper 1999-01-3561, 1999.
Schweizer, 2000	T. Schweizer, H.J. Stein. A New Approach to Particulate Measurement on Transient Test Cycles: Partial Flow Dilution as Alternative to CVS Full Flow Systems. SAE Technical Paper 2000-01-1134, 2000.
Seaton, 1985	A. Seaton, W. MacNee, K. Donaldson and D. Godden. Particulate air pollution and acute health effects, The Lancet, Vol. 345, pp.176-178, 1985.
Shelef, 2000	M. Shelef and R.W. McCabe. Twenty-five years after introduction of automotive catalysts: what next? Catalysis Today. Vol. 62 pp. 35–50, 2000.
Siegmann, 2000	K. Siegmann and H. C. Siegmann. Fast and Reliable "in situ" Evaluation of Particles and their Surfaces with Special Reference to Diesel Exhaust. SAE Technical Paper 2000-01-1995, 2000.
Siegmann, 2000	K. Siegmann, Q. Zhiqiang, A. Keller, U. Matter, L. Scherrer, H.C. Siegmann. Nanoparticle air pollution in major cities and its origin. Atmospheric Environment No. 34, pp. 443-451, 2000.
Silvis, 1999	W.M. Silvis, R.N. Harvey and A.F. Adageforde. A CVF Type Mini-dilution Sampling System for Vehicle Exhaust Emissions Measurement. SAE Technical Paper 1999-01-0151, 1999.
Simons, 1997	S. Simons, A new derivation of the agglomerate size distribution for a constant coagulation kernel. Journal of Aerosol Science Vol. 28, No. 8. pp. 1393-1394, 1997.
Sioutas, 1999	C. Sioutas, E. Abt, J.M. Wolfson and P. Koutrakis. Evaluation of the Measurement Performance of the Scanning Mobility Particle Sizer and Aerodynamic Particle Sizer. Aerosol Science and Technology 30: 84-92, 1999.
Skillas, 1998	G. Skillas, S. Künzel, H. Burtscher, U. Baltenspenger and K. Siegmann. High Fractal-like Dimension of Diesel Soot Agglomerates. J. Aerosol Sci. Vol 29 No. 4, pp411-419, 1998.
Smedler, 1995	G. Smedler, G. Ahlström, S. Fredholm, J. Frost, P. Lööf, P. Marsh, A. Walker and D. Winterborn. High performance diesel catalysts for Europe beyond 1996. SAE Technical Paper 950750, 1995.

Sreenath, 1999	A. Sreenath, G. Ramachandran and J.H. Vincent. An Experimental Approach to Correcting Counting Errors in the Aerodynamic Particle Sizer (APS Model 3310). Particle and Particle Systems Characterisation, Vol. 16, Part 6, pp. 257-265, 1999.
Stone, 1985	R. Stone. Introduction to Internal Combustion Engines. McMillan Press Ltd. London, 1985.
Stradling, 2000	R.J. Stradling, J.F. Unsworth and C. Dodson. The measurement of particle number emissions from diesel engines – a fuel perspective. I. Mech. Eng. Paper C588/029/2000. UK, 2000.
Sturm, 2000	P. Sturm. Introduction to Transport and Air Pollution. Atmospheric Environment 34 pp. 4579-4580, 2000.
Suhre, 1992	B.R. Suhre and D.E. Foster. In-Cylinder Soot Deposition Rates Due to Thermophoresis In a Direct Injection Diesel Engine. SAE Technical Paper 921629, 1992.
Suzuki, 1997	T. Suzuki, T. Kakegawa, K. Hikino and A. Obata. Development of diesel combustion for commercial vehicles. SAE Technical Paper 972685, 1997.
Tach, 1997	Tach. Atmospheric environment, 31 (24): 4193, 1997.
Tanaka, 1999	S. Tanaka and T. Shimizu. A Study of Composition and Particle Size Distribution of Particulate Matter from DI Diesel Engine. SAE Technical Paper 1999-01-3487, 1999.
Tanin, 1999	K. V. Tanin, D. D. Wickman, D. T. Montgomery, S. Das, R. D. Reitz. The influence of boost pressure on emissions and fuel consumption of a heavy-duty, single-cylinder D.I. diesel engine. SAE Technical Paper 1999-01-0840, 1999.
Tapper, 1995	U. Tapper, M. Marjamäki, M. Moisio, E.I. Kauppinen and J. Keskinen. Inversion of Electrical Low Pressure Impactor Data. J. Aerosol Sci. Vol. 26 Suppl. 1, pp. S103 - S104, 1995.
Toy, 2000	E. Toy, J.D. Graham, J.K. Hammit. Fueling Heavy Duty Trucks:Diesel or Natural Gas? Risk in Perspective. Volume 8, No. 1. Harvard Center for Risk Analysis. January 2000.
Tsai, 2001	C.J. Tsai, L.J. Liang. Correlation for thermophoretic deposition of aerosol particles onto cold plates. Journal of Aerosol Science Vol. 32, pp. 473-487, 2001.

Tsai, 2001	C.J. Tsai, C.H. Huang. Effect of gravity on particle collection efficiency of inertial impactors. Aerosol Science 32 pp. 375-387, 2001.
Tsukamoto, 2000	Y. Tsukamoto, Y. Goto and M. Odaka. Continuous Measurement of Diesel Particulate Emissions by an Electrical Low-Pressure Impactor. SAE Technical Paper 2000-01-1138, 2000.
USEPA, 1985	USEPA. Compilation of Air Pollutant Emission Factors, 4th Edition, Vol. II: Mobile Sources. USEPA, Ann Arbor. USA, 1985.
van Beckoven, L.C.	L.C. van Beckoven. Effects of Fuel Properties on Diesel Engine Emissions - A Review of Information Available to the EEC-MVEG Group. SAE Technical Paper 910608, 1991.
van Gulijk, 2000	C. van Gulijk, J.C.M. Marijnissen, M. Makkee and J.A. Moulijn. Evaluation of the ELPI for Diesel Soot Measurements. J. Aerosol Sci., Vol. 31, Suppl. 1, pp. S394-S395, 2000.
Venkataraman, 1994.	C. Venkataraman, J.M. Lyons and K. Friedlander. Size Distributions of Polycyclic Aromatic Hydrocarbons and Elemental Carbon 1. Sampling, Measurement Methods and Source Characterisation. Environmental Science and Technology. Vol. 28, pp. 555-562, 1994.
Venkataraman, 1994.	C. Venkataraman, J.M. Lyons and K. Friedlander. Size Distributions of Polycyclic Aromatic Hydrocarbons and Elemental Carbon 2. Ambient Measurements and Effects of Atmospheric Processes. Environmental Science and Technology. Vol. 28, pp. 563-572, 1994.
Vincent, 2000	J.H. Vincent and C.F. Clement. Ultrafine Particles in Workplace Atmospheres. Phylosophical Transactions of The Royal Society of London, Series A, vol. 358, No. 1775, pp. 2673-2682. 15 October 2000.
Virtanen, 2000	A. Virtanen, M. Marjamäki, J. Ristimäki and J. Keskinen. Secondary Particle Collection Mechanisms in ELPI. J. Aerosol Sci. Vol 31, Suppl. 1, pp. S74-S75, 2000.
Wall, 1984	J.C. Wall and S.K. Hoekman. Fuel Composition Effects on Heavy Duty Diesel Particulate Emissions. SAE Technical Paper 841364, 1984.
Walsh, 1998	Walsh. Global Trends in Diesel Emissions Control – A 1998 Update, SAE Technical Paper 980186, 1998.
Walsh, 1999	Walsh. Global Trends in Diesel Emissions Control – A 1999 Update, SAE Technical Paper 1999-01-0107, 1999.

Wang, 2000	W.G. Wang, D.W. Lyons, N.N. Clark, M. Gautam and P.M. Norton. Emissions from NIne Heavy Trucks Fueled by Diesel and Biodiesel Blend without Engine Modification. Environmental Science and Technology, Vol. 34, No. 6, 2000.
Watt, 1985	I.M. Watt. The Principles of Electron Microscopy. Cambridge University Press, Cambridge, 1985.
Webster, 2000	D. Webster. "Oxidation Catalyst Development" Lecture in the Diesel Particulate and NOx Emissions Course. Department of Fuel and Energy, University of Leeds. Leeds, April 12-16 1999.
Wedekind, 2000	B.G.A. Wedekind, J.D. Andersson, D.E. Hall, R. Stradling, Chris Barnes, G. Wilson. DETR/SMMT/ CONCAWE Particle Research Programme: Heavy Duty Results. SAE Technical Paper 2000-01-2851, 2000.
Weingartner,1997	E. Weingartner, H. Burtscher and U. Baltenspenger. Hygroscopic properties of carbon and diesel soot particles. Atmospheric Environment 31, pp. 2311-2327, 1997.
Westerholm, 1991	R. Westerholm, J. Almén, L. Hang, U. Rannug, K.E. Ege-bäck and K. Grägg. Chemical and biological characterization of particulate, semi-volatile and gas phase associated compounds in diluted heavy duty diesel exhausts: A comparison of three different semi-volatile phase samplers. Environ. Sci. Tech. Vol. 25, 332-338, 1991.
Westerholm, 1999	R. Westerholm, A. Christensen, C. de Serves and J. Almén. Determination of Polycyclic Aromatic Hydrocarbons (PAH) in Size Fractionated Diesel Particles from a Light Duty Vehicle. SAE 1999-01-3533, 1999.
Whitelegg, 1993	J. Whitelegg. Transport for a Sustainable Future - The Case for Europe. Belhaven Press, London and New York, 1993.
Wichmann, 2000	H.E. Wichmann and A. Peters. Epidemiological Evidence of the Effects of Ultrafine Particle Exposure. Phylosophical Transactions of The Royal Society of London, Series A, vol. 358, No. 1775, pp. 2751-2770. 15 October 2000.
Willeke, 1993	K. Willeke and P. Baron. Aerosol Measurement; Principles, Techniques and Applications. Van Nostrand Reinhold, New York, 1993.

Williams, 1988	P.T. Williams, M.K. Abbass, L.P. Tam, G.E. Andrews, K.L. Ng and K.D.A. Bartle. A Comparison of Exhaust Pipe, Dilution Tunnel and Roadside Diesel Particulate SOF and Gaseous Hydrocarbon Emissions. SAE Technical Paper 880351, 1988.
Wilson, 1997	Wilson. Journal of Air and Waste Management Association, 47: 1238, 1997.
Yanowitz, 1999.	J. Yanowitz, M.S. Graboski, L.B.A. Ryan, T. Alleman and R.L. McCormick. Chassis Dynamometer Study of Emissions from 21 In-Use Heavy-Duty Diesel Vehicles. Environmental Science and Technology, Vol. 33, No. 2, 1999.
Yanowitz, 2000.	J. Yanowitz, M.S. Graboski and R.L. McCormick. In-Use Emissions from Heavy-Duty Diesel Vehicles. Environmental Science and Technology, Vol. 34, No. 5, 2000.
Yassine, 1996.	M.K. Yassine, Tagomori, N.A. Henein and W. Bryzik. White Smoke Emissions Under Cold Starting of Diesel Engines. SAE Technical Paper 960249, 1996.
Zaichik, 1995	L.I. Zaichik, B.I. Nigmatulin and V.A. Pershukov. Modelling of Dynamics of Aerosols in Near-Wall Turbulent Flows and Particle Deposition in Pipes. Proceedings of the 2nd International Conference on Multiphase Flow '95 - Kyoto. April 3-7, 1995.
Zelenka, 1998	P. Zelenka, H. Aufinger, W. Reczec and W. Cartellieri. Cooled EGR - A Key Technoloy for Future Efficient HD Diesels. SAE Technical Paper 980190, 1998.
Zhou, 2000	Y. Zhou and Y.S. Cheng. Particle Deposition in First Three Generations of a Human Lung Cast. J. Aerosol Sci., Vol. 31, Suppl. 1, pp. S140-S141, 2000.
Ziemann, 1998	P.J. Ziemann. Particle Mass and Size Measurements Using Mass Spectrometry. Trends in Analytical Chemistry, Vol. 17, No. 6, 1998.
Zieseniz, 1998	Zieseniz, 6th International Highway and Urban Pollution Symposium, ISPRA, May 1998.
Ziskind, 1995	G. Ziskind, M. Fichman and C. Gutfinger. Resuspension of Particulates from Surfaces to Turbulent Flows - Review and Analysis. Journal of Aerosol Science, Vol. 26, No. 4, pp. 613-644, 1995.